ESPOO 2004 VTT SYMPOSIUM 233

BALTICA VI

Life Management and Maintenance for Power Plants Vol. 1

Fortum Helsinki Energy Kunnossapitoyhdistys ry • Finnish Maintenance Society VTT

VTT SYMPOSIUM 233

Keywords:
power plant, maintenance, boiler, machinery, equipment, inspection, monitoring, condition, life, performance, risk, reliability

BALTICA VI

Life Management and Maintenance for Power Plants

Vol. 1

Helsinki – Stockholm – Helsinki
8–10 June, 2004

Edited by

Juha Veivo & Pertti Auerkari

Organised by

VTT Industrial Systems

ISBN 951–38–6291–7 (soft back ed.)
ISSN 0357–9387 (soft back ed.)

ISBN 951–38–6292–5 (URL:http://www.vtt.fi/inf/pdf/)
ISSN 1455–0873 (URL: http://www.vtt.fi/inf/pdf/)

JULKAISIJA – UTGIVARE – PUBLISHER

VTT, Vuorimiehentie 5, PL 2000, 02044 VTT
puh. vaihde (09) 4561, faksi 456 4374

VTT, Bergsmansvägen 5, PB 2000, 02044 VTT
tel. växel (09) 4561, fax 456 4374

VTT Technical Research Centre of Finland
Vuorimiehentie 5, P.O.Box 2000, FIN–02044 VTT, Finland
phone internat. + 358 9 4561, fax + 358 9 456 4374

VTT Tuotteet ja tuotanto, Kemistintie 3, PL 1704, 02044 VTT
puh. vaihde (09) 4561, faksi (09) 456 7002, (09) 456 7010, (09) 456 5875

VTT Industriella System, Kemistvägen 3, PB 1704, 02044 VTT
tel. växel (09) 4561, fax (09) 456 7002, (09) 456 7010, (09) 456 5875

VTT Industrial Systems, Kemistintie 3, P.O.Box 1704, FIN–02044 VTT, Finland
phone internat. + 358 9 4561, fax + 358 9 456 7002, + 358 9 456 7010, + 358 9 456 5875

Otamedia Oy, Espoo 2004

Preface

Market liberalisation and requirements of environmentally benign production continue to shape the framework for successfully managing the condition and life of power plants. Operational demands for fast response and flexibility to benefit from market pricing or from cheap low grade fuels can impose considerable challenge, because the foreseen benefit must also cover for the additional loading and damage to equipment. At the same time, there is an underlying and unchanged need for driving down cost, and continuous technical development in processes, equipment design, manufacturing, materials and maintenance systems (including services) will introduce new solutions to both old and new challenges in the plant.

As the power market, production equipment and technology remain under a continuing transition, the tri-annual BALTICA Conference aims to provide a review on the current status and future expectations on the essential issues on life management and maintenance for power plants. Much of this review is contained in the conference presentations and therefore in the two volumes of this publication. However, to fully benefit from the extensive knowledge and experience of the colleagues and experts, the participants are also strongly encouraged to take the opportunity for personal discussion on further details or particular areas of interest during the conference.

The editors wish to express their sincere gratitude to the authors for providing the excellent state-of-the-art papers and presentations for the conference. The kind effort by the referees, many of them in the Board of the Conference, is very much appreciated for helping to maintain the required quality of the publication. Special thanks are due to Ms Karin Waltari, the Conference Secretary at VTT, for her most valuable contribution in taking good care of the conference arrangements. We would also like to thank Ms Åsa Åvall and Ms Sanni Mustala at VTT for helping to edit the proceedings. Finally, financial and other support by the sponsoring organisations is most gratefully acknowledged.

Espoo, June 2004

Juha Veivo Pertti Auerkari

BALTICA VI Editors

Contents

Contents of Volume 1

Session 2. Developments in boilers and rotating machinery

2 A. Boiler plant

2 B. Rotating equipment

Challenges in application of risk-based approaches: Experiences and examples from the European practice

A. Jovanovic
MPA Stuttgart, Germany

Abstract

Risk-Based Approaches in inspection, maintenance and plant/asset management are nowadays in a well-advanced stage of application and make a well-established part of modern practice. Nevertheless, both current and future application face a number of serious challenges, reviewed and considered in this paper. Their relevance and their application aspects are illustrated mainly on the basis of experiences and results obtained in the European practice, primarily in the work on the EU project RIMAP.

1. Introduction

Risk-based approaches in the area of maintenance started gaining ground in late 80-ties, first in the petrochemical and offshore industry in the USA, spreading later to other areas of application (e.g. power plants) and other countries, notably Europe and Japan. Regulatory basis, technical documentation and tools have been developed, most of them nowadays widely (commercially!) available for virtually all kinds application, on various scales, from very large plants to the very small ones. In the practice we usually talk about terms like RBI (risk-based inspection), RBIM (risk-based inspection and maintenance), RCM (reliability-centered maintenance), RBLM (risk-based life management) or simply, RBM (risk-based management).

However, use and application of risk-based approaches, both for the current and for the future applications may have to deal with and solve a number of serious general challenges, related to the very idea of risk-based approach. Some of them, both those already recognized in the practice and those that may potentially appear yet, have been reviewed and considered in this paper. Their relevance and their application aspects are illustrated mainly based on experiences and results obtained in the European practice, primarily in the work on the large EU project RIMAP.

In addition, the paper looks also at the challenges related to application aspects (e.g. techniques, methods, tools, available data…). Successfully meeting these challenges is condition sine qua non for the further application of the risk-based

approaches. It is only due to extensive plant operating experience, improved understanding of material degradation mechanisms, and the availability of fitness-for-service assessment procedures that these risk-based approaches became feasible at all.

Certain sectors of industry, particularly the refining and petrochemicals sectors, but nowadays increasingly also general process, power, paper and steel industry, set the inspection priorities on the basis of the specific risk of failure. The incentives for the above trend can be found primarily in the potential benefits, which the improved targeting and timing of inspections offer to the industry. The main benefits are (as rightly pointed out also in the HSE report, 2001):

- improvement of the plant safety and reliability, and
- cost savings by eliminating ineffective inspection, extending inspection intervals and greater plant availability.

Concentration of the inspection and maintenance effort onto the right items of the plant, including timely identification and repair or replacement of deteriorating equipment, on one side, and avoiding unnecessary inspection and maintenance actions are the key practical actions leading to the realization of the above mentioned desirable benefits.

2. Risk-based approaches

Risk is nowadays not only a safety issue; neither is it an issue "of rules and regulations" only. It has become also an economic category, "merchandise" in a way, having its price, its market(s), its traders… Who invests in e.g. risk mitigation or reduction, expects an economically measurable benefit, too. This change of paradigm, means in the practice that it is *more important to know and manage the risk, than to necessarily reduce or eliminate it "by all means...".*

Safety limits are usually imposed by law (e. g. radiation related ones in nuclear power plants, or pollutant emissions in chemical plants) – it means that if the risk of certain averse event in the plant must be kept below the limit, otherwise the plant will be shut down. Economic limits (e. g. in conventional thermal power plants) mean that the additional cost due to experienced and/or potential damage (increasing e. g. the insurance costs) will burden the operation so much that the plant will have to be shut down as non-profitable. In the case that the measures have been successful, the plant can be kept in operation for longer time (Figure 1). For example in the case of a power plant only boiler and piping maintenance cost over the lifetime of the plant can reach the level of the 10% of the capital cost for the whole plant. Therefore, the main issue appears to be finding of the right balance between

- gain/profit obtained by risk-reduction measures (e. g. life extension, higher availability and similar), and
- cost of the risk reduction measures.

In the conditions of the liberalized market, the above approach is not sufficient, because it does not take into account the fluctuation of market prices. Therefore, the new market-oriented approaches advocate on-line dynamic analysis of the price cost ratio (Jovanovic 2003).

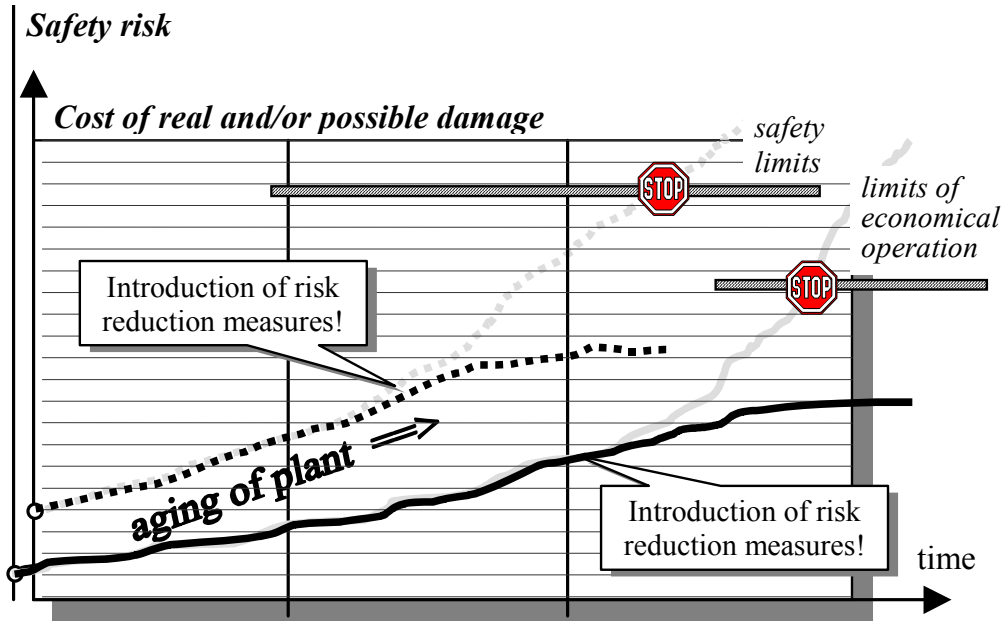

Figure 1. Time-dependency of cost, safety and risk (after introduction of risk reduction measures).

3. Challenges

The situation as described above, however, does not include the issues which can make the whole application of the risk-based approaches questionable. These challenges can be divide into two main groups, namely:

- the general issues and the
- particular, mainly technical issues, specific for RBI, RBLM, RBM,...

In the following text, some of them will be considered. The critical question to answer is the one regarding the self-sustainability of risk-based approaches: are they here to stay or are they just another "fashion of the day" (Figure 2).

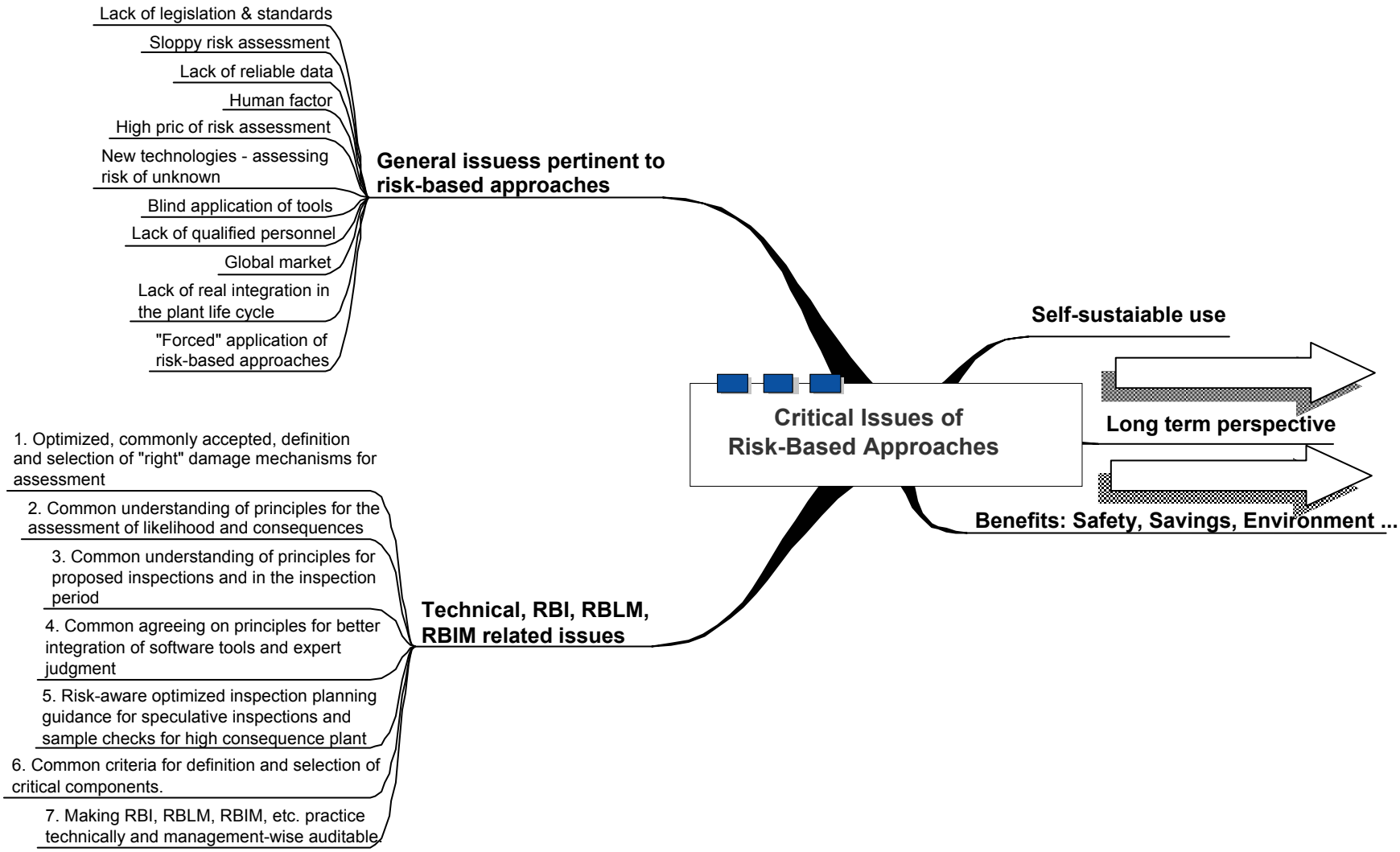

Figure 2. Aspects and possible "futures" of risk-based approaches.

4. Major general challenges ("grand challenges") of risk-based approaches

The following issues have appeared to be of high relevance in the European practice so far (including also, e.g., EU projects like RIMAP, SAFERELNET, FITNET and TRENDS):

Grand Challenge 1. **Legislation, codes, standards**

Lack of unified and consolidated legislation, codes, standards: The codes and standards for design or manufacturing (e.g. PED, 1997, in the area of pressure vessels) have developed in the direction of unification at the European level, whereas those related to inspection and maintenance are still practically exclusively national. In addition risk-based approaches are still allowed in all countries, e.g. in EU (Figure 3).

Grand Challenge 2. **Reliable data**

Do gigabytes of data bring us any closer to the risk assessment we need? How to assess their quality and real scope of use?
While initial versions of RBI/RBLM systems very much stand alone systems, the new generation systems are regularly network or even Intranet oriented (Figure 6). The amount of data can easily reach terabytes levels, especially in integrated (Figure 7, Figure 8), data warehouse oriented systems (i.e. systems storing their own shape in a given moment in time).

Grand Challenge 3. **Human factor**

With further development of systems the known problems might be better under in the control, but the systems often provide an unwanted nice or appealing look/appearance for actually poor analysis – how can one build protection against sloppy risk assessment and management?
Reduction of plant personnel, especially on the level of the highly qualified personnel, has significantly reduced the chances to find right people for performing qualified risk-based analysis. Essentially, it can be very difficult to compose a team comprising of, e.g. following API recommendations:

- Project Manager\Owner
- Personnel with the following expertise:
    - Inspection
    - Metallurgy/Corrosion
    - Mechanical/Reliability Engineering
    - Process Engineering
    - Process Hazards

Figure 3. Spread of risk-based approaches in Europe.

Grand Challenge 4. **Price of risk management**

The relatively high cost of introduction of risk-based approaches is usually covered by the savings achieved in the same stage (i.e. the components not needed to be inspected are removed from the inspection plan). But for the subsequent applications, although the RBI/RBLM cost are often reduced, too, the savings are not guaranteed. This can lead to significant safety problems caused, e.g., by the question who will pay for continued risk management or is business critical the same as safety critical?

Grand Challenge 5. **New technologies**

Introducing more and more decentralized and combined plants, diversifying energy production with renewable energy systems and similar measures lead to completely new issues: How to assess the risks of the unknown? Especially of long term and complex impacts and effects? How to obtain data needed for reliability or risk assessments for the "one-of-the-kind" systems components and systems with virtually no operation record? Some of the issues are covered by the DNV document RP-A203, but the procedure given in the document (DNV, 2001) primarily shows what data are needed and how to collect and analyze them in principle.

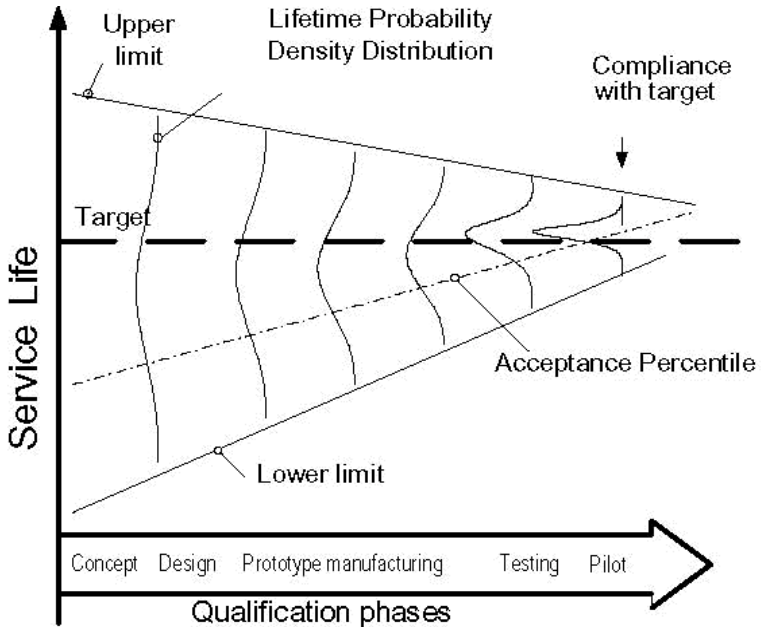

Figure 4. Illustration of the new technology qualification process defined in DNV RP-A203; qualification is achieved when the acceptance percentile crosses the target level for the service life.

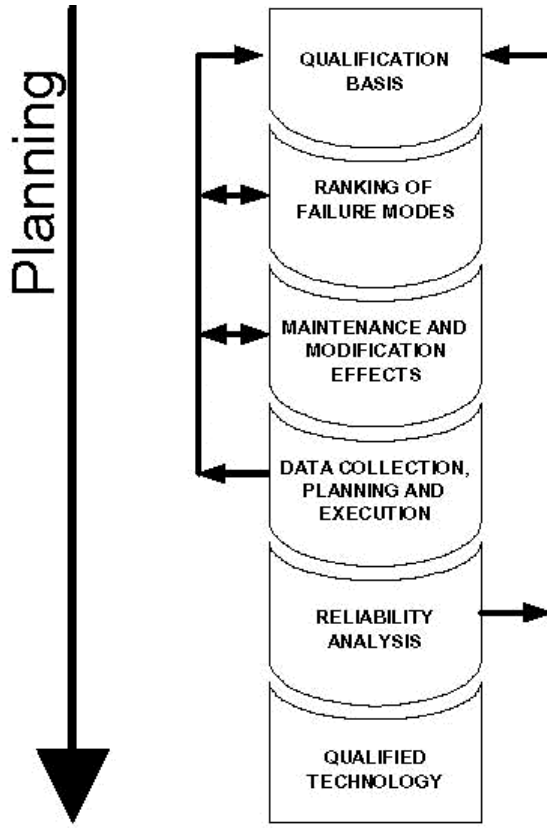

Figure 5. Main activities in the qualification procedure for new technologies as foreseen by DNV-A203.

Grand Challenge 6. **"Blind" application of tools**

Software systems are nowadays widely used and calculations of the consequences made, but it often remains transparent what assumptions were made and details are frequently hidden in the "black box". The same often applies to data coming into the RBI/RBLM system from other software systems (e.g. monitoring systems, plant databases, etc.) – these data are often not really visible for the analyst.

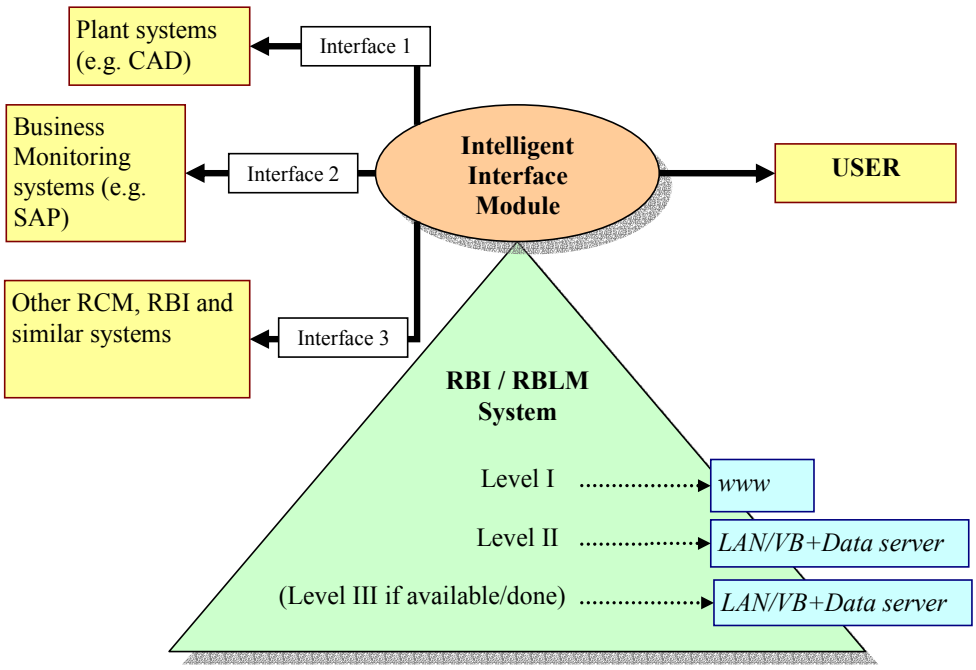

Figure 6. Example of a possible configuration of different database system involved in RBI/RBLM analysis.

Grand Challenge 7. **Old/aged plants**

Old plants are often economists' favorites – economic pressure to increase the plant life can be huge and possible benefits (e.g. no need to ask for new permits, etc.) appealing. But assessing risks of old plants, often to be assessed by the engineers younger than the plant, in the lack of reliable, even basic, data, can be a huge problem.

Grand Challenge 8. **Globalization**

Assessing risks of a plant built on the "globalized" market – multiple and combined vendors, suppliers or subcontractors "disappearing" in mergers and acquisition, language barriers, use of web (imposing often additional challenges to the confidentiality of sensitive data) can become an insurmountable problem for the assessor.

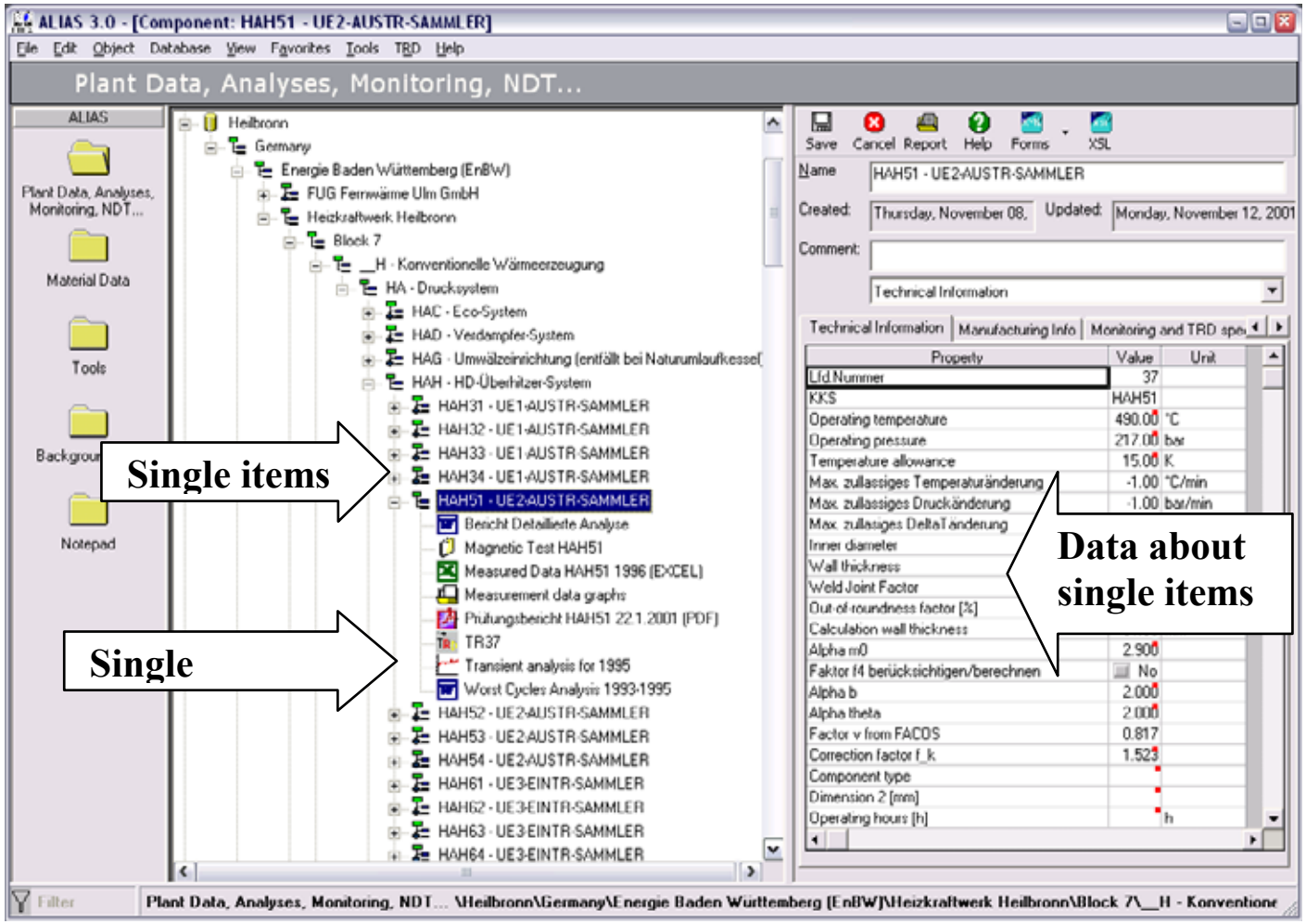

Figure 7. Modeling plant and inspection data.

Grand Challenge 9. **Life cycle**

Real integration in the life-cycle of the plant and of the technology and assessment of medium and long-term risk is not necessarily the priority neither for the owner nor for the inspector. Nevertheless, for the society, especially if combined with new technologies or refurbished plants it can be really a huge problem, in particular, when the one responsible for the risks/causes/consequences (e.g. a bankrupt company) is not accountable any more.

Grand Challenge 10. **"Forced" application**

This is probably the least "grand" of all challenged above, but nevertheless important. It means that using the risk-based approaches is often done without real added value, just because it is "fashionable" or because "others do it, too".

Table 1. Excerpt from the checklist used in RIMAP project regarding the RBI/RBLM personnel qualificatio.

	THE RBIM (RBI/RBLM) MANAGEMENT TEAM AND RESPONSIBILITIES
…	….
3.3	Does the team have knowledge and experience in the key areas?
3.4	Do the team members have adequate qualifications and competence?
3.6	Does the team have wider industry knowledge?
3.7	How is the "competent person" integrated in the team?
3.8	How does the team record meetings and decisions?
3.9	Is access to staff, experts and other resources adequate?
3.10	What are the team's terms of reference?
…	…

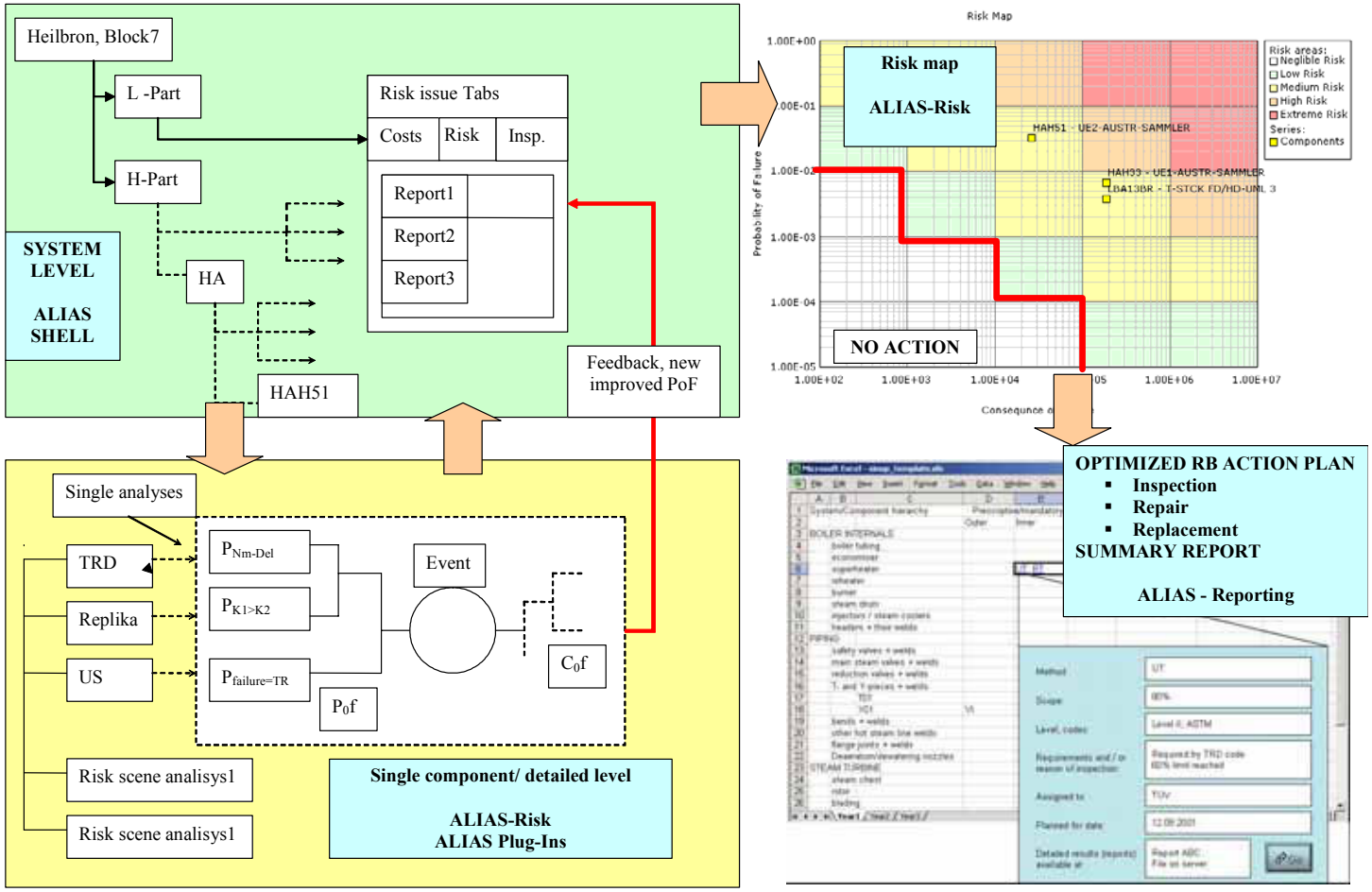

Figure 8. Example of an integrated RBLM system (ALIAS, see [ALIAS] (2003) and Jovanovic, 1999).

5. Major technical challenges of RBI, RBLM, RBIM and RBM

Despite large efforts invested in both USA and EU, as well as in large companies, into the development of general and generally accepted guidelines for RB, RBLM, RBIM and RBM, some technical (purely engineering) issues are still open and will certainly require a lot of attention also in the future work. The most relevant among them are probably:

Technical Challenge 1.

Optimized, commonly accepted, definition and selection of "right" damage mechanisms for assessment – different conclusions, regarding the impact of a damage mechanism, can be drawn from identical data.

Technical Challenge 2.

Common understanding of principles for the assessment of likelihood and consequences. Current methods often benefit of simplicity and ensure conservatism but lack the accuracy. Subjective judgments based on limited information often lead to significant differences in decisions and, e.g., inspection periods. For instance the general applicability and extendibility of the very often used scale given in the example in Figure 9 can often be questioned, as soon as one starts changing the boundary conditions for the analysis.

Technical Challenge 3.

Common understanding of principles for proposed inspections and in the inspection period. In most cases, inspection plans only included procedures for damage mechanisms regarded as active. There was evidence, in a smaller number of plans, of procedures explicitly included for inactive or "unlikely" mechanisms.

Technical Challenge 4.

Common agreeing on principles for better integration of software tools and expert judgment – greater integration of these elements would be beneficial. How for instance to combine the detailed quantitative analysis the flowchart of which is shown in Figure 11 and Figure 10 (risk-based analysis of a header exposed to combined cyclic creep and fatigue loading, suspected nozzle corner crack) with the simplified analysis shown in Figure 9?

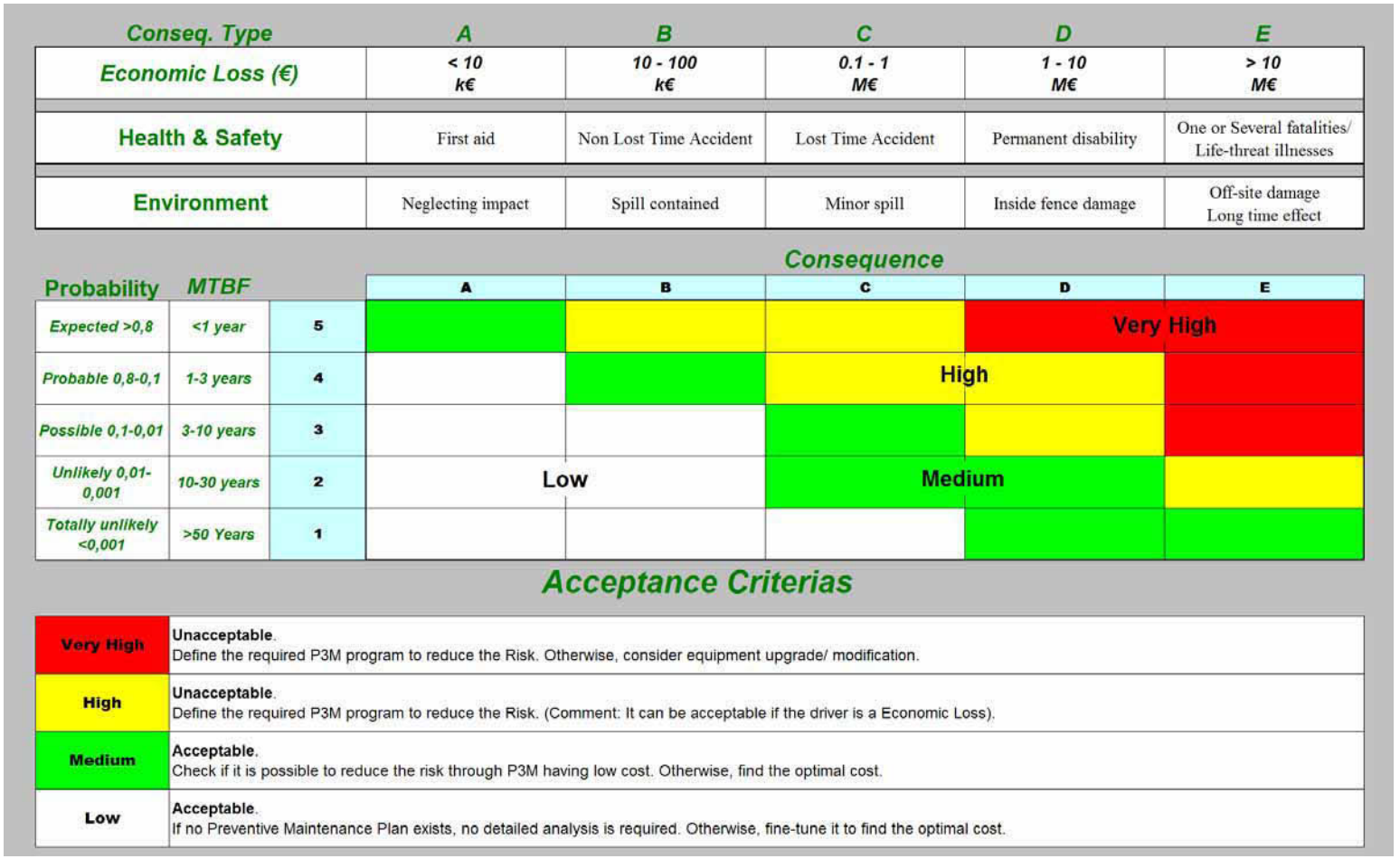

Conseq. Type	A	B	C	D	E
Economic Loss (€)	< 10 k€	10 - 100 k€	0.1 - 1 M€	1 - 10 M€	> 10 M€
Health & Safety	First aid	Non Lost Time Accident	Lost Time Accident	Permanent disability	One or Several fatalities/ Life-threat illnesses
Environment	Neglecting impact	Spill contained	Minor spill	Inside fence damage	Off-site damage Long time effect

Probability	MTBF		Consequence A	B	C	D	E
Expected >0,8	<1 year	5				Very High	
Probable 0,8-0,1	1-3 years	4			High		
Possible 0,1-0,01	3-10 years	3					
Unlikely 0,01-0,001	10-30 years	2	Low		Medium		
Totally unlikely <0,001	>50 Years	1					

Acceptance Criterias

Very High	**Unacceptable**. Define the required P3M program to reduce the Risk. Otherwise, consider equipment upgrade/ modification.
High	**Unacceptable**. Define the required P3M program to reduce the Risk. (Comment: It can be acceptable if the driver is a Economic Loss).
Medium	**Acceptable**. Check if it is possible to reduce the risk through P3M having low cost. Otherwise, find the optimal cost.
Low	**Acceptable**. If no Preventive Maintenance Plan exists, no detailed analysis is required. Otherwise, fine-tune it to find the optimal cost.

Figure 9. Example of the starting risk aggregation plot in terms of probability and consequences of failure (RIMAP).

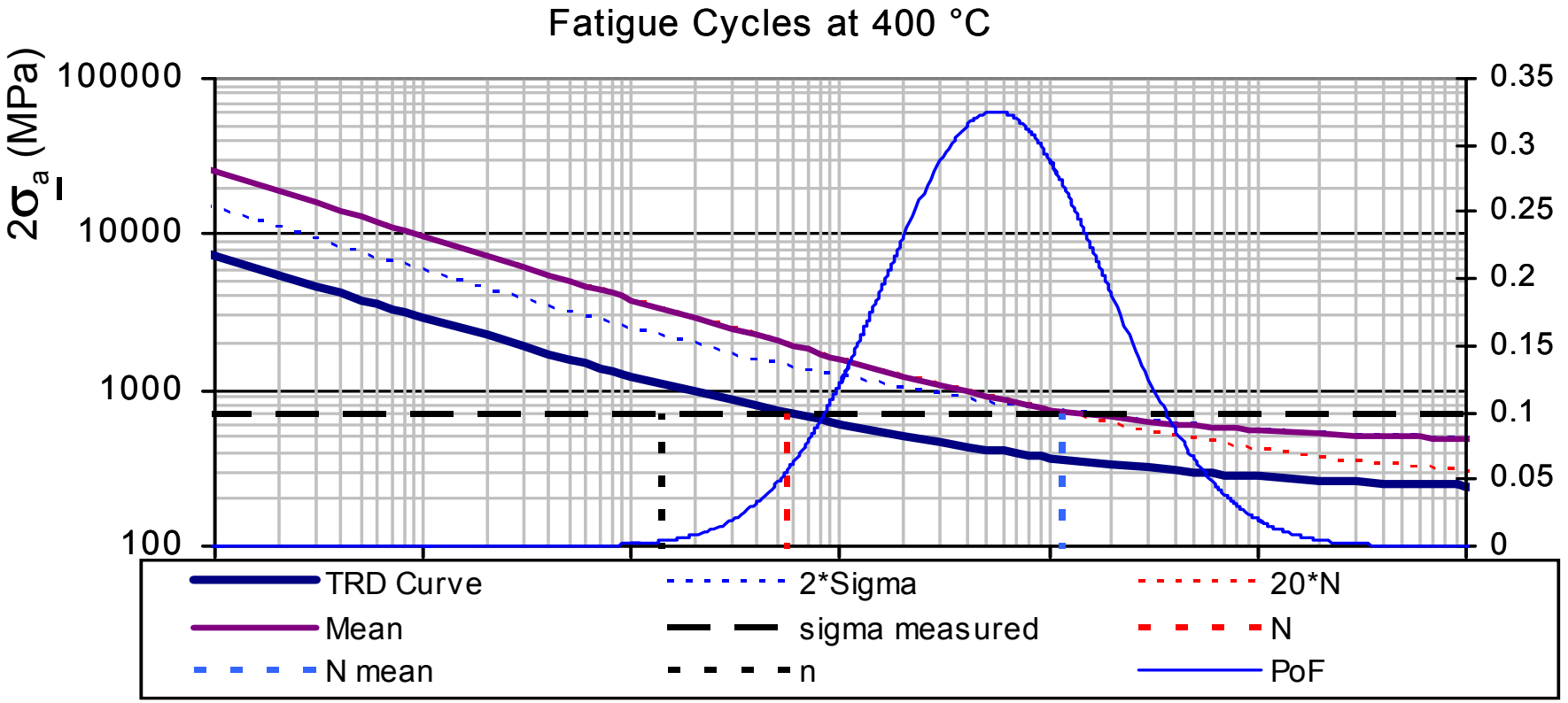

Figure 10. Principle of probabilistic fatigue analysis in PoF calculation.

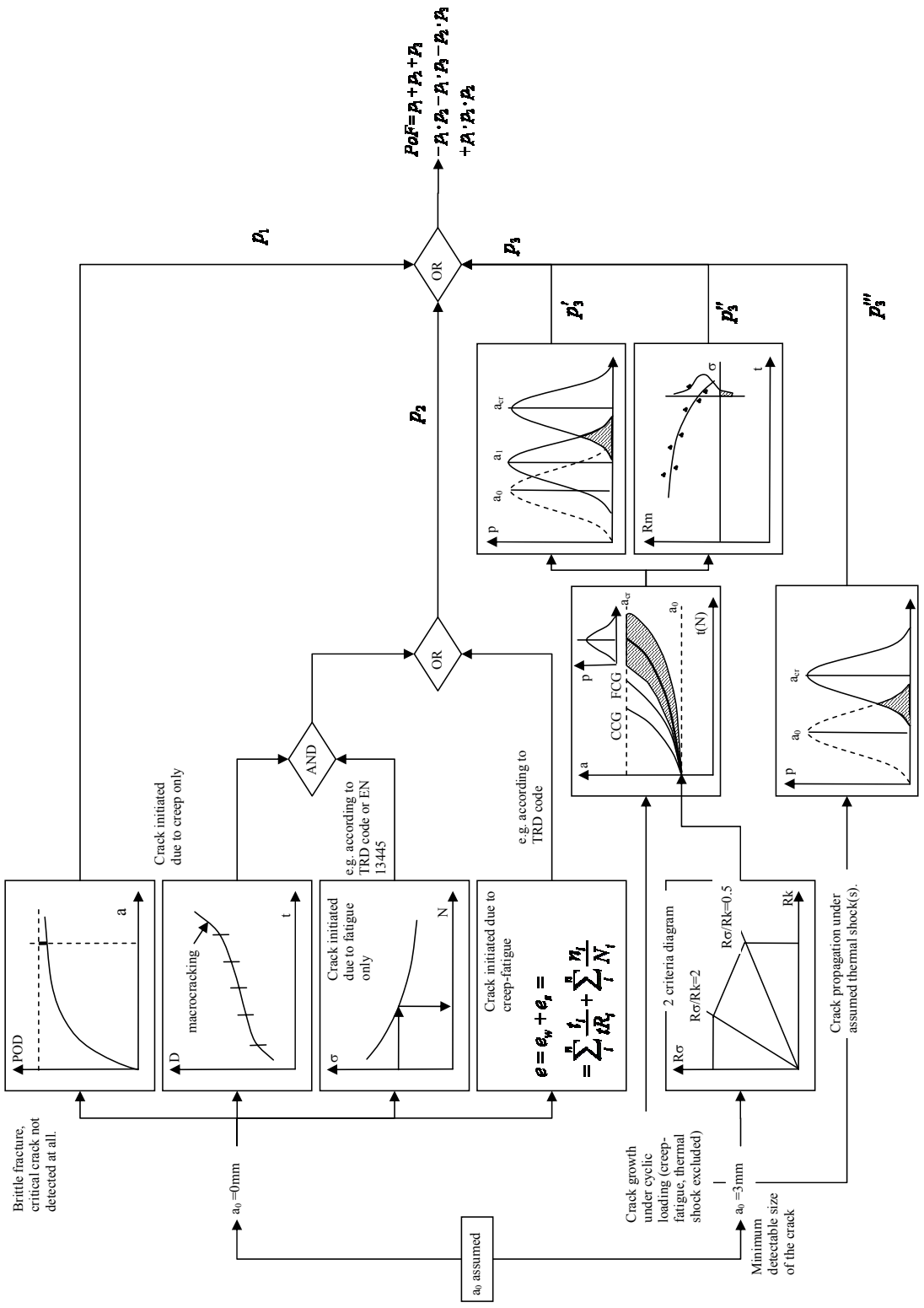

Figure 11. Schematic representation of procedure for probability of failure (PoF) calculation in detailed analysis, more details in Jovanovic et al. (2004).

Technical Challenge 5.

Risk-aware optimized inspection planning guidance for speculative inspections and sample checks for high consequence plant are still missing on virtually all levels: national, company, international.... Reliability and effectives (efficiency) of NDT methods and techniques are of a special importance in this sense (Figure 12).

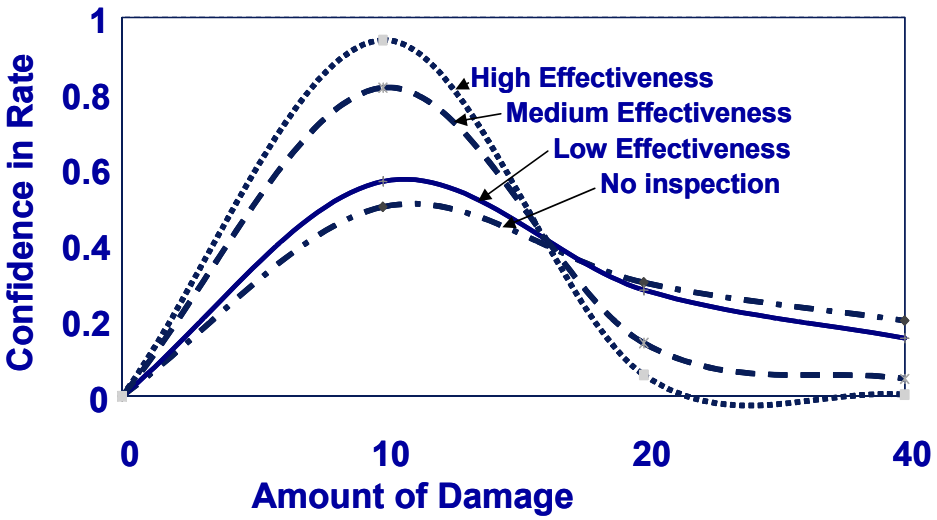

Figure 12. Inspection efficiency as a critical issue for the "future" of RBI/RBLM approaches (API).

Technical Challenge 6.

Common criteria for definition and selection of critical components. One of the main goals of the current practice is to concentrate onto critical components, i.e. components "mostly contributing to the risk". This practically means, that the components that can lead to the extreme, but only hypothetically possible "critical situations" (e.g. disastrous accidents) are not necessarily the most "critical components". They will be that only if the probability of such events can justify this, i.e. cause increase in risk. This approach is often misunderstood by people working in the area of safety, who, correspondingly, tend to create their scales of criticality primarily based on the possible/imaginable consequences, i.e. the worse the possible problem (e.g. accident), the more critical the component.

Technical Challenge 7.

Making RBI, RBLM, RBIM, etc. practice technically and management-wise auditable (Table 1) and its results measurable, e.g. by means of the KPI's (Key performance indicators – an example from RIMAP project given in Figure 13).

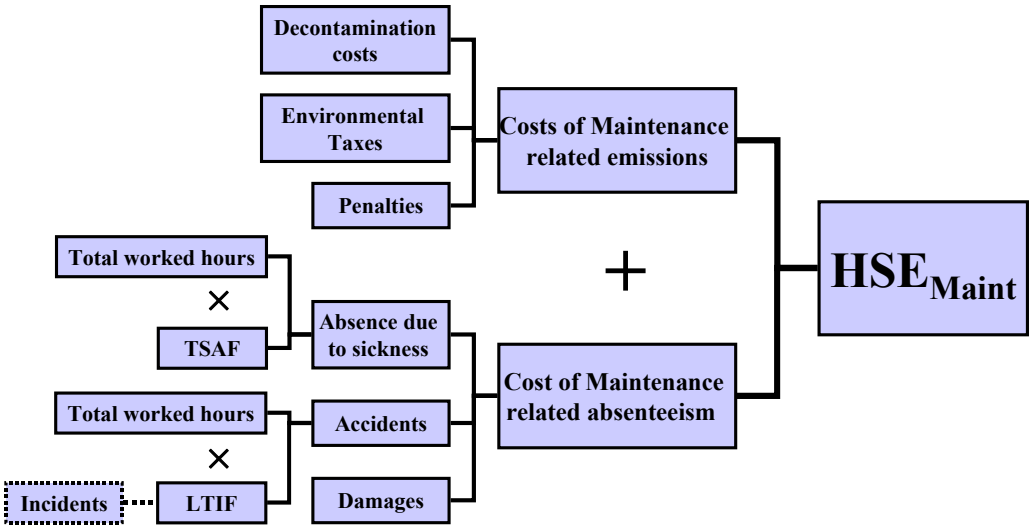

Figure 13. An example of KPI's (RIMAP project).

6. Conclusions: The biggest challenge f all – sustainable application of RBI/RBLM

There have been few issues in the engineering community that have been so much discussed as the issue of risk-based approaches (RCM, RBI, RBLM, RBM…). Large projects on national and international levels have provided a lot of material for these discussions, too.

These discussions have shown the following:

RBI/RBLM is beneficial …

There is a common agreement that a successfully implemented RBLM should lead to a number o benefits. Among them are: avoiding unnecessary redundancy in the scope inspection programs (i.e. avoid unnecessary inspections of the components), avoiding unnecessary conservatism in inspection intervals (skip the complete inspection for certain components during a given overhaul), shortening the overhaul times: avoiding unnecessary outages and/or failures; achieving extra sales are just the most obvious ones.

RBI/RBLM is not easy (and can involve a lot of effort!) …

Making a "successful RBLM application" is, however, not an easy task. The example explained in the works of Jovanovic (2003), Jovanovic et al. (2004) shows how much data, modeling, software tools, and similar is needed, especially for the detailed quantitative analysis. The main RBI/RBLM results for the example (piping system of a power plant) are shown in:

- Figure 14 and Figure 15 (risk map, including situation before and after the inspection)

- Figure 16 (Paretto diagram, showing the critical components, the contribution of which is the most significant)

- Figure 17 (Inspection optimization diagram for different scenarios – in the case on the figure, the optimum can be achieved already after inspecting in detail only 5 our 64 analyzed components – the optimization is based on the cost of inspection/analysis (approx. 57,000 €) and gain in risk reduction (approx. 200,000 €):

	Risk (€)	Inspection Cost (€)	Net savings (€)	D
Before inspection	216259.11	56670.00		
After Inspection	16831.97			
Difference	199427.14		**142757.14**	

Consequently, much of the effort in large past and current efforts / projects (like e.g. RIMAP - www.mpa-lifetech.de/rimap) is being invested in finding the optimal procedures and best practices for performing RBI/RBLM analysis in the most optimal way.

… and can be expensive!

The above optimization includes also finding the best value for the price. Although the initial applications of the RBI are usually very cost-intensive. Up to several million € may be needed for introduction of the risk-based methods and approaches (usually including the software, too) in a large company and up to several hundreds of thousands of € could be the cost for the first full-scale application on one plant. Nevertheless, the cost of analysis tends to go down. For instance, as indication only and for the example of a 3-level analysis like the one in Figure 14 to Figure 17 one should foresee the sums of approx. 10–15,000 € for each level. As in indication only, in such a case one could expect approx. 100 components at the screening level, up to 10 components on the intermediate level and 1–3 components at the detailed analysis level (real respective numbers in the analysis were 64, 8 and 1, as shown in Jovanovic et al. 2004).

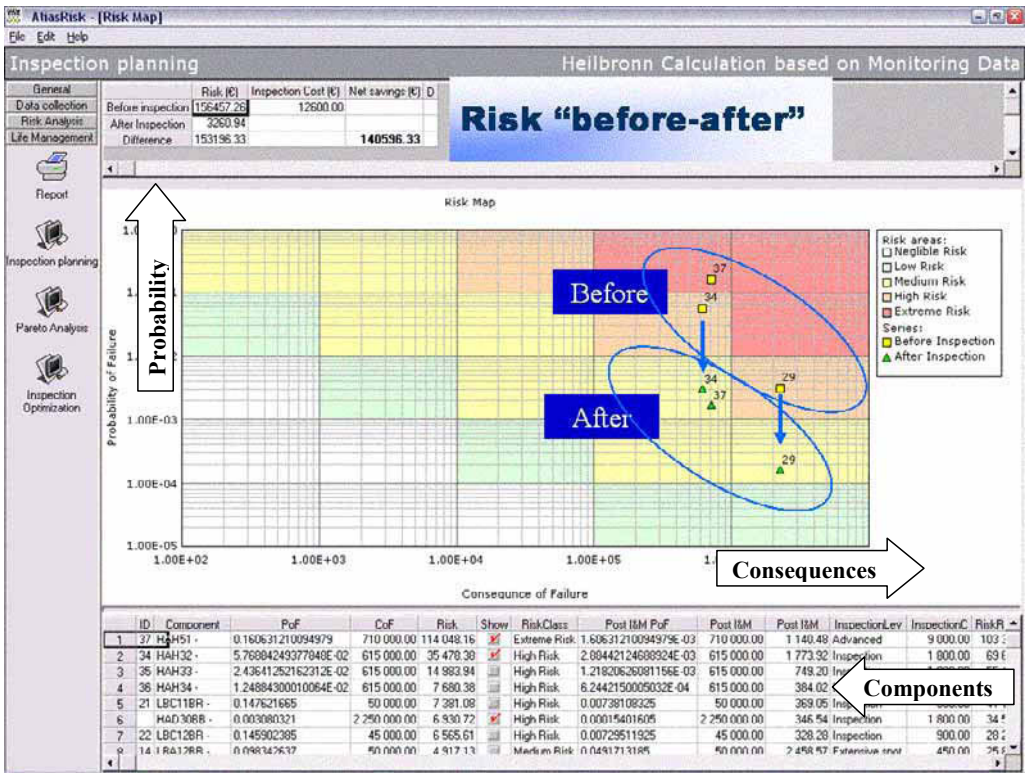

Figure 14. Typical results of a RBLM analysis: a risk map (ALIAS), in this case accompanied by the extract of the cost-benefit analysis and before-after analysis.

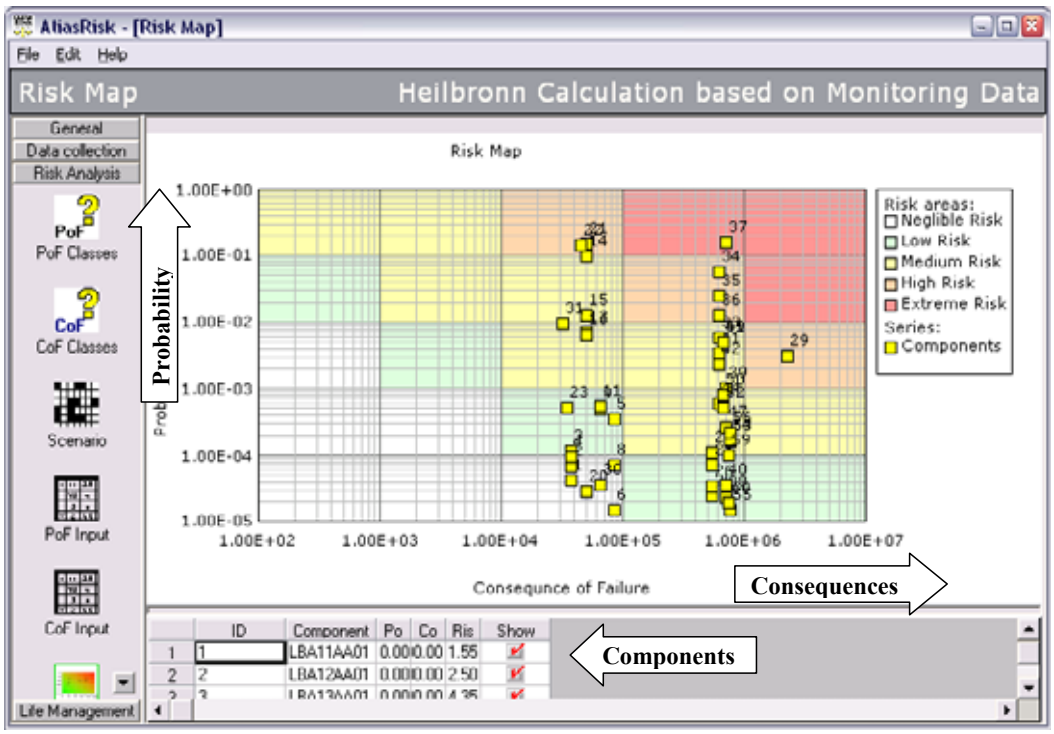

Figure 15. Risk map for the given example, all 64 components (Jovanovic 2003).

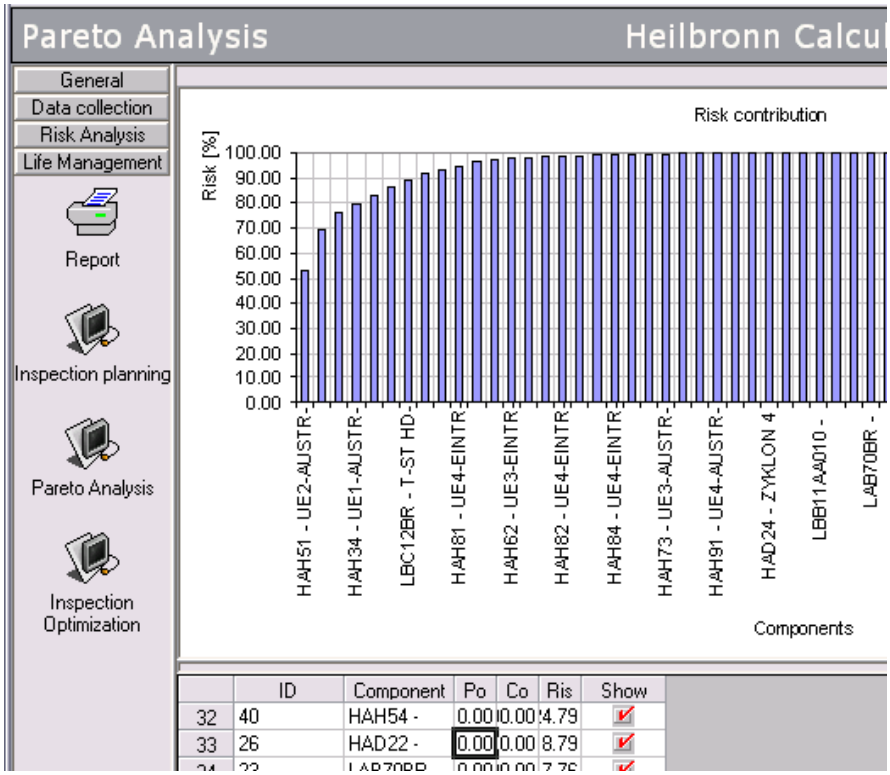

Figure 16. Less typical results of a RBLM analysis: Pareto diagram showing the components mostly contributing to risk (ALIAS).

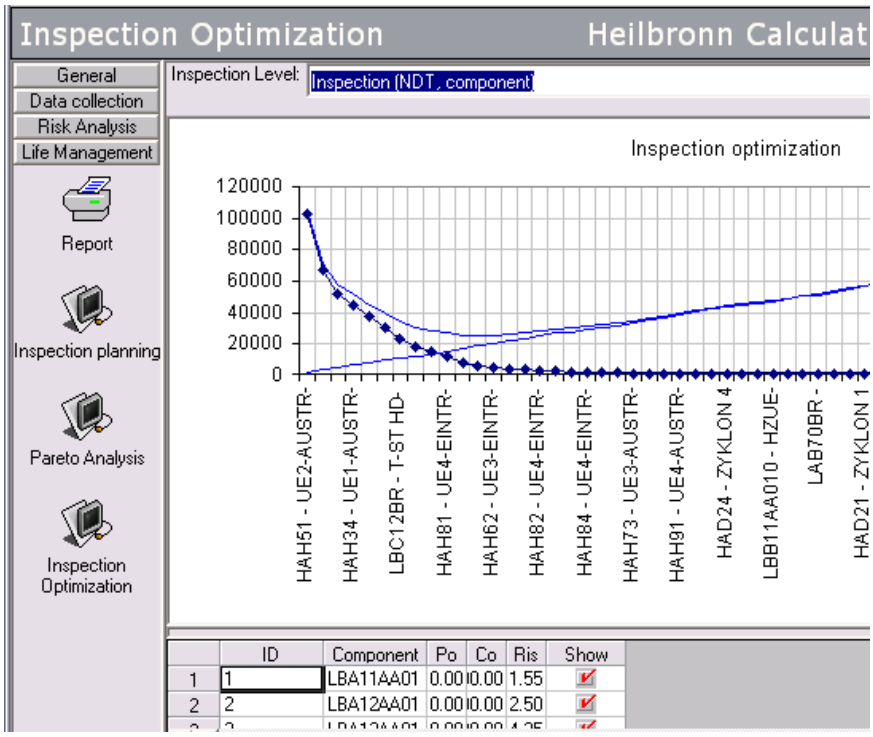

Figure 17. Less typical results of a RBLM analysis: Comparing efficiency of different inspection scenario (ALIAS).

References

[ALIAS] (2003) – ALIAS Info Booklet Advanced Life Assessment System, MPA Stuttgart, revision 15, Sept. 2003.

[API] (2000). API Publication 581, Base Resource Documentation – Risk-Based Inspection, May 2000, © 2000, American Petroleum Institute.

[DNV] (2001). Recommended Practice DNV-RP-A203 Qualification Procedures For New Technology, DNV September 2001.

[FITNET] (2002). FITNET European Fitness-for-service Network, EU-FP6 Project Contract No G1RT-CT-2001-05071, Commission of the European Communities, Revision of June 2002.

Geary, W. (2002). Risk Based Inspection – A Case Study Evaluation of Onshore Plant (MM/02/04), Health and Safety Laboratory, Sheffield.

[HSE] (2001). Best practice for risk based inspection as a part of plant integrity management, Prepared by TWI and Royal & Sun Alliance Engineering for the Health and Safety Executive – Contract Research Report 363/2001, HSE Health & Safety Executive, Crown copyright, Norwich, UK, 2001.

Jovanovic A. (1999). Remaining Life Management Systems: from stand alone to corporate memory systems and Internet (ALIAS System of MPA); Nuclear Engineering and Design 188, 319–329; Elsevier, Amsterdam, 1999.

Jovanovic, A. (2003). Overview of RIMAP Project and its deliverables in the area of power plants, Proceedings of the RIMAP Power Workshop held on Oct. 9th 2003 Stuttgart, Germany. Part of 29th MPA-Seminar, 9th–10th October, 2003, Stuttgart, Germany.

Jovanovic, A. (2003). Risk-based inspection and maintenance in power and process plants in Europe, Nuclear Engineering and Design 226 (2003) 165–182.

Jovanovic, A., Roos, E., Balos, D. & Bareiss, J. M. (2004). Concept of Risk-based Monitoring and its Application for High-temperature Components in Power Plants, to be published by Springer-Verlag London Limited, in the proceedings of PSAM 7 – the International Conference on Probabilistic Safety Assessment and Management, Vienna, June 2004.

[PED] (1997). Directive 97/23/EC of the European Parliament and of the Council of 29 May 1997 on the approximation of the laws of the Member States concerning pressure equipment, Official Journal of the European Communities, N° L 181/1, 9/7/9.

[RIMAP] (2000). RIMAP Project No, GROWTH Project G1RD-CT-2001-03008 "RIMAP", Risk Based Inspection and Maintenance Procedures for European Industry, Commission of the European Communities, Rev. of Oct. 4, 2000.

[SAFERELNET] (2002). SAFERELNET Thematic Network on Safety and Reliability of Industrial Products, Systems and Structures, FP5 Project No. Project Nº: GTC2-2000-33043, Contract Nº: G1RT-CT-2001-05051, Commission of the European Communities, 2002.

[TRENDS] (2002/2003). TRENDS (TRENDS-1 and TRENDS-2) The resource network facilitating QHSE development for a sustainable energy industry (Part 1 and 2), FP5 Contracts No. NNE 5-2001-00379 (TRENDS-1) and ENK6-CT-2002-20651 (TRENDS-2) Commission of the European Communities, Revision of June 2002/2003.

Experience from use of risk-based methods in inspection and maintenance of power plants

Jörg M. Bareiß
EnBW Energy Solutions GmbH
P.O. Box 10 13 11
70012 Stuttgart, Germany
j.m.bareiss@enbw.com

Aleksandar S. Jovanovic, Daniel Balos & Miodrag Perunicic
MPA Stuttgart, University of Stuttgart
Pfaffenwaldring 32
70569 Stuttgart, Germany
jovanovic@mpa.uni-stuttgart.de

Abstract

In the framework of EU project RIMAP (Risk-Based Inspection and Maintenance for European Industries) a new European Guideline for optimized risk based maintenance and inspection planning of industrial plants (RBLM – Risk Based Life Management) is being developed. The RIMAP project consists of the three clustered sub-projects

- research and technological development (RTD)
- demonstration (DEMO)
- thematic network (TN)

The paper presents an overview of the generic Risk-Procedure of the RIMAP project as well as a more detailed insight to the application within the power industry. Also presented in the paper are the experience and results of a full scale application of risk analysis of piping systems and boiler parts at a south German coal fired 760MWe power plant using the concept of risk-based monitoring as part of overall concept of risk-based life management. Shortly the following issues are discussed in the paper

- identification of critical components
- application of a multilevel risk analysis (...from „screening“ to „detailed analysis“)
- determination of PoF – Probability of Failure
- determination of CoF – Consequence of Failure
- optimation of inspection and maintenance plan

1. Introduction

The background for the RIMAP project is that current practice to inspection and maintenance planning in power plants as well as for most industries is nowadays still mostly time oriented and based on tradition and prescriptive rules, rather than being an optimized process where risk measures for safety and economy are integrated. These risk-based approaches help to concentrate onto systems, components and/or locations critical for safety, availability and reliability of industrial plants. However, the very process of finding the „most critical components“, generally denoted as priorization, can be a challenge, especially if done under the time of pressure (e.g. deadlines, production targets, saving targets, etc.). Criticality can to be determined according to different criteria, but in practice, the main criteria generally linked to the following aspects:

- state of component, that, combined with the probability profile of external load/factors, defines the probability that „an adverse event“ happens, and
- importance of the component practically usually expressed in terms of (e.g.) cost, safety consequences, environmental consequences and other consequences.

These aspects are the main elements of risk, defined as a combination (product) of probability of occurrence of certain (usually adverse) event and its consequences, for a given set of scenarios, can be used as basis for the critically-based ranking.

2. The RIMAP Procedure

Risk-based approaches like the RBI/RBLM-concept in RIMAP [1] gain more and more importance and applications in power plants are still in progress. „Risk“ in RIMAP is understood as the product of probability of failure (PoF) and consequences of failure (CoF). Safety, health, environment and economic consequences are considered. An overview of RIMAP procedure [2] is shown in Figure 1. As may be seen, it has five major technical steps, namely

1. Preparatory Analysis
2. Data collection and Validation
3. Multi-level Risk Analysis
4. Decision making and optimization
5. Implementation.

Additionally one techno-organizational (incl. economy-related aspects) step, namely

6. Assessment/Evaluation of Efficiency.

Furthermore, RIMAP procedure is organized as a double cycle: one that is mainly technical and another that is techno-organizational (management related).

Out of these steps, Multilevel Risk Analysis has one more dimension regarding the depth of the required analysis. Corresponding levels are:

(a) screening (low level analysis)
(b) intermediate level (levels of) analysis
(c) Detailed analysis.

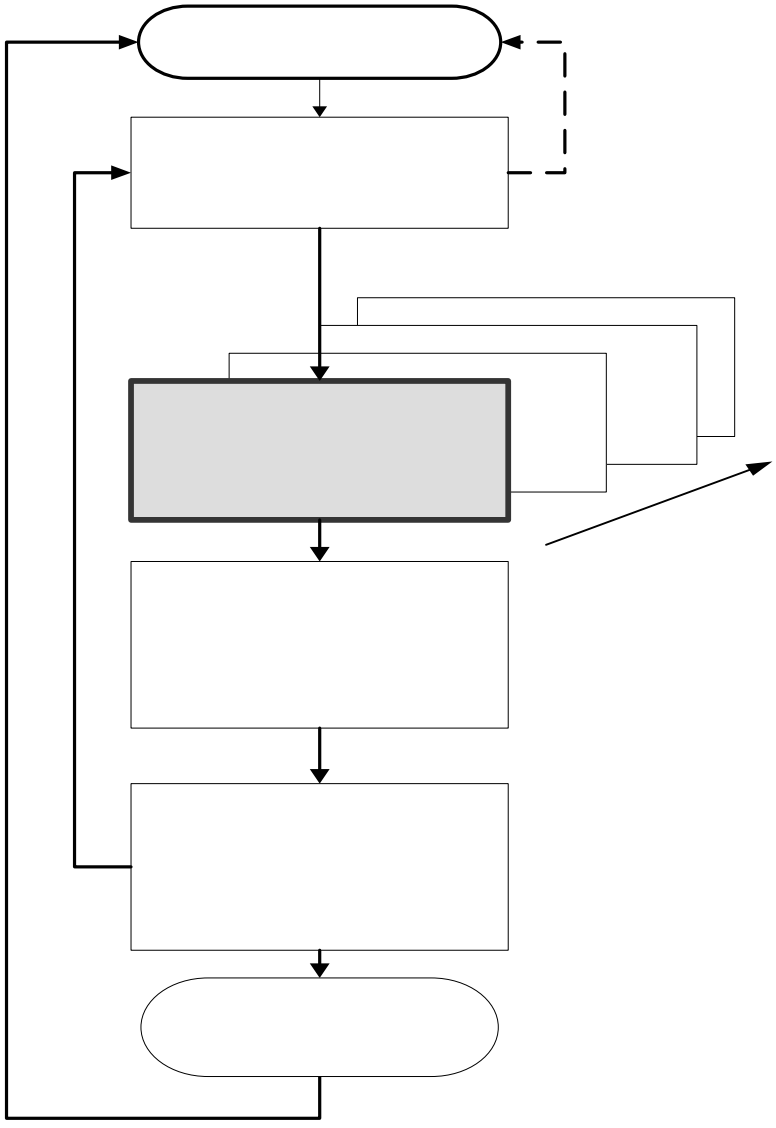

Figure 1. Basic representation of RIMAP procedure [2].

3. The RIMAP application workbook for power plants

The current RIMAP Application Workbook for Power [3] includes two main parts on the methodology application and appendices on supporting information.

Part I

In the first part of the workbook, the following main elements are specified:

- RIMAP procedure, as applied for the given branch of industry.
- Plant breakdown / hierarchy explained together with associated damage mechanisms (possible problems) for systems / subsystems / components.
- Methods for evaluating/calculating Probability of Failure (PoF) and Consequence of Failure (CoF), as applied for the given branch of industry.
- Methods for risk assessment and analysis.
- Considerations regarding benchmarking and decision making.

The most "application-specific" part of workbook is the part on plant breakdown. A recommendation for a standard hierarchy is given (see Table 1) with examples for possible damage related issues (compare Table 2).

Table 1. Extract: Recommendation for the plant systems/subsystems hierarchy.

...
Water systems (G, L)
Feedwater/boiler water systems (G, L)
Feedwater treatment
Feedwater treatment (GA, GB, GC)
Condensate treatment
Condensate polishing (LD)
Boiler water transport
Feedwater pumps (LAC)
Condensate pumps (LCB)
Feedwater piping (LAB)
Feedwater tank, deareator (LAA)
Feedwater heaters (LAD)
HP feedwater heaters
LP feedwater heaters
Conventional power production (H)
...
Steam system (L)
...

In the left most column of Table 2 the plant is broken down to single components, while the table headings give possible damage mechanisms and/or problems. The combinations of components and possible damage mechanisms / problems, which are covered by the workbook are indicated by star-signs (i.e. ★). The number of shown stars (one, two or three) indicates the priority (importance) of the problem – three stars indicate the most important/frequent problem. The systems/subsystems/components in the left most column are

associated with the respective chapters in part II of the Workbook which describes in detail the system/subsystem/ component and corresponding problems.

Table 2. Extract: Plant Hierarchy vs. "typical problems".

Damage Mechanism	**MATERIAL DAMAGE RELATED PROBLEMS**												
	I. Corrosion/erosion/environment related damage, equating or leading to:								**II. Mechanical or thermo-mechanical loads related, leading to:**				
Plant Hieracy	**Volumetric loss of material on surface**		**Cracking (on surface, mainly)**			**Material weakening and / or embrittlement**			**Wear**	**Strain dimen-sional changes**	**Micro void formation**	**Micro cracking, cracking**	**Fracture**
	I.A1 General corrosion	I.A2 localized corrosion	I.B1 stress corrosion	I.B2 hydrogen damage	I.B3 Corrosion fatigue	I.C1 thermal degradation	I.C2 carburization	I.C3 embrittle-ment (strain)	II.A sliding wear, cavit. wear	II.B overloading, creep	II.C creep, creep-fatigue	II.D fatigue (HCH, LCF)	II.E overloading, brittle f.
Conventional steam generation													
Boilers													
Boiler tubes													
▪ *Economiser tubing*	★	☆			☆				★			★	
▪ *Risers/down comers*	☆				☆							☆	
▪ *Waterwall tubing*	★★★	☆☆		☆	☆☆				★★★				
▪ *Superheater /reheater tubing*	☆☆	☆				☆☆			★★	★★★		☆	
▪ *Boiler tube attachments*	☆				☆							☆☆	
.....													

Part II

As mentioned before part II of the workbook gives detailed information –on item per item basis- for the system/subsystem/component considered. This data is given in form of tables and distinguished between system/component related data (component records) and problem/cause related data (problem records).

The main systems and components item that are currently covered to varying extend include:

- Fuel supply and waste disposal system
- Boilers for conventional steam generation
- Steam systems (piping)
- Steam turbines
- Gas turbines
- Generators
- Electric distribution.

Under these heading, different subsystems and components are considered from the point of view of general features and operating conditions, typical damage

mechanisms and failure modes, basic default PoF and CoF data (with references), description of typical preventive and corrective actions, and suggested rating scales on PoF and CoF factors for specific problems on a given component type

Part III

Part III is foreseen for APPENDICES which should provide all additional information and explanations needed (or helpful) for performing a successful risk analysis. For example in RIMAP Application for Power Plants appendices provide like e.g. "Glossary of RBLM", "Supplementary Information on Damage Mechanisms" etc.

4. RIMAP demonstration projects (power industry)

According to the DEMO project workplan several demonstration cases for the involved industry sectors are being planned/negotiated. The cases for the power industry are shown in Table 3.

Table 3. RIMAP demonstration cases (power industry).

No.	plant	Components (number)	Problem / issue	Partner	Time schedule	Status
1	HKW Heilbronn in operation since 1987 110 Th operation 760 MWe	boiler parts, steam piping (64)	creep fatigue	EnBW MPA	01/02 – 12/02	preliminary study finished
					07/03 – 03/04	finished
2	HKW Ulm in operation since 1949 70 ... 350 TBh operation >350 MWth, 20 MWe	boiler, steam piping (40)	creep 350.000 h	EnBW ESB FUG MPA	09/03 – 04/04	finished
3	HKW Altbach in operation since 1985 130 Th equivalent operation	steam turbine (<10)	fracture mechanics	EnBW MPA SIEMENS	02/03 – 06/04	in progress

One full scale application of the RIMAP Power workbook [3] takes place at a South German coal fired power plant, in operation since 1987. The demonstration has as main objectives the following issues:

- to demonstrate applicability and usefulness of the RIMAP-methodology on several practical cases (i.e. systems for power industry: turbine components, boiler parts, steam piping and i.e. most common damage mechanisms: creep, fatigue, corrosion)
- to demonstrate potential economic advantages

- to demonstrate the benefits of standardization
- to give input and feedback to further development/implementation of the methodology and standards for power related issues.

The assessment presented on boiler parts, the main steam pipeline and the hot reheat pipeline (overall 64 components). Systems/components planned for the risk analysis will be fully modelled and all data will be stored in database (ALIAS Software System[1]), see Figure 2.

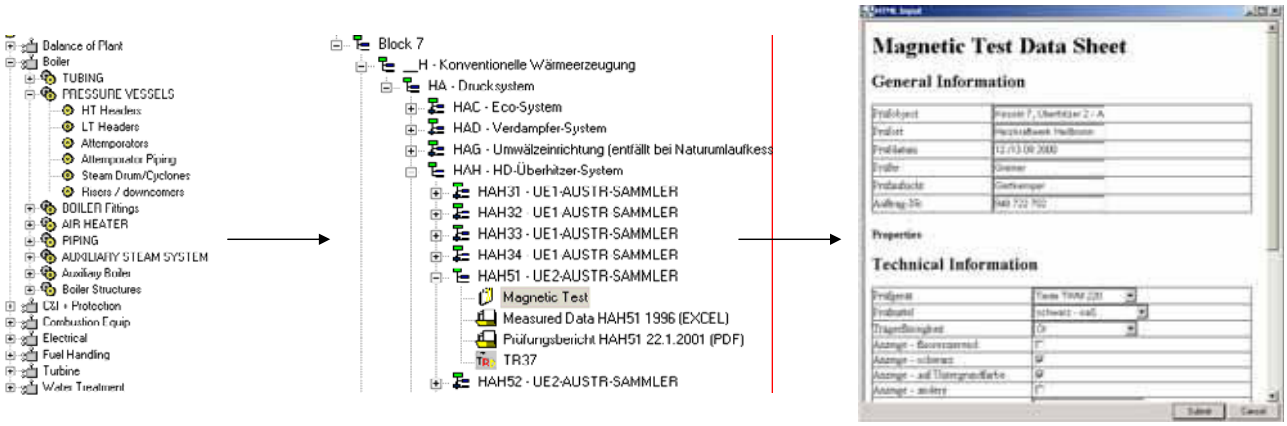

Figure 2. Power plant components in database with all relevant data stored.

Data stored in the database for the chosen 64 components (headers, t-pieces, elbows):

- Material properties
- Data from the on-line monitoring system (e.g. pressure, temperature)
- Test data (e.g. NDT), incl. previous inspection records
- Performed calculations data (e.g. TRD codes 300/301[2]) derived from
  - component geometry
  - design temperature and pressure
  - service time of the component (operational hours).

Risk analysis was done on three levels: “screening”, “intermediate” analysis and “detailed” analysis. On the level of screening, only the general statistical data and the results of TRD on-line monitoring results were taken into account. For this purpose, the existing measurements system (measuring pressure, temperature and temperature difference at the calculation points) and the existing monitoring systems were used. For the purpose of risk analysis, the algorithm was extended for the probabilistic analysis (Monte Carlo simulation). On the level of intermediate analysis inspection results (replica) were introduced and probabilistic assessment of replica findings was done. For the detailed level, the analysis was extended by means of probabilistic high-temperature fracture mechanics and the fatigue-creep crack growth analysis. In addition to the analysis

[1] ALIAS – Advanced Life Assessment Software System, Copyright © 2002, MPA – Stuttgart, Germany
[2] Technical Rules for Steam Boilers TRD300/301 (1919), Vulkan-Verlag, Essen

of recorded data, on the level of detailed analysis also "what-if" analysis for different assumed load cases was done and it was accompanied by the corresponding non-destructive testing on a model (establishing of the minimum detectable nozzle corner crack for the most critical component).

The principle is shown in Figure 3. For detected cracks the real dimensions of which can reach critical crack size, i.e. can be larger than the measured ones (here one 25 mm crack only) are to be assessed. As well as undetected cracks, among which a crack of critical size may appear.

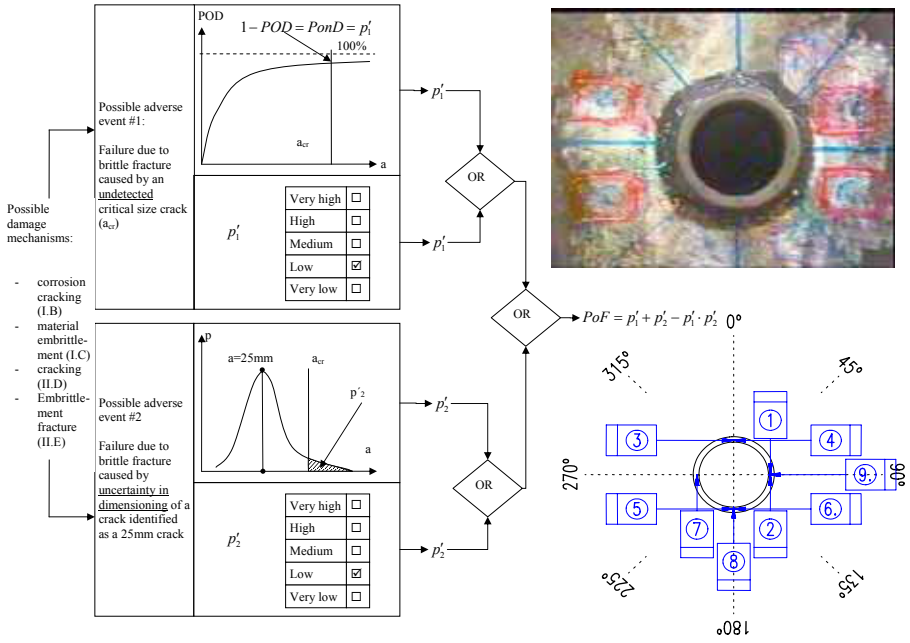

Figure 3. Definition of PoF for the case of a structural failure and its main root cause.

The results of the work clearly show the benefits of the proposed method for concentration on "critical items": out of 64 monitored components analyzed in screening level (see Figure 4), 6 were selected for intermediate analysis and only 1 for the detailed assessment. In addition overall level of risk was managed all the time and the costs and benefits of risk based approach werde made visible, transparent and measurable. Characteristic results are shown in Figure 5.

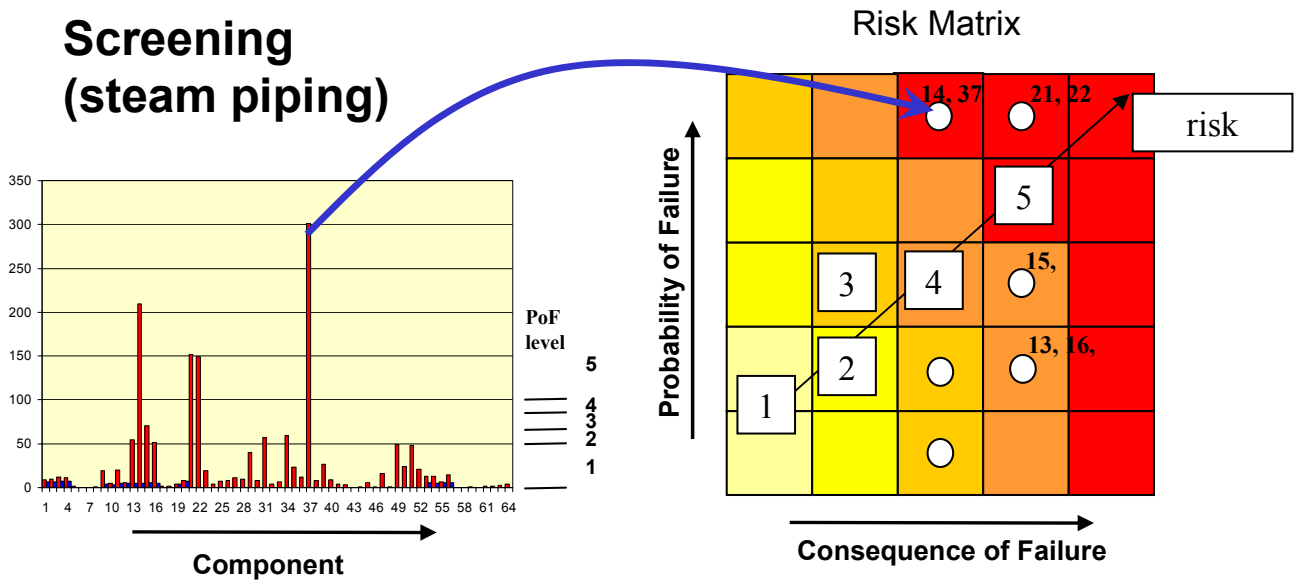

Figure 4. Determination of critical components („screening analysis“).

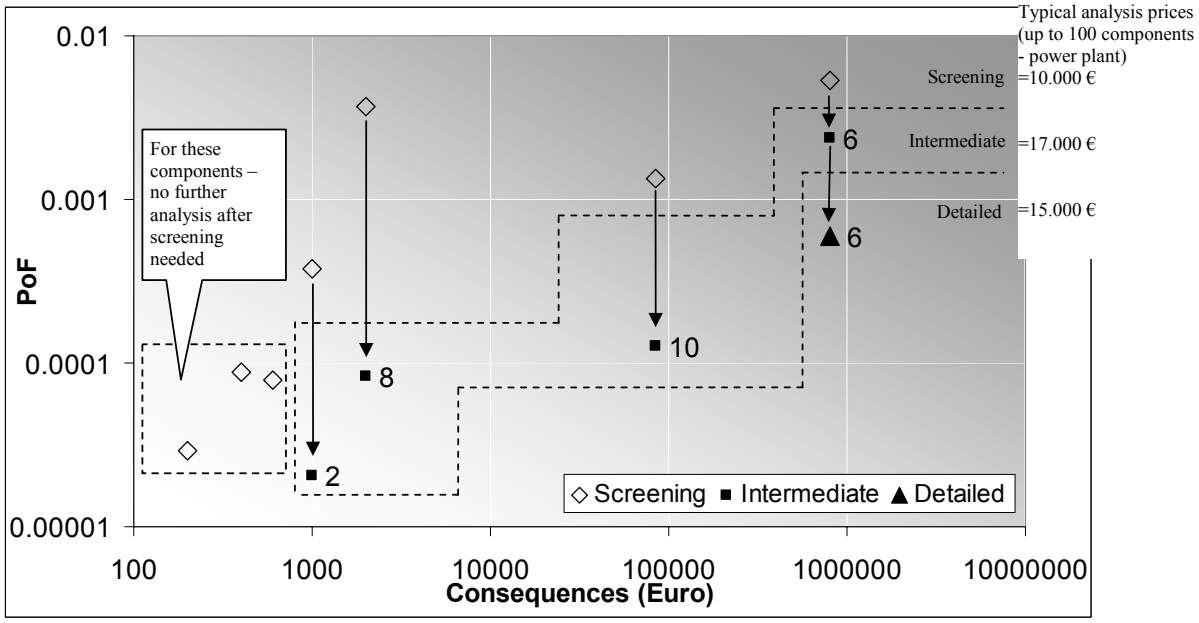

Figure 5. Example of overall results: screening vs. intermediate vs. detailed analysis.

Foreseen goals of the methodology presented above (and overall concept of risk-based life management) are:

- Improved inspection plan (including: method of inspection, scope of inspection, responsible personnel, time scale…), see Figure 6
- Transparency of a utility (e.g. in decision making, risk management…)
- Increased safety
- Optimization of:
  - Plant availability / reliability

- Plant lifetime
- Life cycle costs due to inspections, maintenance and production

- Acceptance (from authorities, other industries)
- Overall economic optimization.

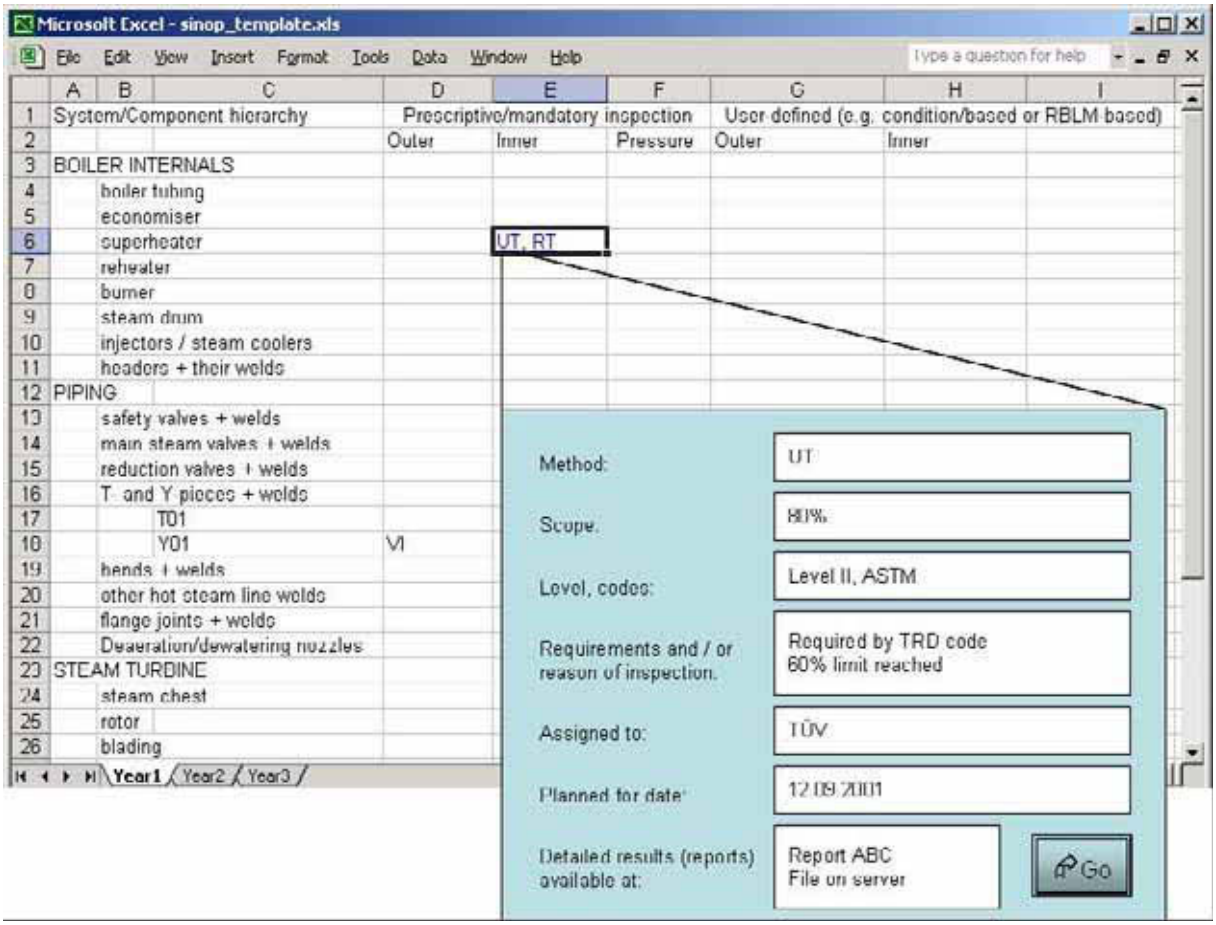

Figure 6. Detailed (improved and optimized) inspection plan.

5. Conclusions

From our experience with the application of the RIMAP methodology for high-temperature components in power plants, boiler parts and piping systems in particular, the following conclusions can be drawn:

- Safety and profitability of a power plant is defined predominantly by a possible failure of individual components. The use of risk-based methods in inspection and maintenance in power plants gives transparency to the decision making process and gives an optimized maintenance policy based on current state/criticality of the components.
- The results of the work clearly show the power and the benefits of the proposed method for concentration on critical items: out of 64 monitored components 6 were selected for intermediate analysis and only 1 for the detailed analysis.

- The work has confirmed that risk-based approach on piping systems makes sense only in system which covers all aspects of life management – materials, monitoring, load analysis, inspection results and analytical tools. Only a system integrating these aspects can assure the confidence needed that no „false alarms“ are triggered and that no real damage location is overseen.

6. Acknowledgements

The support provided for this work by the utility company EnBW HKW Heilbronn, Germany as well as the support of the European Commission to the project RIMAP (Contract GROWTH Project G1RD-CT-2001-03006 „RIMAP“) is gratefully acknowledged and appreciated here.

References

RIMAP RTD or RIMAP Demo project: http://research.dnv.com/rimap
RIMAP TN: http://www.mpa-lifetech.de/rimap

[1] RIMAP Project No, GROWTH Project G1RD-CT-2001-03008 “RIMAP”, Risk Based Inspection and Maintenance Procedures for European Industry, Commision of the European Communities, Rev. of Oct. 4, 2000.

[2] A. S. Jovanovic, S. M. Psomas, P. Auerkari, A. Baecke, J. Bareiß, L. Fabbri, J. Heerings, A. Herring, F. Merlier, A. Ulbrich & G. Våge (2002). RIMAP D2.1 Deliverable – Generic RIMAP Procedure.

[3] A.S. Jovanovic & P. Auerkari (2002). RIMAP D4 Deliverable – RIMAP Application Workbook for Power plants, MPA Stuttgart, Germany.

Risk-based damage assessment and maintenance management for turbine components

Kazunari Fujiyama, Toshihiro Fujiwara, Yujiro Nakatani, Testu Sawa,
Junji Ishii, Masayoshi Horino, Mariko Nishimura & Kazuhiro Kitayama
Industrial and Power Systems & Services Company, Toshiba Corporation
Tokyo/Yokohama, Japan

Abstract

A statistical approach for risk-based maintenance of damage tolerant components is presented. Damage risk is defined here as the expected cost due to repair of damage in the course of component life. The thermomechanical fatigue cracking was studied statistically as the typical damage phenomena for gas turbine nozzles. Probabilities of cycles to critical crack size and cycles to total amount of cracks were calculated through plant inspection data and experimental results of low cycle fatigue. The life cycle cost of damage tolerant components was proved to be optimized by considering the failure risk and the damage risk simultaneously.

1. Introduction

Cost-effective maintenance has been becoming a special concern of utilities in the competitive power generation market. The risk-based approach has been recognized as a useful tool for the optimum maintenance planning [1–3]. The risk has been usually defined as the product of probability of failure and the consequence of failure. Though the maintenance cost has been treated as a definite value, it might depend on damage amount and have statistical uncertainties.

For the components under severe service conditions, some of them are used like damage tolerant ones and imposed repeated repairs until prescribed replace limit. Therefore the risk-based maintenance of such components should be treated from both aspects of failure and damage to be repaired. Damage risk concept is defined here as the product of repair cost multiplied by the probability of damage requiring the repair.

To quantify the statistical characteristics of damage amount, statistical data analyses were conducted for the thermomechanical fatigue cracks of gas turbine nozzles as a case study [4]. Low cycle fatigue test data were utilized as the

reference of damage behavior. Failure parameter and damage parameter were represented by maximum crack length and total length of cracks respectively. Total risk is calculated as the sum of the failure risk and the damage risk.

Life cycle risk cost is estimated using the failure risk cost and the damage repair risk cost. It is shown that the optimum repair intervals can be obtained through the life cycle total risk approach. Some other application of this approach is briefly described for steam turbines and gas turbines.

2. Damage phenomena in turbine components

Figure 1 shows the damage modes of gas turbine components [2, 3]. Hot gas flow may cause oxidation, corrosion and erosion, besides thermal gradient and fluctuation may induce thermomechanical fatigue (TMF) cracks. TMF multiple cracks could be observed typically in gas turbine nozzles. Those cracks are penetrating through wall thickness as the crack length increased. The TMF cracks are weld repaired at scheduled intervals and the components will be used until replace limit.

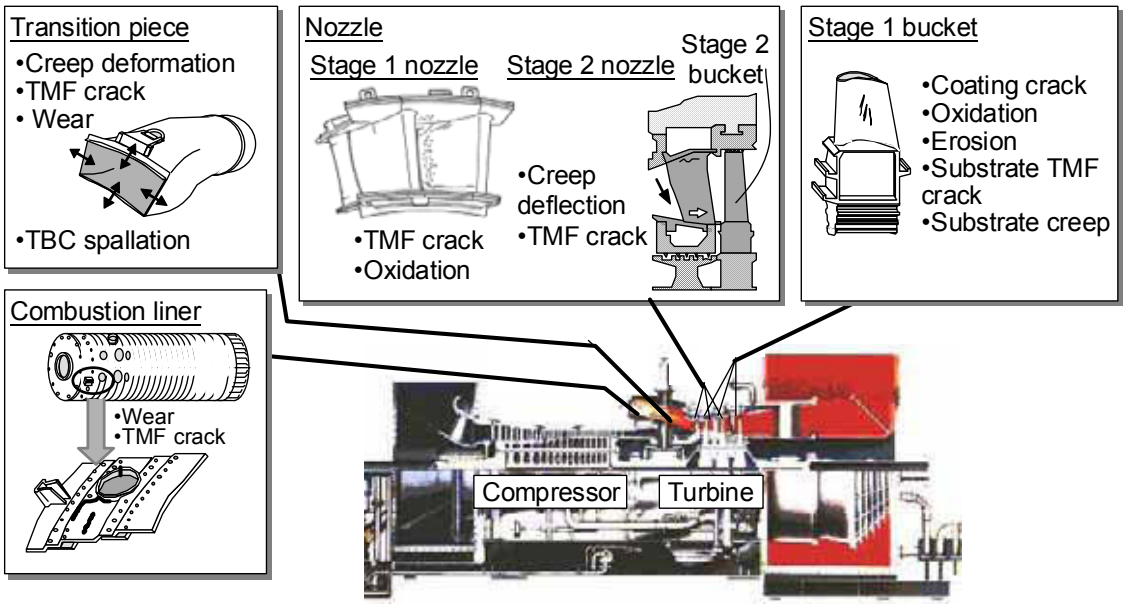

Figure 1. Damage modes of gas turbine components.

Figure 2 shows damage modes of steam turbine components [5, 6]. Steam flow may cause intensive erosion at nozzles and moving blades. Intensive erosion leads to cracking or failure under the vibratory stress. Creep deformation occurs at nozzles, moving blades, bolts, casings and rotors. The major cause of cracking is TMF as well as creep. TMF cracks are induced in the casing nozzle fit radius, in the valve chest corners and in the pipings. The TMF of casings and valves may

be caused by cyclic operation with creep damage, besides the damage in piping may be caused by repeated water induction. Steam turbine components are usually not to be treated as damage tolerant, but actually some TMF cracks might be emerging during operation. TMF cracks are removed or weld repaired so that the remaining ligament satisfies the minimum requirement.

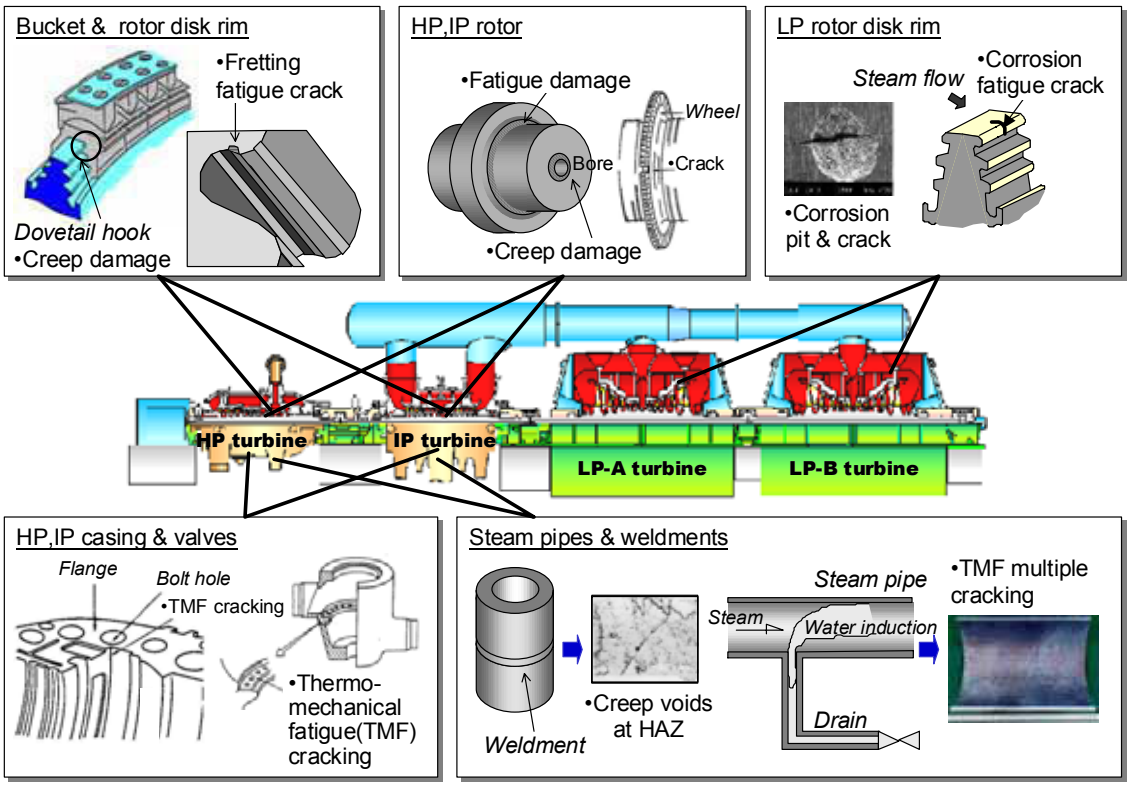

Figure 2. Damage modes of steam turbine components.

3. Risk assessment for damage tolerant components

Figure 3 shows the maintenance steps for damage tolerant components. Initially the inspection intervals are pre-determined by fleet experience or by prevention of failure. Repair action is performed referring the repair criterion and the components are re-installed to operation after the repair. If the condition of the component violates the replace criterion, the component should be replaced.

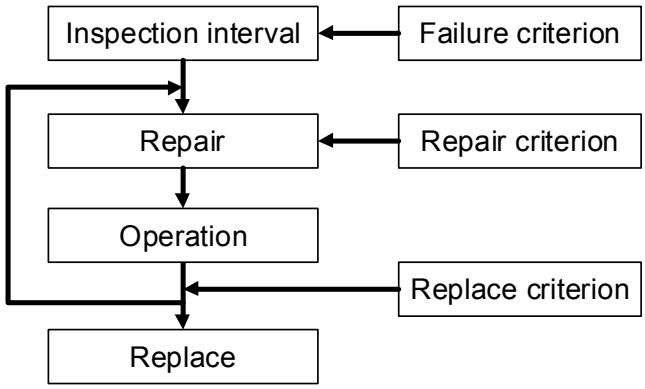

Figure 3. Maintenance steps for damage tolerant components.

Figure 4 shows the concept of risk-based maintenance for damage tolerant components. Both damage probability and failure probability are estimated. The damage risk is defined here as "product of repair cost and probability of damage causing the repair cost". This damage risk can be calculated the damage amount as the total length of cracks which is proportional to repair amount. The failure probability is estimated by the probability of maximum crack length exceeding the critical value for failure.

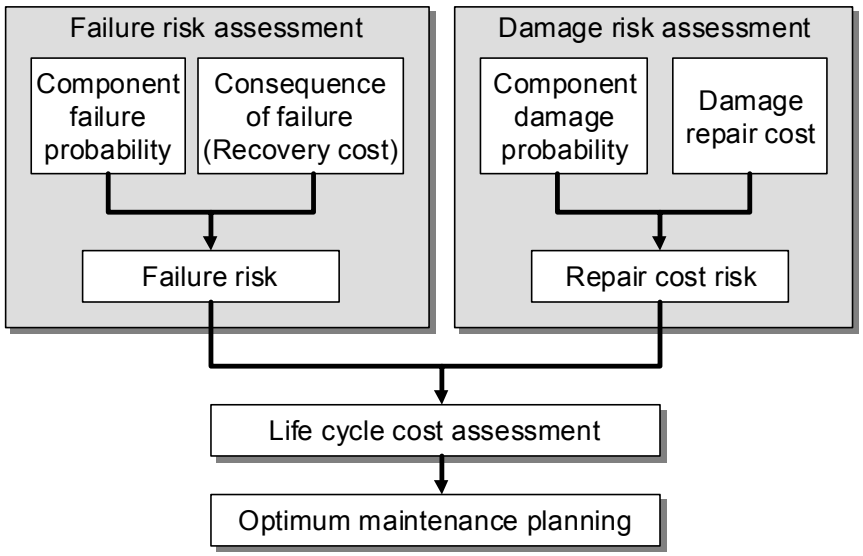

Figure 4. Risk-based maintenance steps for damage tolerant components.

4. Damage data analysis for gas turbine nozzles

A case study is conducted here for the risk-based optimization of maintenance intervals for nozzle vane TMF cracking [3, 4]. The failure risk and the damage risk are calculated using the maximum crack length and the total length of cracks.

4.1 Maximum crack length

Crack length data of gas turbine nozzles were obtained from field inspection records. Those data were related with service histories (start/stop cycles).

Figure 5 shows maximum crack growth trend of nozzle vane area. The maximum crack length is normalized by the chord length *L* of the vane. The maximum crack tends to be located at nozzle vane fillet portions. The crack growth data shows significant scatter possibly due to the variation of stress and temperature distribution for each segment. We can see the initial acceleration stage followed by subsequent retardation stage. Crack growth rate analysis showed the acceleration and retardation stage clearly and similarity for *da*/*dN*-*a* relationship between specimen and actual nozzle vane was observed [6].

In this paper, the crack growth rate approach was not adopted tentatively for the simplicity of statistical analysis.

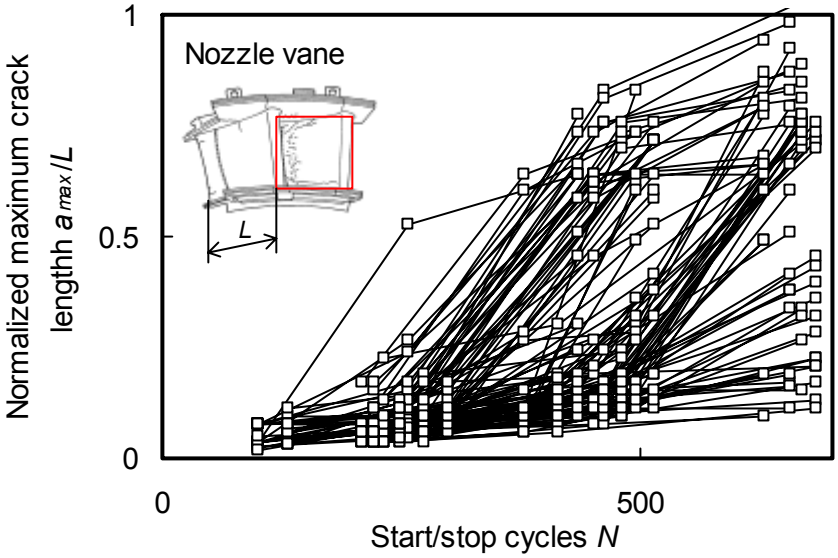

Figure 5. Gas turbine nozzle cracks and maximum crack growth data normalized by chord length L.

To obtain basic properties for nozzle materials are Co-base superalloy *FSX414* for gas turbine nozzle [4]. Tables 1 and 2 show the chemical composition and mechanical properties at room temperature.

*Table 1. Chemical composition of **FSX414**(wt %).*

C	Si	Mn	P	S	Ni	Cr	Co	W	B	Fe
0.25	0.78	0.70	0.005	0.008	10.1	30.2	Bal.	6.94	0.007	0.37

*Table 2. Mechanical properties of **FSX414** at RT.*

Tensile strength (MPa)	0.2% proof stress (MPa)	Elongation (%)	Reduction of area (%)
900	552	13.6	14.4

High temperature low cycle fatigue (HTLCF) tests were conducted for 10mm diameter round bar type specimen of *FSX414* at 1023K, 1123K and 1223K under continuous cycling of full reversed ramp strain wave shape. LCF interruption tests were also conducted on the specimen at 1123K and replica observation was conducted.

Figure 6 shows the relationship between plastic strain range $\Delta\varepsilon_p$ and cycles to failure N_f. The data from 1023K to 1223K are fitted well with Coffin-Manson type law as follows.

$$\Delta\varepsilon_p = C_p N_f^{\alpha p} (C_p, \alpha_p: \text{constants}) \quad (1)$$

Figure 7 shows maximum crack growth data of *FSX414* HTLCF tests conducted at 1123K. The data are fitted irrespective of the strain range with the following equation [3]:

$$a_{\max} = E\exp(FN/N_f), \quad (2)$$

where E and F are constants, and N_f is cycles to failure for LCF specimen corresponding peak stress decreased below 75% of the steady state value.

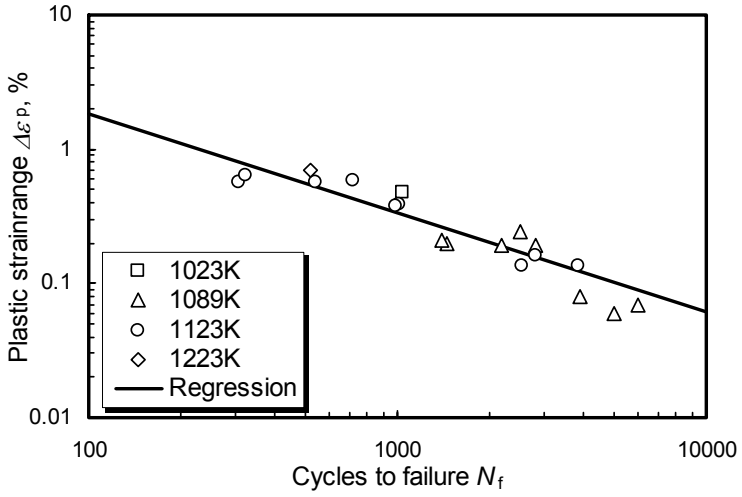

Figure 6. Relationship between plastic strain range and cycles to failure.

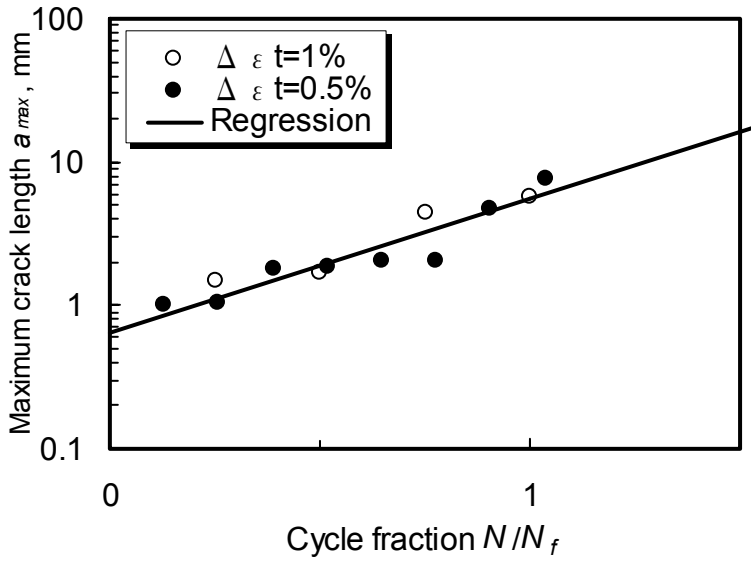

Figure 7. Maximum crack growth data of HTLCF specimen.

Figure 8 shows the log-normal plots of experimental cycles N_{ex} to estimated cycles N_{est}, where N_{est} is obtained from Eqs. (1) or (2). Both a_{max} based N_{ex}/N_{est} and N_f based N_{ex}/N_{est} distributions show similar log-normal distribution.

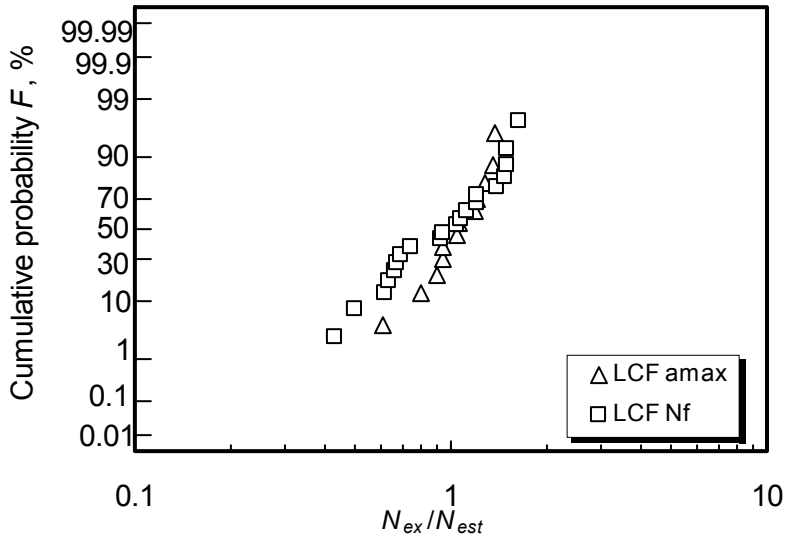

Figure 8. Log-normal distribution of the ratio of experimental to estimated cycles.

Figure 9 shows the regression line for a_{max}/L-N semi-logarithm plot data in the same form of Eq.(2). Figure 10 shows the log-normal distribution of the ratio of actual cycles N_{act} to estimated cycles N_{est}. The distribution of N_{act}/N_{est} is log-normal distribution similar to Fig. 8.

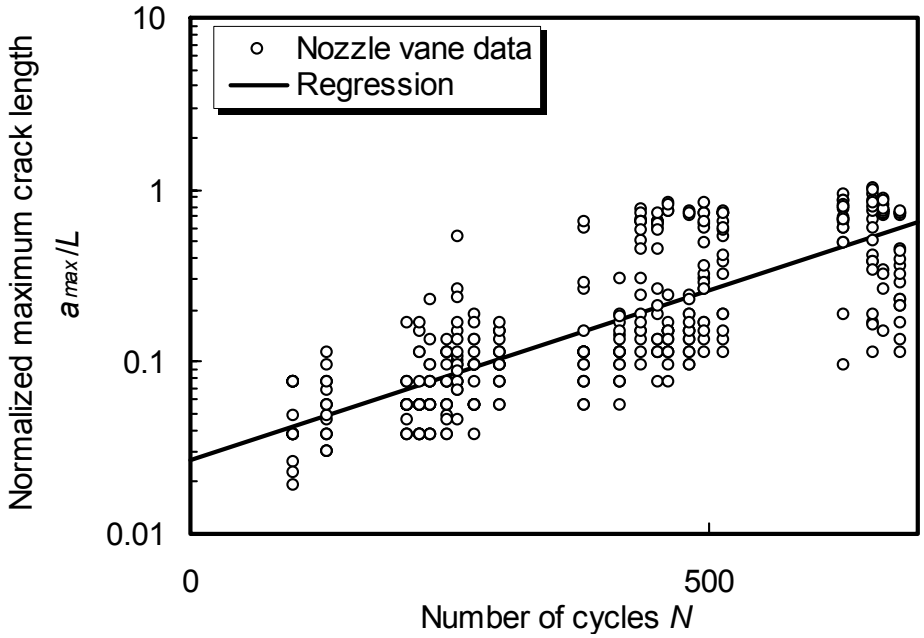

Figure 9. Semi-logarithmic plot of a_{max}/L-N relationship and regression line.

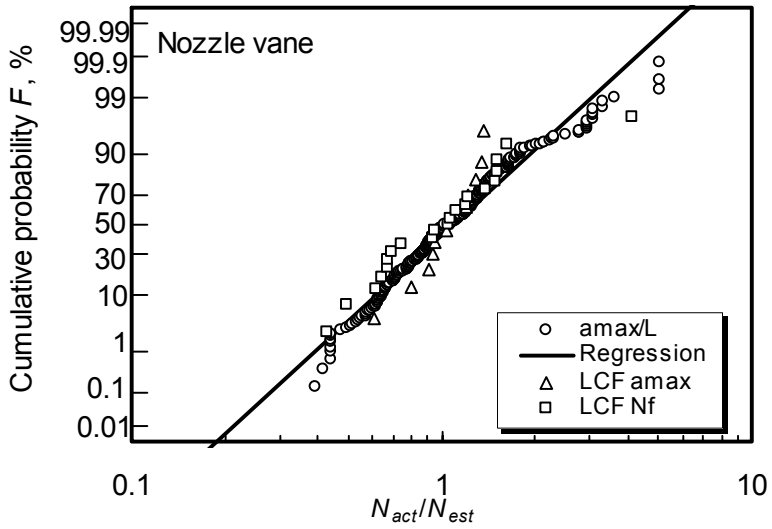

Figure 10. a_{max}/L based N_{act}/N_{est} distribution for nozzle vane.

4.2 Total length of cracks

Figure 11 shows the normalized total length of cracks a_{tot}/L (a_{tot}:sum of all the crack length observed in the subject nozzle vane area) against start/stop cycles. Rather monotonically increasing trend is found for a_{tot}/L-N relationship compared with a_{max}/L. Figure 12 shows the relationship between a_{tot}/L and a_{max}/L. There is a linear correlation between a_{tot}/L and a_{max}/L. Therefore, a_{tot}/L-N relationship can be estimated using a_{max}/L-N relationship. Figure 13 shows the semi-logarithm

plot of a_{max}/L-N relationship and the regression line like shown in Fig. 9. Figure 14 shows the log-normal plot of N_{act}/N_{est} at fixed a_{tot}/L with the a_{max}/L based regression line. Although there is relatively large discrepancy from the log-normal distribution, it still can be used for estimating the damage probability.

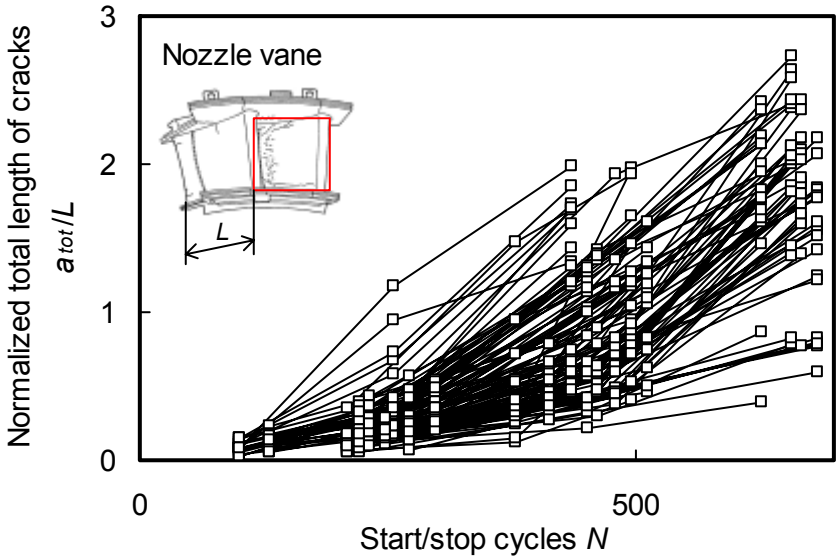

Figure 11. Total length of cracks and start/stop cycles.

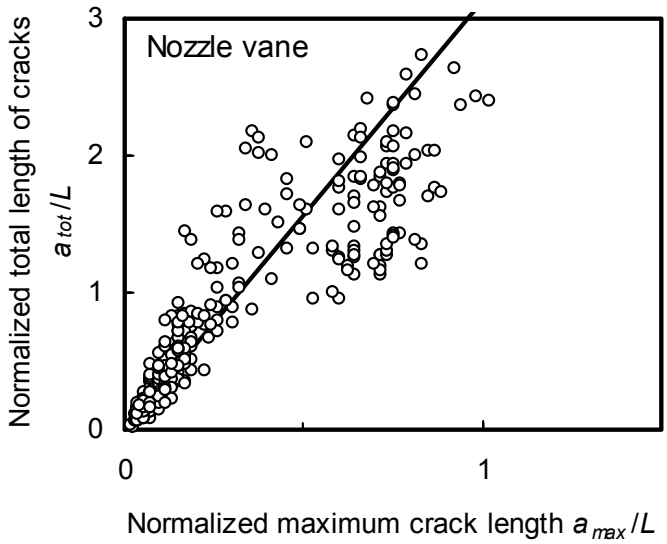

Figure 12. Relationship between a_{tot}/L and a_{max}/L.

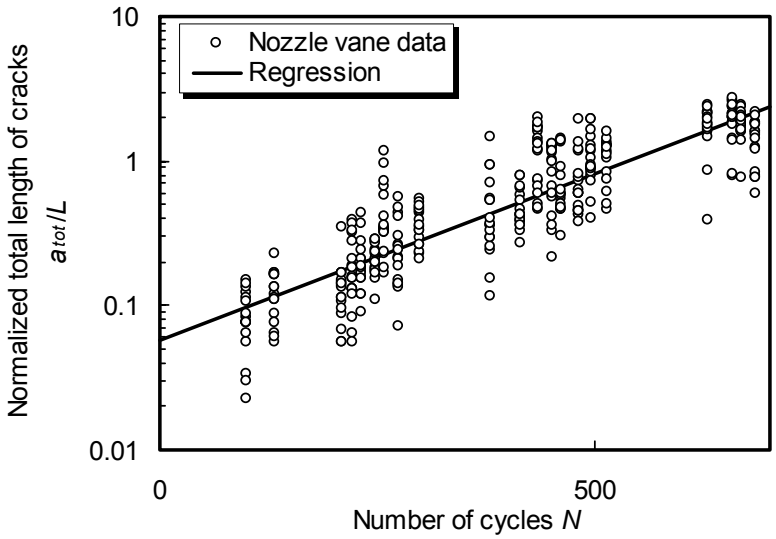

Figure 13. Normalized trend of total length of cracks.

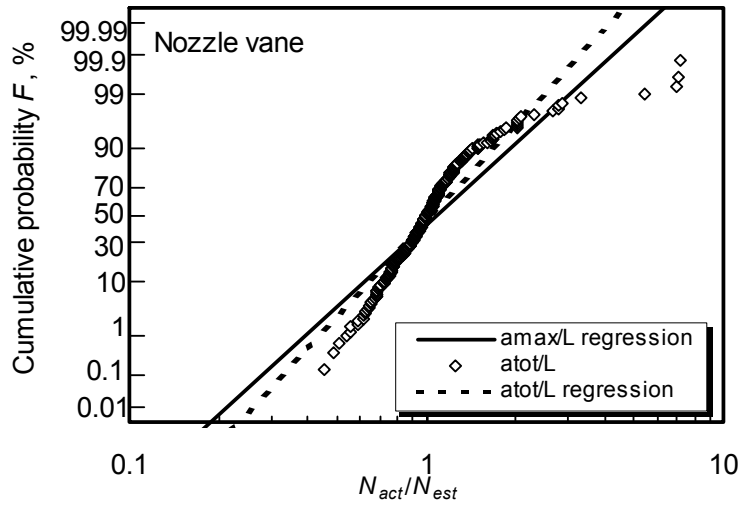

Figure 14. Log-normal distribution of damage probability.

5. Risk assessment and maintenance intervals optimization

The risk assessment of nozzle TMF cracking is performed from both aspect of failure risk and damage risk. Failure probability $F_f(N)$ is described by the following log-normal type distribution function under the failure criterion of $a_{max}/L=1$ (This may be rather safer side condition). This regression line was shown in Fig. 10.

$$F_f(N)=\Phi^{-1}[(\ln N-\mu_{Lef})/\sigma_{Lef}] \quad (3)$$

where, $\Phi^{-1}[]$ is the standard normal distribution function, μ_{Lef} is the mean value of ln$N$ and σ_{Lef} is the standard deviation of ln$N$.

The risk cost of failure, R_{cf} is calculated by the following equation using the cost index of consequence of failure C_f.

$$R_{cf}=C_f F_f(N) \tag{4}$$

The damage probability $F_d(N)$ for prescribed a_{tot}/L is expressed as follows. This regression line was shown in Fig. 13.

$$F_d(N)=\Phi^{-1}[(\ln N-\mu_{Led})/\sigma_{Led}] \tag{5}$$

where, μ_{Led} is the mean value of ln$N$ and σ_{Led} is the standard deviation of ln$N$.

The risk cost of damage, R_{cd} is calculated by the following equation using the cost index of consequence of damage C_d.

$$R_{cd}=C_d \exp(\mu_{Lea}+Z_a\sigma_{Lea})F_d(N) \tag{6}$$

where, μ_{Lea} is the mean value of lna_{tot}, σ_{Lea} is the standard deviation of lna_{tot} and Z_a is the factor modified by inspection information(Initially set as 0).

The distribution of a_{tot} is obtained by Fig. 12 converting into a log-normal distribution of $a_{tot(act)}/a_{tot(est)}$ as shown in Fig. 13.

The total risk cost is calculated by the following equation.

$$R_c=R_{cf}+R_{cd}= C_f F_f(N)+ C_d \exp(\mu_{Lea}+Z_a\sigma_{Lea})F_d(N) \tag{7}$$

R_{cf} is reset at each repair action but R_{cd} is accumulated with repeated repair action. If the cost indexes are assumed as C_f=5 and $C_{Lea}\mu_{Lea}$=1(assuming Z_a=0), Life cycle risk cost curves are obtained for various repair intervals as shown in Fig. 15. Figure 16 shows the total life cycle risk cost at N=1500. The minimum life cycle risk cost is easily found and the optimum maintenance interval is determined.

Once an inspection information is obtained, the Z_a value is determined and to be used to predict the unit specific or component specific life cycle risk cost.

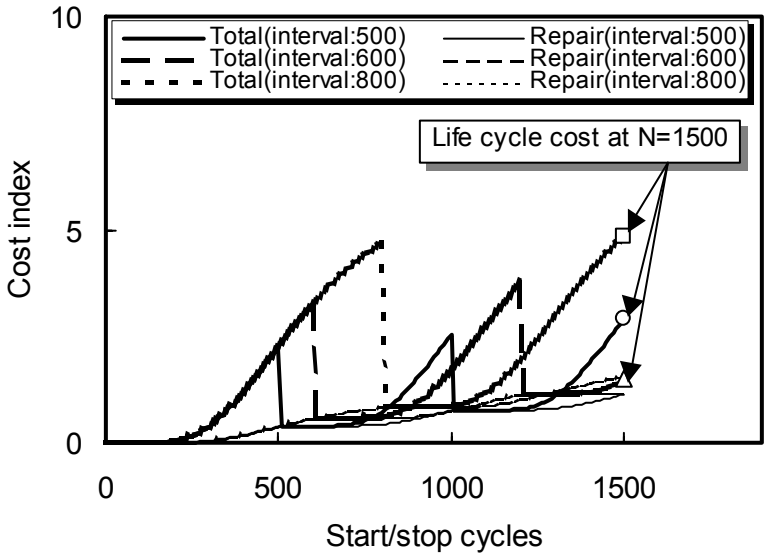

Figure 15. The prior risk assessment for various intervals.

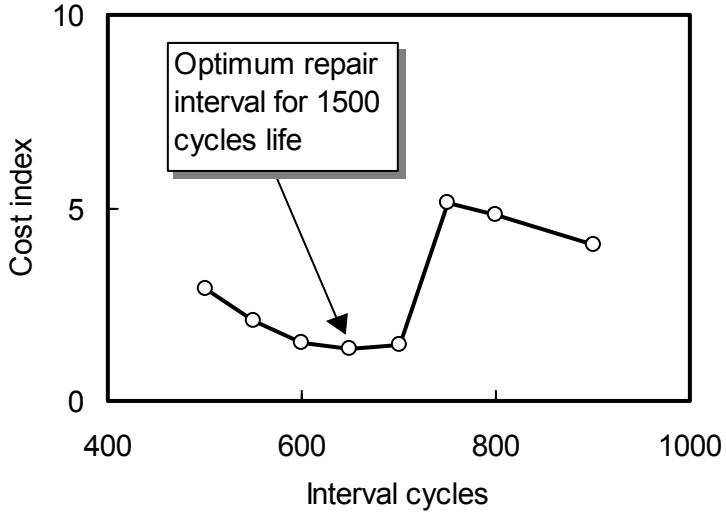

Figure 16. Optimization of total life cycle risk cost.

6. Application for other components

TMF is observed in other components. Other high temperature components of gas turbines, such as blades, combustion liners and transition pieces, are also suffered from TMF cracking damage but have limitations for damage tolerance. Steam turbine casings and valves are also suffered from TMF cracks and might have the optimum repair intervals and life cycle cost. For steam pipes, TMF multiple cracking was induced due to repeated water induction and the same kind of damage analysis was successfully applied [8]. For those cases, damage risk concept could be useful for optimum maintenance planning.

7. Conclusions

The practical method of risk-based maintenance was investigated for damage-tolerant turbine components with the case study for the gas turbine nozzle TMF cracking. Following results were obtained.

(1) The probability of failure and damage for TMF cracks was expressed as the distribution functions of cycles. In this case, the log-normal distribution fitted well.

(2) The log-normal distribution of failure had similar to experimental a_{max}-N relations and LCF life.

(3) The life cycle cost for repeated repair had minimum value and the optimum maintenance interval could be determined.

It was concluded that the life cycle risk cost approach was used to damage tolerant components. Inspection information should be fully utilized for modifying specific components trend.

Product names mentioned here might be trademarks of their respective companies.

References

1. A. Jovanovic & P. Auerkari. Proc. 29th MPA-Seminar, 2(2003) 33.1.
2. K. Fujiyama & T. Fujiwara. Proc. ICF10, Elsevier Science Ltd. (2001) \DATA\CONTENT\0868\PAPER.PDF (CD-ROM).
3. Y. Yoshioka, D. Saito, K.Fujiyama, H. Kashiwaya, T. Kondo, J. Ishii & T. Homma. CIMAC Congress (2001) 249.
4. K. Fujiyama, K. Takaki, Y. Nakatani, Y. Yoshioka & Y. Itoh. Materials Science Research International, JSMS, **8** (2002) 134.
5. K. Fujiyama, T. Kubo, Y. Akikuni T. Fujiwara, H. Kodama, H. Kichise, M. Okazaki & T. Kawabata, Int. Conf. Maintenance & Overhaul Management, (2003).
6. K. Fujiyama, S. Nagai, Y. Akikuni, T. Fujiwara, K. Furuya, S. Matsumoto, K. Takagi & T. Kawabata. Proc. 29th MPA-Seminar, **2**(2003)37.1.
7. K. Fujiyama, N. Okabe, I. Murakami & Y. Yoshioka, CIMAC Congress (1993) G09.
8. Y. Nakatani, K. Fujiyama, N. Ahiko & Y. Ito. Thermal Stress 2001 (2001) 375.

Component life management and cost saving maintenance strategy based on risk-informed decision making

Robert Kauer, Hans-Christian Schröder, Christian Irrgang & Gerhard Klein
TÜV Industrie Service GmbH, TÜV SÜD Group
Germany

Abstract

The words "globalization", "increased competition" and "international business" come to mind when characterizing the present development on a world wide market. A company´s ability to realize innovative concepts will be decisive to satisfy the progressive demands on competitiveness. The objectives of these concepts must always be to achieve high product quality and high productivity with a minimum of expenditure. Maintenance ensures that design-based availability and safety are retained and can be adjusted to current requirements. Maintenance, with its significant influence on life-cycle costs, can be the decisive key to ensure enhanced international competitiveness.

Adapted probabilistic reliability and risk assessment combined with the information extracted from generic and plant specific data as well as from structural analyses yield a solid foundation for decision making in a wide range of usage for maintenance optimization.

For this purpose we have developed adequate risk-informed procedures to provide significant savings. Examples illustrating the procedures demonstrate the benefit

1. Introduction

Process-specific control and operation concepts in combination with a sufficient maintenance strategy significantly influence the economic efficiency of a plant in the same way as the quality of its products. Present-day plant management requires an integral approach to enable decision making, considering the interaction of different systems as well as different phases during a life cycle with regard to cost-effectiveness.

Today, efficient quantitative procedures are available for an integral optimization of maintenance, which in our understanding include not only in-service inspection

aspects but also measures affecting organizational and operational matters as well as considerable interfaces [1]. Special emphasis is given to the risk assessment, which is now the foundation for making a decision. In this connection the term "risk" is not limited to a risk concerning safety but also can be related to a risk concerning availability and ultimately money. How and with which costs is it possible to keep the operation of a system within an acceptable risk? How is it possible to do this even though there are, for instance, defects or flaws on certain components?

2. Typical failure behavior

Maintenance optimization also includes view-points such as spare-part optimization or human factors. This is illustrated in Fig. 1, where the typical failure behavior of technical systems is shown.

Problems, both at the beginning and at the end of the life cycle are characteristic for the well known bath-tub curve. The second curve, for example, is characteristic for fatigue while the third curve with constant increase of failure probability represents corrosive damage.

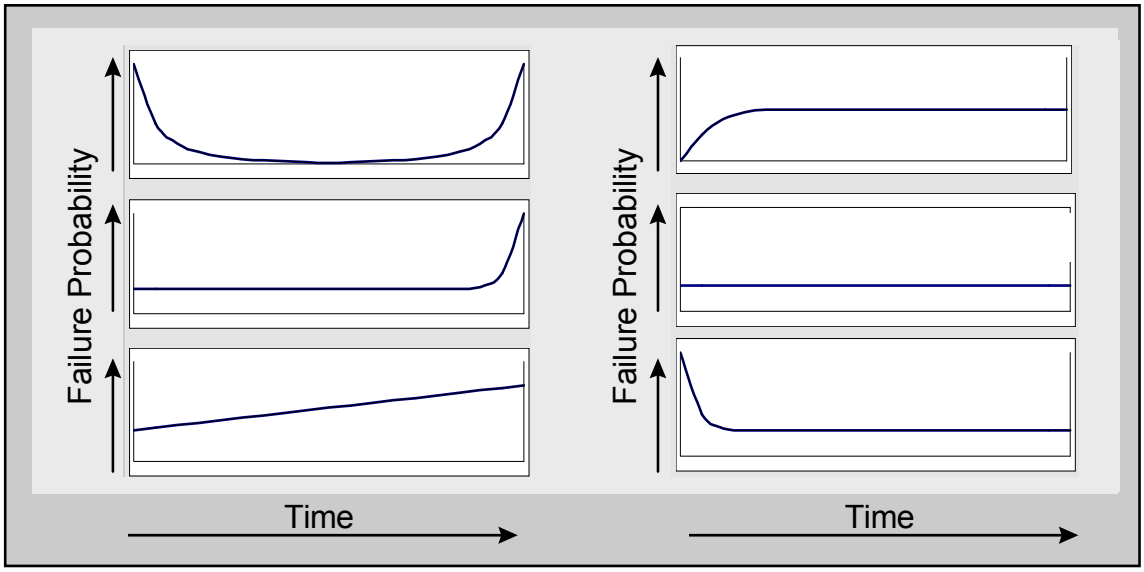

Figure 1. Typical failure behavior with respect to time scale.

Problems, both at the beginning and at the end of the life cycle are characteristic for the well known bath-tub curve. The second curve, for example, is characteristic for fatigue, while the third curve with constant increase of failure probability represents corrosive damage.

Those problems at the start of the life time are caused by circumstances, which are in the system from the very beginning: poor design, insufficient material or mounting failures, etc. A lot of those failures can also be introduced into a well running system through maintenance efforts. Those so called "burn-in" problems are often caused by failures during dismantling or reassembling and are often a human-factor problem.

Systems with a time dependent increase of failure probability (left side of Fig. 1) are not the only types that exist. A lot of systems show time-independent failure rates (right side Fig. 1). Classic in-service inspection methods are not sufficient to reduce those random failures. Here the optimization of the spare part concept can help to reduce these consequences.

The feedback of experience from plant operation shows that the relevant importance of human-factor problems, which are often significant for random failures, has increased. For this reason, measures helping to optimize the reliability of human action many times lead to more effective improvements for availability and safety than an increase of in-service inspection.

In order to realize an economic maintenance strategy, methods having an integral approach as mentioned before are increasingly applied. Risk-informed decision making also becomes more and more significant due to consequent consideration in codes and standards (see for example [2] or [3]). Here the opportunity emerges to question, whether cost intensive former regulations are still necessary. For this purpose, comprehensible and transparent solutions must be generated to be able to be accepted by regulatory authorities.

3. Type of analyses

By using risk-informed decision making, not only the number of failures within a considered period (PoF: Probability of Failure) but also the direct and indirect consequences of failures must be considered. The consequences may be measured in terms of damage to the health and safety of employees or public, damage to the environment, and financial damage to the company due to a loss of production, repair and replacement of equipment. By defining risk as a product of failure probability multiplied by consequences the term risk is not restricted to safety related questions but can also be applied to the assessment of technical facts or modifications from an economic point of view (ROI = Risk-Oriented Inspection and Maintenance).

However, the entire technical process and the used procedures and techniques should be embedded in a quality or safety management system (compare Fig. 2). Herein, the main goals, tasks, and responsibilities should be clearly identified and documented. As risk based inspection and maintenance planning is a multi-

disciplinary task, it requires a team where many competencies are represented and expertise are available (e. g. EN 45004 [4]).

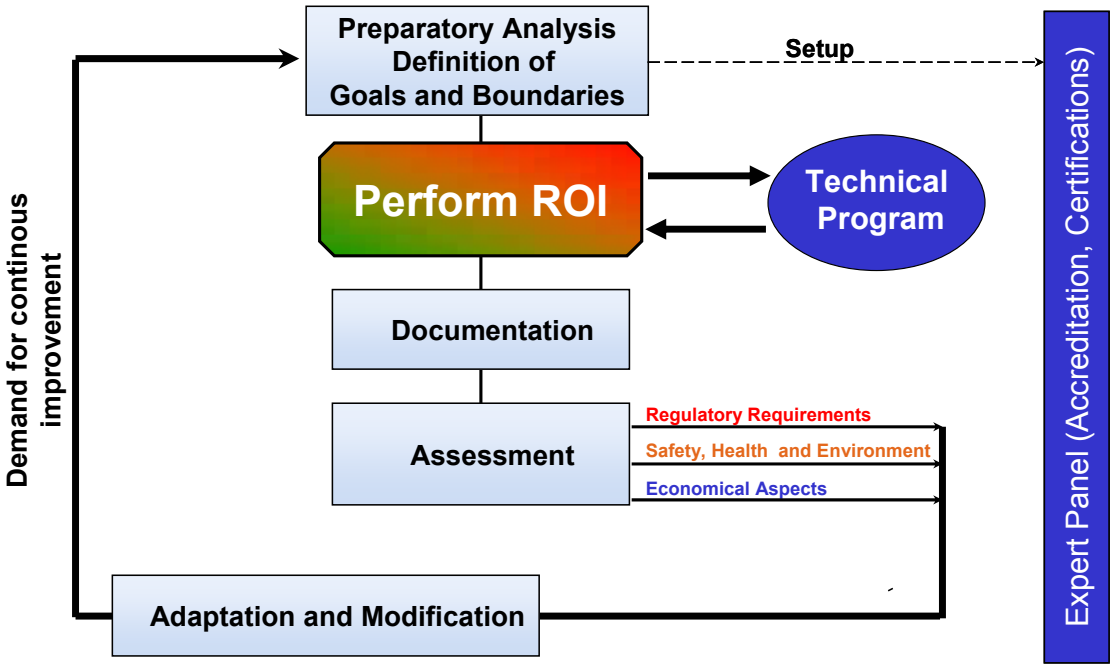

Figure 2. Management loop.

It is also necessary to monitor all influencing parameters (operating window) with respect to the boundary conditions chosen for the original analysis and to ensure the evaluation of any changes by the responsible individuals. Another important issue is the recurrent evaluation at a certain interval to assess all the modifications and new data available to make sure the entire process yields into a loop.

Regarding the (risk-oriented) technical program, it is necessary to provide component dependent flexibility to ensure a adapted seamless transition from screening to detailed analysis and to launch component specific solutions. In Fig. 3 it can be depicted that there are several solutions available for each step to be performed.

So, within the procedure, it is possible to meet the requirements of other already existing risk related programs like EN 1050 [5] for machinery or IEC 61511 [6] for electrical safety systems. In the following, some examples are given how to deal with certain problems.

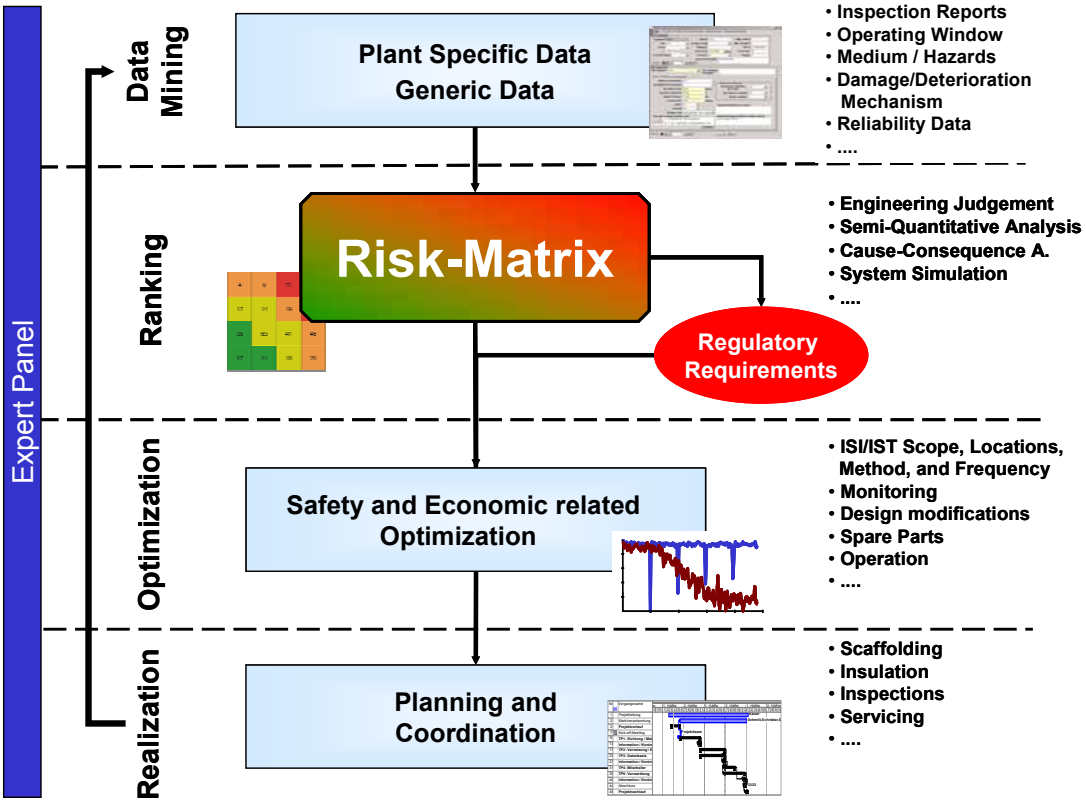

Figure 3. Technical program.

3.1 Example: Fitness for Service / Purpose

To be able to guarantee the safety of components or subcomponents on the one hand and to achieve a very high availability of technical plants on the other, the interaction between material, stress and failure status is of crucial importance for static equipment like pressure vessels and piping.

Of particular interest is this interaction with reference to a justifiable safety-related extension of the service life of a plant or individual components. „Living with defects“. Probabilistic fracture mechanics is an appropriate tool for that kind of task within a risk-oriented surrounding.

Manufacturing caused defects – particularly for welded constructions – as well as operationally caused defects influence safety and availability. Examples for manufacturing defects are: segregations, internal shrinkages, forging defects, weld joint imperfections like slag inclusions, pores, lack of fusion, hot cracks and cold cracks. These defects may increase under certain operating conditions. Operationally caused defects may be created as a consequence from mechanical, thermal or corrosive stress. Typical examples for such defects from operation are: fatigue cracks, creep and stress corrosion cracking or crack areas from thermal shock and alternating stresses.

Non-destructive tests and operational monitoring programs are deployed to locate the status of defects and to trace their development and also to compile stress and material behavior in selected areas.

With the help of probabilistic fracture mechanics, quantitative statements about critical failure factors, limiting creep stress and lowest material toughness can be made taking into account those influential factors divided into type and use of a component or subcomponent. The aforesaid may be used for:

- safety and availability evaluation
- strategy for in-service inspections
- plans for repair or exchange
- extension of duration while in use.

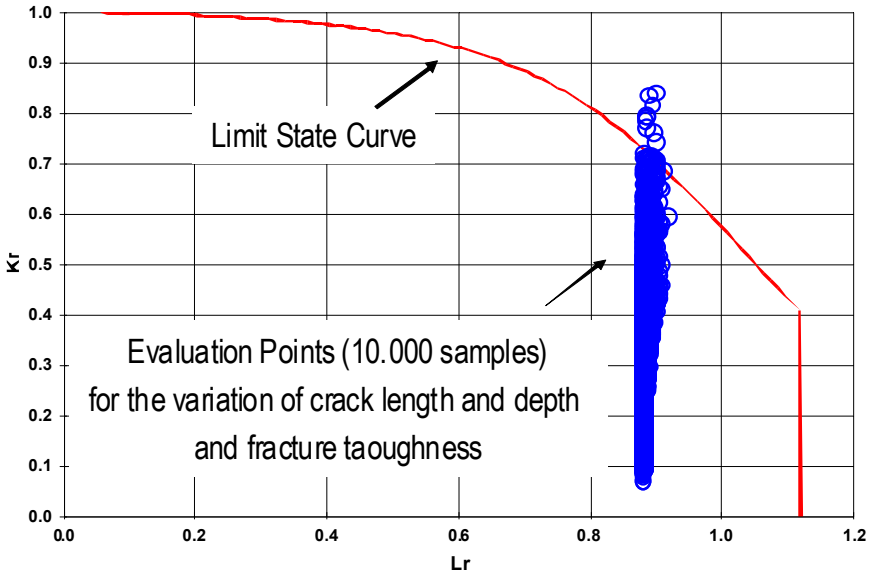

Figure 4. Example: Probabilistic failure assessment (Failure Rate 0.012).

In Fig. 4 the result for an evaluation for a crack regime in a pipe is calculation taking into consideration the variation of the detected cracks as well as a variation of the uncertain fracture toughness.

To decide, whether it is possible to live with these defects, at least for a given period (e. g. next turnaround), it is necessary to establish a proper inspection or monitoring plan, to ensure that all boundary conditions, chosen for the evaluation are within the level of acceptance (influence monitoring) or the existing degradation (e. g. crack propagation) is within the acceptable level (condition monitoring). In the following Fig. 5 the principle procedure is shown.

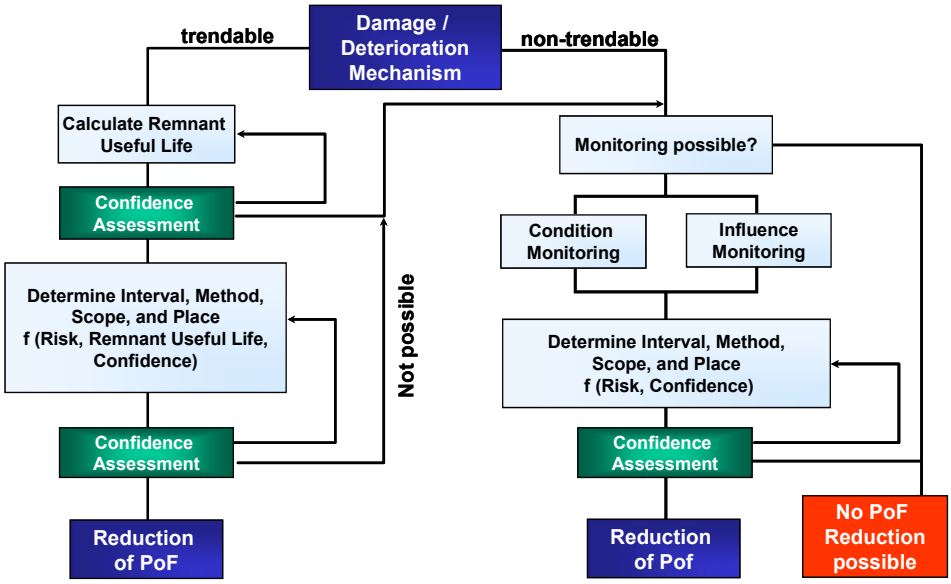

Figure 5. Principle decision strategy for inspection and maintenance.

3.2 Example: E/E/PES Components

Risk-informed decision making is also an integral part of new standards concerning the functional safety of electrical, electronic and programmable electronic (E/E/PES) like IEC 61508 or IEC 61511 (IEC 61511 implements special requirements for the process industry). "Functional safety" is the part of the overall safety relating to the process and the process control system which depends on the E/E/PE safety-related systems, but also on safety-related systems using any other technology or external risk reduction facilities. That is, the IEC requires an *overall* hazard and risk analysis as starting point for deriving *special* requirements on E/E/PES:

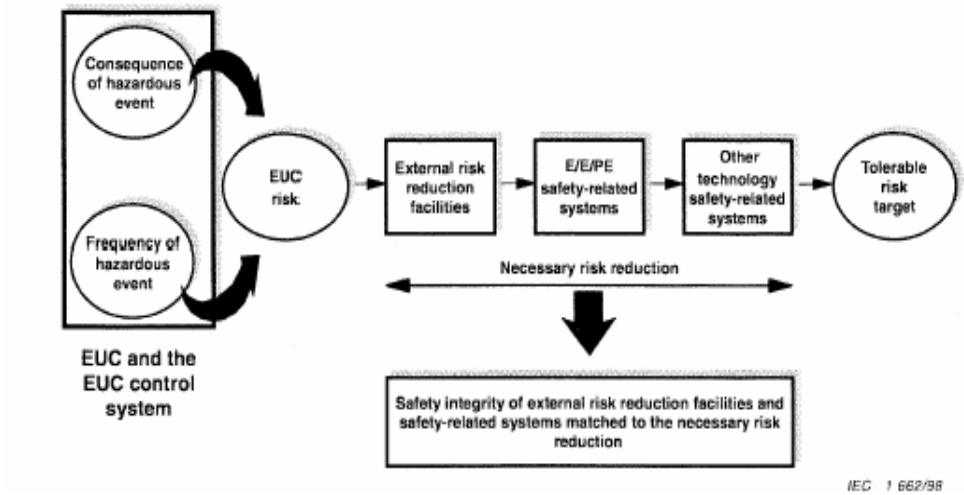

Figure 6. Principle Strategy for Deriving Safety Integrity Levels (from IEC 61508;"EUC" = equipment under control).

These special requirements are called “safety integrity requirements”, where safety integrity is defined as the probability of a safety-related system satisfactorily performing the required safety functions. To characterize the “level of quality” of a system the safety integrity levels (SIL) are introduced, again in a quantitative way:

Table 2 – Safety integrity levels: target failure measures for a safety function, allocated to an E/E/PE safety-related system operating in low demand mode of operation

Safety integrity level	Low demand mode of operation (Average probability of failure to perform its design function on demand)
4	$\geq 10^{-5}$ to $< 10^{-4}$
3	$\geq 10^{-4}$ to $< 10^{-3}$
2	$\geq 10^{-3}$ to $< 10^{-2}$
1	$\geq 10^{-2}$ to $< 10^{-1}$
NOTE – See notes 3 to 9 below for details on interpreting this table.	

Table 3 – Safety integrity levels: target failure measures for a safety function, allocated to an E/E/PE safety-related system operating in high demand or continuous mode of operation

Safety integrity level	High demand or continuous mode of operation (Probability of a dangerous failure per hour)
4	$\geq 10^{-9}$ to $< 10^{-8}$
3	$\geq 10^{-8}$ to $< 10^{-7}$
2	$\geq 10^{-7}$ to $< 10^{-6}$
1	$\geq 10^{-6}$ to $< 10^{-5}$
NOTE – See notes 3 to 9 below for details on interpreting this table.	

Figure 7. Safety integrity levels (from IEC 61508).

From this it becomes clear that the procedure of ROI fits exactly the requirements of IEC: In both cases we have to consider hazards and consequences first, i.e. risks. Moreover, we can identify the potential of risk reduction for systems of “other technology” or “external risk reduction facilities”, as IEC calls it. Of course, due its nature IEC gives no detailed requirements for these “non-E/E/PE-systems”. But because of the overall and overriding view point of ROI *all systems* are treated on a common basis and this means that the necessary “extent of risk reduction” for all these systems can be estimated much more precisely now – *including* E/E/PES. ROI unites the economic and safety-related features of risk and therefore the hazard and risk analysis required by IEC may not be a “stand-alone” solution just for process control systems but can be integrated within the framework of ROI. Furthermore, the (semi-) quantitative procedure of ROI allows us even to formulate targets in terms of SILs. So double working can be avoided.

3.3 Example: System simulation

To get information about time dependent influences on risks system simulations are applied increasingly on maintenance tasks. With the help of this procedure the operational behavior of plants and systems can be simulated. All factors influencing the considered risk can be modeled within one mathematical model (see Fig. 8).

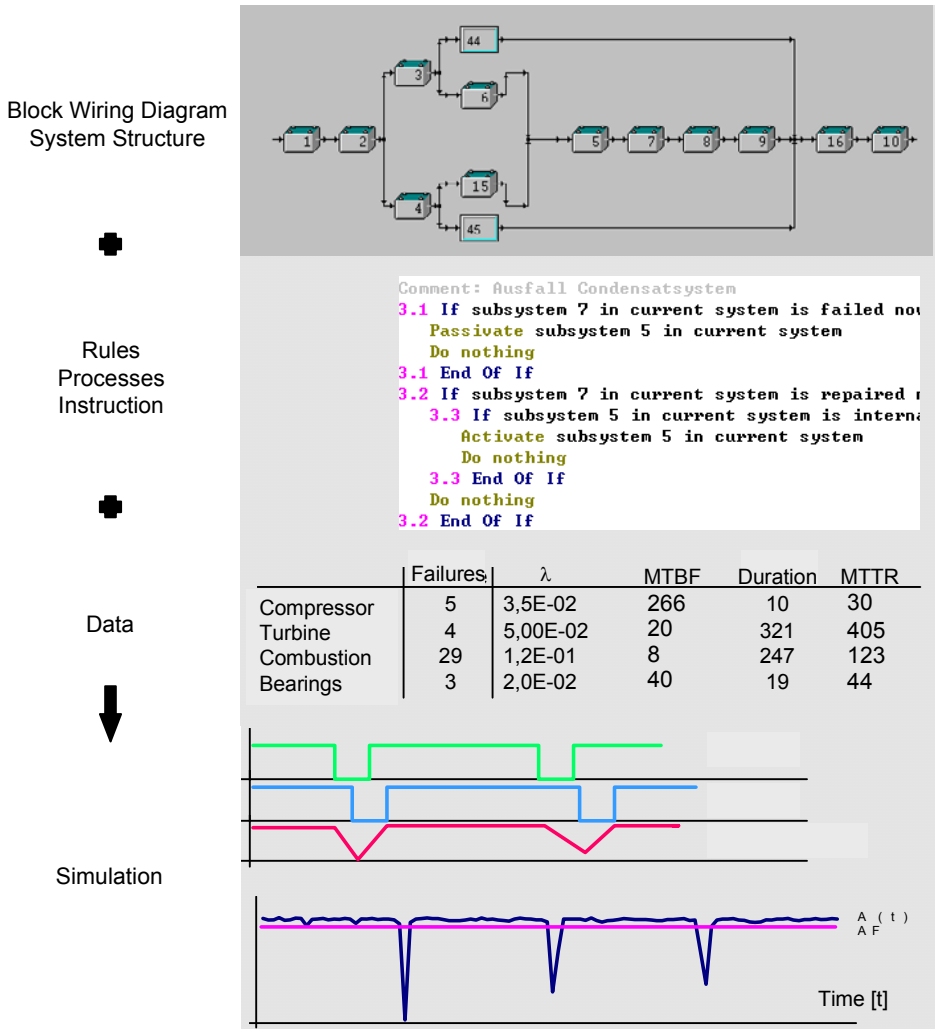

Failure Rate	Basis: 3 years without inspection	4 x more test-start	2 year inspection interval	Improved MTBF 10%	Improved MTTR 50%	E/A redundant	annual burner inspections others 2 year interval
Startsystem	13,2 %	5,8 %	10,4 %	9,7 %	11,2 %	12,1 %	5,7 %
Production-system	3,7 %	1,9 %	2,7 %	2,1 %	2,8 %	3,3 %	1,2 %
Per Demand	1,6 %	1,2 %	1,2 %	0,9 %	1,0 %	1,4 %	0,7 %

Figure 8. System simulation model and results of the evaluation process.

This approach takes implicitly into account interface problems. With Monte-Carlo procedures, availability and safety can be calculated for each point in time within a confined period of time by means of simulation. The results obtained in these analyses show the significance of individual influencing parameters and/or individual components. Thus, a tool is provided which makes it possible to quantify the influence of maintenance measures with respect to time.

The advantages of this procedure by means of maintenance aspects shall be demonstrated for a stand-by internal power supplier in a chemical plant. The main task was to increase the availability for a long term use and per demand by developing an optimized maintenance strategy for this goal. To simulate the behavior of the system 287 Elements were used. The availability of the system per demand should be optimized with respect to the optimization of inspection frequency, repair and replacement strategy and testing procedures. The influence of various possible measures is shown in the table in Fig. 8.

4. Summary

The main objective for launching new maintenance programs is, that individual interests will find a common denominator for the following:

- high operating reliability
- high availability
- high procedure- and process safety
- estimation of life-cycle expenses
- realistic estimation of technical problems, incidents, results
- avoiding unnecessary redevelopment and replacement measures
- understanding the actual aging processes
- cost/economic operation.

Today's range of monitoring and inspecting methods put us in a situation to conduct large-scale plant evaluations. Within the possibilities for optimization safe continued plant operation is feasible using weak point analyses, specific object examination in relevant parts, fracture mechanic and probabilistic analyses. It will be important in the future, that mere registration and evaluation of single statements without looking at a plant/process in its entirety is not the only way.

That is valid in particular for incidents/results, which are not permissible on the basis of regulatory stipulations, but are not cause- and effect-related for subsequent incidents.

In the existing regulations the protection for component integrity is executed mostly on the basis of in-service inspections, in the form of pressure checks and visual inspections. The primary goal should be that all hazardous factors, which could occur during operation be recorded in reality and understood as a protective measure from damages to be expected to happen. From that one may draw the conclusion that avoiding operational damage mechanisms should be at highest priority.

With these instruments plant processes may be controlled technically, economically and in a safety-related way. With control instrumentation as described in V the incidents cannot be understood by only using MSR-protective measures, because they are not designed for it.

In order to establish a successful risk-oriented maintenance program, it is strictly necessary to properly understand which risks has to be measured and the acceptance criteria that should be used.

References

[1] Sacher, H. & Rauh, H.-J. Integral Optimization of Safety and Reliability through Maintenance Strategies. Power-Gen 98, Milano, June 9–11, 1998.

[2] RIMAP (Risk-Based Inspection and Maintenance for European Industries) GRTD Growth Project.

[3] ASME Risk-Based Inspection.

[4] EN 45004 General criteria for the operation of various types of bodies performing inspection, 01.03.1995.

[5] EN 1050 Safety of machinery – Principles for risk assessment, 01.11.1996.

[6] EC 61511 Functional safety of electrical/electronic/programmable electronic safety related systems.

Risk assessment of heat & power plants in Stockholm

Leif Kiessling & Mats Tapper
ÅF Teknik & Miljö AB
Stockholm, Sweden

Abstract

All in all there are about 40 different regulations in Sweden dealing with requirements on risk assessment of critical components and systems in energy plants. The latest also contain requirements on risk management and programs to decrease risk levels. A successful risk management starts with a total mapping of the plant risks. ÅF Teknik & Miljö has developed a risk assessment method that meets several of the authorities' requirements. This method is adjusted to energy plants producing different form of energy such as heat, steam, electricity and cooling. The method has been applied on the largest heat and power plants in Stockholm and the results serves as a basis for systematic reducing the risks and increasing the plant's availability.

1. Introduction

1.1 Swedish authorities' requirements of a risk management

The Swedish authorities have in recent years increased the requirements of risk management in the industrial sector. The authorities in question are Work Environment Authority, Swedish Rescue Service Agency and the Swedish Environment Protection Agency and they cover the three areas often shortened as EHS (Environment, Health and Safety). The purpose of the sharpened requirements is of course to raise the level of protection of the employees, the people and the environment in the plant's surroundings. This session will consider a method to meet several of these requirements.

Over the years the requirements have developed from simple risk inventory to complete risk management. The later means requirements for documented policies, action plans and regular risk follow-ups of the safety work. The risk assessment is one of the most important tools to succeed with the risk management.

1.2 Other actor's requirements on risk management

In addition to the authorities there are other actors on the market with interests in the risks of industrial plants. For example there are unions and customers that don't want to be associated to companies with high rate of accidents or unnecessary environmental impact. Lack of risk management may also results in difficulties to recruit young and well-educated people.

The owner has in addition to the EHS-risks also a high interest of knowing the risk for interruptions in the production causing losses of incomes. Recurring interruptions may result in loss of customers though energy customers are very sensitive to interruptions in the energy supply.

A serious and systematic EHS-risk management is to take good care of your trademark and should also be considered as good marketing.

2. Methodology

Traditionally, the most commonly used key factors for management of plant investment are based on economical and budget issues. A failure of components and accidents also takes an important role. However, significant statistics such as availability and used maintenance man-hours are seldom used for conditioning evaluation of components. It is a strong demand to evaluate the long-term degradation of the systems in the plant and the influence of operation and maintenance. It is important to use a method, which encounter plant personnel to be involved in the long-term aging plant management of the investment. A model for these lifetime analyses (LTA) should include many key factors such as:

- Plant history and present strategy
- Operational data
- Environmental management system data
- Component condition
- Risk of failure
- Environmental risk
- Failure cost
- Personnel hazard.

In a program by Thermal Engineering Research Institute (Värmeforsk) in Stockholm, Sweden several methods for analysis have been studied and it could be concluded that all have both their drawbacks and benefits. For this study we have used Failure Mode and Effect Analysis (FMEA) which i.e. is described by Carina Fritz (1). Ageing programs have also been tested in Japan and elsewhere

(5, 6). We have chosen FMEA because it is easy to use for plant personnel due to its simplicity in theory and it is especially useful for medium and small size companies, which normally is the case for power plant companies in Sweden. An example of a full LTA is given in Figs 1–2 below.

The word risk is an expression for the danger of an unplanned incident or state that could lead to damage of environment, personal or material value. The risk could with this definition be evaluated as a quantitative number as per:

RISK = PROBABILITY X CONSEQUENCE

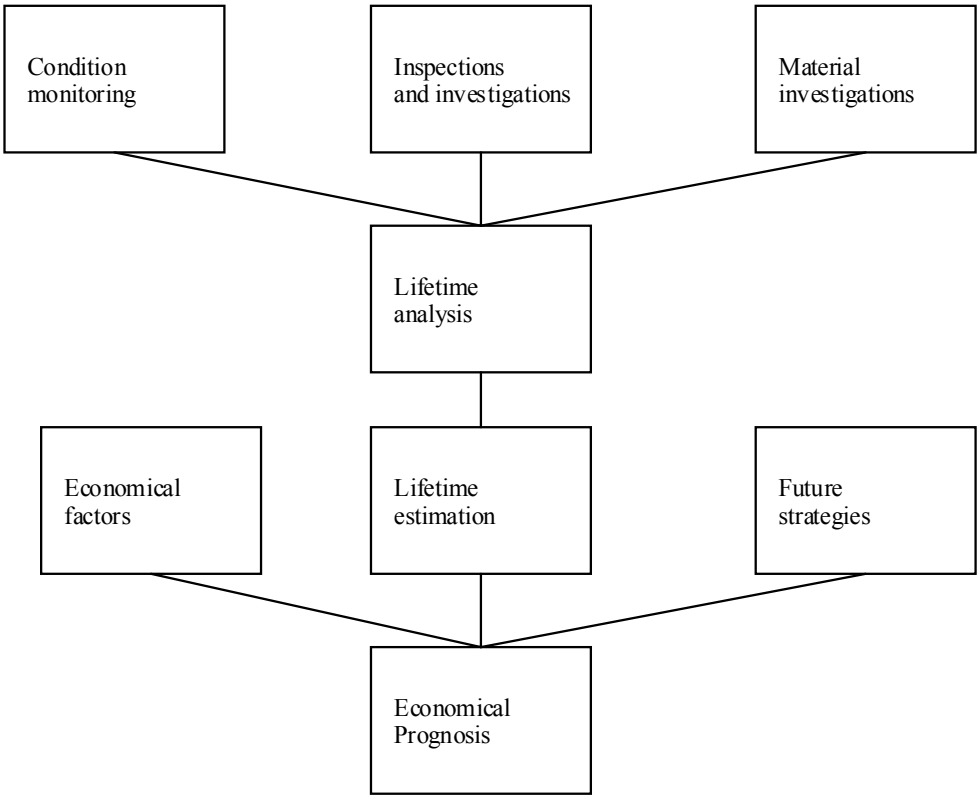

Figure 1. Flow chart of a lifetime analysis (1).

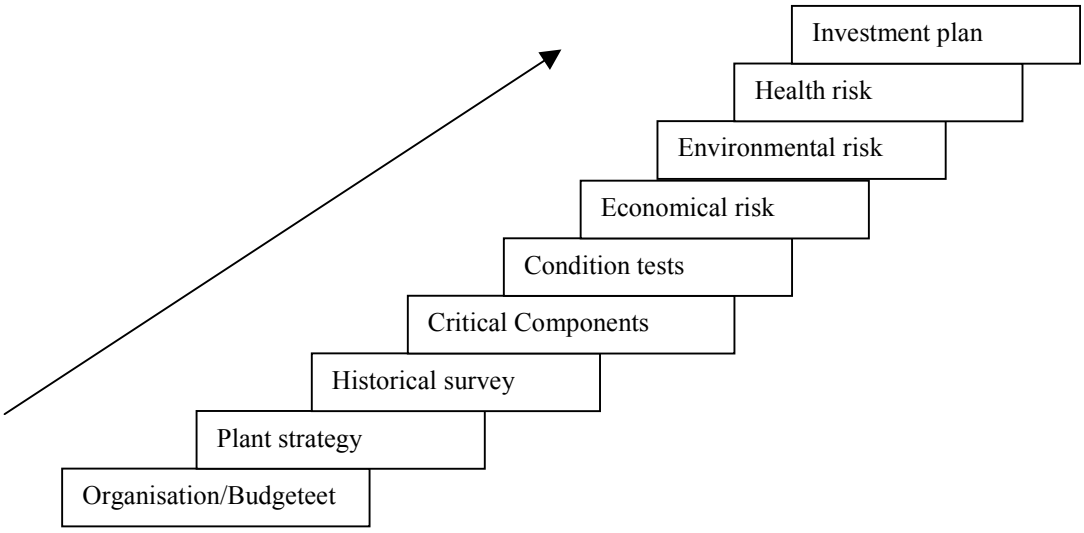

Figure 2. The steps of a lifetime analysis in a power plant.

3. Application on a CHP plant

3.1 Organization of personnel and work

It is important to have a strict project organization for the LTA. A LTM should be regarded as a project itself and be organized accordingly. The work was organized in two working groups and one project leader. The project leader is the key person and was responsible for the project and represented the two different working groups for the plant owner.

One working group was organised with plant personnel and its main task was to work with operating history and interviews of involved personnel. Group number two was a team of specialists with metallurgical and mechanical background being specialists in matters of creep damages, fatigue and other ageing mechanisms. The main task of this group was to determine component condition from historical data and to require further testing for the final analysis.

The two different teams were working quite independent of each other. However, the team with specialists was supporting the team from the plant regarding representative type of data and important issues for the interviews. The two groups had several meetings when experience and complementary data were compared and requested. There was a lot of subjects to analyse, such as reports, operation- and maintenance data. Both groups produced detailed reports with all data from their work. The project leader who controlled the time/cost tables in a manner similar to any project leader catalysed the work. However, his role must also focus on a rather technically initiated leadership were the methodology must be well known by the personnel in the groups at each step in the process.

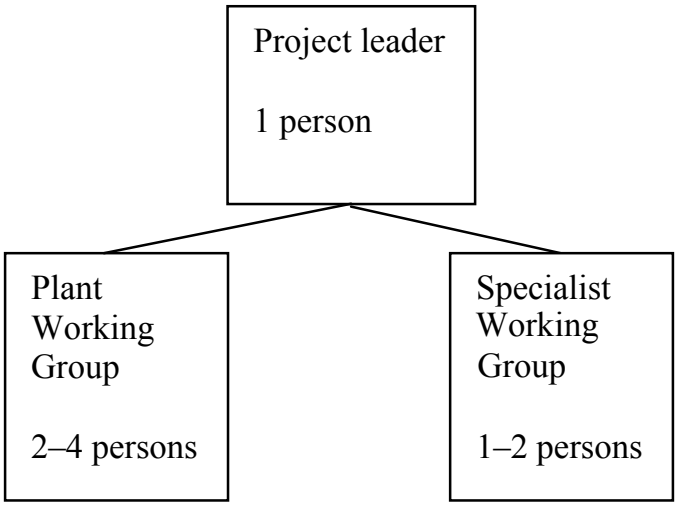

Figure 3. Organisation flow chart.

3.2 Interviews of personnel

A baseline history of transient's cycles and resulting fatigue usage of the plant is of outermost important for the analysis. Most base data could be found in the records and logbooks in the plant archive. However, the logbook data is not always too relevant for data in a program for ageing management. Incidents and other smaller transient that might be important could be foreseen. We thus made interviews with operating personnel with long experience from the plant and we have found a lot of new valuable information. In order to carry out the interviews and history survey more systematic the checklist in Table 1was used.

Table 1. Historical survey – checklist (example for boiler).

Type of data	Data	Checked date
Operating data	Temperature outlet steam °C	
	Pressure outlet steam MPa	
	Number of start/stops per year	
Large failures	Number per year	
	Components	
	Measures	
	Causes(investigations, reports)	
	Consequences	
Small failures	Number per year	
	Components	
	Measures	
	Causes(investigations, reports)	
	Consequences	
Incidents	Number of per year	
	Components	
	Measures	
	Causes(investigations, reports)	
	Consequences	
Regular investigations	Components	
	Intervals	
	Methods	
	Summary of results	
	Measures	
	Consequences	
Rebuilding	New operating data	
	Causes	
Changes of fuel	Strategy	
	Consequences	
	Rebuilding	
	Consequences	

3.3 Determination of critical components

Determination of critical components for each system was carried out by means of empirical knowledge, maintenance program, reported faults and inspection remarks. Latest research data should also be included in the analysis. The plant staff compiled a list of components and parts to be included in the study.

In general the following criteria were used:

- High risk of incidents
- Great impact on plant economy
- Long and short time influence on risk of personnel hazard
- Impact on external environment.

How deep in details each component should be examined was an important factor and was judged from experience of the plant personnel. Thus it was not sufficient to choose individual wall tubes and it was decided to chose left, right and side i.e. 6 items instead of one. The decision how many items that should be included in the list must be based on experience from plant staff after several years of inspections and testing activities. However, if the list contains to many items the analysis will be far to expensive and time-consuming. Highly critical components could be divided into more details in order to evaluate the individual component condition.

3.4 Risk-based inspection and condition evaluation

Inspection of components in the plants is normally carried out in a subjective manner, based on many years of maintenance and know how from the staff. However, the condition and failure risk is then not evaluated in a systematic way. This could cause severe misjudgements to be made during the planning of the yearly inspections. Furthermore the person with the key experience could be retired or simply not present at the right moment. The most obvious investments could be highly ranked instead of more important issues. This could lead to increased operational cost for the plant due to unplanned shut down for failures of systems or components.

Many plants and industries use risk based inspections (7) instead of traditional inspections in order to cut down risks of failures. In many cases they also claims that this has resulted in improved safety, plant reliability and reduced costs. This has been explained by more focused inspections with a decreased number of unnecessary replacements of components.

In order to carry out a risk-based inspection, all high and middle risk components were chosen from the risk analysis of critical components, see Table 2. The material expert engaged in the work chose the accurate technique and extension of inspections. The individual decisions for the components were based on the type of expected failure mechanism and the experience from earlier inspections.

4. Results of a risk assessment

The result of the risk analyze is presented in the table below where the proposed investments for the plant is ranked according to a failure risk and the consequence of the actual failure. The various projects have been analysed according to a "what if" model where the consequences of a neglected investment is discussed. The focus of the discussion is then the failure risk for the most critical component involved in the system. The result is presented in Table 2 below.

Table 2. Investment risk table.

Project No	Component /System	Remedy	Failure	Incident	*Risk* Personal	Econmic.	Environm.	Probability
1	Steam drum	replacement of drum	Leak or failure	Boiler stop and steam outlet	2,15	2,15	0,43	0,43
2	Safety valves steam drum	replacement/renovation	Steam leak	Boiler stop and steam outlet	1,72	0,86	0,43	0,43
3	Floor tubes boiler	replacement of tubes	Tube leak	Boiler stop and steam outlet	1,36	2,04	0,68	0,68
4	Collector Sup. 1	replacement of header	Leak or failure	Boiler stop and steam outlet	2,12	2,65	0,53	0,53
5	Collector Sup 2	replacement of header	Leak or failure	Boiler stop and steam outlet	3	3	0,6	0,6
6	High Pressure preheater	replacement of tubes	Tube leak	Boiler stop and steam outlet	3,2	2,56	0,64	0,64
7	Inspection doors	replacement of doors	Gas leak	Fuel gases outlet	0,63	0,63	1,89	0,63
8	Fixtures economizer tubes	replacement/new design	Tube leaks	Boiler stop	2,6	3,25	0,65	0,65
9	Feed water pumps	replacement of pumps	Pump failure	Boiler stop	0,56	1,12	0,56	0,56
10	Air preheater	replacement of tubes	Clogging of tubes	Effiency decrease	0,52	1,04	0,52	0,52
11	Steam valves main steam	replacement/renovation	Leak	Boiler stop and steam outlet	2,55	2,55	0,51	0,51
12	T-join, main steam line	replacement/repair	Leak or failure	Boiler stop and steam outlet	2,75	2,75	0,55	0,55
13	Bend, main steam line	replacement/repair	Leak or failure	Boiler stop and steam outlet	2,75	2,75	0,55	0,55

The results of the analysis can be presented in a graph as per Fig. 4. If a replacement of the steam drum (investment no 1) is compared with a replacement of a feed water pump (investment no 9) the following interesting conclusions could be drawn. The personal hazard associated with a drum failure is much higher than with a failure of a feed water pump, which would favourite the former investment. However, the probability of the drum failure is lower which makes this investment less pressing than a replacement of the pumps. On the other hand if the drum replacement is compared with a replacement of the high-pressure feeder (investment no 6) it could be concluded that the latter investment has the highest personal risk and should therefore have a higher ranking than the drum replacement.

From the economical point of view, the renovation of the fixtures for the economizer tubes (investment no 8), should have a high ranking due to the high costs involved with the long shut down period caused by an economiser failure. These investments, which involve the main steam line components (investments 11–13), should maybe have the highest ranking due to a combination of high personal and economical risks.

The result of the risk analyse could be carried out on a yearly basis and consequences could be judged accordingly. This could serve as a base for the ranking of the investment and an investment program for the coming period of

years. For the coming periods of operating of the energy plant should then the risk table be updated in order to rank new investment projects in the investment plans for the plant owners. The base data for the analyze could be compiled by the service company responsible for the operation and maintenance of the plant.

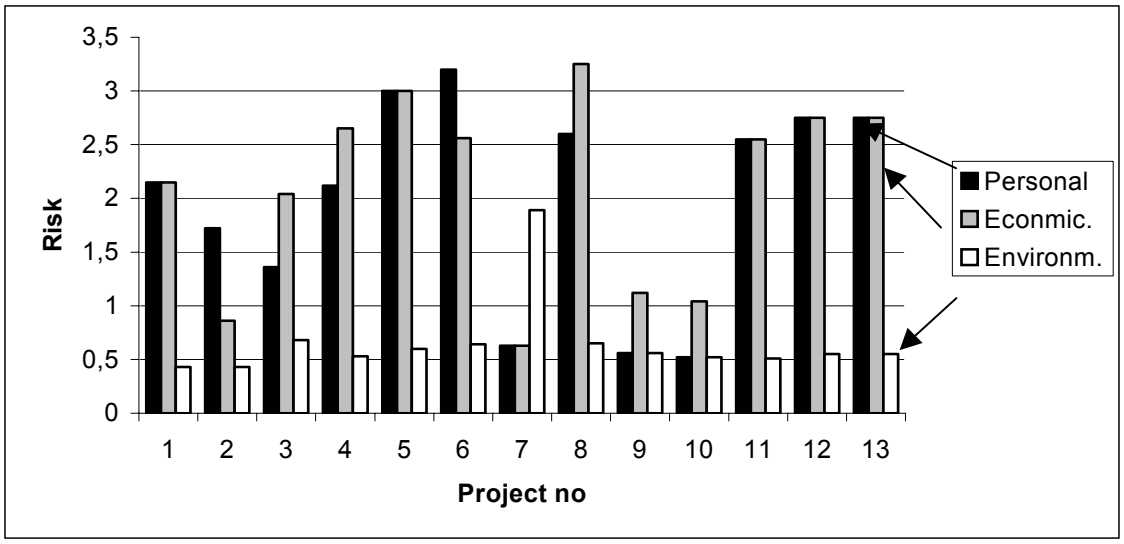

Figure 4. Risk investment graph.

5. Experience from the work

The working groups have gathered the following experience during the study.

- A careful budget and time planning is important before the project starts. Due to the fact that the work is not following normal plant routines there is an evident risk of delays.
- The different working groups should work independently with separate goals and programs. However, the plant personnel must have careful support from the specialists in order to seek the right background data.
- It was difficult to get continuous plant history. Some period was poorly documented and personnel interviews could not fully cover this gap. Some periods are missing and surprisingly not from the first period of operation. This could be a result of hunting for lower plant cost. A computerised system for documentation of maintenance and operating data will certainly improve the situation and increase the available data. However, the demands for relevant data is still the same. A careful documentation of relevant data for LTA is of great value and could not be recapitulated 10 years later.

- Criteria's for determination of critical components must be well prepared in order to avoid a situation when original goals must be changed in the end of the analysis, during the management of the plant investments.
- One person high up in leading position of the plant should be responsible for the risk assessment. Consultants could manage the work but the plant personnel must take an active part in the work. Thus the experience will be kept in the plant for a continuous updating of the long time investment goals. A regular analysis gives a possibility to link the maintenance to the long time goals of the plant.

6. Conclusions

The conclusions below are based on the experience from the risk assessment carried out in a number of energy plants in Sweden.

- The FMEA method used in the study is a practical tool for evaluation of the risk of the investments. The economical, environmental and personal hazard can easily bee viewed.
- It is essential for the result that the study has a well-defined strategy and organization from the start.
- A broad perspective must be kept. Don't dig into details.
- The risk assessment provides improved tool for long time planning with a decreased risk of unnecessary component replacement. Thus improved plant economy is a likely result.
- Today a complete analysis is seldom carried out in a power plant. A LTA must apart from failure risk also include economical, environmental and personal hazard. The result of a LTA shall be a prognosis of all costs for replacement of component over a longer period of time.

References

1. Handbook of Lifetime Analysis of power plants, Thermal Engineering Research Institute (Värmeforsk), Sweden (to be published).
2. Carina Fritz. Failure mode and affect analysis (FMEA) for Swedish industri, IVF-resultat nr 89632, august 1990 (in Swedish).
3. Henrik Bjurström. Livslängdsbedömning – erfarenheter och utveckling in Japan, IVF resultat no 106 (in Swedish).

4. Availability of power plants, report by Vattenfall AB, Sweden. (in Swedish).
5. Shigera Masamori & Hidehito Mimaki. Aging Management Program for PWR Nuclear Power Plants in Japan, Service and Life Management in Operating Plants, ASME 1992, pp. 47–52.
6. Kenneth A. House, Transient Monitoring Program at Sequoyah Nuclear Plant units 1 and 2.
7. Fisher, D. (RSA). Optimising the implementation of a risk based inspection program in a complex facility, CAPE ´99, 12–16 April 1999 (not in proceedings).

Stochastic reliability simulation in power plant life and maintenance management

Mikko Pakarinen
Fortum Service Ltd, Vantaa, Finland

Abstract

This paper describes the conceptual principles, advantages and experiences of using reliability simulation in a competitive power producer environment. In recent years Fortum Service Ltd. has developed and utilized within the joint industry project a new flow-based stochastic reliability and production simulation and modelling tool, Miriam-Regina®. It enables more accurate modelling features, such as storage, operation and maintenance principles, as well as the business-driven results, than earlier analytical methods. Fortum Service Ltd. is applying stochastic simulation within the ProMax approach.

1. Introduction

The liberalisation of the energy market has changed the structure of the power industry. Many local power companies are being combined into larger companies and the competition between power companies is increasing. For each power company the change also means that the effectiveness of the business processes should be improved. Asset management, including maintenance management, is one of the processes to be developed. It seems that for a time the search for effectiveness mainly focused on reducing costs. However, improvements aiming at a lean and effective organization were not enough. In power plant life and maintenance management new value-adding tools and procedures, such as stochastic reliability simulation, are being utilized in the new business environment.

1.1 Fortum in the Nordic markets

Fortum is a leading energy company in the Nordic countries and other parts of the Baltic Rim. Fortum's activities cover the generation, distribution and sales of electricity and heat, the production, refining and marketing of oil, and the operation and maintenance of power plants, as well as energy-related services.

"We provide management, operation and maintenance expertise with performance guarantees for your power plant" is the value proposition of Fortum Service Ltd

TOPGen® services. We offer competitive basic O&M services for reliable daily operations. Our customers can select more value-adding services from our broad Technical Support services portfolio. These services aim at continuous performance and quality improvements to our customers' energy business. The value of these services is enhanced when moving towards higher competitive requirements and open energy markets.

The stochastic reliability simulation tool, Miriam-Regina®, is a tool in Fortum Service's O&M service concept for maximizing the life-cycle profit of power plant investments. Miriam-Regina® is applied to create a stable foundation for cost-effective long-term maintenance and to enhance the risk management of an O&M contract.

The Fortum Service Ltd. way of using stochastic reliability simulation is called the ProMax approach. The approach is based on reliability simulation and Experience-Based Reliability-Centred Maintenance (EBRCM). EBRCM effectively supports the training of O&M staff by producing the best available understanding of the factors governing the maintenance of the plant's critical components and systems.

2. Miriam-Regina® stochastic reliability simulation

Miriam-Regina® is a powerful and flexible reliability and availability analysis program. In recent years Fortum Service Ltd. has developed and utilized it within the joint industry project. It is based on a new-generation simulation system. The program models the stochastic behaviour of a system over time and is suitable for a wide range of studies, from simple trade-offs to complex verifications of integrated production, processing and transportation systems.

2.1 Simulation approach

The stochastic behaviour of the system over time is represented using the Monte Carlo simulation. A simulation run generates a sequence of events, corresponding to system state changes, and performance statistics are gathered as the run proceeds. Output results include system production statistics, production availability and deliverability, planned maintenance, resource and spare parts usage, etc. The results are available both as numerical results and playback of the model. The playback shows how the element status changes throughout the simulation.

The flow algorithm is one of the features that differentiate Miriam-Regina® from other reliability analysis programs. The main advantage of the flow algorithm is the program's ability to handle multiple and different levels of flows and record production availability for several boundary points; the quality of the flow can also be taken into account.

Miriam-Regina® is designed to be as flexible as possible, to allow the user to perform a variety of process analyses. Normally, the program is used to evaluate the operational performance of continuous process plants in terms of equipment availability, production capability and maintenance resource requirements.

2.2 Modelling features

The system to be modelled is defined as a simplified network of elements, boundary points, links and items. The simulation models can easily be made by applying a graphical and user-friendly Reliability Block Diagrams approach. As a multi-user database-supported system, it enables several concurrent tasks to be performed at the same time.

The main sophisticated features are utilised by modelling different flows of network, storage units, and advanced blaming algorithm. The use of many advanced Operation and Maintenance-related features makes it possible to build models that reflect real-world operation better than before.

Different kinds of failures can be taken into account. Items include the failure modes, and failure and repair data, as well as failure distributions. Several probability distributions can be used, depending on the nature of the failure data. Critical failures and deferred failures can also be considered individually. The user may also define several operational rules and production plans that enable more accurate modeling.

Storage units can act as buffers within the system, as they can be filled during downstream restriction of throughput or drained during upstream restriction. Storage units may effectively increase the availability of a production system, depending on their capacity and the rate of throughput.

Spare or resource requirements have a significant impact on the system's availability and economics during the life cycle. Different strategies can easily be studied.

Planned maintenance schedules can be included in the model. The user may choose which items are affected by the planned maintenance, the whole system or a chosen part of the system.

The advanced blaming function is used to identify the events that are responsible for the production loss whenever flow at a boundary point is below demand. It handles simultaneous events, redundant elements and non-critical elements. The list of identified loss contributors provides an important addition to the reliability analysis performed in Miriam-Regina®. This constitutes a vital decision basis for reliability and regularity improvements.

3. ProMax-approach

Reliability modelling and simulation using Miriam-Regina® is the essential feature of the ProMax approach. Fortum Service is using it to create customer-specific production, energy and time-based availability distribution, as well as lists of the most critical equipment and their non-availability effects. It supports a plant's life-cycle management in terms of performance and cost of production, operation and maintenance. It enables effective utilization of the historical information of MMS and expert knowledge. And it effectively supports investment decision-makers.

The main target of the ProMax approach procedure is to identify potential improvements and their economic justifications with combined analyses of accumulated experiences. Potential improvements considered with the procedure include both the content of the maintenance programme and the designed upgrading of the plant's technical concept. To ensure the desired positive impact of the ProMax approach on the plant's productivity, the concept is based on combined analyses of the plant's long-term reliability and maintenance costs. The basic ideas of the ProMax approach are illustrated in Diagram 1

.

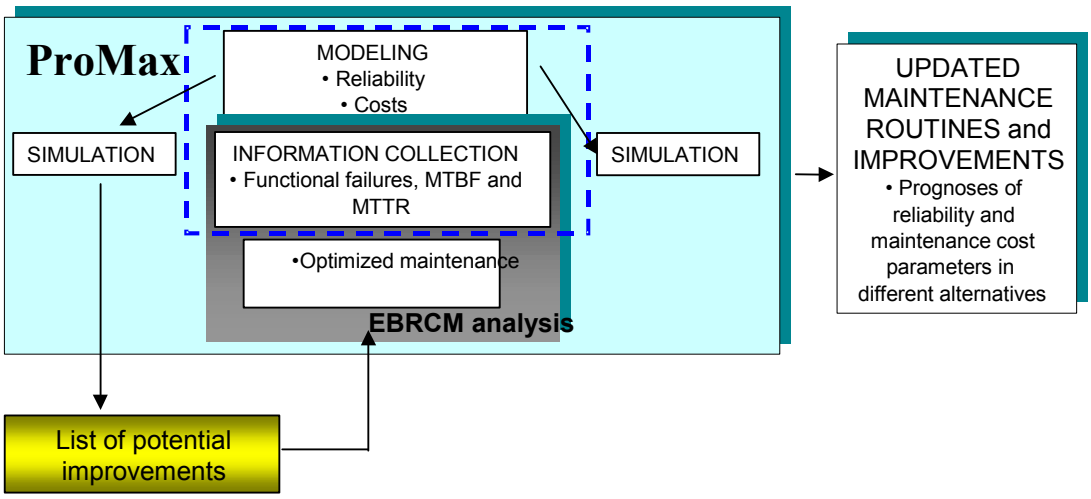

Diagram 1. ProMax approach in maintenance development.

Experience-Based Reliability-Centred Maintenance (EBRCM) is used for maintenance optimisation. The possibility of economic calculation is used to support the balancing of the maintenance programme. The method and the tool developed by Fortum Service Ltd. is a combination of a maintenance-based economic risk analysis and the useful features of a Reliability-Centred Maintenance (RCM) process.

The effects of the improvements to the optimized maintenance can easily be calculated by re-runs of the simulation.

3.1 Applying ProMax

The majority of the information used in the ProMax approach is based on Fortum's own long-term O&M experiences from different power plants. The maintenance templates drawn up by Fortum's O&M specialists for power plant equipment are often utilized. In case Fortum's experiences are not relevant, the data can be supplemented with EPC's and OEM's data. However, experience has shown that this may be difficult at times, if the suppliers have not been contractually obliged to provide this data.

Long-term maintenance costs are generated from the annual man-hours and cost, and spares cost, of preventive and corrective maintenance, which gives a cost model.

Reliability modelling needs several parameters concerning planned O&M practices. Input data include capacities, failure and repair data for each process stage component, and information on supplies of utilities and resources, maintenance schedules and system operating rules. The most essential points are related to failure data and distribution, such as MTBF (Mean Time Between Failure) and MTTR (Mean Time To Repair).

Special Fortum in-house calculation software, REPA, is used for producing failure data. The REPA software enables collectively taking into account the failure data of both the entire equipment population and of each individual piece of equipment, which makes it possible to consider prognoses in the model, including the different modes of operation of the plants and other individual features of the equipment.

The results from the tools are combined with economic studies supporting the O&M contract in the power plant’s investment phase. A huge variety of estimations can easily be simulated and calculated. In many cases the results are availability distributions, durations of disturbances or partial loads, and required amounts of compensation. Special attention is devoted to the effects of the various maintenance and spare parts policies and critical systems for production output.

3.1.1 ProMax in an investment project

The ProMax simulation is used during an investment project to produce estimations of plant productiveness. The estimations may contain figures like availability and shutdown distributions for the plant’s life cycle. The EBRCM-based ProMax approach in investment projects is illustrated in Diagram 2.

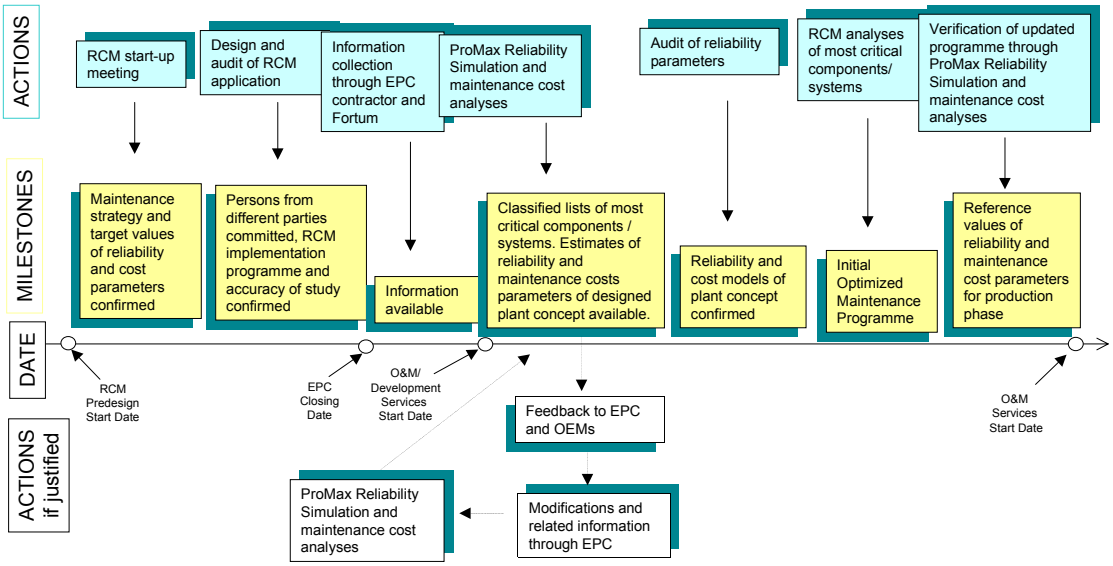

Diagram 2. EBRCM-based ProMax in investment projects.

The Miriam-Regina® simulation is also used, for example, to identify the most critical components and systems to be submitted to more detailed EBRCM analyses. This ensures that the focus of the initial Optimized Maintenance Programme is on those components and systems that have a major impact on the plant's economy and risk management. The outcome of the procedure is not limited to the initial Optimized Maintenance Programme; it also gives reference values of reliability and cost parameters to be traced during a production phase.

3.1.2 ProMax in production phase

In the production phase the use of cumulative experiences from daily operation of various plants is ensured through periodical maintenance audits performed by qualified and experienced maintenance and reliability engineers. The achieved experience, reliability and maintenance cost models, together with the related parameters, are updated and new values are compared with the reference ones. A detailed EBRCM analysis is carried out whenever the comparison suggests a significant deviation has occurred. The EBRCM-based ProMax approach in the production phase is illustrated in Diagram 3.

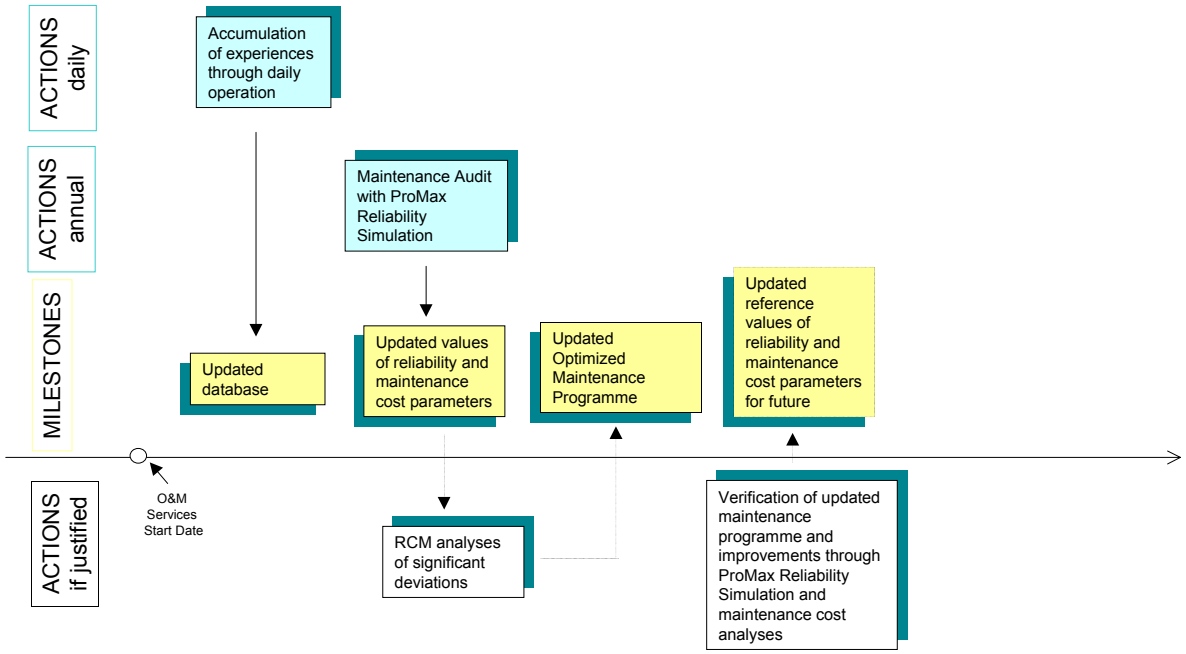

Diagram 3. EBRCM-based ProMax in the production phase.

The results of the maintenance audits are used to control preventive maintenance and condition monitoring programmes, as well as to identify targets for upgrading maintenance. Generally, the same approach can be used to indicate the effect of any designed modification or improvement on the maintenance cost and reliability parameters of the plant.

3.2 Case plant

The following selected case applying the ProMax approach was used in the early phase of a power plant investment project. The target of the case was to estimate the availability distributions and unplanned shutdowns in order to enhance risk management in the O&M tender phase.

The availability model was made for the Miriam-Regina® reliability modelling and simulation program. In order to model the plant for availability estimation, the plant was broken down into components and systems. The main principle was that the systems having an effect on the capacity of the plant were taken into account.

The planned production process, operation principles and maintenance practices were implemented into the model and simulation parameters - during the detailed design phase, the model can easily be updated with detailed design solutions according to the ProMax approach.

O&M cost calculations were combined with the tender process.

The failure data used in the case was a combination of data from Fortum's own sources and from the literature; plant-specific failure data from comparable plants was also used in the process of reliability simulation.

The main result from that ProMax simulation case, the annual availability distribution, is presented in Figure 1.

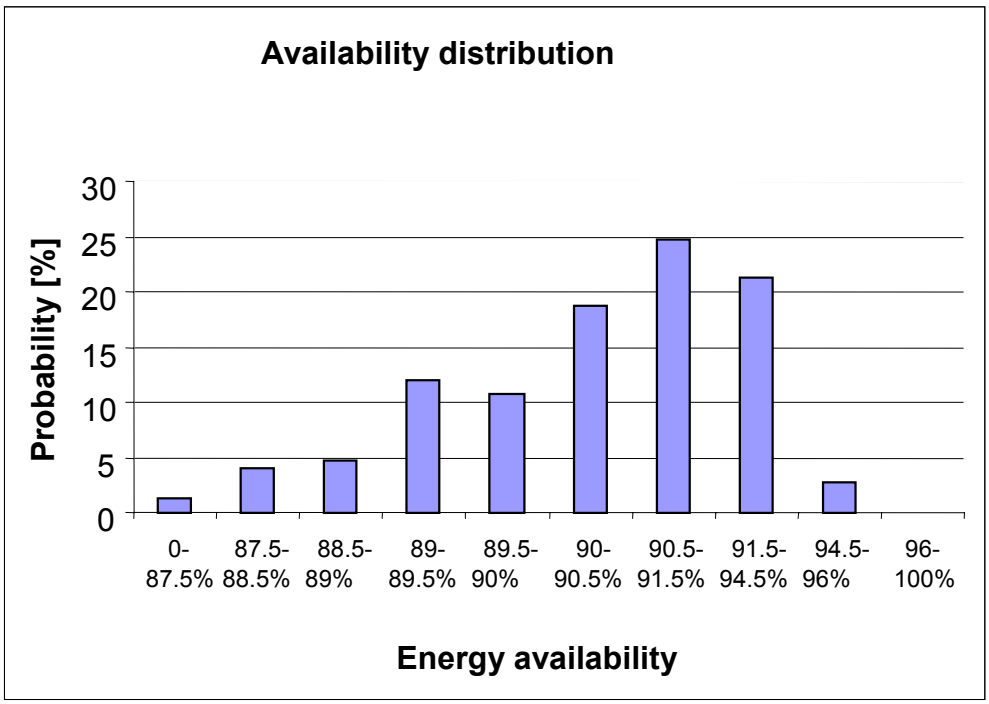

Figure 1. Example of an availability distribution for steam production.

The annual shutdown distribution based on a Miriam-Regina® simulation is presented in Figure 2.

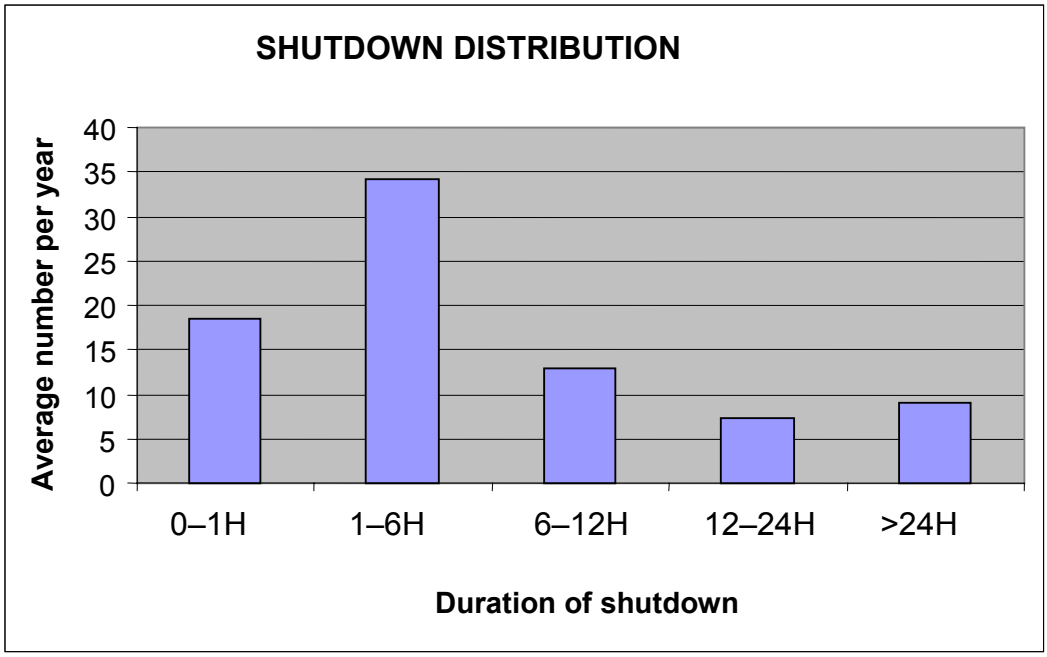

Figure 2. Annual shutdown distribution.

The simulation results revealed the major availability risks and their sizes at the designed plant under review, the critical areas in terms of availability, and the differences caused by the differing modes of operation and the individual features of the equipment with regard to reliability.
The results were used to exchange risk management in the process of identifying the availability-based bonus penalties. Several design changes and their effects were studied by simulating re-runs.

4. Summary

This paper described the main features of the stochastic reliability simulation program Miriam-Regina®, and the ProMax approach the Fortum Service Ltd. way of applying it. Stochastic reliability simulation is used to improve Asset Management and O&M procedures and risk management in the field of the Power Plant O&M offered by Fortum Service Ltd. The ProMax approach is provided by experienced maintenance and reliability engineers using sophisticated software tools to support the service.

In many cases the results from the simulation are like availability distributions, durations of disturbances or partial loads, and amount of required compensation. Special attention is also devoted to the effects of the different maintenance and spare part policies and critical systems for production output by combining the Experience-Based RCM (EBRCM) with the maintenance optimisation. The Miriam-Regina® simulation results will be backed up with the experience of the

plant personnel. The O&M operator will benefit from reduced contractual risks by using the ProMax approach.

Additional simulation results will be run in order to support the plant manager's analytical decision-making for the future.

Remote support and diagnostics – Benefits, experiences and new tools

Tuula Ruokonen, Sakari Kuismanen & Ilkka Salmensaari
Fortum Service Oy
Espoo, Finland

Abstract

Remote support is nowadays one of the services to facilitate efficient co-operation between plant personnel and special experts. By efficient co-operation any problem areas can quickly be identified and solved as well as plant operations developed. A systematic remote performance and condition monitoring program is a valuable tool that can help the plant owners and operators meet their major objectives, i.e. high availability and efficiency with optimised operation and maintenance costs.

The use of performance and condition monitoring brings total cost savings by improved machinery reliability and operation. Condition monitoring information is used to focus the maintenance to the right components at the correct time, thus reducing the risk of additional damage. The remote support makes early detection of incipient failures possible and provides decision-making support at short notice. Combination of the local site knowledge with technical and expert support ensures that the right conclusions are drawn from all the available data, and that this is done in a well-planned and cost-effective way.

Key elements of remote support include a multidisciplinary approach to cover several areas of expertise like thermal condition monitoring, vibration diagnostics and water chemistry monitoring. A Diagnostic Engine concept is being used to enable and automate the utilisation of data in both for early fault detection and trouble-shooting in the Remote Support Centre.

1. Introduction

In most countries, the electricity market has opened or will open in the near future to free competition. New competitors have entered the market and challenged the national power utilities. Profitability is gained through high plant performance, availability and efficiency, and optimum investment and operational costs, i.e. by optimising the plant life-cycle profits. Remote support is

nowadays one of the services offered by the most advanced energy companies to facilitate efficient cooperation between plant personnel and special experts. By efficient co-operation any problem areas can quickly be identified and solved as well as plant operations developed. A systematic remote performance and condition monitoring program is a valuable tool that can help the plant owners and operators meet their major objectives, i.e. high availability and efficiency with optimised operation and maintenance costs.

The use of performance and condition monitoring is expected to bring total cost savings by improved machinery reliability and operation. Condition monitoring information is used to focus the maintenance to the right components at the correct time thus reducing the risk of additional damages. The remote support makes the early detection of incipient failures possible and provides decision-making support at short notice. Combination of the local site knowledge with technical and expert support ensures that the right conclusions are drawn from all the available data, and that this is done in a well-planned and cost-effective way.

2. Remote support

The main goal of the remote support concept is to create an efficient co-operation environment between the plant personnel and selected shared resources and special experts to solve the plant problems together. The support systems include modules at the plant site to gather the essential information, telecommunication network to transmit the data, and intelligent analysis and decision making modules to support the experts at the Performance Centre Network. The newest information and telecommunication technologies provide tools and an efficient infrastructure for this type of service. The technical basis for remote support is the use of computer networks with applications including plant models, simulators, experience data and other support systems. For troubleshooting this enables real-time co-operation based on real-time data.

The capability of incipient failure detection depends on the capability to convert the acquired data to information that is related to machinery condition. The task of the analysis systems is to utilise all the data measured at plants as efficiently as possible. That way, failures are detected in time, and at best they can be predicted.

2.1 Multidisciplinary approach

One of the most important features of the remote support service concept is that all the modules, procedures and systems are working as the entity for the common target. Additionally, the modules must be integrated to business management of the company.

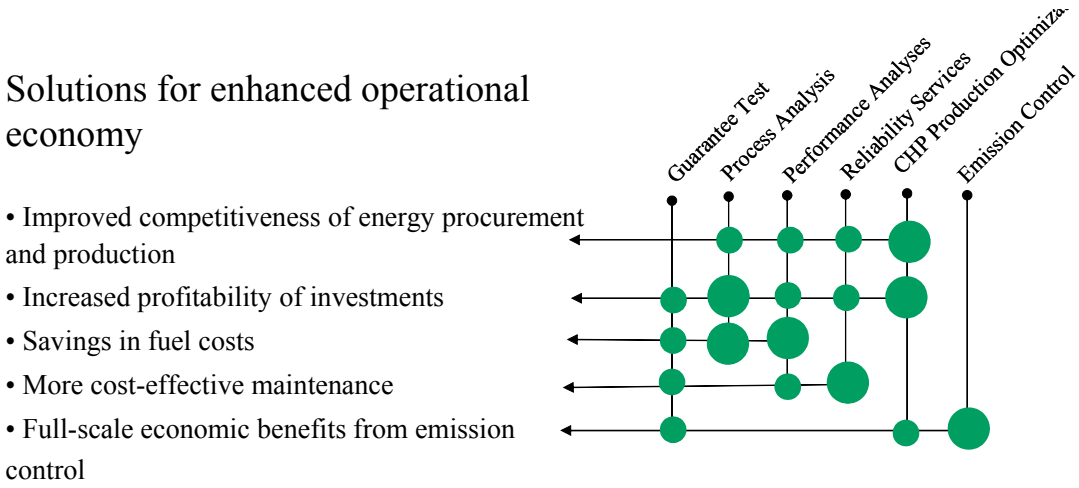

Figure 1. Multidisciplinary approach to utilise plant condition data.

2.1.1 Operational economy monitoring

Operational economy is monitored utilizing the Solvo modelling and analysis package developed by Fortum. On-line Solvo is used to calculate thermal efficiencies etc. and off-line version to simulate different operational situations. Solvo calculates and monitors also individual component performance indicators, such as compressor isentropic efficiency and turbine flow constants. The data also is transmitted to the Performance Centre and analysed periodically by comparing it to the history data and also to the results from other similar type of power plants.

Solvo is a versatile simulation software package for steady state simulation of any kind of power plant processes and main pulp and paper processes. Solvo calculations are based on computational modules' mass and energy balances and specific equations, which describe devices' functions and operations.

In the on-line applications, Solvo works as a tool for an operational economy monitoring and condition monitoring while producing real efficiency values and simulated values. Simulated values correct the real values for standard conditions (ISO-condition). That enables different components real condition monitoring without effect of ambient conditions.

Solvo enables different components to be divided into blocks. The performance of the different parts of boiler, such as evaporator, superheater or economiser, can be monitored individually using this block calculation feature.

2.1.2 Vibration monitoring of rotating machinery

Vibration levels and spectra are measured at site either using a portable or a fixed measurement system. The data is transmitted to the Performance Centre where

the experts analyse the data by using analysis and decision support systems. For fixed measurement systems even continuous monitoring at the Centre is possible. Usually a periodic analysis is done and a report with suggested actions is given to the plant personnel.

2.1.3 Water chemistry monitoring

The quality of water chemistry is analysed based on the relevant plant measurements. The data is monitored by the analysis system at site and the expert at the Performance Centre. If abnormal results appear, the support system suggests corrective actions, and the expert checks and confirms the results.

All the analysis tasks above are crucial in ensuring the best possible performance of the power plant. For analysing them, special expertise or systems are needed. These remote monitoring services can be performed as continuous monitoring or periodic check-ups. The most successful service is not only technical solutions and systems, but real team work between the plant personnel and the experts utilizing both side's know-how and experience.

All service packages include also inspection planning, special measurements at the plant site for determining the "finger prints", performance audits, measurement and analysis training, seminars or problem classes with colleagues from other plants, and trouble shooting in emergency situations.

History information, e.g. operational and maintenance history and reports from the previous analyses, is essential for the experts to draw conclusions. Data bases containing information on similar equipment or incidents at other power plants are also continuously updated to help the experts in their decision making. These data bases can also be used by the plant personnel through Fortum's internal intranet.

3. Diagnostic engine concept

The role for the Diagnostic Applications and Knowledge Base Applications is to automate part of the routine monitoring tasks and to filter data for early fault detection. The tools may include computing applications that combine and process data, rule-based reasoning and helping systems to support troubleshooting.

The effectiveness of incipient failure detection techniques depends on how well they can convert the mass of acquired data to useful information that relates to machinery performance and gives insights into it. The ability to effectively utilise all the acquired data from plants is a key feature of the analysis systems. This

ensures early fault detection and it is preferred to have this kind of diagnostic application tool in Support Centre.

Early fault detection agents can be built by application engineers by defining tests to be carried out as well as timing, warning and alarm limits related to the tests. The Diagnostic Engine carries out routine tasks automatically, giving human experts more time to concentrate on the most challenging analysis tasks.

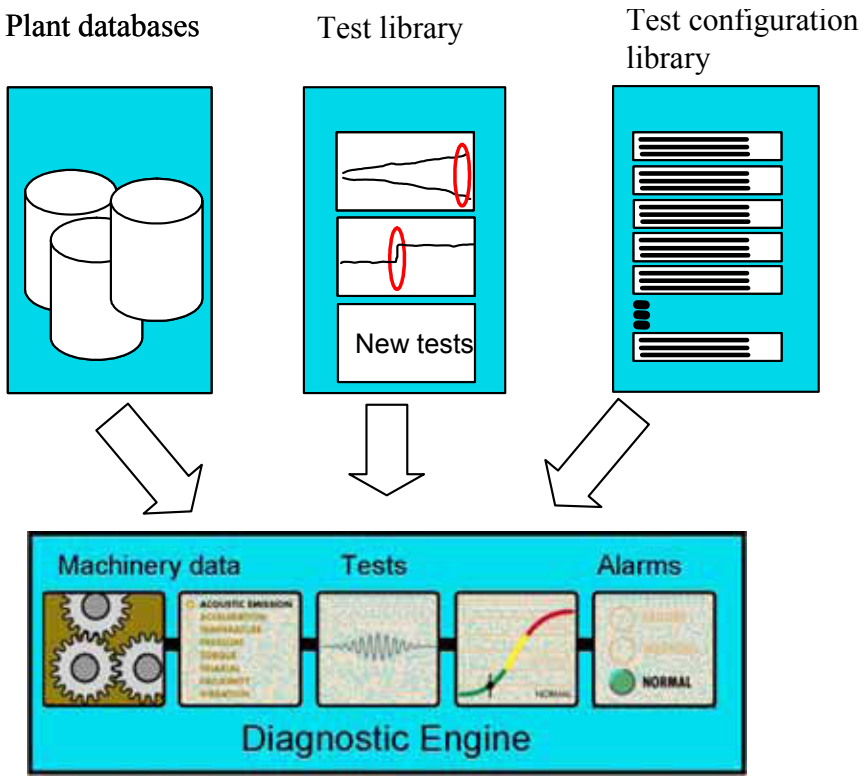

Figure 2. The Diagnostic Engine concept for automating failure detection.

4. Performance monitoring cases

4.1 Gas turbine blade failure

A step change took place in gas turbine vibration readings. The change was small, the vibration amplitude was small even after the change, which meant that there was no alarms at site.

The change was captured in the regular check-ups, which were part of the vibration monitoring support agreement with the Performance Centre. It was found that the step change was seen in most of the vibration readings. The amplitude change mainly in 1xN (machine rotation frequency) indicated, that the

cause was a sudden increase of unbalance. The most likely explanation for this kind of situation is a blade failure.

After this analysis by the vibration experts, the plant manager decided to run the machine down for endoscopic inspection, and the endoscopic inspection revealed a blade failure. This way any further damage of the gas turbine was avoided, for the risk of major breakdown is high, when running with a damaged machine. Furthermore, the material experts at the Performance Centre could analyse the possible reasons for the blade failure.

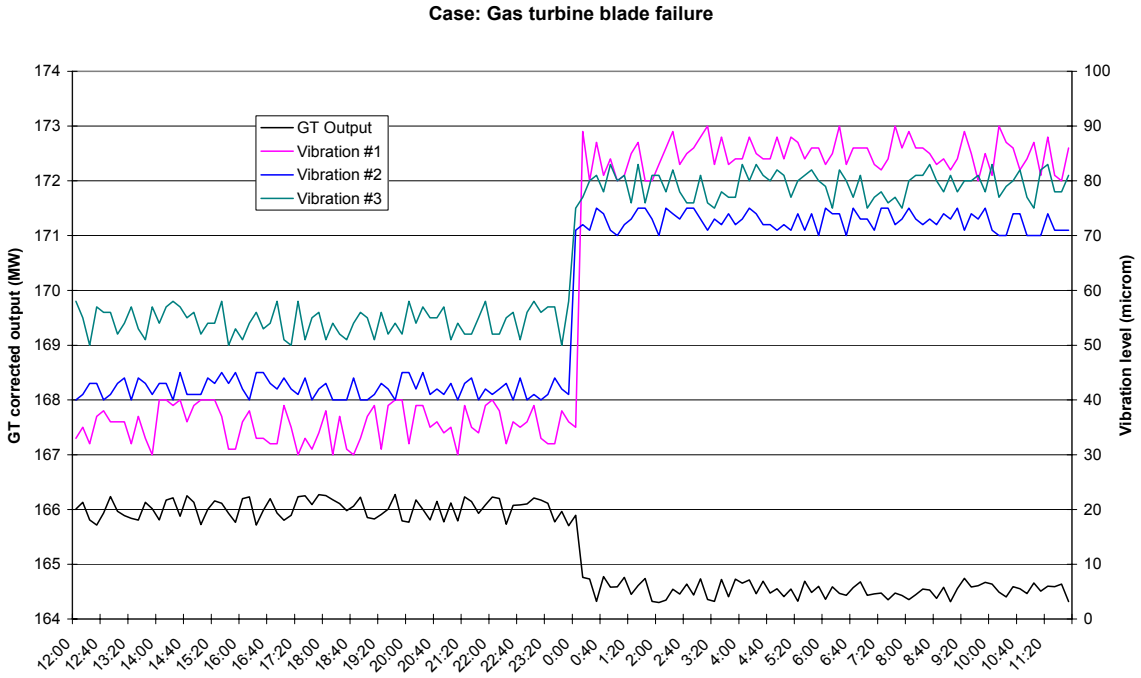

Figure 3. Simultaneous step-changes in gas-turbine vibration and performance data.

4.2 Boiler leak detection

Continuous monitoring revealed gradually a increasing difference in the plant performance of two identical units at a gas-turbine plant. Both plant and boiler efficiencies showed that unit 2 efficiency is decreasing compared to unit 1. The calculations with the thermal model showed clearly performance degradation for the unit 2.

In addition to the regular upper-level measurements and their differences, the sub-processes and their measurements were monitored with the Diagnostic Engine at the Performance Centre. E.g. the low-pressure circuit measurements from feed-water and steam flow rates and the difference between those parameters were monitored for all units. Normal difference between those parameters is about 0.2 kg/s due to blow-down and uncertainty of steam mass

flow measurement. The difference was clearly increasing due to boiler tube leak. Although the difference increased from 0.2 kg/s to over 1.5 kg/s, this plant consists of four similar units and thus the total make-up water consumption stayed within its normal variation. Thus it was very difficult for the plant operators to notice the change, or locate the failure.

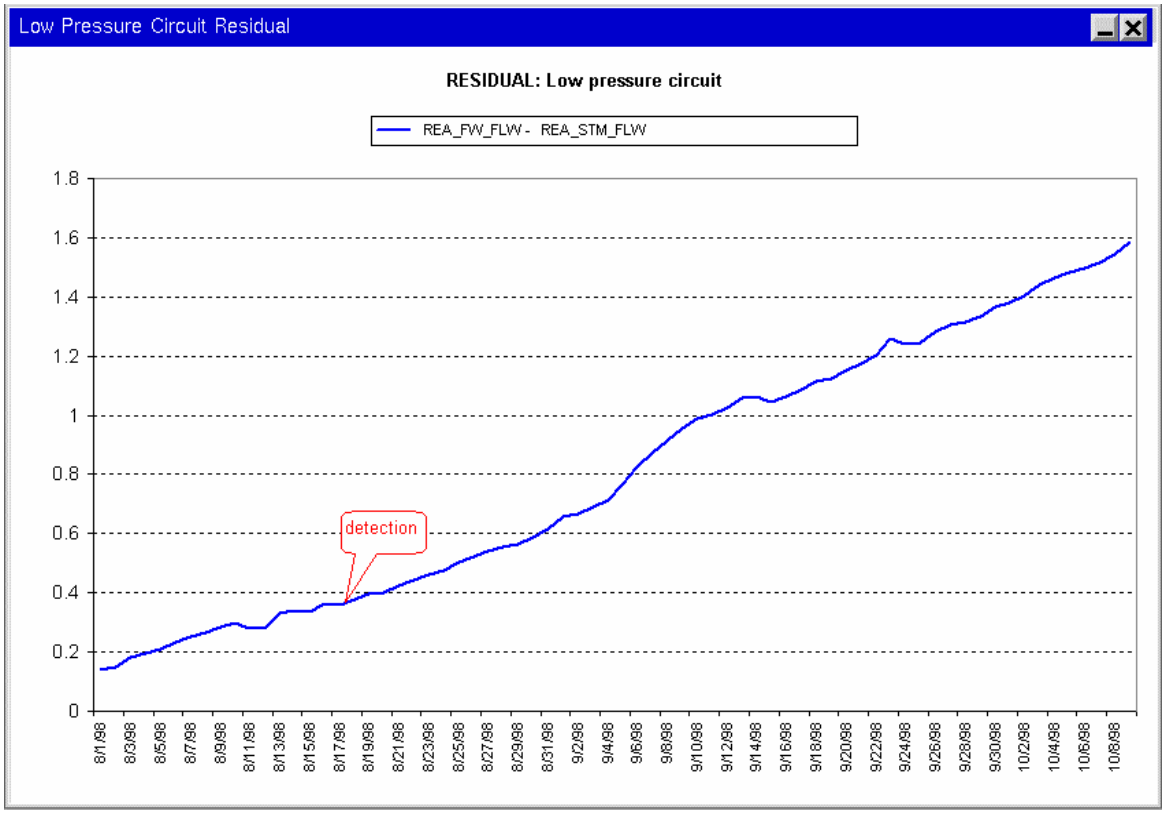

Figure 4. Boiler leak detection.

Naturally the boiler leak was detected faster and easier from the low-pressure circuit difference than from the plant or boiler efficiencies, for it revealed the original failure reason and location. In this case, the boiler leak could be detected from the low-pressure circuit as early as two weeks before the changes could be observed from the plant or boiler efficiency figures. In addition to giving the plant personnel knowledge of the real condition of the boiler, this method gives them more time to plan and prepare for the needed actions to repair the failure situation.

With these model-based methods, failures can even be localised simultaneously as they are detected. In some cases, the failures can be predicted utilising the sub-models and lower-level measurements, before their symptoms can even be detected in the upper-level measurements.

Materials for ultrasupercritical coal-fired power plant boilers

R. Viswanathan, EPRI, Palo Alto, USA
J. F. Henry, Alstom, Chattanooga, USA
J. Tanzosh, B&W, Barberton, USA
G. Stanko & Foster Wheeler, Livingston, USA
J. Shingledecker, ORNL, Oak Ridge, USA
B. Vitalis, Riley, Worcester, USA

Abstract

The U.S. Department of Energy (DOE) and the Ohio Coal Development Office (OCDO) have recently initiated a project aimed at identifying, evaluating, and qualifying the materials needed for the construction of the critical components of coal-fired boilers capable of operating at much higher efficiencies than current generation of supercritical plants. This increased efficiency is expected to be achieved principally through the use of ultrasupercritical steam conditions (USC). The project goal initially was to assess/develop materials technology that will enable achieving turbine throttle steam conditions of 760°C (1400°F)/35MPa (5000 psi), although this goal for the main steam temperature had to be revised down to 732^{o}C (1350^{o}F), based on a preliminary assessment of material capabilities. The project is intended to build further upon the alloy development and evaluation programs that have been carried out in Europe and Japan. Those programs have identified ferritic steels capable of meeting the strength requirements of USC plants up to approximately 620°C (1150°F) and nickel-based alloys suitable up to 700°C (1300°F). In this project, the maximum temperature capabilities of these and other available high-temperature alloys are being assessed to provide a basis for materials selection and application under a range of conditions prevailing in the boiler. This paper provides a status report on the progress to date achieved in this project.

1. Introduction and background

1.1 Project objectives

The principal objective of this project is to develop materials technology for use in ultrasupercritical (USC) plant boilers capable of operating with 760F (1400°F)/ 38.5 MPa (5500 psi) steam.

In the 21st century, the world faces the critical challenge of providing abundant, cheap electricity to meet the needs of a growing global population, while at the same time preserving environmental values. Most studies of this issue conclude that a robust portfolio of generation technologies and fuels should be developed to assure that the United States will have adequate electricity supplies in a variety of possible future scenarios.

The use of coal for electricity generation poses a unique set of challenges. On the one hand, coal is plentiful and available at low cost in much of the world, notably in the US, China, and India. Countries with large coal reserves will want to develop them to foster economic growth and energy security. On the other hand, traditional methods of coal combustion emit pollutants and CO_2 at high levels relative to other generation options. Maintaining coal as a generation option will require methods for addressing these environmental issues.

This project, through a government/industry consortium, is undertaking a five-year effort to evaluate and develop materials that allow the use of advanced steam cycles in coal-based power plants. These advanced cycles, with steam temperatures up to 732°C (1350°F) will increase the efficiency of coal-fired boilers and reduce emissions substantially. In addition to a reduction in all fuel related emissions, there are additional benefits to higher efficiency that favorably impact carbon management. Studies have shown that the unit could easily and economically (assuming inexpensive oxygen) be designed to allow startup with air but operate with oxygen and recirculated flue gas blend (to replace the nitrogen). This so-called oxy-fuel combustion option produces a concentrated stream of carbon dioxide which is sequestration-ready. It also requires little additional equipment and may actually eliminate some of the currently required air quality control equipment depending on the purity requirements for sequestration. Even if amine scrubbing or other carbon- dioxide removal technologies are used, the size and cost of the device would be significantly reduced by the lower gas flow resulting from the higher plant efficiency. The USC technology is thus completely compatible with the goals of achieving near zero emissions in future energy systems.

At the current time, the lead in the manufacture of the key materials for USC plants clearly lies in Japan and Europe. More than a dozen plants operating at steam conditions close to 593°C (1100°F)/27 MPa (4000 psi) are in operation worldwide and plants operating at 620°C (1150°F) is a near-term possibility. Research, development and demonstration programs are underway in Europe and Japan aimed at materials capable of withstanding steam conditions up to 650°C (1200°F) and over the next decade to 700°C (1300°F). It is imperative that the domestic boiler manufacturers in the US match their capabilities in this advanced technology area. This is one of the objectives of the US DOE/OCDO project. Furthermore, materials technology is generic in nature and cuts across many

energy systems operating at high-temperature. Consequently, materials technology developments for high temperature applications are expected to be of enduring value. In the near term, materials developed for USC plants can be confidently used for retrofit application in currently operating plants to increase their reliability.

1.2 Comparison of US and European approaches

Under a project known as "Thermie" (or AD 700) aimed at 700°C (1300°F)/ 4500psi steam conditions, research work has been carried out in Europe for several years. The question naturally arises, how the US project is different from the European union project. Firstly, the steam conditions chosen in the US Project are more ambitious than the EU project resulting in higher efficiency. Secondly, operating parameters and designs are different in different countries, and EU results cannot be directly translated to operating conditions in the US. While European plants generally utilize low sulfur coals, coal quality is widely variable in the US. The US program therefore, calls for evaluation of materials under several different levels of sulfur contents in the coal. Many new alloys have come into the market place since the inception of the Thermie project. These alloys will be evaluated in the US program. Lastly, results from the EU program are available only to the EU participants and not to the US domestic boiler manufacturers. Therefore, there is a need to develop indigenous capabilities in the US.

There are many differences between the U.S and European practice such as differences in fuel heating value estimations, site specific ambient conditions, fuel quality, plant design and operation that contribute to higher efficiency assessments for European plants. Specifically, there are four main areas where this study and the European approach differ. They are fuel heating value; air heater exit gas temperature, condenser pressure, and number of reheat stages. The most obvious difference is that the U.S conventionally reports heat rates and efficiencies based on the Higher Heating Value (HHV) of the fuel, whereas the European convention is to use Lower Heating Value (LHV). For instance, the Ohio coal, which is a commonly used grade of coal in the US, has a LHV that is 95.91% of the HHV so the calculation will show 1.0427 times better net plant efficiency for the LHV basis. The same power output is produced for the same coal flow even though the heating value is only 95.91% of the HHV content. As a result , the net plant efficiency can be higher by nearly 2% on a LHV basis.

In general, the European plants use lower sulfur, higher ash fusion temperature international merchant coals as compared to the U.S wider usage of higher sulfur coals such as Illinois #6 and Pittsburgh #8 (2–3.5% S). A more recent development in the U.S has been the increase in the usage of the low sulfur Powder River Basin coals. High moisture and high ash contents in US coals

reduce boiler efficiency. Concern over corrosion in the cold end of the air heater and downstream ductwork sets a minimum on the permissible boiler outlet temperature when higher-sulfur coals are used, and thereby reduces the achievable boiler efficiency. Flue gas temperatures typically are about 133^{o}C (272^{o}F) in the US as opposed to a value of 105^{o}C (221^{o}F) in Europe. This gives the European plants an efficiency advantage of 0.8% compared to a US Plant burning Ohio coal.

The condenser operating pressure is another major difference between the United States and Europe. Colder latitudes and the availability of colder seawater cooling permit the condenser back pressure to be lower and the turbine expansion line end point (ELEP) enthalpy is lower so more expansion work is available from the steam turbine. An improvement of condenser pressure from 67.7 mBar (2.0" Hg) typical of US plants to 21 mBar (0.62" Hg) typical of European plants. European plant can improve plant efficiency by about 0.7% for the cycle under this study.

The availability of once-through cooling water also has a beneficial effect on heat rate by eliminating the auxiliary power requirements for pumping cooling water to the towers. This can typically reduce heat rate by about 0.6%. The overall auxiliary power consumption in US plants is nearly 6% of the gross power generated. This number is lower in European plants, once again contributing to higher plant efficiency.

Changing the turbine cycle to double reheat from a single reheat configuration would improve the LHV efficiency by about 1.7%. Using double reheat is relatively expensive in that the turbine casing configuration is more complicated and the steam leads increase by two more, one lead is required to be high temperature nickel-base alloy.

In any case, these differences in power plant practice described above are the major issues in comparing the efficiency predictions between the European Union Thermie Project and this United States Department of Energy program. They can account for 4 to 5% difference in the % point values of efficiency or 8 to 10% difference in reported heat rates. These factors should be kept in mind in comparing the goals of the US project with those of the Thermie project.

1.3 Project structure

The USDOE/OCDO project is based on an R&D plan developed by the Electric Power Research Institute (EPRI) that supplements the recommendations of several Department of Energy (DOE) workshops on the subject of advanced materials, and DOE's Vision 21. The project is of five years duration, and runs from 6/1/2001 to 12/31/2006. The total project funding is, approximately $20 million with the US DOE providing nearly $15 million, the OCDO providing $2

million and the rest being secured in the form of cost sharing by the participating organizations.

In view of the variety of skills and expertise required for the successful completion of the proposed work, a consortium that includes EPRI and the major domestic boiler manufacturers (Alstom Power, McDermott Technology, Babcock & Wilcox, Riley Power, and Foster Wheeler Development Corporation) has been developed. Energy Industries of Ohio (EIO) provides overall Program Management and fosters participation by other Ohio entities such as the Edison Welding Institute, University of Akron and University of Cincinnati. Oak Ridge National Laboratory has been separately funded by the DOE to provide augmenting efforts to the project. and works closely with the project team. Co-operation of utility stakeholders, alloy vendors and other National Labs has also been secured via advisory roles for their staff.

2. Project tasks

The project objective is expected to be achieved through 8 tasks as listed below:

Task 1. Conceptual Design and Economic Analysis
Task 2. Mechanical Properties of Advanced Alloys
Task 3. Oxidation Resistance
Task 4. Fireside Corrosion Resistance
Task 5. Welding Review
Task 6. Fabricability
Task 7: Coatings
Task 8: Design Data and Rules.

3. Project results

3.1 Preliminary design and economic studies

Conceptual design and economic studies have been completed. Alloy selection, component sizing, delineation of temperature/stress profiles have been completed. Economic viability has been shown. Material procurement has been completed.

Based on creep strength and allowable stress considerations, Haynes 230, Inco 740, CCA 617, HR 6W, Super 304 H. and SAVE 12 alloys have been selected for heavy section and tubular applications. Alloys T 92 and T 23 will be considered for application in waterwall tubing. The composition and intended application of the alloys is shown in Table1.

Table 1. Candidate alloys for USC boiler.

Alloy	**Nominal Composition**	**Developer**	**Application**
Haynes 230	57Ni-22Cr-14W-2Mo-La	Haynes	P, SH/RH Tubes
INCO 740	50Ni-25Cr-20Co-2Ti-2Nb-V-Al	Special Metals	P, SH/RH Tubes
CCA 617	55Ni-22Cr-.3W-8Mo-11Co-Al	VDM	P, SH/RH Tubes
HR6W	43Ni-23Cr-6W-Nb-Ti-B	Sumitomo	SH/RH Tubes
Super 304H	18Cr-8Ni-W-Nb-N	Sumitomo	SH/RH Tubes
Save 12	12Cr-W-Co-V-Nb-N	Sumitomo	P
T92	9Cr-2W-Mo-V-Nb-N	Nippon Steel	WW Tubes
T23	2-1/4Cr-1.5W-V	Sumitomo	WW Tubes
P - pipe			

The feasibility of designing an ultrasupercritical 750 MW boiler operating at 732^{o}C (1350^{o}F)/35 MPa (5000 psi) HP turbine throttle steam conditions with existing material technology is encouraging. The initial goal of 760°C (1400°F) 38.5 MPa (5000 psi) for the main steam had to be compromised in view of the need for large thicknesses for the tubing and piping systems, which would disallow cyclic operation. Reheat temperature could however be maintained at 760^{o}C (1400^{o}F), since reheat pressure is only 7.8 MPa (1128 psi). This design will increase the plant efficiency from an average of 37% (HHV) (current domestic sub-critical fleet) to approximately 46% (HHV) see Table 2. For a double reheat configuration the efficiency will reach 48%. Expressed in terms of European parameters, this would correspond to nearly 52% LHV. This efficiency increase from 37 to 48% HHV is expected to save nearly $12 million annually in fuel costs or $240 million over a 20-year plant life for a 750MW plant operating at 60% capacity factor at a coal cost of $1.5/Mbtu. The CO_2 and other fuel-related emissions will be reduced from 0.85 to 0.67tonnes/MWh, a reduction of nearly 22% as shown in Figure 1. This amounts to an annual reduction of nearly 700,000 tons of CO_2, which is very significant in view of worldwide agreements to reduce CO_2 emissions by year 2010. If carbon taxes were imposed on a pulverized coal power plant, the USC plants will become even more attractive, economically. Throttle temperature increase has been concluded to be much more advantageous than throttle pressure increase for improvement of efficiency at minimal cost impact.

Based on a 20-year breakeven consideration, assumed capacity factor of, 80% and coal cost of $1.42/GJ ($1.50/MBtu). It is estimated that an ultrasupercritical plant can be cost competitive even if the total plant capital cost is 12 to 15% more than a comparable scale facility built using conventional subcritical boiler and cycle designs, due to the fuel cost savings over the 20-year period, as shown in Figure 2, balance- of- plant costs are expected to be 13 to 16% lower than those for existing boiler and cycle designs due to smaller coal handling and pollution control systems, resulting from the improved plant efficiencies. As a result of these reductions in fuel and balance-of-plant (BOP) costs, boiler and

steam turbine capital costs can be permitted to be higher compared to subcritical plant by 40 to 50%. It should be noted that the above economic trade-off study does not take into account benefits resulting from reduction of emissions due to increased efficiency. If a potential "carbon tax" were also taken into account, the advantage of the USC plant becomes even more substantial. For an assumed tax of $7 per ton of CO_2 emitted, the total annualized savings in going from a 37% efficiency subcritical plant to a 48% efficiency USC plant is estimated to be $4.9 million. The allowable capital cost for a USC plant in this case is considerably higher than when the carbon tax is not taken into account.

Table 2. Estimated plant efficiencies for various steam cycles (P. Weitzel, B&W & M. Palkes, Alstom).

Description	Cycle	Reported at European Location (LHV/HHV)	Converted to U.S. Practice[2]
Subcritical	16.8 MPa/538°C/538°C		37
Supercritical	24.5 MPa/565°C/565°C/565°C[1]		
ELSAM (Nordjylland 3)	28.9 MPa/580°C/580°C/580°C	47/44	40.9
State of the Art Supercritical (LEBS)	31.5 MPa/593°C/593°C/593°C[1]		42
Thermie	38 MPa/700°C/720°C/720°C	50.2/47.7	46/43
EPRI/Parson	37.8 MPa/700°C/700°C/700°C		44
DOE/OCDO USC Project	38.5 MPa/760°C/760°C 38.5 MPa/760°C/760°C/760°C		46.5 47.5–48

1. Eastern bituminous Ohio coal. Lower Heating value, LHV, boiler fuel efficiency is higher than higher heating value, HHV, boiler fuel efficiency. For example, an LHV net plant heat rate at 6205.27 Btu/kWh with the LHV net plant efficiency of 55% compares to the HHV net plant heat rate at 6494 Btu/kWh and HHV net plant efficiency of 52.55%.

2. Reported European efficiencies are generally higher compared U.S. due to differences in reporting practice (LHV vs HHV), coal quality, auxiliary power needs, condenser pressure and ambient temperature and many other variables. Numbers in this column for European project numbers are adjusted for U.S. conditions to facilitate comparison.

Based on the material specifications listed above, a material take-off was developed. To obtain the total boiler cost, current market level pricing was applied to the standard ASME materials used in the design. For the non-ASME nickel based super alloys, the vendor estimated pricing was used. The super alloy pricing is the greatest unknown because there is no way of knowing the ultimate commercial mass-produced pricing. Other unknowns are the fabrication and construction costs associated with the new super alloys. For the purposes of this study, the fabrication cost is assumed to be equal to the fabrication cost of a conventional supercritical boiler. The construction cost was based on the cost of a conventional supercritical unit increased proportionally by the weight ratio of the ultra supercritical to the conventional supercritical unit.

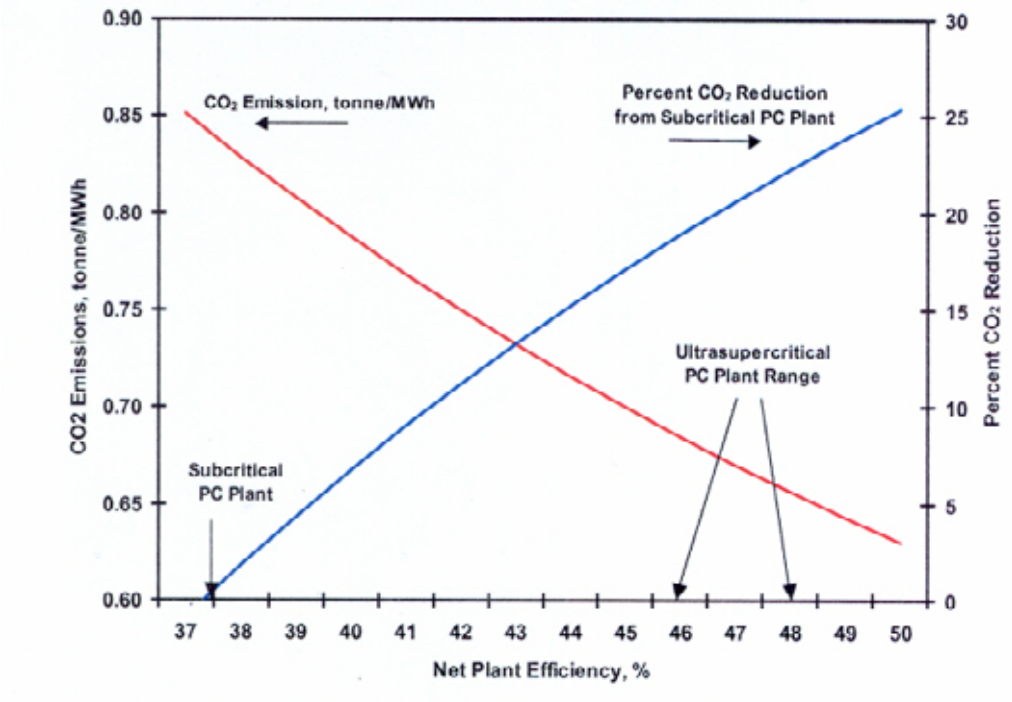

Figure 1. Carbon Dioxide Emissions vs Net Plant Efficiency (G. Booras, EPRI) CO_2 emissions from a USC plant can be reduced by 22% by increasing net plant efficiency from 37 to 47%. This amounts to a reduction of 700,000 tons of CO2 per annum (750MW plant at 60% Capacity factor, using Pittsburgh #8 coal).

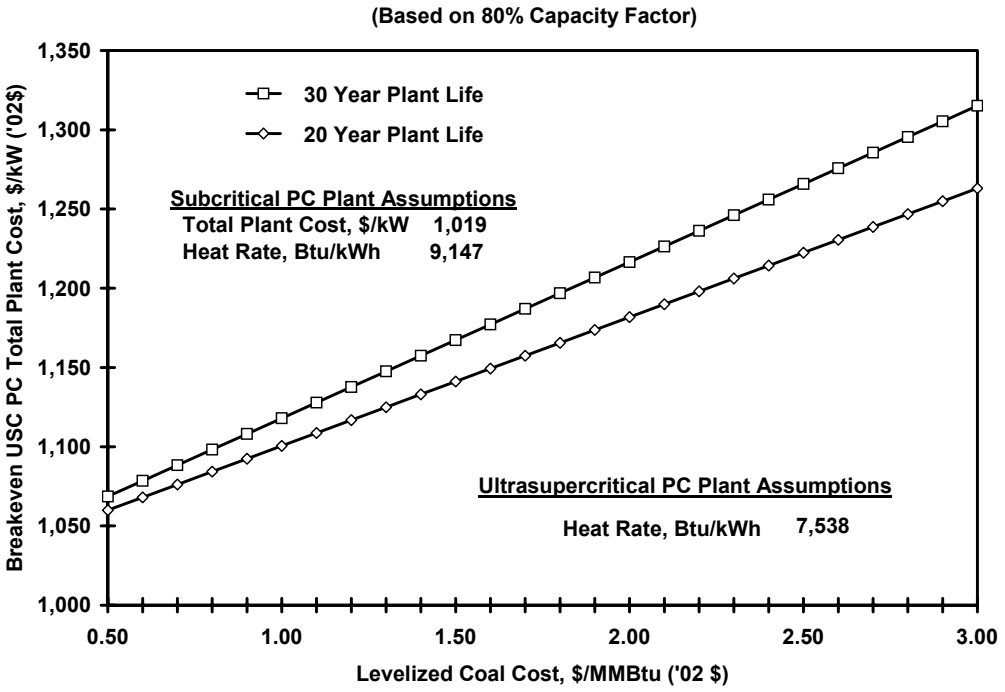

Figure 2. Breakeven total plant cost and fuel cost – 20 vs 30 year life (G. Booras, EPRI).

The material tabulation for the ultrasupercritical unit was compared to both a subcritical and conventional supercritical unit of approximately the same megawatt output. The ultrasupercritical boiler was found to have approximately 7% more suspended weight than a conventional supercritical boiler with the same plant output. This is interesting to note because the ultra supercritical boiler is actually smaller than conventional supercritical unit. The ultra supercritical unit is nearly 20% narrower than the conventional supercritical unit. Because the ultrasupercritical unit is narrower, the total header and piping weight does not increase over the conventional supercritical unit. However, there is approximately 13% increase in overall tubing weight for the ultrasupercritical unit. The cost used for the super alloy materials were $20/lb for both Haynes 230 and Inco 740.

Ultimately the ultrasupercritical design was found to have approximately a 28% increase in cost over the PC subcritical unit. As noted above, the cost comparison is based on a delivered and erected price for the boiler island only. While this analysis indicates that the percentage increase in cost over a PC subcritical unit is below the 40% value for economic viability, the assumptions stated and the preliminary nature of the evaluation must be taken into account when drawing any conclusions.

An alternative to review in light of the high cost of the superalloys would be to evaluate a design which increases throttle temperature without a major increase in throttle pressure. As mentioned above, increasing steam temperature is much more economical than raising steam pressure. Reducing throttle pressure may allow the use of much more standard austenitic materials while maintaining the plant efficiency gains of higher throttle temperature. Input and plant design studies with steam turbine manufacturers is needed.

3.2 Mechanical properties

Six alloys were identified by the consortium for extensive mechanical property analysis. The alloys include: one ferritic material (SAVE12), two austenitic alloys (Super 304H and HR6W), and three Ni-based alloys (Haynes 230, CCA617, and Inco 740). The austenitic materials are candidates for boiler tubing while the other materials are being tested in both tube form and heavy wall thick sections for headers and piping. Creep rupture tests have been completed, up to 5000 hours on all the materials. The temperature capabilities for a rupture criterion of 100MPa /10^5 hours for several alloys is shown in Figure 3. Preliminary investigations on Inco 740 produced an optimum heat treatment for creep-rupture strength. which exceeds expectations based on prior reported data, see Figure 4. Alloy CCA 617 exhibited rupture strengths well in excess of those for conventional Inco 617.

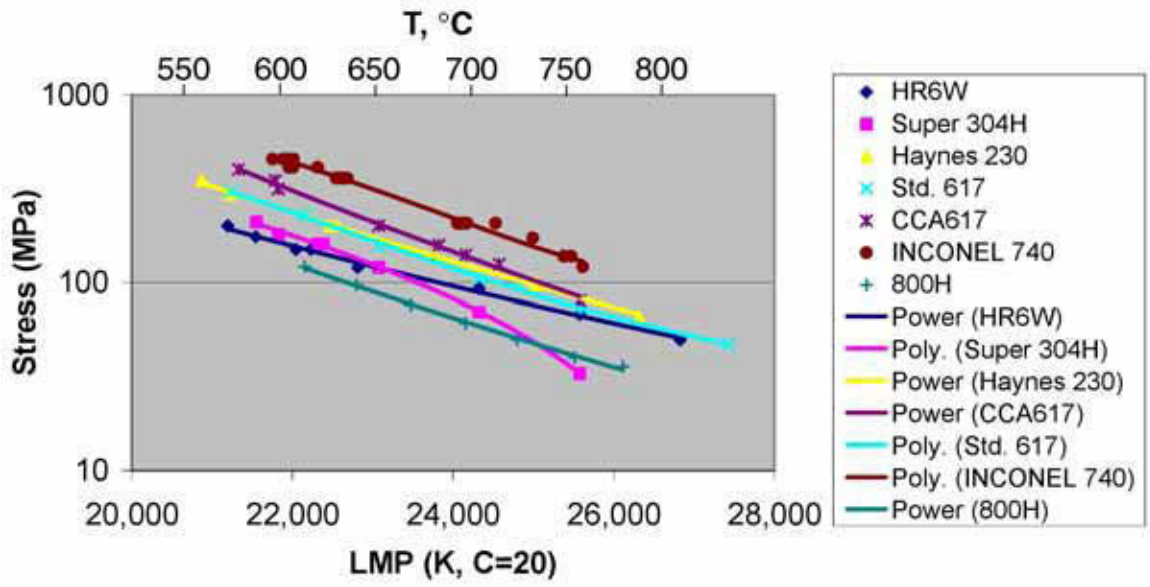

Figure 3. Temperature limits for superalloys for rupture in 10^5 hr. at 100 MPa Stress (J. Shingledecker & R.W. Swindeman, ORNL).

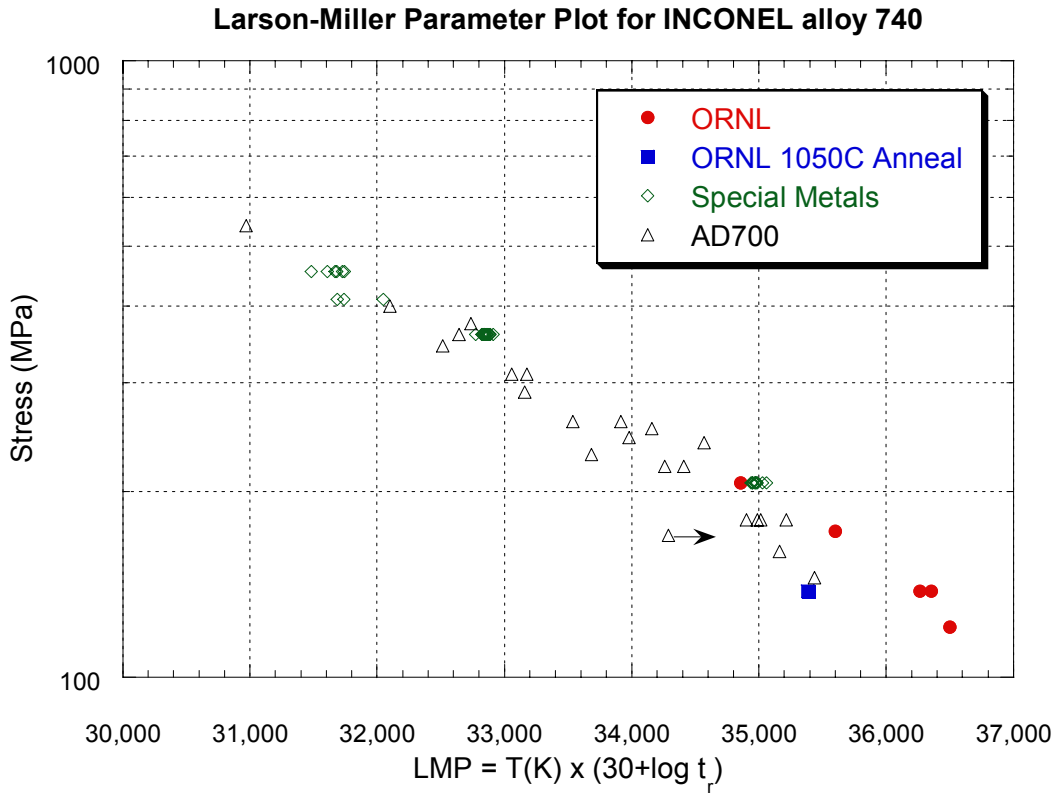

Figure 4. Larson-Miller parameter plot for inconel alloy 740 (J. Shingledecker & R.W. Swindeman, ORNL).

Future mechanical property work includes: long-term creep tests on all the materials, notched bar creep tests, creep-fatigue testing, the testing of weldments and dissimilar metal welds, the mechanical characterization of thick section materials (including 3" thick welded plates), cold work limits (U-bend tubes under pressure), and model validation tests (creep testing on deeply notched thick sections). A new 9% Cr alloy developed by NIMS (National Institute of Materials Science) of Japan is alleged to have rupture life that is two orders of magnitude higher compared to the strongest known 9% Cr alloy T 92, see Figure 5. Samples of this alloy have been procured and are under evaluation.

3.3 Steamside oxidation tests

Steamside oxidation tests show that oxides of T92 and T122 apparently undergo oxide breakaway behavior in < 500 hours to form iron-rich oxides. Tests at 700°C (1300°F)/1.75MPa (250psi) steam show that results are in line with European data. The high-Cr alloys are found to form chromium-rich oxide scales. Less spallation of oxide scales was observed under pressurized oxidation conditions. Corrosion rate data for alloys have been established.

Steamside oxidation tests have been completed up to 4000 hours at 650°C (1200°F). It has been found that oxidation resistance is predominantly controlled by the chromium content of the alloy, with some exceptions, see Figure 6. Two alloy versions of 9%Cr steel provided by the National Institute for Materials Science (NIMS), Japan, were found to have oxidation resistance that was superior compared to the other 9 Cr alloys and comparable to high- Cr austenitic steels. Interestingly, these alloys were found to form protective chromium oxide scales on the surface, in contrast to other 9Cr alloys which typically formed iron oxide scales. The nickel-based alloys were consistently superior to all other alloys, the top of the pack being CCA 617, Haynes 263 and Inco 740. Chromized coatings on T92 performed better than Electroless Nickel or Cereblack coatings, but the chromized T92 specimens did not perform as well as austenitic alloys.

Calculated weight change derived from weight loss results compared to measured weight gain results show clear evidence of spallation of oxide in the course of the 2000 hr tests at 650°C (1200°F) in the ferritic steels T23, T91, and T92. Other ferritic steels, two of the steels supplied by NIMS and SAVE 12 were much superior. No spallation was observed in the austenitic steels and Ni-based alloys after 4000 hr. Based on the weight loss results up to 2000 hours, the oxidation rates were calculated to be parabolic at 650°C, thus rate constants could be readily calculated and compared with prior literature data. The constants calculated for T23 and T91 from the data are consistent with the predicted rate constants indicating that test results for baseline ferritic materials are in good agreement with results generated by other organizations. For the three austenitic materials (SAVE25, Inco740 and HR120) tested at two different laboratories, the

calculated rate constants were similar. An excellent correlation was obtained between the oxidation rate constant at 650°C based on weight loss and a compositional parameter consisting of Cr, C and B for the ferritic steels.

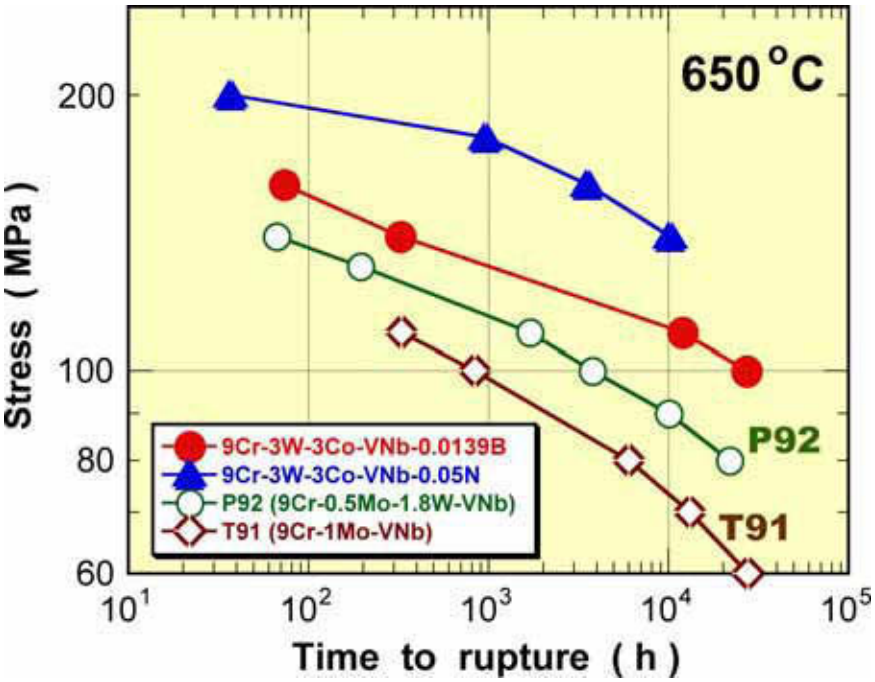

Figure 5. Present Status of Steel Development (9Cr-3W-3Co-0.2V-0.05Nb steels) (F. Abe, NRIM).

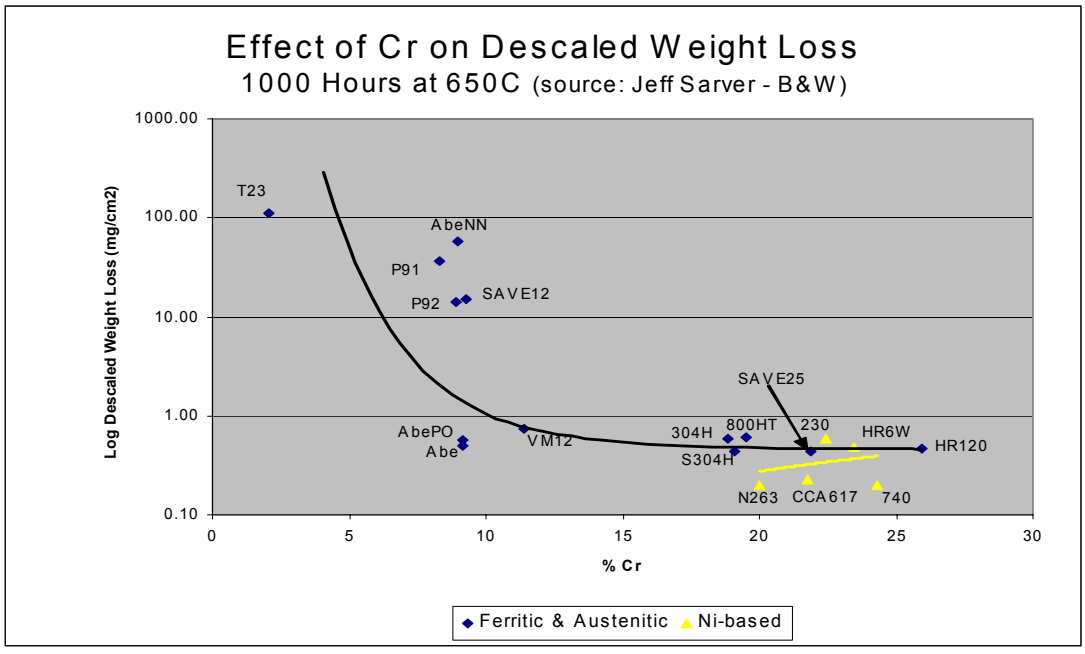

Figure 6. Weight Change Results (from steam oxidation tests at 650oC/1000 h) (Jeff Sarver, B&W).

3.4 Fireside corrosion

Test matrices and environmental conditions relevant to both superheater/reheater applications and waterwall applications have been finalized. Two USC test loops were fabricated, hydro-tested, and installed at a utility power station during a scheduled outage. Figure 7 shows one of the loops being hydro tested prior to installation in a boiler. Testing of the loops at the plant, which burns high-sulfur coal, has been initiated. Throughout the planned 18-month test of the loops, steam flow will be throttled to simulate USC boiler design operating conditions where metal surface temperatures up to 760^{o}C (1400°F) will be maintained. Operating parameters during the test will be continuously monitored using an on-line remote access computer system. During outages at the plant, the test loops will be physically examined within the boiler, diametrically measured for hot corrosion wastage, photographed and assessed for performance. Other host utility sites have been identified for air-cooled probe testing.

3.5 Weldability studies

Preliminary results indicate that submerged arc welding (SAW) a high deposition rate process favored by boilermakers for thick sections, might not be feasible for nickel-based materials. Tests on Haynes 230 and Inco 740 have been unsuccessful, and the process has been temporarily suspended, at least on these alloys. A 3 in. thick plate of Haynes 230 was successfully welded using pulsed Gas Metal Arc Welding (GMAW) technique as shown in Figure 8.

An orbital Gas-Tungsten Arc Welding (GTAW) process has been qualified for Super 304H and test specimens are being fabricated. Attempts to weld tubing using an automatic GMAW process were unsuccessful. Switching to type 347 filler produced acceptable welds. An orbital GTAW process was qualified for tubing of alloy CCA 617. SAW process was qualified for plate and test specimens are being fabricated. Attempts to perform Shielded Metal Arc Welding (SMAW) using matching filler were unsuccessful due to slag control problems with CCA 617 electrodes. On the other hand, successful SMAW Welds were achieved using conventional 617 electrodes. Weldability evaluations for HR6W and SAVE12 have not yet been started. Weld processes and filler metals have been selected. Collaboration is being pursued with the alloy vendor, Special Metals, in view of their experience in welding 1 in. thick plates of Inconel 740 using GMAW.

3.6 Fabricability studies

Experience in welding, machining, cutting, boring and grinding USC alloys Haynes 230, Inco 740, HR6W, CCA 617 and super 304 H stainless steel has been gained in the course of fabrication of two USC test loops. Protective weld

overlay claddings with alloys Inco 52, Inco 72 and Inco 622 were also successfully applied to tube sections that form the loops. Field welding of the USC materials was additionally demonstrated during installation of the test loops at the Niles plant. Controlled straining (ranging from 0 to 50%) of special tapered tube specimens was conducted to produce strained materials needed to conduct studies in characterizing the recrystallization/precipitation behavior of USC alloys. Fabrication of multiple U-bends produced from Haynes 230 and HR6W tubing (2 in. OD X 0.4 in. MW) was successfully demonstrated using production equipment. Tube U-bends with strains of 15%, 20% and 35% were produced as shown in Figure 9. Swaging trials of two of the USC alloys were also completed. Technical data on recrystallization behavior, phase precipitation and dissolution in USC alloys is being compiled to assist in the understanding and development of USC boiler fabrication procedures. A questionnaire relating to fabricability and heat treatment of USC alloys has been prepared and circulated to alloy vendors to gain from their experience with these materials.

3.7 Coatings

Several specimens with claddings, spray coatings (cold spray, High-Velocity Oxygen Fuel (HVOF)) and diffusion chromium, chromium-silicon, chromium-aluminum coatings have been prepared and subjected to steam oxidation tests in the lab. Results show that ferritic steels benefit most from coating; austenitic steels may benefit; Nickel-based alloys are not likely to need coatings at all. Process scale-up activities are being pursued. The scale-up tests for the chromizing process have been completed and the evaluation of results revealed excellent reproducibility for both types of materials, Super 304 H and T 92. Development of parameters for depositing HVOF and cold spray techniques for 50Ni/50Cr coatings is complete. Based on these results, optimal parameters have been selected and used to coat, Haynes 230 tubes. Developing plasma transferred arc parameters for deposition of 50Ni/50Cr has begun. Laser cladding parameters for depositing 50Ni/50Cr alloy are in the process of being developed.

3.8 Design approaches

A detailed review of literature pertaining to the reference stress approach has been completed and a topical report has been issued. An example problem of the reference stress concept has been applied to an ASME geometry. New cylinder design rules have been developed and submitted to the ASME design committees. These rules will remove some of the conservatism in the current design codes and therefore permit use of thinner wall materials or, alternately, permit use of materials that might otherwise not meet the allowable stress requirements.

Figure 7. Hydrotesting of Test Loops Prior to Installation in a Boiler (Walt Mohn & Denny McDonald, B&W).

Figure 8. End View of Completed 3" Thick Haynes 230 Alloy Weld (John Sanders, B&W).

Figure 9. Cold U-bending Trials (Alloy 230 results: R = 3", 5", 7-1/2" (Walt Mohn, B&W).

4. Summary

The technical and economic feasibility of designing an ultrasupercritical 750 MW boiler operating at 732/760°C (1350/1400°F) and 35 MPa (5000 psi) with existing materials technology is encouraging. This design would be capable of achieving a net plant efficiency of about 46% HHV based on US design practice. With a double-reheat configuration a plant efficiency of 48%, could be achieved. Materials needed for construction of various parts of the boiler have been identified. Studies pertaining to mechanical properties, steamside oxidation resistance, fireside corrosion resistance, weldability, fabricability and the use of coatings/claddings are being pursued. Design approaches that are less conservative and more robust are being explored, with a view to extend the range of applicability of available materials to higher temperatures/stresses.

5. Acknowledgements

The sponsorship and guidance of this work by Dr. Romanosky and Dr. Udaya Rao of NETL, and by Howard Johnson of OCDO is gratefully acknowledged. The project manager is Robert Purgert of EIO. The technical results reported are based on contributions by numerous investigators including Paul Weitzel, Mark Palkes, George Booras, Robert Swindeman, John Shingledecker, Jeff Sarver, Ian Perrin, John Sanders, Mike Borden, Walt Mohn, Steve Goodstine, John Fishburn, and many others. Their contributions are appreciated.

General References

R. Viswanathan. Supercritical Power Plants – An Overview, Proc. of International Conference on Thermal Power Generation, organized by NTPC/USAID, New Delhi, October 13–15, 2003, Vol. 2, pp 23–43. Also see POWER, April 2004 issue.

G. Booras et al. Economic Analysis of Ultrasupercritical PC Plants, Pittsburgh Coal Conference, 2003.

J. Sarver. Preliminary Results From Steam Oxidation Tests Performed On Candidate Materials for Ultra-Supercritical Boilers, EPRI International Conference on Materials and Corrosion Experience for Fossil Power Plants, Charleston, S.C., 2003.

B.K. Schimmoller. Boiler Industry: Surviving Rough Waters, Power Engineering Magazines, 2003. Citation to USC work.

DOE Launches Project to Improve Materials for use in Ultrasupercritical Coal Plants, DOE TechLine, 2003, http://www.netl.doe.gov/publications/press/2001/tl_ultrasupercritical.html.

Updated Cost and Performance Estimates for Clean Coal Technologies including CO_2 Capture – 2003, EPRI, Palo Alto, CA, 2003. 1004482.

Supercritical circulating fluidized bed technology for Łagisza 460 MW_e power plant

Ilkka Venäläinen
Foster Wheeler Energia Oy
Varkaus, Finland

Abstract

Circulating Fluidized Bed (CFB) boiler technology has established its position as utility scale boiler technology. Plant sizes up to 300 MW_e are in operation today and designs for larger boilers are being developed. The next natural step for CFB technology is to go for supercritical steam parameters. A Polish utility company Południowy Koncern Energetyczny SA (PKE) placed an order to Foster Wheeler Energia Oy for a 460 MW_e supercritical CFB boiler for their Łagisza power plant. This will be the first supercritical once-through CFB boiler in the world.

The boiler design for 460 MW_e Łagisza power plant utilizes the Benson Vertical Low Mass Flux Technology developed and licensed by Siemens. CFB boiler with low and uniform furnace heat flux is extremely well suited for the Benson technology providing a stable operation of the boiler also during load changes and abnormal operation conditions. The supercritical once-through technology combines a high plant efficiency with the other well known benefits of CFB technology, such as fuel flexibility, low emissions and high availability.

1. Introduction

Target for high efficiency in modern power plants is set not only because of economical reasons but also for enhanced environmental performance in terms of reduced fuel needs, quantity of ash generated and pollutants emitted. Cutting CO_2 -emission has become increasingly important after the Kyoto Protocol. As coal will remain an important source of energy the focus has been set to improve the efficiency of coal fired power plants. To achieve this goal, supercritical steam parameters have been applied. Most large European thermal power plants built for fossil fuels such as coal and brown coal over the last decade have had supercritical steam parameters and have been based on pulverized coal fired once-through boiler technology.

Circulating fluidized bed (CFB) technology has emerged as a growing challenger to conventional pulverized coal-fired boilers in energy generation. Over the last

decade, CFB boiler technology based on natural circulation has reached utility scale. There are several CFB boilers in operation with sizes between 200–300 MW_e. The largest units in operation are two 300 MW_e CFB boilers at Jacksonville Energy Authority (JEA) in Jacksonville, Florida, U.S.A delivered by Foster Wheeler. These boilers burn either 100% coal or 100% petroleum coke or any combination of the two. The largest units in terms of physical dimensions are two 262 MW_e CFB boilers at Turow power plant in Poland (units 4 and 5, unit 6 under construction). The fuel for these boilers is brown coal with 45% moisture content, which increases the flue gas flow considerably.

Now CFB technology is taking a step further, to larger sizes with supercritical steam parameters and once-through technology. The detail engineering work for 460 MW_e supercritical CFB boiler for Południowy Koncern Energetyczny SA (PKE) in Poland is about to be finalized. This is a result of a continuous and determined development work conducted by Foster Wheeler including an experience database of over 200 reference boilers in operation. Emphasis has been given to mechanical design issues and understanding the process conditions affecting heat transfer, flow dynamics, combustion characteristics, gaseous emission control and thermohydraulics among others. Understanding these processes has been gained by the work done in bench-scale test rigs, pilot plants, field testing of operating units, model development, and simulation using developed semi-empirical models or more theoretical models.

PKE is located in southern Poland in Katowice and it is the largest utility in Poland, operating eight power plants within a 50 km radius from Katowice with installed capacity of over 5055 MW_e. In year 2001, PKE announced a bidding process for supercritical once-through boiler delivery for 460 MW_e unit in their Łagisza plant, with two alternative combustion technologies: pulverized combustion and circulating fluidized bed combustion. Foster Wheeler submitted proposals for both combustion alternatives and was selected as the boiler supplier on December 30, 2002, with both combustion technologies. Finally CFB technology were chosen by PKE after detailed technical comparisons, as well as economical studies with following conclusions:

- Total plant investment cost is lower. The installation of wet desulfurization and SCR systems that are essential for a PC-based solution can be eliminated, and all emission requirements are still fulfilled.
- Overall plant performance is better. Net plant efficiency using CFB technology and an advanced flue gas heat recovery system is approximately 0.3 percentage points better than with PC solution.
- Fuel flexibility provides a useful safety margin for the future. The unique multi-fuel capability of the CFB provides a wider fuel range and the additional possibility of using opportunity fuels.

2. PKE Łagisza 460 MWe project

The new 460 MW_e (gross) Unit will replace old power blocks of Łagisza Power Plant. The existing blocks were erected in 1960's and consist of seven units (110–125 MW_e each). Two of them will be shut down after the new 460 MW_e unit is commissioned. The new unit will not be built at place of old boilers, although many of existed renovated plant systems like coal handling and water treatment will be utilized for the new CFB unit.

The scope of Foster Wheeler's delivery includes the boiler island supply based on an EPC delivery basis: engineering and design, civil works and foundations for the boiler, boiler house enclosure with steel structures, boiler pressure vessels with auxiliary equipment, main steam piping to turbine and reheated steam piping, coal bunkers and fuel feeding equipment, electrostatic precipitator and cold end flue gas heat recovery system, erection, construction, start up, and commissioning. The time schedule of the project is as presented in Table 1.

Table 1. Project execution schedule.

Contract Signing	December 30, 2002
Notice to Proceed:	
I Stage – Basic Engineering	March 1, 2003
II Stage – Execution	After financing closing, not later than 30.06.2004
Hand Over	36 months after Stage II starting

Main fuel for the boiler is bituminous coal. The source of fuel consists of 10 local coal mines with wide range of coal parameters, proving once more the fuel flexibility of the CFB technology. Table 2 is presenting parameters of design fuel and overall fuel range.

Table 2. Fuel specification.

		Bituminous Coal		Coal Slurry
		Design fuel	Range	Range
LHV (a.r.)	MJ/kg	20	18–23	7–17
Moisture	%	12	6–23	27–45
Ash (a.r.)	%	23	10–25	28–65
Sulfur (a.r.)	%	1.4	0.6–1.4	0.6–1.6
Chlorine (dry)	%	max 0.4	max 0.4	max 0.4

a.r. = as received

Boiler design is made with a possibility for combustion of additional fuels. Main additional fuel is coal slurry that is available in large amounts in local coal mines. Due to CFB technology characteristics, wet coal slurry can be combusted with 30% share by fuel heat input. Coal washing rejects can also been burned in form of dry coal slurry granulates with a share up to 50% of heat input. Boiler is designed also to utilize biomass fuels up to 10% of fuel input. The biomass feeding equipment is included in the delivery as an option.

The steam parameters for the boiler were specified by the customer. The selected steam pressure and temperature are proven in other supercritical units and conventional boiler steel materials can be used. Table 3 presents main steam parameters of this 460 MW_e CFB boiler.

Table 3. Steam parameters at 100% load.

SH flow	kg/s	361
SH pressure	MPa	27.50
SH temperature	°C	560
RH flow	kg/s	305.7
RH pressure	MPa	5.48
Cold RH temperature	°C	315.1
Hot RH temperature	°C	580
Feed water temperature	°C	289.6

The plant net efficiency is naturally dictated by the selected steam parameters, steam cycle, wet cooling tower conditions and boiler efficiency. In Łagisza design the boiler efficiency is improved by including a flue gas heat recovery system, which cools the flue gases down to 85°C thus improving the plant net efficiency. The calculated net plant efficiency for Łagisza is 43.3% and net power output 438.9 MW_e.

The emission requirements for Łagisza boiler are according to European Union directive for Large Combustion Plants (see table 4). The emissions for sulfur dioxide are controlled with limestone feeding into the furnace. The required sulfur reduction of 94% with design coal is easily achieved with calcium to sulfur molar ratio of 2.2. Nitrogen oxide emissions are controlled with low combustion temperature and staged combustion. There are also provisions made for ammonia injection system (SNCR), however that is not required on normal design coals. Particulate emissions are controlled by electrostatic precipitator.

Table 4. Emission limits.

Emission (6% O_2, dry)	mg/m^3n
SO_2	200
NO_x	200
Particulates	30

3. Łagisza CFB boiler design

3.1 General

The boiler design for Łagisza design is based on well proven Foster Wheeler CFB –technology. It utilizes the experience of over 200 reference units starting from the first generation CFB boilers with conventional cyclone design which typically had a thick multi-layer refractory linings. These heavy refractory linings are known to cause high maintenance, decreased availability and limiting operational flexibility, such as long start-up times. Few of these first generation units have been made with a steam or water cooled structure, however the manufacturing of such construction is laborious and some sections with thick refractory linings remained together with few expansion joints.

The second generation CFB technology was developed to integrate the solids separator with the combustion chamber and to get rid of heavy multi-layer refractory linings. This was achieved with water or steam cooled panel wall construction that allowed the whole solids separator construction including the solids return channels to be made of panel walls with thin refractory linings. Also the number and size of expansion joints could be minimized, with water cooled separator construction no expansion joints are needed. The first of the second generation CFB boilers was started already 1992 and thereafter the number and size of this advanced technology grown steadily. The largest of the second generation CFB boiler are the units delivered to Turow power plant in Poland for units 4, 5 and 6. The power output of these units is 262 MW_e. Figure 1 shows the development CFB boiler size for the first and the second generation CFB boilers.

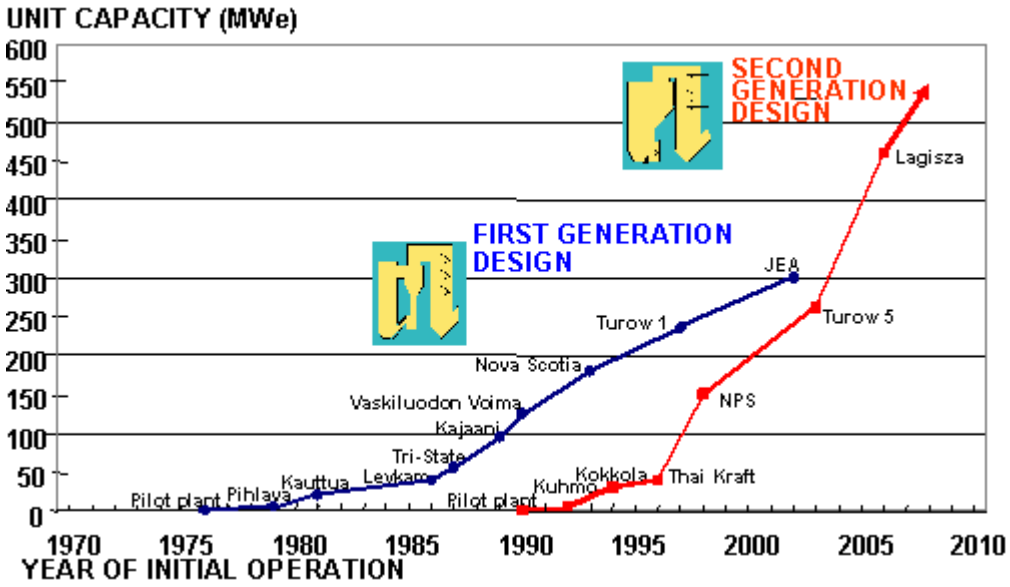

Figure 1. The increase of the size of CFB boilers.

3.2 Water and steam circuitry

In Łagisza CFB boiler the feed water enters the boiler at a temperature of 290°C for preheating in a bare tube economizer. From there the water is divided to the enclosure walls of the INTREX™ heat surfaces and thereafter to distribution headers of the evaporator (furnace) walls. During boiler start-up and shut down the circulation pump is used to secure minimum water flow through the evaporator. The fluid from the outlet headers of the evaporator walls is collected to the vertical water/steam separators. During boiler start-ups and shutdowns water is separated from the steam in these separators and led to a single the water-collecting vessel. Dry steam from the water/steam separators is led to the furnace roof, which is the first part of superheating system. The excess water from the water-collecting vessel is recovered to the condensate system.

When the boiler load exceeds the so called Benson-point at approximately 32% of MCR the steam exiting the evaporator walls is slightly superheated. Hence the circulation system can be closed and the boiler is in full once-through operation.

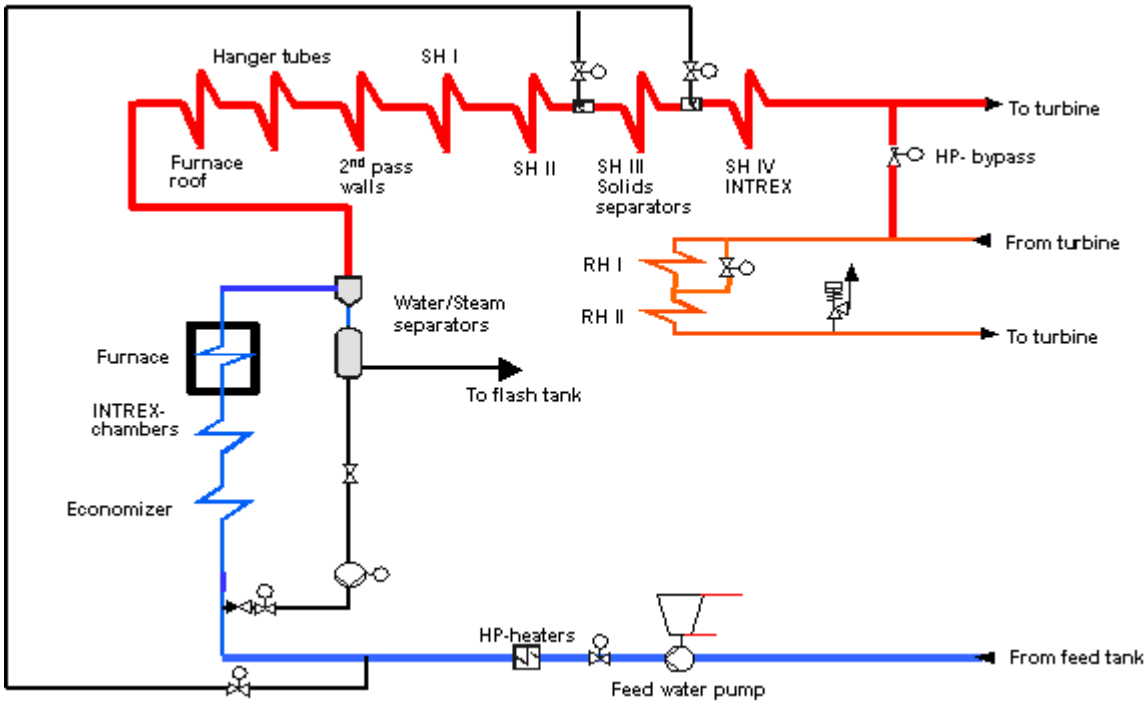

Figure 2. Steam circuitry.

After the furnace roof the steam is taken to superheater support tubes, walls of the convection pass and tube coils of the convective superheater I. Thereafter the steam is superheated in heat surfaces in the furnace. This superheater II is located in areas where the solids densities are low and it's lower ends are protected against any possible erosion. In location and arrangement this superheater is similar to several wing wall superheaters that have been successfully used in several boilers.

After superheater II the steam is divided to eight parallel solids separators that form the superheater III. The separator walls are formed of the gas tight membrane walls and they are covered with a thin refractory lining with high heat conductivity.

Final superheating is performed in superheater IV located in four parallel INTREX superheaters at the one side of the furnace. The INTREX superheater is a fluidized bed heat exchanger that is integrated to the lower part of the furnace, see Figure 5. The main steam temperature is controlled with a two stage feed water spray as well as by adjusting fuel feeding.

Steam after the high pressure turbine is brought back to the boiler for reheating. The first stage reheater is located in the convection pass. The reheater I (RH I) is equipped with a steam side bypass which is used for reheat steam temperature control. At higher loads part of the reheat steam is bypassed the RH I which reduces the heat pick-up and hence the inlet steam temperature to RH II is

decreased. This patented reheat steam control method avoids using a spray control for reheat side and therefore do not cause a decrease in plant efficiency. There are over 20 CFB boilers utilizing this control method, e.g. Turow CFB boilers in Poland. In Łagisza the final reheater stage is located in INTREX heat exchanger similar to the final superheater.

The plant is operated with sliding steam pressure so the boiler pressure is following the turbine load. Hence at lower loads (below 75%) the main steam pressure below critical pressure (221 bar) and at higher loads the boiler is operating at supercritical pressures.

3.3 Furnace design

3.1.1 Flue gas side

The flue gas side furnace design for Łagisza CFB boiler is based on extensive analysis of the fuels and limestones that are going to be used. These have given the required data for the design models to make predictions for circulating material particle size distribution, solids densities and finally the heat transfer with gas temperatures. The design resulted with a furnace cross section of 27.6 x 10.6 m and height of 48.0 m. The furnace dimensions are only slightly larger than the experience from the operating units, see comparison to the key reference boilers shown in Table 5. The Łagisza CFB boiler is presented in Figure 3.

Table 5. Comparison of furnace dimensions.

		Łagisza	Turow 4–6	JEA	Turow 1–3
Furnace					
- Width	m	27.6	22.0	26.0	21.2
- Depth	m	10.6	10.1	6.7	9.9
- Height	m	48.0	42.0	35.1	43.5

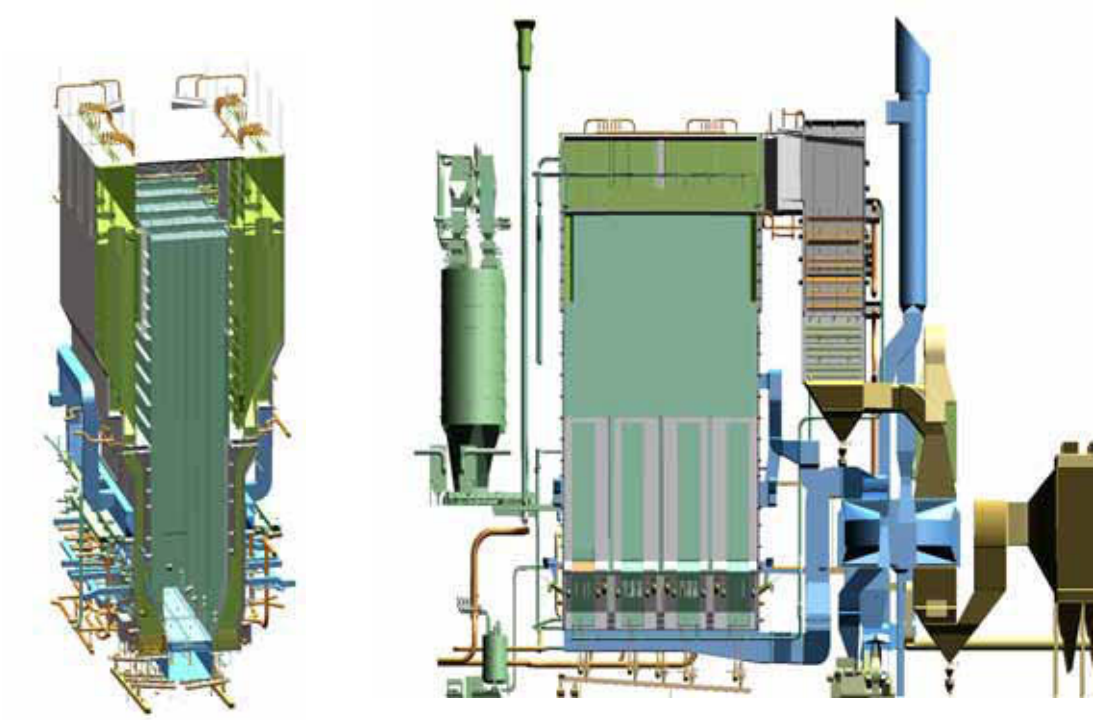

Figure 3. Łagisza CFB Boiler.

The furnace has one single fluidizing grid under which there are four separate air plenums introducing primary air to furnace. The primary air flow for these four air plenums is measured and controlled separately to insure equal air flow to all sections of the grid and uniform fluidization. The single continuous fluidizing grid ensures simple control as well as a stable and uniform operation of the furnace.

The lower furnace is tapered so that the grid area is approximately 50% of the upper furnace cross section. This provides high internal turbulence of the fluidized bed and enables efficient mixing of fuel and secondary air. The operation of the furnace has been verified with measurements in the similar units in operation as well as with 3D computer modeling. The furnace is very insensitive for operational disturbances such as unbalanced fuel feeding. The studies for such cases have been presented in [1].

Fuel feeding is arranged on the long walls of the furnace. The grid area per one fuel feed point is the same as used in other boilers. Secondary air is introduced also on long furnace walls at three elevations to provide stage combustion for minimizing the NO_x emissions.

3.3.2 Water / steam side

The water and steam side design in based on the low mass flux BENSON once-through technology licensed by Siemens AG, Germany. This technology is ideal for CFB conditions as it utilizes vertical furnace tubes, opposed to spiral wound tubing used in many other once-through designs [1]. For the CFB technology the vertical tubing is the normal arrangement in natural circulation designs and hence the similar design can now be used for supercritical, once-through boilers.

The heat transfer rate in CFB and boilers is very low and uniform compared to pulverized coal (PC) and therefore the required water mass fluxes are rather low [1]. The low heat fluxes allow also using normal smooth tubes in furnace walls with a mass flux of 550–650 kg/m^{2}s at full load.

In addition to furnace walls there are also additional evaporation surfaces in a form of wing walls inside the furnace. These wing wall panels are required because furnace wall area is not sufficient to provide required evaporation duty with a reasonable furnace height. These wing walls are heated on both sides (opposed to one sided heating of furnace walls). Therefore these tubes are internally rifled.

The fluid temperatures after each evaporator tube system have been analyzed in different load conditions. Due to low and uniform heat flux of the CFB furnace and the BENSON low mass flux technology the fluid temperatures are very uniform [1].

3.4 Solids separator design

The solids separator design for Łagisza CFB boiler is based on the second generation CFB design with steam cooled panel wall construction. The solids separator design is optimized for high collection efficiency with low flue gas pressure loss. The advanced separator inlet design with tall and narrow shape provides a uniform flow of flue gas and solids avoiding high local velocities. This results in equal collection efficiency as the best conventional cyclones with considerably lower pressure loss, see Figure 4.

There are eight (8) solids separators arranged in parallel, four (4) separators on two opposite furnace walls. The separator size only slightly larger than in Turow units 4–6 and even larger separators are in commercial operation. Hence there is no scale-up in the separator size.

The separators are designed with panel wall sections and have a thin refractory lining anchored with dense studding. This minimizes the required amount of refractories. The separators are manufactured with panel welding machines and

hence extensive manual welding is avoided. The separator tubes are steam cooled forming a third superheater stage. Also the gas ducts (two pcs) after the solids separators are steam cooled and connected to the separator tubing.

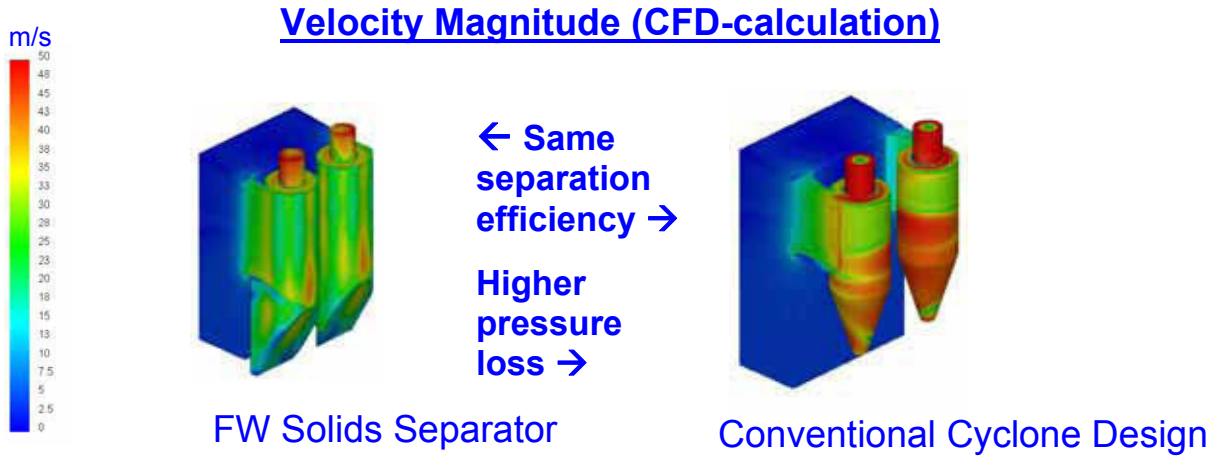

Figure 4. Comparison of solids separator designs.

3.5 INTREX™ heat exchanger design

INTREX is a fluidized bed heat exchanger extracting heat from the hot circulating bed material that is collected in the solid separators. Additional bed material is taken to INTREX chambers directly from the lower part of the furnace. This provides sufficient amount of bed material at wide load range. A unique feature of the INTREX superheater is it's ability to control the heat transfer by changing the fluidization velocities. This special capability is utilized for example during load changes to trim the steam temperature. Also in case of fuels having high chlorine contents INTREX superheater provides enhanced protection against corrosion.

Łagisza boiler design incorporates altogether eight INTREX heat exchangers, one for each solids separator. Four of the INTREX heat surfaces are serving as final superheater and other four as final reheater. Also this part of the boiler the refractory linings are minimized due to water cooled casing of the INTREX surfaces. This allows the integration of the INTREX casings to the furnace thus eliminating expansion joints and minimizing distances to transfer hot solids. Controlling of the flow of hot solids is done only with fluidization, therefore no valves or other mechanical devices are required.

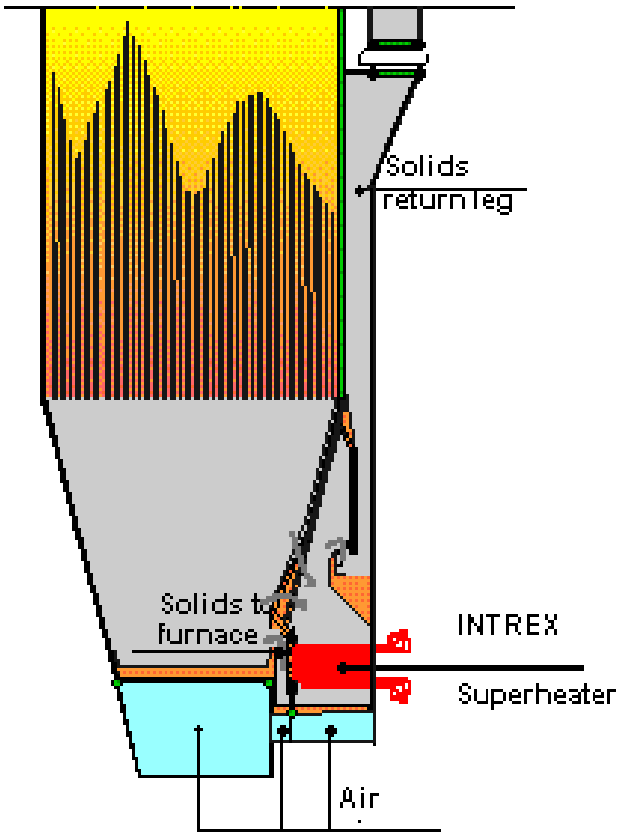

Figure 5. INTREX heat exchanger.

Another benefit of the INTREX heat exchanger is a high heat transfer rate, which decreases the amount of heat surface required thus making the actual dimensions smaller. The design of INTREX heat exchangers is similar to those of the previous boilers.

3.6 Boiler materials

The material requirements for most sections of the boiler are very conventional and normal boiler materials can be used. The furnace and solids separator panels can be manufactured of materials that do not require post-weld heat treatment. Material for INTREX heat exchangers is austenitic steel material, TP347HFG. That material has been successfully used previously in many existing Foster Wheeler CFB Boilers.

Table 6. Selected boiler materials.

Heat exchanger tubes:		
Heat surface	Tube material	Header material
Economizer	15Mo3	15NiCuMoNb5
Furnace walls	13CrMo44	15NiCuMoNb5 13CrMo44
Superheaters and reheaters	13CrMo44 7CrMoVTiB1010 X20CrMoV121 TP347HFG	13CrMo44 X10CrMoVNb91 X11CrMoWVNb911
Steam piping:		
Main steam pipe		X11CrMoWVNb911

3.7 Flue gas heat recovery system

The flue gas heat recovery system (HRS) improves the boiler and power plant efficiency by decreasing the flue gas temperature down to 85 °C. The system recovers heat from the flue gases which results in an improvement of 0.8%-units in total plant efficiency.

HRS is operating in the clean gas after the ESP and ID fans. The flue gas temperature is approximately 125°C in front of the HRS. The cooling of the flue gas takes place in a heat exchanger made of PF-plastic tubing to avoid corrosion problems. After the HRS, the flue gas is conducted to the cooling tower via glass fiber duct.

A primary water circuit transfers the recovered heat to the combustion air system and heat is transferred to both primary and secondary air. As the combustion air temperature before the rotary air preheater is increased, the air flow is not able to absorb all the heat available from the flue gases. Therefore part of the flue gases is conducted to a separate low-pressure bypass economizer where the heat from the flue gases is used for heating of the main condensate. Part of main condensate is taken before the latest LP-Preheater and conducted to the feed water tank, see Figure 6.

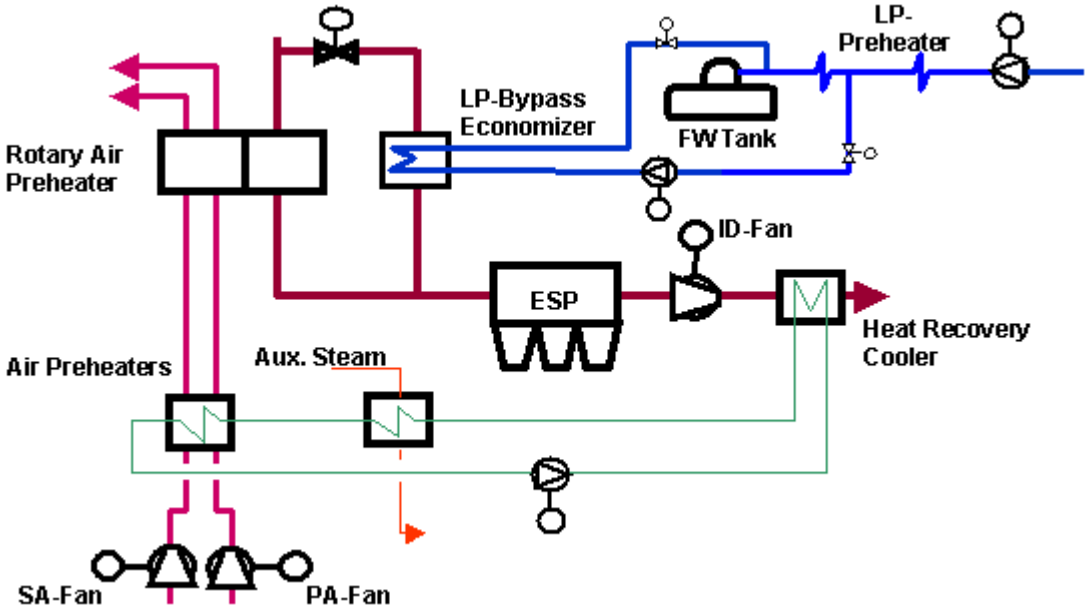

Figure 6. Flue gas heat recovery system.

4. Future designs

Now when the design for Łagisza 460 MW_e CFB boiler is almost completed, the next logical step is to reach for larger boiler sizes and higher plant efficiencies. To accomplish this goal Foster Wheeler together with few European partners has launched a development program to develop a CFB boiler design for 800 MW_e. The design for the 800 MW_e boiler will be based on the Łagisza design with the necessary scale-up modifications.

In this project the steam parameters are selected to represent the state-of-the-art material technology and hence an improvement in the plant efficiency. The selected steam temperature for fresh steam will be 600°C and 620°C for reheat steam. The steam pressure will be approximately 300 bar.

Bituminous coal as a fuel and using direct sea water cooling, a net efficiency exceeding 45% is estimated.

5. Conclusions

Circulating fluidized bed (CFB) boiler technology has established its position as utility scale boiler technology. Now the CFB technology is ready to go for supercritical steam parameters and larger boiler sizes. A Polish utility company Południowy Koncern Energetyczny SA (PKE) placed an order to Foster Wheeler

Energia Oy for a 460 MW_e supercritical CFB boiler for their Łagisza power plant. This will be the first supercritical once-through CFB boiler in the world.

With supercritical once through technology CFB boilers are able to provide a basis for high efficiency power plant with reduced emissions including CO_2 together with high fuel flexibility. The CFB boiler for Łagisza power plant utilizes a wide range of coals and is also able to burn coal wastes in form of coal slurry and granulates. Even biomass can be utilized.

The boiler design for 460 MW_e Łagisza power plant is based on proven solutions that are already used in other large CFB boilers delivered by Foster Wheeler. Only a modest scale-up has been required. It can be concluded that CFB technology is today commercial to boiler sizes of 500 MW_e and programs exist to scale-up the technology up to 800 MW_e.

References

[1] R. Lundqvist, R. Kral, P. Kinnunen & K. Myöhänen. The Advantages of a Supercritical Circulating Fluidized Bed Boiler. Presented at PowerGen 2003, Düsseldorf, Germany.

Issues of importance for availability of a waste-fuelled CFB boiler

Göran Eidensten & Mathias Edelborg
Fortum Service Öst AB, Stockholm, Sweden

Julia Sundberg & Ulla McNiven
AB Fortum Värme samägt med Stockholms stad, Stockholm, Sweden

Abstract

With energy producers searching for more economic ways to serve communities in production of electricity and heat, waste has become an attractive fuel option. In Stockholm at Fortum's site in Högdalen, a modern CFB boiler built in 1999 is fuelled by industrial waste. Fortum's experience shows that it is very important to take into account the choice of fuel in the beginning of the plant lifecycle. If the power plant is not well-suited for the fuel, major availability problems can be introduced in four areas: fuel preprocessing, fuel feeders, boiler, and flue gas cleaning.

Good availability can be achieved by (1) active fuel monitoring and management, and updated specification of fuel; (2) predictive and preventive maintenance programmes with systematic inspections and refurbishment; and (3) updated instructions and competence in operations. The drive towards the most economic production constantly sets new challenges to the technology, but with continuous development efforts by manufactures and users together with supportive research facilities the technologies can be adapted to serve the new demands.

1. Introduction

In order to meet demands for efficient production of heat and electricity, energy producers are looking at low-quality fuels like waste. In Finland, interest in waste fuels has rapidly grown and several EfW projects have been forecast within the near future. In Sweden, the use of waste fuels continues to experience remarkable growth. However, the fuel choice has to be taken into account in the plant design.

Fortum's power plant in southern Stockholm in Sweden consumes over 500 000 tons of waste annually. By the end of 2005 this will increase to 700 000 tons. At the site, a modern CFB boiler built in 1999 is fuelled by industrial waste. This paper describes Fortum's recent experiences with the waste-fuelled CFB plant in Stockholm.

1.1 The CFB plant

Boiler 6 (P6) at the Högdalen plant consists of an external and an internal fuel management system, a CFB boiler (91.2 MW) and a flue gas cleaning system with condensation (approx. 15 MW). The fuel burned in P6 is industrial waste comprising combustible residual products primarily from industry in the Stockholm area.

By the 2003 overhaul, the boiler had been in operation for 21,388 hours. The unit is the first Foster Wheeler compact boiler specially designed for the combustion of biomass and recovered fuels (Blomberg et al. 2001). In order to reduce the risk of fouling and corrosion in the convection pass, the boiler is equipped with an idle pass prior to the convection superheaters, as is conventional for waste incineration (Figure 1). In order to reach the desired final steam temperature of 480 °C, the unit has two INTREX™ superheaters (Blomberg et al. 2001).

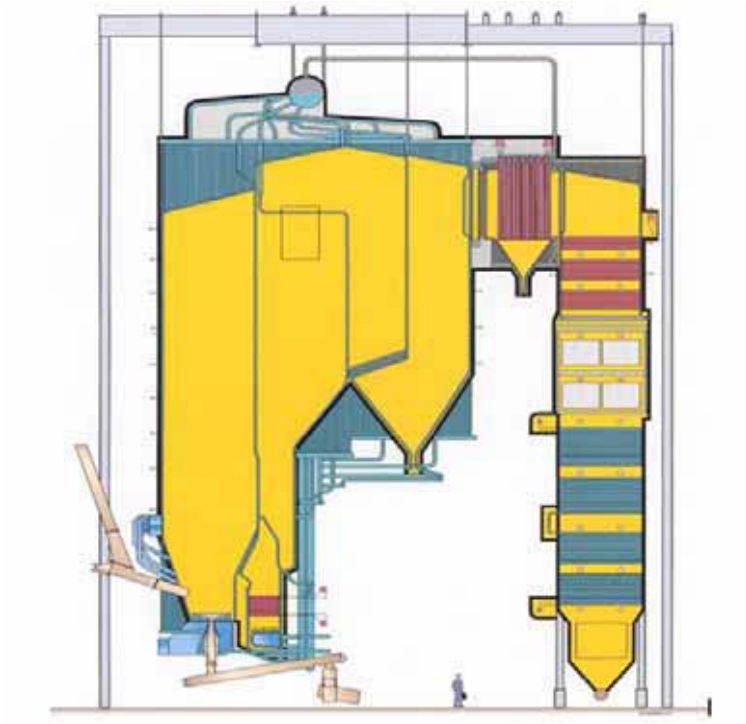

Figure 1. General layout of the waste-fuelled CFB boiler (P6).

1.2 Flue-gas cleaning

Alstom Power has supplied the flue-gas cleaning system, which consists of a semi-dry cleaning process, NID reactor and bag filter, a wet cleaning process, scrubber, and a flue-gas condenser with accompanying water purification (Figure 2).

As part of the semi-dry cleaning, quicklime mixed with re-circulated fly ash and water is added to the flue gas stream. To enhance the separation of heavy metals and dioxins, activated carbon is induced to the stream prior to the semi-dry step. The wet cleaning process, the scrubber, consists of a quencher, acid stage and neutral stage. The flue gas is washed in a spray tower using circulating streams of acid and neutral liquid. In the quencher, the flue gases are cooled to saturation point, about 60°C.

After the scrubber, the flue gases enter the condenser, where water vapor is condensed by means of returning district heating water. The condensing process further purifies the gases, as impurities tend to condense with the moisture.

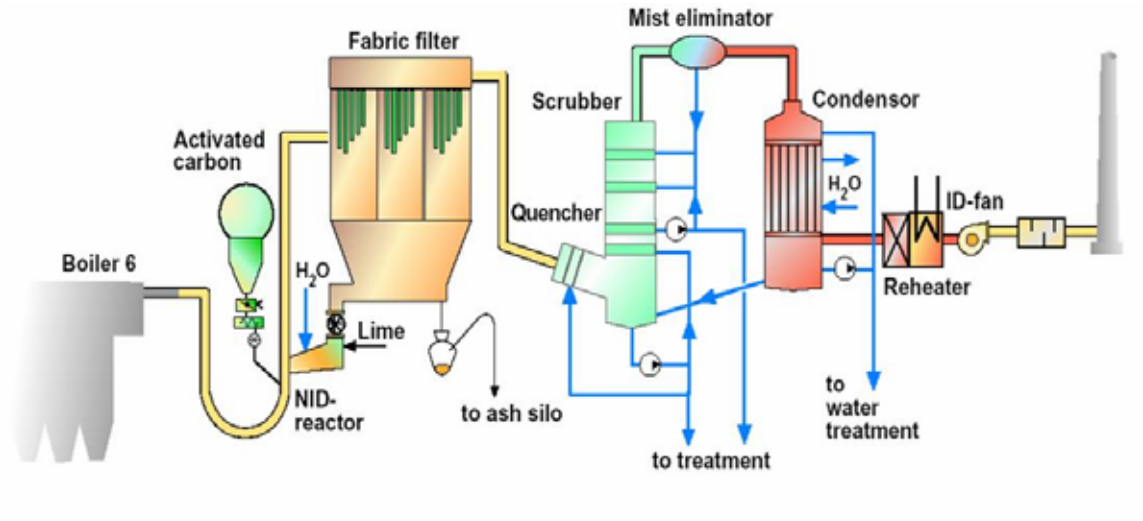

Figure 2. Process diagram of flue-gas cleaning in P6.

2. Major availability problem areas

Unexpected disturbances have occurred during the first operating years of the boiler plant. Problems limiting availability have included the following:
External and internal fuel handling system,

- Deposits in the boiler,
- Tube leaks,
- Sintering of the bed,
- Flue gas cleaning.

2.1 Fuel

The majority of the fuel arrives pre-treated according to specifications, in lorries that tip it into a feeding hopper. From the feeding hopper, the fuel is transported by conveyors, magnetic separator, sieve and a crusher to two storage silos that

hold 4000 m^3 each. The intake for the storage silos is designed to feed in 600 m^3/hour (Eidensten 2003).

Waste, even industrial waste, is a heterogeneous and problematic fuel. External and internal fuel handling are subject to capacity problems, and breakdowns and stoppages. During the 02/03 operating season, the fuel composition used was as follows (Table 1, Figure 3.).

Table 1. Fuel composition.

Material fraction analysis [%]						
Soft plastic	Hard plastic	Paper	Wood	Textiles	Metal	Other
7	4	20	55	3	1	10

Figure 3. Fuel: industrial waste.

Since commencing operation in 1999, blockages caused by oversize material and non-magnetic metals have been reduced as a result of refined delivery checks and cooperation with suppliers. A great deal of wear and tear damage has occurred on the fuel equipment, primarily on feeding screws from the silo.

The capacity problems involve transport components not being capable of supplying the required fuel quantity. Feeding screws from the silo have difficulties in maintaining a 100% supply rate over prolonged periods, which has resulted in load limitations.

2.2 Fuel feed

From the storage silos, the fuel is then fed out by means of rotating screws in the bottom to 3 day silos via a belt conveyor, magnetic separator, belt elevator, screw and a chain conveyor (Figure 4). From the day silo, the fuel passes along three parallel fuel lines into the boiler. Each line consists of a rotating screw in the bottom of the silo, a chain conveyor with levelling, a feeder and a screw conveyor into the boiler.

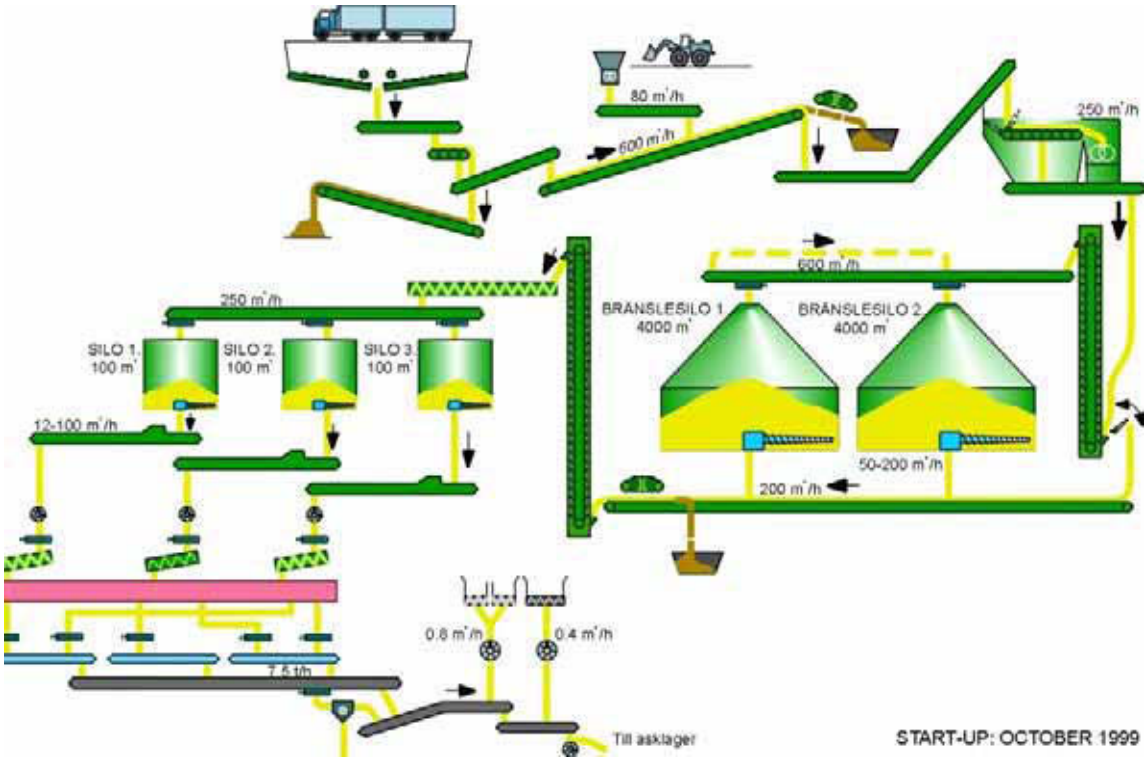

Figure 4. Fuel feeding system of the boiler P6.

It is very important that the fuel used in such a CFB boiler is well prepared and that the size and quality of the fuel fractions are according to the specification. Fuel which does not correspond to the specification tends to wind around the screws and clog cell feeders and the hopper (Svedenkrans 2000).

2.3 Boiler

The availability problems of the boiler in Högdalen have been due to:

- Deposits – there are large quantities of thick deposits in the boiler, primarily in the idle pass, which results in the steam temperature after superheater 1 being too high so that it is not possible to run the boiler with a full load.

- Sintering – The boiler bed has sintered several times. Most of these events are due to numerous disruptions in the fuel management system between the day silos and the boiler.
- Tube leaks – An example follows. In December 2002, around 10 m2 of tubes were replaced in the roof above the cyclone. This area was in the wall thickness measurement programme with more intensive inspections planned for 2004. On inspection of the roof, it was discovered that approximately half the tube thickness had deteriorated due to high temperature corrosion, see Figure 5. During the 2003 overhaul, Foster Wheeler replaced 10 m^2 tubes and coated the roof with silicon carbide.

Figure 5. Roof tube surfaces after sand blast cleaning.

The tests carried out earlier in the boiler show remarkable differences in the corrosion behaviour with different fuels (Makkonen 2002). With recovered fuels, the risk of fireside corrosion is evident at as low a temperature as 300°C (Makkonen 2002) (Figure 6). This explains a lot of the challenges with the fuel used in Högdalen, compared with, e.g., forest residue, where corrosion according to the measurements starts at temperatures above 500 °C.

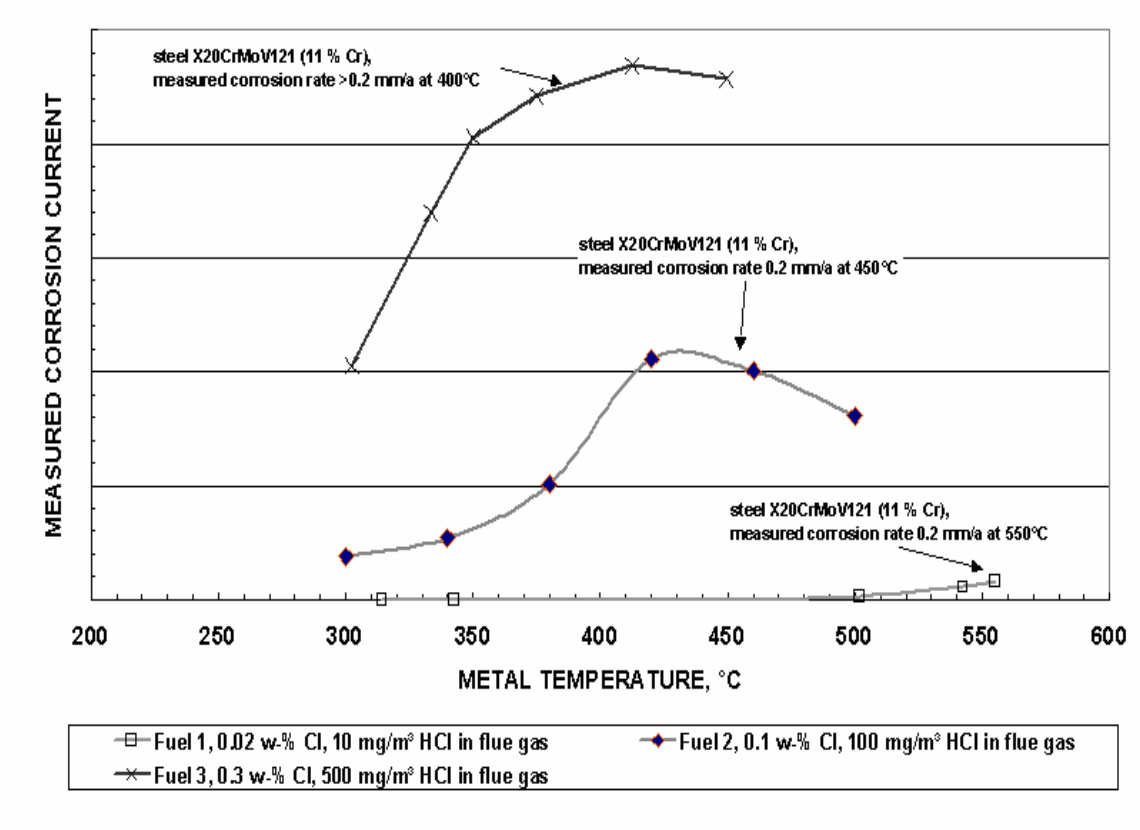

Figure 6. Measured relative corrosion risks by combustion of different fuels at the Högdalen CFB boiler. Fuel 1 is forest residue, fuel 2 is recovered wood and fuel 3 is selected industrial waste (Makkonen 2002).

The tests carried out in Högdalen have confirmed that the boiler operation differs remarkably with different fuels. Recovered fuels caused most feeding instabilities, and it was noticed that despite aggressive bed regeneration, the amount of coarse particles in the bed material increased rapidly, indicating risk of fluidization difficulties (Makkonen 2003).

With suitable additives it is believed that the sulphur/chlorine ratio can be improved to lower the corrosive impact of chlorine in the fuel (Svedenkrans 2000).

2.4 Flue gas cleaning

The problems in the flue gas cleaning were mainly caused by the bag filters and the erosion in the flue gas channel. Due to high content of halogens such as chlorine in the fuel, the bag filters were prematurely deteriorated and a higher quality of textile had to be chosen.

3. Solutions

The measures implemented in the action plan have been aimed at increasing the availability by reducing stoppages resulting from the aforementioned problems. The major measures implemented are:

- The feed from both storage and day silos has been altered by enlarging the chute from the silos.
- The feed screws have been redesigned, with an extra thread, so that the fuel will be more easily released from the screw.
- The fuel conveyors have been altered to avoid having to clean them in every shift.
- Trials to reduce the rate of deposit accumulation in the boiler by mixing additives with the fuel.
- Installation of soot removal systems using water in the idle pass.
- Design improvements on superheater tubes and panel walls to reduce the risk of tube leaks.
- Status checks on tubes through analyses and thickness gauging.
- Selection of the most suitable type of bag filters.

The fuel handling procedure and the quality control of the fuel have been reviewed. Further training has been arranged both internally and for the fuel suppliers. The preventive maintenance programmes have been improved and will be further improved according to the results of the follow-up programme. The operational procedures have been updated.

4. Operational achievements

The improvement initiatives of the owner/operator, maintenance contractor, boiler manufacturer and research associates have been successful. The fuel and the local conditions have challenged the solutions. With the development programme, satisfying operational results have been achieved. In early 2004 boiler 6 achieved monthly record production. The steady operation in 2004 can be seen in Figure 7, which compares performance before and after the improvement programme. The problems in the fuel feed have been minimised. This has led to minimum chances for bed sintering. The improvements in the flue gas cleaning have been fully successful. However, due to heavy loading and increased operation time caused by increased availability - the need for further improvements has been recognised.

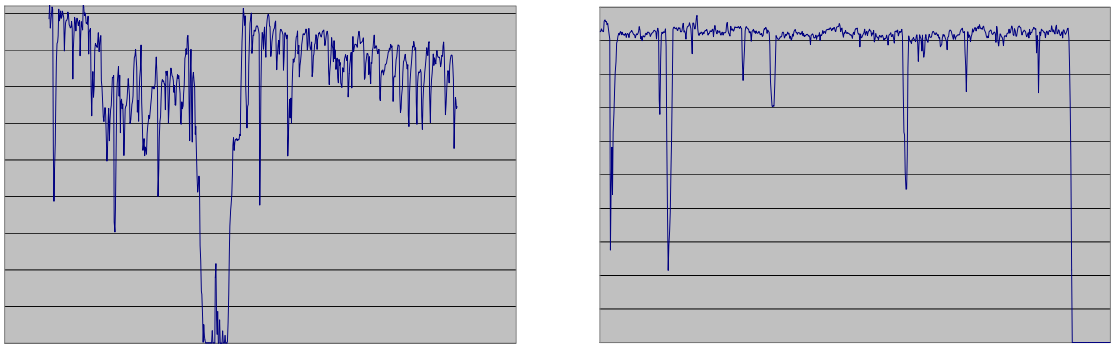

(a) (b)

Figure 7. Monthly output graphs of boiler 6 (a) before improvements in 2003, (b) after an improvement programme in 2004.

5. Continuous development

One of the characteristic features of the O&M practices in Fortum's power plants is continuous development. In Högdalen, besides investments in better solutions in problem areas, a research and development programme continues. In particular, the basics in maintenance processes are thought through thoroughly. Fortum's experience in systematic approaches (McNiven 2000) and high temperature components (Auerkari et al. 1997) is applied. The improvement team has defined the critical components and the preventive maintenance programme will be modified according to the results. The combustion process will be further studied in co-operation with the manufacturer and a research organisation. Several national level research projects improve parts of the process. The projects are looking at, e.g., possible additives, soot blowing, metal separation and bed sand improvements. Continuous development will be even better integrated to normal O&M practices.

6. Summary

Fortum's experience with a CFB boiler in the EfW site in Högdalen in Stockholm has been described. The experience shows that it is very important to take into account the choice of fuel in the beginning of the plant lifecycle. If the power plant is not well-suited for the fuel, major availability problems can occur in the areas of fuels, fuel feeding, boiler performance, and flue gas cleaning.

Fuel composition can introduce thick and sticky deposits. Elements in fuel can be corrosive. Fuel handling can be disturbed by fuel clumping. When dealing with feeding of fuel, capacity problems and possible lack of redundancy must be taken into account. Possible availability problems with the boiler can be due to (1)

deposits that limit efficiency, (2) short life due to environment/materials, (3) sintering in the bed, and (4) structural/construction limits. Flue gas cleaning can trigger high demands on filters due to corrosive flue gases and new challenges regarding semi-dry and wet processes.

Good availability can be achieved with (1) active fuel monitoring and management, and updated specification of fuel; (2) predictive and preventive maintenance programmes with systematic inspections and refurbishment; and (3) updated instructions and competence in operations. The drive towards the most economic production constantly sets new challenges to the technology, but with continuous development efforts by manufactures and users together with supportive research facilities, the technologies will be suited for the new demands.

References

Auerkari, P., McNiven, U., Rönnberg, J., Heimsch, J. & Poloni, M. 1997. Applications of advanced systematic concepts towards managing the performance of high temperature components in coal fired power plants. In: Jovanovic, A.S. (ed.), Proceedings of Intelligent Software systems in inspection and life management of power and process plants, Paris, France, 25–27 August 1997.

Blomberg, T., Hiltunen, M. & Makkonen, P. 2001. Modern CFB Concept for Combustion of Recovered Fuel: Design for Improved Availability. 16th International Conference on Fluidized Bed Combustion, Reno, USA, 2001.

Eidensten, G. 2003. Tillgänglighetshöjande åtgärder för panna P6 i Högdalen. (Availability improvements.) Foster Wheeler panndag. Stockholm, Sweden, 24 September 2003. (In Swedish)

Makkonen, P. 2003. Corrosion Tests in Combustion of Recovered Fuels in a Modern CFB Boiler, VGB Conference "Operating Experience with Fluidized Bed Systems", Köln, Germany, 2002, also available in VGB PowerTech No. 8/2003.

Makkonen, P. 2002. Erfahrungen aus neuer Wirbelschichtteknologie mit hochkalorischen Abfällen (Experiences from New CFB Units in Heat Recovery from Recovered Fuels Containing High Heating Value), VDI Conference, Mannheim, Germany, 2002.

McNiven, U. 2000. Systematics and methodology in boiler plant life and plant condition management. Fortum – Research Reports – 01/00. Dissertation. Helsinki University of Technology. Espoo, Finland. ISBN 951-591-074-9

Svedenkrans, C. 2000. Mätningar och utvärdering avseende sambandet mellan bränslesammansättning, pannfunktion och materialkorrosion i en CFB-panna konstruerad för returbränsle. (Measurements regarding fuel, boiler performance and corrosion.) Examensarbete i Kraft- och värmeteknologi. Institutionen för Energiteknik. Kungliga Tekniska Högskolan. Stockholm, Sweden. (In Swedish)

Reducing superheater corrosion in wood-fired power plant

P. J. Henderson, C. Andersson, H. Kassman & J. Högberg
Vattenfall AB, Stockholm, Sweden

Abstract

One of the major drawbacks to the combustion of 100% wood and waste wood fuels in power station boilers is the increase in the fouling and corrosion of superheaters, which increases operation and maintenance costs. Wood fuels have a high content of potassium and chlorine, but they contain very little sulphur compared to fossil fuels. To combat corrosion, boiler tests have been performed with ammonium sulphate which is sprayed into the flue gases after combustion but before the superheaters and effectively converts gaseous KCl into potassium sulphate, K_2SO_4. This is much less corrosive than KCl. Long-term probe measurements showed that the corrosion rates were reduced by 50%. This concept, together with an instrument for measuring alkali chloride levels in the flue gas has been patented and is known as "ChlorOut". Probe tests with different steels showed that superheater corrosion can also be greatly reduced by the choice of the right material.

1. Introduction

In the last few years, there has been a move away from burning fossil fuels through the co-utilisation of biomass and coal and finally to 100% biomass such as wood and waste wood products. Unfortunately, burning of biomass causes widespread fouling of superheater tubes and corrosion can occur rapidly under the sticky alkali chloride deposits. Even at today's maximum steam temperatures of 500 to 540°C there are some severe corrosion problems when burning 100% wood-based fuel [1]. It is also desirable to be able to burn other environmental fuels such as straw, demolition wood or other wood-waste products, to reduce production costs and avoid dumping waste at landfill sites. This, however, makes the corrosion and fouling problems even more serious, [2, 3].

A complete set of superheaters for a 100 MW combined heat and power boiler costs about 1.5 MEuro. The durability of superheaters is thus an important factor in determining the long-term production costs. Unplanned outages due to leaking superheaters are also very expensive. As well as causing corrosion problems, the build-up of deposits reduces the heat uptake to the superheaters which leads to lower efficiency. Consequently, ways are being sought to reduce superheater corrosion.

Most biomass fuels have a high content of alkali metals and chlorine, but they contain very little sulphur compared to fossil fuels. Potassium chloride, KCl, is found in the gas phase, condenses on the superheater tubes and forms complex alkali salts with iron and other elements in the steels. These salts have low melting points and are very corrosive. Vattenfall has developed and patented an instrument for *in-situ* measurement of gaseous alkali chlorides which gives an indication of how corrosive the flue gases are, [4]. This instrument is called an *in-situ* alkali chloride monitor (IACM). Vattenfall has also developed and patented a concept with a sulphate containing compound called ChlorOut, [5], which is sprayed into the flue gases after combustion, but before the superheaters, and effectively converts KCl into potassium sulphate, K_2SO_4. This is much less corrosive than KCl.

This paper reports on measures taken to reduce superheater corrosion in two fluidised bed boilers burning wood-based fuels, using the ChlorOut additive to control the KCl levels and by using more corrosion resistant steels.

2. Experimental

2.1 Descriptions of plants used for testing

105 MWtot boiler in Nyköping, Sweden

This plant is situated about 120 km south of Stockholm. The plant consists of a Bubbling Fluidised Bed (BFB) steam boiler (Boiler 3) for Combined Heat and Power (CHP) operation, two circulating Fluidised Bed (CFB) boilers for hot water production and a hot water accumulator. Tests were performed in Boiler 3, for CHP production.

The CHP unit produces 35 MW of electricity and 69 MW of heat and has been in operation since the end of 1994. The final steam temperature is 540°C and the pressure 140 bar. The fuel mix consists of wood chips (logging residues), demolition wood and coal.

The ChlorOut was sprayed into the flue gases upstream of SH2, the first superheaters that the flue gases meet on their passage through the boiler. Deposit and corrosion probe testing were performed immediately before SH2 and flue gas measurements immediately after, see Figure 1.

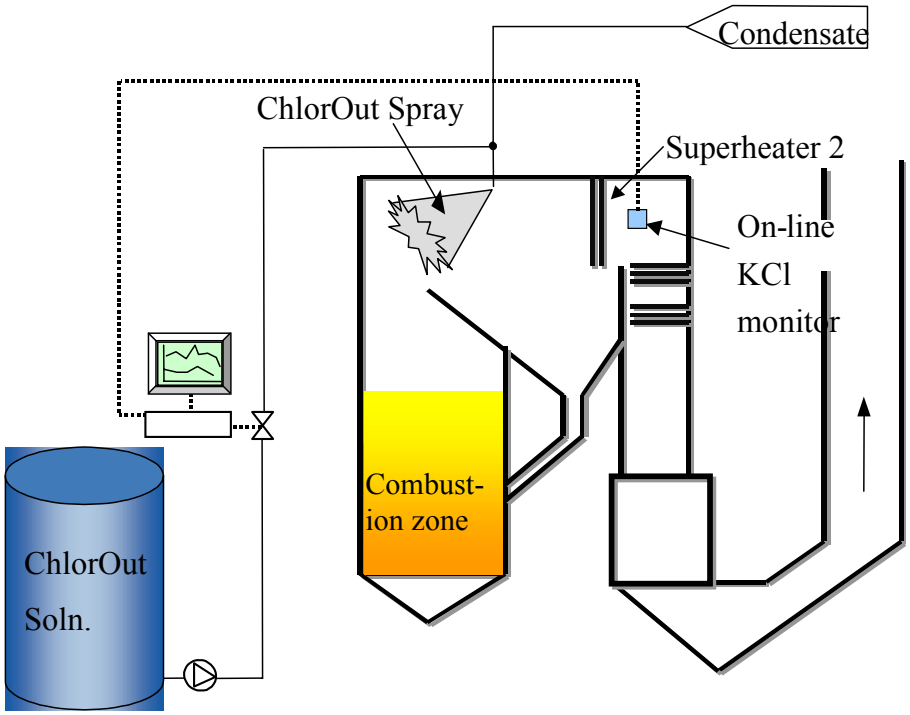

Figure 1. Schematic diagram of the ChlorOut system in BFB boiler, Nyköping.

The signal from IACM was used to control the amount of ChlorOut sprayed into the boiler. A fuel like demolition wood will increase the KCl level in the flue gas, which means that more ChlorOut has to be injected into the boiler to bring the KCl levels under control. The ChlorOut solution was diluted with water from flue gas condensation unit. The ChlorOut patent covers a number of sulphates, in this case ammonium sulphate was used to aid the reduction of NOx.

98 MWtot boiler in Munksund, Sweden

This is a Circulating Fluidised Bed (CFB) boiler situated at SCA's pulp and paper mill in Munksund, near Piteå, in the north of Sweden, about 75 km south of the Arctic Circle. The boiler was taken into operation in 2001 and can produce up to 25 MW electricity as well as process steam. The final steam temperature is 480°C and pressure 60 bar. The boiler is fired mainly with bark (>80%), but also sawdust, woodchips and approximately 6% of waste from cardboard recycling.

The ChlorOut was sprayed into the flue gases at the entrance to the cyclone, and deposit and corrosion probe testing were performed immediately before SH2 where the flue gas temperature is 680°C, see Figure 2.

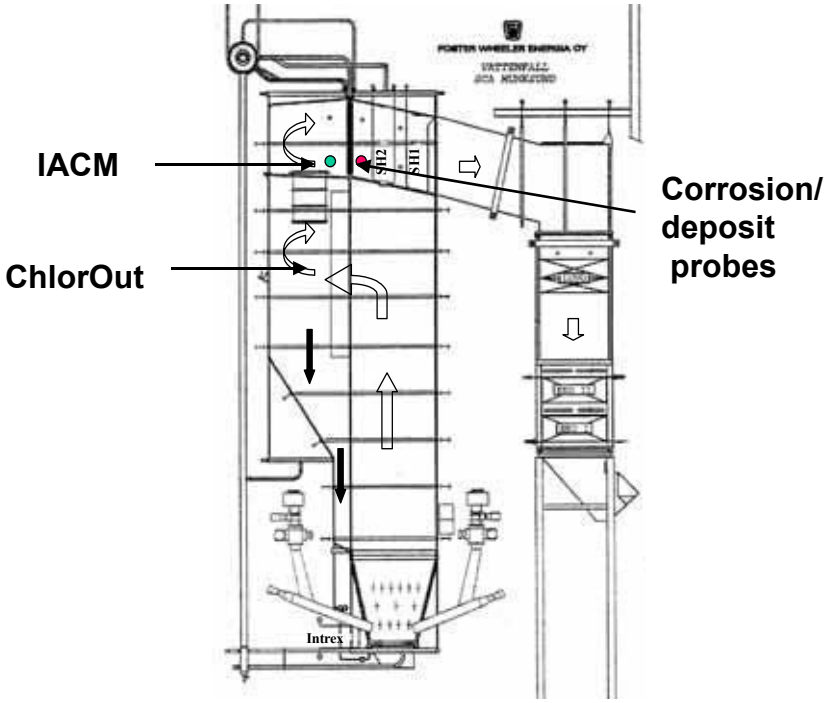

Figure 2. Schematic diagram of the ChlorOut system in the CFB boiler, Munksund.

2.2 Measurement techniques

Deposit, corrosion and flue gas measurements were performed under normal conditions (without ChlorOut) in Nyköping and Munksund. Deposit and flue gas measurements were also performed with ChlorOut in Nyköping and Munksund, but long-term corrosion tests with ChlorOut were only performed in Nyköping.

The chemical composition of the flue gas at the superheaters/corrosion probes was determined by several measurement techniques, including *In-situ* Alkali Chloride Monitoring (IACM). IACM is a new method, developed and patented by Vattenfall AB, for continuous and in-situ measuring of alkali chlorides in the gas phase in the area around the superheaters in power stations [4]. IACM measures the overall concentration of NaCl and KCl, which during wood fuel firing can be expressed as the level of KCl. IACM was also used to measure SO_2 in these tests. IACM works on the principle of optical absorption and has a sampling time of 5–10 seconds.

Deposits were collected on stainless steel rings on temperature controlled deposit probes for a period of 3 hours and were analysed by energy dispersive x-ray analysis in a scanning electron microscope (ASEM), which penetrates several microns. Some deposits were analysed by time-of-flight secondary ion mass spectrometer (TOF-SIMS) The secondary ion mass spectrum gives information

about the elemental and chemical composition of the material. Since the secondary ions originate only from the 1–5 outermost atomic/molecular layers of the material, this technique is highly surface sensitive. Chemical profiles through the depth of the oxide, formed *under* the deposit on ring specimens of 13CrMo44, were obtained by Glow Discharge Optical Emission Spectroscopy (GDOES). In this technique, a plasma bombards the surface of the specimen (the cathode) and sample erosion occurs by cathode sputtering. The atoms are excited in the plasma and subsequent photoemission from electron de-excitation is analysed by optical spectroscopy. Thus simultaneous material removal and multi-element acquisition is obtained. It was not possible to perform GDOES on the deposits.

Corrosion specimens were exposed as rings on internally cooled probes placed near the superheaters. Details of probe construction can be found in Ref. 6. Each ring was measured at 15° intervals on two circumferences before and after testing to obtain values of metal loss caused by corrosion or oxidation. Internal corrosion (or selective corrosion such as grain boundary attack) was also measured. The total corrosion is the sum of metal loss and internal corrosion values. The microstructures of the exposed rings were examined by light optical- and scanning electron microscopy and energy dispersive x-ray analysis. The chemical compositions of the steels used are shown in Table 1.

Table 1. Chemical composition in wt % of the steels tested. The balance is Fe.

Steel	**Cr**	**Ni**	**Mo**	**Mn**	**Other**
15Mo3	--	--	0.30	0.52	C 0.16, Si 0.26
13CrMo44	0.86	0.07	0.48	0.46	C 0.12, Si 0.21
10CrMo910 (T22)	2.1	--	0.92	0.43	C 0.12, Si 0.22
X20CrMoV12 1	10.45	0.70	0.88	0.6	C 0.18, Si 0.22, V 0.26
T92	9.15	0.26	0.5	0.46	W 1.7, Si 0.22, Nb 0.6, N 0.05, V 0.2, B 0.003, C 0.11
Esshete 1250	14.9	9.65	0.94	6.25	C 0.084, Si 0.58, Nb 0.86, V 0.22, B 0.004
TP 347 H	17.6	10.7	--	1.84	Si 0.29, C 0.05, Nb 0.6

3. Results

3.1 Results from Nyköping

ChlorOut drastically reduced the growth rate of deposits measured in 12 hour exposure tests with a ring temperature of 500°C. The fuel used in these tests was 50% logging residues and 50% demolition wood. Without ChlorOut the growth rate was 21 g/m^2/h; this was reduced to 6 g/m^2/h when ChlorOut was used.

During the three hour test period ChlorOut reduced the average gaseous alkali chloride levels in the flue gases from 30 to 17 ppm. Chemical analyses of deposits collected for three hours at 600, 500 and 400°C showed that ChlorOut removed or greatly reduced the Cl content of the deposit by converting KCl into K_2SO_4. The key elements from the analyses are shown in Tables 2 and 3. During these tests the fuel burnt was 5% coal, 47.5% demolition wood and 47.5% logging residues.

Table 2. Deposit analyses of key elements, in wt % (by ASEM) and corresponding KCl levels in the flue gas, in Nyköping. Ring temperatures 500 and 600°C. Fuel 5% coal, 47.5% demolition wood and 47.5% logging residues.

	With ChlorOut: KCl (g) 17 ppm				No ChlorOut: KCl (g) 30 ppm			
Element	600°C wind	600°C lee	500°C wind	500°C lee	600°C wind	600°C lee	500°C wind	500°C lee
Na	1.5	1.4	1.1	1.8	0.3	1.0	0	0.7
S	11.4	9.7	10.3	8.0	5.8	13.0	5.7	6.8
Cl	0	0	0	0.1	1.3	0.3	2.9	2.2
K	17.4	11.9	16.5	9.9	8.4	21.4	8.0	11.2
Ca	6.4	6.7	6.3	4.2	19.5	12.3	19.3	17.2

Table 3. Key elements and compounds found on leeward side of deposits collected at 400°C, in Nyköping. Same conditions as in Table 2. Elements in wt% by ASEM and compounds by TOF-SIMS. The results show that KCl has been converted into K_2SO_4 by ChlorOut.

Element	No ChlorOut In wt %	With ChlorOut In wt %		Compound	No ChlorOut Relative conc. (total = 1)	With ChlorOut Relative conc. (total = 1)
Na	1.0	1.5		NaCl	0.044	0.055
S	5.2	8.9		Na_2CO_3	0.005	0.007
Cl	7.5	0		Na_2SO_4	0.022	0.063
K	20.7	6.7		KCl	0.628	0.067
Ca	10.4	2.2		K_2CO_3	0.016	0.021
				K_2SO_4	0.284	0.787

The results of corrosion probe testing of superheater steels are shown in Figure 3.

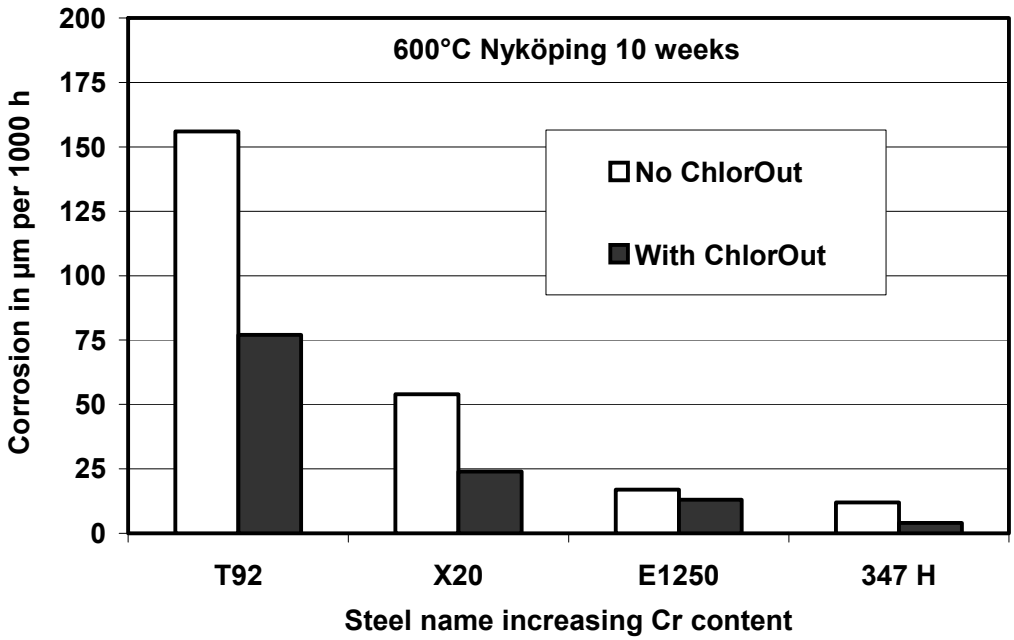

Figure 3. Corrosion per 1000 hours for various steels tested in Nyköping. Exposure time was 10 weeks. Average metal temperature was 580°C without ChlorOut and 602°C with ChlorOut. In spite of a 20°C higher temperature the corrosion rates were lower with ChlorOut.

The ChlorOut additive reduced corrosion by 50% for the 9–12% Cr martensitic steels T92 and X20. The 2 austenitic stainless steels Esshete 1250 and TP 347 H show much lower corrosion rates, with or without ChlorOut. T92 (a development of the 9% Cr steel T91) or T91 itself, are sometimes chosen as replacements for X20; they have higher strengths and can therefore be used with thinner wall-thicknesses. Fig. 3 shows that it is not a good idea to use 9% Cr steels for biomass plants with 540°C steam. In the plant in Nyköping the original X20 superheaters were replaced with Esshete 1250 in 1998, because of corrosion problems and have since shown low corrosion rates.

When ChlorOut was in use it was noted by the staff that operational problems were generally fewer than in previous years and it was easier to control the steam temperatures in the superheaters. In addition, NOx emissions were reduced by 20 mg/MJ. When ChlorOut was switched off, temporarily, an increase in the amount of fouling was seen on SH 2 and 3. After ChlorOut was switched off for the 10 week corrosion tests, the inlet of SH 3 became completely blocked.

The air pre-heaters in Nyköping are made of the austenitic stainless steel AISI 316 (SS 2343, WNr 1.4436) which contains 16–18% Cr, 11–14% Ni and 2.5–3%

Mo. Corrosion probe tests near the air pre-heaters, with a temperature gradient of 60–130°C, showed that corrosion with and without ChlorOut was negligible in both cases. However, the corrosion rate with ChlorOut was slightly lower than without ChlorOut, below about 100°C [7].

3.2 Results from Munksund

ChlorOut reduced the growth rate of deposits measured in 3 hour exposure tests by at least 50% in all cases. The key elements from the deposit and flue gas analyses are given in Table 4.

Table 4. Deposit analyses in wt % (by ASEM) and KCl and SO_2 (by IACM) in the flue gas, in Munksund. Chloride levels by dissolving the deposits in de-ionised water, analysing by ion chromatography and compensating for deposit mass. Ring temperatures 400 and 500°C; the f*uel is bark with 6% waste from cardboard recycling.*

	With ChlorOut: SO_2 22–40 ppm KCl (g) 0.5–1.9 ppm.				No ChlorOut: SO_2 23–28 ppm KCl (g) 14–19 ppm			
Element	400°C wind	400°C lee	500°C wind	500°C lee	400°C wind	400°C lee	500°C wind	500°C lee
Na	2.4	1.3	2.5	1.6	2.4	1.7	2.4	1.7
S	10.0	6.1	10.1	5.8	5.5	2.6	5.5	3.1
Cl	0	0	0	0	13.8	4.2	9.6	4.3
K	6.9	5.0	8.3	5.0	17.2	7.2	14.0	7.4
Ca	12.3	24.7	13.0	24.5	13.8	21.4	15.4	21.6
Chloride	0.14		0.22		3.6		6.6	
Weight gain	31 mg		24 mg		66 mg		50 mg	

Table 4 shows that during short-term tests ChlorOut greatly reduced the amount of $KCl_{(g)}$ in the flue gas from about 20 to 2 ppm. This led to a large decrease in the chloride content of the deposits. The Cl level was below the limit of detection by ASEM. Deposit growth rates, as measured by weight gains, were approximately halved by ChlorOut.

In Figures 4 and 5 the results are shown of GDOES profiling through the surface of 13CrMo44 rings. The oxide layer is approximately 2 µm thick in the case with no ChlorOut, but only 0.5 µm thick with ChlorOut. Cl has diffused much further into the oxide in the former case.

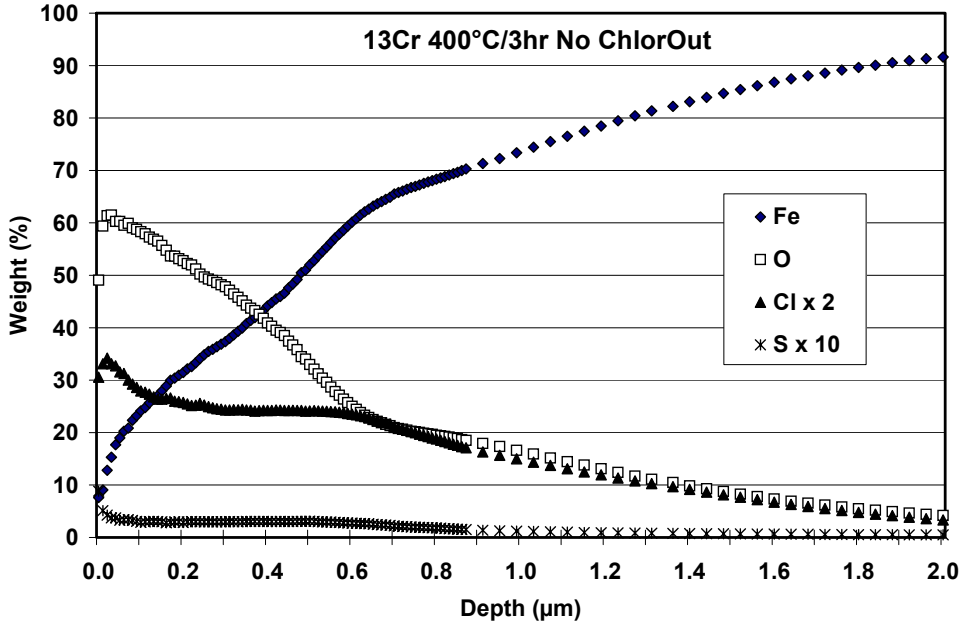

Figure 4. Composition profiles for Fe, O, Cl and S from the surface into the steel after exposure for 3 hours. Fuel is bark with 6% waste.

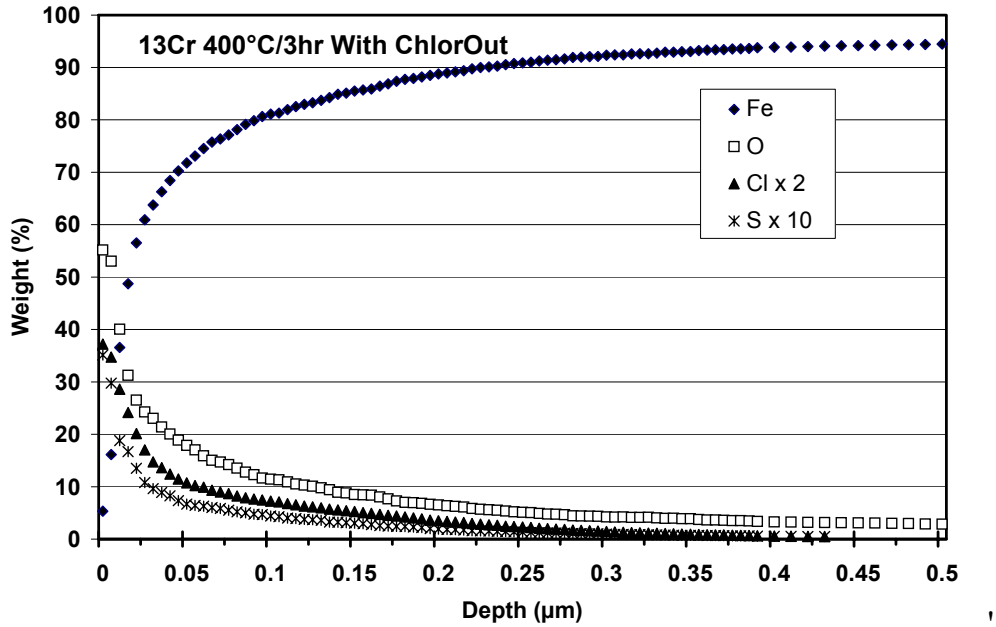

Figure 5. Composition profiles for Fe, O, Cl and S from the surface into the steel after exposure for 3 hours with ChlorOut. Fuel is bark with 6% waste.

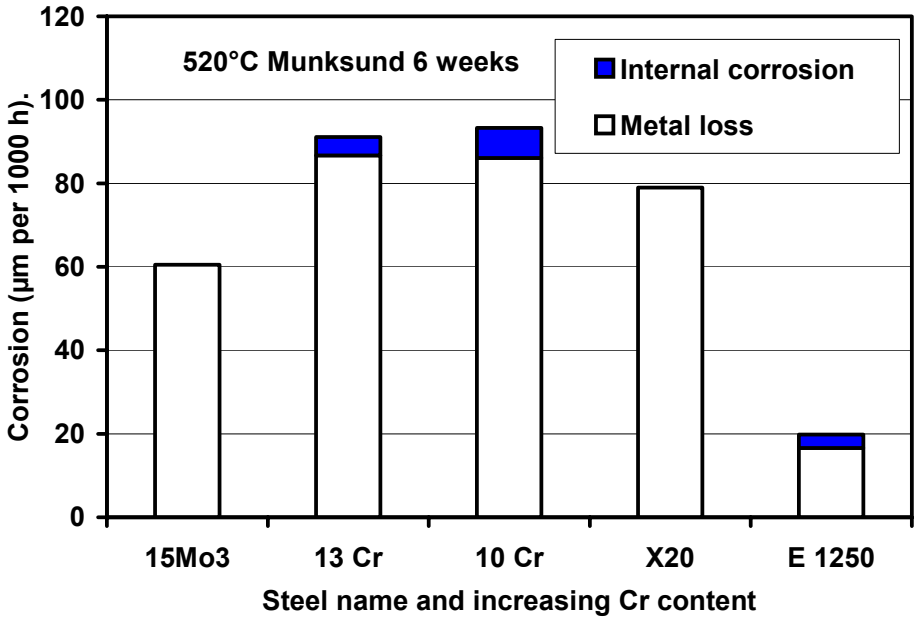

Figuree 6. Corrosion rates per 1000 hours for various steels tested in Munksund.

Figure 6 shows that increasing the chromium content of steels from the 0% of 15Mo3 to 1% in 13Cr, 2% in 10Cr or even 10% in X20 did not lead to a reduction in corrosion rates. However the stainless steel Esshete 1250, containing 15% Cr, showed very low corrosion rates. Examination with analytical SEM showed that in Esshete 1250 Cl was found in the deposit on top of the oxide, but in the other steels Cl was found at the metal-oxide interface.

4. Discussion

The use of "ChlorOut" reduced the corrosion rates of the steels in Nyköping. The overall gaseous reactions in the case of ammonium sulphate and KCl are as follows with KCl being converted into HCl and K_2SO_4. (The ammonia produced is used to reduce NOx).

$$(NH_4)_2SO_4 \rightarrow 2\ NH_3 + SO_3 + H_2O$$
$$SO_3 + H_2O + 2KCl \rightarrow 2HCl + K_2SO_4$$

A deposit containing only alkali sulphates has a higher first melting point than a deposit containing alkali chlorides, [8] and as molten phases increase the corrosion rate, alkali sulphates are preferred to alkali chlorides in the deposits.

It is known that co-firing wood fuel with sulphur containing fuels like coal decreases the corrosion rate, [9]. It has been shown that the addition of SO_2 to a He-O_2-HCl mixture led to a decrease in corrosion under deposits made from waste incinerator fly-ash and that no chlorides were found in the deposits after

the experiments [10]. It has also been shown that the addition of SO_2 to pure oxygen reduced the oxidation rate of T22 in the range 500–600°C when no deposits were involved [11]. In this case the suppression of oxidation was suggested to be due to the formation of small amounts of iron sulphate which interfered with the oxidation process.

Elemental sulphur, mixed directly with the wood fuel is the most obvious source of sulphur for use in 100% biomass firing, but it has been previously shown that sulphur leads to a great increase in the SO_2 level of the flue gases at the superheaters and an increase in the acidity and sulphate content of water from condensed flue gas at the cold end of the boiler [12]. This carries with it an increased risk for low temperature corrosion. In Nyköping ChlorOut showed only positive effects in terms of reduced corrosion and fouling and none of the negative effects like increased low temperature corrosion. This is probably because ChlorOut is sprayed as a liquid into the flue gases after combustion, thus ensuring good mixing.

In Nyköping, the corrosion rate of steels decreased with increasing alloying content, principally Cr and Ni. In Munksund, no such trend could be seen. This lack of correlation between alloying content and corrosion behaviour in biomass or waste fired boilers has been seen before e.g. [6, 13]. However the 15% Cr steel Esshete 1250, which also contains 6% Mn, performed well in both boilers.

In Nyköping when superheater 3, previously made of X20, was due to be replaced, the 9% Cr steel X10/T91was offered as a replacement at a total cost of 0.25 MEuro. Esshete 1250 was instead chosen at a total cost of 0.4 MEuro. Inspite of a higher investment cost the long-term savings in using E1250 are in the range of 20–60 kEuro per year because of increased lifetime.

ChlorOut resulted in a 50% reduction in the corrosion rate of ferritic/martensitic steels. Because ChlorOut also reduces NOx, the additional cost of ChlorOut is offset by a reduction in the use of ammonia. ChlorOut also reduces fouling, leading to a reduction in unplanned outages.

5. Conclusions

Superheater probe testing showed that ammonium sulphate halved the corrosion rate of ferritic/martensitic steels in a wood-fired boiler and reduced the fouling rate. The stainless steel Esshete 1250, which contains only 15% Cr also showed very low corrosion rates compared with other common superheater steels.

6. Acknowledgements

We thank Mattias Mattsson and Annika Stålenheim, Vattenfall Utveckling, for their invaluable work in this project. We also thank Thomas Björk, Institute for Metals Research, Stockholm, for the GD-OES measurements and Peter Sjövall, SP, Borås, for the TOF-SIMS results. This work was financed jointly by Vattenfall's "Renewable Fuels and Tools" programme and the EU project CORBI, no. ENK5-CT2001-00532.

References

1. P. Henderson, A. Kjörk, P. Ljung & O. Nyström. Värmeforsk report 700. June 2000. Värmeforsk Service AB, Stockholm. (In Swedish).
2. P. J. Henderson, A. Karlsson, C. Davis & P. Rademakers *et al.* Proc. 7th Liège Conf. Materials for Power Engineering. Pp. 785. Eds. J Lecomte-Beckers *et al.* Forschungszentrum Jülich, Germany, 2002.
3. H.P.Nielsen, F.J. Frandsen, K. Dam-Johansen & L.L. Baxter. *Progress in Energy and Combustion Science,* 2000, 26, pp. 283–298.
4. IACM. Swedish Patent SE 9903656-8, 2001. International Patent application PCT/SE 00/01866 (2000)
5. ChlorOut. Swedish Patent SE 0100220-3, 2003. International Patent application PCT/SE 02/00129 (2002)
6. P.J. Henderson, P. Ljung, S-B Westberg & B. Hildenwall. Proc. Conf. *Advanced Materials for 21st Century Turbines and Power Plant*. Pp. 1094–1104. Eds. A. Strang *et al*. IOM, London. Book 736, 2000.
7. B. Hildenwall. Vattenfall Utveckling. Private communication, 2002.
8. K. Iisa, Y. Lu & K. Salmenoja. *Energy & Fuels*, 13, pp. 1184–1190, 1999.
9. P.J. Henderson, Th Eriksson, J. Tollin & T. Åbyhammar. Proc. Conf. *Advanced Heat Resistant Steels for Power Generation*. Eds. R. Viswanathan & J. Nutting. IOM Communications, London, 1999. Pp. 507.
10. M. Spiegel. *Materials at High Temperatures,* 1997, 14, pp. 221.
11. A. Järdnäs, J.-E. Svensson & L.-G. Johansson. Materials Sci. Forum 2001, 369–372, pp. 173.
12. P. Henderson, H. Kassman & C. Andersson. Proc. Conf. "Power Plants in Competition" VGB Conference, Cologne, March 2003. To be published in VGB Power Technology June 2004.
13. P. Makkonen. *VGB Power Tech* 2003, No 8, pp. 80.

Trends of fluidized bed boiler industry to meet the requirements of future power generation

Jouni Hämäläinen, Antti Tourunen & Jaakko Saastamoinen,
VTT Processes, P.O.Box 1603, FIN-40100 Jyväskylä, Finland

Abstract

The age profile of the existing power plants results in a high demand for new power production capacity within the next years. The replacement or the modernisation of the old power plants utilising modern technology with high steam parameters and high efficiencies would contribute to the saving of the resources and to the reduction of all kind of emissions. The new investments must be able to compete decades forward in order to secure competitive power production. CFB combustor with high fuel and operational flexibility including wide range of coals would give an extra opportunity for the operators to improve competitiveness in power generation business.

Currently circulating Fluidized Bed (CFB) boilers with conventional design have been successfully demonstrated at the < 300 MWe scale. The net efficiency of those plant designs are on level of 38–40% depending on fuel and condenser conditions. During the past years, the once through supercritical (OTSC) CFB technology has been developed and readiness to propose commercial projects at medium scale < 500 MWe has been created. The CFB technology has many advantages also in utility scale (fuel and operational flexibility, multifuel capability, low emissions, in-situ sulphur reduction, etc), that would fulfil the requirements of utility operators at deregulated energy markets. In addition the foreseen need for new power production capacity which should first compensate the retirement of the older units and second cover the forecasted increase in electricity demand will require new clean coal technologies to secure coal competitiveness and improve acceptance of coal utilisation in power production. New plants with supercritical steam parameters can now achieve overall net efficiencies in the 43–45% range but even higher efficiency, up to 50%, is achievable due to development of new superheater materials.

1. Introduction

Fluidized bed combustion has well-known advantages including fuel flexibility, multifuel capability, low emissions, in-situ sulphur reduction, etc. that have proven viability of the technology at industrial scale applications. In the future power plant operators must act at deregulated energy markets that will emphasize competitiveness of utilities in operation. Naturally this means actions to improve cost-effectiveness of power generation. Solid fuel fired power plants have a balanced cost structure, i.e. investment, fuel and operation and maintenance (O&M) costs contribute almost equally to the electricity generation costs. Therefore, one way to improve cost-effectiveness of power generation is improved fuel flexibility if feasible. Usually the enlarged fuel flexibity means use of more demanding fuels on manner of ash behaviour. Also the physical characteristics may differ from the traditional fuels and cause unstability on fuel handling and feeding processes. The fluidized bed technology is very fuel flexible but still one the main trends is to enlarge the fuel selection and achieve high plant availability also with demanding, opportunity, fuels. This means R&D activities not only on combustor design itself but also much attention on fuel receiving, handling and feeding processes too. At the same time high environmental performance with even tighter emission limits must be quaranteed.

The other trends of fluidized bed technology address to scaling up the technology and improve the power generation efficiency. At present fluidized bed boilers represent the market for relatively small units, in terms of utility requirements. Today the largest circulating fluidized bed in operation is 300 MWe. However, the development even larger boilers up to 600–800 MWe is going on. Those large scale fluidized bed boilers will apply supercritical once through steam cycle achieving clearly higher power generation efficiency compared to current natural circulation boilers.

2. Widening the fuel selection

There is a growing interest in utilising renewable fuels in multifuel applications. Main reasons for this are environmental; reduction of CO_2 emissions as well as emissions of NO_x and SO_2. Widening the fuel selection is, however, one way to improve plant competitiveness by utilising fuels with lower cost, industrial residues etc. Usually enlarging the fuel spectrum sets new demands not only for operators but also for boiler design and process control as well as fuel handling systems. The physical and chemical characteristics of biofuels affect highly on fuel combustion behaviour compared to “traditional” fuels. Figure 1 below shows the fuel selection that can be used in fluidized bed boilers.

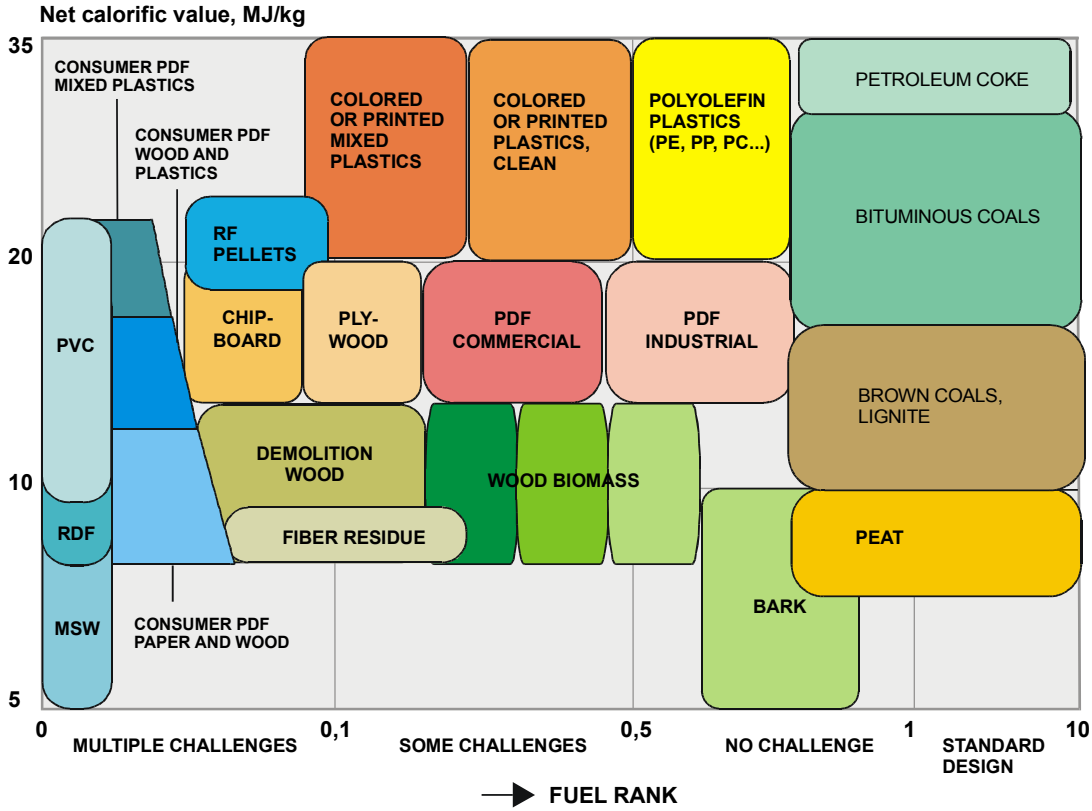

Figure 1. Fuel range applicable for fluidized bed combustion. Right hand fuel that have standard boiler design but moving to left side the fuel characteristic cause more challenge for multifuel operation and boiler design.

Due to ash properties the biomass based fuels set new requirements for boiler design and operation to achieve high plant availability and performance. The chemical composition of the ashes, such as alkali metal, phosphorous, chlorine, silicon and calcium contents affects on ash melting behaviour and further on may contribute to the fouling and durability of the heat transfer surfaces in the boiler. However, the behaviour of a biomass fuel is affected by an existence of other fuels. It has been shown that fouling tendency of biomass ash can be prevented by co-firing biomass based fuels with sulphur-containing fuels like peat or coal. Also the other ash composition in peat and coal, like aluminium silicates, may react with alkaline metals released from biomass and, therefore, prevent formation of ash deposition.

The biomass physical characteristics also affect largely on plant operation and performance. The biomass based fuels has lower bulk density compared to “traditional” fuels. They also have much more varied particle size distribution as well as moisture content. These all affects on fuel production, transport, receiving and handling systems and sets therefore additional demand to fuel handling and feeding systems at the plant. Below, in Figure 2, is shown measured stability of the fuel feeding rate for peat (up) and for peat/bark mixture (down).

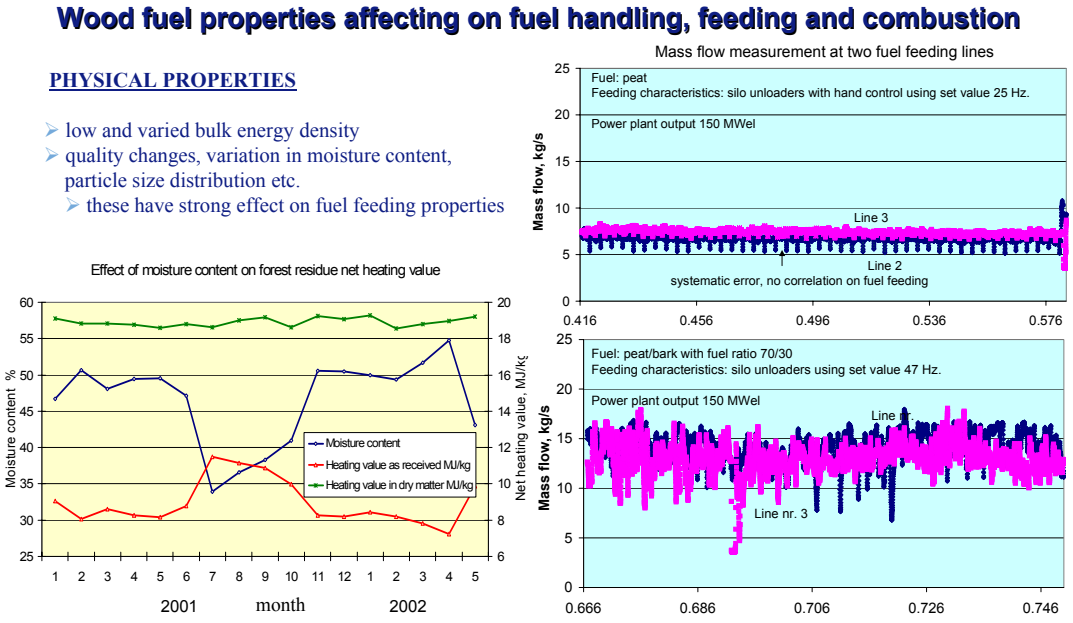

Figure 2. Seasonal variation of biomass heating value (moisture content). Example of biomass blending on fuel mass flow rat.

Obviously the fluctuation of fuel feeding flow will effect on stability of plant operation increasing the emissions of power generation but also operation and maintenance costs as well. To improve the fuel mass flow control by advanced feeder designs and on line control methods the overall plant operation can be improved in multi-fuel applications.

3. Scaling up the technology and improving the efficiency

Currently circulating Fluidized Bed (CFB) boilers with conventional design have been successfully demonstrated at the < 300 MWe scale. The net efficiency of those plant designs are on level of 38–40% depending on fuel and condenser conditions. During the past years, the once through supercritical (OTSC) CFB technology has been developed and readiness to propose commercial projects at medium scale < 500 MWe has been created (See Figure 3.). Scaling up the technology further up to 800 MWe size is logical step to fulfill the requirements needs of utility operators.

CFB technology has many advantages in utility scale, as have discussed above also, that would fulfil the requirements of utility operators at deregulated energy markets. New plants with supercritical steam parameters can now achieve overall net efficiencies in the 43–45% range but even higher efficiency, up to 50%, is achievable due to development of new superheater materials. Currently the

largest fluidized bed boiler under construction is a 460 MW_e power plant based on CFB supercritical OTU technology. Location of the plant is in southern Poland at the Poludniowy Koncern Energetyczny (PKE) Łagisza. The boiler applies high fuel flexibility burning coal from 10 different coal mines and coal slurry (washery reject) up to 30% and dried coal washery reject up to 50%. There exists also a provision to burn 10% biomass in the future. The power plant meets EU large combustion plant (LCP) directive without selective catalytic reduction (SCR) system for NO_x or flue gas desulphurization (FGD) unit. Sulphur reduction is performed applying in furnace sulphur capture.

These inherently favourable combustion conditions for emission performance guarantee competitive investment cost that together with high fuel flexibility and multi-fuel capability secure cost-effective power generation and improved competitiveness for operator.

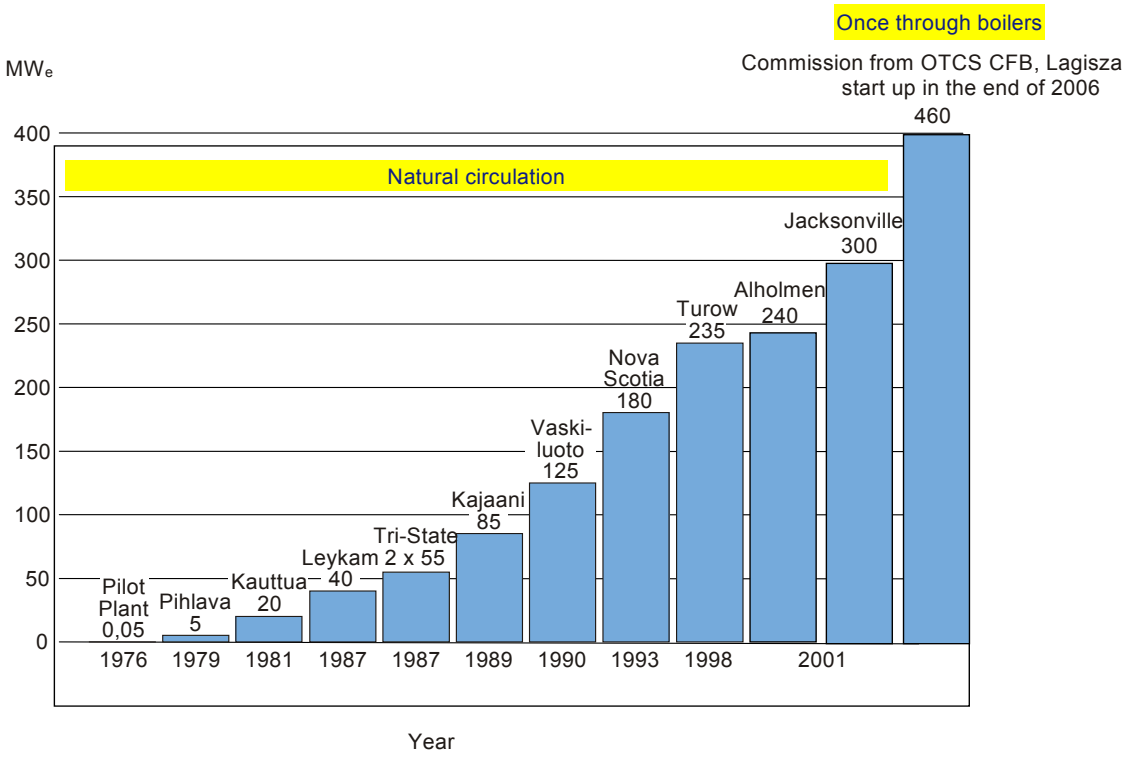

Figure 3. Scale up of CFB technology during 30 years.

4. Conclusion

Fluidized bed combustion has well-known advantages including fuel flexibility, multifuel capability, low emissions, in-situ sulphur reduction, etc. that have proven viability of the technology at industrial scale applications. In the future power plant operators must act at deregulated energy markets that will emphasize competitiveness of utilities in operation. Solid fuel fired power plants have a

balanced cost structure, i.e. investment, fuel and operation and maintenance (O&M) costs contribute almost equally to the electricity generation costs. Therefore, one way to improve cost-effectiveness of power generation is improved fuel flexibility if feasible. Currently circulating Fluidized Bed (CFB) boilers with conventional design have been successfully demonstrated at the < 300 MWe scale. During the past years, however, readiness to propose supercritical (OTSC) CFB technology has been created at medium scale < 500 MWe. Scaling up the technology further up to 800 MWe size is logical step to fulfill the reguirements needs of utility operators.

Literature

Hämäläinen, J., Orjala, M., Järvinen, T., Kärki, J. & Vainikka, P. Variation, effect and control of forest chip quality in CHP, BIOENERGY2003, International Nordic Bioenergy Conference, Jyväskylä, Finland, 2nd–5th September, 2003, pp. 225 – 232.

Tourunen, A., Saastamoinen, J., Hämäläinen, J., Paakkinen, K., Hyppänen, T. & Kettunen, A. Study of Operation of a Pilot CFB-reactor in dynamic conditions, Proceedings of 17th International Conference on Fluidized Bed Combustion 18–21.5.2003, Jacksonville, Florida.

Fuel blend characteristics and performance of co-fired fluidised bed boilers

Markku Orjala, Pasi Vainikka, Janne Kärki & Jouni Hämäläinen
VTT Processes
P.O.Box 1603, FIN-40101 Jyväskylä, FINLAND
Tel. +358 14 67 2611, Email: name.surname@vtt.fi

Abstract

When co-firing biomass fuels with fossil fuels, following implications may be expected: increased rate of deposit formation, shorter sootblowing interval, bed material agglomeration, increased risk of corrosion, higher in-house power consumption etc. Deposit formation inhibits heat transfer and reduces boiler efficiency, additionally chlorine rich deposits induce hot corrosion of heat transfer surfaces. Due to this operating and maintenance costs can increase, but this can be diminished or even avoided with appropriate fuel blend and process control.

Effect of different fuels on deposition and corrosion have been studied by deposit and material testing probes, both in VTT Processes' test facilities and in power plant boilers. To support plant operators in daily decision-making and in plant operation optimisation advanced methods for combining data from deposit formation monitoring and process calculations are being developed. These methods will help operators to achieve better boiler performance with improved fuel flexibility.

Use of biomass fuels reduces emissions but may cause harmful forming of deposition. Depending on the boiler type, it is recommended to combust 10–20% of peat with wood fuels in order to reduce above mentioned operational problems. If wood fuels consist mainly of new tree growth, like logging residue, it is favourable to use even higher share of peat, 30–40%, as co-firing fuel.

1. Background

Taxation, legislation and market competition increasingly promotes use coal and renewable energy sources more efficiently and with wider range. National and international emission regulations, concerning especially the level of greenhouse gas emissions, and the introduction of emission trading systems can play important role in the future's energy business. This has lead to an increase in the

use of solid biomass based fuels in Fluidesed Bed Boilers and might do it also in Pulverised Coal-fired plants. Co-firing, however, poses new challenges for power plant operators. Particularly, the nature of biomass ash causes boiler fouling, which in turn decreases boiler efficiency. In order to increase fuel flexibility and achieve the most economical way for power generation, many operation parameters must be taken into account. Advanced on-line methods for ash behaviour and deposition formation monitoring as well as on-line process performance calculation methodologies have been developed and these can be implemented into power plant control systems for operators' support.

In Finland, the main provider and user of wood-based energy is the forest industry, which acquires wood fuels at a competitive price in connection with raw material procurement or as a by-product of wood processing. About 35 million cubic metres of solid wood (271 PJ) is used annually for energy production in Finland, covering the aforementioned 20% of the total consumption of primary energy. Most of wood-based energy is recovered from liquid (black liquor) and solid industrial wood residues (bark, sawdust etc.). During the recent five years more than 100 district heating plants and 500 MW_e of new additional capacity for electricity production from wood-based fuels have been commissioned in Finland (total capacity more than 2 000 MW_e).

In larger CHP plants, FBC technology has become a dominant technology. Simultaneously, fuel-handling technologies have been developed. Also a lot of effort has been focused on utilising wood residues from the forest industry. In recent years, use of forest residues has been increasing. Integrating the fuel and raw material supply chains has decreased the costs of forest fuels.

Utilisation of biomass fuels and wastes may, however, cause unexpected problems during power production. The quality of ash in biomass fuels differs remarkably in chemical manner from ashes of coals and peat. Alkaline metals, that are usually responsible for fouling of heat transfer surfaces, are abundant in biomass and will be easily released during combustion in gas phase. In addition, several observations have shown that alkali metals and chlorine in biomass cause hot corrosion especially at low sulphur conditions. Characterisation of fuel behaviour during combustion, fuel blend control and deposit formation monitoring is therefore needed to avoid decrease in power plant availability.

2. Blending of fuels equals blending of fuel properties

Biomass fuel properties, which vary in wide ranges, and the constituents of the fuel set demanding requirements for the optimisation of in-furnace conditions, and for the materials and structure of furnace membrane walls and superheaters. These properties include ash content, the chemical composition of the ash and

ash behaviour characteristics. Chemical composition of ash, such as alkali metal, phosphorous, chlorine, silicon and calcium contents, as well as the chemical composition of the compounds, affect melting behaviour of ash. This will contribute to the fouling and durability of the heat transfer surfaces in the boiler. In biomass fuels alkaline metals are in the form of salts or are bound in organic matter, but for example in coal inorganics are bound in silicates which are more stable. Chlorine can also be bound in organic matter. Deposit formation inhibits heat transfer and reduces boiler efficiency, additionally, chlorine rich deposits induce hot corrosion of heat transfer surfaces

Throughout the combustion process, the behaviour of a biomass fuel is affected by an existence of other fuels. It has been shown that even a small concentration of chlorine in logging residue chips will result in the harmful formation of alkaline chloride compounds on boiler heat transfer surfaces. This could be prevented by co-firing sulphur and aluminium silicate -containing fuel: when peat or coal is blended with biomass fuel such deposition formation can be prevented. In the latter case, vaporised alkaline metals of biomass ash are bound in sulphur and aluminium silicate compounds, the amount of alkaline chlorides in deposits is reduced or these are not formed at all, and chlorine is released as HCl to flue gases. The risk of bed agglomeration usually grows as the amount of alkaline metals (sodium and potassium) increases. When logging residue chips are combusted, the particle size of the bed material has been detected to grow. When peat is added, this phenomenon disappears.

Ash characteristics have important role also in boiler design, because deposit formation, erosion, corrosion and defluidisation of the bed sand should be minimised. Ash-forming matter in biomass fuels can be present in several forms: as soluble ions, associated to organic matter or as minerals. The form in which the ash-forming matter is present affects the behaviour of fuel ash. There are significant differences in how ash-forming elements are distributed in different fuels. In older fuels, ash-forming elements are present as minerals. In relatively young fuels, up to half of the ash-forming elements can be organically associated or present as easily soluble salts or as minerals.

According to present knowledge, control of the rate of deposit formation in biomass combustion is associated with the reactions between compound that contain chlorine, sulphur, aluminium silicate and alkaline substances. High-risk chlorine compounds are of the type NaCl or KCl. These alkaline chlorides can, however, react with sulphur and aluminium silicate compounds releasing HCl.

$$2KCl + SO_2 + ½\ O_2 + H_2O \rightarrow K_2SO_4 + 2HCl \quad (1)$$

$$Al_2O_3 \cdot 2SiO_2 + 2KCl + H_2O \rightarrow K_2O \cdot Al_2O_3 \cdot 2SiO_2 + 2HCl \quad (2)$$

One parameter that has been often referred to is the sulphur-to-chlorine atomic ratio (S/Cl) in fuel or fuel blend. It has been suggested that if the S/Cl ratio in fuel is less than two, there is a high risk for superheater corrosion. When the ratio is at least four, the blend could be regarded as non-corrosive. The mechanism suggests therefore, that sulphur in the system is able to bind alkalis in sulphates (K_2SO_4, Na_2SO_4) through reactions in gas phase. However, limestone feeding, especially in fluidised bed combustion, changes the sulphur-to-chlorine balance of the gas phase. Calcium oxide, CaO, from limestone feeding or wood fuel co-firing, binds sulphur to calcium sulphate, $CaSO_4$. For this reason there is less sulphur available for sulphating potassium and sodium than fuel blend's sulphur-to-chlorine ratio indicates. In cases where there is plenty of calcium available in the system, i.e. with limestone feeding and biomass co-firing, fuel's sulphur-to-chlorine ratio should not directly be used. [1, 2]

3. Power plant availability and operation cost analysis

VTT Processes has studied the availability of wood-fired boilers in twelve Finnish power plants: four CFB and eight BFB plants with thermal output 100-300 MW. Special attention in the questionnaire was paid on the following issues:

- the connection between the reported failures and the fuels used
- fouling of heat transfer surfaces and the material effects
- behaviour of bed material; need for bed sand replacement, blockages interfering fluidisation, slag formation
- need for soot blowing
- the effects on smooth fuel feed, the homogeneity of fuels and on how fuel distributes in the furnace
- temperature fluctuations in the furnace caused by heterogeneous fuel quality and fuel feeding.

The questionnaire supported the previous experience where it was noticed that wood fuels may cause operational problems in multi-fuel operation. Many plants have faced problems with stock discharging gears, fuel conveyers and feeding gears. Usually problems originate from unsuitable equipment and their tendency to get stuck due to the unexpected nature of wood fuels. Fluid bed related problems involving bed sintering due to fluctuation of bed temperature were also common during the use of wood fuels. To decrease these problems plants replaced bed material frequency. Majority of the respondents has discovered also that wood fuels affected the rate of furnace deposition as the share of wood fuels increased. However, it was not generally found that wood fuels would increase the need for soot blowing. Adequate and functional soot blowing supports the use of wood fuel and it should be carefully recognised when plant is planning to increase the use of wood fuels. Half of the respondents noted that wood fuels

have changed the nature and composition of ash residues the reason why it is very difficult to find further use for co-combustion residues (for example in cement industry). All of the respondents stated that flue gas emissions, especially SO_2, have decreased significantly during the use of wood fuels and the need for lime usage therefore decreased. Due to high moisture content of wood fuels, the capacity of conveyers and feeder as well as flue gas fans majority of the plant operators stated that after starting the use of wood fuels the maximum power generation capacity is more difficult to achieve.

All the aforementioned aspects effect on the operating and maintenance costs of the plant in multi-fuel operation. VTT collected operating experiences from power plants in a questionnaire for a period of two years. In year 1 of the study only peat was combusted and in the year 2 wood fuels were blended with peat. For both of the periods unit costs (€/MWh_{fuel}) were calculated. The difference between those costs gives some indication about the influence of wood combustion on power plant running costs and it is possible to establish cost comparisons between the two cases. The effects of different factors were analysed separately in every plant, and the costs caused by these factors in combustion of pure peat and co-combustion of peat/wood blends were determined. Following factors were analysed:

- need for soot blowing
- need for changing bed sand
- changes in ash composition
- changes in plant's power consumption
- fuel storage.

When all the above factors affecting the costs are taken into account, the increment of the costs equals to 0.26 €/MWh_{fuel}. This corresponds to 70% wood share in the fuel blend. The results indicate, however, that even with as low wood share as 25–30% the effect of increased unit cost starts to have influence on the annual utilisation of the boiler. When small amounts of wood are used, the share being about 10%, the plants had no problems and the costs did not increase.

4. Methods for optimisation of multifuel-based bioenergy production

Understanding of deposit formation and ash behaviour is a key issue in optimising boiler operation and in securing good level of plant performance and high availability. Boiler fouling has effect on several factors at power plants. The increase in operating and maintenance costs caused by boiler fouling can increase the total energy production costs significantly. The formation of harmful deposits can be reduced or even avoided with appropriate fuel blend control. To develop

methods for optimisation of multifuel operation, combustion and co-firing properties of fuels can be studied both at VTT Processes' test facilities and at industrial-scale power plant boilers. The formation of alkaline chloride compounds in biomass combustion and their effect on deposit formation and corrosion have been monitored by deposit formation and material monitoring probes. The objective is to characterise deposit build-up and its effect on heat transfer in biomass (especially wood) combustion. With the knowledge gained it is possible to develop methodologies and mathematical models to better understand the changes in heat transfer caused by biomass co-combustion. With mathematical models and simulations, the interrelation between fuel composition and deposit formation tendency can be studied and the causalities between heat transfer, in-furnace conditions and fuel & fuel-ash characteristics correlated. The results from these calculations can be applied in estimating and optimising the factors that have effect on plant availability.

4.1 Pilot-scale combustion tests

The Bubbling Fluidised Bed (BFB) test rig has 13–15 kW fuel capacity. The height of the FB reactor is 4.1 m and it has inner diameter of 16 cm. The reactor can be heated up to the desired temperature levels by using electrical heaters and it can be cooled down by applying cool air to lower parts of the reactor. The BFB pilot plant was used for characterisation of fuel combustion behaviour at fluidised bed combustion conditions. The main focus was on establishing the effect of change in the fuel mix, in this case the share of aspen bark with peat and spruce bark and the effect of fuel blends quality on flue gas emissions and on deposition formation. According fuel analysis of used fuels: aspen bark, spruce bark and peat, Table 1, properties of spruce and aspen bark seem to be quite similar.

Table 1. Proximate and ultimate analyses of aspen bark, spruce bark and peat.

	Aspen bark	*Spruce bark*	*Peat*
Moisture content before pretreatment (%)	56.4	62.3	-
Moisture content after processing (%)	6.2	10.4	23.6
Ash content at 500℃ (%)	3.91	4.06	4.77
Ash content at 815℃ (%)	2.73	3.11	4.76
Calorimetric heating value (kJ/kg)	21422	20309	22078
Effective heating value in dry matter (kJ/kg)	20069	19055	20859
Effective heating value of wet fuel (kJ/kg)	18668	16812	15350
C-content (%)	52.5	51.1	54.7
H-content (%)	6.20	5.75	5.59
N-content (%)	0.68	0.48	1.73
O-content (%)	37.82	39.5	33.0
S-content (%)	0.06	0.03	0.16
Cl-content (%)	0.02	0.02	0.05
Moisture of fuel blends during the tests varied from 35 to 37 %			

Fuel ash analyses reveal that there are significant differences in aspen and spruce bark elemental composition. Aspen bark contains nearly two times more sodium, manganese, potassium and notably less calcium, aluminium and silicon than spruce bark. Spruce bark's ash composition is typical when compared to values found in literature. Peat ash is rich in aluminium, sulphur, iron and silicon in comparison to spruce and aspen bark, see Table 2. In terms of deposit formation propensity high Cl, Na and K contents and coincident low Al, Si and S contents can be considered as a potential risk.

Table 2. Elemental composition of ashed fuels from BFB experiments. Ashing in 500℃ prior to XRF-analysis

wt-% in ash	*Aspen bark*	*Spruce bark*	*Peat*
K	12.29	5.37	1.48
Na	0.51	0.30	1.37
Mg	3.09	1.89	1.11
Ca	26.94	31.23	7.38
Al	0.64	1.22	8.15
Mn	0.36	1.59	0.12
Fe	0.37	0.63	9.90
S	0.87	0.46	1.17
Cl	0.07	0.07	0.14
Si	2.01	4.01	21.60
P	1.38	1.09	0.93

It was found that it is advantageous to combust aspen bark with peat as a homogeneous mix. In the experiment where the fuel mix consisted of equal proportions of aspen and spruce bark, bed sand agglomeration was observed. Agglomeration was not observed when peat was added to amount for 50% of the fuel's energy content. The materials between the sand particles, suggested to cause the agglomeration, were potassium, calcium and silicon compounds. Bed-material analyses showed that Ca-, K-, Mn-, P- and Mg-concentrations increased linearly during the tests.

Deposit samples collected from the experiments with different fuel blends were analysed with SEM-EDX. In the analysis differences were found only in sulphur concentrations. In co-firing peat with bark deposit layers were mainly formed of calcium and potassium together with sulphur. When peat was not used deposits contained oxides and silicates. Phosphorus was found in small concentrations and in selected locations also chlorine. According to the elemental analysis of fly ash samples the increase of aspen bark share from 0 to 50% resulted in clearly higher concentrations of S, Ca, Mg, Na and K in filter ash, as well as higher Ca and Mg concentrations in cyclone ash.

4.2 Full-scale combustion tests

Deposit formation monitoring at full-scale boilers provides unique information on the rate of deposit formation, the effect of sootblowing and consequent changes in heat transfer. Additionally, the data from deposit formation monitoring has been shown to correlate with boiler performance, which gives basis for studying the interrelation of fuel blend characteristics – deposit formation – boiler performance. This enables the development of on-line methods for maximising boiler efficiency and quantifying the implications of applied fuel blend on boiler performance.

Power plant operators have only few ways to diminish deposition rate on the heat surfaces in the boiler. By using controlled fuel blend, the amount of the harmful substances effecting on deposit formation are also controlled. Optimising process conditions e.g. keeping furnace flue gas temperatures low enough makes it easier to avoid melting of ash. When deposits are already formatted on the surfaces, can problems be reduced by optimising cleaning of heat transfer surfaces (usually soot-blowing).

The main effect of deposits on boiler operation is the decreased heat transfer from flue gases to water and steam. This causes higher flue gas exit temperature and thus lower boiler efficiency (see Figure 1). The other effects can be listed as follows:

- deposits increase the flue gas pressure losses thus increasing the power demand for flue gas fans
- boiler operators might have to limit the boiler load so that live steam temperatures don't drop (when spray water has already reached it's minimum)
- fouling increases the need for soot blowing (or other on-line cleaning)
- the work amount during maintenance shut-downs may increase because of increased need for cleaning
- deposits have effect on life-time of boiler equipment (erosion, corrosion)
- deposit formation can cause unwanted boiler shut-downs.

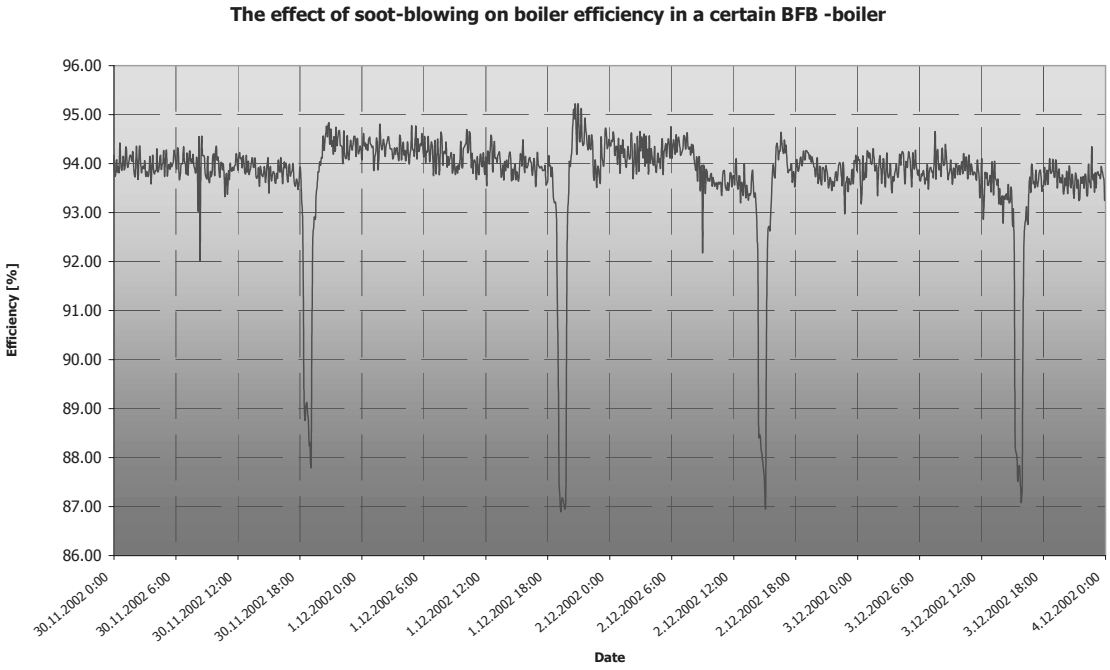

Figure 1. The effect of deposit formation and soot-blowing on boiler efficiency.

If we can achieve on an average of 0.5%-unit higher annual boiler efficiency by optimising the performance of the boiler through fouling control, we can achieve significant annual savings. The fuel saving potential for typical 300 MW_{fuel} BFB-boiler can be estimated as follows:

- Total use of fuels 2.1 TWh
- Estimated costs: 10 €/MWhfuel * 2.1 TWh/a = 21 Milj. €/a
- 0.5%-unit higher annual boiler efficiency means that we can save fuel as much as: 0.005*2.1 TWh/a = 10.5 GWh/a
- This means 10 €/MWh * 10 500 MWh/a = <u>105 000 €/a</u>.

Power plant operators examine deposit formation usually during the maintanence shut-down, which is usually done only once a year. Camera surveillance and visual observation through the holes in the boiler shows the magnitude of the deposits, but they aren't very convinient methods for on-line monitoring. Direct deposit probe measurement, however, gives on-line data on deposit formation on the heat transfer surfaces. This is also the case with data from process measurements: temperatures and pressures from the flue gas side, steam temperatures, cooling need of steam and heat transfer magnitudes calculated from the monitoring data give some kind of idea of deposition rate.

A specific deposit-monitoring probe has been developed at VTT Processes based on design, which is applied in corrosion measurements. There are several temperature and heat flux measurements in these air/water cooled heat transfer probes. During the tests the 3 metre casing remains cool whereas the temperature of the thinner 48 mm diameter head (with the bright test material rings in Figure 2) is adjusted to the level of superheater tube temperatures.

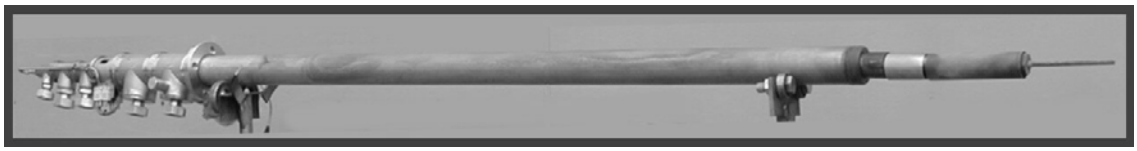

Figure 2. The deposit-monitoring probe can be applied in analysing both short- and long-term deposition build-up.

Deposit monitoring probe has many advantages:

- Probe gives continuous (on-line) information of deposition formation and the changes in deposition rate are rapidly detected.
- Changes in fuel blends are easy to see on probe data and therefore it can be used to evaluate the risks of poorly known or new fuels.
- Power plant process data contains disturbances and cannot be used to monitor short time deposition formation as well as probe data.
- Probe data is more stable than process data and results are easier to interpret.
- Deposit formatted on the probe surface can be analysed and at the same time corrosion on different materials can be studied.
- Deposit probe can be used in different parts of the boiler to find out deposit formation on the heat transfer surfaces.

As the flow rate of coolant is reduced, the side and leeward temperatures of the probe tend to increase. This is due to the reduced rate of heat transfer into the probe resulting from the long-term deposit formation. Long-term deposition build-up varies according to fuel used. In Figure 3 are presented deposit monitoring probe temperature measurements during six week campaign at BFB-boiler combusting wood, peat and REF (Recovered fuel). REF significantly increases deposit formation rate (see dotted trend-lines in figure). Boiler operators are able to do longer soot-blowing intervals when using pure peat at the end of the period.

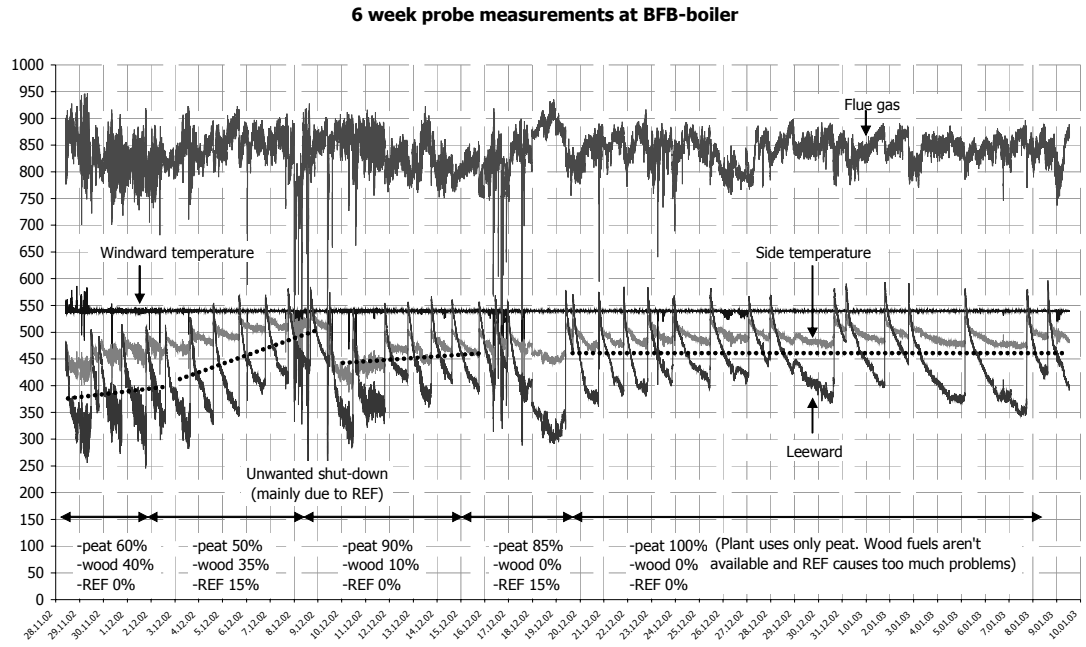

Figure 3. Temperature fluctuation on the three sides of the deposit monitoring probe during six week measurement campaign at BFB-boiler. Fuels were wood, peat and REF.

The fouling information from probe data can be compared with the measurements from the process. The coolingwater need for steam is one good indicator of the status of a superheater fouling (see Figure 4 for comparison with the spray and probe data). With the measured temperatures and heat fluxes from the probe we can obtain overall heat transfer coefficient and further on the overall thermal conductance can be obtained with overall heat transfer coefficient and the surface area. We can calculate overall thermal conductance also for real heat exchanger with logarithmic mean temperature difference and heat transfer rate. As we compare these calculations we can see that they are quite similar (Figure 5).

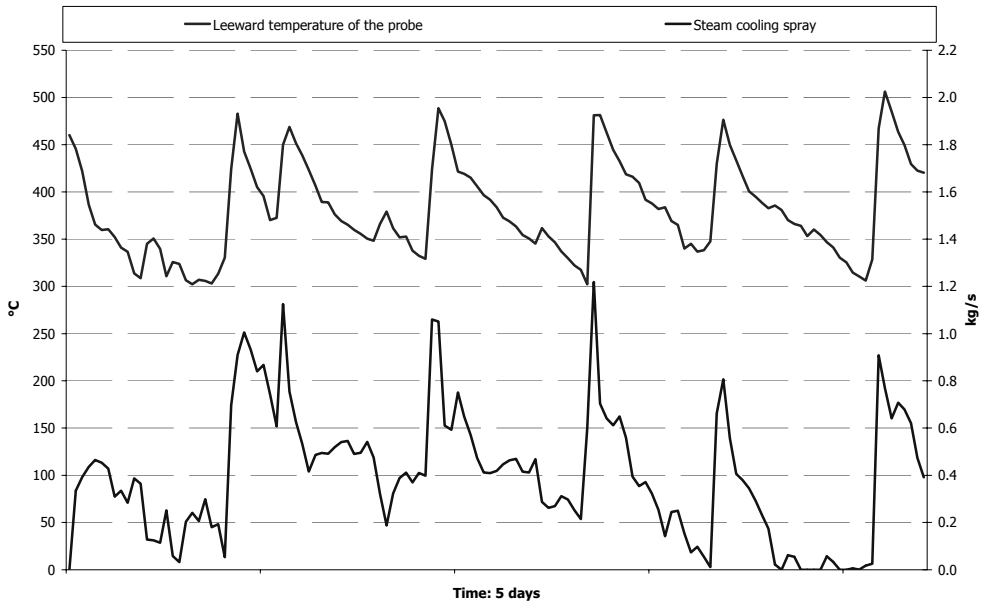

Figure 4. Probe temperature measurements (above) vs. boiler data (below).

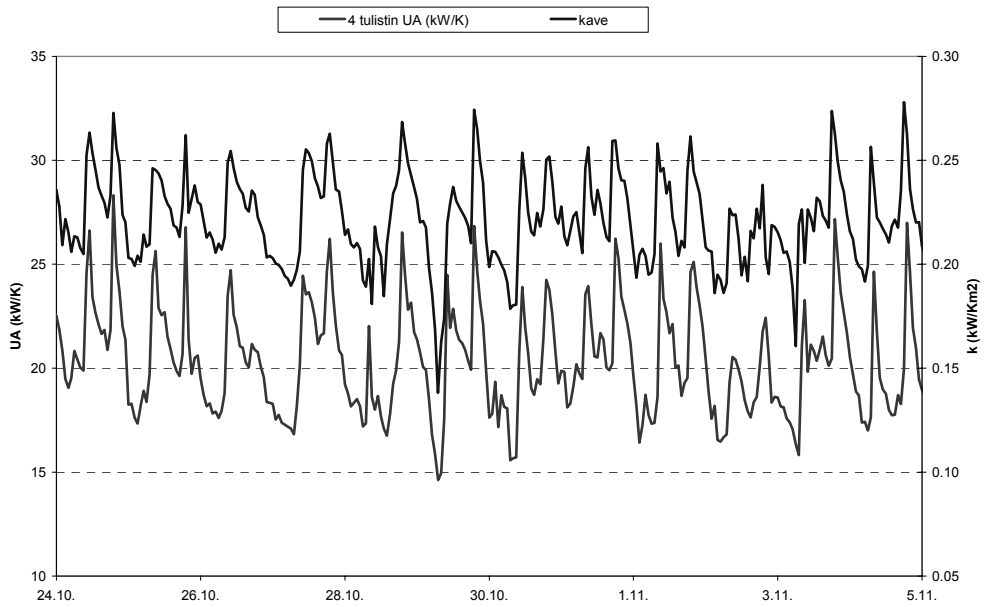

Figure 5. Overall thermal conductance from process data (below) vs. overall heat transfer coefficient from probe data (above) in a four week measurement campaign at CFB-boiler. Fuels were bark, sludge and some coal.

The rate of change in the probe's temperatures over the soot blowing intervals change according to fuels used. The rate of change in temperatures was examined together with elementary analyses of fuel and fly ash and boiler operational parameters. Correlation was detected between the rate of change in the temperatures and presence of some elementary substances. The model was developed further by widening the database of measured information, making use of previously measured data and by taking into account process conditions in the

form of heat transfer correlations. From the probe temperature data we obtain relative thermal resistances for different sides of the probe, R/R_t. This can be formulated as equation:

$$\frac{R}{R_t} = Y = Y_\infty + \left(Y_0 - Y_\infty\right) e^{-t/\tau} \tag{3}$$

On-going modelling challenge is to find correlation between parameters (Y_∞, Y_0 and τ) and deposit properties and process conditions. Such evolution gives basis for developing a tool for evaluating optimal fuel blends and soot blowing intervals without any probe measurements. In addition, it is possible to quantitatively estimate how much different fuel types inhibit heat transfer in the furnace and consequently boiler operation. With the aid of measurements, analysis and modelling methods the impact of fuel blend and fuel-ash on deposit formation and heat transfer has been established.

5. Conclusions

Fuel and process optimisation is needed when substituting ordinary fuels with solid biomass fuels. As fuel blending changes the behaviour of fuels in combustion, optimisation of the proportion of fuels in the fuel blend is required. Several approaches are available for the optimisation work. Pilot-scale reactors have been applied in studying the interaction of sulphur – chlorine – aluminium silicate species in order to find optimal shares of fuels in terms of safe and efficient combustion. At large-scale plants deposit formation monitoring methods have been developed for optimising boiler performance from heat transfer point of view. The primary goal of future work is to develop monitoring methods for boiler users, so that they can use produced fouling and slagging information in fuel and process optimisation and thus achieve better boiler efficiency and operation economics.

References

[1] Makkonen P. Artificially Intelligent and Adaptive Methods for Prediction and Analysis of Superheater Fireside Corrosion in Fluidized Bed Boilers. Acta Universitatis Lappeenrantaensis 98, Lappeenranta University of Technology, 1999, PhD Thesis. ISBN 951-764-375-6.

[2] Salmenoja, K. Field and laboratory studies on chlorine-induced superheater corrosion in boilers fired with biofuels. Faculty of Chemical Engineering, PhD Thesis, Report 00-1, Åbo Akademi University, 2000. 102 p.

Gasifier for biofuels and recycled fuels – A way to extend existing boilers' fuel mix

Juha Palonen
Foster Wheeler Energia Oy
Varkaus, Finland

Timo Eriksson
Foster Wheeler Energia Oy
Varkaus, Finland

Abstract

Gasification offers a number of energy options for supplementing and diversifying the coal-fired generating base, and for dealing with the waste based fuels in Europe when new directives on landfills come into force soon. Foster Wheeler has steadily developed its CFB gasification technology and recently completed a unit for Electrabel in Belgium.

1. Introduction

The Foster Wheeler Circulating Fluidized Bed (CFB) Gasification Technology was developed in the early 1980's, the development work being driven by very high oil prices. The first commercial scale CFB gasifiers, using 17 to 35 MW of dry waste wood as feedstock, were delivered for the pulp and paper industry in the mid 80's for substituting oil in the lime kiln process. During the 1990's, a gasification process producing raw gas from a variety of biomass and recycled fuels to be co-combusted in a pulverized coal (PC) boiler was developed. Additionally, three commercial scale atmospheric CFB/BFB gasifiers with fuel inputs from 40 to 70 MW have been delivered in the years 1997–2003.

Based on the recent success and evaluation of the future needs, Foster Wheeler Energia Oy (FW) has during the recent years been developing a gasification concept for converting difficult, mainly waste derived solid fuels into clean gas to be co-combusted in existing boilers. The first project with this concept, including an 80-MW gasifier, hot gas cleaning equipment and co-combustion in a PC boiler is in the design phase. However, there will be a delay in this project: The administrative court returned the permitting issue to the lower authority that had earlier given the permit. But an appeal to the high court has been prepared and provided to. However, the process will take another 6–12 months, but the readiness for the investment is being kept all the time by the customer.

2. Gasification advantages

With fluidized bed gasification, cheap and potentially CO2 neutral solid fuels can be converted into combustible gas for replacing expensive oil, natural gas or coal. Locally available low-grade fuels such as wood chips, wood waste, bark, demolition wood, straw and wastes such as REF (in-origin classified recycled fuel) and RDF (refuse-derived fuel) have been successfully gasified. A CFB gasifier is a true multifuel unit with good fuel flexibility, i.e. the above-mentioned fuels can be used in the same unit - though the heat output varies with the heat value of the fuel. By connecting a gasifier for instance to a PC boiler, cheap solid fuels can be converted to power and heat at very high efficiency, compared with stand-alone units with the same fuel input. The gasifier – PC boiler process connection also offers low investment and operation costs, utilization of existing power plant capacity with small modifications to the main boiler, high plant availability and reduction of the boiler emissions.

When using the clean gas concept, i.e. by cleaning the product gas prior to the combustion, it is possible to utilize in a safe way difficult, e.g. waste based fuels in a high efficiency PC boiler without fear of fouling risk or possible DeNOx catalyst poisoning risk which both can possibly result from direct co-firing of difficult solid fuels in PC boilers (See chapter 5).

Table 1 summarizes the Foster Wheeler atmospheric gasifier references.

3. FW CFB gasification

The atmospheric CFB gasification system developed by FW is relatively simple. It consists of a reactor where gasification takes place, a cyclone to separate the circulating bed material from the gas, and a return pipe for returning the circulating material to the bottom part of the gasifier. All these components are entirely refractory lined. From the cyclone, the hot product gas flows into an air preheater located below the cyclone. Gasification air is blown with a high-pressure air fan to the bottom of the reactor, below a bed of particles through an air distribution grid. Air enters the gasifier at a velocity high enough to fluidize the bed particles and convey some of them out of the reactor and into the cyclone. In the cyclone, gas and circulating solid material flow in the same direction – downwards – and both the gas and solids are extracted from the bottom of the cyclone. The following figure shows the main components of a CFB gasifier.

Fuel is fed into the lower part of the gasifier, above the air distribution grid. The incoming biofuel typically contains 20–60% of water, 40–80% of combustibles and 1–2% of ash. Depending on the fuel and application, the operating

temperature in the reactor is 800–1000°C. When entering the reactor, the biofuel particles start to dry rapidly, and a primary stage of reaction, namely pyrolysis, occurs. During this reaction, fuel converts to gases, charcoal, and tars. Part of the charcoal flows to the bottom of the bed and is oxidized, generating heat. The products flow upwards in the reactor, and a secondary stage of reactions take place. These reactions can be divided into heterogeneous reactions, where char is one ingredient in the reactions, and homogeneous reactions where all the reacting components are in the gas phase. A combustible gas produced from these and other reactions then enters the cyclone and escapes the system together with some fine dust.

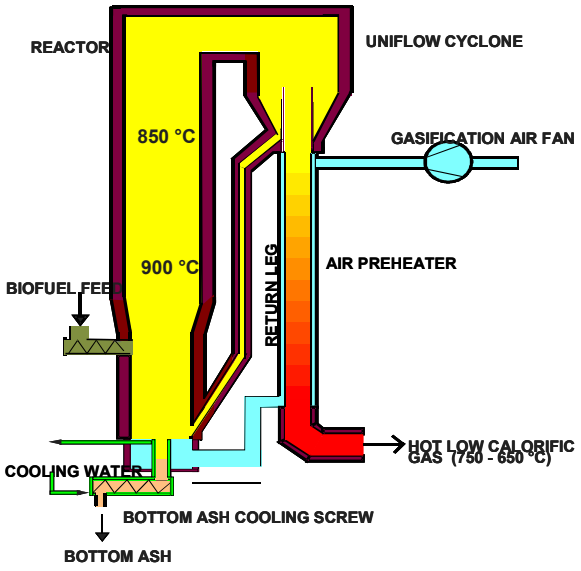

Figure 1. The foster wheeler gasifier.

Most of the solids in the system are separated in the cyclone and returned to the lower part of the gasifier. These solids contain char, which is combusted with the fluidizing air. This combustion process generates the heat required for the pyrolysis process and subsequent, mostly endothermic gasification reactions. The circulating bed material serves as a heat carrier and stabilizes the temperatures in the process. Coarse ash accumulates in the gasifier and is removed from the bottom with a water-cooled bottom ash screw.

Table 1. Foster Wheeler atmospheric gasifier references.

Customer	Size MW	Fuel	Application	Year
Hans Ahlstrom Laboratory, Finland	3	Misc.	Test unit	1981
Oy W. Schauman Ab, Finland	35	Bark, sawdust	Lime kiln fuel	1983
Norrsundet Bruks Ab, Sweden	25	Bark	Lime kiln fuel	1984
ASSI Karlsborg, Sweden	27	Bark	Lime kiln fuel	1984
Portucel, Rodao, Portugal	15	Bark	Lime kiln fuel	1985
Kemira Oy, Vuorikemia, Finland	4	Coal, peat	Test unit, clean gas	1986
Lahden Lämpövoima Oy, Finland	40–70	Biofuels	Hot raw gas to boiler	1997
Corenso United Ltd., Finland	40	Aluminious plastic waste	Cyclone cleaned gas to boiler	2000
Electrabel, Belgium	50	Biofuels	Hot raw gas to boiler	2002

3. The Lahti gasifier, a showcase for the technology

The first CFB gasifier connected to a PC boiler was constructed in 1997 at the Kymijärvi power plant of Lahden Lämpövoima Oy. The Kymijärvi power plant produces electric power (167 MWe) and district heat (240 MW) for the city of Lahti, Finland. The Lahti gasifier was connected to a 20-year-old Benson-type once-through boiler, the steam data of which are 125 kg/s, 540°C/170 bar/540°C/40 bar. The boiler was converted from heavy oil firing to coal firing in 1982, and typically it operates about 7000 h/a, depending on the heat demand and electricity prices.

The Lahti gasifier started commercial operation in 1998 and initially used biofuels such as bark, wood chips, sawdust and uncontaminated wood waste. Other fuels have also been tested subsequently, including in-origin classified waste fuel (REF), railway sleepers and shredded tyres. As a result of availability and price changes, the share of REF fuel has gradually increased at the expense of cleaner biofuels. The gasifier has operated well with varying fuel mixes, with availabilities of 96% or higher. Table 2 shows the fuels used in 1998–2002 and table 3 summarizes the annual availabilities as well as the energy produced in years 1998–2001.

Table 2. The fuels used in the Lahti Gasifier 1998–2002.

Fuels used at Lahti		**1998**	**1999**	**2000**	**2001**	**2002**
Biomass	%	71	57	63	61	56
REF	%	22	23	29	26	31
Plastics	%	-	13	7.4	12	11
Paper	%	-	6	0.1	0.3	2
Railway sleepers	%	5.5	0.1	0.2	-	-
Shredded tires	%	1.5	0.9	-	-	-
Total	tons	79 900	106 200	91 800	11 6100	103 800

Table 3. Annual operating availabilities of the Lahti Gasifier 1998–2002.

		1998	**1999**	**2000**	**2001**
Availability	%	99.3*	98.9	97.1	96.1
Energy produced**	GWh	223	343	295	449

* Second half of the year.
** Design value 300 GWh/a

The effects of gasification on the main boiler were studied with comprehensive measurements during a one-year monitoring program. The changes in the boiler emissions were measured to be as follows: NO_x, decrease by 10 mg/MJ; SO_x, decrease by 20–25 mg/MJ (fuel effect); CO, no change; HCl, increase by 5 mg/MJ (fuel effect, low base level); particulate matter, decrease by 15 mg/m^3n; heavy metals, increase in some (fuel effect, low base level); dioxins etc., no change. In the future, the reduction of CO_2 emission will increase in importance.

Table 4. Summary of the gasifier effect to the main boiler emissions.

Emission	**Change caused by gasifier**
NOx	Decrease by 10 mg/MJ (5–10%)
SOx	Decrease by 20–25 mg/MJ
HCl	Increase by 5 mg/MJ *
CO	No change
Particulates	Decrease by 15 mg/m3n
Heavy metals	Slight increase in some elements, base level low
Dioxins, Furans, PAH, Benzenes, and Phenols	No change

4. The Ruien gasification project

Following the success in Lahti, a gasification plant based on the same concept was constructed at the Electrabel Ruien power plant, which is the largest fossil fuel -fired power plant in Belgium. The gasifier was connected to the tangentially fired once-through boiler (steam values 180 bar / 540°C) of Unit 5, which has a power output of 190 MW_e. The new plant increases the use of renewable energy, thus reducing CO_2 emissions. The Flemish legislation includes a system of green certificates to encourage the use of renewable energy, so that the share of it in electricity production would rise to 5% in 2010.

The design fuel for the gasifier is fresh wood chips, but the gasifier can also utilize other types of fuel, such as bark, hard and soft board residues and dry, recycled wood chips, and the fuel moisture may vary between 20 and 60%. Depending on the fuel mix, the heat input to the boiler is normally 45–70 MW. The plant has been in commercial operation since May 2003. A drawing illustrating the gasifier connection to the boiler, and a photograph of the gasifier built in the middle of existing power plant structures are shown below.

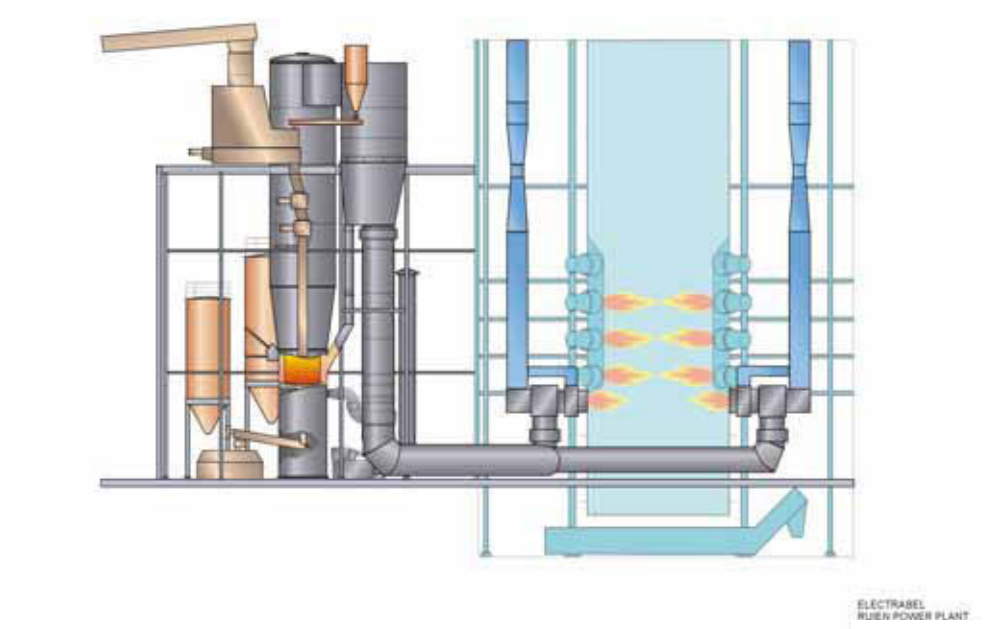

Figure 2. The layout of the Ruien gasification plant connected to the PC boiler.

Figure 3. The Ruien gasifier building.

5. Gasification experiences of difficult biofuels

The basic concept with combustion of the raw (uncleaned) product gas in a PC boiler is simple and works very well with relatively clean biofuels. However, such fuels are not always abundantly available. In the near future, co-firing of secondary, more difficult fuels is expected to be extended significantly. This is of increasing interest because substitution of fossil fuels by biomass will reduce the CO2 emissions. On the other hand, coal-fired boilers are likely to be equipped with SCR to reduce NOx emissions. However, the results show that the direct co-combustion of bio-residues such as RDF, sewage sludge, waste wood or meat and bone meal in existing coal fired power plants leads to increased deactivation of SCR catalysts. Also an increased risk of fouling and possible corrosion in the superheater section of the boiler has to be taken into the consideration in direct co-combustion applications. Analyses of deactivated catalyst samples indicate that the high concentration of phosphorus and sodium compounds as constituents of bio-residues has a significant influence on the deactivation rate. This deactivation problem can be avoided by, instead of direct secondary fuel combustion in the PC boiler, combining the boiler with a gasifier producing clean gas. FW fluidized bed gasifier can be equipped with product gas cleaning equipment, where harmfull components such as alkalies, trace metals, etc can be removed. Clean gas is then lead to the main boiler and co-combusted in a safe way. The following chapters describe examples of clean gas applications.

5.1 Gasification of straw

Straw gasification technology including gas cooling and cleaning was developed further and found technically feasible by Foster Wheeler and Energi E2 (Denmark) in 1999–2001. The work also included development of the straw feeder technology of TK-Energy (Denmark).

5.1.1 Straw as a fuel

The alkaline and chlorine contents of straw may vary a lot, but the following values are typical for Danish straw: sodium (Na) 0.03% in d.s., potassium (K) 1.8% in d.s. and chlorine (Cl) 0.6% in d.s. Several test runs with pelletized and loose straw were carried out at a 3 MW_{th} CFB gasification pilot plant at the Karhula R&D Center of Foster Wheeler Energia Oy. In the first test series, pelletized straw was found to guarantee trouble-free fuel feeding and steady gasification process. The main objectives of the tests were to study the conditions for gasification, gas cooling, dust separation and gas combustion. It was confirmed that pelletized straw could be gasified in spite of its high alkali contents and low melting point of the ash.

5.1.2 Tests carried out

In the first test series, a secondary cyclone located after the gas cooler was used for particle separation from the synthesis gas before it was combusted. Afterwards, a high-temperature baghouse filter was installed in the syngas line after the gas cooler. The tar contents of the syngas were high, in the range of 10–20 g/m^3n, and the baghouse operation temperature was selected to be in the range of 300–400°C to avoid filter blinding by condensing tars.

In the second gasification test series, loose straw was gasified. A newly developed straw feeding system was also tested in practice, and the syngas was cleaned in the new baghouse filter before combustion. In these tests it was confirmed that also loose straw could be successfully fed into gasifier and gasified to produce a steady flow of combustible gas. The ranges of applicable process conditions were found.

The third straw gasification test series was supported by the European Commission. The experimental research consisted of three main validation tasks: the capability of the developed feeding system to feed loose straw into the gasifier, the optimal process conditions and additives for gasifying loose straw and the capability of the selected gas cleaning system to make the gas suitable for co-combustion in large CHP plants. Co-gasification of straw and wood chips was also tested.

5.1.3 Test results

During the three test campaigns, more than 220 tons of pelletized and loose straw were gasified, and the total operational hours were over 400. Based on the pilot test program, the following conclusions could be drawn:

- Gasification of loose straw is technically feasible,
- Smooth, stable operation with high alkaline fuel was achieved,
- Wood and straw may be gasified together and trouble-free operation was reached,
- Carbon conversion was in the range of 95–97%,
- It was possible to keep the gas cooler clean both by soot blowing and by spring hammering,
- The hot gas filter operated well without blinding by tars and it removed also alkalis and chlorides quantitatively at 350–370°C from the synthesis gas,
- In the gasification conditions, PAH were formed, dioxins and furans were not formed,
- The optimal gasification conditions were validated in the project.

5.1.4 A Full scale 100 MWth straw gasification plant

A design study was carried out for a full-scale straw gasification plant of 100 MW_{th} integrated with an existing large CHP plant. A schematic of the process is shown below. The practical solutions of all unit operations were developed. The budget for a complete plant was calculated and consequently the overall project economy was assessed. The results of the process validation and design study offered a technical and economical basis for the decision-making about a demonstration plant.

The design study indicated that the economy of a 100 MW_{th} gasifier integrated with an existing large CHP plant is sensitive to the fuel and energy prices. At the price level of 2001 (e.g., straw price 5.6 €/GJ or 83.1 €/ton; market price of electricity 21.4 €/MWh), a biomass fuel slightly cheaper than straw would have been required to make the investment profitable in Denmark. Technical and economical evaluations have been continued for straw and other biofuels with high alkali and chlorine contents, but so far no plants based on this concept have been built. However, the economics appear to favor the lowest cost waste based fuels that can be converted to power and heat with nearly identical systems.

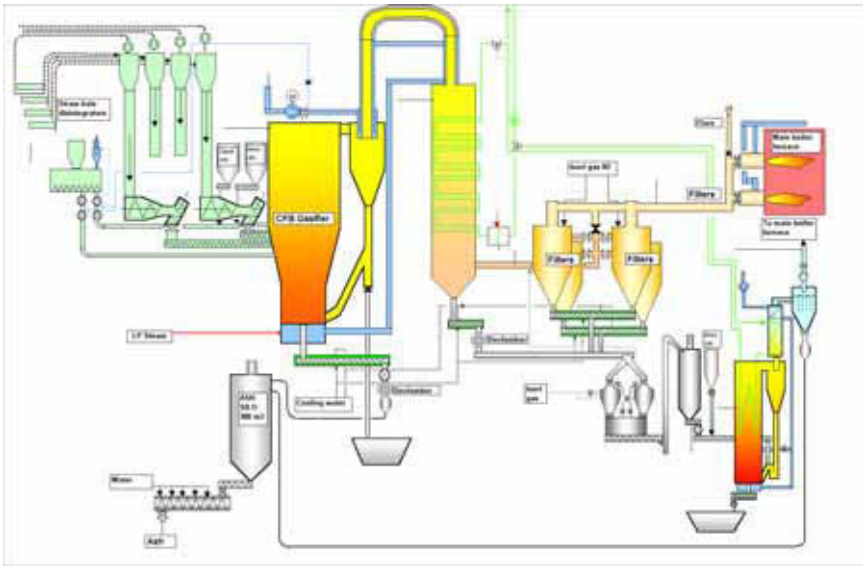

Figure 4. The process schema of the 100 MWth straw gasification plant.

5.2 Energy production from recycled fuels through gasification

Energy recovery from industrial and municipal wastes has become an important option for waste management and power production. The Kyoto protocol and EU's target to increase the share of renewable energy favor this trend. In the future, materials that can be composted or contain combustible fractions cannot be landfilled any more. Also the requirement of more efficient recycling and energy recovery favors technologies utilizing combustible fractions at the highest efficiency.

Building on the successful demonstration of CFB gasification and co-combustion in Lahti, FW has been developing gasification-based solutions for turning waste fuels into energy. Figure 5 shows the layout of the gasification plant produsing clean gas from recycled fuels. Besides pilot plant tests with gas cleaning, long term testing has been carried out with slipstream equipment at the Lahti gasification plant. This slipstream unit is provided with a FW gas cooler and a commercial hot gas filtration system. In September 2003, it had logged about 1500 operation hours with product gas, and testing continued. This development project led by FW has been co-funded by TEKES (National Technology Agency of Finland), and the other partners have been Lahti Energia Oy and Energi E2.

Simultaneously, Powest (subsidiary of Pohjolan Voima Oy in Finland) and Vapo Oy (Finnish biofuel, power and heat producer) together with VTT (Technical Research Centre of Finland) developed further both the Vapo MBT (mechanical-biological treatment) waste pre-treatment concept and gas cleaning technologies.

Several tests were carried out with PDU and pilot scale test rigs at the VTT laboratories.

In March 2003, FW and Powest-Vapo-VTT decided to join their waste treatment, gasification, gas cleaning and co-combustion technologies to establish a strong team for the realization of the first commercial scale project. At the moment the Martinlaakso 80 MW gasification plant project is under the design phase, but some delay will be in this project: The administrative court returned the environmental permiting issue to the lower authority that had earlier given the permit. But an appeal to the high court has been prepared and provided to. However, the process will take another 6–12 months, but the readiness for the investment is being kept all the time by the customer.

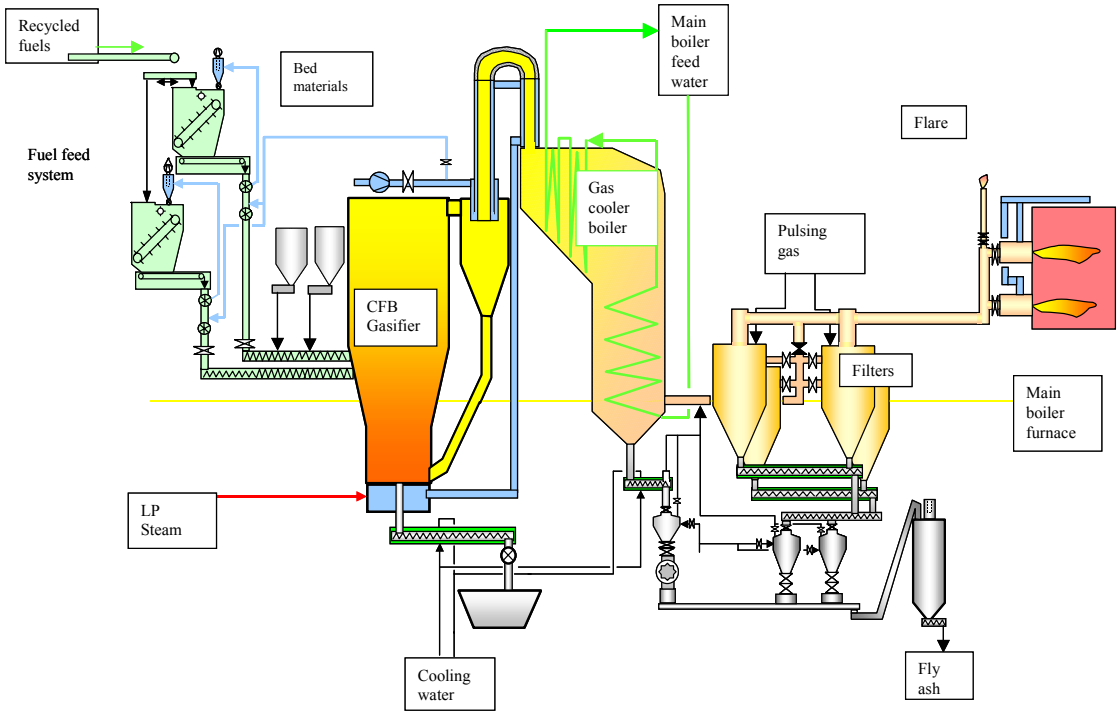

Figure 5. The Foster Wheeler gasifier concept for recycled fuels.

6. Conclusions

Since the early 1980's Foster Wheeler has steadily developed its CFB gasification technology and recently completed a unit for Electrabel in Belgium. Gasification offers a number of energy options for supplementing and diversifying the coal-fired generating base.

A CFB gasifier is a true multifuel unit with good fuel flexibility, i.e. very different fuels can be used in the same unit - though the heat output varies with the heat value of the fuel. By connecting a gasifier for instance to a PC boiler, the boiler fuel mixture can be extended and cheap solid fuels can be converted to power and heat at a very high efficiency, compared with stand-alone units with the same fuel input. The gasifier – PC boiler process connection also offers low investment and operation costs, utilization of existing power plant capacity with small modifications to the main boiler, high plant availability and reduction of the boiler emissions.

Corrosive-erosive wear mechanism of boiler heat transfer surfaces

Arvo Ots
Tallinn Technical University, Thermal Engineering Department
Tallinn, Estonia

Abstract

The mechanism of wear of steam boiler heat transfer surfaces in the conditions of periodical cleaning of ash deposit is presented. The wear is considered as high-temperature corrosion process of boiler tubes where the accelerating factor is the periodic destruction of protective oxide film on the tube surface during the cleaning cycles. The basic formula is given to determinate the intensity of wear of boiler tubes and to analyse individual parameters on the depth of wear. The influence of cleaning method of heat transfer surfaces is characterized by the degree of destruction of the protective oxide film. The depth of wear of boiler tubes also depends upon the type of metal, chemical composition of the ash deposit covering the metal surface, metal temperature and the period between the cleaning cycles.

1. Introduction

Heat transfer surfaces of steam boilers under the influence of the flue gas containing complex inorganic compounds are being covered with gradually increasing ash deposit, which cause additional thermal resistance to heat transfer from the combustion products of the fuel to the medium being heated. To reduce the influence of ash deposit on heat transfer, steam boilers are provided with cleaning devices of various types. In cleaning cycles not only ash deposit removal, but also destruction of the protective oxide layer takes place. This will diminish the oxide layer diffusion resistance to corrosion active components and lead to increasing corrosion intensity of tubes.

The method of calculation and analysis of high-temperature corrosive-erosive wear of boiler heat transfer surfaces in the conditions of periodical cleaning of ash deposits is presented. The wear of material is considered as the process of high-temperature corrosion of metal during which periodical destruction of oxide film on the tube surface. The cycles of cleaning appear to intensify the process. Proceeding from this, the method for calculating the depth of wear of boiler tubes and the analysis of the influence of individual parameters, for instance, such as type of metal, temperature, period between cleaning cycles, cleaning method on the intensity of wear, are given.

2. High-temperature corrosion intensity of metal

At high-temperature corrosion of metal under the influence of ash deposit on oxide film is formed on the boiler heat transfer surface tubes. This prevents the transfer of oxygen and other corrosive active components to the metal surface. With the increase in thickness of oxide film its diffusion resistance also increases and the intensity of corrosion goes down.

High-temperature corrosion of metal, which begins on a clean surface, can be divided into initial and basic stage. During the initial period the formation of oxide film with stable properties occurs. Therefore the corrosion intensity in the initial state is usually more intensive compared with basic stage.

The depth of corrosion of metal in basic stage depending on time is usually expressed by power-law

$$\Delta s_0 = A\rho_{\mathrm{M}}^{-1}\tau^n, \tag{1}$$

where Δs_0 – depth of corrosion during time τ; A – temperature dependent coefficient; ρ_{M} – density of metal; T – absolute temperature; n – exponent of oxidation.

High-temperature corrosion would occur in the following three regimes: kinetic, diffusion and kinetic-diffusion.

When the oxide film has a well protective nature and adjoins on metal surface closely the corrosion is controlled by diffusion and exponent of oxidation $n = 0.5$. However, if the oxide film on the surface has small diffusive resistance, the process is controlled by kinetic regime and determined on intensity of chemical reactions and exponent of oxidation $n = 1$. Between the above-mentioned two extreme regimes there exists an intermediate control regime where the corrosion rate of metal is determined by both – diffusion and kinetic factors. In this case coefficient n lies between 0.5 and 1.

Arrhenius law expresses the temperature dependent coefficient A by following formula

$$A = k_0 \exp\left(-\frac{E}{RT}\right), \tag{2}$$

where k_0 – pre-exponential factor; E – activation energy; R – universal gas constant; T – absolute temperature of metal.

The ratio between diffusion and kinetic factors on corrosion intensity of metal often depends on temperature. It directly influences the value of the oxidation exponent n. The n depends on temperature of metal and is usually expressed as a linear function $n = \gamma + \varepsilon T$. Then the depth of corrosion in the basic state

$$\ln \Delta s_0 = \ln (k_0 \rho_{\mathrm{M}}^{-1}) - \frac{E}{RT} + (\gamma + \varepsilon T) \tag{3}$$

where γ and ε depend on composition of metal and physical and chemical characteristics of ash deposit.

3. Influence of cyclic cleaning on corrosion of metal

Figure 1 demonstrates the wear of boiler tube heat transfer surface under the influence of cleaning force. The vertical axis indicates the depth of wear of tube (Δs), and horizontal axis the cleaning force (P) that may remove the ash deposit from the surface. Figure expresses the depth of wear at a given moment of time and at a fixed metal temperature. If the period between the cleaning cycles is τ_0, then time $\tau = \sum_{\mathrm{i}=1}^{m} \tau_{0\mathrm{i}}$, where m is number of cleaning cycles with period τ_0.

At small cleaning force the oxide film on the tube surface is unharmed. At the first approximation the depth of wear in the region of the influence of the insignificant cleaning force may be considered as independent of P (section A–Z in Fig. 1). Actually, however, the Δs in mentioned region may to certain extent depend on P because the corrosion activity of deposit can be influenced by the cleaning force. Two possible situations in Figure 1 are expressed as curves Z–A' and Z–A", respectively. Consequently, in the region between P-P'_{cr} the acceleration of wear of the tube does not occur by influence of cleaning force on oxide film, but may change chemical and structural composition of ash deposits on metal surface.

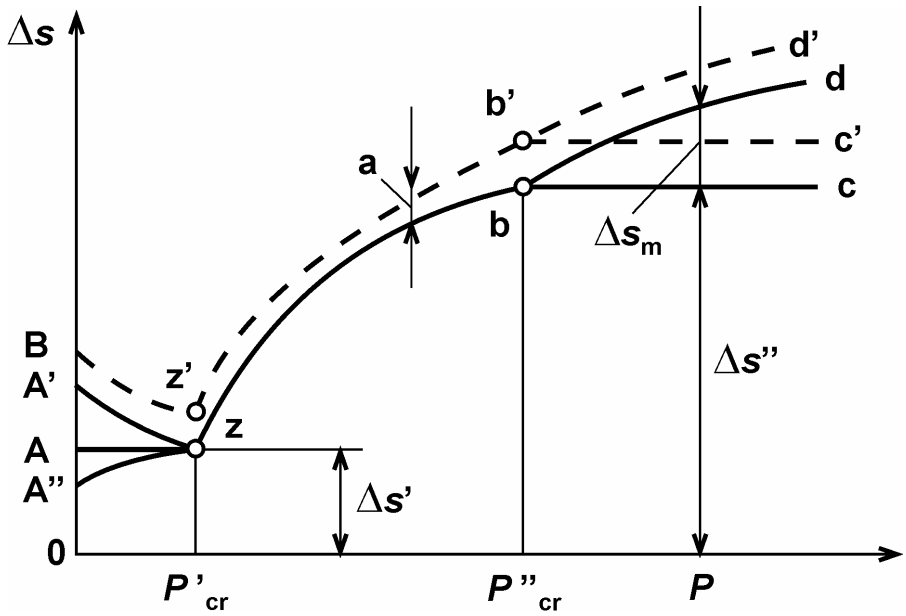

Figure 1. Depth of wear depending upon cleaning force.

The destruction of oxide film begins from the cleaning force P'_{cr} (the first critical cleaning force) and corrosion process is accelerated. If the depth of wear is denoted as $\Delta s'$ at the force P'_{cr} (point Z in Figure 1) then according to equation (1)

$$\Delta s' = A\rho_M^{-1}(m\tau_0)^n, \tag{4}$$

where $m = \tau/\tau_0$ – number of cleaning cycles during the time τ.

If the cleaning force increases from P'_{cr} to P''_{cr} (the second critical cleaning force), a partial destruction of the oxide film takes place during the cleaning cycle (section Z–b in Figure 1). In the extreme case, when $P = P''_{cr}$, the oxide film on the metal surface is totally destroyed in each cleaning cycle and the corrosion process begins on the clean surface under the influence of initial ash deposit. The depth of wear by force P''_{cr} is denoted as $\Delta s''$.

In the case of very great cleaning force $P > P''_{cr}$ the metal itself may be removed from the surface of the tube together with the oxide film during cleaning cycles. The wear is described in the region b–d and Δs_m is added to $\Delta s''$. Such a situation, for instance, occurs when steam lancing is used for cleaning of heat transfer surface. Also possible is another situation, for instance by water lancing, when metal does not remove from tube surface in cleaning cycles (line b–c).

With the metal high-temperature corrosion sometimes also concurs between crystals of metal or thermal fatigue crack formation takes place. In this case to the depth of wear must be added the corrosion depth between crystals of metal

and depth of fatigue cracks. This is reflected in Figure 1 as curve B–Z'–d' or B– Z'–b'–c'.

The depth of wear in the case that oxide film on the metal surface is totally destroyed (point b) is expressed as

$$\Delta s'' = BA\rho_{\mathrm{M}}^{-1} m \tau^{n}. \tag{5}$$

The factor B in formula (5) describes the influence of processes occurring in the initial stage of corrosion and takes into account the differences between corrosion activities in stable and initial ash deposit on heat transfer surfaces. The value of B depends on composition of the deposit, period between the cleaning cycles, temperature and type of metal.

The accelerating influence of cleaning on the wear of the tube under conditions of the total destruction of the oxide film during each cleaning cycle is expressed by formula

$$\nu = \frac{\Delta s''}{\Delta s'} - 1 = Bm^{1-n} - 1. \tag{6}$$

In practice the oxide film on the metal surface is usually not destroyed totally during the cleaning cycle. Under such conditions it is convenient to use the degree of destruction of the protective oxide film as a characteristic of the influence of cleaning action of heat transfer surface from ash deposit on the corrosive-erosive wear of tube

$$\xi = \frac{\Delta s - \Delta s'}{\Delta s'' - \Delta s'}, \tag{7}$$

where Δs – actual depth of wear.

The degree of destruction of the oxide film is equal to the ratio of the depth of wear caused by the action of the cleaning force (Δs–$\Delta s'$) to the maximum possible depth of wear ($\Delta s''$–$\Delta s'$). The degree of destruction of oxide film depends mainly on the value of the cleaning force and on the resistance of the oxide film to the action of this force.

Figure 2 shows the character of dependence of ξ on the cleaning force. If the cleaning force is small, the oxide film on the tube is not destroyed and $\xi = 0$, but when the oxide film is totally destroyed, then $\xi = 1$. With very great cleaning force, when some part of the metal itself with oxide is removed from the tube surface during the cleaning cycle, the depth of wear consists of sum $\Delta s = \Delta s'' + \Delta s_{\mathrm{m}}$ and the degree of destruction of the oxide film becomes more than 1.

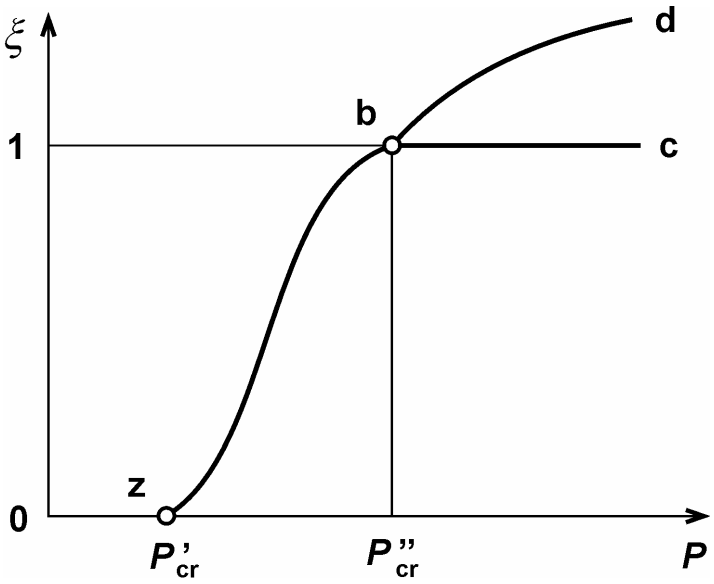

Figure 2. Degree of the destruction of oxide film depending upon cleaning force.

With the help of formulae (6) and (7) the depth of wear can be expressed as

$$\Delta s = [1 + \xi\,(B\,m^{1-n} - 1)]\,\Delta s'. \tag{8}$$

Equation (8) is the basic formula for calculating the depth of wear of the boiler heat transfer surfaces under the conditions of periodic cleaning from ash deposit. It follows that the absolute value of the depth of corrosive-erosive wear under the periodic destruction of the oxide film on tube surface in cleaning cycles is proportional to the depth of high-temperature corrosion under the influence of stable ash deposit $\Delta s'$. The accelerating effect of the cleaning force on the wear intensity of the metal is expressed by the relation $\xi\,(B\,m^{1-n} - 1)$.

The influence of cleaning of boiler heat transfer surface on the depth of wear increases with the rise of the degree of destruction of oxide film and the rise in the number of cleaning cycles. The exponent of oxidation n also strongly affects the depth of wear. It is necessary to mention that n depends mainly on the composition of fuel ash and on type of steel. With the increase of n the depth of wear approaches the value of $\Delta s'$. Hence, the higher the exponent n is, the less sensitive the metal is to the periodic destruction of the oxide film.

Figure 3 shows the influence of the accelerating factor of wear $1 + \mu = \Delta s/\Delta s'$ on the number of cleaning cycles at various values of ξ.

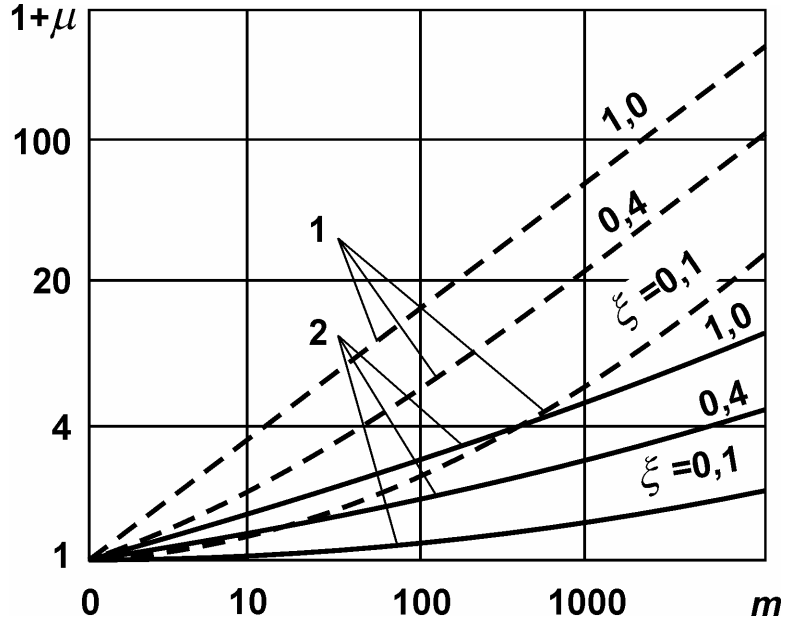

Figure 3. Dependence of the acceleration factor of wear upon the number of cleaning cycles and the degree of destruction of oxide film. 1 – n = 0.4*;* 2 – n = 0.75.

4. Experimental study

The intensity of corrosive-erosive wear of steam boiler heat transfer surfaces in the conditions of their periodic cleaning from ash deposit depends to a large extent on the method of cleaning. A complex of experimental studies was carried out to determine the rate of wear of steam boiler heating surfaces. On the basis of these data, the degree of destruction of oxide film on the tube surface was calculated by using different methods of cleaning when burning fuels (oil shale and brown coal) with different corrosion activities of the ash deposit. This is evident on the comparative diagram of the high-temperature corrosion depth of two metal types (pearlitic and austenitic steel) under the influence of brown coal ash with low alkali metal content and absence of chlorine (Na_2O = 0.4 %; K_2O = 0.6 %; Cl = 0 %) and oil shale ash with high content of alkali metals and chlorine (Na_2O = 0.2 %; K_2O = 6.0 %; Cl = 0.5 %) in Figure 4. Similar experiments were carried out also in pure air atmosphere. It becomes clear that both metals corrode with greater intensity under the influence of Cl containing ash. The relative acceleration of corrosion impact by oil shale ash on Cr-Ni austenitic steel is more notable than on Cr pearlitic steel, in spite of the fact that the absolute value of corrosion depth in the first case is lower.

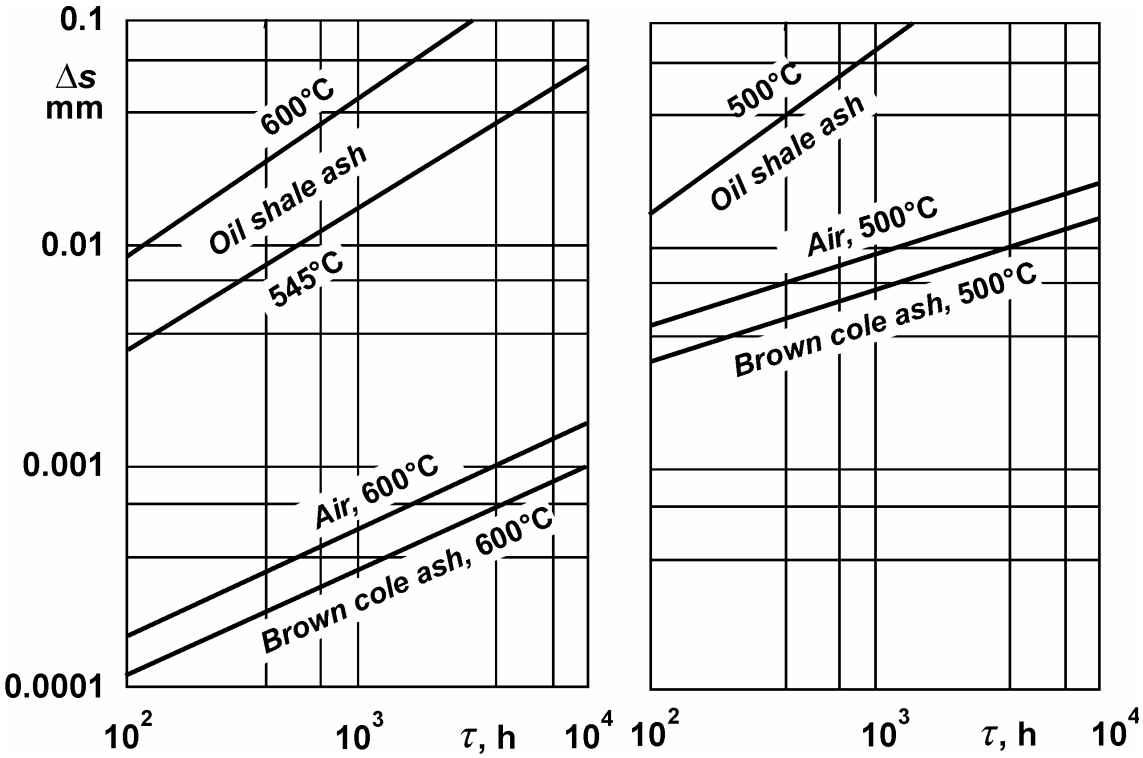

Figure 4. Comparative diagram of high-temperature corrosion of steels (left, austenitic steel; right, pearlitic steel).

Figure 5 shows the dependence of the degree of destruction of oxide film on the platen superheater tubes made of pearlitic steel 12Cr1MoV at different external tube surface temperatures on the radius of the steam lancing (on the distance of the axis of travel of the lance) by burning of pulverized oil shale.

It is obvious that with an increase in the lancing radius, ξ rapidly decreases due to reduced dynamic action of the steam jet on oxide film. With an increase of tube surface temperature, the resistance of the oxide film to the steam jet increases and the degree of destruction of oxide film is reduced. The 12Cr1MoV steel due to higher exponent of oxidation n is more sensitive to the periodic destruction of oxide film than the austenitic steel Cr18Ni12Ti.

Figure 6 shows the dependence of the degree of destruction of the oxide film on the tubes made of 12Cr1MoV and Cr18Ni12Ti steels in platen superheater when burning brown coal and oil shale on water lancing radius. It is obvious that the value of ξ decreases with lancing radius but does not actually depend on type of steel, corrosion activity of ash on temperature of metal.

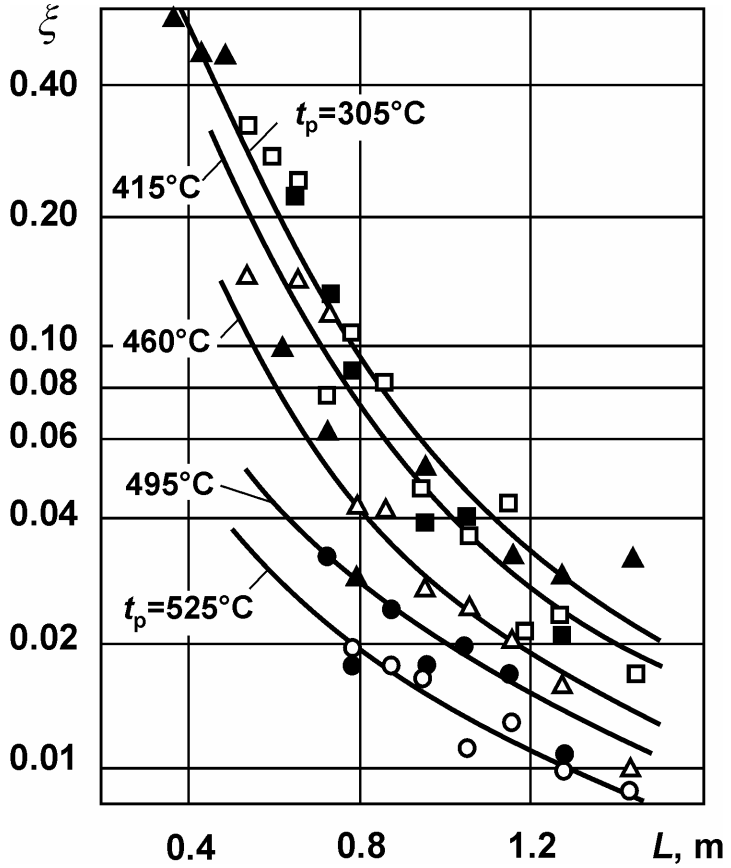

Figure 5. Dependence of the degree of destruction of oxide film on the tubes made of pearlitic steel upon the steam lancing radius and metal temperature.

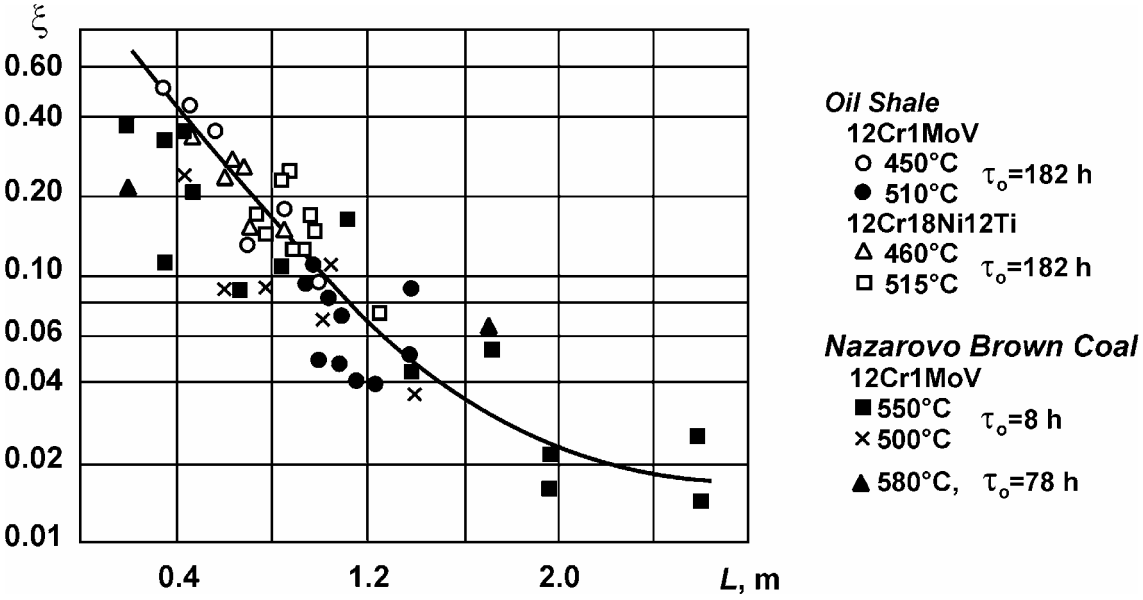

Figure 6. Dependence of the degree of destruction of oxide film upon the water lancing radius and metal temperature.

5. Lifetime of tubes

The solution of equation (8) on the given depth of wear Δs, the period between the cleaning cycles τ_0, the temperature of the metal T and the degree of destruction of oxide film ξ permit to obtain the lifetime of the boiler heat transfer surfaces on the basis of corrosive-erosive wear. For instance, Figure 7 gives the dependence of the lifetime of the tubes made of 12Cr1MoV steel depending on external surface temperature and the period between the cleaning cycles when burning oil shale. This Figure has been made for the depth of wear Δs = 0.77 mm and for two values of the degree of destruction of oxide film.

The curves in Figure 7 characterize the general nature of corrosive-erosive wear of heat transfer surface tubes, making it possible to determine the quantitative connections between the parameters of the process. For example, the lifetime of the tubes rapidly increase with the increases in the period between the cleaning cycles and decreases when the temperature of the metal increases. Wear also depends to a great extent upon the degree of destruction of oxide film on the tube surface.

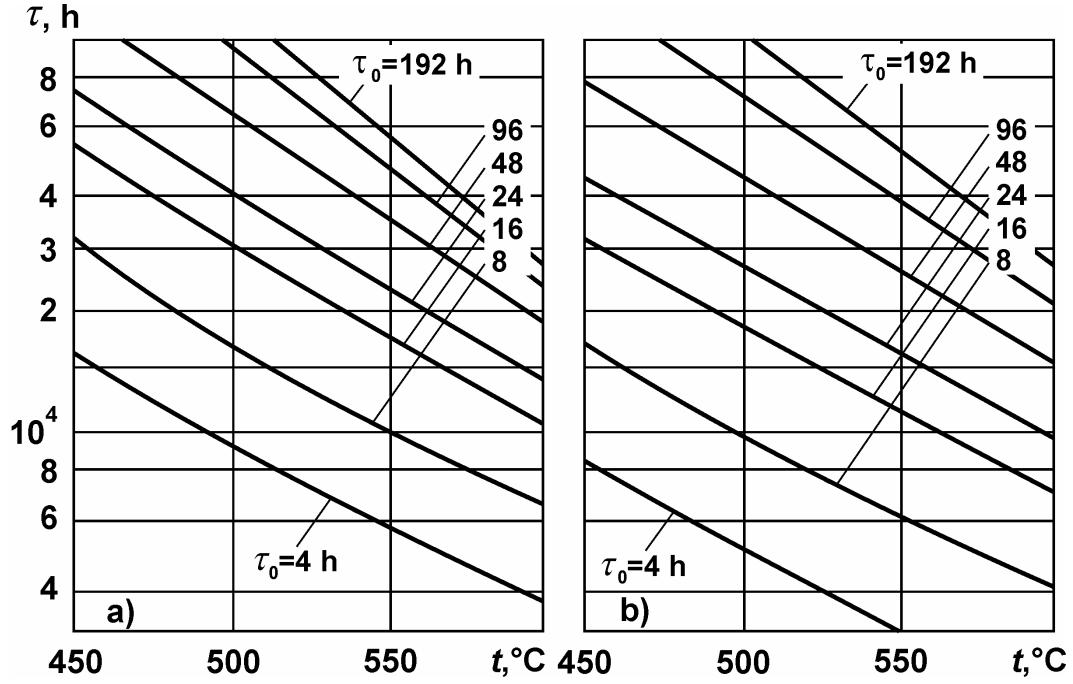

Figure 7. Dependence of the lifetime of the tube made of 12Cr1MoV steel on the temperature and the period between cleaning cycles by burning oil shale.

With the help of Figure 7 we can also establish the limiting temperature of the tube metal. By this we mean the highest temperature of tube wall, which can be used in consideration of the high-temperature corrosion and cleaning conditions of heat transfer surface.

Materials for fluidized bed heat exchangers

P. Makkonen & M. Mäkipää
VTT Processes, Biologinkuja 5, P.O. Box 1601, FIN-02044, VTT, Finland

Abstract

In order to increase the steam parameters in combustion units, several new approaches have been proposed. New materials have been tested, but they seldom have been a sufficient solution. Metallic coatings sprayed on superheater tubes have been noted to reduce erosion and corrosion in selected cases. New plant designs have been tested. However, most of these solutions have at least one special feature, which prevents using them as a general solution applicable to all new boiler units. Fluidised bed combustion units, and especially circulating fluidised bed (CFB) combustors have gained reputation as one of the most feasible means of solid fuel combustion. These units have one major benefit over other technologies: possibility to utilise the re-circulated solids for heat generation. This allows using fluidised bed heat exchangers (FBHE), which are one of the most promising novel solutions to improve the efficiency of solid fuel combustion units. Selecting optimal materials for such heat exchangers is not straightforward due to several special demands, such as high heat flux and continuous erosion.

1. Introduction

Corrosion of heat transfer elements is the limiting factor in attempts to increase plant efficiency with higher steam values. Renewable energy sources, such as biomass and recovered fuels generate need to shield superheaters from different corrosive components. Traditional heat transfer elements, which are located in the flue gas duct, face almost all the chlorine and sulphur brought into the furnace along with the fuel. Deposits that are eventually created on these tube surfaces may contain components, which have very low melting points. If the deposit starts to melt, even partially, the conventional steels will start to suffer from local or general corrosion, and the only ways to prevent this are changing fuel or limiting steam temperature. The idea of using a different approach in the placing of heat transfer elements is a relatively old one. Superheater elements have been located in the bed region of bubbling fluidised bed boilers (BFBs), but the fluidisation has been noted to cause high erosion losses, and the presence of burning fuel has caused metal carbonisation and local high temperatures, eventually resulting in high material loss rates. Due to this material loss, such approach has been abandoned.

In circulating fluidised bed units, the solids return provides a possibility to install an external heat exchanger, which is practically safe from corrosive components. This is due to the fact that nearly all the corrosive components are easily volatilised, and thus carried out from the furnace with the flue gas. However, the operating principle of taking heat from fluidised solids causes high thermal stresses in the materials, and thus sets new needs for proper material selection. At the same time, the corrosion reactions noted in the fluidised bed superheaters are not similar to those of found from superheaters located in the flue gas channels. This paper presents the idea of fluidised bed heat exchangers, gives some calculated examples of thermal stresses present in real applications, and gives information about the possible corrosion mechanisms, summing this data into recommendations for material selection.

2. Fluidised bed heat exchanger (FBHE)

The boilers equipped with FBHE units have one or more superheater sections located in separately fluidised chambers, into which the circulated bed material is brought from the solids separator. There are several ways to locate such chambers, and each boilermaker has selected the location according to their own boiler design. The most usual place to put the chamber is where the solids return from the solids separator, see Figure .

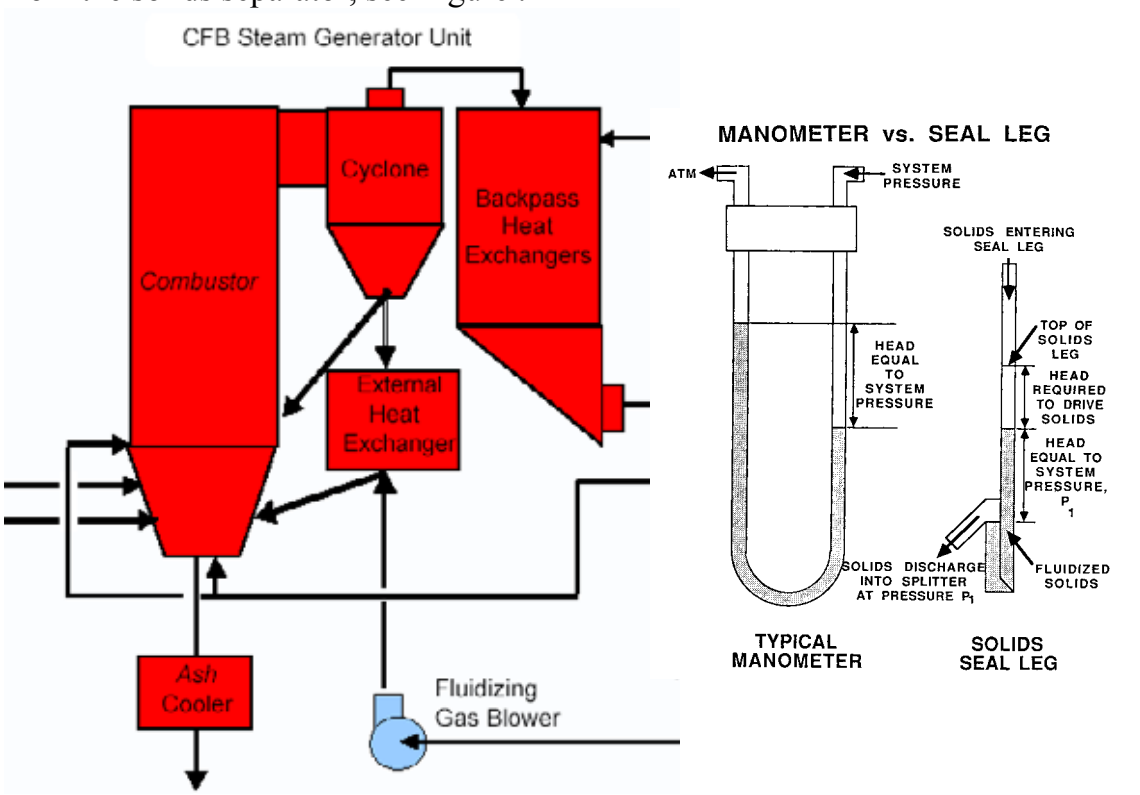

Figure 1. An external superheater located in the solids return, and the operating principle of the gas seal between furnace and the solids separator. (Marion 2002, Hill, Mallory and McKinsey 1985).

The operating principle of a FBHE is relatively simple: hot solids are brought into a chamber, in which they are fluidised with air or re-circulated flue gas as a slowly bubbling fluidised bed. Heat exchanger elements, often in the form of tube coils, are located inside this fluidised bed, see Figure .

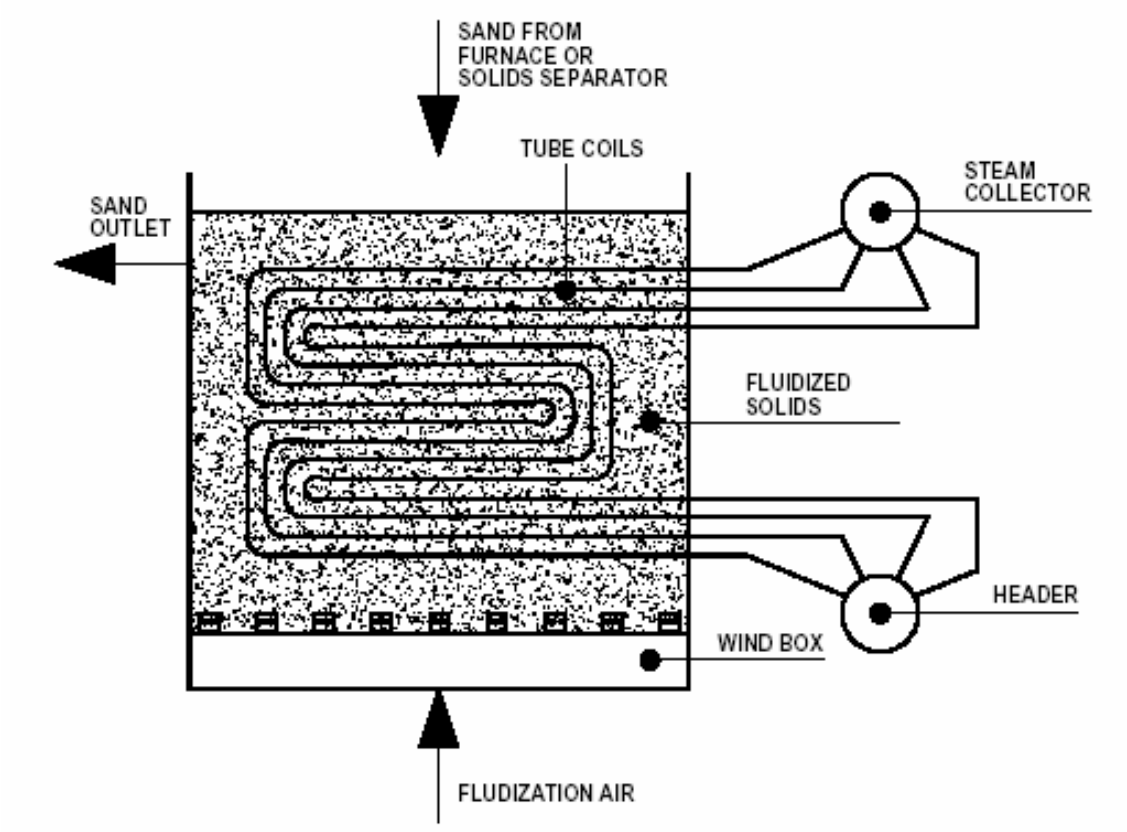

Figure 2. Principle of external superheater (Makkonen 2000).

The hot particles colliding with the heat transfer surfaces effectively release their thermal energy, thus increasing significantly the external heat transfer coefficient. At the same time, the continuous collisions slightly erode the surface, thus preventing deposition of harmful ashes. The benefits of such heat exchanger are clear:

- more efficient heat transfer than in the gas channel => smaller heat transfer area is required
- possibility to control the heat transfer, both by the bed temperature in the chamber and the fluidisation velocity
- the atmosphere contains much less harmful substances than the gas-phase in the flue gas channel.

3. Heat transfer in fluidised bed heat exchanger

The main difference between the heat transfer in a conventional and a fluidised bed heat exchanger is in the particle convection. Gas convection and radiation also form a significant part of the total heat transfer. A simplified description of heat transfer phenomena is shown in Figure .

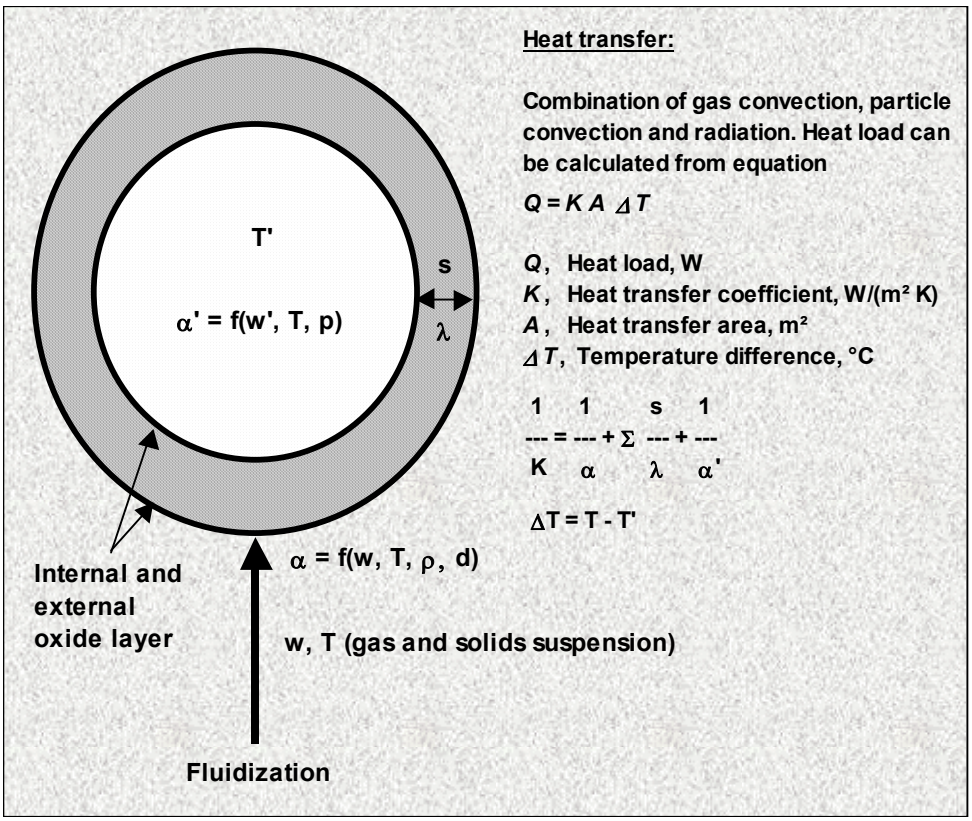

Figure 3. A simplified illustration showing the main elements affecting heat transfer in a fluidised bed.

The total heat flow from fluidised sand into steam is mainly dependent on:

- fluidisation velocity, which determines both the gas convection and particle collision frequency
- temperature of solids entering the chamber, which determines radiation and temperature difference between the bed and steam
- characteristics of the solids (particle size and shape, density, thermal conductivity)
- suspension density of the fluidised bed
- tube geometry and placing of tubes.

There are several semi-empirical correlations, which can be used to estimate the inside and outside heat transfer coefficients. Few of these are directly applicable

to the external heat transfer coefficient (Iacob and Vigier 2002), while the heat transfer coefficient inside a steam tube has been well established. The outside heat transfer coefficient is in any case much higher than in a gas channel, because the convective and conductive heat transfer from fluidised particles brings a very high increase in the heat release rate. This causes high heat loads per unit area, which leads to a high temperature gradient through the tube wall. It is generally estimated that in the gas channel superheaters, the tube surface temperature is from 5°C to 30°C higher than the steam temperature inside the tube, depending on the design and material. In a fluidised bed heat exchanger, the difference may be as high as 100°C, see calculations in Table.

Table 1. Theoretical temperature differences [K] between steam inside a tube and the tube surface in different cases.

	External heat transfer coefficient, W/m² K						
	Conventional				FBHE		
	50	100	150	200	400	600	800
Clean tube, K	6	12	18	24	44	62	77
+ Internal oxide 100 µm, K	8	15	22	29	53	73	89
+ External oxide 200 µm, K	9	18	26	34	61	83	102

This temperature increase has a significant effect on the erosion and corrosion mechanisms that can affect the lifetime of the tubes. Due to this, some special materials have been considered as the most feasible materials to be used in fluidised bed heat exchangers.

4. Erosion and corrosion in fluidised bed heat exchangers

The term erosion-corrosion is used for describing cases in which the metal or the protective oxide is first weakened by corrosion, and the corrosion products are then removed by erosion. According to Meuronen (1997), erosion of heat transfer surfaces is dependent on process conditions, particle flow density, mass flow and velocity, angle of collision and material properties of both the colliding particle and the heat transfer surface. When combined with parameters affecting corrosion rate and mechanism, combined erosion-corrosion may unexpectedly result in a very complex and rapid metal degradation (Reponen et al. 1999). This type of corrosion is very difficult to detect reliably, because there are few detectable corrosion products left on the sample. General rules for estimation of the rate and reduction of erosion-corrosion are not available. Currently, the best means of protecting heat transfer surfaces from erosion-corrosion is proper boiler design. Tube shields can also be used to protect the most eroding areas.
Erosion and erosion corrosion may put additional brackets on the applicability of various materials used in fluidised bed heat exchangers. Material degradation

will occur depending on the actual conditions at different regimes as erosion, corrosion enhanced erosion, erosion enhanced corrosion, and corrosion. Oxide scales of optimal properties provide protection both for corrosion and erosion. The rate of degradation of metals and alloys by solid particle impaction may decrease as temperature is increased, because surface oxides come more elastic at the higher temperatures, (Stephenson and Nicholson, 1990). Thus, a maximum of erosion-corrosion rate occurs in regard of material temperature for metals and alloys exposed in fluidised bed conditions, (Wright, Krause and Carlton 1980, Hall and Saunders 1992). Figure illustrates erosion behaviour of some steel grades. It may be noted that the erosion rate may behave unexpectedly as the material temperature increases.

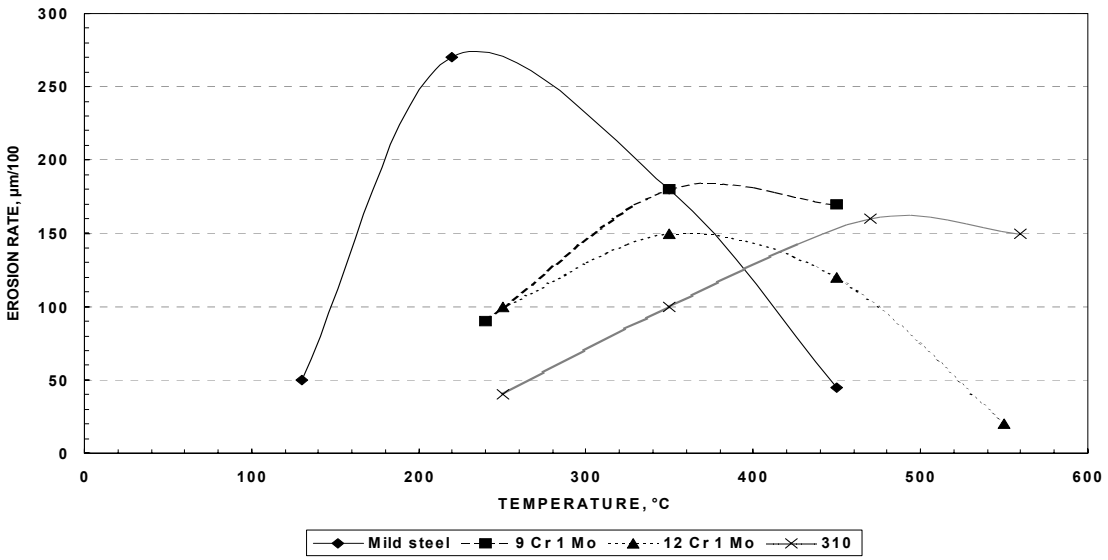

Figure 4. Pure erosion rates of selected steels (data from Hall and Saunders 1992).

The environment in a fluidised bed chamber differs significantly from the one in a gas channel. The corrosive components in fuels, such as sulphur, chlorine and alkali metals, are almost fully carried out from the furnace with the flue gas. However, some of these are carried into the fluidisation chamber, whether as gas phase substances or components formed in reactions with ash and bed material. Some of these components may decompose thermally or due to attrition, and thus release aggressive elements. The tubes may have a thin, hard deposit layer, which the constant erosion caused by the fluidised particles cannot remove. If this occurs, the corrosion rates depend on the composition and renewal of the deposit. If the tube surfaces stay clean, the material loss rate is mostly dependent on the characteristics of the oxide layer. Three different cases can be separated: combustion of wastes and other recovered fuels, combustion of biomasses and co-combustion, and combustion of fossil fuels, such as coal and peat.

4.1 Erosion and corrosion in combustion of recovered fuels

Fuels, which may release high amounts of hydrogen chloride and/or volatile heavy metal species in flue gases, such as wastes and recovered fuels create a risk of flue gas side chlorine corrosion. This limits the allowable steam temperatures to about 450°C. In fluidised bed heat exchangers, the risk of corrosion due to hydrogen chloride and/or volatile heavy metal species is significantly lower due to much lower concentrations. However, even low quantities of these substances may have a significant effect on the structure of the oxide scale, and thus affect the material loss rates. There are few studies about materials performance in such environment, and further studies are strongly recommended to find the actual corrosion mechanisms and to select the right steels for each application. As an example, corrosion tests in a CFB burning industrial waste in Stockholm, Sweden have been reported in 2002 (Makkonen 2002). The test results show a clear difference in the corrosion rate between the flue gas channel and the fluidised bed environment. During the two years of exposure in the flue gas channel at material temperature of 400°C, steel AISI TP347H had corroded 0.6 mm. In the fluidised bed heat exchanger, the same steel showed no clear signs of corrosion at material temperature of 530°C. Some oxide scaling was detected during the cooling of the tube coils. This indicates that the oxide scale had been very uniform, thus being able to resist both erosion and corrosion. Steels, which have the capability to create such a solid oxide scale seem very promising for the fluidised bed heat exchangers, especially in combustion of very demanding fuels.

4.2 Erosion and corrosion in co-combustion

For fuels like biomass or mixtures of biomass and coal, there is a risk of hot corrosion due to deposition of alkali metal salts. These deposits can be found from practically all superheater and re-heater surfaces located in the flue gas channel. The composition and amount of the deposits mainly depend on the fuel mixture. It has been noted in several publications that if the fuel mixture contains sufficient amount of sulphur and other components, which can react with the reactive alkali metals, and thus prevent the formation of alkali chlorides, both the amount of the deposits and their composition will change. In these cases, especially the amount of chlorine in the deposits is greatly lower, and thus the risk of fireside corrosion is reduced. Alloying highly with chromium is usually considered as useful in order to combat deposit corrosion. However, cleaning superheater tubes using steam blowing may be a risk for high-chromium alloys due to the formation of volatile chromium species. This cleaning is not necessary in the fluidised bed heat exchangers due to continuous erosion by bed particles. In the co-combustion applications, the highest allowable steam temperature is about 560°C, depending on the boiler type and fuel mixture. This high a temperature already sets special demands for the material strength.

4.3 Erosion and corrosion in coal combustion

For clean fuels like coal, the main design parameter limiting materials performance is the material temperature, which adversely affects both the steam side and the fire side oxidation. Highly alloyed metallic materials having good oxidation and corrosion properties have complex and unstable material microstructure, are difficult to manufacture, and may not possess sufficiently good mechanical properties at high temperatures. Planned new designs with ultrasupercritical steam parameters (345 bar, 650°C) set very high demands for the material properties, and especially resistance to oxidation and sulphur induced corrosion become very important. It has to be noted that sulphur induced corrosion may become a serious problem at this high temperatures.

5. Applicable materials

Due to the high thermal load and the special environment, the materials for fluidised bed heat exchangers have to be selected according to different criteria than in conventional units. Figure shows an illustration of boiler type and steam parameter selection based on fuel characteristics. Table lists some candidate materials for modern power plants with high steam parameters. The materials used for heat transfer surfaces are usually selected according to their creep strenght, see Figure . Resistance to internal or external oxidation is also among the selection criteria.

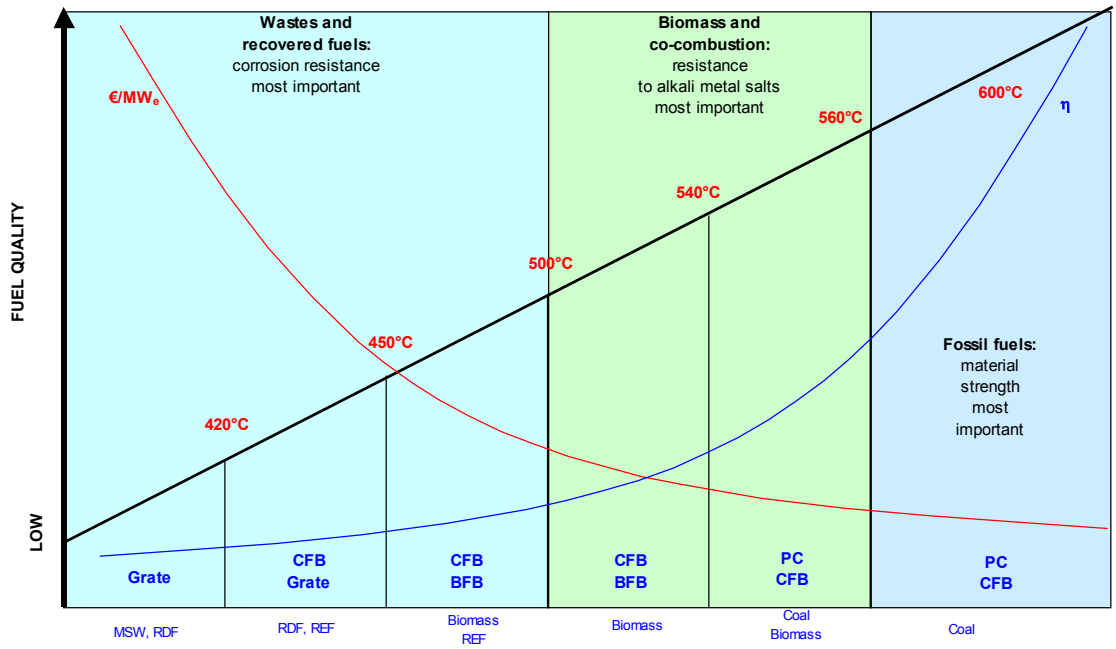

Figure 5. Relative dependency between boiler type and applicable fuels, investment cost (produced electricity) [€/MW$_e$], allowable steam temperature, and boiler efficiency [η].

Table 2. Candidate materials for advanced supercritical plants for various steam conditions. The same materials are of interest for co-combustion plants (Viswanathan and Bakker 2000).

Component	Phase 0 31MPa (4500 psi) 565/565/565°C (1050/1050/1050°F)	Phase 1 31MPa (4500 psi) 593/593/593°C (1100/1100/1100°F)	Phase 1B 31MPa (4500 psi) 620/620/620°C (1150/1150/1150°F)	Phase 2 34.5MPa (5000 psi) 650/650/650°C (1200/1200/1200°F)
Headers/steam pipes	P22, HCM2S (P23) P91, P92, P122	P91, P92, P122, E911	P92, P122 E911, NF12, SAVE12	SAVE12+ NF12+
Finishing SH non-corrosive	T91, 304H, 347	TP347 HFG Super 304 H/P-122*	NF 709 Super 304 H	NF 709 Inconel 617
Corrosive	310 NbN (HR3C)	310 NbN (HR3C) SS347/IN72**	310 NbN (HR3C) Super 304H/IN72**	Cr 30A NF 709/IN72**
Finishing RH	Same as SH	Same as SH	Same as SH	Same as SH
Water wall Lower wall Upper wall For low NOx Boilers + High S coal	 C steel T11, T12, T22 Clad with alloy containing >20% Cr or chromized	 T11, T12, T22 T23 (HCM12) Same as Phase 0	 Same as Phase 1 Same as Phase 1 Same as Phase 0	 Same as Phase 0

* High strength ferritic alloys with 9%Cr are suitable for steam piping and headers, but may suffer excessive fire side oxidation. 12Cr steels may be suitable, but further testing is needed.

** IN72 (44Cr, bal Ni) weld overlay for corrosion protection

+ Developmental Alloy

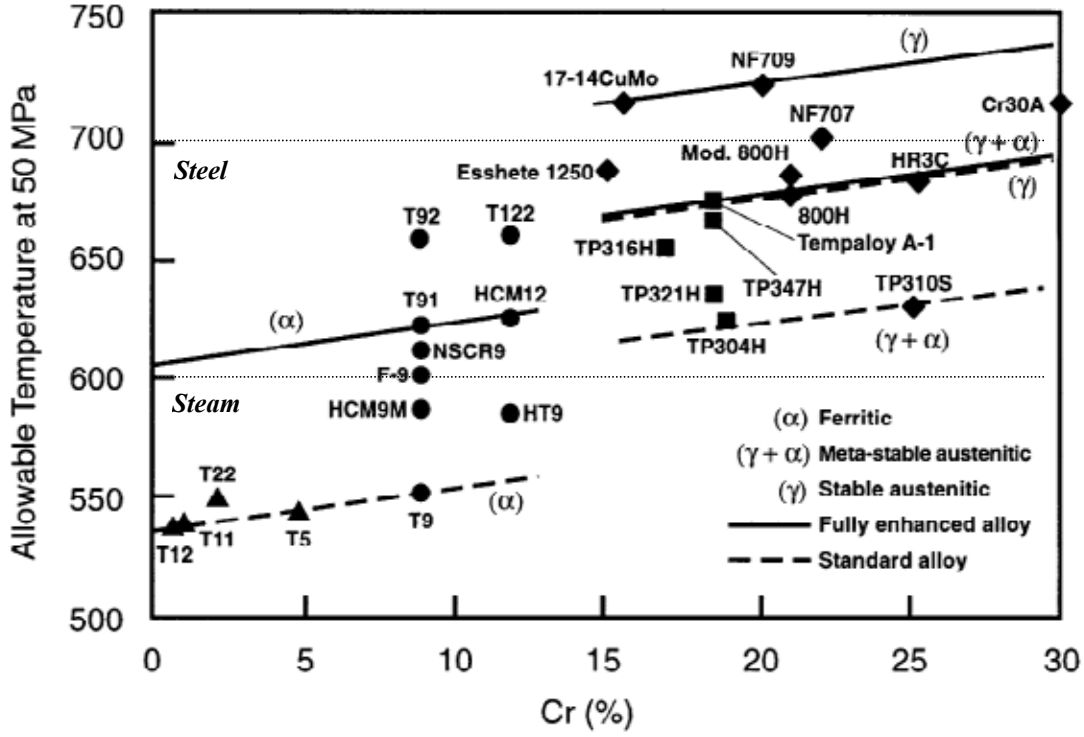

Figure 6. Allowable metal temperatures at constant allowable stress of 49 MPa (7 ksi) as a function of chromium content for various alloys (Masuyama et. al. 1988).

Lines drawn in Figure show that if the steam temperature is selected to be 600°C, and the tubes in a fluidised bed heat exchanger have to be selected according to the "worst case" scenario of steam temperature + 100°C, there are only few applicable materials. The material NF709 is one of the most promising solutions to be used for the high-efficiency once through steam generators equipped with fluidised bed heat exchangers. In waste combustion, the focus must be set according to erosion-corrosion resistance. In combustion of biomass and co-combustion, the material selection needs also special attention. Those steels, which generate a uniform and solid oxide scale perform generally better than the ones forming a more brittle oxide. Well balanced steels, such as TP347H and TP301S, have promising characteristics for waste and co-combustion, but more tests in laboratory conditions and real applications are strongly recommended.

6. Conclusions

Fluidised bed heat exchangers have proven to be one viable solution in attempts to increase boiler efficiency in fluidised bed combustion. This approach includes a fluidisation chamber, into which hot solids are introduced, usually from the solids separator. Heat transfer tubes are located inside the fluidised solids, and thus the heat transfer rates are higher than in conventional gas channel superheaters. Simultaneously, the solids entering the chamber contain only low amounts of corrosive substances. This leads to lower material loss rates than in other superheater types. However, the continuous erosion by the fluidised particles and the high thermal load set special needs for the materials that are used in the tubes. At the same time, the demand for higher steam parameters and increasingly difficult fuels set additional demands to the proper selection of steels. New supercritical steam parameters create demands for creep strength up to 750°C temperatures. Such steels that can handle so high temperatures are rare, and if the environment is corrosive, risks of too high material loss rates have to be taken into account in the plant design.

References

Evald, A. & Jakobsen, H.H. *Recent developments in Denmark.* dk-TEKNIK ENERGY & ENVIRONMENT, 2003.

Hall, D.J. & Saunders, S.R.J. *Corrosion-Erosion of Alloys Exposed in Fluidised Bed Combustors*. Final Report COST 501-Round II, Work Package 4, UK5, 1992.

Hill, M.K., Mallory, R.G. & McKinsey, R.R. *Development of the Seal Leg Char Recycle System*. In 1987 International Conference on Fluidized Bed Combustion, Volume Two, Mustonen, J.P., (Ed.), New York, 1987.

Iacob C. 6 Vigier P. *Heat Transfer in Fluidized Bed For a Low Gas Flow Rate*. Available at http://www.lifco-industrie.com/ (February 2004).

Makkonen, P. *Corrosion Tests in Combustion of Recovered Fuels in a Modern CFB Boiler*. VGB Conference "Operating Experience with Fluidized Bed Systems", Köln 2002.

Makkonen, P. *Latest Improvements in CFB Boiler Design for Combustion of Difficult Fuels*. The Second Annual Seminar of the KESTO -Technology Programme, Helsinki, 14.11.2000.

Marion, J.L. *Combustion Technology Development Needs and Opportunities*. Combustion Technology University Alliance Workshop, Salt Fork Lodge, Cambridge, OH, 2002.

Masuyama, F., Haneda, H. & Roberts, B.W. *Update Survey and Evaluation of Materials for Improved Coal-Fired Power Plants*. Report CS-5181-SR, EPRI, Palo Alto, 1988, pp. 5.85–5.108.

Meuronen, V. *Ash Particle Erosion on Steam Boiler Convective Section*. Doctoral Thesis, Lappeenranta University of Technology, Lappeenranta 1997. ISBN 951-764-181-8

Reponen, P., Liu, X., Hellman, J. & Lindroos, V. *Erosion-Corrosion at Elevated Temperatures*. Report TKK-MOP-C10, Helsinki University of Technology, Laboratory of Physical Metallurgy and Materials Science, Espoo 1999. ISBN 951-22-4500-0

Stephenson, D.J. & Nicholls, J.R. *Role of Surface Oxides in Modifying Solid Particle Impact Damage*, Materials Science and Technology, Vol. 6, January 1990, pp. 96–99.

Viswanathan, R. & Bakker, W.T. *Materials for Boilers in Ultra Supercritical Power Plants*. Proceedings of 2000 International Joint Power Generation Conference Miami Beach, Florida, July 23–26, 2000.

Wright, I.G, Krause, H.H. & Carlton, H.E. *Observations of the Low-Temperature (400 to 910°F) Corrosion/Erosion Behavior of Selected Alloys in an Atmospheric Pressure Fluidized-Bed Coal Combustor*. J. Materials for Energy Systems, Volume 2, December 1980, pp. 33–48.

Sulphidation attack of the heat transfer surfaces in boilers: Materials performance and views on future prospects

Martti Mäkipää[1], David Baxter[2], Erja Turunen[3] & Maria Oksa[3]
[1]VTT Processes, Espoo, Finland
[2]JRC, Institute for Energy, Petten, Holland
[3]VTT Industrial Systems, Espoo, Finland

Abstract

Sulphidation attack of the heat transfer surfaces in boilers may be due to the presence of reduced sulphur compounds in gaseous phase, or due to the result of adverse deposit conditions. Under reducing conditions in the furnace, the safe upper temperature limit of heat transfer surfaces made of low alloyed steels may be no more than about 300–330^{o}C. The use of austenitic stainless steels or high chromium – high nickel alloys may allow metal temperatures that are 50 to 80 degrees or more higher. However, deposition of alkali and heavy metal salts may create corrosion conditions where protective chromium oxide or chromium sulphide scales fail. Materials design for the mixed fuel or high-pressure boilers must be considered carefully. High wastage rates of heat exchangers made of highly alloyed metallic materials or claddings may not be feasible for economic and environmental reasons. New developments in the manufacturing of austenitic stainless steels, however, may provide economic solutions for the superheater steel tubes. Corrosion resistant thermal spray coatings may fail due to their porous or discontinuous structure, or due to the thermal mismatch with the substrate. Prospective technologies based on the application of nanosized raw materials aiming to manufacture of gas-tight, temperature cycling resistant coatings are in the development stage.

1. Introduction

Sulphidation attack of heat transfer surfaces of boilers is in most cases related to the presence of reduced gaseous sulphur compounds such as hydrogen sulphide in the combustion zone. At present, sulphidation of heat transfer surfaces has been identified as a major problem in waste incinerators, kraft recovery boilers, but less so in pulverised coal fired boilers. In large utility boilers using pulverised coal as fuel, combustion is usually under good control and enhanced corrosion of water wall tubes due to reducing conditions is thus of no concern in the majority

of plants. Operation conditions, where heat flux is high, reducing conditions may prevail from time to time close to the water wall, and the chlorine content of the fuel used is high, may lead to increased corrosion rates of water wall tubing even in the case of large coal fired boilers.[1, 2] Because of the recent developments in the fuel and boiler technology, e.g., mixed fuel combustion and increased steam values, corrosion attack of heat transfer surfaces will be of more concern in the foreseeable future. This paper refers to some recent works on materials performance under sulphidizing conditions. Future prospects in materials and coatings technology for better control of sulphidation type of corrosion attack will be discussed.

2. Sulphidation of steels and alloys

2.1 Gas phase attack

Corrosion failures of water wall tubing made of carbon steel and low alloy steels may be avoided by proper control of operation conditions and/or applying diffusion chromium coatings or composite tubes with outer cladding made of austenitic stainless steel. Practical experiences show that diffusion chromium coatings may suffice for protection but under relatively mild temperature conditions. On the other hand, corrosion performance of alloys and steels alloyed with high concentrations of nickel and chromium critically depends on the material temperature and partial pressure of sulphur and oxygen in the environment. At the relatively low material temperatures typical of water wall tubes, protective scale growth and possible deterioration take appreciable amounts of time. Long-term corrosion tests reported refer to only a limited range of key parameters.[3, 4]

2.1.1 Experimental

Experiments were performed under simulated Kraft recovery boiler lower furnace conditions, which were chosen to be closely similar to the test conditions used by other research groups studying materials performance in recovery boiler conditions.[5] Materials to be tested were SAN 38 (UNS N08825 Mod), SAN 63 (UNS N06625) and San 65 (similar to SAN 63 but with a higher content of iron). Samples of St 45.8 and 304L were tested concurrently for comparative purposes. Two types of corrosion tests were made. Short-term tests with duration of 200 h were made at 360^{o}C and 400^{o}C under a flowing N_2 atmosphere with 0.5% H_2S. Long-term tests at an exposure temperature of 380^{o}C were made in an autoclave having a total pressure of 1.5 bar, applying discontinuous testing method with intermediate weighing. The total test times were about 1100 h and 1500 h. Calculated equilibrium partial pressures of sulphur in the test atmospheres (H_2S-H_2O-Ar mixtures) were, as targeted, about 10^{-9} atm and 10^{-4} atm at the exposure

times 1100 h and 1500 h, respectively. Specimens exposed were prepared by making cross-sections and studied using SEM/EDS.

2.1.2 Results

The mass gain of chromium-alloyed stainless steels and alloys was found to be only a small fraction of that of carbon steel under all test conditions. Corrosion rate behaviour observed in the long-term discontinuous tests for austenitic steel and high-Ni-Cr alloys depended on sulphur partial pressure, time, and the material tested.

With the lower sulphur partial pressure gas, the corrosion rate of austenitic stainless specimens was almost parabolic in the beginning, but after 1100 h exposure time it was almost linear with an equivalent metal loss of about 0.015 mm/a. This was only about 1/10 of the linear corrosion rate determined for carbon steel. Different tested specimens of austenitic steel showed somewhat different linear corrosion rates. This variation was most pronounced in the case of the material SAN 38. The mass change of high-nickel high-chromium molybdenum alloys SAN 63 and SAN 65 was very small after the initial weight gain, and for many specimens within the weighing accuracy.

With the higher sulphur partial pressure gas, the corrosion rate of austenitic stainless steel increased with time. Corrosion rate of high-nickel alloys remained typically low, but there was substantial variation between different specimens in the case of SAN 65, the alloy that occasionally performed worse than SAN 38, Fig. 1. Furthermore, corrosion scale morphologies on the SAN 63 and SAN 65 specimens showed features of localised attack, Fig. 2.

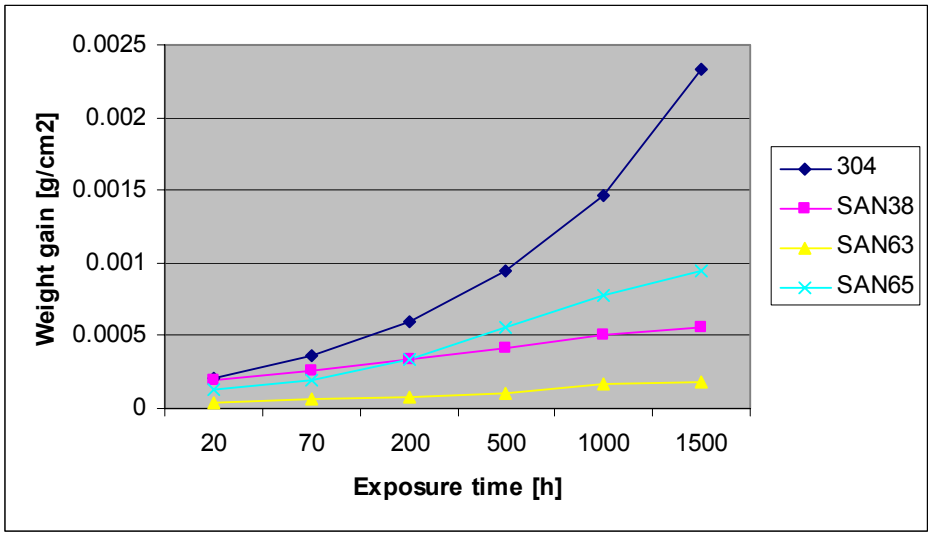

Figure 1. Weight gain of specimens made of austenitic stainless steel type 304L and various nickel alloys in discontinuous corrosion testing for up to 1500 hours under wet hydrogen sulphide -argon atmosphere at 380°C.

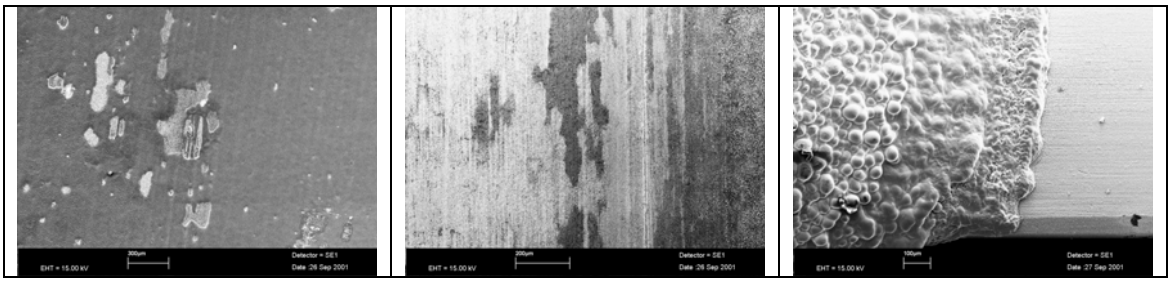

Figure 2. Corrosion scale morphology of various nickel alloy specimens after total exposure time of 1500 hours under wet hydrogen sulphide -argon atmosphere at 380°C. On the left, specimen (a), SAN63. In the middle, specimen (b), SAN65. On the right, specimen (c), SAN 65. (all secondary electron images).

In most cases, variations in the corrosion scale morphology was not related to significant corrosion. Exceptionally, one SAN 65 specimen suffered from sulphide scale growth, which did lead to significant mass gain of the specimen (Fig. 2, specimen (c)).

2.1.3 Discussion

Corrosion resistance of austenitic stainless steel of type 304L was found to be in terms of specimen weight gain about ten times lower than that of carbon steel under a dry or wet hydrogen sulphide-containing test atmosphere. A similar relationship holds in practice between long-term corrosion rates for recovery boiler water wall panels made of austenitic stainless steel composite tubes and that of carbon steel tubes, respectively. Sulphidation resistance of composite tubes with type Alloy 825 claddings (SAN 38) may be sufficient up to the temperature range from 350°C to 360°C, whereas composite tubes with type Alloy 625 claddings (SAN 63, SAN 65) may perform well enough up to the material temperature range from 360 to 380°C, if the partial pressure of sulphur is relatively low, i.e., clearly less than 10^{-4} atm. However, the sulphidation resistance of steels and alloys with high concentrations of nickel may be put in doubt if still higher exposure temperatures are considered. The experience from earlier laboratory tests performed under conditions simulating coal gasification atmosphers ($pS_2 = 10^{-10}$-10^{-5} atm), suggests that austenitic stainless steels and high-nickel alloys become susceptible to breakaway corrosion above the temperature range from 482 to 650°C. In a study reported by Norton et al. discontinuous corrosion tests were performed at 450°C and 550°C under similar conditions as in this work to study sulphidation resistance of ferritic model alloys with 12% chromium and variable amounts of silicon. Commercial austenitic alloys 800 H and HR3C were used as reference materials. Sulphidation resistance of the above mentioned austenitic alloys was found to be at least ten times lower than that of a commercial ferritic chromium alloy steel HCM 12, and similar to that of silica sub-scale forming model alloys with ≥ 2–4% Si. Alloying of austenitic stainless steels and nickel alloys with silicon has been shown to be

beneficial, e.g.[29] A brief look at the phase stability diagrams of the system Ni-S-O suggests that alternating sulphating and sulphidizing conditions may be detrimental to high-nickel alloys. Alloying with chromium is beneficial to suppress this type of attack, but the percentage of chromium needed to guarantee safe operation may be very high (about 50% or more). In practice, such a requirement will be achieved economically only by applying coatings such as chromizing.

2.2 Deposit attack

Very complex corrosion and stress related materials degradation phenomena might occur when sulphidizing conditions form under heat transfer surface deposits. For example, it has been shown that material wastage and/or stress corrosion cracking of austenitic stainless steel cladding of composite floor tubes in Kraft recovery boilers is related to enrichment of sulphur and chlorine species close to the floor tube surfaces. [7] Conditions causing under-deposits sulphidation attack of austenitic stainless steels and alloys may be created even in the superheater area. [8, 29]

2.2.1 Experimental

An aggressive molten salt deposit was applied on test specimens, simulating under laboratory test conditions the high temperature corrosion of superheaters in boilers. The corrosion medium was an alkali chloride – alkali sulphate salt mixture of eutectic composition, prepared from Na_2SO_4, KCl and NaCl. The specimens were exposed in air and half-immersed into melt at 520–530°C for 65 hours. A detailed description of the test method has been presented in Oksa et al. (2001). [9] Actual boiler testing was performed in a recovery boiler and in a biomass boiler. In the latter, fuels used were wood, peat and a small amount of REF (refuse derived fuel). Test rings fabricated from different low alloyed, stainless steels and high-Ni-Cr alloys were installed into the superheater area in an air-water-cooled probe. The material temperatures of different probes were in the range from 530 to 560°C. The metallurgical cross-sections of the specimens were investigated with scanning electron microscopy (SEM), and analyzed by energy dispersive X-ray analysis (EDX).

2.2.2 Results

Corrosion under laboratory testing was substantial, especially with the low alloyed steels. However, the stainless steels and high-Ni-Cr alloys experienced localised corrosion, which resembled corrosion of specimens from actual boiler exposures. The chemical compositions of the alloys in question, SAN28, AC66, and HR3C are presented in Table 1. A thin, about 20–30 μm thick chromium and sulphur rich layer was found under molten deposits in both laboratory tests and in actual boiler exposures.

Table 1. Chemical composition of the tested materials

Alloy	Cr	Ni	Fe	Mo	V	Si	Mn	P	S	Nb	Al	Ce	Co	Cu
AC66	27.3	32.2	Bal.			0.21	0.64	0.014	0.011	0.78	0.006	0.055		
San28	26.65	30.60	Bal.	3.32		0.42	1.73	0.015	<0.001				0.059	0.87
HR3C	24.8	19.2	Bal.	0.13	0.05	0.39	1.15	0.020	0.003	0.39			0.47	

An example of a test specimen of AC66 material with corrosion attack described above, is presented in Fig. 3. The dark corroded area was composed mainly of chromium (Cr) and sulphur (S). Nickel (Ni) and iron (Fe) were depleted from the layer. Small amounts of chlorine (Cl) and potassium (K) were detected in the area. The dotted corroded area next to the dark layer was depleted in chromium and enriched in nickel.

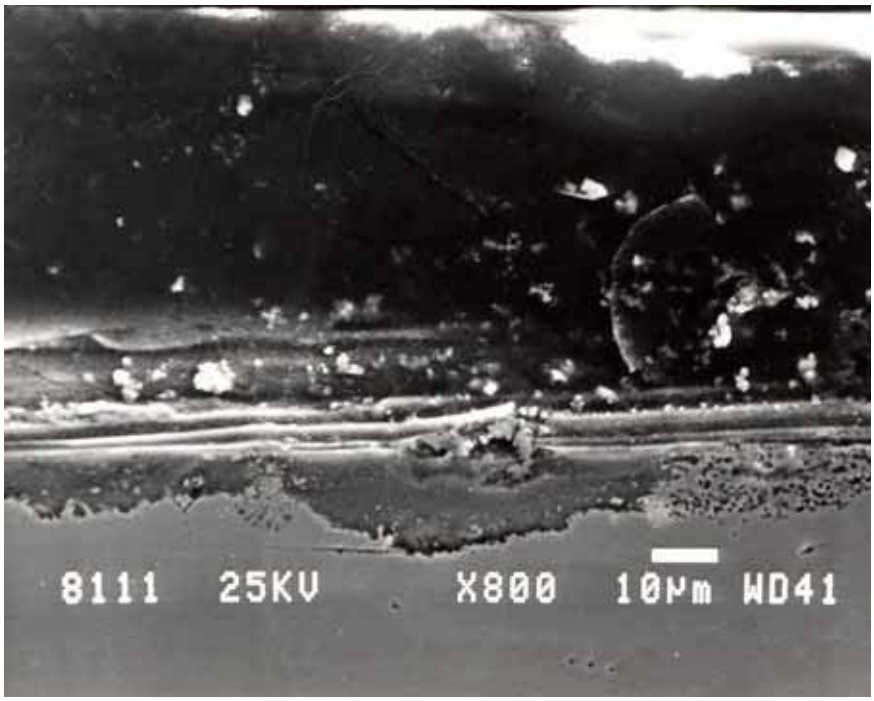

Figure 3. AC66 material after exposure to alkali sulphate – alkali chloride melt. SEM image of cross-section (secondary electron image).

Similar behaviour of another high-Ni-Cr alloy (SAN 28) is presented in Fig. 4. The material was corroded in actual biomass boiler conditions, the time of exposure being about 450 hours. A typical corroded area contained sulphur, nickel, chromium and iron. The dark spot below the deposit is enriched with chromium.

It was evident from the laboratory and boiler testing that in most cases the thin chromium and sulphur rich layer, which might have been protective, became detrimental in the presence of alkali metals and/or chlorine. In the investigated specimens, next to the chromium rich area in the metal surface was an area depleted in chromium, and enriched with nickel.

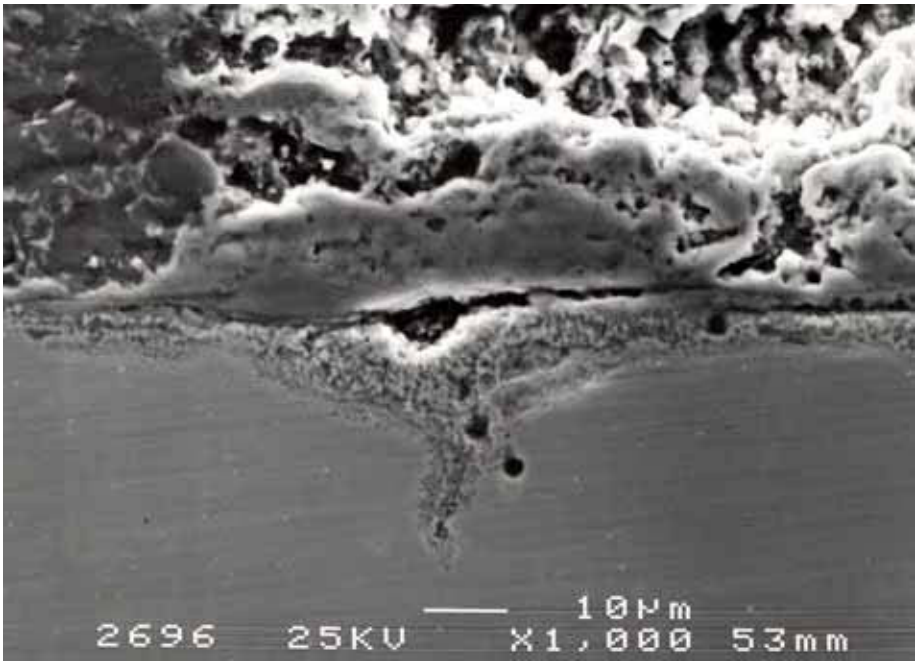

Figure 4. San28 material after exposure in a biomass boiler (wood, peat, and less than 10% of REF) conditions. SEM image of cross-section. Corroded area consists of sulphur, nickel, chromium and iron. Dark spot below the deposit is enriched with chromium, which is present with sulphur, chlorine and potassium (secondary electron image).

2.2.3 Discussion

According to the results, alloying with chromium affords limited protection to internal corrosion in the presence of mixtures of alkali sulphates and chlorides. Chromium depletion renders the sub-scale metal surface as well as grain boundaries susceptible to sulphidation attack. Accordingly, under actual boiler operation conditions the most harmful type of corrosion attack may be considered to be grain boundary attack, see, e.g., [10, 11, 29]. However, it has been shown that alloying suitably with silicon may enhance protective chromium oxide scale formation and suppress grain boundary carbide sulphidation of chromium steels and alloys. [12, 13, 30] It is thus interesting to see if development of nickel-lean austenitic stainless steels with increased silicon content will provide a real competitive alternative for austenitic stainless and high-nickel alloys as superheater steel tube materials. The results of short-term tests are indeed encouraging. [14, 11]

3. Protection of heat transfer surfaces

3.1 Coating technologies

Coatings offer a tempting possibility to change the material and properties of a surface. The high cost and difficult fabrication of some special materials in bulk form have favoured coatings as an alternative to produce more corrosion and wear resistant tubing. When applying coatings some critical factors such as porosity, residual stresses and mismatches in CTE (coefficient of thermal expansion) must be optimised carefully in order to produce high quality solutions with long lifetime. Careful design and manufacturing of the coating are very important in order to apply the most suitable coating to the application. With wrong design and faulty manufacturing, the coating may peel off without giving any protection to the coated surface. Minimal porosity is critical, especially in the case of attack by gaseous and liquid corrosive elements, as found under boiler conditions.

3.1.1 Thermal spraying

The thermal spray industry has been one of the fastest growing fields in coating technology. It is an effective and low cost method to apply thick coatings to change surface properties of the component. Thermal spray is a general term to describe all methods in which coating is formed from the melted or semi-melted droplets. The most common methods in boiler applications are HVOF (High Velocity Oxy Fuel), APS (Atmospheric Plasma Spray) and wire arc spray. HVOF process has been recognised as the most significant development due to its capability to produce very dense coatings with low oxygen content, good adhesion and compressive residual stress stages. [15]

3.1.2 Weld cladding

Providing added protection or repair of boiler components is commonly achieved by weld overlay or weld cladding. Weld cladding is carried out on site or on components in the workshop during fabrication and most commonly uses alloy 625 as the consumable for corrosion protection of low-alloy boiler steels [30]. While the process is widely known and carried out commercially, there are many potential problems limiting the quality of the welded product. The main problems include, excessive dilution with the base metal, entrapment of slag, excessive porosity and segregation of certain elements [31]. While alloy 625 is the most commonly used consumable alloy, development work with other alloys has been carried out to both minimise the problems with alloy 625 and to tailor claddings for specific applications [32].

3.1.3 Laser technology

Rapid growth in high power laser technology, especially with diode lasers, has increased the scope of application of laser cladding. Manufacturing and performance of different types of metal alloy coatings are widely reported. [16] However this technology is not yet used extensively for protection of boiler tubes.

Laser surface melting has shown growing potential to re-melt the thermally sprayed surface and improve the performance of the coatings. It is one of the most promising surface modification techniques to improve the surface properties of materials to resist corrosion and wear. In laser treatment a thin surface of the coating is melted and re-solidified into a compact, homogenous, non-porous layer. [17]

3.2 Coating materials

3.2.1 Metallic and composite coatings

The most common coating solutions are based on metal alloys and cermets. High chromium content nickel alloys (Cr-Ni, Cr-Ni-Ti) have shown the best potential in boilers that are exposed to highly corrosive sulphur-rich gases. [18] Another group with good resistance in sulphur-rich atmospheres is iron aluminide, mainly Fe_3Al, manufactured by HVOF or APS methods. [15, 17, 19] Chromium additions (Fe-Cr-Al–alloys) have shown even better corrosion resistance. [19]

3.2.2 Ceramic coatings

Ceramics, such as Cr_2O_3 and Al_2O_3, offer an interesting solution due to the good chemical resistance of these materials. Recently the performance of dicalcium silicate (Ca_2SiO_4) coatings has shown some interesting properties in sulphur atmospheres. [20] Ceramic coatings are mainly manufactured by APS, which produces porosity of 2–8%, and hence sealing as post-treatment is needed. HVOF technology has been used to produce denser, more protective coatings from ceramics. [21] The main disadvantages of ceramic coatings are poor mechanical properties and mismatches in CTE. The concept of functionally graded (FG) coatings was introduced some years ago. In this concept, material properties such as CTE and elastic modulus are designed to gradually change in order to decrease the thermal stresses within the coating. [22, 21]

3.2.3 Nanostructured coatings

It is recognised that nanocrystalline materials have special mechanical properties. Typically, the strength of crystalline materials is increased with decreasing grain size, and materials with very small grain size often also exhibit superplastic

behaviour at elevated temperatures. [23, 24] The use and interest for nanostructured materials is increasing rapidly, and it is estimated that the biggest steps forward in material science will be achieved using nanostructures. Nanocomposites that incorporate mainly nanostructured ceramic particles in a metallic nanocrystalline matrix have been studied intensively over the last few years. Among them one can find the nanostructured WC-Co and Cr_3Cr_2-NiCr composites. [25] Amorphous structures manufactured by HVOF or arc spray have been introduced to improve mechanical properties of metal alloy coatings. [26] Sustained efforts have been made to develop nanocrystalline ceramic powders and their plasma spraying. The major attempt is focused on the development of alumina-titania coatings, which have proved to possess superior toughness and adhesion along with high wear and spallation resistance. [27]

3.2.4 Sealing

Due to the porosity of thermal spray coatings corrosion resistance is lowered in critical applications. By sealing the thermally sprayed coating porosity can be minimised from 1–2% to zero, thus preventing the corrosive agents from penetrating to the substrate material. Sealing can either be done with different sealants, which are applied by painting onto the substrate closing the open porosity of the coating surface, or by laser treatment. [28]

4. Conclusions

According to the test results presented above, austenitic stainless steels and high-nickel-alloys provide protection to sulphidation attack which is, however, is an uncommon cause of failure. Highly alloyed metallic materials or claddings may not be feasible for economic and environmental reasons. Recent developments in the manufacturing of nickel-lean austenitic stainless steels as well as of metallic chromium-rich (Cr-Ni, Cr-Ni-Ti) coatings system may in the near future provide economic solutions for the extended life required. Prospective technologies based on the application of ceramic coatings and nanosized raw materials aiming at the manufacture of gas-tight, temperature cycling resistant coatings are in the development stage.

References

1. Daniel, P.L. The Effect of Coal Chlorides on Furnace Wall Corrosion. In: J. Stringer & D.D. Banerjee (Ed.), Chlorine in Coal. Elsevier Science Publishers, New York, 1991. 511 p.

2. Davis, C.J., James, P.J., Pinder, L.W. & Mehta, A.K. Furnace Wall Fireside Corrosion in PF-Fired Boilers: The Riddle Resolved. UEF/EPRI Conference, "Effect of Coal Quality on Power Plant Maintenance", Park City Utah, May 2000.

3. Lai, G. High-Temperature Corrosion of Engineering Alloys. ASM International, Materials Park OH, 1990. 231 p.

4. Simms, N.J., Saunders, S.R.J., Osgerby, S. & Oakey, J.E. Measurement and Compilation of Materials Degradation in the COST522 Programme. Materials at High Temperatures, 20(2)2003, pp. 137–151, 2003.

5. Moberg, O. Recovery boiler corrosion. In: Pulp and paper industry corrosion problems. NACE, Houston 1974.

6. Norton, J.F., Maier, M. & Bakker, W.T. The addition of Si to Fe-based alloys as a means of enhancing sulfidation resistance in complex mixed atmospheres. Materials at High Temperatures, 17(2)2000, pp. 327–337.

7. Mäkipää, M., Mäkinen, S., Backman, R. & Hämäläinen, M. Corrosion of BLRB floor tubes in reduced kraft smelts: Experimental and theoretical studies. 1996 Engineering Conference, Chicago, IL, USA, September 16–19. (Proc.), TAPPI PRESS, Technology Park/Atlanta, 1996.

8. Mäkipää, M., Oksa, M. & Koivisto, L. Superheater Tube Corrosion in Changing Operation Conditions of Recovery Boilers. CORROSION2001, Paper 01424. NACE, Houston, Texas, USA, 2001. 14 p.

9. Oksa, M. & Mäkipää, M.Comparative laboratory testing of molten salt attack of superheater tube materials. 10th International Symposium on Corrosion in the Pulp and Paper Industry. Helsinki, 21–24 August 2001. Helsinki 2001. Pp. 523–537.

10. Liu, C., Little, J.A., Henderson, P.J. & Ljung, P. Corrosion of HR3C heat exchanger alloy in a biomass fired PF utility boiler. Materials and Corrosion, 51(11)2000, pp. 765–773.

11. Mäkipää, M., Jokiniemi, J., Lind, T., Mikkanen, P., Pyykönen, J., Kauppinen, E., Oksa, M., McKeough, P., Koivisto, L., K. Saviharju, K. & Kytö, H. In: Superheater tube corrosion in recovery boilers, Proc. 10th Int. Symp. Corrosion in the Pulp and Paper Industry (10th ISCPPI). Helsinki 21–24 Aug. 2001. VTT Symposium 215, Hakkarainen, T. (Ed.).

12. Dunning, J.S, Alman, D.E. & Rawers, J.C. Influence of Silicon and Aluminum Additions on the Oxidation Resistance of a Lean-Chromium Stainless Steel. Oxidation of Metals, 57(5–6)2002, pp. 409–425.

13. Sho, A., Isomoto, T., Toyama, K., Urabe, T. & Yoshiba, M. Corrosion Performance of Newly Developed Stainless Steels for Superheater Tubes of High-Efficiency MSW-to-Power Plants. J. Japan Inst. Metals, 66(6)2002, pp. 554–562.

14. Fujukawa, H., Makiura, H. & Nishiyama, Y. Corrosion behavior of various steels in black liquor recovery boiler environment. Materials and Corrosion, 50(10)1999, pp. 154–161.

15. Totemeier, T.C., Wright, R.N. & Swank, W.D. Microstructure and stresses in HVOF sprayed iron aluminide coatings. Journal of Thermal Spray Technology 11 (2002), pp. 400–408.

16. Conde, A., Zubiri, F. & Damborenea, J. de. Cladding of Ni–Cr–B–Si coatings with a high power diode laser. Materials Science and Engineering A, 334 (2002), pp. 233–238.

17. Sidhu, B.S., Puri, D. & Prakash, S. Characterisations of plasma sprayed and laser remelted NiCrAlY bond coats and Ni3Al coatings on boiler tube steels. Materials Science and Engineering A 368 (2004), pp. 149–158.

18. Yamada, K., Tomono, Y., Morimoto, J., Sasaki, Y. & Ohmori, A. Hot corrosion behavior of boiler tube materials in refuse incineration environment. Vacuum 65 (2002), pp. 533–540.

19. Tortorelli, P.F. & Natesan, K. Critical factors affecting the high-temperature corrosion performance of iron aluminides. Materials Science and Engineering A 258 (1998), pp. 115–125.

20. Jansen, F., Wei, X., Dorfman, M., Peters, J. & Nagy, D. Performance of dicalcium silicate in hot-corrosive environment. Surface and coatings Technology 149 (2002), pp. 57–61.

21. Turunen, E., Varis, T., Gustafsson, T., Hannula, S.-P., Antila, E. & Gasik, M. Functionally Graded HVOF Sprayed NiCr-Al2O3 Coatings for Demanding Applications. International Thermal Spray Conference, ITSC 2003. Pp. 1531–1534.

22. Miyamoto, Y., Kaysser, W.A., Rabin, B.H., Kawasaki, A. & Ford, R.G. Functionally Graded Materials: Design, Processing and Applications, Kluwer Academic Publishers, Bosten, Dordrecht, London, 1999. 320 p.

23. Mohammed, F.A. & Li, Y. Creep and superplasticity in nanocrystalline materials: current understanding and future prospects. Mater. Sci. Eng., Vol. 298A (2001), pp. 1–15.

24. Hannula, S.-P., Koskinen, J., Haimi E. & Nowak, R. Nanoencyclopedia, Ed. R. Navi. In print. 2004.

25. He, J. & Schoenung, J.M. Nanostructured coatings. Materials Science and Engineering A, 336, 2002, pp. 274–319.

26. Seong, B.G., Hwang, S.Y. & Kim, K.Y. High-temperature corrosion of recuperators used in steel mills. Surface and Coatings Technology, 126, 2000, pp. 256–265.

27. Gell, M., Jordan, E.H., Sohn, Y.H., Goberman, D., Shaw, L. & Xiao, T.D. Development and implementation of plasma sprayed nanostructured ceramic coatings. Surface and Coatings Technology, Vol. 146–147, 2001, pp. 48–54.

28. Oksa, M., Turunen, E. & Varis, T. Sealing of thermally sprayed coatings. EUROCORR 2003 The European Corrosion Kongress, Budapest, HU, 28 Sept. – 2 Oct. 2003, European Federation of Corrosion (EFC), Hungary 2003. 291 p.

29. Viswanathan, R. & Bakker, W.T. Materials for Boilers in Ultra Supercritical Power Plants. Proc. of 2000 International Joint Power Generation Conference, Miami Beach, Florida, July 23–20. 2000, IJPGC2000-15049. 22 p.

30. Brill, U., Klower, J., Maassen, E., Richter, H., Schwenk, W. & Venkateswarlu, J. Effects of chromium and silicon on the behaviour of heat-resistant alloys in simulated waste incineration environments. Proceedings of the Conference Materials for Advanced Power Engineering, 3–6 October 1994, (Part II). Liege. D. Coutsouradis et al. (eds.). Kluwer Academic Publishers 1994. Pp. 1585–1596.

31. Lai, G., Hulsizer, P., Brooks, R. Life Extension of Boilers using Weld Overlay Protection. Baltica IV, Helsinki, September 1998. Espoo 1998. VTT Symposium 184. Pp. 309–330.

32. .DuPont, J.N. Solidification of an alloy 625 weld overlay. Met. & Materials Trans. 27, (1996), pp. 3612–3620.

33. Goodwin, G.M. Weld Overlay Cladding with Iron Aluminide. Proc. of 11th Annual Conference on Fossil Energy Materials, Knoxville, May 20–22, 1997. Pp. 217–224.

The new hybrid protective coating for hot corrosion applications

M. Danielewski[1], S.Środa[2], Z. Żurek[3], R. Gajerski[1] & I. Lalak[4]

[1]University of Science and Technology, AGH, Kraków, Poland
[2]European Commission Joint Research Centre, Institute for Energy, Petten, The Netherlands
[3]Cracow University of Technology, Institute of Chemistry and Inorganic Technology, Kraków, Poland
[4]Warsaw Combined Heat and Power Plants S.A., Warsaw, Poland

Abstract

A new hybrid protective coating has been developed to extend the lifetime of power plant boiler water walls and other parts of the boiler affected by hot corrosion. The base layer of the coating (30–80 μm thickness) consists of non-organic bounding agents and a specially processed Al filler. The top layer contains spherical and/or flake-like Al, Si and/or Al-Si fillers (25–60 μm thickness). The bonding is a mixture of organic resins.

The coating has been tested using laboratory salt-recoat corrosion tests and cyclic-oxidation tests up to 2000 hours, mainly at the temperature range of 400–550^{o}C. The best of the hybrid coating variants outperformed several commercial products at 500, 550 and 600^{o}C. The first plant corrosion tests were started in Power Plant "Siekierki" in Poland in 2001. From that time several trial plant tests have been made to optimise the coating composition and the application process. The results of the laboratory scale and power plant tests show that the coating provides active chemical and passive mechanical protection of the outer metal surface. The coating limits access of the corrosive atmosphere to the base metal, protects against erosion and decreases the deposit/ash adhesion. The coating shows satisfactory oxidation resistance up to 500^{o}C in oxidizing as well as in reducing atmospheres. Additionally, special application procedure provides protection in high humidity environments at room temperature. At present stage the hybrid coating has been tested in the corrosion laboratory at JRC IE Petten in several simulated combustion atmospheres to investigate aptitude for waste incinerator application.

1. Introduction

This project has been a collaborative venture between the University of Science and Technology (AGH), Cracow University of Technology and several Polish commercial companies undertaken within the State Committee for Scientific Research funded Targeted Project framework. Close collaboration was developed between the universities and industrial partners consisting of two SMEs: EnterEko, Remak and the end-user: Power Station "Siekierki". The project was started in September 2001 and will be ended in August 2004.

The principal objectives of the proposal were:

- to design a hybrid overlay coating which would offer protection over a range of hot corrosion conditions likely to be experienced in coal fired boilers and industrial gas turbines
- to develop a manufacturing route for the application of such coatings on boiler components, which could improve the operational flexibility of the boiler.

Initial fundamental studies were undertaken using several base and overlay coatings to define the optimal thickness and composition offering optimum resistance to hot corrosion over the temperature range of 350–550^{o}C. Samples of tested materials have been coated with a family of these graded structures and their corrosion resistance has been evaluated using laboratory salt-recoat corrosion tests and cyclic-oxidation tests up to 2000 hours over the temperature range of 400–550^{o}C. The industrial partners undertook substantial development of the coating technology in the second half of the project in order to define a thermal treatment route for on-site coating procedure. The obtained coating responds to corrosion environment to form the optimum protective layer for the corrosion environment, i.e. an alumina layer at high temperatures and a compact thin magnetite layer at lower temperatures.
Finally the coating with the generic name HybrideMD has now been applied to the complex geometry of an industrial coal-fired boiler (750m^2) in "Siekierki" Power Plant.

2. Experimental

2.1 Laboratory tests

The samples for the tests were first cleaned by 8 bar pressured air and the surfaces were polished by corundum powder. Then immediately the first layer of the hybrid coating was applied by air spray method. After drying, the second layer was applied by the same method. Finally the samples were pre-heated for

24h at a temperature of 200°C. The obtained multi-layer protective coating has a base layer of 60 μm thickness consisting of non-organic binding agents and specially processed Al filler, while the top layer contains spherical and/or flake like Al, Si and/or Al-Si fillers 40 μm thick. The bonding was a mixture of organic resins. Fig. 1 shows the microphotograph of hybride coating before the tests.

Salt-recoat corrosion tests and cyclic-oxidation tests were made up to 2000 hours over the temperature range 400–550°C using NaCl + Na_2SO_4 deposit in 10%H_2O + 1% SO_2 gas mixture. Fig. 2 presents SEM microphotograph of the cross section of the scale formed on carbon steel protected by hybrid coating with NaCl + Na_2SO_4 deposit in 10%H_2O + 1% SO_2 gas mixture for 2000 h.

The multi-sample exposure tests were carried out under isotermal conditions at temperature of 500°C in N_2-8% O_2-15% H_2O-2000 vppm HCl atmosphere for 360 hours. The exposure test was carried out in a vertical tube furnace, tube diameter 80 mm. The gas flow was 10 l/h. The gas before the furnace was passed through the humidifier at appropriate temperature to obtain 15% of water vapour in the gas mixture. Fig. 3 shows SEM micrographs of the sample protected with HybrideMD coating exposed to N_2-8% O_2-15% H_2O-2000 vppm HCl atmosphere at 500°C for 360 hours.

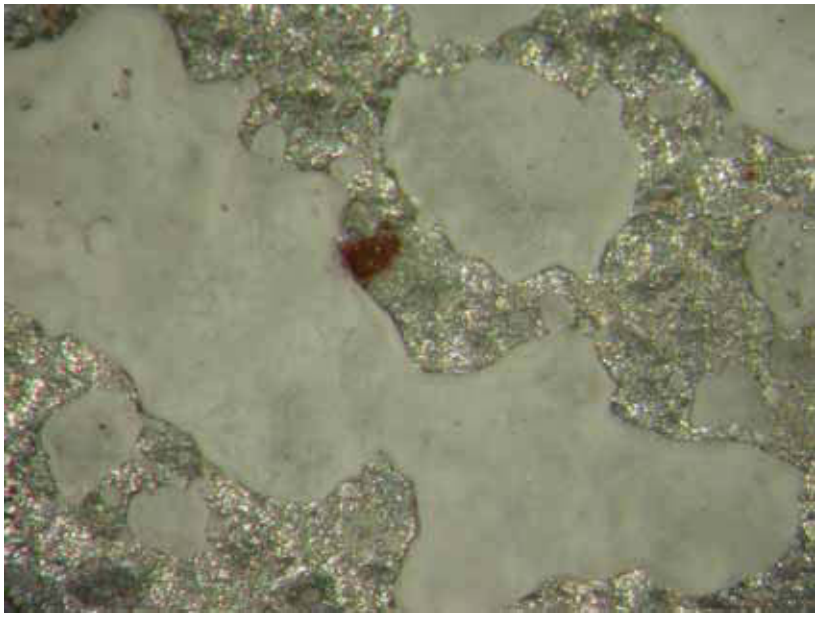

Figure 1. SEM micrograph of the surface of the MD hybrid coating before the exposure test.

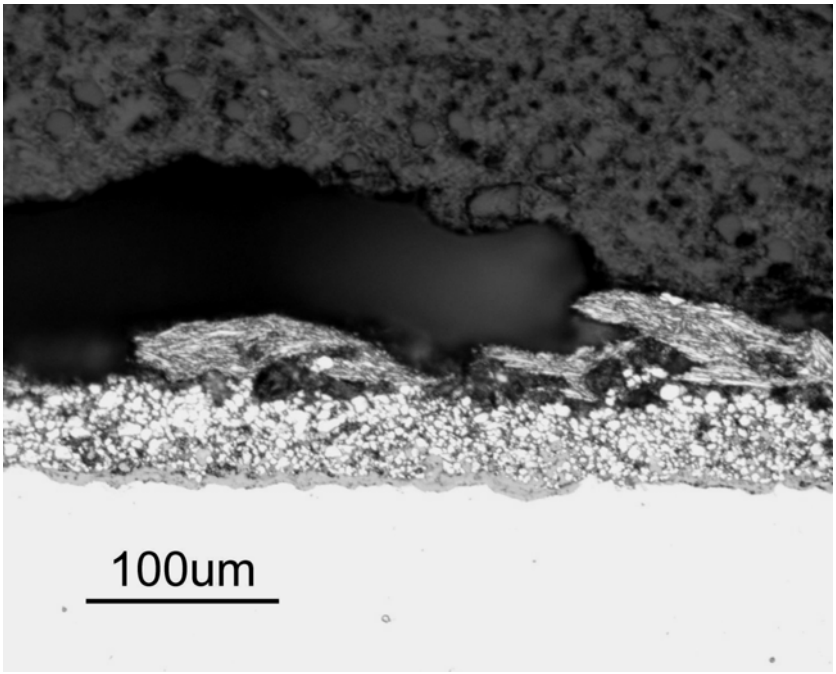

Figure 2. SEM micrograph of the cross section of the scale formed on carbon steel protected by hybrid coating with NaCl + Na_2SO_4 deposit in 10%H_2O + 1% SO_2 gas mixture for 2000 h.

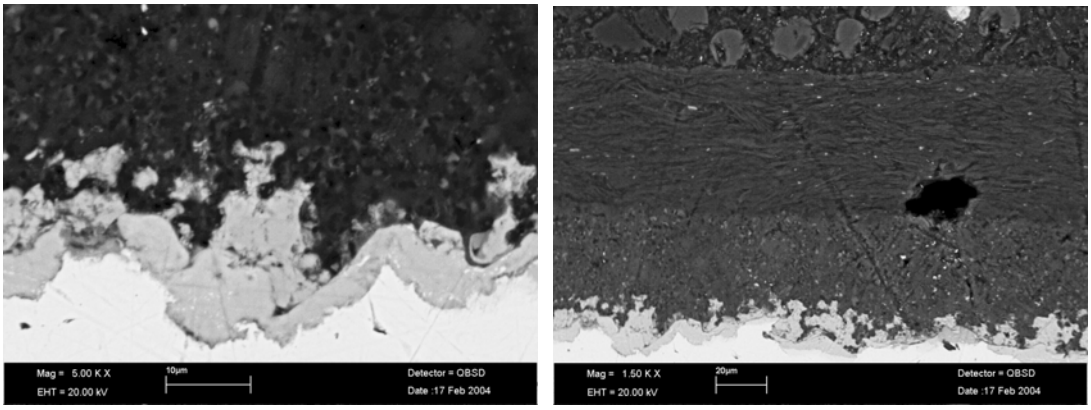

Figure 3. SEM micrographs of the sample protected with HybrideMD coating exposed to N_2-8% O_2-15% H_2O-2000 vppm HCl atmosphere at 500^oC for 360 hours.

2.2 Plant tests

The first plant corrosion tests were started in Power Plant "Siekierki" in Poland in 2001 (Figs. 4–8). From that time several trial plant tests have been made to optimise the coating composition and the application process.

Application consists of the following steps:

- shot/sand blasting of boiler tubes exposed to hot corrosion,
- air-less application of the base coat,
- thermal treatment at 300–350°C,
- air-less application of the top layer(s).

Figure 4 presents the uncoated wall after operation in "Siekierki" Power Plant.

Figure 4. Uncoated wall after operation in "Siekierki" Power Plant.

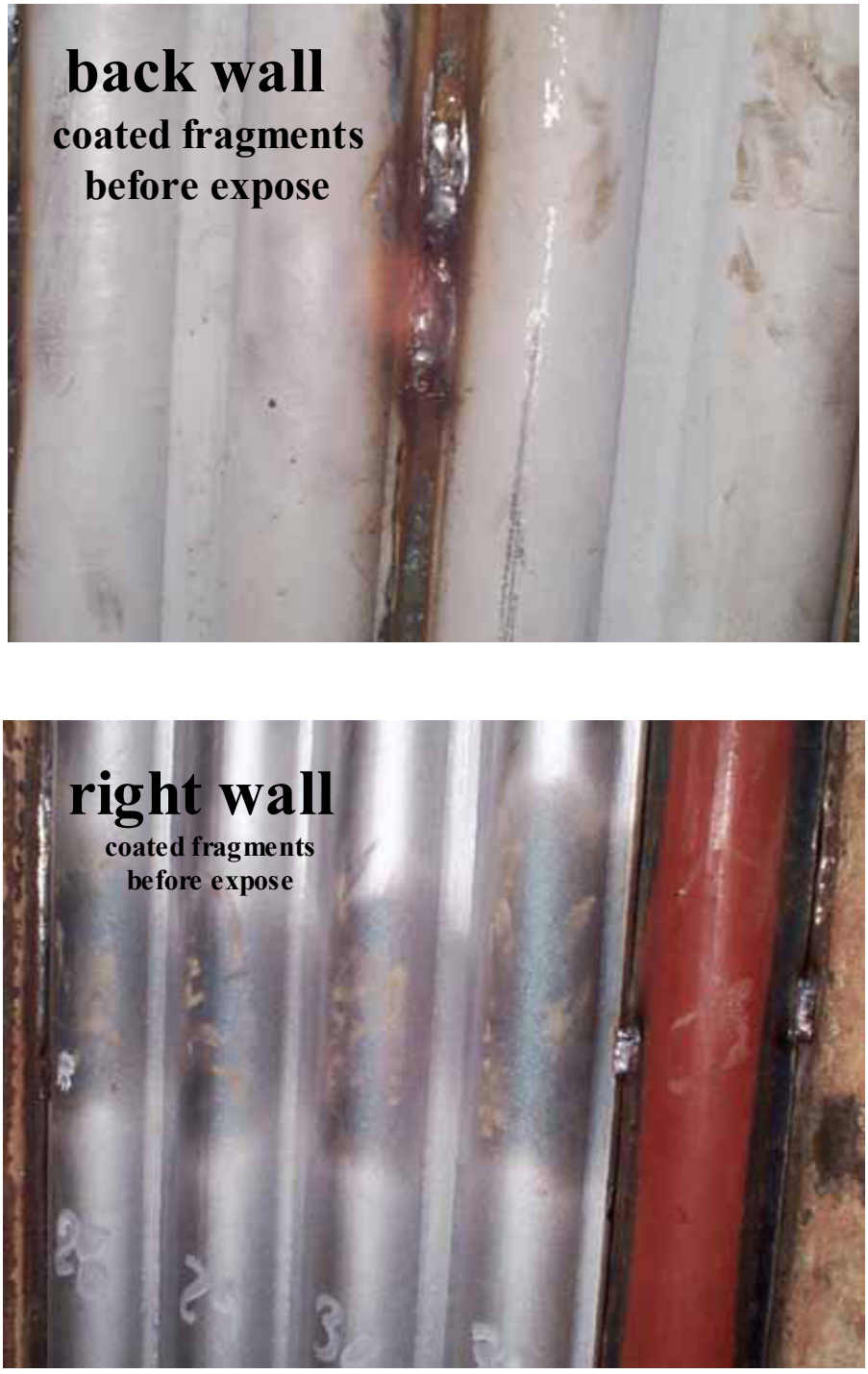

Figure 5. Photographs of the water walls in "Siekierki" Power Plant with hybrid coating before exposure testing.

a)

b)

Figure 6. Photographs of the water walls in "Siekierki" Power Plant protected with hybrid coating a) after 4000 h operation, b) after more than 8000 h of operation.

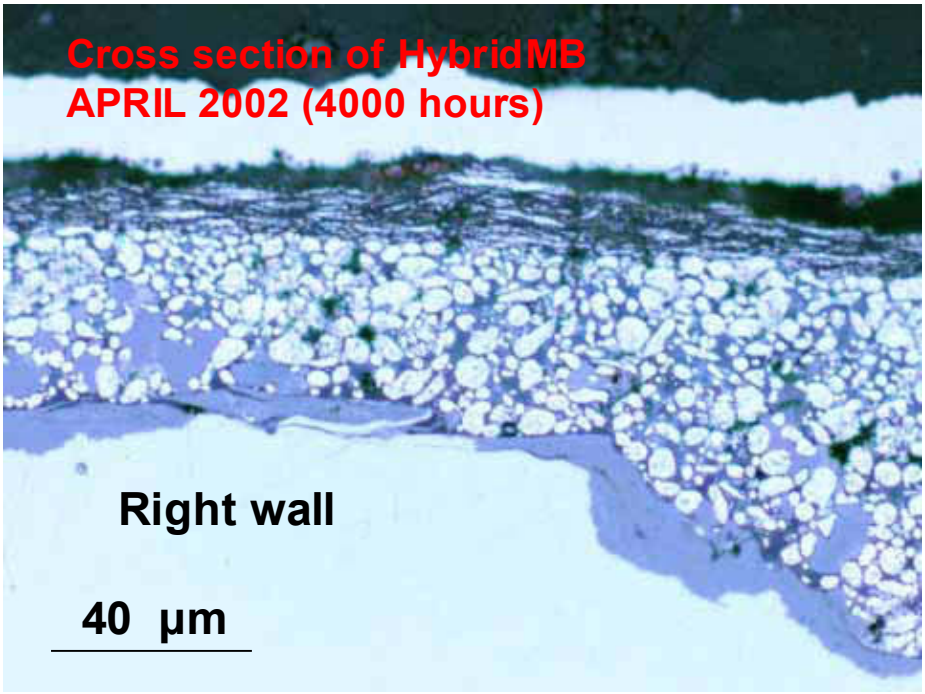

Figure 7. SEM micrograph of the cross section of a tube protected by HybrideMD coating after 4000 h of operation in "Siekierki" Power Plant.

Figure 8. Photograph of the water wall tubes protected by HybrideMD coating after 8000 h operation in "Siekierki" Power Plant.

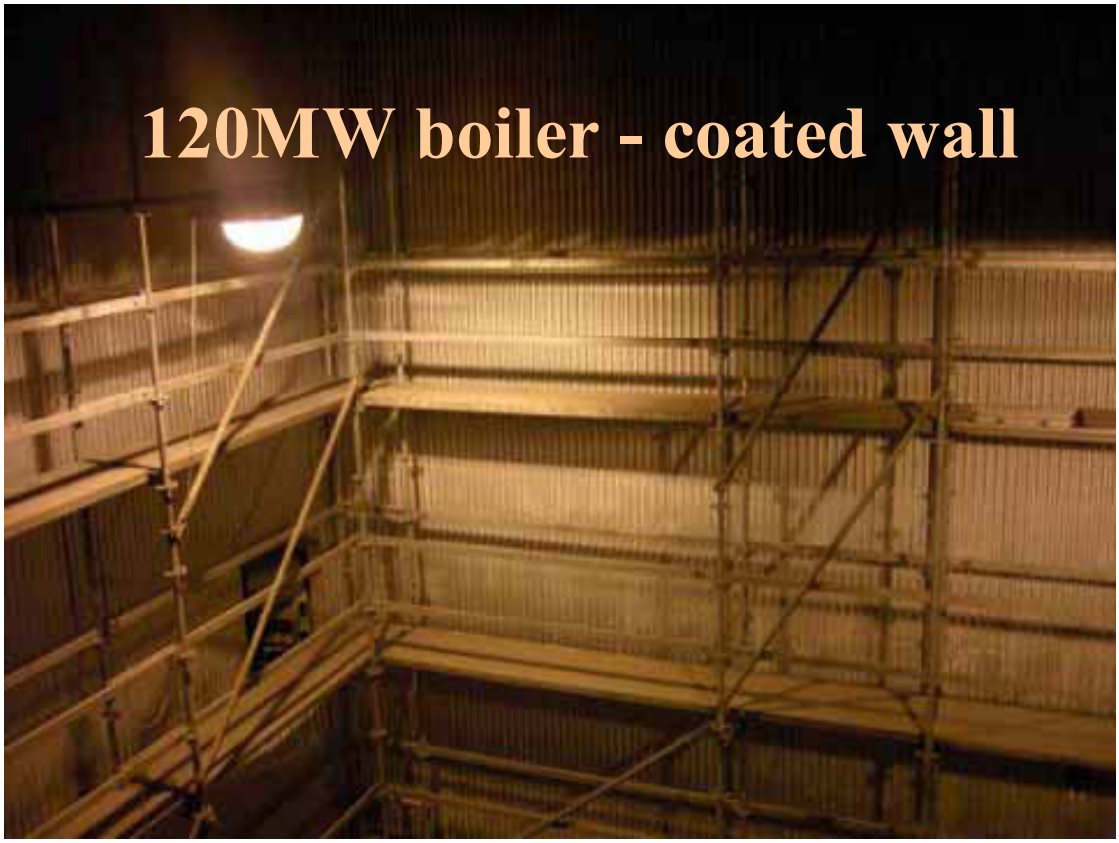

Figure 9. HybrideMD variant has been applied in 2003 to the complex geometry of an industrial coal-fired boiler (750m^2).

3. Summary

Based on several different laboratory tests and finished and ongoing plant tests the HybrideMD coating shows advantages as follows:

- Protects against hot corrosion, decreases oxidation rate,
- Does not affect:
  - boiler performance,
  - boiler construction,
  - working conditions,
- Decreases deposits/ash adhesion,
- Protects against erosion,
- Can be reapplied or renovated,
- Simple on-site procedure,
- Low cost (components, first application and renovation).

Disadvantages or limitations of the coating are:

- Dimensions of the samples should be more than 20x20 cm
- Application of this coating is laborious
- Failing on the edges
- Leakage of the coating.

4. Acknowledgements

This work has been supported by Polish Scientific Committee (KBN) Grant No.6 T08 0116 2001 C/05691

The effect of HCl and SO_2 on gas phase corrosion of boiler steels

Satu Tuurna[1], Szymon Sroda[2] & Liisa Heikinheimo[1]

[1]VTT Industrial Systems, P.O. Box 1704, 02044 VTT FINLAND
[2]European Commission Joint Research Centre, Institute for Energy, P.O. Box 2, NL-1755 ZG Petten, The Netherlands

Abstract

The high temperature corrosion kinetics and mechanism of different steel types, typically used in boiler applications, were investigated. Materials were exposed in simulated moist air atmosphere (8%O_2 + 15%H_2O) with 200 ppm SO_2 and 2000 ppm HCl addition at temperatures of 500 and 600°C. The measured mass mass change for different exposure times up to 360 h shows that in the conditions used the oxidation rate of studied samples obeys parabolic rate law. Corrosion products, growing on tested materials, were analysed by SEM/EDS and XRD techniques. The obtained results indicated a significant influence of gas composition and temperature on the morphology and growth rate of the corrosion product. The presence of chlorine in simulated combustion atmosphere accelerates the oxidation process. In general, the oxidation layers formed in moist air with HCl addition are more prone to spallation, exhibits large porosity and several cracks. The observed morphology and composition of the oxide scales suggest that in this case the corrosion mechanism could be described as *active oxidation* process. Active oxidation assumes that the oxide scale contains physical defects through which the gas phase chlorine and oxygen can diffuse to reach the scale/metal interface. Then the iron is chlorinated, and volatile or condensed $FeCl_2$ can form. In contrast, in the most of the studied cases the presence of sulphur seems to slow down the corrosion rate. The growing scales are more dense and adherent to the base metal. The sulphides, which were formed mainly at metal/scale interface, may play the significant role in ion transport through the scale

1. Introduction

Boiler tubes have a finite lifetime because of prolonged exposure to an aggressive service environment, high temperature and stresses. Analysing plant operating data and characterising service exposed tubes failure mechanisms and degradation processes can be concluded. This information is valuable in predicting the remaining lifetime of a component. However, since this data is not produced

under controlled environments and several parameters have synergetic effects, the exact reason for a failure cannot be identified. Laboratory tests at controlled environments are used to characterise and identify an individual failure mechanism and its dependency on test parameters varying preferable only one parameter at a time. The laboratory experiment data can be utilised with a long-term operating data to obtain wider process knowledge for the background of lifetime predictions.

The presence of chlorine, sulphur, alkali metals and moisture in combustion gases is the main reason for high temperature corrosion of boiler materials [1]. The water vapour accelerates severely the oxidation of metal surfaces in combustion gases. Sulphidation reactions are one of major factors in high temperature corrosion. Combustion of fuels containing sulphur produces SO_2, which can be partially oxides to SO_3. Alkali and heavy metal impurities in the fuel react with SO_2/SO_3 at the combustion temperature forming different sulphates/sulphites, which are highly corrosive when depositing on the tube surfaces. Even in small amounts, sulphur in various forms can accelerate corrosion at high temperatures. Sulphur together with oxygen forms much more aggressive environment than oxygen alone. In many metals the reaction rates with sulphur are much faster than the reaction rates with oxygen [2–5]. Chlorine activated corrosion is the most detrimental corrosion process in energy conversion systems. Chlorides and hydrochloric acid increase the oxidation rate, and also cause cracking and spallation of the oxide layer formed on the metal surface. Metal chlorides are formed by inward diffusion of chlorine to the metal/oxide interface, at where they evaporate and subsequently are oxidised to non-protective oxides releasing chlorine, which can return into the oxide layer [6–8].

The low alloyed ferritic/martensitic steels are traditionally preferred boiler materials due to their low thermal expansion coefficient, good thermal conductivity, creep strength and relatively low cost. However, the high temperature properties of these materials are adequate only up to 600°C and these materials have a quite poor high temperature corrosion resistance. Recent demands for higher steam temperatures and pressures have created a need for materials with higher strength properties. High-alloyed steels have better resistance against high temperature oxidation and corrosion than ferritic steels and these are used if ferritic steels cannot resist the atmosphere in question. The nickel-based alloys seem to have the best resistance against high temperature corrosion in those atmospheres [4, 9, 10].

The results presented here are a part of the study aiming at control and optimisation of in-service performance of boiler materials, EU-OPTICORR project [11]. The laboratory tests are aiming to characterise and identify an individual failure mechanism of several alloys and steels at simulated combustion atmospheres. In this study, the high temperature corrosion behaviour of different steel types were investigated at temperatures of 500 and 600°C under moist air atmosphere with 200 ppm SO_2 or 2000 ppm HCl.

2. Experimental

Three ferritic, one austenitic steel and one nickel based alloy were chosen for the studies. The chemical compositions of studied materials are presented in Table 1.

The samples were cut from the plates into rectangle shape coupons of 10 x 10 x 2–5 mm dimensions. Their surfaces were bright polished with SiC paper of 1000 grit, then ultrasonically degreased in ethanol.

Table 1. Chemical composition of studied materials (wt-%).

Steel grade	Fe	Cr	Mo	Ni	Mn	Al	Si	Cu	C
71518	bal	0.6		0.8	1	0.04	0.4	0.4	0.076
4X60	bal	1.4		0.04	0.6	0.04	0.2	0.01	0.058
2.25Cr1Mo	bal	2.25	1	0.4	0.6	0.01	0.2	0.15	0.059
TP347H	bal	17.6		10.7	1.8		0.3		0.048
Alloy 625 Si	2.8	19.0	8.9	bal		0.24	1.2		

The multi-sample exposure tests were carried out under isothermal conditions at temperatures of 500 and 600°C in N_2-8% O_2-15% H_2O-200 vppm SO_2 and N_2-8% O_2-15% H_2O-2000 vppm HCl atmospheres up to 360 hours. The test gases were based on the TESTCORR recommendations. The exposure tests at 500°C were carried out in a vertical tube furnace, tube diameter 80 mm. The gas flow was 10 l/h. The tests at 600°C were carried out in a horizontal tube furnace, tube diameter 75 mm. The gas flow used was 6 l/h. Before entering the furnace, the gases were passed through the humidifier unit at an appropriate temperature to obtain 15% of water vapour in the gas mixture.

The composition and sequence of the growing reaction layers on exposed samples were studied using SEM/EDS and XRD analyses. To monitor the corrosion phenomena mass change measurements were carried out.

3. Results

3.1 Mass change measurements

Fig. 1 shows the mass change per unit area for studied ferritic and austenitic materials oxidised in moist synthetic air, N_2-8% O_2-15% H_2O-200 vppm SO_2 and N_2-8% O_2-15% H_2O-2000 vppm HCl atmospheres at 500 and 600°C. The mass change of nickel based alloy samples in used, relatively short, exposure times was almost negligible.

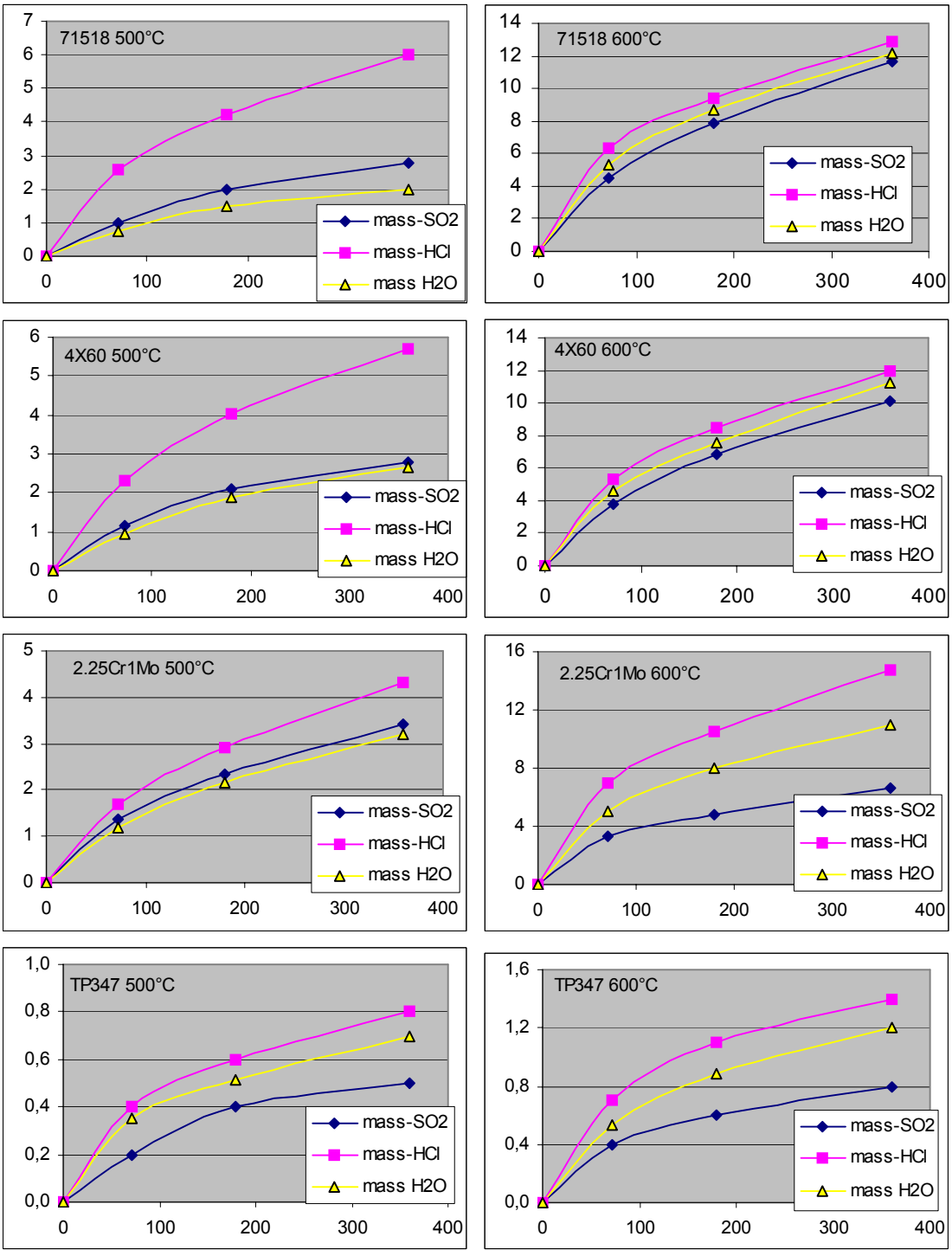

Figure 1. Mass change [mg/cm^2] of studied samples oxidised in N_2-8% O_2-15% H_2O, N_2-8% O_2-15% H_2O-200 vppm SO_2 and N_2-8% O_2-15% H_2O-2000 vppm HCl atmospheres at 500 and 600°C up to 360 h.

3.2 Oxide scale composition and morphologies

The composition and sequence of the growing reaction layers on exposed samples were studied using SEM/EDS and XRD analyses. Fig. 2 presents the oxide scales formed on 2.25Cr1Mo samples after 360 h exposure at 600°C in N_2-8% O_2-15% H_2O-200 vppm SO_2 and N_2-8% O_2-15% H_2O-2000 vppm HCl.

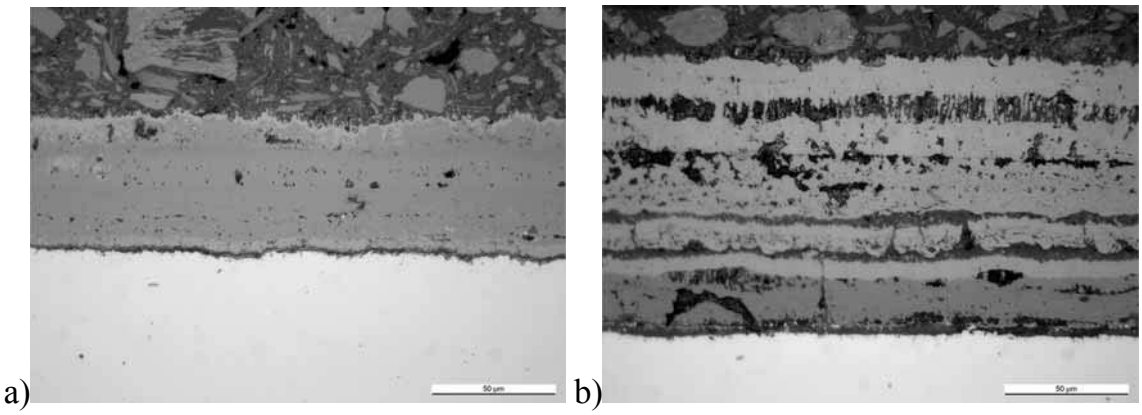

Figure 2. The oxide scales formed on 2.25Cr1Mo samples after 360 h exposure at 600°C. a) N_2-8% O_2-15% H_2O-200 vppm SO_2 and b) N_2-8% O_2-15% H_2O-2000 vppm HCl. Scales 50 µm.

Fig. 3 shows the microphotograph and the SEM/EDS analysis of surface oxide scales formed on steel TP347 after 360 h exposure at 500°C in moist synthetic air containing SO_2 and HCl.

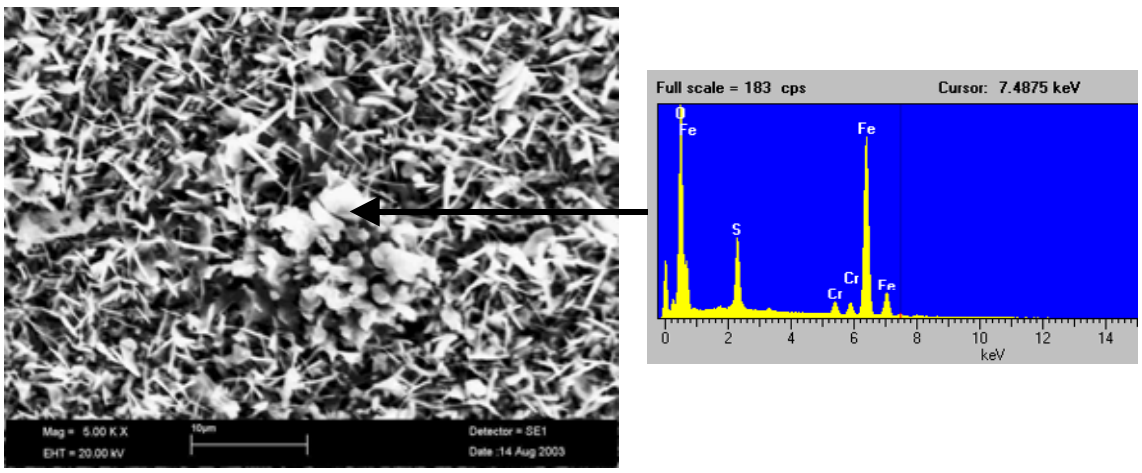

Figure 3. The microphotograph and the SEM/EDS analysis of surface oxide scales formed on steel TP347 samples after 360 h exposure at 500°C in N_2-8% O_2-15% H_2O-200 vppm SO_2 atmosphere.

Fig. 4 shows the oxide crystals growing at Alloy 625 surface after 360 h exposure at 500°C moist synthetic air containing SO_2 and HCl.

a) 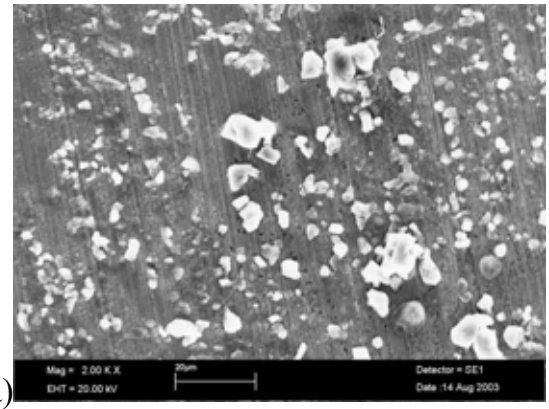 b) 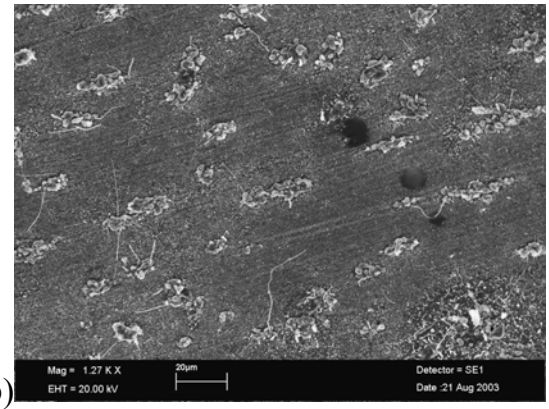

Figure 4. Oxide crystals at Alloy 625 surface after 360 h exposure at 500°C. a) N_2-8% O_2-15% H_2O-200 vppm SO_2 and b) N_2-8% O_2-15% H_2O-2000 vppm HCl. Scales 20 μm.

Figs. 5 and 6 present the X-ray maps of the elements in oxide scales formed on steel TP347 after 360 h exposure at 500°C in N_2-8% O_2-15% H_2O-200 vppm SO_2 and N_2-8% O_2-15% H_2O-2000 vppm HCl.

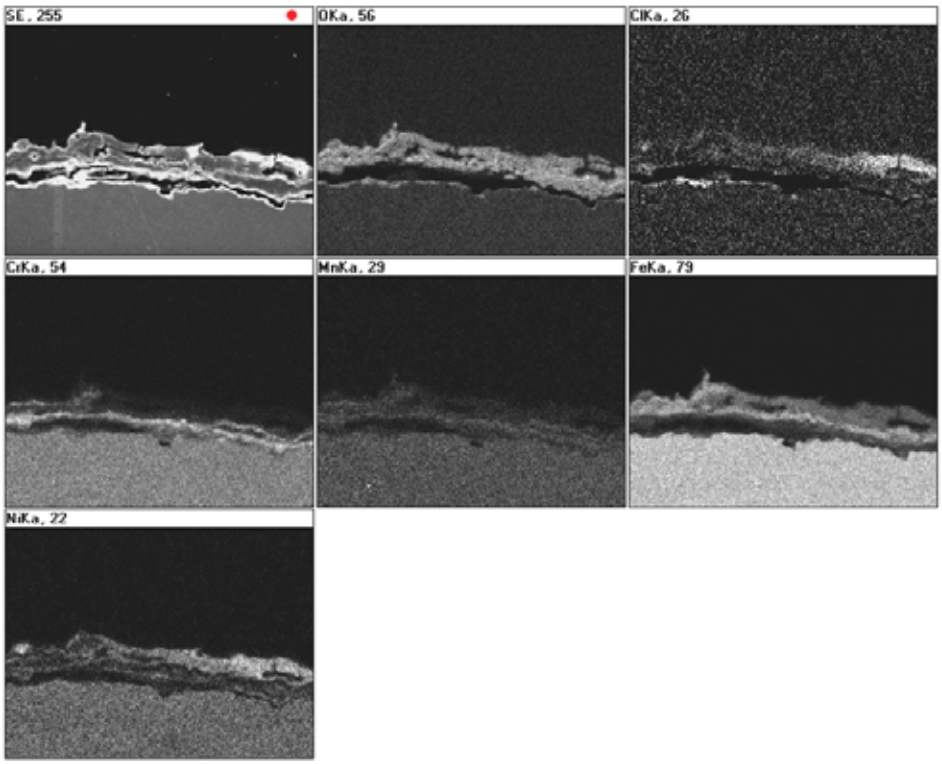

Figure 5. X-ray maps of the elements in oxide scales formed on steel TP347 after 360 h exposure at 500°C in N_2-8% O_2-15% H_2O-200 vppm SO_2.

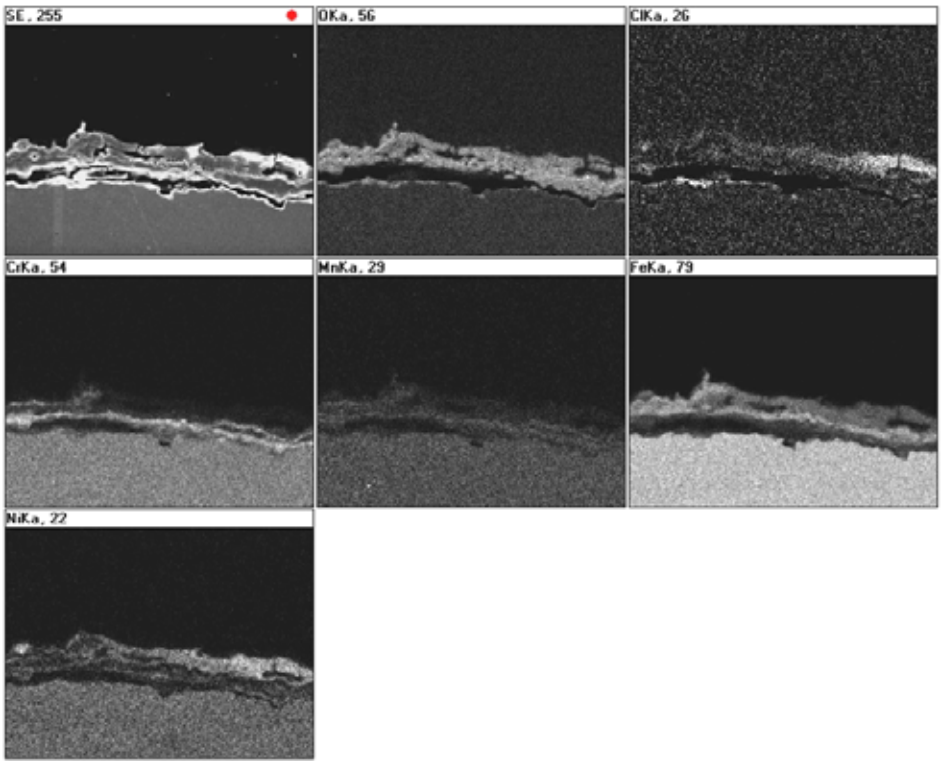

Figure 6. X-ray maps of the elements in oxide scales formed on steel TP347 after 360 h exposure at 500°C in N_2-8% O_2-15% H_2O-2000 vppm HCl.

4. Discussions

The mass change measurements combine with SEM/EDS and XRD analyses presented show that the oxidation rate and mechanism depend strongly on the temperature and the gas composition.

Measured mass change for different exposure times up to 360h (Fig. 1) shows that in used conditions the oxidation rate of studied samples may be described by the parabolic law (Eq. 1). It means that the oxidation and thereby the scale build-up process is controlled by diffusion of the reagents within the reaction products phase.

$$\left(\frac{\Delta m}{A}\right)^2 = 2k_p t + C' \qquad (1)$$

where $\Delta m/A$ is a mass increase per unit area [g/cm^2]

k_p is the parabolic rate constant, which is proportional to the diffusivity of the rate-controlling ionic species [g^2/cm^4s]

t is duration time of the process [s] and C' is the integration constant.

In all cases the mass change of samples exposed in SO_2 gas was smaller than the mass change in HCl containing exposure gas (Fig 1). Table 2 presents the parabolic rate constants calculated from mass change results after 360 h exposure. For all materials tested the rate constants are increasing with the exposure temperature and also with the change of exposure atmosphere from SO_2 containing gas to HCl containing gas.

Table 2. Parabolic rate constants for exposed materials after 360 h [$g^2cm^{-4}s^{-1}$].

Material/ Conditions	**500°C-SO_2**	**600°C-SO_2**	**500°C-HCl**	**600°C-HCl**
71518	6.0E-12	1.0E-10	2.8E-11	1.3E-10
4X60	6.0E-12	7.9E-11	2.5E-11	1.1E-10
2.25Cr1Mo	8.9E-12	3.4E-11	1.4E-11	1.7E-10
TP347H	1.9E-13	4.9E-13	4.9E-13	1.5E-12

In general, the oxide scales formed on the studied alloys had a multi-layered structure. Similar scale structures have been reported in the literature [12, 13].

Fig. 7 illustrates the schematic structures of oxide scales formed in moist air with the SO_2 and HCl additions on studied materials.

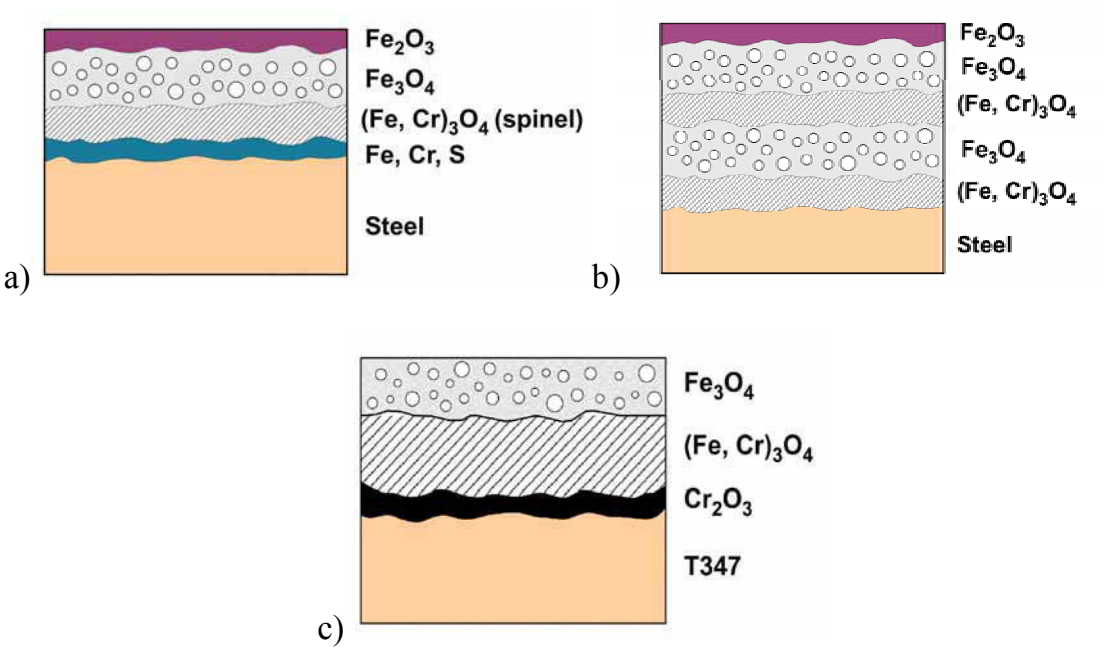

Figure 7. Schematic drawings of oxide structures formed on different types of steels. Scales formed on a) low Cr steel in gas containing SO_2 and b) HCl, and c) on austenitic steel.

Oxide scales formed on the ferritic steels in moist air with SO_2 addition had a multi-layered structure (Fig. 7a), basically similar to the oxide structures observed on ferritic steels exposed in moist air [14]. The thin outer layer is hematite. The middle scale consisted of magnetite. The inner scale contained mainly iron-chromium oxide with small amounts of alloying elements as Si and Mo. Sulphur was found at the metal/scale interface (Fig. 5) and also coincidentally on the surface on the growing scale (Fig. 3).

The morphology of the outer scales after oxidation in moist air with HCl was quite similar as in moist air with SO_2 (Fig. 7b). In this case, however, minor amounts of Cl were found at the metal/scale interface probably as $FeCl_x$. At 600°C, the scale showed a layer-by-layer structure. In particular, the oxide layer formed on the 2.25Cr1Mo material had a repeating structure of inner iron-chromium oxide and outer iron oxide scales (Fig. 2b).

The effect of chromium concentration on the oxidation resistance can be seen from the exposure results. Higher Cr concentrations result in lowered oxidation rate. The formation of $(FeCr)_3O_4$ islands reduce the outward diffusion of iron [12]. Only a thin oxide layer was formed on the surface of austenitic steel TP347H during 360 h exposure. However, also this oxide scale had a multi-layer structure with the outer layer of Fe_3O_4 and inner layer of Fe_3O_4-$(Cr,Ni)_2O_3$ mixture (Fig. 7c). After the exposure test in moist air with SO_2 sulphur was found at metal/scale interface probably as a nickel sulphide (Fig. 5) while after exposure in moist air with HCl addition chlorine was found in the metal scale interface (Fig. 6). Corrosion of Alloy 625+Si was almost negligible in all exposure atmospheres, however some oxide crystals could bee seen on its surface (Fig. 4).

Generally, the oxide scales formed in moist air containing HCl were more porous with several cracks than oxides formed in moist air with SO_2; more spallation of the scales was also observed. Although only small amounts of Cl was detected in reaction product layers, the observed morphology and composition of the scales suggest that in this case the corrosion mechanism was an *active oxidation* process [4, 15], which assumes that the oxide scale contain physical defects through which the gas phases chlorine and oxygen can diffuse to reach the scale/metal interface at which the iron is chlorinated, and volatile or condensed $FeCl_2$ can form.

The corrosion behaviour of studied samples in moist air with SO_2 shows that the sulphides (on ferritic steels – iron sulphide, on austenitic steel preferably the nickel sulphide), which were formed mainly at metal scale interface, can have a significant impact on ion transport through the scale.

5. Conclusions

The results presented here are a part of the project aiming to control and optimise the in-service performance of boiler materials and development of simulation tools for high temperature oxidation of steels under service conditions (EU FP5 OPTICORR Project).

The presence of HCl in moist gas at temperatures of 500°C and 600°C accelerates the oxidation process of the studied ferritic steels. In contrast, the presence of SO_2 seems to suppress this process. The effect of HCl on the oxidation rate of more alloyed materials is not so evident in used, relatively short, exposure times.

This study is continued to cover more tests in moist air with the mixture of SO_2 and HCl to clarify corrosion behaviour of materials under controlled simulated combustion environments. Proper data is needed for processing and quantification of the kinetic data, modelling the oxidation kinetics and the development of computer-based simulation methods for lifetime analyses.

References

1. Otsuka, N. Effects of Fuel Impurities on the Fireside Corrosion of Boiler Tubes in Advanced Power Generating Systems – a Thermodynamic Calculation of Deposit Chemistry. Corrosion Science, Vol. 4 (2002), pp. 265–283.

2. Kofstad, P. High temperature corrosion. Elsevier Applied Science, 1988. 558 p.

3. Bakker, W. The Effect of Deposits on Waterwall Corrosion in Fossil Fueled Boilers. Materials at High Temperatures 20 (2003), pp. 161–168.

4. Srivastava, S. & Godiwalla, K. Review - Fuel Ash Corrosion of Boiler and Superheater Tubes. Journal of Materials Science, 32 (1997), pp. 835–849.

5. Gawel, J. & Wyczesany, A. Equilibrium Gas Compositions for the SO_2-O_2 System and Their Application to the Sulfidation of Copper. Corrosion Science, Vol. 28 (1989), pp. 867–872.

6. Grabke, H.J., Reese, E. & Spiegel, M. The Effects of Chlorides, Hydrogen Chloride, and Sulfur Dioxide in the Oxidation of Steels Below Deposits. Corrosion Science, Vol. 37 (1995), pp. 1023–1043.

7. Kawahara, Y. High temperature corrosion mechanisms and effect of alloying elements for materials used in waste incineration environments. Corrosion Science, Vol. 44 (2002), pp. 223–245.

8. Mayer, P. & Manulescu, A. Influence of Hydrogen Chloride on Corrosion of Boiler Steels in Synthetic Flue Gas. Corrosion – NACE, Vol. 36 (1980), pp. 369–373.

9. Viswanathan, R. & Bakker, W. Materials for Ultrasupercritical Coal Power Plants – Boiler Materials: Part 1. Journal of Materials Engineering and Performance, Vol. 10 (2001), pp. 81–95.

10. Iseda, A., Sawaragi, Y., Teranishi, H., Kubota, M. & Hayase, Y. Development of New 12% Cr Steel tubing (HCM12) for Boiler Applications. The Sumimoto Search, No. 40 (1989), pp. 41–56.

11. Heikinheimo, L., Hack, K., Baxter, D., Spiegel, M., Krupp, U., Hämäläinen, M. & Arponen, M. Optimisation of in-service performance of boiler steels by modelling high temperature corrosion – EU FP5 OPTICORR project. 6th International Symposium High Temperature Corrosion and Protection of Materials, 16–21 May 2004, Les Embiez France.

12. Ueda, M., Nanko, M., Kawamura, K. & Maruyama, T. Formation and Disappearance of an Internal Oxidation Zone in the initial Stage of the Steam Oxidation of Fe-9Cr-0.26Si Ferritic Steel. Materials at High Temperatures, 20 (2003), pp. 109–114.

13. Marino, L. & Bueno, L. High-Temperature Oxidation Behavior of 2.25Cr-1Mo Steel in Air - Part 1: Gain of Mass Kinetics and Characterization of the Oxide Scale. Journal of Pressure Vessel Technology, Vol. 123 (2001), pp. 88–96.

14. Sroda, S., Tuurna, S., Penttilä, K. & Heikinheimo, L. High Temperature Oxidation Behaviour of Boiler Steels under Simulated Combustion Gases. 6th International Symposium High Temperature Corrosion and Protection of Materials, 16–21 May 2004, Les Embiez France.

15. Spiegel, M., Zahs, A. & Grabke, H.J. Fundamental Aspects of Chlorine Induced Corrosion in Power Plants. Materials at High Temperatures, 20 (2003), pp. 153–159.

Structural analysis and lifetime assessment of steam drums

Otso Cronvall, Satu Tuurna, Heli Talja, Liisa Heikinheimo & Pertti Auerkari
VTT Industrial Systems
P.O. Box 1704, FIN-02044 VTT
Espoo, Finland

Abstract

Structural analysis and lifetime assessment of steam drums in conventional power plants are discussed in this article. The analyses involve damage and structural mechanics, heat transfer analyses and fracture mechanics, and are connected to fluid mechanics. The used input data was from two steam drums in a Finnish fossil fuel power plant. Structural mechanics analyses were performed with FEM code ABAQUS. The lifetime analyses were performed using fracture mechanics analysis code VTTBESIT1.0. The primary considered damage mechanism was crack growth by corrosion-fatigue. Conclusions of the analysis results are summarised.

1. Introduction

A steam drum is a cylindrical high-energy pressure vessel, usually located at the top of the boiler. The primary purpose of a steam drum is to collect the generated steam, before it is being superheated, and separate water from the steam. The steam drum also serves as a storage for boiler water, which is recirculated through downcomer tubes for steam generation. During normal operation the steam drum is about half-filled with water. Nonvolatile solutes originated from the feed water are accumulated in the water and are removed periodically by blow down [1]. The steam drum material is usually a carbon or low allow steel. Primarily damage to the drum material is due to internal metal loss including corrosion and oxidation. Mechanical and thermal stresses can also create cracking in the drum [2]. As long as it is intact, the magnetite layer that forms at operating temperatures on the internal metal surfaces prevents the contact of water and metal and thus protects the metal from further corrosion.

2. Characteristics of the examined steam drums

The data presented in this chapter are taken from reported design and other information of the example power plant and its steam drums [3], located at the Mertaniemi power plant of Lappeenranta Energy Oy in Lappeenranta, Finland.

2.1 Geometry

The relevant geometry data of the examined two steam drums, K1 and K2, are very similar. The overall geometry of the steam drum K1 is shown in Figure 2.1. According to current edition of the design codes (TRD 301, EN 12952-3 or EN 13445), the wall thickness is slightly below the requirements. This is due to the fact that the design codes before 1970's did not provide limits to the strength of the protective oxide layer, and consequently it was possible to accept lower drum wall thickness than today when using high strength drum materials.

The principal dimensions of the steam drum are:

- nominal total length is 7630 mm
- nominal outer diameter is 1600 mm
- nominal wall thickness of the cylinder part is 38 mm
- nominal wall thickness of the head parts is 32 mm
- measured wall thickness of the head parts is 35 mm

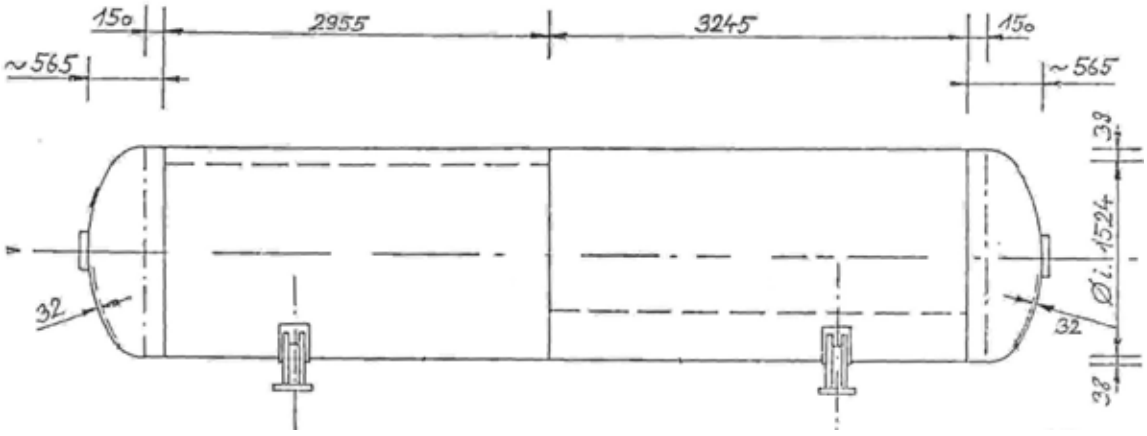

Figure 2.1. The overall geometry of the steam drum K1 [3].

The steam drum is oriented horizontally, and it is supported by two support legs, which are situated symmetrically at the cylinder part. The distance between the midpoints of the legs is 4200 mm, and the distance from each leg midpoint to the nearest steam drum endpoint is 1565 mm. Both steam drums contains also 12 nozzles, 8 small tubes and two manholes. The nozzles are situated at various locations in the cylinder part, and the tubes and the manholes are situated at the head parts.

The wall thickness of the collar of the manhole is 72 mm. The manhole is closed at its inner end with an end plate of 10 mm wall thickness. The length, outer diameter and wall thickness of each of the four small tubes in the head part are 350 mm, 70.0 mm and 10.0 mm, respectively. All of these tubes are closed at their outer ends with tube plates of 6.0 mm wall thickness.

The outer surfaces of the steam drums are thermally insulated with mineral wool, the thickness of which is approximately 250 mm. The mineral wool is also covered with aluminium plates.

2.2 Materials

The material of the cylinder and head parts as well as of the nozzles and manholes of the steam drums is ferritic steel ATM NiMoV, manufactured by Vöest-Alpine at Linz (Austria), 1975. The materials of the small tubes at the head part and the flanges are ferritic steels 15Mo3 and ATM 55, respectively. Some relevant material properties of the main material ATM NiMoV are given in Table 2.1.

Table 2.1. Relevant material properties of ferritic steel ATM NiMoV as a function of temperature [3, 4].

Material property	Symbol	Unit	Temperature [°C]			
			20	100	200	310
Yield strength	σ_y	MPa	440	431	412	368.7
Rupture strength	σ_u	MPa	590	590	590	590
Young's modulus	E	GPa	211	204	196	184.4
Poisson's constant	ν	-	0.3	0.3	0.3	0.3
Density	ρ	kg/m^3	7850	7850	7850	7850
Coefficient of heat expansion	α_T	$\cdot 10^{-6}$/°C	11.1	11.1	12.1	12.9
Thermal conductivity	λ	W/mK	33	33	33	33
Specific heat	c	J/kgK	460	460	460	460

The inner surfaces of the steam drum head parts were thermally sprayed with NiCr-alloy (CorCure TE-50) in 2000after detecting and grinding off severe cracking. To the knowledge of the power plant staff [0], this is the first time that this treatment has been applied to protect steam drums from the formation and growth of cracks. In the following yearly inspections no cracks or other degradation was detected in the NiCr-alloy coating.

2.3 Loads and boundary conditions

The loads considered in the analyses are mechanical and thermal. The pressure in the steam drums is caused by hot steam and water. Compared to steam pressure, the magnitude of water pressure is at all times practically insignificant. The maximum values of pressure and temperature used in the lifetime analyses are taken to correspond the mean values of maximum loading caused by start-up in steam drums K1 and K2 between 1994 and 1999 [3]:

- pressure: 94.9 bar
- temperature: 307 °C.

The total number of shutdowns and start-ups for steam drums K1 and K2 between start of the operation in 1975 and 2000/ summer 2003 are [3]:

- K1: 705/ 747 times
- K2: 667/ 701 times.

It was assumed that the temperature outside of steam drums is 50°C during summer, and 40°C during winter. In the state of shutdown the temperature and the pressure inside the steam drums correspond to conditions outside of the steam drums. The two support legs allow to some extent longitudinal displacement. Displacements in other directions are prevented.

2.4 Degradation characteristics of the steam drums

Severe cracking was detected on the inner surface of both steam drums in 2000. These cracks had formed at the head parts below the water level and they were oriented in the circumferential direction [3]. The largest detected crack was 4 mm deep and 18 mm long. At the wall depth of 3 mm from the inner surface the length of this crack was 4 mm. All detected cracks were straight without branching. In the examined areas the density of the cracks was higher in the drum K1 than in the drum K2. In the head parts of both steam drums the cracks continued with considerably diminished density and size deeper than the maximum grinding depth, which had been approximately 2.2 mm in K1 and 2.4 mm in K2. In the examined sections of K1 and K2 the maximum crack depths were approximately 2.5 mm and 1.1 mm, respectively. A small fraction of the detected cracks were deeper than 3 mm. The crack tip geometry varied from very sharp to rounded and continuously changing from one shape to the other. The tip of one crack in the drum K2 had clearly experienced plastic deformation, in all other cases plastic deformation was not observed. The measured wall thickness of the head parts before grinding was 35 mm [3].

Based on metallographic examinations it was concluded that the degradation mechanism causing the initiation and growth of cracks is corrosion-fatigue [3]. The load cycles causing fatigue were assumed to be stresses that occur due to shutdowns and start-ups. The considerable width of the cracks suggests that they are quite old, due to which they have most likely grown slowly at least initially, and that corrosion plays a significant role in the crack growth. Copper and chlorine that were found from the inner drum surfaces were also considered as a reference to corrosion [3].

3. Structural mechanics analyses

3.1 Description of the simplified analysis model

The structural mechanics analyses in this study have been performed with FEM code ABAQUS/Standard Version 6.3.

Due to symmetries in geometry, loads and boundary conditions it was not necessary to form a FEM model of the complete structure. Hence only a such quarter of the structure was modelled that remains left when the original structure is cut from the middle in two with vertical symmetry planes in both longitudinal and cross sectional directions. As the areas of interest in the steam drums were head parts, it was not necessary to model those nozzles which are situated in the cylinder part, as their effect to the stress and strain distributions of the head part is negligible. For the same reason it was not necessary to model the support leg, instead the effect of the support leg was taken into account as a boundary condition. However, the small tubes and the manhole which are located in the head part were modelled. The effect of the thermal insulation (mineral wool) covering the steam drums was taken into account as a temperature distribution in the outer surface, so it was not necessary to model it. Also, the structure was modelled as undamaged, i.e. no cracks were modelled. The finite element mesh and the global co-ordinate system of the structural model are shown in Figure 3.1.

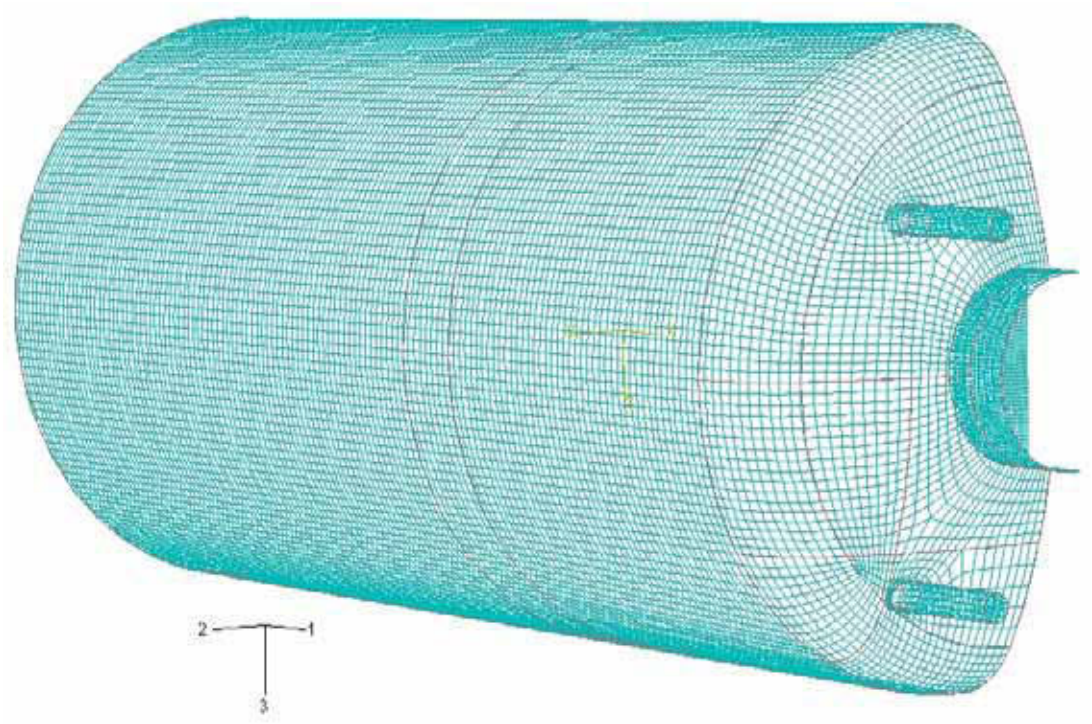

Figure 3.1. Finite element mesh of the steam drum model, seen from the outside, and the global co-ordinate system.

The considered loads in the analyses were:

- steam pressure inside the steam drum
- hydrostatic pressure caused by water inside the steam drum
- temperature
- weight of the steam drum.

The model was meshed with shell elements. The number of the elements in the model was 16174 and the type of the element was S4R. This element is a 4-node, three-dimensional, quadrilateral, stress/ displacement shell element with reduced integration [6].

3.2 Description of the two static analysis cases

In order to calculate the cycling of stresses for corrosion-fatigue analyses, it was decided to examine the steam drum model under two conditions: shutdown and start-up. One load cycle was considered to consist of one shutdown and one start-up. Static analyses were performed for both shutdown and start-up conditions.

In Analysis case 1, shutdown, the pressure and the temperature both inside and outside the steam drums correspond to atmospheric conditions. It was assumed, that during shutdown there is no water in the steam drums. This analysis case corresponds to minimum loading.

In Analysis case 2, start-up, both inner pressure and temperature are mean values calculated from the corresponding yearly peak values from years 1994 to 1999, see Chapter 2.3. Conditions outside the steam drums correspond to atmospheric conditions. It was assumed, that during start-up the water level in the steam drums is at the mid-height of the steam drum. This analysis case corresponds to maximum loading.

The pressure and temperature loads of both analysis cases are given in Table 3.1. In addition to these loads the weight of the steam drum was also considered in both analysis cases.

Table 3.1. The two considered analysis cases, 1: shutdown and 2: start-up.

	Load	Unit	Analysis case	
			1: Shutdown	2: Start-up
Inside steam drum	Water pressure	bar	0.0	0.07
	Steam pressure	bar	1.0	94.9
	Temperature	°C	40.0	307.2
Outside steam drum	Pressure	bar	1.0	1.0
	Temperature	°C	40.0	40.0

Due to modest heating and cooling rates during the load cycles the thermal gradients across the steam drum wall were not considered in the static FEM analyses.

3.3 Results from ABAQUS analyses

The primary interest in the ABAQUS analyses was to calculate the stress distributions in the head parts of the steam drums. As the cracks located in the inner surface of the head parts were circumferentially oriented, the most important stress component was longitudinal stresses. These stresses cause the growth of the cracks when only mode I crack growth is considered. The distributions of longitudinal stresses in Analysis case 2, start-up, in the inner surface of the head part, taken from the results of the ABAQUS analyses, are shown in Figure 3.2. As can be seen from the Figure, the longitudinal tension stresses at the inner surface of the head part reached their maximum values at the area where the radii of curvature is smallest. This was also the area where most of the cracks were detected.

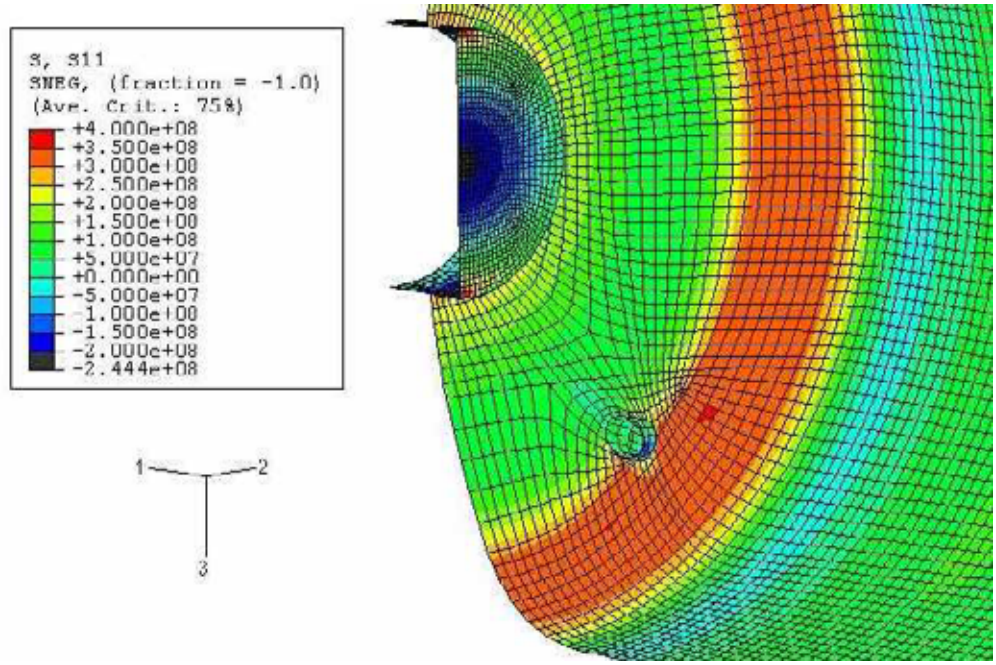

Figure 3.2. Longitudinal stresses at the inner surface of the head part, Analysis case 2: start-up. The dimension of stresses is Pa.

The longitudinal stresses in the inner and outer surfaces of the head part in the location where maximum longitudinal tensile stress in the inner surface of the head part takes place during start-up are shown in Table 3.2. The variation of these stresses across the head part wall is linear.

Table 3.2. Longitudinal stresses in the head part surfaces in the location where maximum longitudinal tensile stress in the inner surface of the head part takes place during a start-up.

Longitudinal stress	Unit	Start-up	Shutdown	Extraction
Stress at the inner surface	MPa	346.5	1.0	345.5
Stress at the outer surface	MPa	-119.8	-0.6	-119.2

4. Structural lifetime analyses

This chapter deals with fracture mechanics based lifetime analyses of the steam drum case. In general, the nature of lifetime assessment models of structural components can be deterministic, probabilistic or a combination of these two types. Due to a very limited amount of available degradation data, deterministic fracture mechanics based ageing models were applied in this study. The crack growth analyses concerned only the head parts of the steam drums.

4.1 Fracture mechanics procedure for lifetime analyses

In the lifetime analyses crack growth due to corrosion-fatigue was estimated by applying Paris-Erdogan equation, which has the form [7]:

$$\frac{da}{dN} = C \cdot (\Delta K)^n \tag{4.1}$$

where a is the crack depth, N is the number of loading cycles, ΔK is the stress intensity factor range, i.e. $K_{max} - K_{min}$, C and n are material, temperature and environment dependent constants and the dimension of da/dN is mm/load cycle.

The Paris-Erdogan equation contains the following assumptions: the crack growth depends only on the stress intensity factor range, the stress amplitude is constant and small enough for linear elastic fracture mechanics (LEFM) to be applicable, and that the crack growth rate is independent of the previous load history [8]. In the fracture mechanics based analyses it was assumed that cracks grow according to mode I.

The material, temperature and environment dependent constants for the application of crack growth equation were chosen so that they take into account the effect of corrosion. Modified values of the constants presented in ASME XI [9], Division 1, Article A-4000, Paragraph A-4300(b), (2) were used in the analyses. The application of the Paris-Erdogan equation together with the constants in ASME XI [9] simulates the fatigue crack growth behaviour of

pressure vessel steels exposed to light water reactor (LWR) environments. The values of the ASME constants were modified because when the original values of the constants were used in the analyses the results showed clearly too modest crack growth compared to actual observed crack growth.

The modification of the material, temperature and environment dependent constants taken from ASME XI [9] was based on the observed crack growth and realised load cycles between 1975 and 2000. However, as no data of the speed of the crack growth was available and the available crack data was all in all very limited. Therefore, it was decided to base the modification of the ASME constants on three cracks all of which were detected from the steam drum K1. The first one of these cracks is the largest detected crack, the dimensions of which were: a x l = 4.0 x 18.0 mm. It was also decided to modify only the values of coefficient C, because the response of the Paris-Erdogan equation is much more sensitive to changes in exponent n. The value of ΔK_I based on which the set of C and n values was changed was also kept the same as in ASME XI [9], namely at 21 MPa·√m. When such values for constants C and n were used under lower values of ΔK_I that the crack growth was within a realistic scale, the cracks started to grow unrealistically fast when ΔK_I exceeded 21 MPa·√m. As all available measured crack data was from year 2000, the initial depths of the examined cracks had to be somehow estimated. Because the cracks were estimated to be old, see Chapter 2.4, it was assumed that the initial cracks had existed in the steel drum from the start of the operation in 1975. It was also assumed that the maximum initial crack depth was 1.0 mm. After a considerable amount of preliminary crack growth analyses had been performed, the following values were estimated for coefficient C:

- $0 < \Delta K_I < 21$ MPa·√m $\Rightarrow$ $C = 8.8747 \cdot 10^{-11}$
- $\Delta K_I \geq 21$ MPa·√m $\Rightarrow$ $C = 2.095 \cdot 10^{-05}$

With these values for coefficient C and with original values for exponent n, and when the initial crack depth varied between 0.4 mm to 1.0 mm, the growth of the examined three cracks in the realised number of load cycles in the crack growth analyses matched exactly their actual measured depths. Both estimates for coefficient C were several times higher than the respective original values defined in ASME XI [9].

4.2 Applied analysis tool – VTTBESIT1.0

The fracture mechanics based crack growth analyses were performed with the analysis program VTTBESIT1.0. This analysis program comprises parts developed by the Fraunhofer-Institut für Werkstoffmechanik (IWM), Germany and by VTT.

The stress intensity factor calculation is done using the program BESIT60 developed by IWM. It is based on the weight function method and on the influence function method. Solutions are provided for "infinite" and half-elliptical crack cases in plates and cylinders. The theoretical background and analysis procedures of BESIT60 are presented in references [10, 11, 12].

VTTBESIT1.0 uses the BESIT60 program code as a pure stress intensity factor computing subroutine. With the present version of VTTBESIT1.0 it is possible to calculate the crack growth caused by fatigue and stress corrosion cracking (SCC), based on solutions of stress intensity factors along the crack front. During a single crack growth analysis the aspect ratio is kept as constant.
At present the achievements of the VTTBESIT1.0 code development by VTT Industrial Systems are:

- The creation of a visual interface.
- The addition of the capability to calculate the crack growth due to fatigue.
- The addition of the capability to calculate the crack growth due to SCC.
- The addition of the calculation of the allowable crack sizes according to ASME XI [9].

4.3 Description of the lifetime analyses

The crack growth analyses performed with VTTBESIT1.0 were limited to that area in the head parts of the steam drums where the longitudinal tensile stresses in the inner surface reached their highest values. This is the same area from which cracks were detected in the inspections in 2000. The detected cracks were circumferentially oriented surface cracks. As the measured wall thickness of the head parts and the measured grinding depth inevitably vary at least to some extent, the wall thickness of the head part was conservatively taken in the analyses as: h_{wall} = 35 - 3 = 32 mm. The effect of the thermally sprayed NiCr-alloy covering the inner surfaces of the head parts was not considered in the analyses. The NiCr-alloy coating was conservatively not considered in the analyses.

The following stress ranges, presented in Table 3.2, were used in all crack growth analyses:

- longitudinal stress range at inner surface: 345.5 MPa
- longitudinal stress range at outer surface: -119.2 MPa.

The variation between these two values was considered to be linear.

Due to lack of crack data assumptions were made concerning the dimensions of the initial cracks. To be reasonably conservative the postulates of the initial

cracks were based on the largest detected crack, see chapter 2.4. At the wall depth of 3 mm, measured from the inner surface, the depth of this crack was 1 mm. As it was assumed in the crack growth analyses that 3 mm of the wall depth was ground off, the maximum depth of the initial cracks was taken as: a_0 = 1.0 mm. In all crack growth analyses the examined cracks were circumferential, half-elliptic surface cracks.

The values of the material and environment dependent constants used when applying the Paris-Erdogan equation in the crack growth analyses were:

- $0 < \Delta K_I \leq 21$ MPa·√m $\Rightarrow$ $C = 8.8747 \cdot 10^{-11}$ and $n = 5.95$,
- $\Delta K_I \geq 21$ MPa·√m $\Rightarrow$ $C = 2.095 \cdot 10^{-05}$ and $n = 1.95$.

The dimensions of the initial cracks were varied in the analyses. The initial crack depths were: a_0 = 0.4, 0.7 and 1.0 mm, and the initial aspect ratios were: a_0/c_0 = 1/1, 1/2, 1/3, 1/4, 1/5 and 1/10. Sensitivity of the crack growth model response for variation of other input parameters was not examined.

4.4 Results from the crack growth analyses

The results from the structural lifetime analyses presented in this chapter show the growth of cracks having various initial depths and lengths as a function of the number of load cycles. Starting time in the crack growth analysis results is year 2000. As the modification of the constants used in crack growth equation is based on crack data from steam drum K1, the presented results do not depict as well the expected growth of cracks in steam drum K2.

The mean values of the total number of load cycles (shutdowns and start-ups) for steam drum K1 from the start of the operation in 1975 to 2000, and from 2000 to 2003 are: 705/25 = 28.2 load cycles/year, and (747-705)/3 = 14.0 load cycles/year, respectively. Correspondingly, the same mean values for the same time periods for steam drum K2 are: 667/25 = 26.7 load cycles/year, and (701-667)/3 = 11.3 load cycles/year, respectively. The actual number of load cycles per year for the steam drums in question has varied over the years in operation, however this data was not available. These mean numbers present, however, a reasonable relation between the load cycles and the elapsed time.

For cracks having aspect ratio 1/1 the amount of crack growth was very modest, after 1000 load cycles the depth of the largest crack was just below 1.5 mm. In the case of other aspect ratios the amount of crack growth was considerably bigger. It should also be kept in mind, that the length of several of the analysed initial cracks exceeded the measured length, at wall depth of 3 mm, of the largest detected crack, namely 1.0 mm. The growth curves of some of the analysed initial cracks as a function of number of load cycles are shown in Figures 4.1 and 4.2.

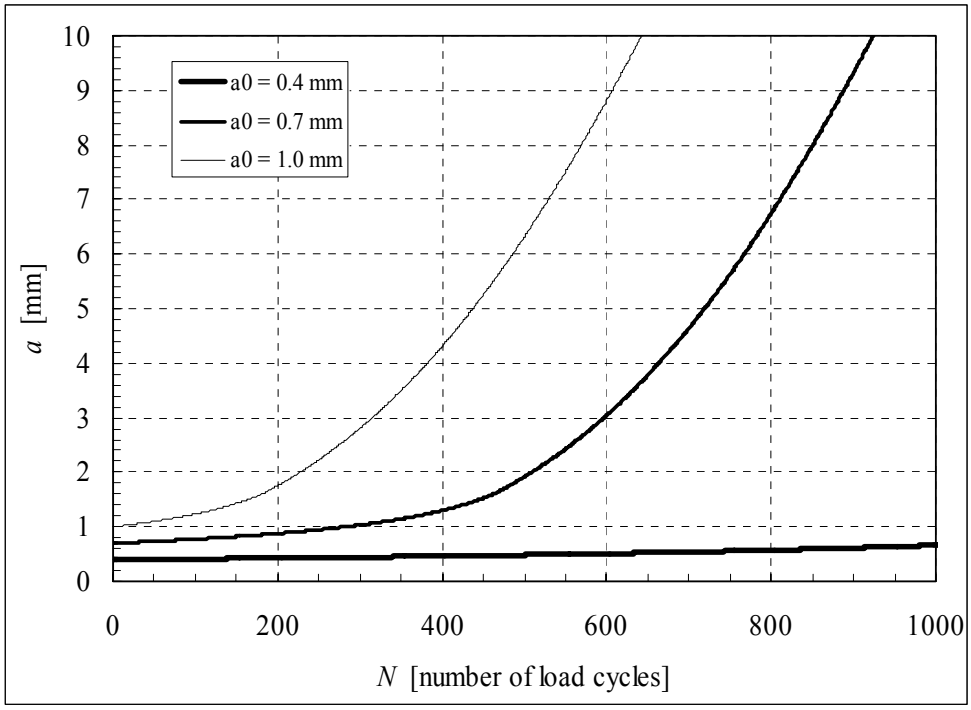

Figure 4.1. Crack growth as a function of number of load cycles for initial cracks with aspect ratio 1/2.

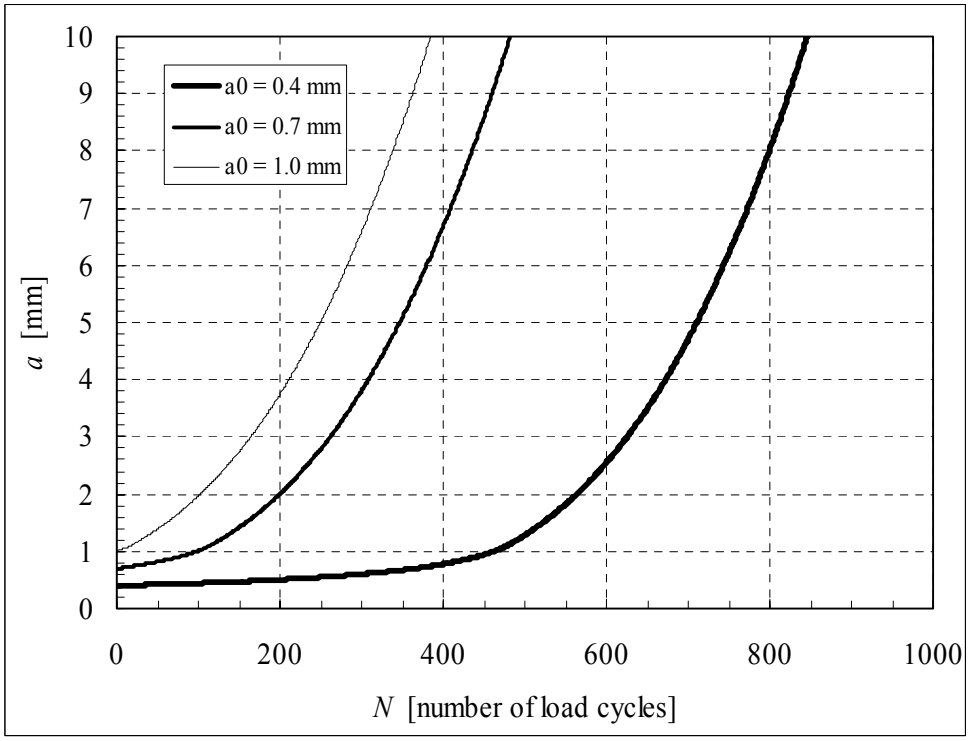

Figure 4.2. Crack growth as a function of number of load cycles for initial cracks with aspect ratio 1/5.

4.5 Lifetime estimates based on the analysis results

The numbers of load cycles, together with corresponding time estimates, it took from the assumed initial cracks to grow to the depth of 2.6 mm are presented in Table 4.1 for those cracks the growth of which reached or exceeded this crack depth within 1000 load cycles. As mentioned earlier, the starting time for the crack growth is year 2000. The crack depth estimates for all assumed initial cracks after they have experienced the estimated number of load cycles between summers of 2000 and 2004, which is: 4×14 = 56 load cycles, are presented in Table 4.2.

The estimated values for coefficient C used in the Paris-Erdogan equation should not be used when analysing other steam drums or power plant components, because these estimates are based on very limited and component specific data that does not really have statistical relevance. Also, as quite many assumptions had to be made when estimating values for coefficient C, one should view the analysis results that have been achieved using these coefficient values with caution. In addition, the crack growth equation is quite sensitive to some of the input data, e.g. the size of the initial crack.

Table 4.1. The numbers of load cycles, together with corresponding time estimates, it took from the assumed initial cracks to grow to the depth of 2.6 mm within 1000 load cycles. The depths of the four assumed initial cracks excluded from here did not reach 2.6 mm within 1000 load cycles.

Aspect ratio a_0/c_0 [-]	Initial crack depth a_0 [mm]	No. of load cycles [-]	Time estimate [year]
1/2	0.7	565	20.04
1/2	1.0	284	10.07
1/3	0.4	901	31.95
1/3	0.7	333	11.81
1/3	1.0	182	6.45
1/4	0.4	693	24.57
1/4	0.7	268	9.50
1/4	1.0	154	5.46
1/5	0.4	603	21.38
1/5	0.7	240	8.51
1/5	1.0	142	5.04
1/10	0.4	498	17.66
1/10	0.7	206	7.30
1/10	1.0	128	4.54

Table 4.2. The crack depth estimates for all assumed initial cracks after they have experienced the estimated 56 load cycles between summers of 2000 and 2004.

Aspect ratio a_0/c_0 [-]	Initial crack depth/crack depth a_0/a [-]					
1/1	0.4/0.40		0.7/0.71		1.0/1.02	
1/2	0.4/0.41		0.7/0.74		1.0/1.12	
1/3	0.4/0.41		0.7/0.78	*)	1.0/1.25	*)
1/4	0.4/0.42		0.7/0.81	*)	1.0/1.39	*)
1/5	0.4/0.42		0.7/0.84	*)	1.0/1.45	*)
1/10	0.4/0.43		0.7/0.88	*)	1.0/1.54	*)

*) The lengths of these assumed initial cracks exceeded the measured length of the largest detected crack, which is 1.0 mm.

5. Conclusions

The steam drum analyses involve damage and structural mechanics, heat transfer analyses and fracture mechanics, and are also connected to fluid mechanics. The studied damage mechanism is crack growth by corrosion-fatigue.

The allowable nominal minimum thickness of the head part wall is 29.4 mm [3]. This leaves 32–29.4 = 2.6 mm of wall thickness margin for cracks to grow, which includes the initial crack depth. The numbers of load cycles together with corresponding time estimates that it took from the analysed initial cracks to grow to the depth of 2.6 mm are presented in the study for those cracks the growth of which reached or exceeded this limit depth within 1000 load cycles.

Another noteworthy aspect is the estimation of how much the examined initial cracks have grown from the summer 2000 to the present time (2004). The crack depth estimates for the assumed initial cracks after they have experienced the estimated number of load cycles between summers of 2000 and 2004 are presented for initial crack depths of 0.4, 0.7 and 1.0 mm.

The maximum predicted depth of the crack corresponding to the largest detected crack would be 1.12 mm in summer 2004 for an initial depth of 1.0 mm and aspect ratio of 1/2. However, if the assumed initial crack depth is the same and the aspect ratio 1/10, the predicted maximum crack depth in summer 2004 is expected to be 1.54 mm. It should be noted, that in reality a protective nickel-chromium coating has been applied to the internal surface of the drum head. This can be expected to considerably retard the crack growth by corrosion-fatigue. The actual condition of the drum will be subject to in-service inspections.

6. Acknowledgements

This article is part of the VTT research project KOKOMO. The project is funded by VTT Industrial Systems, which is gratefully acknowledged. The authors of the article are also grateful to Mr. Heikki Tanttari from Lappeenranta Energy Oy for the input data on the case study and for most pleasant co-operation.

References

1. Office of Industrial Technologies Energy Efficiency and Renewable Energy U.S. Department of Energy, 2003. Improving Steam System Performance: A Sourcebook for Industry.
2. Hovinga, M.N. & Nakoneczny, G. J. 2000. Standard Recommendations for Pressure Part Inspection During a Boiler Life Extension Program. BR-1701, ICOLM. China.
3. Heikinheimo, L., Salonen, J. & Auerkari, P. 2000. Cracking of Steam Drums (in Finnish). Technical Research Centre of Finland (VTT), Manufacturing Technology, Research Report VAL72-001382. 30 p.
4. Vöest-Alpine-Baustähle. Sondergüte Altherm. Techn. Lieferbed. 2001, 77.03., 1977. Germany. 11 p.
5. Tanttari, H. 2004. Personal communication, Lappeenranta Energy Oy.
6. ABAQUS Inc. 2002. ABAQUS/Standard User's manual, Version 6.3. Pawtucket, Rhode Island, U.S.A.
7. Paris, P. & Erdogan, F. 1960. A Critical Analysis of Crack Propagation Laws. Journal of Basic Engineering, Vol. 85, pp. 528–534.
8. Sanzo, D. et al. 1994. Survey and Evaluation of Aging Risk Assessment Methods and Applications, NUREG/CR-6157. U.S. Nuclear Regulatory Commission, Washington D.C. 159 p.
9. The American Society of Mechanical Engineers (ASME). 2001. ASME Boiler and Pressure Vessel Code, Section XI.
10. Varfolomeyev, I. et al. July 1996. BESIF 1.0: Stress Intensity Factors for Surface Cracks under 2D Stress Gradients. IWM-Report T 14/96, Fraunhofer-Institut für Werkstoffmechanik (IWM). 42 p.
11. Busch, M. et al. 1994. K_I-Factors and Polynomial Influence Functions for Axial and Circumferential Surface Cracks in Cylinders. IWM-Report T 18/94, Fraunhofer-Institut für Werkstoffmechanik (IWM). 41 p.
12. Busch, M. et al. January 1995. Polynomial Influence Functions for Surface Cracks in Pressure Vessel Components. IWM-Report Z 11/95, Fraunhofer-Institut für Werkstoffmechanik (IWM). 88 p.

Influence of casting flaws on the operational properties of turbine casings and valve chests

K.H. Mayer, ALSTOM Energie GmbH, Nürnberg, Germany
S. Sheng, Siemens Power Generation AG, Mülheim, Germany
Klenk & H. Theofel, MPA Stuttgart, Germany

Abstract

From pilot castings with typical flaws (open and partly healed hot tears) large specimens were taken. The behaviour of flaws under service-like conditions, creep, creep-fatigue and fatigue at 530°C, was then investigated, accompanied by intensive non-destructive testing. The achieved results allow a better evaluation of existent defects. A significant improvement was achieved in ultrasonic test specifications for the inspection of new and service exposed components.

1. Introduction

Heat-resistant ferritic cast steels are providing an ideal trade-off between functional shape, design depending strength and economic production for HP- and IP-components in modern steam turbines. The weight proportion of cast steels in the HP- and IP-area is approx. 60%, while it is only 20% for forgings. This positive application of cast steels was possible due to continuous improvements in the techniques of melting, casting, heat treatment, welding and non-destructive testing.

Experience with long-term stressed turbine casings and valve chests of HP and IP turbines shows that the inspection findings are depending on the state of the art at the time of design, manufacture, inspection and commissioning. An example in Figure 1, published by General Electric, demonstrates the percentage of turbine casings with cracks in response to the operating period and the year of commissioning (1). A striking fact is the high proportion of cracks found in turbines which were designed and built in the 1950s and early 1960s. After twenty years of operation it was established that 40–60% of the turbines had developed cracks in the casings. The experience in Germany is generally comparable (2).

For the application of castings in steam turbines it was a great challenge in the past to accept ultrasonic indications due to hot tears. Uncertainties mainly occurred about the fracture mechanics effect of these indications. A research

programme of the foundries, turbine manufacturers and MPA Stuttgart were initiated in the 1990s to clarify the influence of open and partly healed hot tears on the life time of turbine casings and valve chests.

The results of the investigations helped the NDT inspectors to gain experience in determining allowable and not allowable US indications which were identified in new and long-term service loaded steel casting turbine components. Finally the results of the investigations helped, to set up the limits for the registration of allowable and not allowable ultrasonic indications of highly-stressed steel cast components in the new European Standard EN 12680-2 (3).

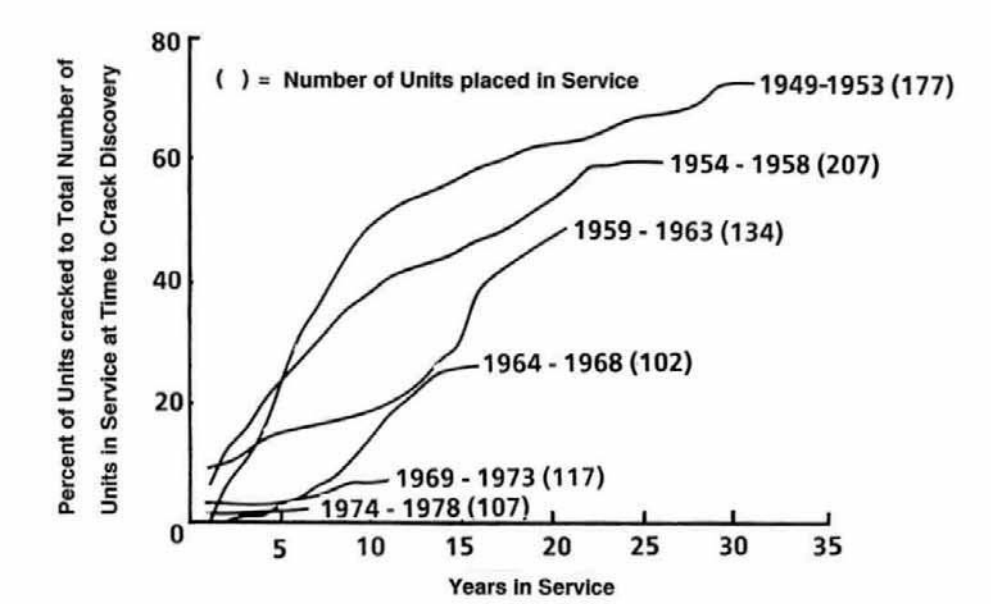

Figure 1. History of crack appearance in casings (1).

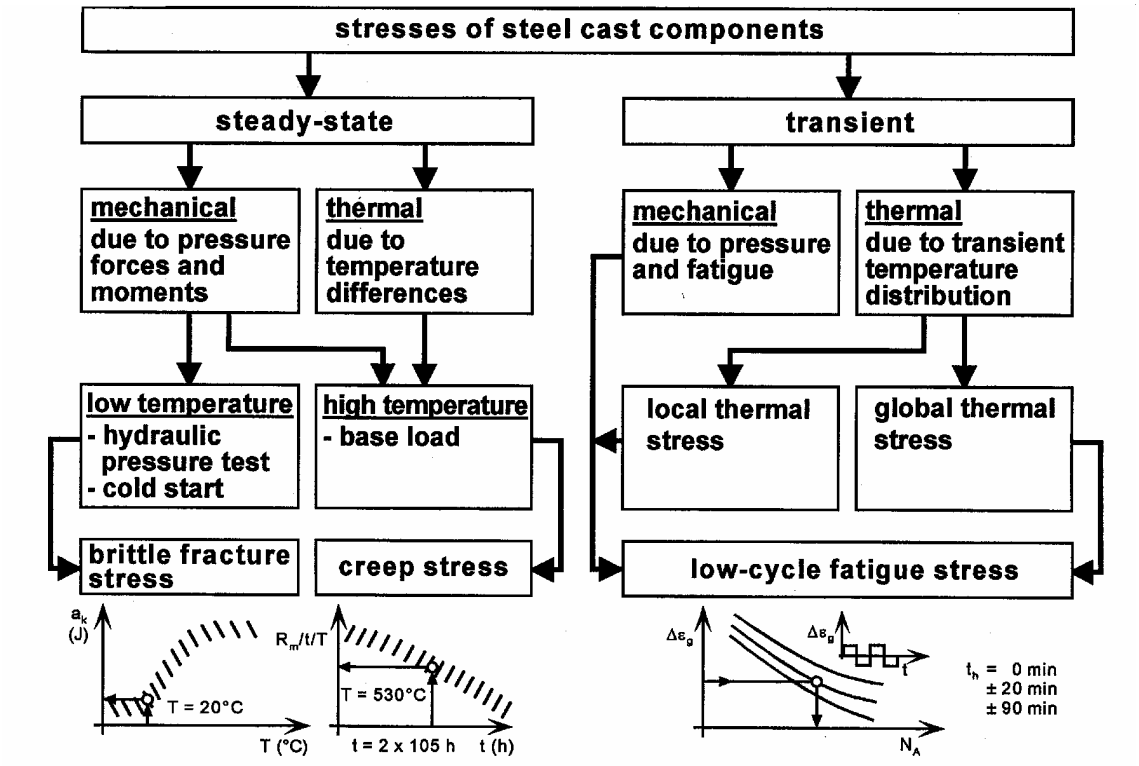

Figure 2. Stresses of cast steel components in steam turbines (2).

2. Stresses in turbine casings and valve chests

In principle the various types of stresses in steel cast turbine components are similar to those of hot pressure vessels, as shown in Figure 2 (2). A distinction must be made between steady-state and transient stresses, both caused by mechanical and thermal stresses. An important factor in the mechanical part of the steady state stresses is the internal pressure, which results in creep stresses at temperatures exceeding 400°C.

At low temperature there are exceptional cases i.e. brittle failure can occur during hydrostatic testing in the virgin condition and start-up. The transient mechanical stresses are caused by pressure variations and fatigue. Superimposed on these mechanical stresses is a transient thermal load, resulting in low-cycle fatigue stress.

A particular risk potential for cracks exists in the area of local concentrations of expansion, due to factors associated with the shape of the component. In addition to these locally limited thermal stresses directly caused by temperature differences in the area under review, there are also cases under transient operating conditions, where temperature differences over larger areas of the component cause additional global thermal stresses between thinner and thicker

sections of the components. These examples demonstrate that the designer of modern steam turbines cannot succumb to give the component any shape he would wish; he must make sure that the components offer good thermal flexibility and low stress concentrations. By doing so we also obtain more calculable stress patterns and better interpretation of non-destructive test indications.

3. Typical casting defects

As an example, in Figure 3 the zones and regions of a lower part of a IP outer casing are revealed, which have a tendency to develop shrinkage cavities, hot tears and surface flaws. Modern foundry practice contributes towards prevention of such defects by using appropriate feeder positions and dimensions, padding and external chills (4). Typical defects are:

- Shrinkage cavities, developed due to shrinkage, i.e. due to the volume deficit between liquid and solid state. They can largely be avoided by correct feeding.
- Hot tears, developed while casting is cooling down in the temperature range between liquid and solid, i.e. while it is in a doughy state just at the temperature at which the material solidifies completely. The cracks occur due to obstructed shrinkage at cross-sectional transitions. The cracks are particularly dangerous because they are perpendicular to the surface and start just beneath the surface.
- Surface flaws, defects in form of accumulations of non-metallic inclusions. They occur predominantly in areas where the rising hot metal contacts the underside of moulds and cores.

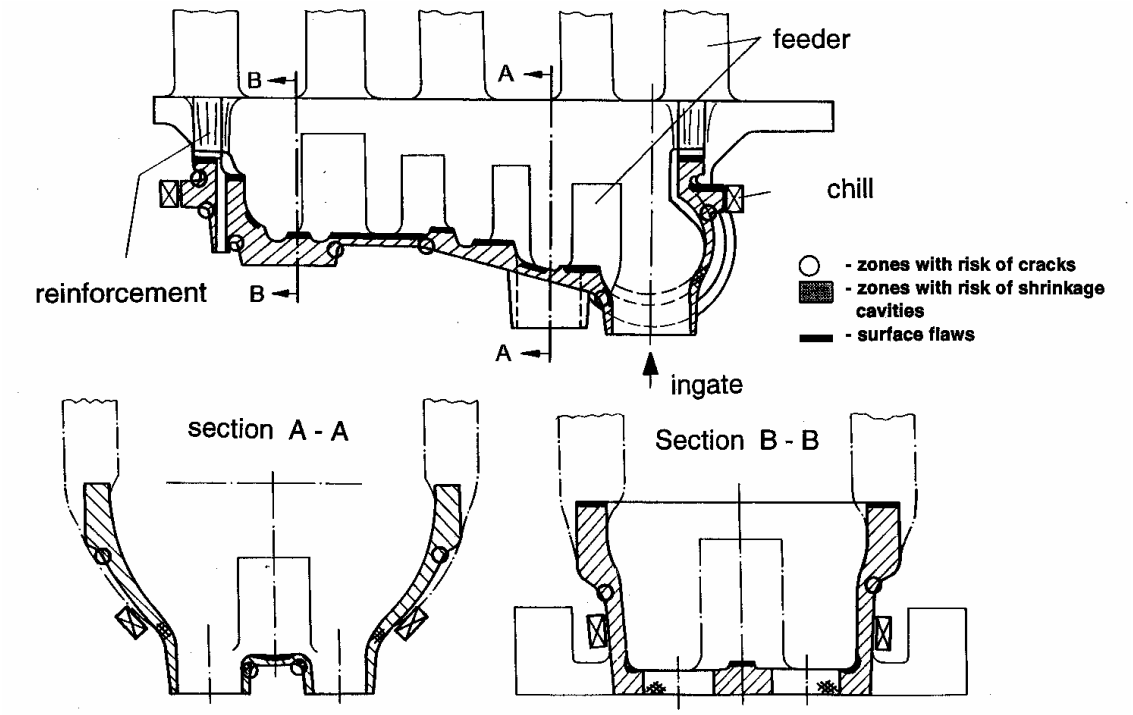

Figure 3. Casting areas with increased flaw risk (4).

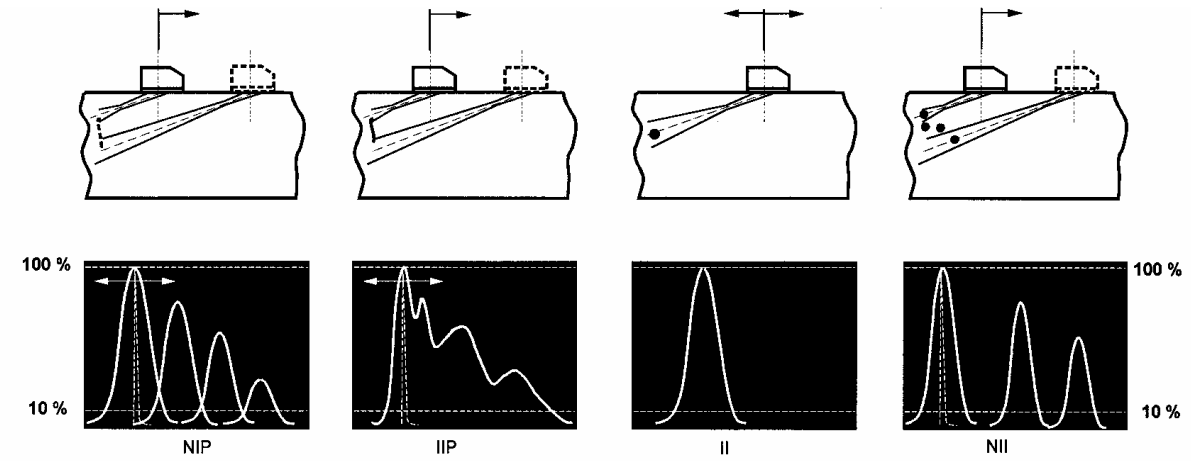

NIP Numerous planar indications with measurable dimensions perpendicular to the surface. (partly healed hot tear)

IIP Individual indication with measurable dimensions perpendicular to the surface (hot tear)

II Individual indication with non-measurable dimensions perpendicular to the surface (pores, shrinkages, non metallic inclusions)

NII Numerous indications without measurable dimensions but with measurable dimensions of the indication range. (pores, shrinkages, non metallic inclusions)

Figure 4. Typical echo dynamics of sub-surface indications in steel castings.

4. Non-destructive testing

Present-day non-destructive testing of turbine casings and valve chests calls for a 100% magnetic particle test and 100% ultrasonic test. The radiographic test is only performed to obtain supplementary results to the ultrasonic test if the findings cannot be interpreted satisfactorily. The ultrasonic tests provide relatively dependable information on non-healed and partly healed thermal cracks, Figure 4. For the detection of these hot tears, specifically selected angle probes are used, whose focus area allows to characterise and determine the size of these near surface defects by means of their echo-dynamic. The characterisation of possible indications depend on their echo-dynamic as follows:

- NIP: Numerous planar indications with measurable dimension perpendicular to the surface (partly healed hot tears)
- IIP: Individual indications with measurable dimension perpendicular to the surface (open hot tears)
- II: Individual indications with non-measurable dimensions perpendicular to the surface (pores, shrinkages, non-metallic inclusions)
- NII: Numerous indications without measurable dimension but with measurable dimensions of the indications range (pores, shrinkages, non-metallic inclusions).

Shrinkage cavities can also be detected and determined by ultrasonic inspection. This requires a high amplification and an inspection without any recording threshold for ultrasonic indications (5). In the new Standard EN 12680-2 (3) the ultrasonic inspection of highly stressed steel castings, like turbine casings and valve chests is specified.

5. Investigations on flaw behaviour

A joint research project initiated by German turbine manufacturers and carried out with the support of foundries at MPA Stuttgart in the 1990s has the following objectives (6–8):

- to determine the crack initiation and crack propagation behaviour of open and partly healed hot tears experimentally under conditions of fatigue, creep fatigue and creep stress,
- to correlate the ultrasonic inspection results with the true flaw sizes,
- to define the crack initiation and crack propagation behaviour by applying fracture mechanics methods.

The test principle is shown in Figure 5. Tests are carried out using large specimens (40 x 40 mm cross section area) taken from five pilot 5t castings of cast steel grade GS-17CrMoV5-11. As a result of various casting techniques they show open and partly healed hot tears at the cross-sectional transition to the thick-walled flange. After locating the flaws and determining their size by ultrasonic and magnetic particle inspection methods, specimens were taken from the flaw zones and then loaded under conditions similar to service. Finally they are subjected to brittle fracture at -150°C in the flaw zone, to identify the type, size and shape of the flaws, as well as of any cracks resulting from the loading conditions by means of metallographic examinations of the fractured areas.

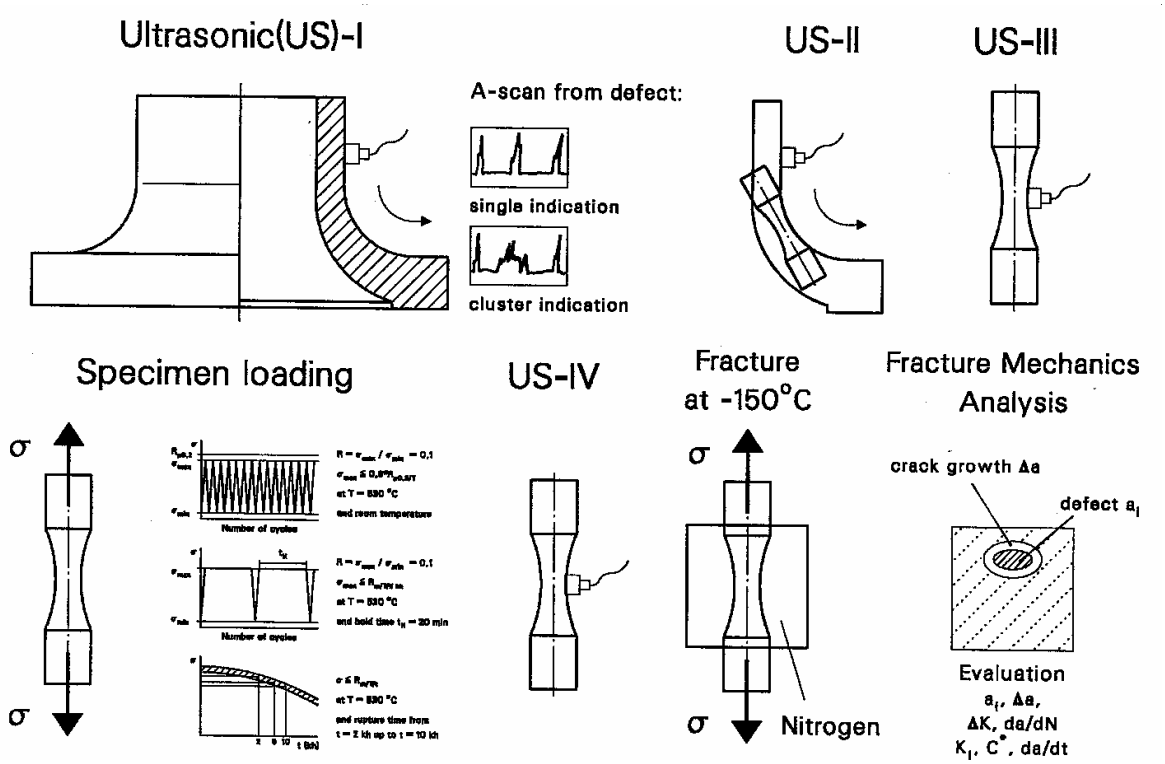

Figure 5. Inspection, removal, loading and evaluation of specimens from flaw-bearing castings.

5.1 Non-destructive testing

Figure 6 demonstrates as an example the flaw depth versus the flaw area determined by ultrasonic inspections at specimens from the pilot casting S. It compares the findings before and after loading, i.e. simulation of the operational stress at 530°C. Casting S was the one with the highest rate and size of ultrasonic indications. The test results are marked with the type of indication before and after loading. The figure also contains the acceptance limit of ultrasonic indications as specified in pre EN 411-1 for quality class 2 (pre-standard to EN12680-2). The figure reveals that the flaws of all specimens exhibit a

substantial crack propagation due to the simulated creep and creep-fatigue stress conditions. It is surprising that there also is a significant crack propagation for some relatively small flaws, initially accepted as allowable indications acc. to the above mentioned limit. This was also observed at some specimens of another pilot casting with a similar higher rate and size of indications.

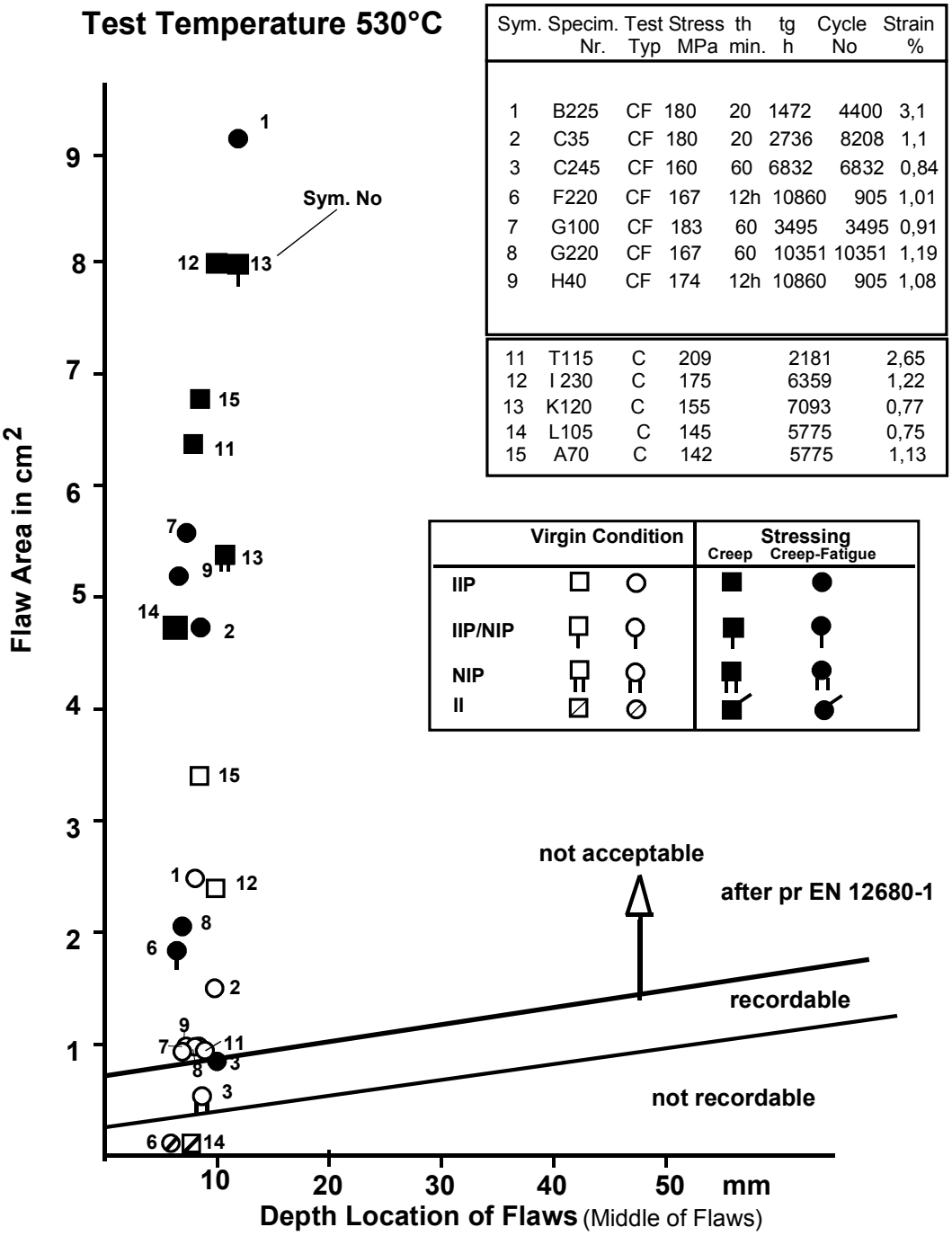

Figure 6. Flaw sizes in cast steel specimens before and after creep and creep fatigue loading.

The growth of the flaw sizes, indicated by ultrasonic testing, is plotted in Figure 7 versus the remaining deformation caused by creep or creep-fatigue stresses. Again specimen results from casting S are shown, for details about loading conditions compare legend in Figure 6. The area of the defects increases with increasing deformation with a similar grade, independent of the type of loading and also from the initial amount of the ultrasonic indication.

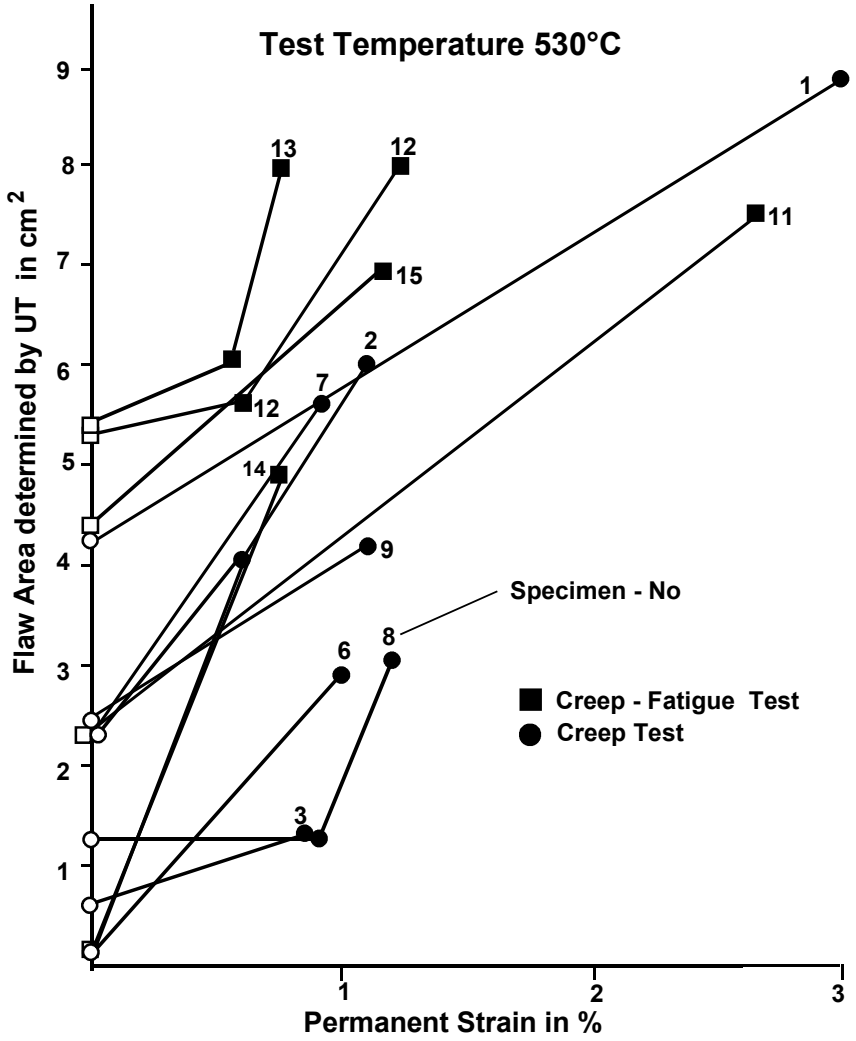

Figure 7. Flaw sizes in cast steel specimens, depending on permanent strain.

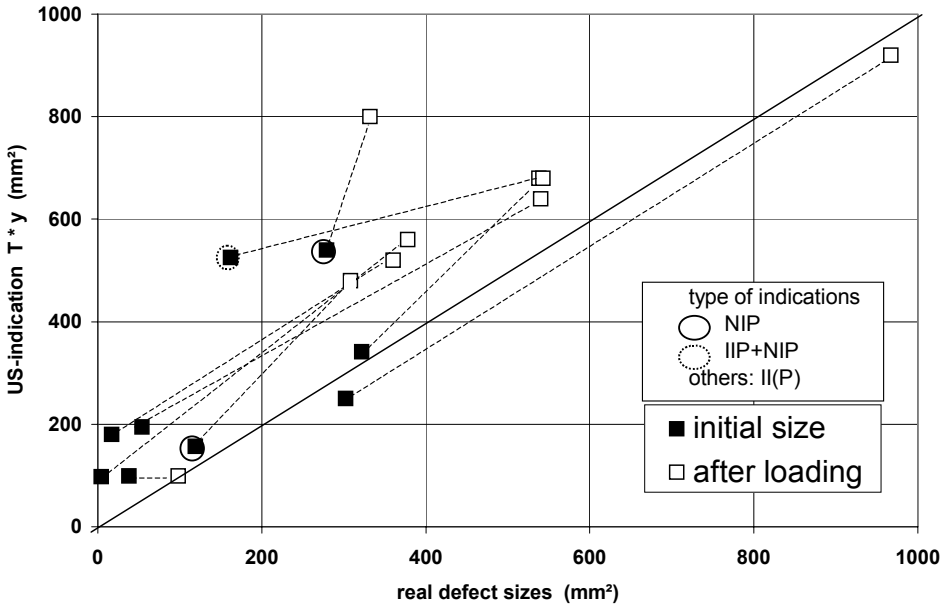

Figure 8. Area of US-indications, compared with real defect sizes (casting S).

Figure 8 shows a comparison between the flaw areas of specimens from casting S determined by means of ultrasonics and metallography. The diagram shows, that the initial flaw sizes before loading and also the defect sizes after loading are situated in the area above the straight line with the gradient 1:1. This means that the real defect sizes are described conservatively by US-testing. This result was also found in the investigations at the other castings.

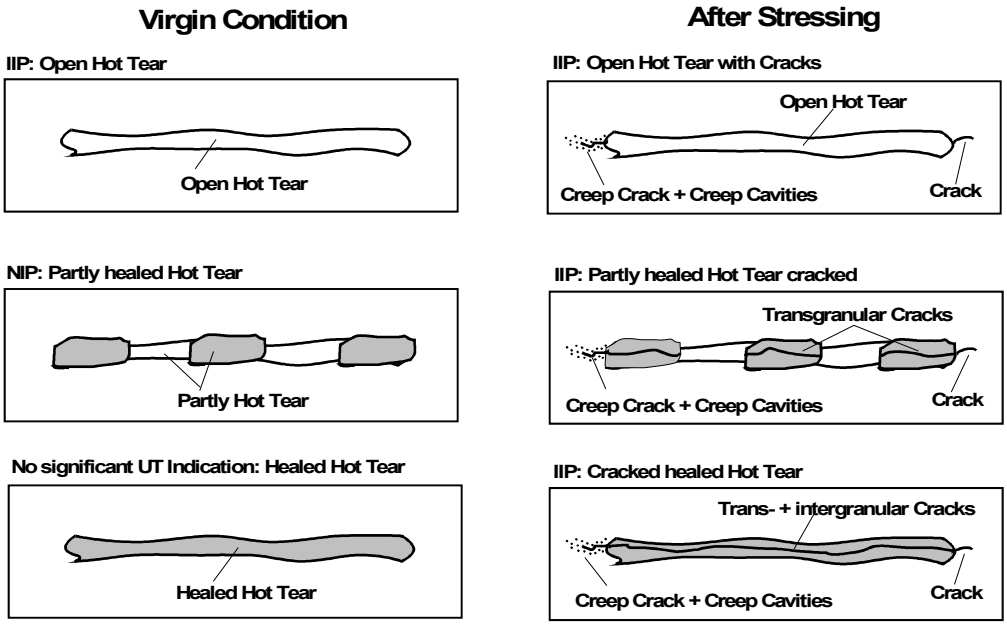

Figure 9. Appearance of flaws and defects before and after loading, schematically.

The damage behaviour of the flaw areas, caused by creep or creep-fatigue loading, was identified by metallographic examination. It is shown schematically in Figure 9 for each flaw type and kind of ultrasonic indication. The appearance in the initial state is shown in the charts on the left and the state after loading is shown in the charts on the right. In the initial state it can be distinguished between:

- An open hot tear which causes an ultrasonic indication IIP
- A partly healed hot tear (partly filled with remnant melt) that causes to an ultrasonic indication NIP, and
- A healed hot tear which is almost completely healed/filled with remnant melt. This flaw only causes a small and/or no clear ultrasonic indication (within the remnant melt the portion of non-metallic inclusions, e.g. dendritic MnS-zones, and contents of C, Si, Mn, S, P, Cr, Mo and trace elements are considerably higher than in the parent material (9)). The strength of this healed hot tear is considerably lower than that of the surrounding material.

As far as crack propagation occurred during the simulation of the service conditions, depending on the type of stresses it was found that:

- Open hot tears show fatigue cracks and/or creep damage in form of cavities and intercrystalline cracks at the edges of the flaws.
- Tear connections between small open areas were cracked transcrystalline in partly healed hot tears. At the outer borders of these hot tear zones fatigue cracks and/or creep damage were present.
- In completely healed hot tears trans- and intercrystalline separations of almost the whole healed area occurred. After these separations, at the borders to the base material again fatigue cracks or creep damage emerge. This type of damage was found on specimens having small ultrasonic indications in the initial state and then shows larger amounts of indications after simulated service conditions.

5.2 Fracture mechanics methods

For the assessment of defects a two-criteria approach was developed (11), to take into account the effect of local stresses as well as ligament stresses. Therefore, the two parameters stress intensity at the defect (K_{Imax}, to consider the crack tip situation) and the nominal stress (σ_n, to consider the ligament stress) have to be determined. They are then compared with the corresponding time dependent values for creep crack initiation (stress intensity K_{IAC}) and for creep rupture strength (R_m). These data were evaluated with creep tests at standard specimens (CT and tensile), taken from flawless material.

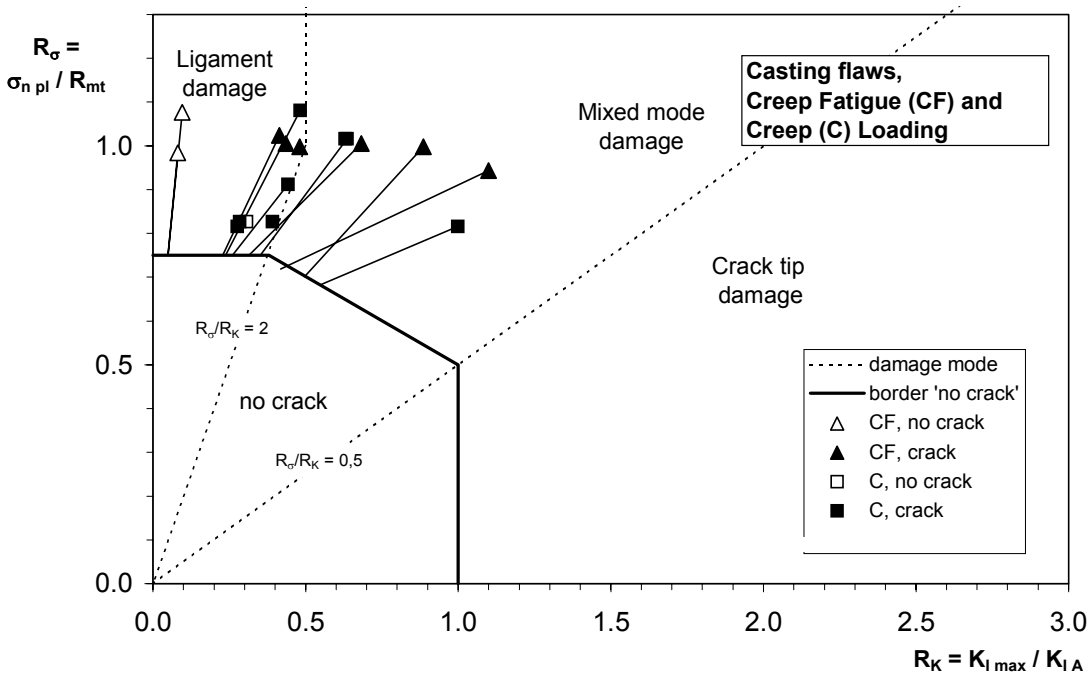

Figure 10. Two Criteria Diagram for flaws in steel cast specimens, test results at 530°C.

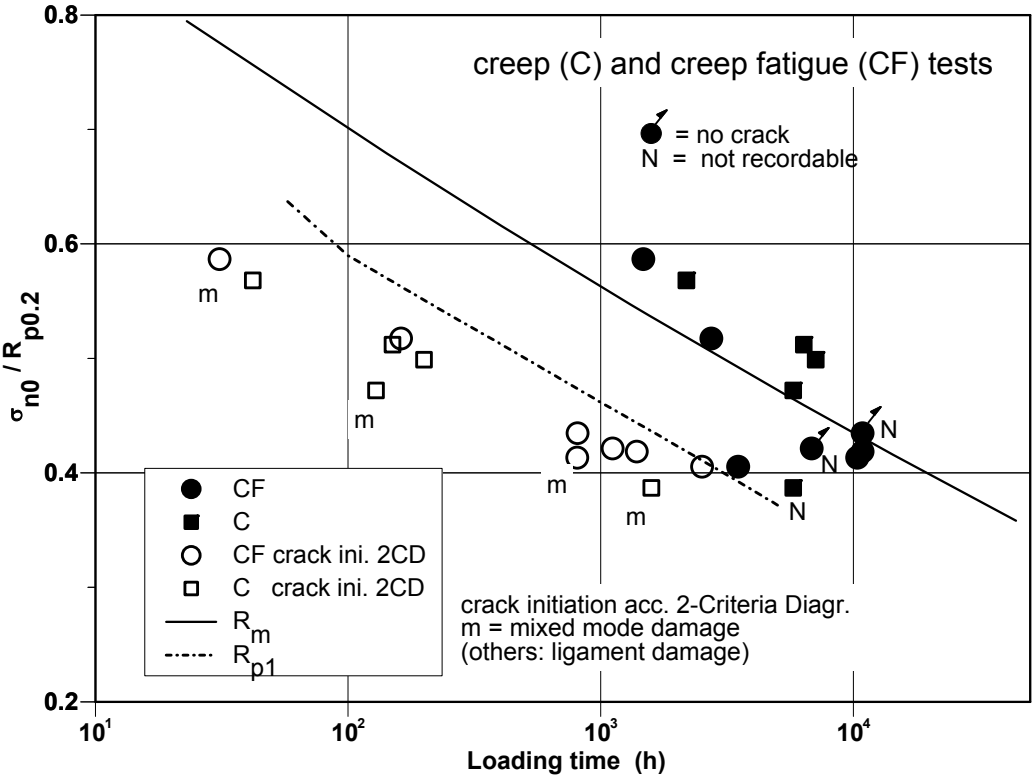

Figure 11. Normalised stresses versus loading time, limits for crack initiation in flaw-bearing specimens, creep and creep-fatigue tests at 530°C.

For the two-criteria-diagram, the stress intensity ratio $R_K = K_{Imax}/K_{IA}$ and the stress ratio $R_\sigma = \sigma_{npl} / R_{mt}$ are used. The two-criteria approach was originally valid only for static creep load conditions. For the application to creep-fatigue conditions, a modification is given in (12), by evaluating K_{Iid} and R_m at a time reduced by 40%, taking into account the influence of load cycles on damage.

With this method all tested specimens from casting S with creep and creep-fatigue loading could be plotted into the two-criteria diagram, Figure 10. For each specimen the ratios R_σ and R_K for theoretical crack initiation times due to the initial defect sizes were calculated. From that point at the border for crack initiation, a straight line was drawn to a symbol, which gives both ratios for the situation after loading. In most of the specimens crack initiation after loading was found, and all points are laying outside the border for crack initiation. Thus the two-criteria diagram is conservative with its prediction of crack initiation and propagation.

The evaluated defects are mostly in the region of the damage mode 'ligament', partly in 'mixed mode'. So the net stress is dominant for the failure behaviour of these embedded defects. In Figure 11 the standardized net stress is plotted over time for crack initiation, calculated with the two-criteria diagram (open symbols). Closed symbols show the same stress level for the end of the test. The creep rupture strength and 1% creep strength curve for defect free small scale specimens is also shown. Again it can be seen, that the crack initiation time determined by the two-criteria diagram is conservative. The R_{p1} curve can be taken as a lower bound to assess the crack initiation behaviour for specimens having defects.

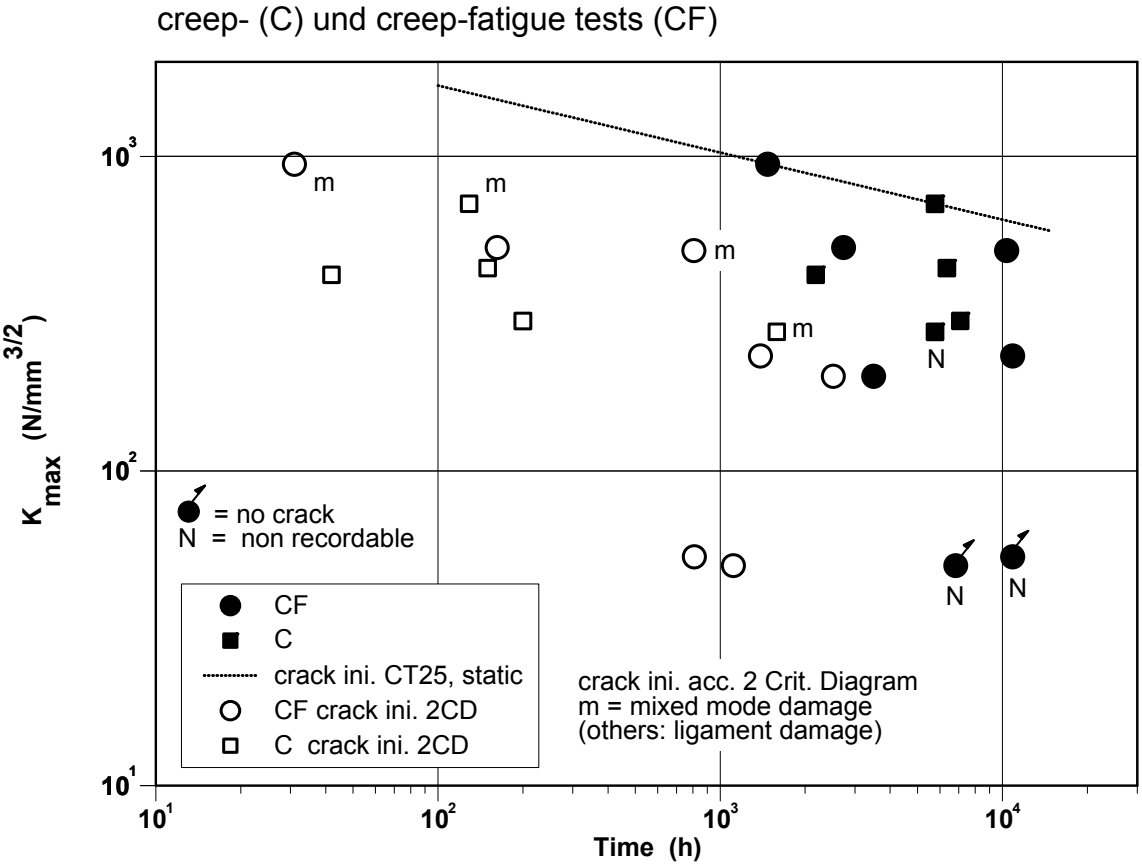

Figure 12. Stress intensity at initial flaws versus loading time, tests at 530°C.

In a similar way in Figure 12 the stress intensity K for all defects (K calculated with standard formulas and with idealised elliptical defect forms) is plotted versus crack initiation time and loading time, respectively. The dashed line was obtained from static tests with defect free CT25-specimens. For all investigated defects ligament or mixed mode damage was determined, which means that damage appears mainly due to creep in the ligament. Therefore, for specimens with internal defects, the stress intensity K is below the crack initiation curve. This applies for crack initiation and after creep and creep-fatigue loading of specimens.

6. Summary and Conclusions

Investigations on hot tears in cast steel components revealed the following results:

- The correlation between the true size of open and partly healed hot tears and the ultrasonic inspection results (echodynamic evaluation) permits improved determination of the true size of flaws in turbine cast components.

- Valuable experience was gained about the identification of the types of ultrasonic indications and casting flaws and their influence on the crack propagation under service-like stresses. Acceptance limits for the ultrasonic inspection of highly stressed cast components in standards could be specified.
- The evaluation of crack initiation at specimens with defects with the two-criteria diagram is conservative. As an approximation, the curve R_{p1} (stress to achieve constant creep strain) curve can be used.
- The majority of the investigated hot tears behave like cracks and can thus reliably be assessed on the basis of fracture mechanics laws with regard to their crack propagation behaviour, under conditions of fatigue, creep and creep-fatigue loading.

References

1. S.J. Woodcock. Upgrading opportunities for high temperatur steam turbines. EPRI Sem. on fossil plant retrofits for improved heat rate and availability, S. Diego, USA, Dec. 1–3, 1987.

2. K.H. Mayer, W. Schneider, K. Stark & D. Tremmel. Experiences with long-term stressed turbine casing and valve bodies made of heat-resistant cast steel. VGB Kraftwerkstechnik 9 (1991).

3. EN 12680-2, June 2003. Founding – Ultrasonic examination – Part 2: Steel casting for highly stressed components.

4. K.H. Mayer, W. Gysel, A. Trautwein & D. Tremmel. Die Anwendung des warmfesten Stahlgusses im Dampfturbinenbau – seine Anforderungen und Eigenschaften. VGB Kraftwerkstechnik 60 (1980), Heft 5, pp. 398–405.

5. D. Christinaus, W. Prestel und H. Bächthold. Ultraschallprüfung von Stahlguß nach DIN 1690, Teil 2 und SEP 1922, beide Ausgabe 1985. Konstruieren und Gießen 12 (1987) Heft 2, pp. 19–30.

6. J. Bareiß, C. Berger, K. Maile, K.H. Mayer & M. Weiß. Untersuchungen zur Charakterisierung des Verhaltens von Fehlstellen in Gußstücken unter Kriech-, Ermüdungs- und Kriechermüdungsbeanspruchung. DVM-AK „Bruchvorgänge“, Magdeburg, Februar 1994.

7. J. Bareiß. Gußfehlstellen I, Verhalten von Fehlstellen im warmfesten Stahlguß bei betriebsähnlichen Belastungen. Vorhaben AiF-Nr. 8338, Abschlußbericht 10/95, MPA Stuttgart.

8. K.H. Mayer, C. Berger, C. Gerdes, T. Kern & K. Maile. Influence of flaws on the operational properties of rotors and casings of steam turbines. VBG Kraftwerkstechnik 77 (1997), Heft 10.

9. J.M. Motz et al. Einfluß oberflächennaher Fehlstellen im Stahlguß auf die Rißeinleitung bei Schwingsungsbeanspruchung – Teil 1, Giessereiforschung 43, 1991, Nr. 1.

10. K. Maile, H. Theofel, C. Weichert, K.H. Mayer, C. Gerdes & S. Sheng. Assessment of hot tears in cast steel components. International Journal of Pressure Vessels and Piping 78 (2001), pp. 865–874.

11. J. Ewald, K. Maile & R Tscheuschner. Beurteilung des Rißwachstums im Kriechbereich mit Hilfe eines Rißspitzen/Fernfeld-Konzeptes. 13. MPA-Seminar, Stuttgart, 1987.

12. J. Granacher et al. Ermittlung und Berechnung des Kriechermüdungs-verhaltens zweier Kraftwerksstähle, 22. Vortragsveranstaltung AG warm-feste Stähle / Hochtemperaturwerkstoffe, Düsseldorf, 26.11.1999

Occasional underloads and fatigue

B. Roger Rabb
Wärtsilä Finland Oy
Vaasa, Finland

Abstract

The fatigue strength of a machine part, nominally subjected to a constant amplitude load and designed for an infinite lifetime, can suffer greatly by a few occasional peak loads if they cause stress amplitudes beyond the fatigue limit. This phenomenon has been given much attention by researchers in recent years. Interest in this question at the author's company was aroused in the 1980's when the cylinder liner of a medium speed diesel engine tested in the company laboratory developed fatigue cracks in the orifices of the cooling bores. These cracks was found to be caused by large underloads as a result of temperature stress variations during engine start-up and stopping. Underloads are especially detrimental for the fatigue limit because of the residual tension stresses caused in a notch by them. These residual stresses cause a decaying acceleration of the damage accumulation. A surprisingly low number of underloads can be enough to initiate a propagating fatigue crack, although the basic dynamic stress amplitude is well below the fatigue limit. The effect of occasional underloads is highlighted in this paper by presenting the results of extensive fatigue testing with a constant amplitude stress containing a few large periodic underloads on three different material types, i.e. grey cast iron, nodular cast iron, and quenched and tempered steel. The transformation by an appropriate statistical analysis of the evaluated sample values to population values are shown in some cases to facilitate the application of the new knowledge to the fatigue analysis.

1. Introduction

Medium speed diesel engines are mostly operated at a virtually constant power output. The fatigue analysis of most engine parts can therefore be made, assuming a constant amplitude load. However, due to engine start-ups and stoppings, engine parts affected by temperature stresses, i.e., the cylinder head and liner, can then experience a much higher stress amplitude. Also some other engine parts, such as the screws of the cylinder head and the connecting rod, will be subjected to large stress amplitudes due to regularly repeated engine overhauls.

A section through an in line medium speed diesel engine is shown in Fig. 1. This engine operates at a nominal speed of 750 rpm. During an engine lifetime of about 200 000 operational hours it can be estimated that the engine will be started and stopped about 20 000 to 40 000 times. The cylinder head is made of nodular cast iron, and particularly its flame deck is exposed to a variable amplitude stress history consisting of about 4.5 billion high cycle loads due to the firing pressure, as well as a maximum of 40 000 low cycle loads due to engine start-ups and stoppings. The high cycle stress amplitude, which can be considered to be quite constant, must of course be below the fatigue limit. Cumulative damage will result when the low cycle amplitude, which can also be considered constant, is much larger than the high cycle amplitude and exceeds the fatigue limit. The cylinder liner is made of centrifugally cast grey cast iron. Due to wear it has to be replaced at least once during the lifetime of the engine. Accordingly, the number of load cycles on the liner is only half the amount of load cycles on the cylinder head.

The typical load spectrum in Fig. 2 for a cylinder liner, for example, is simple to handle. It consists of a number of n_{hc} high cycle loads with mean stress $\sigma_{mean,\,hc}$ and amplitude levels $\sigma_{a,\,hc}$. Correspondingly, it has a number of n_{lc} low.

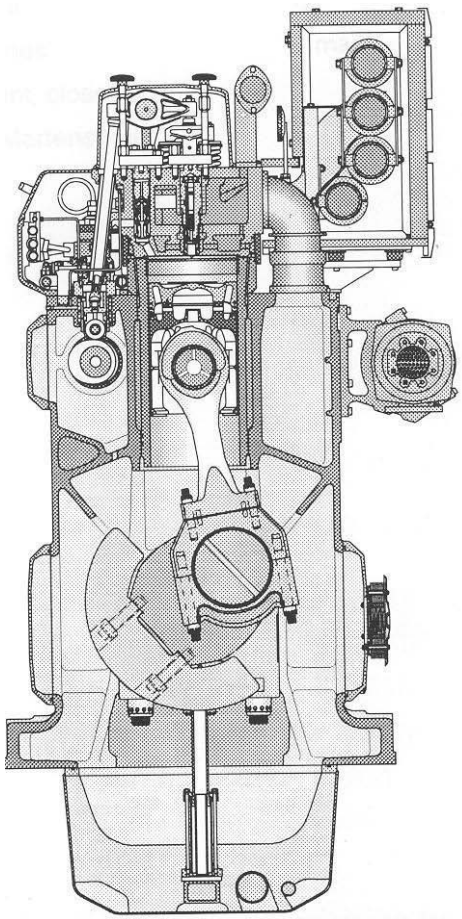

Figure 1. Wärtsilä 32 medium speed diesel engine.

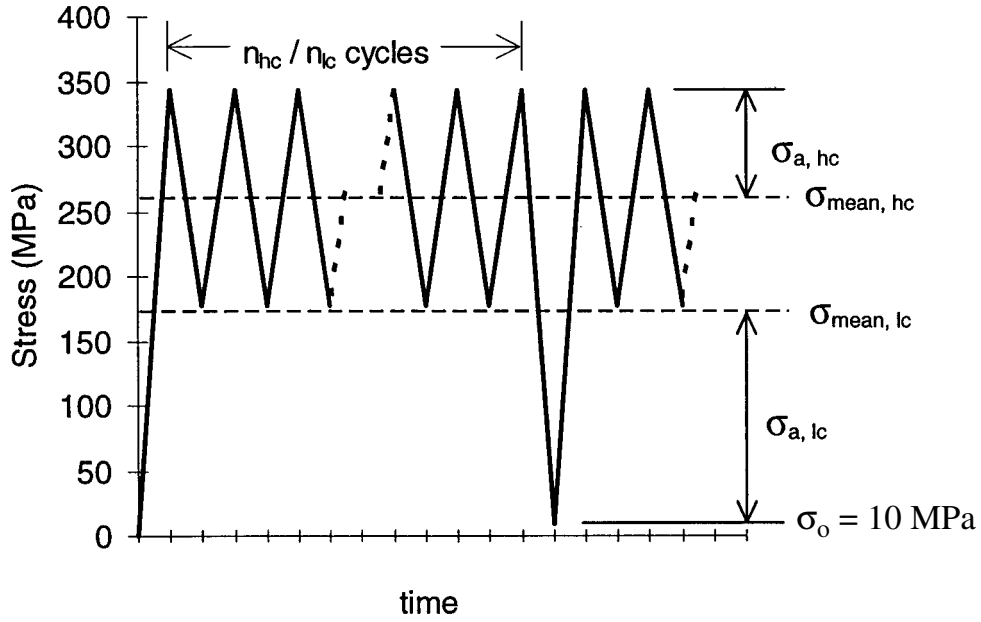

Figure 2. Definitions of the quantities in the stress history with high cycle and low cycle loads in the test of nodular cast iron grade 500-7/ISO 1083.

cycles with mean stress $\sigma_{mean,\,lc}$ and amplitude levels $\sigma_{a,\,lc}$. The cycle ratio in one block of the spectrum test is thus n_{hc}/n_{lc}.

The cumulative fatigue damage caused by a variable amplitude load has long been known, and much research has been done on this issue. Already in the 1920's, the Swedish researcher, A. Palmgren, examined the fatigue life of bearing rollers [1]. But not until M. A. Miner published his investigations [2] in the 1940's on this subject did this phenomenon become more known. The linear damage rule according to Miner is quite simple and in its original form it only considered amplitudes over the fatigue limit. If n_i denotes the number of cycles with amplitude σ_{ai} and N_i denotes the lifetime taken from the constant amplitude S-N curve at this stress amplitude, the Miner rule is as follows.

$$D = \sum_i n_i / N_i \tag{1}$$

However, it has long been known that cycles with amplitudes below the fatigue limit must also be included in some way to this damage sum. Many attempts have been made to construct a correction of the constant amplitude S-N curve to account for amplitudes below the fatigue limit. H. T. Corten and T. J. Dolan [3] were among the firsts to attempt a correction, which was basically an extension of the constant amplitude S-N curve with the same slope into the high cycle domain. Also the correction suggested by E. Haibach [4] deserves a mention. He suggested that the slope exponent k in the power expression for the S-N curve of steels should be

replaced in the high cycle domain by the slope exponent $2k-1$. If N denotes the life in the number of cycles at amplitude σ_a, and if N_{fa} is the number of cycles where the S-N curve reaches the fatigue limit σ_{fa}, then this correction is as follows for steel.

$$N = N_{fa}\left(\frac{\sigma_{fa}}{\sigma_a}\right)^{k} \qquad \text{basic S-N curve for } \sigma_a \geq \sigma_{fa} \tag{2}$$

$$N = N_{fa}\left(\frac{\sigma_{fa}}{\sigma_a}\right)^{2k-1} \qquad \text{extended S-N curve for } \sigma_a < \sigma_{fa} \tag{3}$$

However, the linear damage rule has many weaknesses. It is not possible, for example, to consider the sequence of load amplitudes. More crucially still, in cases where the number of under- or overloads are few, it fails to give the correct estimates of the expected lifetime. It is known from many experiments, References [5], [6] and [7], that an occasional overload tends to retard the crack growth due to the generated compression residual stresses in the crack wake. In the same manner, an occasional underload will accelerate the crack growth due to the tension residual stresses it will generate.

The modern understanding of fatigue, References [5] and [8], makes no strict distinction between crack nucleation and crack propagation. Also the crack nucleation phase consists of a growth of a small inherent defect, whether it starts from an internal material defect or from a slip band intersecting the surface in a bad direction. In principle the whole fatigue process with crack nucleation and propa-

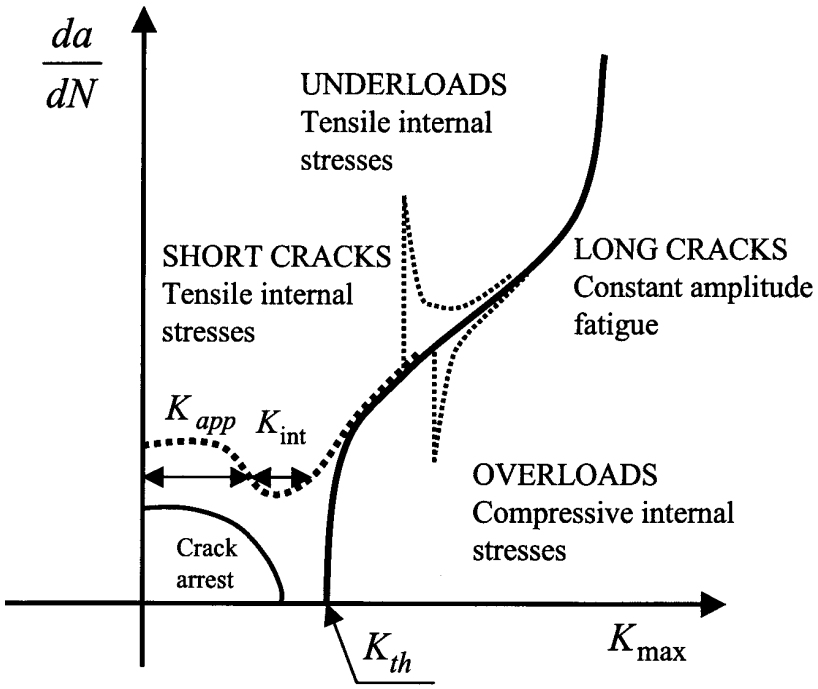

Figure 3. Crack nucleation and propagation at a certain stress intensity range, Refs. [5] and [8].

The meaning of the symbols in Fig. 3 is as follows:

da/dN	crack growth rate in m/cycle
K	stress intensity factor in MN/m$^{3/2}$
K_{th}	threshold value for a growing crack at a certain stress intensity range
K_{app}	stress intensity due to an applied external load
K_{int}	stress intensity due to an internal stress

Crack growth when the maximum stress intensity factor exceeds the threshold at a given intensity range. i.e. $K_{app} + K_{int} > K_{th}$

gation can be illustrated in a $da/dN - \Delta K$ plot as in Fig. 3. The vast majority of the testing in question was performed using a programmable resonant test machine manufactured by RUMUL. This machine can perform constant amplitude testing at frequencies between 80 and 300 Hz. The axial specimens tested in these projects were fatigued at a frequency of about 150 Hz.

2. Tests on nodular cast iron

The fatigue tests made to determine the behaviour of nodular cast iron grade 500-7/ISO 1083 in the high cycle regime when occasional underloads are present are given in detail in Reference [9]. The geometry and dimensions of the smooth test specimens are shown in Figure 4a.

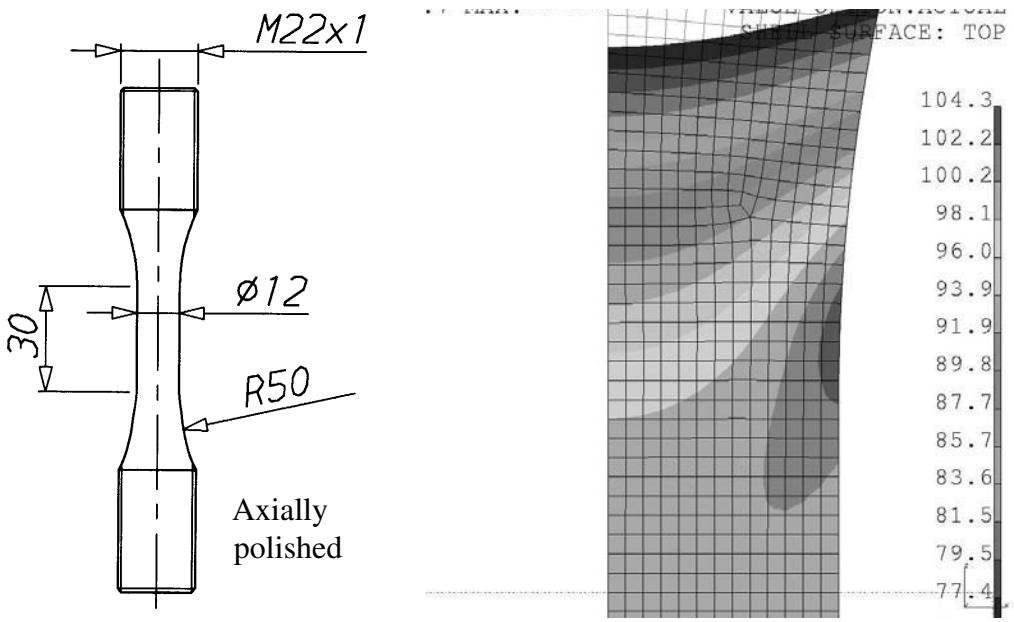

a) specimen b) stress distribution in the notch

Figure 4. Test specimen used in the fatigue tests and in the test of the static strength.

The material in the specimen in Fig. 4 was nodular cast iron grade 500-7/ISO 1083 with the following strength as an average of 10 tensile tests:

$R_m = 625\,\text{MPa}$ mean tensile strength with unbiased standard deviation 15.0 MPa

$R_{p0.2} = 338\,\text{MPa}$ 0.2 % proof stress with unbiased standard deviation 4.1 MPa

and with the following properties

$K_t = 1.043$ theoretical stress concentration factor of the specimen

$A_{eff} = \sum_i \frac{\log R_i}{\log 0.5} \cdot A_i = 909\,\text{mm}^2$ effective stress area of the specimen for a relative standard deviation of the fatigue limit of $s_r = 0.09$

The effective stress area of this specimen at a certain relative standard deviation of the fatigue strength is given to facilitate the application of the test data to actual components with different effective stress areas. The important concepts effective stress area and the related concept statistical size factor are explained in References [10] and [11].

To be able to determine the appropriate high cycle stress amplitudes in the fatigue test with occasional underloads, the fatigue limit at high cycle mean stress had first to be tested with a staircase test. The basic S-N curve at high cycle mean stress also had to be tested to be able to compare it with its extension into the high cycle domain.

On the one hand, actual stresses should be used in a modern fatigue analysis since these are the stresses that are calculated in an FE analysis, and their transformation to nominal stresses are both unnecessary and sometimes even impossible. On the other hand, in order to calculate the effective stress area, the actual stress distributions must be used. Because the test specimen in Fig. 4a has a simple geometry, it is easy to calculate the actual stresses from the nominal stresses by multiplying the nominal stresses by the theoretical stress concentration factor, $\sigma_{actual} = K_t \sigma_{nom}$. In the following, actual stresses are therefore mostly used. On the other hand, it is more convenient to conduct the tests using nominal stresses.

2.1 Staircase test at the high cycle mean stress

The outcome of the staircase test with 17 specimens and with the intended actual high cycle mean stress $\sigma_{mean,\,hc} = 271.2\,\text{MPa}$ is shown in Fig. 5. The sum of the mean stress and the evaluated actual fatigue limit $\sigma_{fa} = 111.9\,\text{MPa}$ is 383.1 MPa, i.e. the yield strength is slightly exceeded. A nonlinear plastic FE analysis showed that the actual maximum principal stress 367.3 MPa after yielding was in the smooth shaft and not in the notch. The corresponding true mean stress is thus about 255.4 MPa. This has to be considered when the fatigue diagram is constructed.

Generally, yielding in the test specimens makes it more difficult to correctly interpret the test data. However, in this case the shift of the mean stress due to this yielding is rather small and only the correction of the mean stress explained above is made.

The evaluation of the sample mean and sample standard deviation from the test outcome in Fig. 5 is made with a maximum likelihood fitting of the density function, Refs. [10] and [11].

$$P(n, m|\sigma_{ao}) = K\prod_{-\infty}^{\infty} p_i^{n_i} q_i^{m_i} \qquad \text{where} \tag{4}$$

$$p_i = \frac{1}{s\sqrt{2\pi}} \cdot \int_{-\infty}^{\sigma_{ai}} e^{-\frac{(x-\bar{\sigma}_a)^2}{2s^2}} dx \qquad \text{and} \qquad q_i = 1 - p_i \tag{5}$$

In Equations (4 and 5) the meaning of n_i is the number of failures on the level with stress amplitude σ_{ai} and m_i is the corresponding number of runouts. The constant K is neither dependent on the mean, nor on the standard deviation. The mean of the trial density function is $\bar{\sigma}_a$ and its standard deviation s. The cutoff limit in this staircase test was 10^7 cycles, which is the usual value. The evaluated standard deviation cannot really be trusted in this case because of the small number of specimens in this test, Reference [11].

In order to construct the entire fatigue diagram in Fig. 6, use was made of an earlier test on nodular cast iron grade 500-7, Reference [11]. The same specimens as in Fig. 4a were used in this test, but they were taken from a batch with an average tensile strength of $R_m = 517$ MPa. The fatigue ratio, i.e. the ratio between the

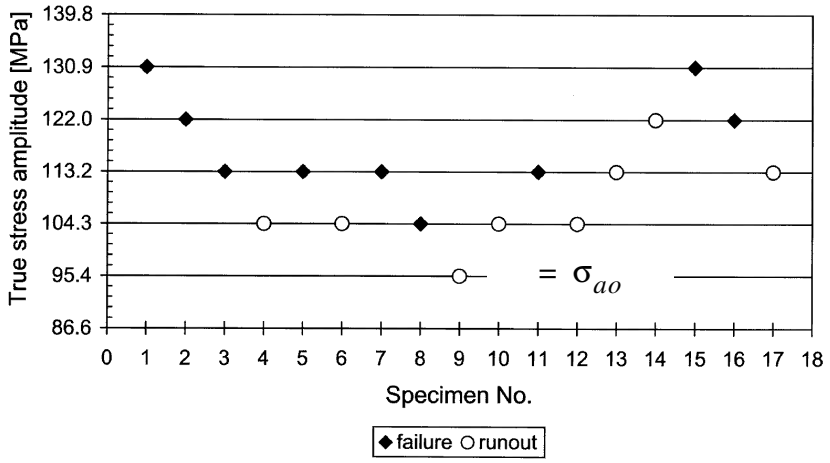

Figure 5. Staircase test with the specimens of nodular cast iron at a true mean stress considering also the yielding of about 255.4 MPa.

The following sample values were evaluated in the staircase in Fig. 5:

$\bar{\sigma}_a$ = 111.9 MPa sample mean fatigue limit at a true mean stress of about 255.4 MPa

s = 10.6 sample standard deviation

fatigue limit in fully reversed tension compression to the average tensile strength was then evaluated to f_R = 0.378. The Haigh diagram in Fig. 6 has been constructed using this fatigue ratio and the evaluated data in Fig. 5. However, according to the tested S-N curve at zero mean stress, see Fig. 9, the fatigue ratio could be a little lower, or about 0.37. It is worth noting how steep the diagram in fact is. The Haigh diagram for nodular cast iron is often presented wrongly, i.e. much flatter, in older literature.

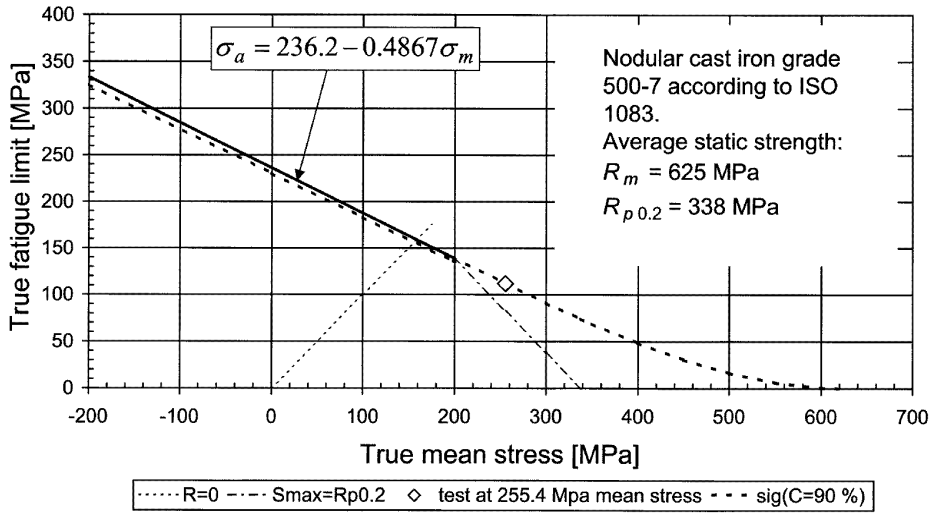

Figure 6. Haigh diagram for nodular cast iron. The dotted line corresponds to the 90 % confidence value to be used in the fatigue analysis and is valid for 25 test specimens according to Fig. 4a and for a typical sample standard deviation of 10 % . The effective stress area of this specimen is A_{eff} = 909 mm^2 *at a relative standard deviation of* s_r = 0.09

2.2 Basic S-N curves

Most of the tests of the basic S-N curve at a nominal high cycle mean stress of 260 MPa were made at three different nominal stress amplitude levels, i.e. 110, 130, and 240 MPa. Because a different amount of yielding in the specimens will take-place at each different level, the actual mean stress will shift more downwards for higher amplitude levels. Because the basic S-N curve is used only as a reference,

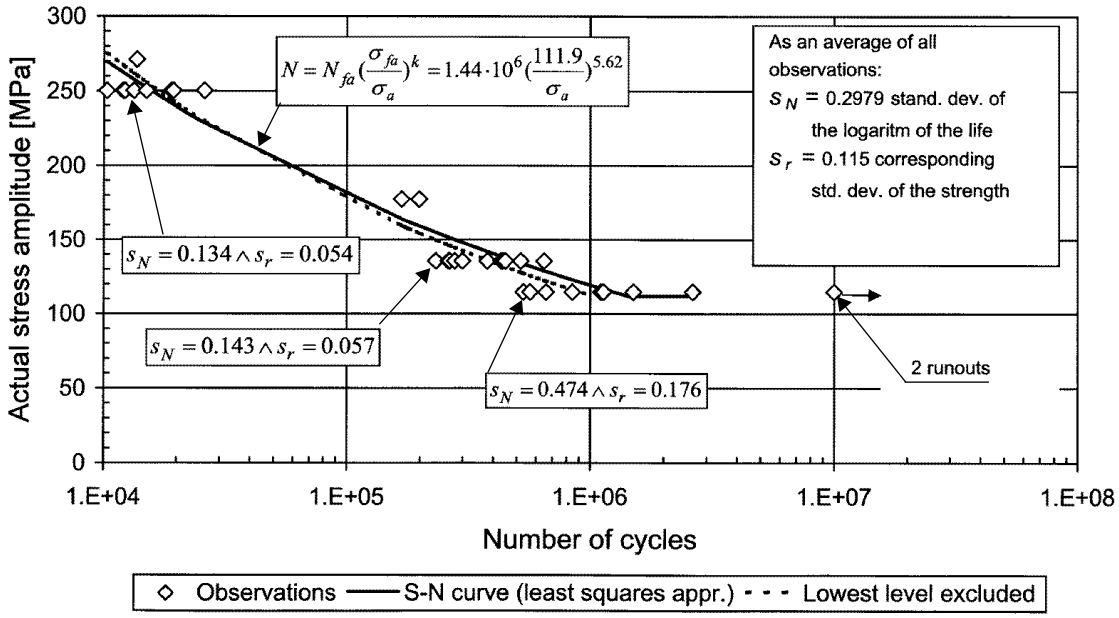

Figure 7. S-N curve for nodular cast iron grade 500-7/ISO 1083 at the high cycle mean stress 255.4 MPa.

this shift will not be considered here, but the evaluation is made as if the actual mean stress at each level would be the same and equal to $\sigma_{mean} = \sigma_{mean,\,hc} =$ 255.4 MPa. The outcome of this test is shown in Fig. 7.

In Fig. 7, the symbol s_N denotes the standard deviation of the lifetime logarithm. The symbol s_r denotes the corresponding approximate standard deviation of the fatigue strength according to Equation (6).

$$s_r \approx 1 - \frac{1}{10^{s_N / k}} \tag{6}$$

The curve fitting of the S-N curve to the test outcome is done with the method of least squares, Reference [12]. It is worth noting that the scatter in the S-N curve increases towards the fatigue limit. Because the allowed stress amplitude in the fatigue analysis is decided by a reduction of the mean fatigue limit to the maximum allowed probability of failure, this means that it is possible to use smaller safety factors in the finite lifetime domain than when designing in relation to the fatigue limit. However, the S-N curve obtained by excluding the observations on the lowest test level indicates that the S-N curve has started to plain out on this level. Accordingly, the relative standard deviation on the lowest level could in fact be less than the one determined with Equation (6).

It is seen in Fig. 2 that the actual low cycle mean stress will be about 190.3 MPa, although it will slightly change depending on the high cycle stress amplitude. The outcome of a test of the S-N curve corresponding to this mean stress is shown

in Fig. 8. Especially on the highest test level, with a maximum stress $\sigma_{max} = \sigma_{mean,\,lc} + \sigma_a = 427.6$ MPa, the yield stress has been exceeded. The small shift of the mean stress due to this shift has not been considered in this evaluation.

A test of the S-N curve in fully reversed tension compression was also made, see Fig. 9. The scatter of the lifespans in this test is very high. Especially, the obser-

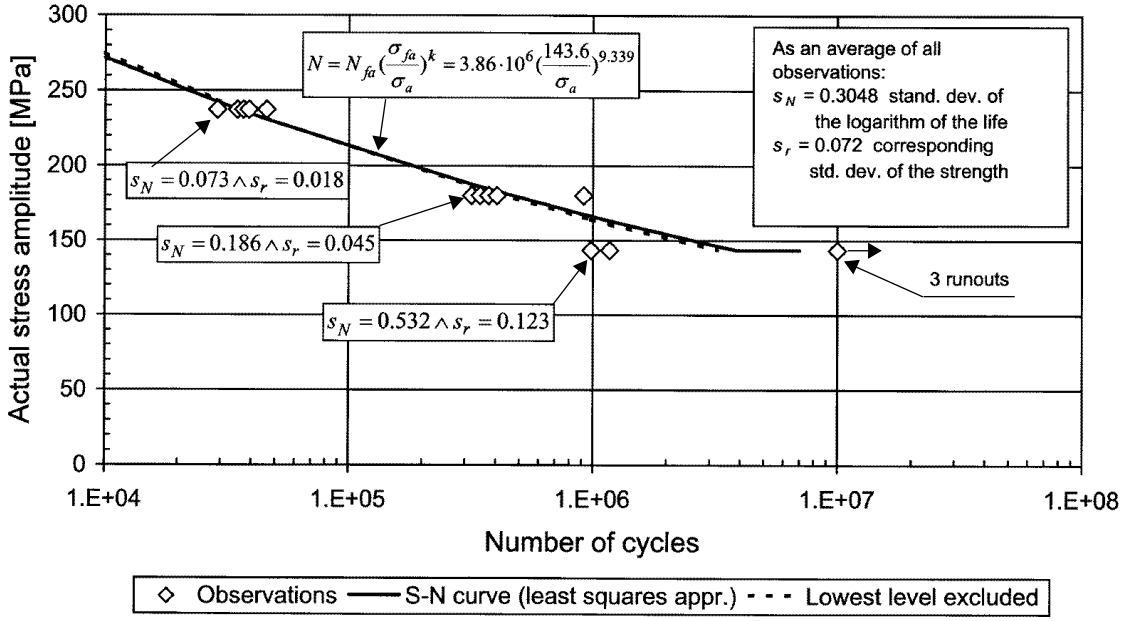

Figure 8. S-N curve for grade 500-7/ISO 1083 at the approximate low cycle mean stress of 190.3 MPa.

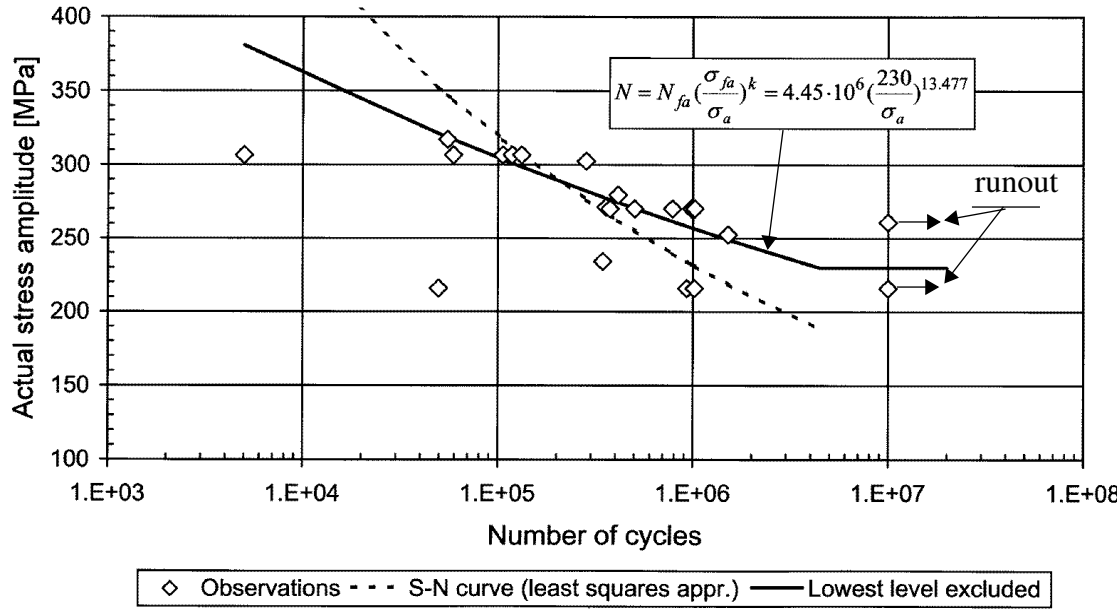

Figure 9. S-N curve for grade 500-7/ISO 1083 at fully reversed tension compression.

vations on the lowest test level 215.9 MPa, do not at all agree with the test data on the higher test levels. The observations on the lowest test level are therefore considered unreliable and excluded from the calculation of the best fit of the S-N curve according to the method of least squares. Generally it is seen from Figs. 7, 8 and 9 that the slope exponent varies from 5.6 to 13.5 and that the S-N curve is steeper for higher mean stresses.

2.3 Spectrum tests

One block of the test with an occasional underload is shown in Fig. 2. The same smooth specimens made from the same batch as shown in Fig. 4 were used. The test matrix is shown in Table 1. A small nominal positive minimum stress of 10 MPa was maintained constant during all the tests, see Fig. 2. The cutoff limit, i.e. the cycle limit where the single test was stopped if the specimen had not failed before that, was chosen to be approximately 150 million cycles.

The original idea, when determining the cycle ratios for different high cycle test amplitudes, was to try to obtain in all tests an approximately constant proportion of damage caused by the underload cycles. However, the outcome of the test showed that low cycle damage was negligible in each case.

The effect of the underloads is to accelerate the damage accumulation due to the high cycle load, as illustrated in Fig. 3. The outcome of this spectrum test is shown in Fig. 10. It can be deduced that occasional underloads have a very severe damage accelerating effect on the fatigue limit. For more frequent underloads, or a cycle ratio of about 10 000 to 20 000, the extension of the S-N curve has almost the same slope as the basic S-N curve, as once suggested by H. T. Corten and T. J. Dolan. However, the starting point of the extension is to the left of the end point of the basic S-N curve. With the higher cycle ratio of about 220 000 to 300 000, the

Table 1. Test matrix in the spectrum test of nodular cast iron grade 500-7/ISO 1083.

Test No.	Number of specimens n	Actual high cycle stresses		Actual low cycle stresses		Cycle ratio $\frac{n_{hc}}{n_{lc}}$
		$\sigma_{mean,\,hc}$	$\sigma_{a,\,hc}$	$\sigma_{mean,\,lc}$	$\sigma_{a,\,lc}$	
1	9	255.4	115.8	190.8	180.4	3 300
2	3	255.4	94.7	180.3	169.8	10 000
3	10	255.4	87.1	176.5	166.0	20 000
4	6	255.4	87.1	176.5	166.0	220 000
5	10	255.4	67.8	166.8	156.4	300 000

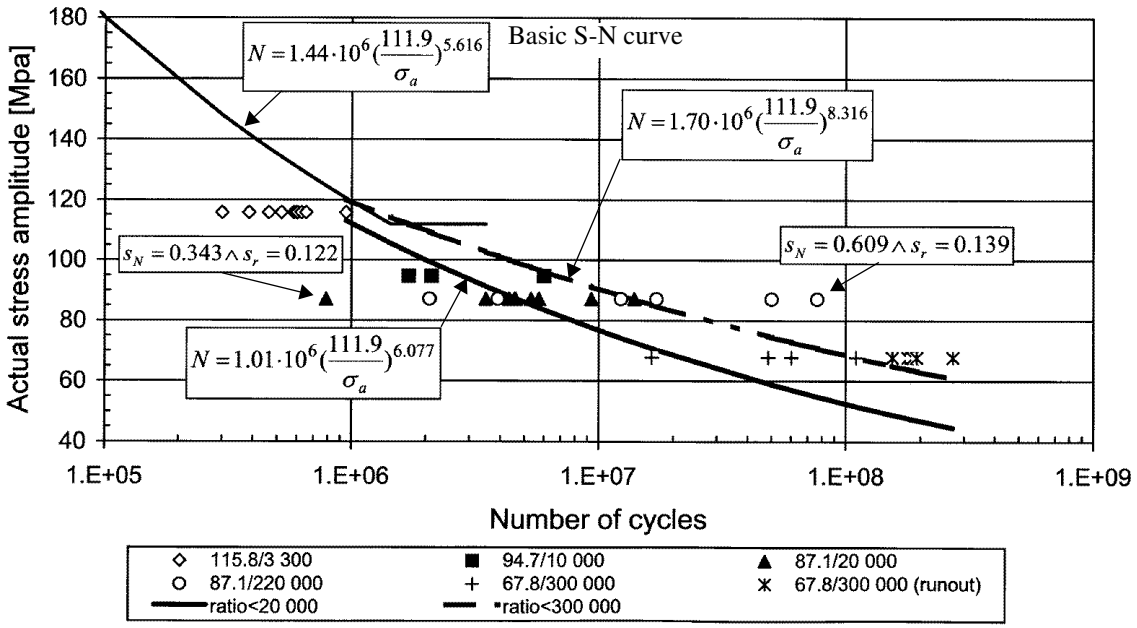

Figure 10. Extension of the S-N curve for grade 500-7/ISO 1083 due to occasional underloads at a high cycle mean stress of 255.4 MPa.

Table 2. Life and scatter (sample values) at different test levels and with different cycle ratios in the spectrum test on nodular cast iron grade 500-7/ISO 1083.

Test No.	Average number of high cycles $\overline{N} = 10^{\overline{\log N}}$	Number of low cycles n_{lc}		Average amount of low cycle damage $\frac{n_{lc}}{3.9 \cdot 10^6 \left(\frac{143.6}{\sigma_{a,\,lc}}\right)^{9.3}}$	Stand. dev. of log. life s_N	Relative standard deviation of the fatigue strength $s_r \approx 1 - \frac{1}{10^{s_N/k}}$	
		Average	Min.			s_r	Comm. k
1	544000	164	90	$5.3 \cdot 10^{-4}$	0.137	0.051	6.08
2	$2.79 \cdot 10^6$	278	170	$5.3 \cdot 10^{-4}$	0.292	0.105	6.08
3	$4.64 \cdot 10^6$	232	39	$3.6 \cdot 10^{-4}$	0.343	0.122	6.08
4	$13.7 \cdot 10^6$	62	9	$9.6 \cdot 10^{-5}$	0.609	0.139	9.35
5	$109.9 \cdot 10^6$	366	54	$3.3 \cdot 10^{-4}$	0.374	0.088	9.35

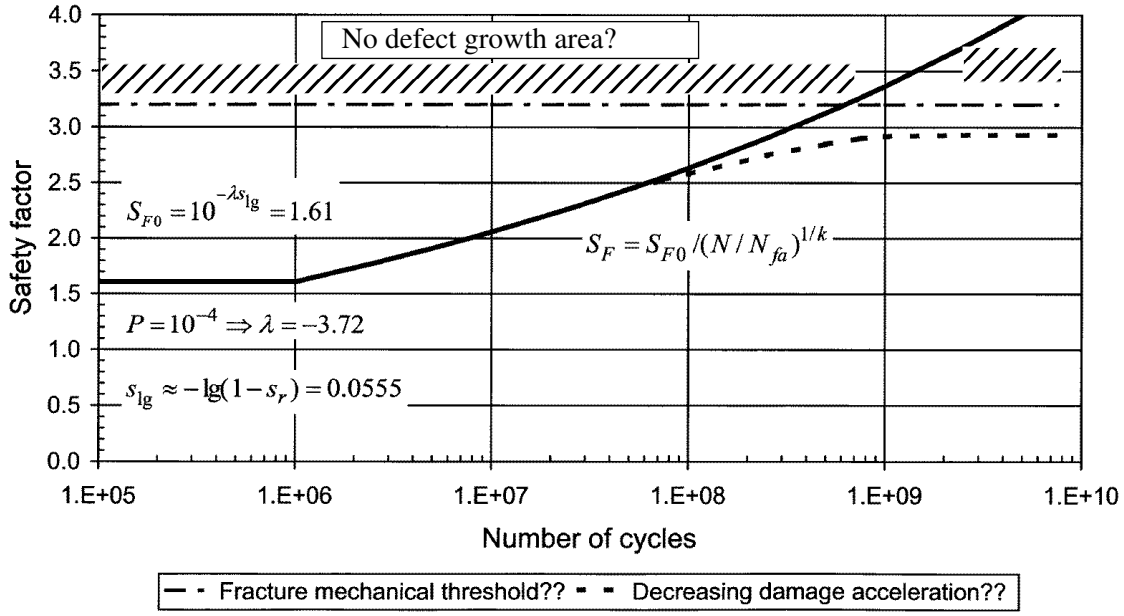

Figure 11. Effect of ccasional underloads on the required safety factor in relation to the normal fatigue limit . Maximum allowed probability of failure $P = 10^{-4}$ *and relative population standard deviation with 90 % confidence* $s_r = 0.12$.

extension is more flat and more in line with the suggestion made by Erwin Haibach [4]. The extended S-N curve according to the full line (ratio<20 000 in Fig. 10) has been evaluated by the method of least squares applied on the observations on amplitude level 94.7, cycle ratio 10 000, and on amplitude level 87.1, cycle ratio 20 000. For the evaluation according to the dotted line, the observations on level 87.1 with cycle ratio 220 000 and on level 67.8 with cycle ratio 300 000 have been used (ratio<300 000 in Fig. 10).

It is important to notice that the required number of occasional underloads to cause fatigue failure at a high cycle stress amplitude below the fatigue limit is surprisingly low. In test No. 4, a minimum number of 9 underloads has been enough to cause fatigue failure in one specimen. The failure of the cumulative linear Miner rule to predict this phenomenon is illustrated in Table 2 by the calculated low cycle damage, which in itself is negligible. The calculated standard deviations are quite high. This must be considered when the appropriate factor of safety is determined in the fatigue analysis. Much testing must still be done to be able to determinate the correct safety factor in variable amplitude conditions with occasional underloads, especially in the ultra high cycle regime, i.e. with cutoff limits up to one billion cycles. The present situation with its open questions is sketched in Fig. 11. It seems logical to assume that there must be some limit to the required safety factor. In addition to testing in the ultra high cycle domain, this limit could perhaps also be estimated by using the fracture mechanical stress intensity threshold value and some upper limit of the possible initial defect, see Figs. 12 and 13.

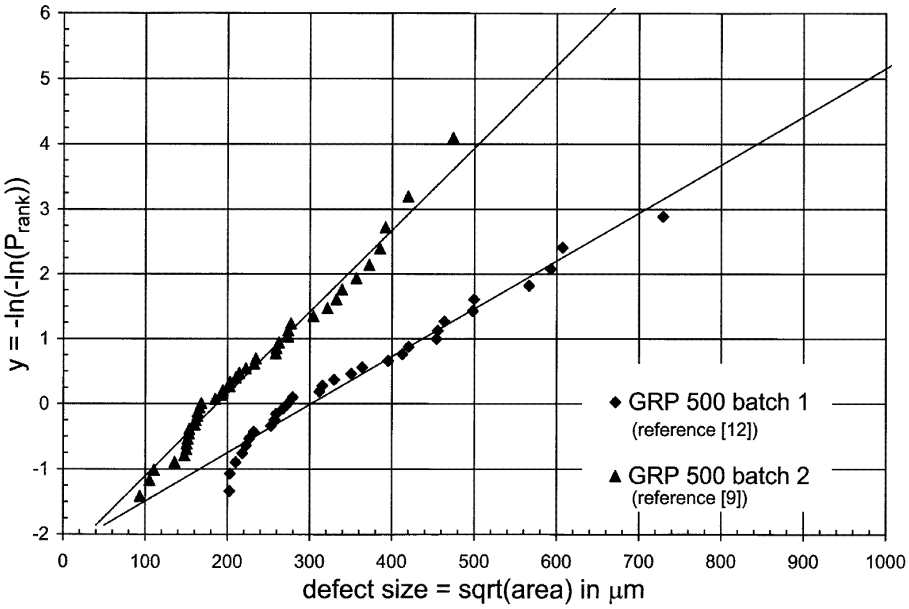

Figure 12. Defect distribution in the broken test specimens of nodular cast iron.

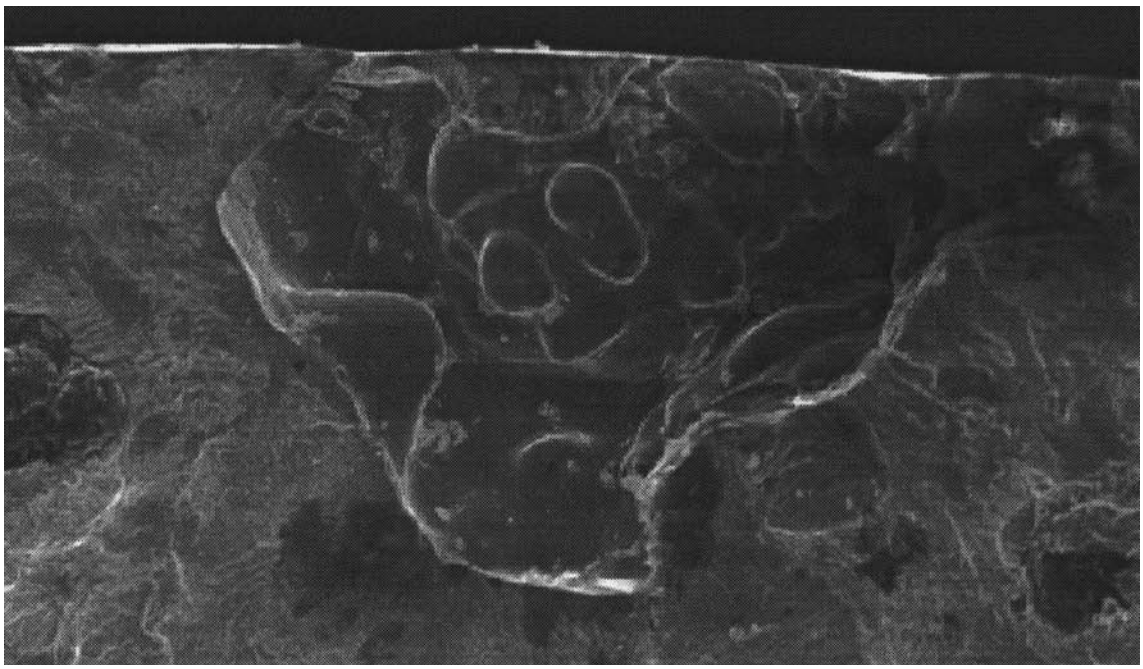

Figure 13. Crack nucleation from a shrinkage pore in one of the broken specimens.

3. Tests on grey cast iron

The fatigue tests that were made on specimens of grey cast iron grade 300/ISO 185 and their evaluation are explained in more detail in References [12] and [13]. Therefore, only a brief summary of these tests will be given here. These tests were the first spectrum tests ever planned by the author, and therefore due to lack of ex-

perience they are not as complete as the corresponding tests on nodular cast iron. The biggest weakness is that the cycle ratio was different on all the three tested levels and exact information about how the cycle ratio will influence the slope exponent was not obtained. The same specimens as those according to Fig. 4a were also used in these tests. The ultimate tensile strength, as an average of 10 tensile tests, of these specimens was R_m = 339 MPa with an unbiased standard deviation of 18.6 MPa. The same type of spectrum as shown in Fig. 2, but with the values given in Table 3, was used in these fatigue tests with occasional overloads.

The basic S-N curve measured in this test at the actual high cycle mean stress of 166.9 MPa is shown in Fig. 14. Staircase tests were also made to obtain the Haigh diagram of the specimens in this material, see Figs. 15 and 16.

The outcome of the fatigue tests with occasional underloads according to Table 3 is sketched in Fig. 17.

Table 3. Test matrix in the spectrum test of grey cast iron grade 300/ISO 185.

Test No.	Number of specimens n	Actual high cycle stresses		Actual low cycle stresses		Cycle ratio $\frac{n_{hc}}{n_{lc}}$
		$\sigma_{mean,\,hc}$	$\sigma_{a,\,hc}$	$\sigma_{mean,\,lc}$	$\sigma_{a,\,lc}$	
1	5	166.9	31.8	104.6	94.1	5000
2	5	166.9	29.2	103.3	92.8	27 500
3	5	166.9	26.6	102.0	91.5	200 000

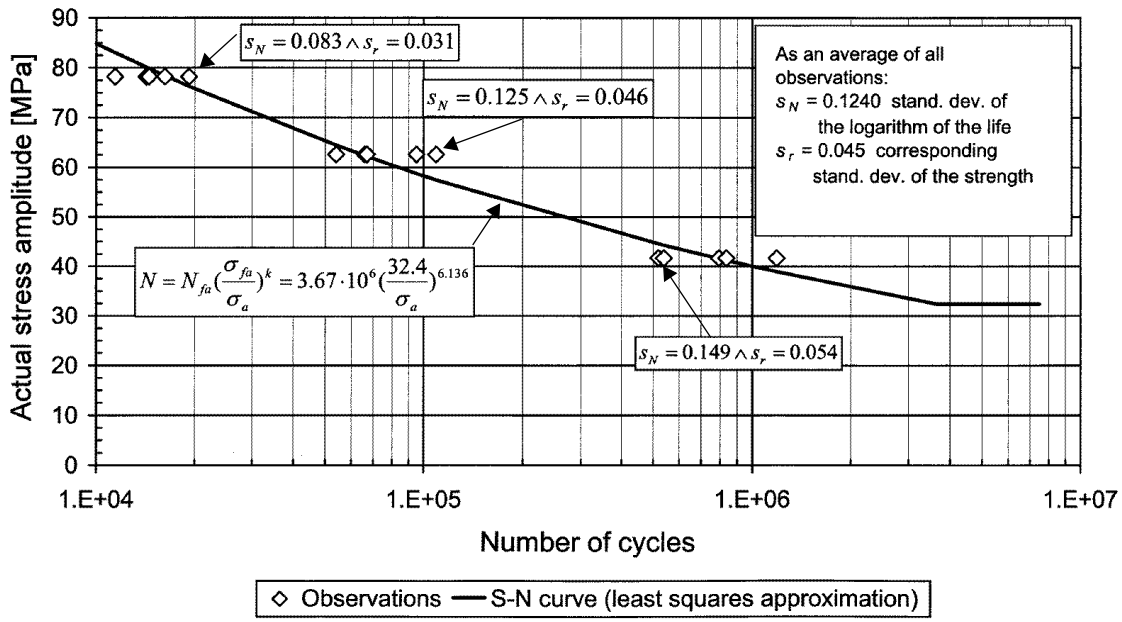

Figure 14. S-N curve for grey cast iron grade 300/ISO 185 at the high cycle mean stress 166.9 MPa.

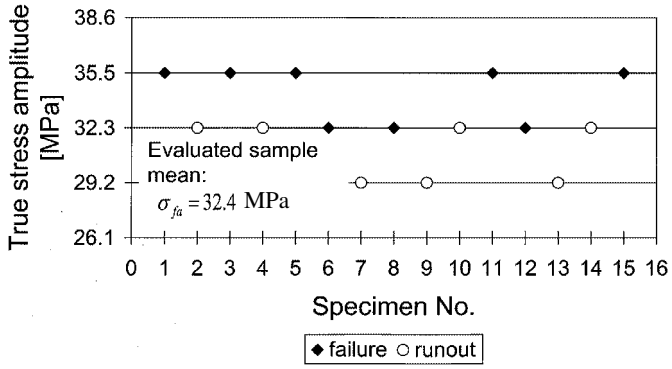

Figure 15. Staircase test on grey cast iron grade 300/ISO 185 at the high cycle mean 166.9 MPa.

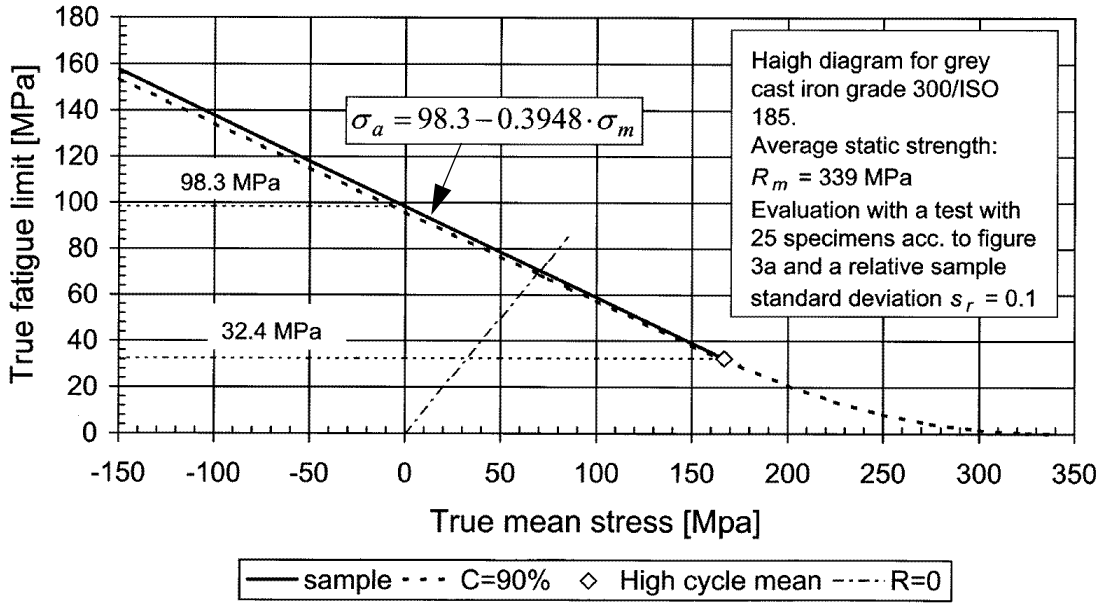

Figure 16. Haigh diagram for grey cast iron grade 300/ISO 185.

It can be seen that even in this case a very low number of occasional underloads will promote an acceleration of the damage caused by the high cycle loads. Besides, it is also evident that the cycle ratio will influence the slope of the extended S-N curve. A summary of the outcome of this test is given in Table 4. The amount of low cycle damage is also in this case negligible. The scatter in the lifetime logarithm is comparable to the one found for nodular cast iron. However, the corresponding scatter in the fatigue amplitude is much smaller due to the flatter curve . This fact can be utilized when the appropriate safety factor with regard to the fatigue limit is defined. To determine the population standard deviation it is recommended to put a 90 % confidence on the sample value. The distribution of the sample standard deviation is characterised by the Chi squared distribution, see

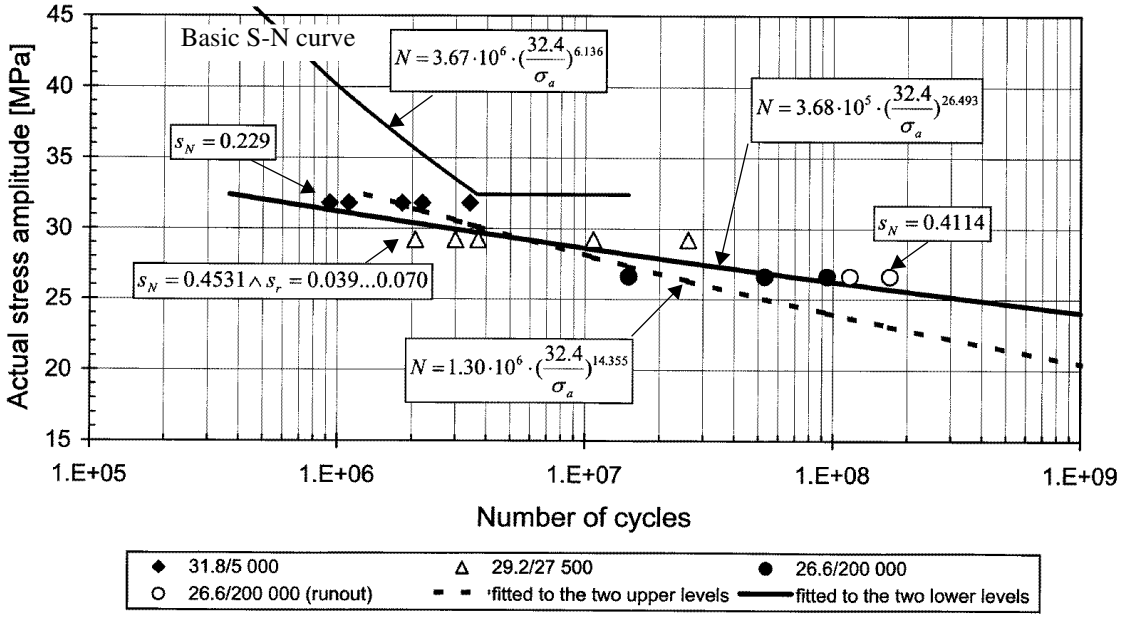

Figure 17. Extension of the S-N curve for grey cast iron grade 300/ISO 185 due to occasional underloads at a high cycle mean stress of 166.9 MPa.

Table 4. Life and scatter (sample values) at different test levels and with different cycle ratios in the spectrum test on grey cast iron grade 300/ISO 185.

Test No.	Average number of high cycles $\overline{N} = 10^{\overline{\log N}}$	Number of low cycles n_{lc}		Average amount of low cycle damage, ref. [12] $\frac{n_{lc}}{3.7 \cdot 10^6 \left(\frac{54.6}{\sigma_{a,\,lc}}\right)^{7.3}}$	Stand. dev. of log. life s_N	Relative standard deviation of the fatigue strength $s_r \approx 1 - \frac{1}{10^{s_N/k}}$	
		Average	Min.			s_r	Comm. k
1	$1.70 \cdot 10^6$	379	186	$4.0 \cdot 10^{-3}$	0.229	0.036	14.36
2	$5.78 \cdot 10^6$	332	75	$3.2 \cdot 10^{-3}$	0.453	0.039	26.49
3	$6.84 \cdot 10^7$	452	75	$3.9 \cdot 10^{-3}$	0.411	0.035	26.49

Reference [11]. Because there have only been 5 specimens per level, the following population standard deviation can be calculated, e.g., for level 2, Table 4:

$$s_{rC90} = \sqrt{\frac{n-1}{h_1}} \cdot s_r = \sqrt{\frac{5-1}{1.064}} \cdot 0.039 = 0.076 \qquad (7)$$

The required safety factor, at e.g. a maximum allowed probability of failure $P = 10^{-4}$ which corresponds to a standard normal variable $\lambda = -3.72$, is then as follows:

$$s_{lg} \approx -\lg(1 - s_{rC90}) = 0.0343 \text{ and } \quad S_F = 10^{-\lambda s_{lg}} = 1.34 \tag{8}$$

For instance, at a high cycle number $n_{hc} = 10^9$, the extended S-N curve in Fig. 17 gives a fatigue amplitude of $\sigma_{a,\,hc} = 24.0$ MPa, and the allowed value is hence $\sigma_{all} = \sigma_{a,\,hc} / S_F = 17.9$ MPa. Calculated in relation to the fatigue limit the equivalent safety factor would then be $S_F = 32.4 / 17.9 = 1.81$.

4. Tests on quenched and tempered steel

These fatigue tests with occasional underloads were planned in the still ongoing project FADEL (Fatigue Design for Long Life). Project FADEL is a joint project between 5 Finnish companies and the testing is mainly made at VTT, the Technical Research Centre of Finland, and partly at the Lappeenranta University of Technology. The material in the specimens shown in Fig. 18 is quenched and tempered steel EN 10083-1 - 34CrNiMo6+QT. The Haigh diagram for this material had first to be tested, and the resulting diagram is shown in Fig. 19 with the actual high cycle test points and the approximate low cycle test point of the spectrum test sketched.

As seen in Fig. 19, the stress amplitude of the low cycle load of the test spectrum is rather high. The reason for this choice of load spectrum is that it in fact resembles the load spectrum in the thread roots of pretensioned screws. For instance, the connecting rod and cylinder head screws will experience even higher low cycle stress amplitudes due to the loosening and tightening during periodic engine overhauls. One of the main purposes of this test was to determine whether there is a risk that the already low number of such overhauls during the engine lifetime could initiate this kind of accelerated fatigue crack nucleation. The final test matrix for the tests with occasional underloads is given in Table 5 and sketched in Fig. 20.

4.1 Staircase tests

The Haigh diagram for the chosen material EN 10083-1 - 34CrNiMo6+QT had first to be determined by two staircase tests, one at the high cycle mean stress and the other at the low cycle mean stress. The outcome of these staircase tests are shown in Figs. 21 and 22. Due to a perhaps too large stress increment in the tests at the high cycle mean stress, there is a distribution of failures and runouts on only the level in the middle. It is not possible to calculate any sensible standard deviation from such an outcome. However, the evaluated actual fatigue limit $\sigma_{fa} = 428.0$ MPa at the high cycle mean stress can be trusted. The staircase test at an actual mean stress of 207.2 MPa, which is close to the low cycle mean stress

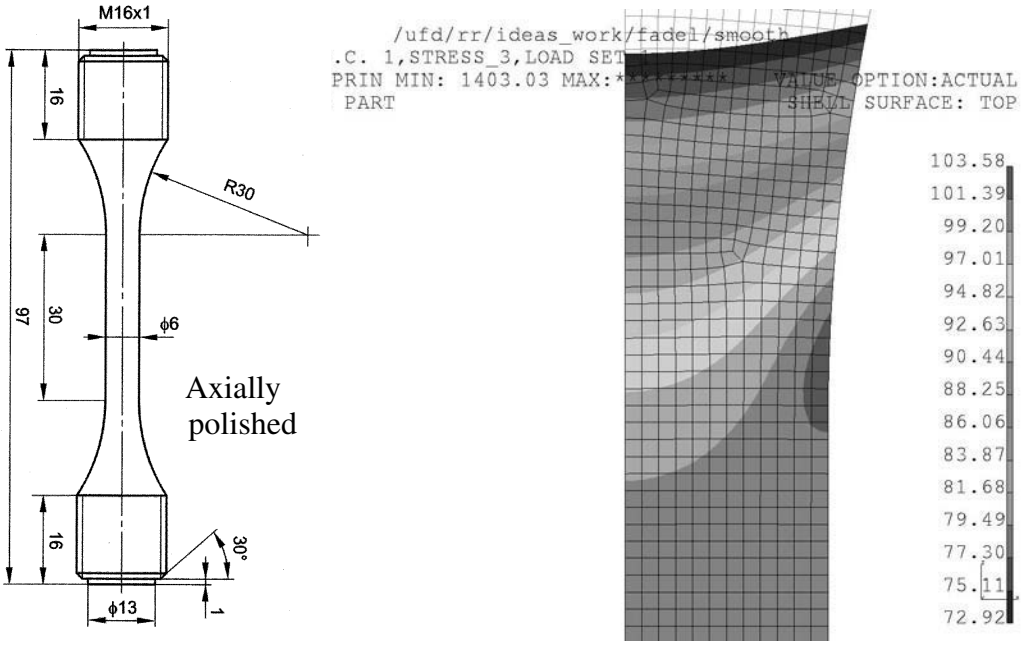

a) specimen b) stress distribution in the notch

Figure 18. Test specimen used in the fatigue tests and in the test of the static strength.

The material in the specimen in Fig. 18 was EN 10083-1 - 34CrNiMo6+QT with the following strength as an average of 2 tensile tests:

$R_m = 1165\,\text{MPa}$ mean tensile strength

$R_{p0.2} = 1064\,\text{MPa}$ 0.2 % proof stress

and with the following properties

$K_t = 1.036$ theoretical stress concentration factor

$A_{eff} = \sum_i \frac{\log R_i}{\log 0.5} \cdot A_i = 367\,\text{mm}^2$ effective stress area of the specimen for a relative standard deviation of the fatigue limit of $s_r = 0.07$

looks rather good. The calculated sample standard deviation in this test is 34.2 MPa, i.e. the relative sample standard deviation is $s_r = 0.064$, which is quite typical for quenched and tempered steels. However, it should be considered that the evaluation of staircase test outcomes of this type can systematically lead to a somewhat too small sample standard deviation, see Reference [11]. Therefore, based on also other tests on quenched and tempered steel of the same type, a value of $s_r = 0.07$ has been used in Fig. 19. This value is valid for a staircase test with 25 specimens, which means that the transformation to a population value with 90 % confidence gives a value of $s_{rC90} \approx 0.09$. This value should be used in the reduc-

tion of the mean fatigue limit to the required probability of failure.
These two staircase tests allowed the construction of the complete Haigh diagram, with the testing points of the spectrum test schematically included, as shown in Fig. 19.

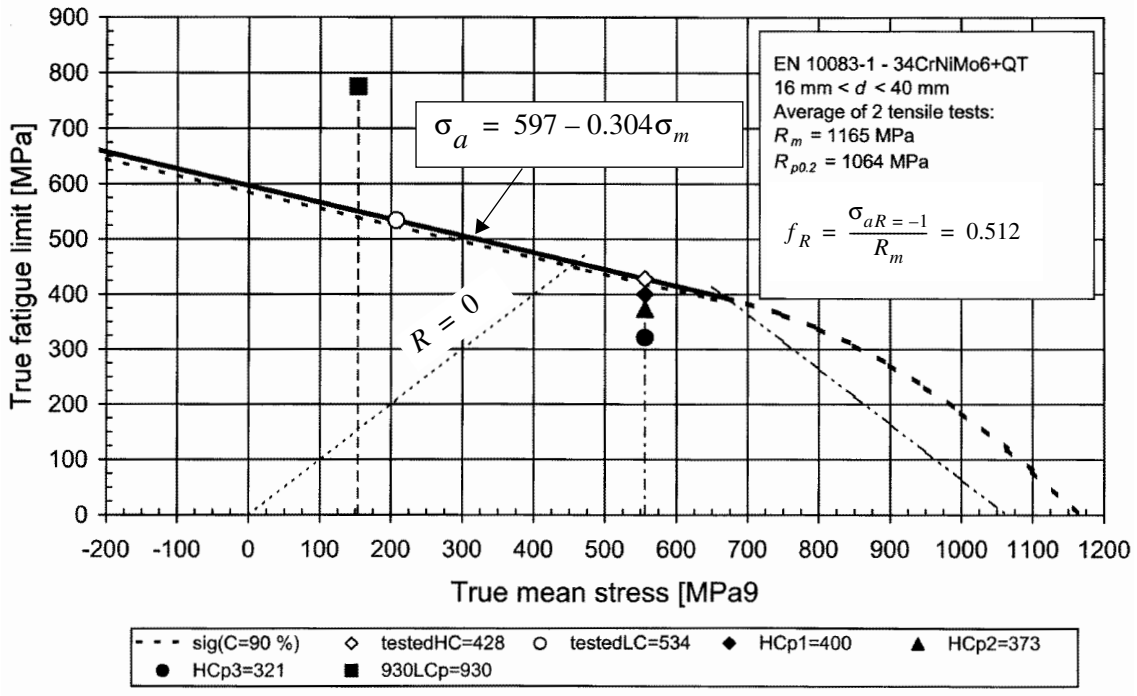

Figure 19. Haigh diagram with the approximate test points for the spectrum tests sketched. The dotted line corresponds to the 90 % confidence value to be used in the fatigue analysis. The confidence line is valid for 25 specimens and a typical sample standard deviation of 7 %. This diagram is tested with specimens according to figure 18a.

Table 5. Test matrix in the spectrum test of quenched and tempered steel EN 10083-1 - 34CrNiMo6+QT

Test No.	Number of specimens n	Actual high cycle stresses		Actual low cycle stresses		Cycle ratio $\frac{n_{hc}}{n_{lc}}$
		$\sigma_{mean,\,hc}$	$\sigma_{a,\,hc}$	$\sigma_{mean,\,lc}$	$\sigma_{a,\,lc}$	
1	5	556	400.4	167.4	789.0	10 000
2	5	556	400.4	167.4	789.0	100 000
3	5	556	373	153.7	775.3	10 000
4	5	556	373	153.7	775.3	100 000
5	5	556	321.2	127.8	749.4	100 000

4.2 Basic S-N curve at the high cycle mean stress

The basic S-N curve at the actual high cycle mean stress of 556 MPa was tested with a total of 15 specimens at three different levels above the corresponding fatigue limit 428 MPa. The outcome of this test is shown in Fig. 23. For a comparison, the broken specimens on the highest level 454.8 MPa of the corresponding staircase test, Fig. 22, are also included to this figure.

It is seen from Fig. 23 that the scatter increases towards the fatigue limit, from a standard deviation $s_N = 0.112$ on the lifetime logarithm on the highest test level

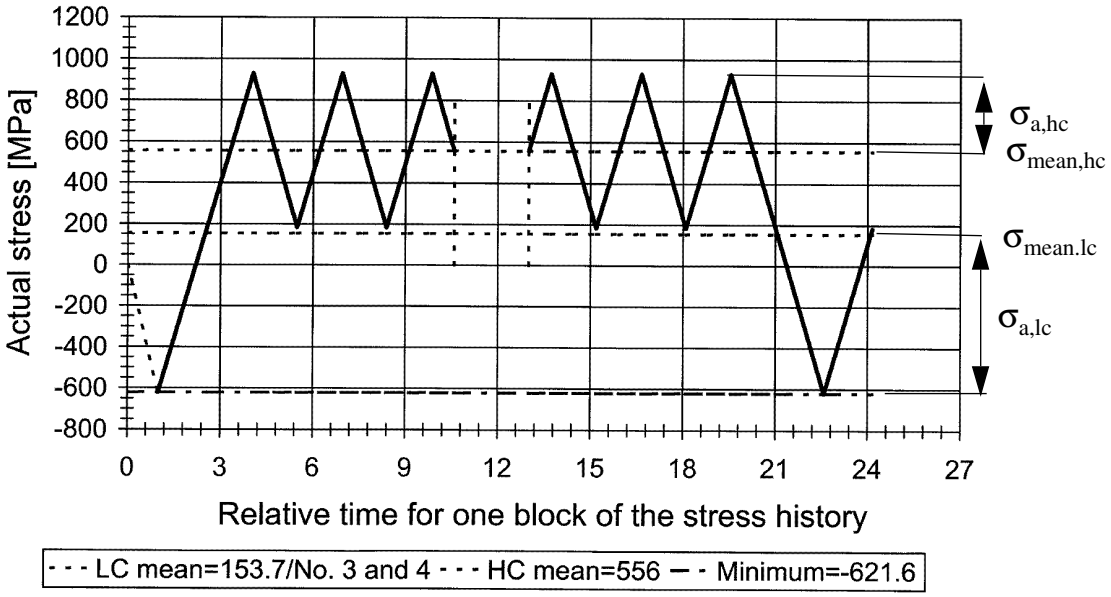

Figure 20. Stress history in one block of the spectrum test on quenched and tempered steel specimens.

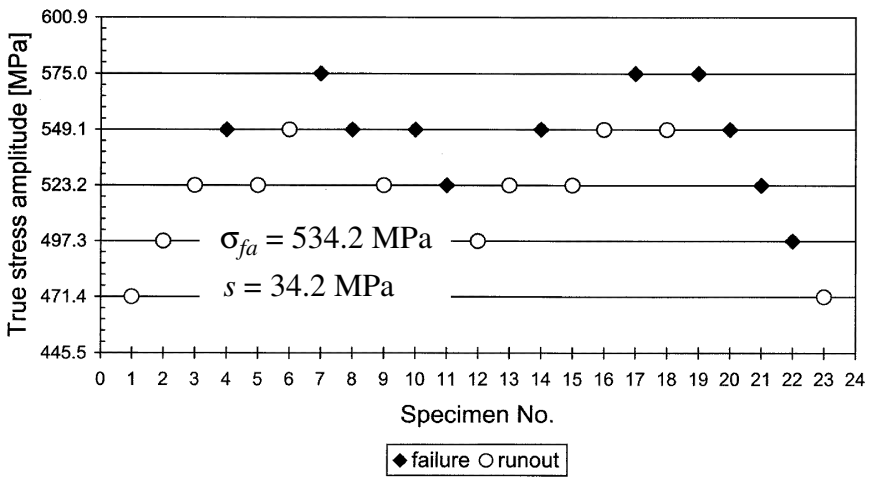

Figure 21. Staircase test to determine the fatigue limit at the low cycle mean stress.

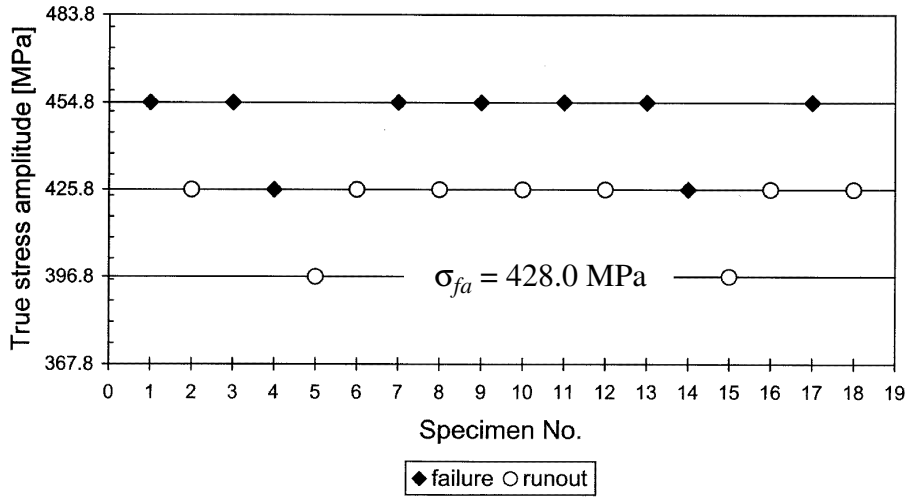

Figure 22. Staircase test to determine the fatigue limit at the high cycle mean stress.

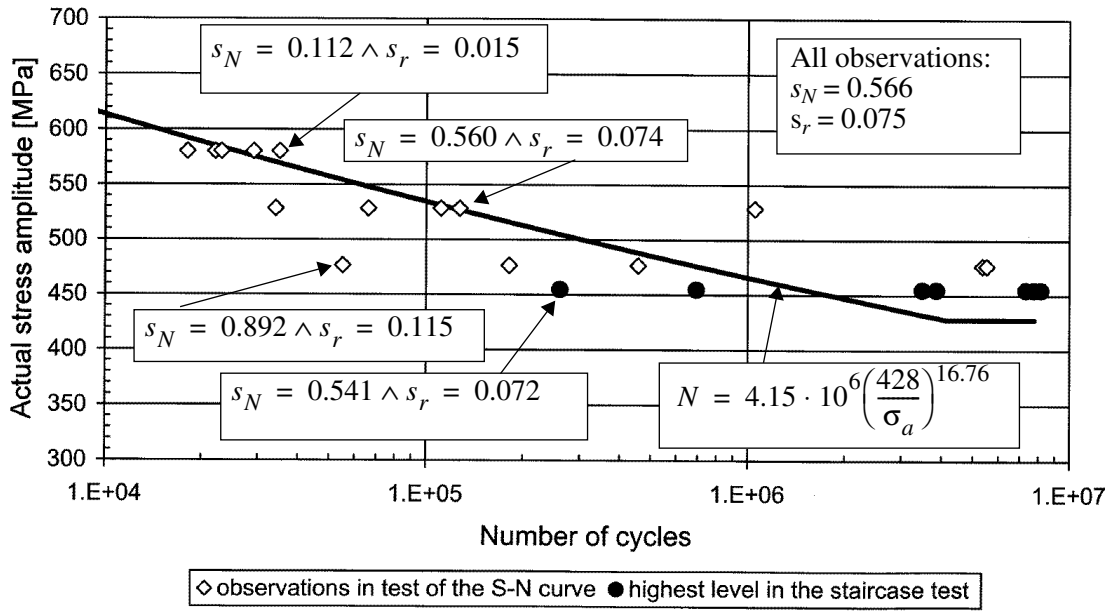

Figure 23. Tested S-N curve at the actual high cycle mean stresses 556 MPa.

to a value of $s_N = 0.892$ on the lowest level at 476.6 MPa. It is clear that this can be considered when the appropriate safety factors are determined. A more alarming fact is that the scatter in the S-N curve close to the fatigue limit is larger than the one calculated in the corresponding staircase test. This was also true for nodular cast iron, Fig.7, and it will arouse fears that it is wrong, as is now common, to estimate the standard deviation to be used in the fatigue analysis from the staircase test.

4.3 Spectrum tests

The outcome of the test with occasional underloads is shown in Fig. 24 and Table 6. Quenched and tempered steel 34CrNiMo6+QT will, according to the test results in Figure 24 and Table 6, be extremely sensitive to such kinds of occasional underloads. This came as a total surprise, because it had been assumed before these tests that E. Haibach's suggestion should work quite well. However, the extension of the S-N curve starts shifted one decade or more to the left in comparison to the end point of the basic S-N curve. The extension of the S-N curve continues even somewhat steeper than the basic curve and with small sensitivity to the different cycle ratios. Moreover, an extremely low number of occasional underloads, on average about 30 and at a minimum of only 3 pcs, is needed to initiate this accelerating damage. Regrettably, the S-N curve corresponding to the low cycle mean stress was not tested. If the damage due to the underloads is calculated using the tested S-N curve for the high cycle mean stress, then considerable low cycle damage will take place in this case. However, this could be an illusion, because according to the low cycle fatigue curve for 34CrNiMo6 found in Reference [14], the lifetime at this low cycle strain amplitude $\approx \sigma_{a,\,lc}/E = 789/206000 = 0.0038$ should be about 10^4 to 10^5 cycles. The scatter in the extension is quite high and it must be concluded that it is necessary to use at least the same relative standard deviation as for the fatigue limit in the fatigue analysis. The outcome on the lowest test level 321.2 MPa is very strange with unexpectedly short lifetimes. This is illustrated with the steep extension obtained by fitting it to all the three test levels with cycle

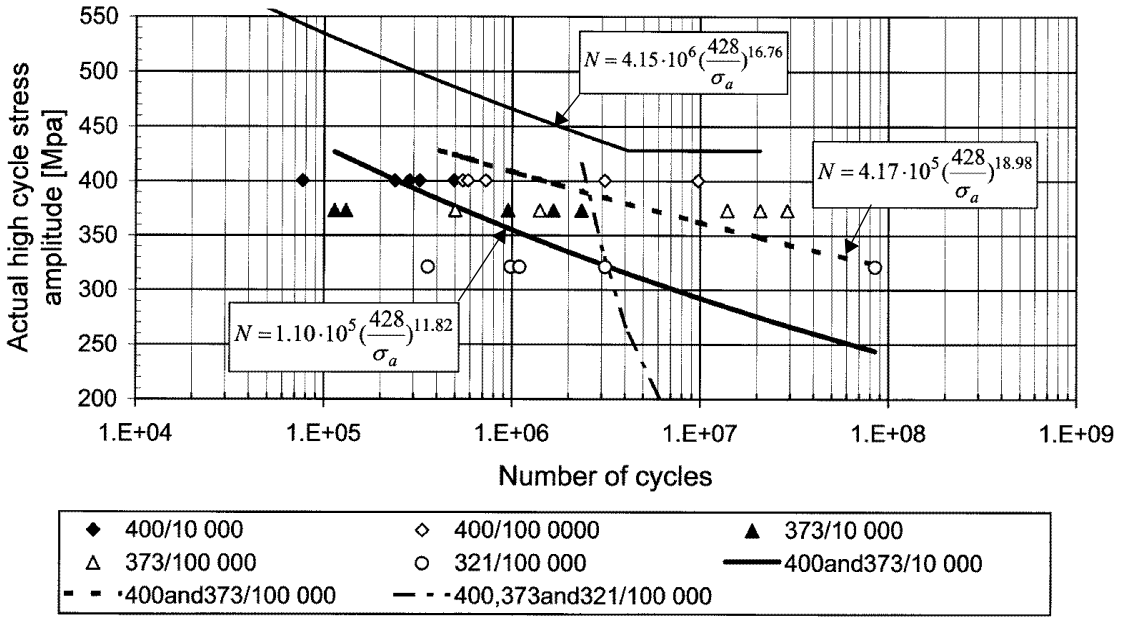

Figure 24. Extension of the S-N curve for quenched and tempered steel EN 10083-1 - 34CrNiMo6+QT due to occasional underloads at an actual high cycle mean stress of 556 MPa.

Table 6. Lifetime and scatter (sample values) at different test levels and with different cycle ratios in the spectrum test on quenched and tempered steel EN 10083-1 - 34CrNiMo6+QT.

Test No.	Average number of high cycles $\overline{N} = 10^{\overline{\log N}}$	Number of low cycles n_{lc}		Average amount of low cycle damage[a] $\frac{n_{lc}}{4.2 \cdot 10^6 \left(\frac{428}{\sigma_{a,\,lc}}\right)^{16.8}}$	Stand. dev. of log. life s_N	Relative standard deviation on fatigue strength $s_r \approx 1 - \frac{1}{10^{s_N/k}}$	
		Average	Min.			s_r	Comm. k
1	242 600	24	7	0.165	0.302	0.057	11.82
2	$1.48 \cdot 10^6$	14	5	0.102	0.552	0.065	18.98
3	560 800	56	11	0.288	0.620	0.114	11.82
4	$5.67 \cdot 10^6$	56	5	0.194	0.783	0.091	18.98
5	$2.53 \cdot 10^6$	25	3	0.084	0.917	-	-

a. The S-N curve at the high cycle mean stress is used because the S-N curve at the low cycle mean stress was not tested.

ratio 100 000. Because only 5 specimens have been tested on each level it could perhaps be a slump, but it could also be that this combination of low cycle and high cycle stress amplitudes will give the most unfavourable internal residual stresses.

5. Conclusions

It has been shown above with spectrum tests on three different material types, namely, nodular cast iron, grey cast iron, and quenched and tempered steel that the damage accelerating effect due to occasional underloads with amplitudes beyond the fatigue limit is a very real problem. The severity of this phenomenon seems to increase with increasing strength. The extension of the S-N curve for grey cast iron is much flatter than the basic curve. Nodular cast iron is more sensitive and the extended S-N curve has about the same slope as the basic curve. However, the extension of the S-N curve due to occasional underloads for quenched and tempered steels can be even steeper than the basic curve.

These findings cannot be explained by any old theory about cumulative damage. It is even hard to quantitatively explain it with the fracture mechanical reasoning in chapter 1. Before a consistent theory can be developed it is necessary to

conduct more testing on the three decisive factors, namely a) the influence of the cycle ratio, b) the influence of the total life, i.e., will the extended curve flatten during ultralong lifetimes, and c) the influence of the amplitude of the underload.

In general, the scatter in the extended S-N curves are quite high and when the safety factor corresponding to the maximum allowed probability of failure is determined, it is recommended to use the same relative standard deviation as for the fatigue limit, at least for nodular cast iron and quenched and tempered steel .

References

1. A. Palmgren. Die Lebensdauer von Kugellagern. VDI-Z 69 (1924). pp. 339–341.

2. M. A. Miner. Cumulative damage in fatigue. Trans. ASME. J. Appl. Mech. 12 (1945) A159–A169.

3. H. T. Corten and T. J. Dolan. Cumulative fatigue damage. Proc. Int. Conf. Fatigue of Metals, Inst. Mech. London. New York 1956. Pp. 235–246.

4. Prof. Dr.-Ing. Erwin Haibach. Betriebsfestigkeit. Verfahren und Daten zur Bauteilberechnung. 2. Auflage. Springer–Verlag Berlin Heidelberg 2002.

5. A. K. Vasudevan, K. Sadananda and G. Glinka. Critical parameters for fatigue damage. International Journal of Fatigue 23 (2001) S39–S53.

6. Gary B. Marquis, B. Roger Rabb and Päivi Karjalainen-Roikonen. High Cycle Variable Amplitude Fatigue of a Nodular Cast Iron. “Fatigue Testing and Analysis Under Variable Amplitude Loading Conditions”. ASTM STP 1439. P. C. McKeighan and N. Ranganathan, Eds., American Society for Testing and Materials, West Conshohocken, PA, 2003.

7. J. C. Newman, Jr. and E. P. Phillips. Prediction of Crack Growth under Variable-Amplitude and Spectrum Loading in a Titanium Alloy. “Fatigue Testing and Analysis Under Variable Amplitude Loading Conditions”. ASTM STP 1439. P. C. McKeighan and N. Ranganathan, Eds., American Society for Testing and Materials, West Conshohocken, PA, 2003.

8. K. Sadananda, A. K. Vasudevan, R. L. Holtz and E. U. Lee. Analysis of overload effects and related phenomena. International Journal of Fatigue 21 (1999) S233–S246.

9. Gary Marquis & Jussi Solin. Long-life fatigue design of GRP 500 nodular cast iron components. VTT Technical Research Centre of Finland, Research Notes 2043, Espoo 2000.

10. Roger Rabb. Interpretation and Evaluation of the Statistical Size Effect. Proceedings Vol. 3 from the 23rd CIMAC World Congress on Combustion Engine Technology, May 7–10, 2001 Hamburg. Pp. 1125–1140.

11. B. Roger Rabb. Staircase testing – confidence and reliability. Fatigue Damage of Materials. Experiment and Analysis. Editors: A. Varvani-Farahani and C. A. Brebbia. WITpress 2003.

12. B. Roger Rabb. Fatigue Testing and Its Statistical Evaluation into Design Rules. Tampere University of Technology. Publications 253. Doctoral thesis, Tampere April 1999.

13. Roger Rabb. Fatigue Life Evaluation of Grey Cast Iron Machine Components under Variable Amplitude Loading. ESIS Publication 23, Fatigue Design and Reliability. Editors: G. Marquis & J. Solin. 1999 Elsevier Science Ltd.

14. Chr. Boller and T. Seeger. Materials Data for Cyclic Loading. Part B: Low-alloy Steels. Elsevier 1987.

Life prediction of gas turbine hot section components – an Italian – French cooperative project

V. Bicego[1] & L. Lelait[2]
[1]CESI, Milan, Italy
[2]EDF-EIFER, Karlsruhe, Germany

Abstract

In the frame of a cooperative EUREKA scheme, EDF and CESI have been carrying out a four year project, entitled Gas Turbine Life Prediction (acronym TULIP), intended to develop a life prediction methodology for the rotating blades of large industrial gas turbines. In the CESI approach, a blade Life Management System was developed in the form of a software tool for predicting the blade lives under typical operational transients (normal and also abnormal) and stationary periods, utilising results of previous thermomechanical finite element and fluid mechanics analyses. The EDF approach is tailored to steady state (base load) operation, as most of the gas turbines exploited by the EDF group are currently working in this mode.

1. Introduction

Gas turbines (GT) are the race horses of electrical power generation. As maintenance on such power generation systems is quite expensive (i.e. compared to running operation cost, mainly for fuel, and to initial investment; for example the cost of periodical critical parts maintenance and replacements is typically 2 times larger than the GT initial price), efficient use is extremely important; as well as availability, particular when GTs are used in peak loading. To obtain a reliable, cost–effective and efficient energy production with a low polluting level it is very important that the engine remains as long as possible in a good condition. Normally maintenance and overhaul intervals are prescribed by the gas turbine Original Equipment Manufacturers (OEM) based on the design know-how and on the feedback collated from users' experience. Sufficiently wide statistics to derive reliable predictions of component lives are normally available only to the manufacturers; on the opposite each individual user is generally unable to obtain sufficient statistics on a particular GT model, unless he has several similar machines in his fleet and several years of operation experience. Moreover in several plants gas turbines are operated in variable conditions, so that the scheduled time intervals originally suggested by the OEM do not result to be the best ones to minimise maintenance costs while optimising plant availability and safety.

Differently from steel components, methods to evaluate by direct means the damage state and the expected residual life of hot GT components, which are the most critical ones in terms of cost, non accessibility, and impact on the machine performance, are still far from fully developed and validated. However, some damage monitoring tools are currently available, during off load operations for major maintenance (overhaul), which, coupled to theoretical methods of damage modelling, have demonstrated to have promising capabilities of life prediction. The first theoretical tool for hot parts life prediction in GTs was a code produced by EPRI[1–3], able to combine turbine history with mechanical analysis algorithms and actual, measured engine parameters, to calculate the residual life of the components. With the support of such a system it was shown possible for a user to predict the consequences of the different types of turbine operation (start/stop, baseload, trip etc.). This concept was originally proven with General Electric Frame 7 and 6 gas turbines in EPRI developments in the last decade, leading to the development of the so called Life Management System (LMS) called REMLIF.

Following those early developments, the concept has been expanding worlwide in the last decade. In the frame of a cooperative EUREKA scheme, EDF (Electricitè de France) and CESI (an R&D organisation for the electricity industry in Italy) have been recently completing a four year collaboration, entitled Gas Turbine Life Prediction project (acronym TULIP). Initially the intention was to develop a life prediction methodology for the first stages of both rotating and static blades of large industrial gas turbines; however the focus (and the budget) was then concentrated on the rotating parts only, having the larger criticality for an efficient machine use. The basic work consisted of using several tools of analysis (i.e. blade life theories, material properties direct measurements of a number of parameters etc.) as an input to damage algorithms, and using operational and historical data to validate the algorithm predicted parameters. The methods developed in TULIP project, of general applicability to all GT models, have been developed with reference to the particular geometries, materials and service conditions of three gas turbines which the partners consider having the largest perspectives for their business strategy of services to gas turbines operators: namely the ABB 13E2 model was investigated in the French part of the project, and the Fiat TG50D5 (Westinghouse designation M701) and Nuovo Pignone MS9001E (GE designation PG917E) models in the Italian part. Blade materials are IN738 coated with SV20, U520 with ANDRY995, and GTD111EA with GT33+ respectively.

Advantages, merits and limitations of the several tools and methods utilised for GT life prediction by CESI and by EDF are described in this paper, as well as some examples of the findings on the prediction capabilities in comparison to some relevant cases of service experience in GT units.

2. Methodologies for damage analysis & life prediction

Different objectives were pursued by the two developers, as a result of the different needs/industrial use.

The intention of CESI was to develop a blade Life Management System (LMS) in the final form of a software tool (for a normal PC) for predicting the blade lives under typical operational transients and stationary periods. The traditional consideration of cyclic damage in the evaluation of the Equivalent Operating Hours is often still via a simple rule, e.g. assuming a cycle equal to 10 hrs of operation, clearly a very rough estimate; it was developed for all GTs, before the advent of the coatings, and is now applied identically to all coating systems. Coating families of different generations have quite different strength capabilities to resist cyclic damage: typically the distance between best and worst cases may be more than a decade in life, and this is therefore the wide margin of approximation in life prediction which a modern LMS has the objective and the possibility to strongly reduce. The CESI approach to LMS development utilised results of previous thermomechanical finite element and fluid mechanics analyses. Investigations were related to in-situ temperature measurement (by pyrometry), heat transfer from gas to blade and blade to cooling channels (by computational fluid dynamics), material properties (creep and thermo-mechanical fatigue tests), and coating behaviour (coating degradation under steady and cyclic conditions). The LMS is therefore suited for predicting damage development in any type of GT operation mode, from heavy duty to peak loading only.

On the other hand, in the EDF approach the priority was to address the damage developments under steady state (base load) operation, as most of the GT turbine exploited by the EDF group are currently working in this mode. Moreover for well designed machines the steady degradation of the coating life is the main parameter controlling maintenance. In this context as an alternative to aerothermal and structural FEM analysis, which would require massive OEM proprietary information to evaluate blade temperature profiles, EDF was focussing on temperature values from destructive metallurgical information: from these temperature values and having a model for degradation of coating with time, the remnant life time of the coating can be calculated. In practive, an "Inverse Problem Solution" technique is used to lifetime analysis allowing determination of the quantitative values of the model parameters.

A consistent use was made in both approaches of coating parameters as measured by a F-SECT system developed by CESI (Frequency Scanning Eddy Current Technique [4], as an input to the Inverse Problem Solution method for EDF, and as a validation means for the cyclic oxidation model in the LMS software of CESI. The full list of the several tools considered by the two project partners in

their development of a hot gas path components damage analysis system are summarised in the comparative scheme reported in Table 1.

Table 2. The ingredients utilised in the development of the life prediction methodologies by the two partners.

Tools	CESI	EDF
Pyrometry	used, for calibrations/corrections to the aerothermal analysis results	no
F-SECT	thickness d (mm), % β phase content in the coating, input to starting conditions for LMS life prediction	d (mm), % Al content in the coating, to estimate Teq. via life models
Inverse Problem Solution	no	in life models, to derive Teq
TMF damage	yes, strain ranges vs. cycles to failure curves, from TMF lab testing, LOP cycles	no
Creep damage	yes, FEM viscous	indirectly (from elastic thermal analysis and Teq)
Oxidation and coating degradation	yes, cyclic and stationary	isothermal
γ'	no	under evaluation
LMS software	user friendly, on PC	no
approach suited for GT operation:	cyclic operation and heavy duty	heavy duty
international frames of this research	TULIP	TULIP, and links to a NATO project
validations	substantial activity done, continuing	started

2.1 CESI approach

The Life Management System (LMS) developed at CESI is a PC software tool able to predict the gas turbine components lives under stationary and transient conditions. The LMS development work was consisting of a comprehensive list of investigations as follows.

a. Damaged components and damage mechanisms identification: based on service experience, the critical regions on components and the relevant damage modes (creep, fatigue, Thermo-Mechanical Fatigue (TMF), coating damaged features, role of hot corrosion, embrittlement etc.) were analysed in order to identify the correct approach in the development of a LMS; attention was also paid to the refurbishment cycles, repair and heat treatment features and coating details.

b. Computational fluid dynamics: geometrical parameters were taken for original component, including the inner cooling channels details, and the operating conditions were reviewed and collected, both normal stationary service and the most typical start up and shut down transients; these data were then processed by means of fluid dynamics codes.

c. Thermo-mechanical analyses: temperature data in the component from the aerothermal analyses were processed via a thermal-structural finite element (visco-elasto-plastic) code to provide patterns for temperature, stress and strain at the several locations in the component.

d. Materials relevant data gathering: in a few cases, sufficient material information can be found in literature (traditional alloys and simple physical and mechanical parameters, such as thermal conductivity, Young's modulus...); on the other hands materials resistance to high temperature damage mechanisms, particularly for coated elements, had to be determined by important testing activities: creep, TMF and cyclic oxidation mainly. In CESI laboratories several cyclic oxidation tests were performed at different temperatures (1 hour cycle); through metallography, quantitative image analysis and X-ray microanalysis, an analytical model was formulated, taking into account the aluminum depletion mechanisms active during operation and based on literature studies [5–9].

e. Damage models: this is the key element in the LMS development. The materials data had to be processed by suitable methods to provide the numerical coefficients (temperature, stress, strain and time dependent) in the damage growth rate models and end-life criteria, specific for the damage mechanisms and maintenance philosophy under consideration (e.g. end life defined as component failure, or maximum tolerated damage suitable to be repaired, ...). Namely three damage mechanisms were accounted for:

   TMF (coated material specimens were tested);
   creep (base material specimens);
   cyclic oxidation (coated material specimens).

   For TMF damage analysis, a TMF strain-life formula of EPRI in [2], taking into account strain R-ratio and hold time (HT) effects was used; for creep, a simple stress dependent and Arrhenius type stress – life curve was used; and

for cyclic oxidation, a complex model, based on a physical description of oxidation kinetics, elements (mainly Ni) diffusion (inwards and outwards), Alumina formation kinetics, and spalling kinetics during thermal cycles was used, following similar modeling in the literature [4–8]. Finally, the three ingredients of damage (TMF, creep and cyclic oxidation) were summed up via a normal Linear Damage Summation rule.

f. LMS software: the several damage models and end life criteria were implemented in a software tool, containing the input and output interfaces for a friendly use by the plant operator; it is pointed out that this software carries out a number of different damage evaluations, for a preselected grid of component conditions (new/refurbished) and operational scenarios (including transients), as provided by the user. In the LMS software some options exist to take advantage of directly measured (i.e. experimentally obtained) parameters; e.g the results from the aerothermal analysis can be tuned to the actual temperature values by pyrometry of from metallurgical studies.

g. Validation: the code and its prediction capability have to be verified against case histories, namely damage evidence after certain operational histories, for which the LMS tool is applied to derive comparative damage evaluations.

2.2 EDF approach

The EDF approach is focused on steady state (base load) operation, because most of the GT turbine exploited by the EDF group are currently working on this type of functioning. Moreover EDF considers that the coating life time is the main feature that controls the maintenance of the gas turbine for well a designed machine. This means that in a first step it is not needed to develope in this case a software tool taking into account all the mechanical aspects (creep, fatigue,…) of the damage to the superalloy. In this context as an alternative to aerothermal and structural FEM analysis, which would require special know-know and knowledge of constructor design information to calculate by theoretical models the temperature profile in the blades, EDF was focussing on a tool to evaluate the temperature values which have been seen by the blade using metallurgical information coming from non-destructive evaluation. From such temperature and having a model for degradation of coating with time, the remnant life time of the coating can be calculated.

The inverse problem solution technique has been used to lifetime analysis and monitoring of overlay coatings in stationary gas turbines for electric power generation, because it allows an easily feasible determination of the quantitative values of the degradation model parameters [10–12]. The basic idea of the inverse technique is to use easily obtainable experimental data like the measured Al or/and β or γ’ phase concentration profiles after a defined experimental time t_e as input values for the model parameters estimation. All other parameters needed

for the modelling like effective diffusion coefficients are then determined by the inverse problem technique and used for the life time calculation.

Then the characteristics of the degradation state of a coating on site are determined by a non-destructive method like Frequency Scanning Eddy Current, as an input to the residual lifetime prediction. In previous works it has been shown that Eddy Current is a suitable method for the non-destructive measurement of the degradation state of MCrAlY coatings [13, 14]. The approach by the Inverse Problem Solution technique is not only able to analyse and predict the lifetime of a coating, but furthermore, having understood the degradation mechanisms of a coating, it is able to deduce the operating temperature from a given oxidation and degradation state of a service exposed turbine blade. There is a close relationship between blade temperature and the conditions of the overlay coating on the blade. With the determined values of coating thickness and degradation state measured at different positions along the turbine blade, a residual lifetime mapping can be performed monitoring the performance potential of the blade for the next operating period. Alternatively, a temperature distribution mapping can be determined allowing the power plant operator to obtain more precise information about the temperatures in the engine.

All in all, the aim is to provide a new tool which is utility-oriented because this tool does not need any design proprietary information nor destructive examination of real components for lifetime analysis as well as for degradation state evaluation. This tool will result in a long term innovation in electric power generation with an impact on plant reliability and costs savings, safety, performance and more efficient use of primary resources.

3. Achieved results

Validation activities are ongoing by the authors (incidentally: with good results) and will not be covered here in detail, as the discussion of case histories of GT blade damage analysed by the life prediction tools here described would need a dedicated presentation, beyond the scope of this paper. It is appropriate to show at least some views of the types of results which are obtained.

In figure 1 the actual evidence of damage is shown for a TG50D5 blade, after 8,800 firing hours and 450 operational cycles (about half being trips from load; similar types of graphs can be obtained also for the other two mechanisms, creep and TMF, and are not shown here). This case is related to an abnormal operating period, with a lot of component scrapping due to heavy damage of the coating, its complete failure and hot corrosion damage of the base alloy at the leading edge and on the pressure side. This happened at the beginning of the plant history, trying to reach the nominal efficiency levels (the LMS code was not yet prepared

at that time). By destructive metallographic examinations the coating was found absent in two regions outlined in Fig. 1. Based on the measurements of the γ' particle size in the hottest regions of the blade an overtemperature of about 50°C was estimated. In Fig. 2 the predicted levels of oxidation damage are reported.

The LMS code provided the component life was exceeded in terms of both cyclic oxidation and TMF damages, even if in different regions. The comparison between Figs. 1 and 2 is a good view of the agreement between real and calculated damaged regions in the hottest zones of the component airfoil (pressure side) and at the leading edge.

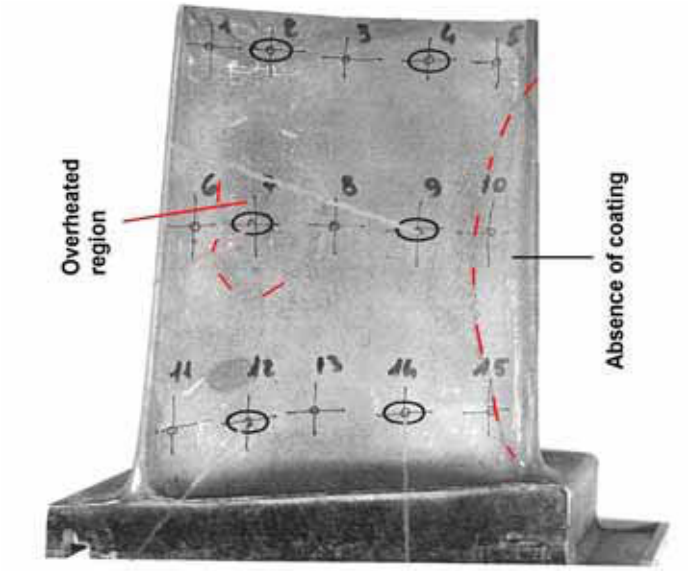

Figure 1. Observed damage findings for the TG50D5 blade (modeled in Figure 2).

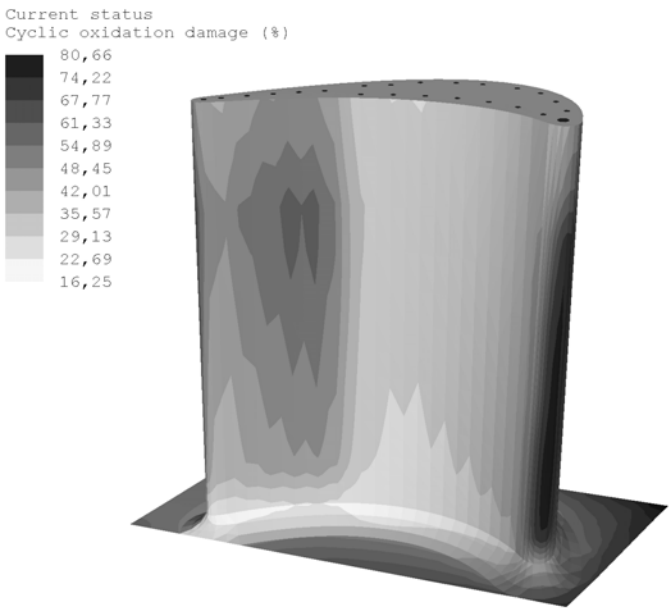

Figure 2. Distribution of cyclic oxidation damage levels as predicted by the LMS developed for the TG50D5 blade.

More in general according to the CESI experience with the developed TULIP software applied in several cases of TG50D5 damage findings, the following scenario was consistently observed (and confirmed by LMS predictions) for the first row blades:

- creep damage is a minor element in the damage budget;
- TMF damage is often significant, but it reaches important levels only at blade root positions, not along blade edges;
- oxidation damage in the coating (with combined β phase depletion) is the main life limiting factor on the blade foils.

Currently the LMS developed at CESI is still in the validation phase, i.e. it is intended than a number of details are checked and progressively optimised from the feedback of application to service exposed GT components. Nevertheless, from the comparative analyses of predicted and actual damage amounts so far obtained, the prediction capability seems quite significant already at this stage. It has to be mentioned that creep and cyclic oxidation damage models are reasonably well established; on the other hand, the larger uncertainties are within the TMF damage prediction part, as the TMF strength model presently utilised was determined from a limited source of TMF data, from tests carried out in a previous CESI programme. As in these experiments no account was made for investigating HT nor R-ratio effects, the coefficients for such terms in the TMF strength model were not available for our alloy U520 and had to be taken identical to those reported in the TMF model of EPRI in ref. [2], for another Ni-base alloy. Predicted results were non-conservative in our TMF analyses, by a constant factor in life (predicted damage being 50% when fatigue macrocracking was observed, i.e. not a large discrepancy); in any case an experimental programme devoted to define the HT- and strain ratio-dependence of the TMF damage equation for the alloy here considered, U520, is intended to remove this marginal lack of knowledge.

Figure 3 presents the comparison between destructive measurements using Frequency Scanning Eddy Current Technique and destructive measurements using scanning electron microscopy made on 13E2 coating. One can see the very good correlation, meaning that the non destructive measurements could be used as an input for the inverse model to identify the medium temperature observed by the blade at this localization.

Concerning the modeling of the composition evolution of the coating, Fig. 4 presents the correlation between calculated Al profile and real destructive measurements: a good correlation is observed. That means that knowing the temperature and time one is able to calculate the thickness evolution of the coating. In the near future we would like to make the reversed calculation: knowing the thickness (measured by Non Destructive Eddy Current Techniques,

see above) and time (operation at base load of the gas turbine) the temperature is estimated.

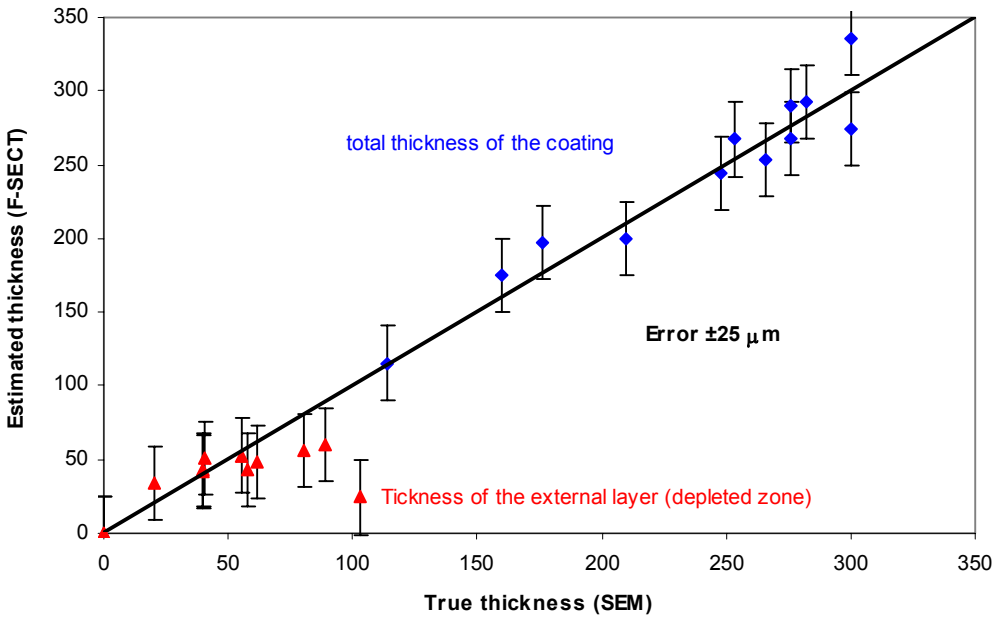

Figure 3. Comparison between non-destructive and destructive measurement.

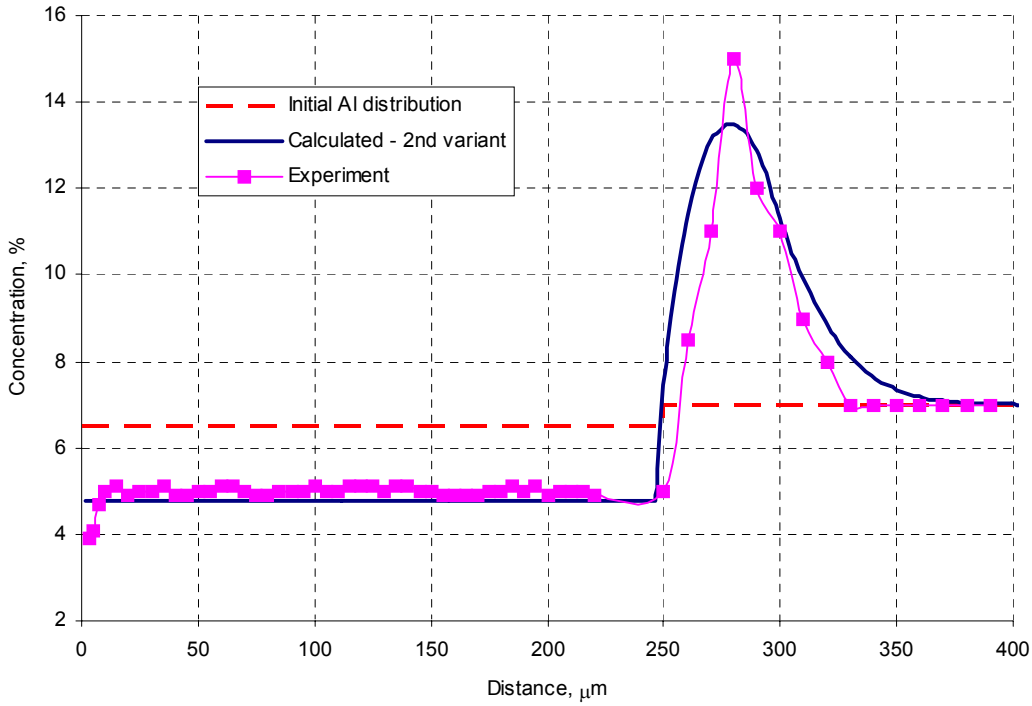

Figure 4. Measured and calculated Al concentration profile across the coating (SV20) and base alloy (IN738) after 1970 h at 950 °C.

4. Needs and perspectives

The method of life prediction accounting for damage contributions due to transients allows analyses of blade durations under several operation scenarios, from steady state to daily cycling. So far, full development of the LMS was achieved only for the blades of the relatively old model TG50D5 (U520 coated with AMDRY995; metal temperature 800°C).

A modest effect of cyclic oxidation damage is generally found in these machines, which might be explained by the modest coating properties at high temperature: the coating is aged and degraded by steady oxidation during isothermal operation, and cyclic oxidation in transients is less important. And in cases when consistent damage from cycling is found to occur, this is due to TMF, not to cyclic oxidation. It is believed that with better materials and coating systems, e.g. GTD111 with GT33+, having superior resistance to isothermal oxidation, the damaging effects of transients on cyclic oxidation and oxide spalling are more important, therefore this is the area where an accurate model for cyclic oxidation in the LMS becomes essential. This is the area where current study at CESI is moving in.

It is becoming progressively clear that pyrometers will not become applied as normal ancillary tools included in all GTs, clearly for cost penalties due to casing modifications, pyrometry cost per sè, and also the complications of additional data acquisition / monitoring needs in the machine control system. It is believed that pyrometry is at least important in the initial validation phase of a LMS on a machine (aerothermal FEM results have to be checked against real data). However, increasingly accurate models of coating oxidation analysis, via Inverse Problem Solution techniques as used by EDF in this study, are providing an alternative means to evaluate the temperature.

A more systematic integration of FSECT data in the life prediction activities, i.e. essentially the possibility to have actual measurements at inspection intervals of the residual coating resistance to oxidation (amount of beta phase, as % of original coating volume or as an equivalent thickness of the coating), is judged beneficial to pinpoint the theoretical predictions over actual data. Not simply as a validation scope, but allowing a new approach in the GT life prediction: from damage evolution predicted from beginning “0” to current “i” state, to damage evolution from i-1 to i, i.e. incrementally and linked to initially measured data.

Damage evolution models as soon as they will become confidently ready for blade parts coated with TBC will need to be implemented in the life prediction methods for the new GT models making use of such materials. Here in addition to the intrinsic difficulty of modelling the complex damage phenomena occurring in a TBC coated material, the additional complications of several TBC systems

(materials and processes, bonding layers and bulk materials), in new blades and in re-processed blades, greatly increase the complexity however.

In all cases it appears that in addition to materials characteristics usually available from several sources of information, such as physical properties and thermal properties, other materials data (creep, TMF and oxidation resistance) are needed which are not easily available in literature and in data banks. In recent years such characteristics are increasingly regarded as confidential know how in a competitive market of GT services to utilities, so these data are no more reported in scientific papers available in the open literature. Materials variability and test method uncertainties may also be relevant, and might need to be accounted by statistical re-formulations of the life prediction methods here described.

5. Conclusions

The results obtained by CESI and EDF via a cooperation in an EUREKA scheme in the field of hot gas path components life predictions, for relevant GT models used in their fleets, have been presented, showing the advantages and the potential of the approach.

Currently the partners are considering extentions to other components (namely the static vanes), and to other GT models, including components where ceramic coatings are used, this requiring the largest step forward in the basic modelling research.

References

1. H.L. Bernstein. “Life Management System for General Electric Frame 7E Gas Turbine”. Proc. of an Int. Conf. on Life Assessment and Repair Technology for Combustion Turbine Hot Section Components, ASM, EPRI GS-7031, 17–19 April 1990, Phenix USA. Pp. 111–118.

2. H.L. Berstein, T.S. Grant, R.C. McClung & J.A. Allen. “Prediction of Thermal-Mechanical Fatigue Life for Gas Turbine Blades in Electric Power Generation”. ASTM STP 1186, H. Sehitlogu, Ed., Philadelphia, 1993. Pp. 212–238.

3. R. Viswanathan, J. Scheibel & D.W. Gandy. “Life Management System for Combustion Turbine Buckets and Nozzles”. Int. Conf. Life Assessment of Gas Turbine Hot Section Components, Edinburgh, The Institute of Materials, London, October 1999.

4. G. Antonelli, Ruzzier & F. Necci. 1997. “Thickness Measurement of MCrAlY High-Temperature Coatings by Frequency Eddy Current Technique”. ASME Paper No. 97-GT-1.

5. K.S. Chan, N.S. Cheruvu & G.R. Leverant. “Coating Life Prediction for Combustion Turbine Blades”. In International Gas Turbine & Aeroengine Congress & Exibition, Stockholm, 2–5 June 1998, paper 98-GT-478, Transaction of the ASME, Vol. 121, 1999. Pp. 484–488.

6. K.S. Chan, N.S. Cheruvou & G.R. Leverant. “Coating Life Prediction Under Cyclic Oxidation Conditions”. J. of Eng. for Gas Turb. and Power, Vol. 120, 1998, pp. 609–614.

7. K.S. Chan, N.S. Cheruvou & G.R. Leverant. “Coating Life Prediction for Combustion Turbine Blades”. J. of Eng. for Gas Turb. and Power, Vol. 121, 1999, pp. 484–488.

8. D.J. Chellman & A.J. Ardell. “The Coarsening of γ’ Precipitates at Large Volume Fractions”. Acta Met., Vol. 22, 1974, pp. 577–588.

9. J.A. Nesbitt. “Predicting Minimum Aliminum Concentration for Protective Scale Formation on Ni-base Alloys”. J. of Electrochemical Society, Vol. 136, 1989, pp. 1518–1527.

10. Mesures effectuées sur des ailettes de turbine à gaz de combustion (TAC GT13E2 d’Azito) par tomographie à rayons X et par méthodes optiques et impacts sur le programme de travail du projet. Frank Meissonnier, 15/03/2002, CR-AMA-02.072 (classified).

11. V. Kolarik, P.G. Keukovsky & A.I. Rybnikov. Life time modelling for McrAlY coatings for industrial gas turbine blades, SfP – Coating life time. 7th Six-Monthly Progress Report, N° SfP-972631, 14.05.2002 (classified).

12. Etude du vieillissement de revetements pour aubes de turbines à gaz, Laurent Gourgeon, Stage de Mars à Aout 2002, DESS Corrosion Dégradation et Protection des Matériaux (classified).

13. L. Lelait. Life time modelling of AZITO coating, EIFER Report N° HK-42/02/013, 10 Jan. 2003.

14. L. Lelait. Gas turbine blade coating assessment at the Azito Power Plant by Frequency Scanning Eddy Current Technique, EIFER Rep. N° HK-42/02/013, 10 Dec. 2002.

The degradation mechanisms of combustion turbine vanes and blades made from nickel base alloy after approx. 120 000 h of service

Bernasovský P.[1], Brziak P.[1], Domankova M.T.[2] & Zifcak P.[1]
[1] Welding Research Institute, Bratislava, SLOVAKIA
[2] Slovak University of Technology,
Faculty of Materials Science and Technology
Trnava, SLOVAKIA

Abstract

The mechanical properties and microstructural analysis up to TEM microscopy are performed in order to evaluate the possibility for further service of selected vanes and blades removed from a 6 MW combustion turbine after about 120 000 h of service. The blades and vanes are made of the creep resistant alloy EI893 (67Ni16Cr9W4Mo). Secondary particle coarsening was the main degradation mechanism observed in the investigated specimens. The mechanical properties varied on lower threshold prescribed for virgin materials.

1. Introduction

The blades and vanes of the first and second rotor stage and the first stator stage of 6 MW gas turbines type GT 750-6 of (formerly) Czechoslovak provenience are made of Russian hardenable nickel alloy designated as EI 893. The chemical composition of EI 893 alloy is given in Table 1.

Table 1. Chemical composition of EI 893 alloy (weight %).

C	Al	Si	Ti	Cr	Mn	Fe	Ni	Mo	W
0,074	1,3	0,22	1,46	15,8	0,03	0,27	67,5	4,2	9,02

After the specified heat treatment (950°C/1.5 h + 1160°C/2 h + 1000°C/4 h + 900°C/8 h + 840°C/15 h) the microstructure of EI 893 alloy is formed of polyhedral grains with non-uniformly distributed $Ni_3(Al,Ti)$ phase (also called as gamma prime - γ′) and $M_{23}C_6$ carbides, which are distributed mainly on the grain boundaries. The high strength of EI 893 alloy is mainly due to hardening by γ′. Two types of γ′ can be distinguished in matrix: coarse butterfly-like γ′ introduced during solution heat treatment; and fine spheroid γ′ introduced in between coarse γ′ during ageing. The minimum specified mechanical properties of the EI 893 alloy are given in Table 2.

Table 2. The minimal tensile properties of EI 893 alloy after prescribed heat treatment together with measured tensile properties of as serviced blades and vanes (those results not matching minimal values are highlighted).

Note		**Spec. iden.**	**Spec. loc.**	**Temp. [°C]**	**$R_{p0,2}$ [MPa]**	**R_m [MPa]**	**A_5 [%]**	**Z [%]**
EI 893 after heat treatmet		-	-	20°C	min. 490	min. 833	min. 20	min. 25
		-	-	750°C		min. 637		
EI 893 after app. 120 000 service	1st stage vane	1S3B	Bottom	20	605	1086	**18,3**	**24,8**
		1S2C	Top	20	541	1008	**17,0**	27,8
		1S2B	Bottom	500	460	852	29,3	33,3
		1S2D	Top	500	453	838	28,7	30,6
		1S2A	Bottom	750	404	**593**	38,9	49,3
		1S3A	Root	750	472	**624**	25,2	30,6
	1st stage blade	1R9	-	20	736	1195	28,3	30,6
		1R8	-	20	640	1160	27,3	33,3
		1R7	-	500	676	1026	29,0	30,6
		1R6	-	500	661	1015	29,3	30,6
		1R5	-	750	537	650	27,6	34,3
		1R4	-	750	505	664	21,7	30,8
	2nd stage blade	2R9	-	20	725	1132	31,0	36,0
		2R8	-	20	615	1036	-	-
		2R7	-	500	580	884	36,0	36,0
		2R6	-	500	559	867	37,0	36,0
		2R5	-	750	493	**611**	20,4	30,6

Loading of blades is dynamic, by flow of combustion products and in case of rotor blades also by axial load induced by centrifugal force. The working temperature of the first rotor and stator stage is around 730°C, whereas at the second stage it is around 715°C. The main degradation mechanism of blades and vanes is simultaneous coarsening of γ´ phase and $M_{23}C_6$ carbides controlled by the time and service temperature leading to plasticity drop and an increased risk of brittle fracture initiation or formation of creep cracks. The accepted safe time of blade service is around 50 000 h. Then the blades and vanes must be heat treated (regenerated) to restore the mechanical properties because of the probability of breakdown at service of the non-treated blades servicing for over 100 000 h would be up to 40%. The presented contribution deals with the study of 120 000 h service on the structural and mechanical properties of stator and rotor blades of the first stage and the rotor blades of second stage that were not heat treated and should thus be at the limit of their service life.

2. Experimental

The mechanical properties of blades were analyzed by the following tests:

- creep tests at 750°C and 250, 230 and 210 MPa,
- tensile tests at temperatures of 20, 500 and 750°C,
- CVN tests at temperatures of -20, 20, 100 and 400°C.
- hardness measurement by Vickers at the load of 98.1 N (HV10) on metallographical cross sections in the blade foot and top. On each blade, 7 indents were made gradually from the leading edge, see Fig. 1ab.

The way of sampling is shown in Fig.1ab. Only one test piece could be machined from the 1st and 2nd stage blades, position of which is shown in Fig. 1a, designation 1R for 1st stage blade and 2R for 2nd stage blade.

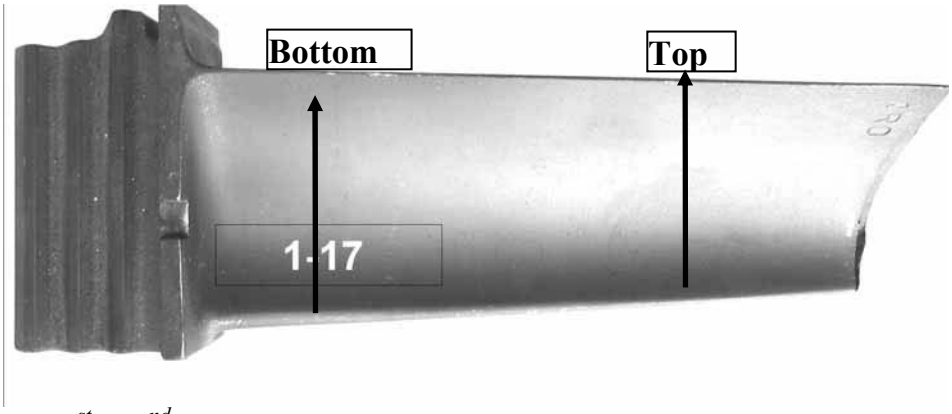

Figure 1a. 1st + 2nd stage blade. The principal location of specimens for mechanical tests (1–17), hardness measurements + microstructure analysis (black arrows).

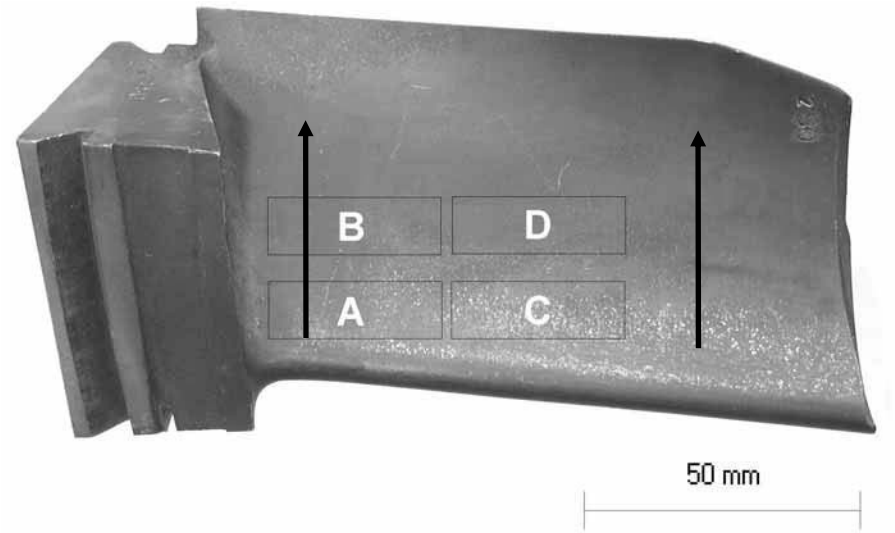

Figure 1b. 1st stage vane. The location of specimens for mechanical tests (A, B, C, D) hardness measurements + microstructure analysis (black arrows).

From the 1st stage vane, 4 pieces were machined from one blade, designated as 1S + serial No. of the blade + piece location (A, B – blade bottom; C, D – blade top), see Fig.1b.

The samples for microstructural analyses performed by light microscopy were ground, mechanically polished and electrolytically etched in 20% HCl. On each blade microstructure in the foot and on the top was documented. For TEM microscopy metallographical cross sections were used, from which carbon replicas were taken and observed by use of JEOL 200CX microscope.

3. Results and discussion

3.1 Tensile tests

The results of tensile tests are given in Table 2 together with minimum specified values for 20˚C and 750˚C. The EI 893 alloy preserved its mechanical properties also at elevated temperatures. In 1S blades the elongation and reduction of area values at 20˚C and ultimate tensile strength at 750˚C were below the admissible level set for the safe service. From comparison of results from tensile tests of 1S blade performed in the foot and on the top of blade certain difference was observed. The values of tensile strength and yield point in the foot zone are higher whereas the ductility and reduction in area are in turn lower. The 1S vanes are thermally most loaded with the upper limit of service temperature of 730˚C. In the vane blade ageing of alloy was observed, in the vane foot (with lower temperature) on the contrary an additional hardening of alloy was observed.

The 1R vanes meet the requirement of minimum strength properties in all cases. However, the minimum yield point is much higher, which may be connected with the additional hardening of the vane in certain zones of vanes. A significant drop in toughness was observed in 2R4 sample and lower Rm value at 750˚C in 2R5 sample. Significant degradation of properties in material of these vanes occurred, mainly the low values of ductility increase the risk of initiation of fatigue or brittle fracture.

3.2 Impact tests

The impact bend test at different temperatures was aimed at study of KCU3 impact toughness in vane material EI 893. The impact toughness is not guaranteed in this type of vane and in comparison to tensile tests it has less testimonial power regarding the state of material and degree of its degradation. In spite of that it may depict the state in vane material embrittlement, to eventually assess the risk of damage at the start-ups and shutdowns. Table 3 shows the results.

Table 3. The minimal accepted Charpy U notch impact energy of EI 893 alloy together with measured values of as serviced blades and vanes.

Note		Spec. iden.	Spec. loc.	Temp. [°C]	KCU3 [J.cm^{-2}]	min.– KCU 2 [J.cm^{-2}]
EI 893 after app. 120 000 service	1st stage vane	1S4A	Bottom	-20	39	32
		1S4C	Top	-20	43	
		1S4B	Bottom	20	45	
		1S4D	Top	20	46	
		1S5A	Bottom	100	58	
		1S5C	Top	100	63	
		1S5B	Bottom	400	78	
		1S5D	Top	400	79	
	1st stage blade	1R10	-	-20	38	
		1R17	-	-20	38	
		1R12	-	20	41	
		1R13	-	20	43	
		1R14	-	100	45	
		1R15	-	100	46	
		1R16	-	400	61	
		1R11	-	400	63	
	2nd stage blade	2R10	-	-20	66	
		2R11	-	-20	68	
		2R12	-	20	60	
		2R13	-	20	59	
		2R14	-	100	71	
		2R15	-	100	64	
		2R16	-	400	98	
		2R17	-	400	98	

The results proved that the notch toughness values at ambient temperature are relatively low, but still higher that the minimum specified values. From the results it can be concluded that the increased risk of fracture formation is at the shutdowns and/or temperatures lower than 400˚C. These results are considered appropriate from the viewpoint of impact toughness.

3.3 Hardness measurements

The results of HV 10 hardness measurements of 1S, 1R, 2R specimens are given in Table 4. In zonal dependence across the blade from leading edge to tapered end of vane/blade we measured increasing hardness with reducing cross section of the vane. Different hardness values are the result of thermal gradients in the

vane/blade, what was expected. The measured values (correspond to attained strength values) were considered as acceptable.

Table 4. The minimal accepted hardness HV10 of EI 893 together with measured values of as serviced blades and vanes.

Note	Spec. iden.	Spec. loc.	Hardness HV 10	
			Measured values 1–7	Average
1st stage vane	1S3	Bottom	254, 264, 253, 276, 285, 268, 272	267.5
		Top	287, 272, 281, 274, 284, 289, 294	283
1st stage blade	1R6	Bottom	342, 339, 339, 333, 327, 333, 333	335.2
		Top	312, 314, 312, 314, 319, 317, 325	316.1
2nd stage blade	2R2	Bottom	292, 292, 283, 302, 302, 306, 309	298
		Top	292, 314, 309, 299, 304, 327, 327	310.3

3.4 Creep tests

Table 5 shows the results of creep tests of specimens 1S, 1R and 2R. In order to allow comparison of creep tests with the specified values, it was necessary to extrapolate these values towards lower stresses and longer times. We selected for creep the widely used linear extrapolation in σ_{TPt} – log t coordinates. For better comparison, Table 5 shows theoretical time to rupture expressed from the equation of extrapolated values, according to widely accepted values for EI 893.

Table 5. The results of creep tests of as serviced blades and vanes together with widely accepted values for EI 893 (results not matching minimal values are highlighted).

Note	Spec. iden.	Temp. [°C]	[MPa]	Time to rupture [h]	Extrapolated time to rupture [h]
1st stage vane	1S1A bottom	750	250	1012	543
	1S1B bottom	750	230	1280	1115
	1S1C top	750	210	6100	4019
1st stage blade	1R1	750	250	1060	543
	1R2	750	230	**913**	1115
	1R3	750	210	**1842**	2288
2nd stage blade	2R1	750	250	1114	543
	2R2	750	230	1292	1115
	2R3	750	210	2532	2288
	EI 893 values	750	170	10 000	
		750	120	50 000	
		750	105	100 000	
		750	100	120 000	

When considering that the times at which specimen fracture occurs are just informative, we may suppose that the results of creep tests of specimens 1S and 2R met the EI 893 conditions. Creep tests of specimens 1R did not meet the calculated requirements.

The creep tests suggest a great scatter of creep values between the individual vanes and blades, as was also proved at assessment of tensile tests. Thus the scatter in values is very important for us from the viewpoint of correct evaluation of the measure of safety. The creep properties of 1S and 2R vanes was evaluated as acceptable even after about 120 000 h of service.

3.5 Microstructural analysis

The microstructural analysis was aimed at evaluation of structure and composition after long-time service of 1S, 1R, 2R materials.

Microstructure at 200 times magnification by means of light microscopy is shown in Fig. 2ab – 1S vanes, Fig. 2cd – 1R blades; and Fig. 2ef – 2R blades. The structure of both vanes and blades is characterized by a high degree of intergranular and transgranular precipitation of coarsened particles of γ´ and carbides. This precipitation is less pronounced in 1S vanes compared to 1R and 2R blades.

The grain size varies within 60 to 75 μm in all measured specimens. However, significant heterogeneity of grain size was observed.

Microstructure observed by TEM is shown in Fig. 3ab – 1S vanes, Fig. 3cd – 1R blades; and Fig. 3ef – 2R blades. In all specimens, the particles with different morphology can be observed. The coarse $M_{23}C_6$ particles were observed on the grain boundaries and also in the matrix of all specimens. Several particles of $M_{23}C_6$ carbides attained the size around. 2μm. In the grain boundary vicinity of 1R specimens, needle-like particles were observed, precipitated in the colonies with a characteristic shape, see Fig. 3d. According to the shape and rich chromium content, the needle-like particles would be brittle σ phase. Due to its shape, it was difficult to extract the γ´ coarse particles to carbon replicas, these were observed only on specimen 1S. The same precipitation of coarse precipitates over the grain boundary and inside the grains was observed in all specimens investigated. The virgin EI893 material was not available; anyway the coarsening of secondary particles has been reported as main degradation mechanism during service of nickel base alloys [1]. Since other degradation mechanisms (corrosion, creep, fatigue) have not been observed in specimens investigated, the lowered ductility of specimens 1S (and R2 to some extent) can be attributed to overall coarsening of secondary particles.

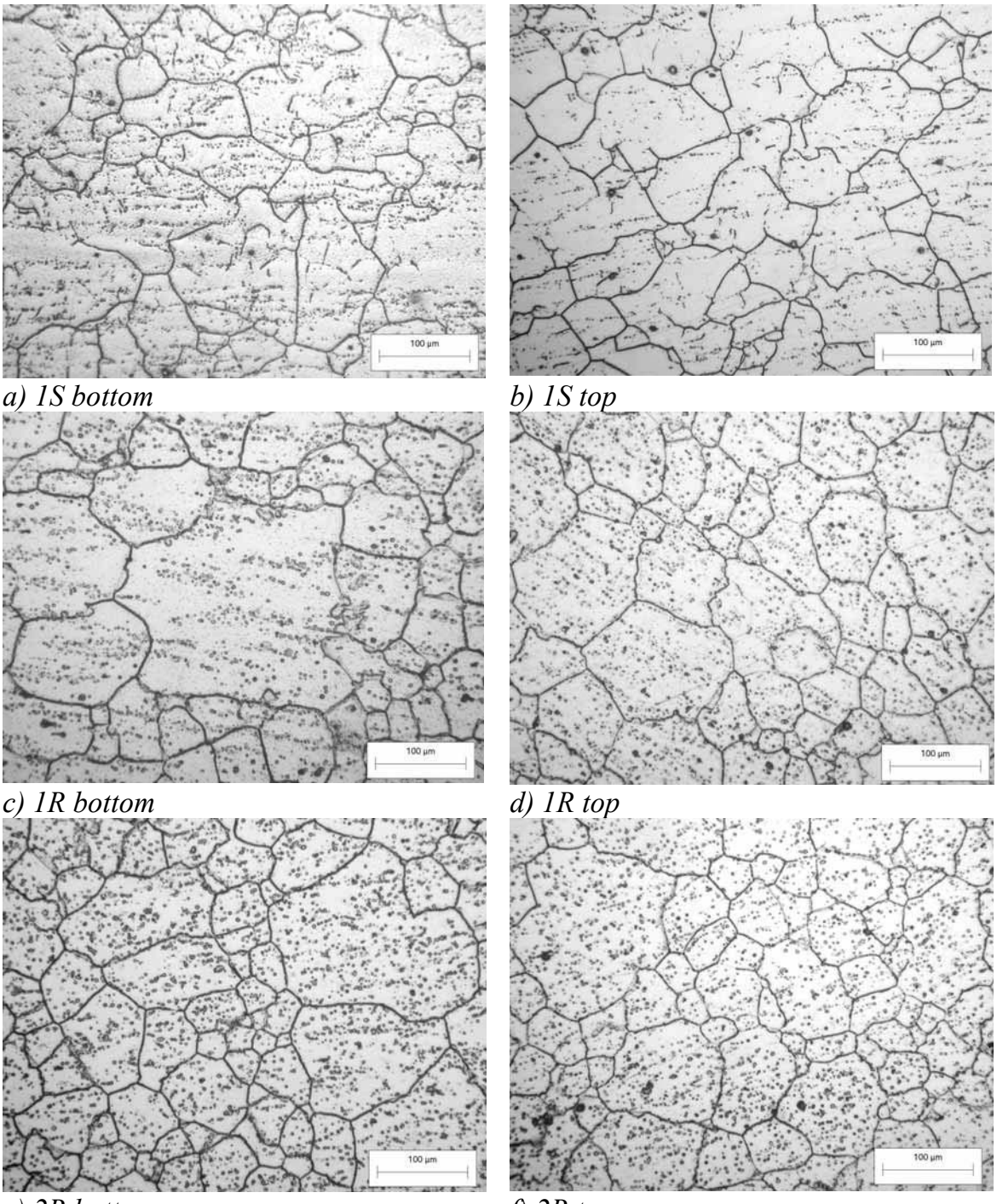

a) 1S bottom *b) 1S top*

c) 1R bottom *d) 1R top*

e) 2R bottom *f) 2R top*

Figure 2. The microstructure of specimens 1S, 1R and 2R. EI893 after service of about 120 000 h, light microscopy.

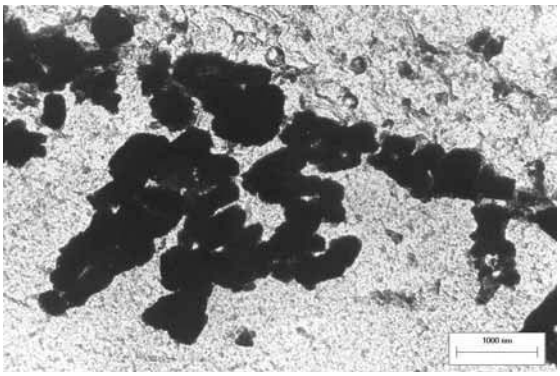

a) 1S bottom, grain boundary, $M_{23}C_6$ + M_6C carbides.

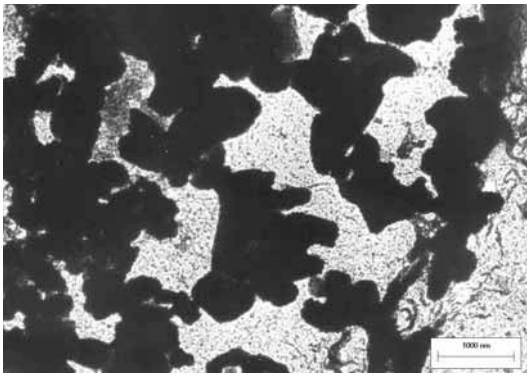

b) 1S top, matrix, γ´.

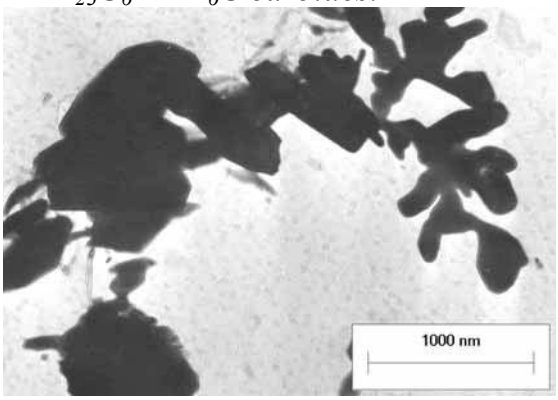

c) 1R bottom, grain boundary, $M_{23}C_6$ + M_6C carbides.

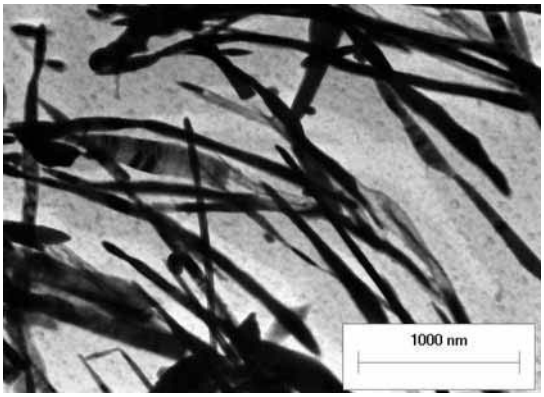

d) 1R top, matrix, $M_{23}C_6$ carbides+ σ phase.

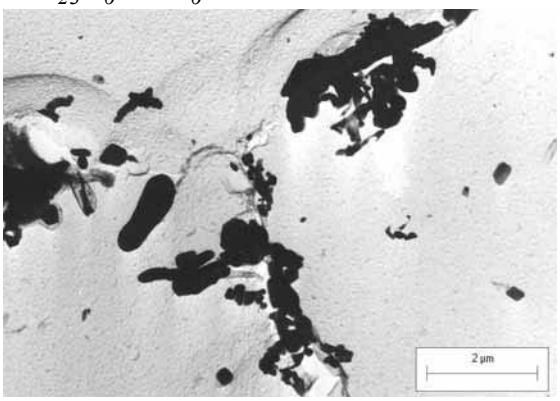

e) 2R bottom, grain boundary, $M_{23}C_6$ + M_6C carbides.

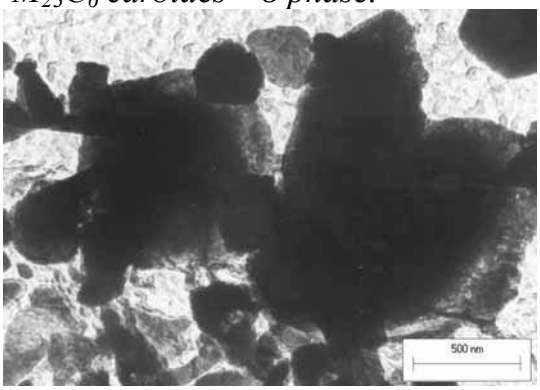

f) 2R top, $M_{23}C_6$ carbides.

Figure 3. The example of microstructure observed in specimens 1S, 1R and 2R. EI893 after service of about 120 000 h, TEM.

4. Conclusions

Based on mechanical tests and microstructural analyses the following can be stated:

1. Strength properties after long-term service for 120 000 h are acceptable for 1S vanes and 1R + 2R blades.
2. The impact bend tests have shown certain degradation of impact toughness in 1S vanes and 1R and 2R blades. The toughness values are considered as favorable for the next service period.
3. The measured hardness values correspond to measured strength values.
4. The creep tests of 2R blades and 1S vanes were assessed as acceptable. In case of 1R blades, degradation of creep properties, perhaps due to σ phase was observed.

It may be finally concluded that in spite of certain degradation of mechanical properties (strength and toughness of same samples), the measured creep properties of the 1S and 2R specimens were above supposed values and only the creep properties of the 1R specimen were slightly lower than supposed.

However it must be stressed that the supposed values of creep properties were just theoretical and were calculated for a new alloy. Based upon the actually measured values the 1S vanes were recommended to use in service for another 20 000 h. The 1R and 2R blades we recommend to use in service for another 10 000 h.

Literature

[1] Viswanathan, R. Damage Mechanisms and Life assessment of High Temperature Components, ASM International, Metals Park, Ohio 44073.

Negative creep in nickel base superalloys

Kristian V. Dahl, TU Denmark, Lyngby
John Hald, Elsam/Energy E2/TU Denmark, Lyngby

Abstract

Negative creep describes the time dependent contraction of a material as opposed to the elongation seen for a material experiencing normal creep behavior. Negative creep occurs because of solid state transformations that results in lattice contractions.

For most applications negative creep will have no practical implications but under certain conditions it may become critical. For bolts and fasteners, which are highly constrained during service, negative creep may lead to dramatically increased stresses and eventually to failure.

The article was inspired by a recent failure of Nimonic 80A bolts in German gas turbines. As a result of this failure similar bolts from Danish gas turbines of the same type were investigated and it was found that the bolts had experienced negative creep during service.

1. Introduction

At elevated temperatures metallic materials may undergo solid-state reactions as a result of microstructural instability. These reactions are frequently accompanied by density changes, e.g. precipitation from solid-state can promote an expansion or contraction in alloys. In some cases, length changes may be observed at zero applied stress or an alloy may exhibit a contraction in spite of an applied tensile stress. The term “negative creep” is used to describe a time-dependent contraction of a material rather than the extension normally seen during creep tests.

If a microstructural transformation occurs during a creep test then the observed creep curve will be a sum of two contributions, one from normal creep and one from length changes due to the transformation. Figure 1 shows a series of schematic diagrams of different material behaviour during creep tests and stress relaxation tests for a material that contracts during the testing because of a microstructural transformation.

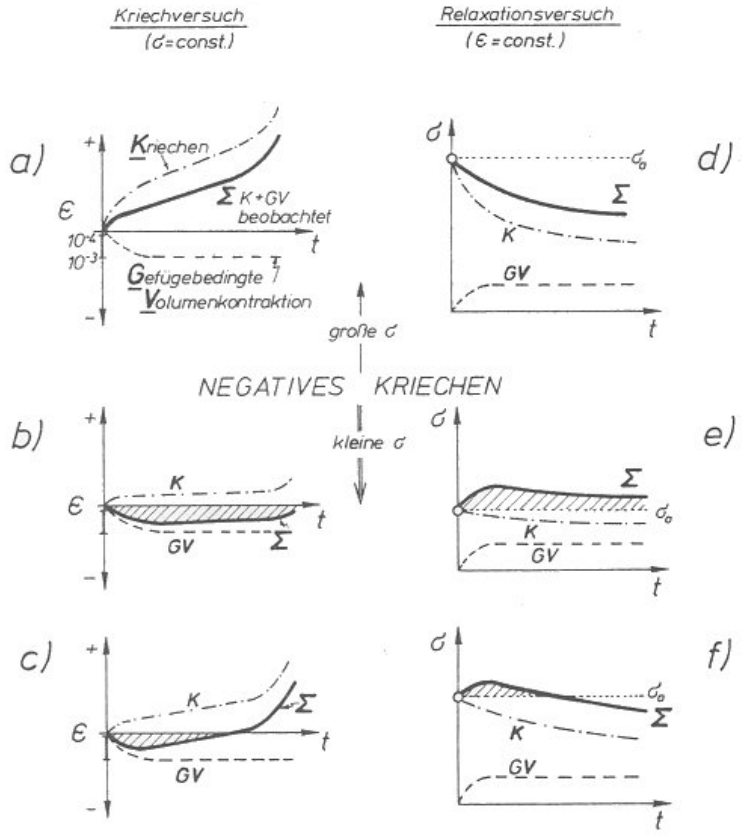

Figure 1. Schematic drawings of negative creep behaviour (hatched areas). Normal creep behaviour (K) and volume contraction due to a solid-state transformation (GV) for normal creep tests (a to c) and for stress relaxation tests (d to f). [1]

At high stresses normal creep behaviour (K) will dominate and the contribution from the microstructural transformation (GV) will be concealed within the sum curve (∑) (pictures a) and d) in Figure 1). At low stresses the contribution from the microstructural transformation may dominate and negative creep behaviour may be observed (pictures b) and e) in Figure 1). During creep tests a solid-state transformation may result in sample contraction in spite of the applied tensile stress and during stress relaxation tests there will be an increase in stresses in order to maintain the imposed constant strain. Pictures c) and d) in Figure 1 show a mixed behaviour, where negative creep is observed after short times, while normal creep behaviour dominates after long times.

A quantitative treatment of the negative creep phenomenon is complicated because of the interaction between the two opposing processes. The plastic strain may accelerate the progress of the solid state reaction, while the resistance to plastic flow is dependent on the structural changes produced by the metallurgical reaction. [1]

For most applications the density changes introduced by a microstructural transformation will have no practical implications but under certain conditions it may become critical. For bolts and fasteners a situation close to that of the constant strain stress-relaxation tests can arise during service.

Negative creep can occur in many different alloys. The first observations of negative creep were done by Fountain and Korchinsky [2] in 1959 during their work on iron-molybdenum and iron-tungsten alloys. In later work negative creep behaviour has been found for several different Ni-based superalloys and can be connected with solid state transformations such as the precipitation of carbides or order-disorder transformations. For superalloys that often contain numerous different alloying elements, long time exposure at elevated temperatures results in microstructural evolution and it has in fact been found that negative creep behaviour is more the rule than the exception. Kloos, Granacher and Bartsch found negative creep behaviour for the alloys IN713C, IN738LC and IN939 [3] (see Figure 2), and similar behaviour was found for Waspaloy [1]. The most comprehensive investigations on negative creep have been done for the alloy Nimonic 80A [4, 5, 6, 7, 8, 9], where lattice contraction occurs due to an ordering transformation.

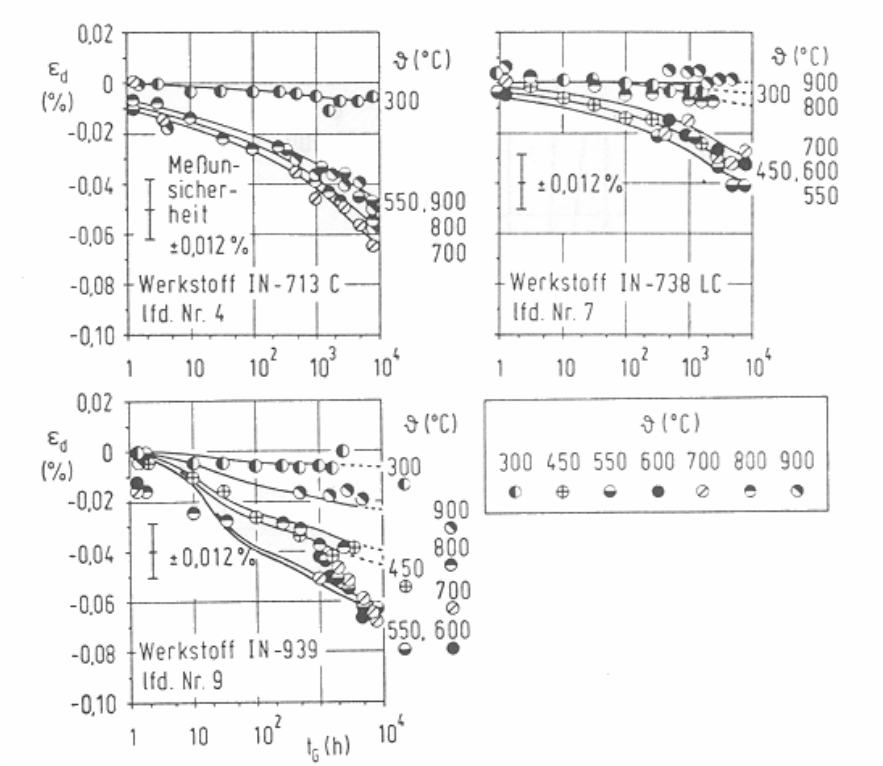

Figure 2. Density dependent strain due to structure induced density changes, measured in annealing tests [3].

2. Nimonic 80A

Nimonic 80A is a widely used superalloy, e.g. for bolting material, and is widely treated in the literature. Nimonic 80A was introduced as a turbine blade alloy already in 1944 and was adopted as a bolting material for steam turbines in the mid 1960s for operating metal temperatures of 370–570ºC. The nominal composition of Nimonic 80A is shown in Table 1.

Table 1. Composition of Nimonic 80A (weight percent).

C	**Si**	**Cu**	**Fe**	**Mn**	**Cr**	**Ti**	**Al**	**Co**	**Mo**	**B**	**Zr**	**Ni**
0.04	1.0	0.2	1.0	1.0	18.0	1.8	1.0	2.0	0.3	0.0015	0.04	bal
0.10	max	max	max	max	21.0	2.7	1.8	max	max	0.005	0.10	

Failures of Nimonic 80A steam turbine bolts have been relatively infrequent. Approximately 0.4% of the bolts in service have failed much earlier than the expected stress rupture life [9]. Nimonic 80A does not normally experience creep in the temperature regime up to 600ºC and when failed bolts were investigated it was found that instead of normal creep extension the bolts had contracted during service.

Stress relaxation testing and subsequent metallurgical investigation [4, 5] revealed that this unusual behaviour was due to an ordering transformation. Formation of the Ni_2Cr ordered phase resulted in a general lattice contraction and gave rise to negative creep.

Out of ~10,000 steam turbine bolts manufactured by Parsons Power Generation Systems 75 failures have been recorded and 34 of these were found to be a result of overload when ordering increased the stress levels in the bolts. For these bolts an initial overtightening combined with the lattice contraction caused the failure [6]. Usually the failure occurs as a brittle intergranular fracture [7].

2.1 Ordering of Ni-Cr matrix phase in Ni-based superalloys

Superalloys are normally strengthened by precipitation of the ordered γ′-phase (Ni_3Al) which has a very high resistance against coarsening, but at very long exposure times and rather low temperatures ordering of the otherwise disordered γ FCC matrix (Ni and Cr) can also take place.

The degree of ordering has a maximum when the Ni:Cr ratio of a given material corresponds to the stoichiometric composition of the ordered phase (Ni_2Cr). When the composition deviates from the ideal ratio (2:1) the kinetics of the ordering reaction become sluggish (formation is delayed) and ordering only appears after several thousands of hours of aging [10].

The unit cell of the Ni_2Cr phase is orthorhombic. The orientation relationship between the ordered phase and the fcc matrix is shown in Figure 3.

The presence of the ordered phase in a given sample can be established by electron diffraction in a transmission electron microscope. The superlattice reflections marked 1 and 2 in Figure 4 clearly indicates the presence of the Ni_2Cr ordered phase.

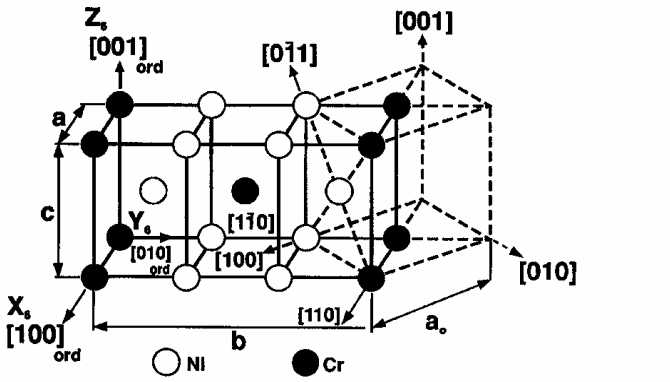

Figure 3. Ordered structure of Ni_2Cr. The broken lines refer to the original fcc unit cell [1].

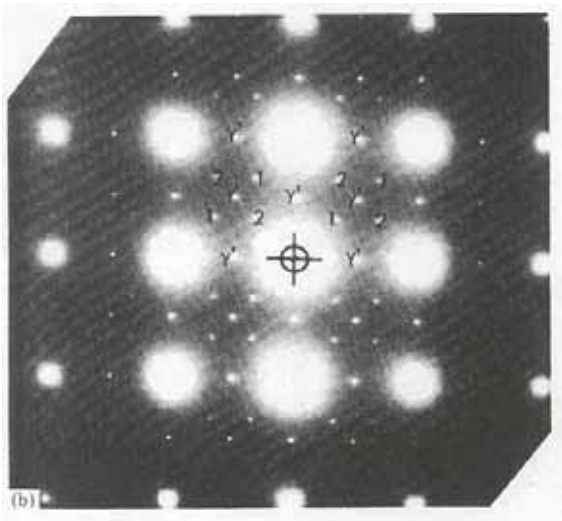

Figure 4. Diffraction pattern from Nimonic 80A thin foil containing the ordered Ni_2Cr phase [4].

For the Nimonic 80A alloy the ordering transformation introduces a general lattice contraction of approximately 0.1%, which can produce an increase in stress [4] and therefore can result in negative creep. Figures 5 and 6 show the stress relaxation behaviour of Nimonic 80A during a constant-strain stress relaxation test at different temperatures.

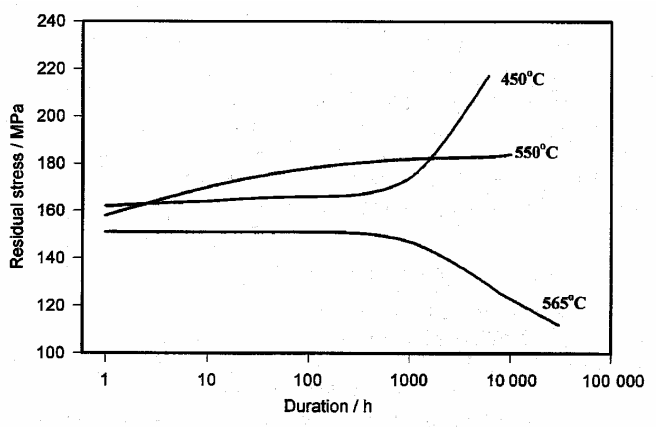

Figure 5. Stress Relaxation of Nimonic 80A at a constant strain of 0.1% [11].

At temperatures above 550ºC Nimonic 80A exhibits normal stress relaxation behaviour in that the stress decreases with increasing test duration (Figure 5 and 6). Below 550ºC the contraction due to the ordering transformation becomes the dominant factor, and negative creep behaviour is observed.

The ordering transformation does not occur immediately due to sluggish kinetics because of deviation of the Ni-Cr matrix composition from the ideal 2:1 Ni:Cr ratio. The larger the deviation the more sluggish the kinetics become. This has been shown by Marucco in investigations on Ni-Cr-Fe alloys with varying composition [12].

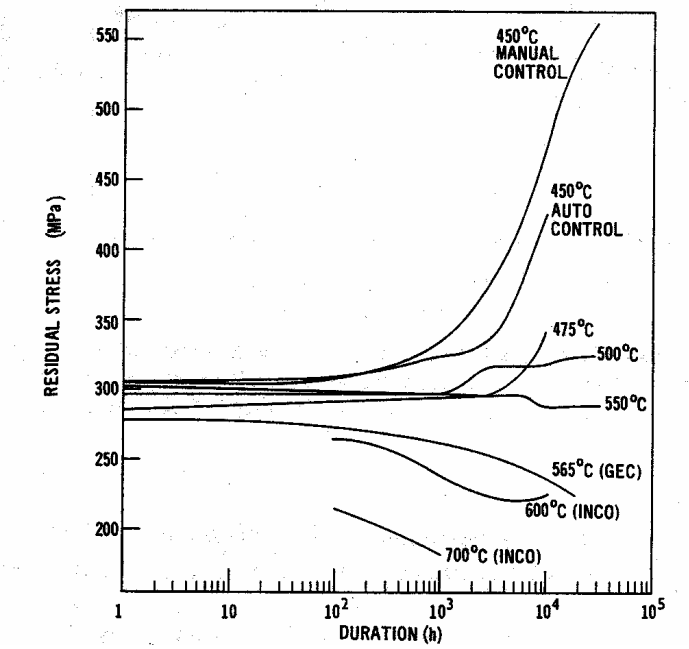

Figure 6. Stress relaxation of Nimonic 80A at a constant strain of 0.15% [4].

Total lattice contractions of up to 0.16% have been reported for a service time of 50,000 h [6].

The ordering transformation has also been reported to result in an embrittlement of the bolting material. In failed bolts a lower charpy impact value and a higher microhardness value compared to virgin stock have been found [7]. However there is some doubt whether this effect is caused by the ordering transformation or by segregation of phosphorous to grain boundaries. [13]

3. Analysis of bolt specimens

In German gas turbines two failures of Nimonic 80A bolts used for fixation of IN939 heat shields in the hot gas ducts of the turbines have recently been reported. The failure mechanism appeared to be creep and the failure occurred at a notch right below the bolt heads.

Three bolts originating from Danish gas turbines of similar type in Hilleroed and Svanemoellen were studied at the Materials department (IPL-MPT) at the Technical University of Denmark in order to establish if these bolts had indications of creep failure. Figure 7 shows the setup used in the gas turbines.

The estimated temperature of the bolt heads is 500−550°C. The lower part of the bolts is expected to be cooler than the bolt heads due to the flow of cooling air coming from the bottom.

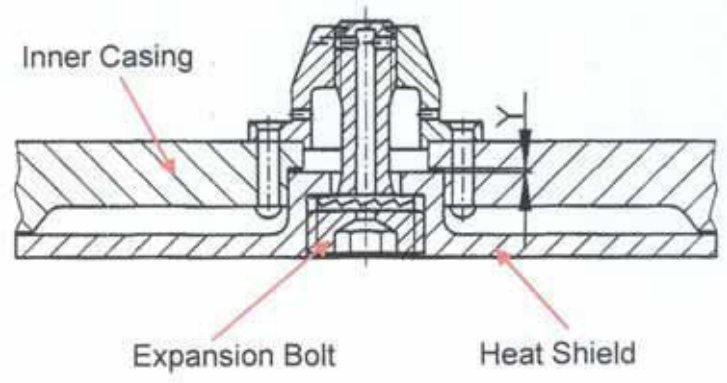

Figure 7. Geometry of the heat shield and bolt-setup.

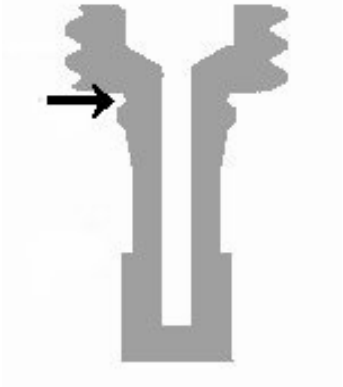

Figure 8. Schematic drawing of a bolt; the notch where failures have been found in German gas turbine bolts is marked with an arrow.

The failure was reported to happen at a notch right below the bolt head as shown in the schematic drawing in Figure 8.

An overview of the specimens available for metallurgical studies is shown in Table 2. Bolts B1 and B2 were as shown in Figure 8 while B3 had an extra cooling hole in the bottom of the bolt.

Table 2. Test specimens.

	Cooling hole	**Eqv. service hours / EOH**	**Number of starts**	**Estimated service temperature at bolt-head**
B1	no	89198	2279	500–550°C
B2	no	57100	543	
B3	yes	57100	543	
ref		0	0	N/A

3.1 Experimental procedures

Cross sections were prepared from all four bolts and studied in a light optical microscope (LOM) in order to look for signs of creep damage, and the oxidation of the surface of the service exposed bolts was studied in the scanning electron microscope (SEM).

The presence of the ordered Ni_2Cr phase described in the literature was investigated in a transmission electron microscope (TEM) using diffraction mode. TEM thin foils were prepared from different locations in all the bolts. Thinning of the foils was done by electropolishing in perchloric acid.

Finally part of the bolt B3 was sent to the materials research department (AFM) at Risoe National Laboratory for dilatometer testing.

3.2 Stereo microscopy and light optical microscopy

Investigation in the stereo microscope and in the light optical microscope indicated no presence of creep cavities or beginning creep failure neither at the notch where it has been found in German Nimonic 80A gas turbine bolts or anywhere else in the bolts. Figure 9 shows the microstructure of one of the service exposed bolts.

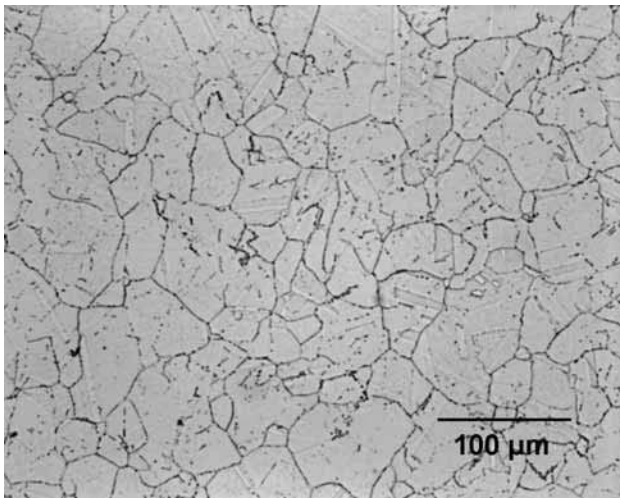

Figure 9. LOM micrograph of the microstructure of bolt B2; discrete carbide particles are located at grain boundaries.

3.3 Transmission electron microscopy (TEM)

TEM specimens revealed the presence of the ordered Ni_2Cr phase in all the bolts that have been in service. In the bolts that did not have a cooling hole running through the entire length of the bolt the ordered phase was only present in the lower part of the bolt, while it was present in the entire body of B3. The ordered phase was not found in any of the bolt-heads where the temperature has probably been too high for the ordered phase to be thermodynamically stable; also the ordered phase was not present in the reference bolt.

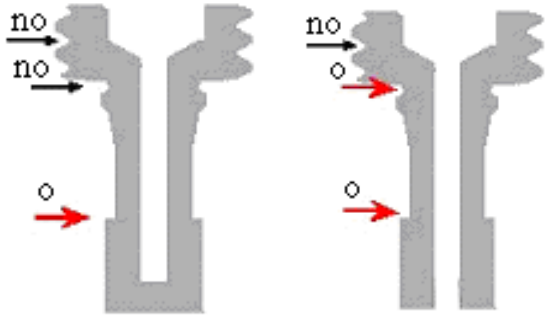

Figure 10. Schematic drawing of the bolts. The arrows indicate the locations from which TEM thin foils were prepared; arrows marked "no" indicates areas where ordering was not found (No Ordering) and arrows marked "o" indicates areas where the ordered phase was found.

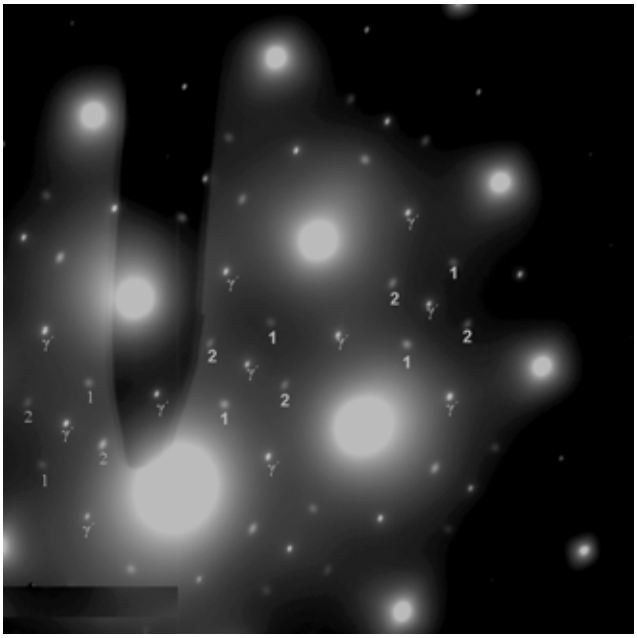

Figure 11. [001] Electron diffraction pattern from the lower part of bolt B1. 1 and 2 indicate diffraction points from two different Ni_2Cr super-lattices. γ′ indicates super-reflections from the Ni_3Al ordered phase.

The fact that the ordered phase is not present in the upper part of bolts B1 and B2 indicates that the temperature of this part has been above the critical temperature for the formation of the ordered Ni_2Cr phase. The extra cooling of bolt B3 has brought the temperature down to an area below T_c making the ordered phase energetically favorable.

3.4 Scanning electron microscopy (SEM)

Investigation of cross sections in the scanning electron microscope shows that the head of the bolts have seen a substantially higher temperature than the body of the bolts. It is clear that the heads are much more attacked by oxidation. Both surface and internal oxidation can be seen in the bolt heads (Figure 12), while the bolt body only shows signs of surface oxidation (Figure 13). This implies that the bolt heads have seen a higher service temperature than the other parts of the bolt.

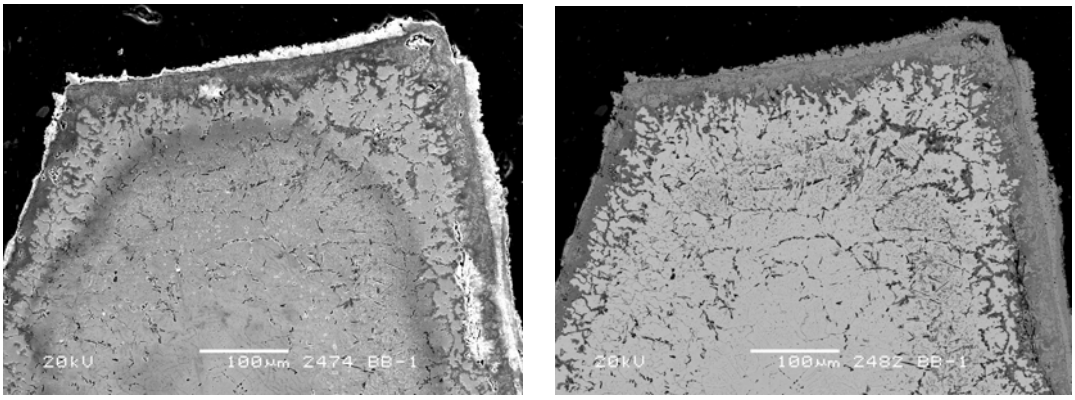

Figure 12. SEM images of part of the bolt head. The bolt head is heavily oxidized. (left) SE image and (right) BSE image of the exactly same area.

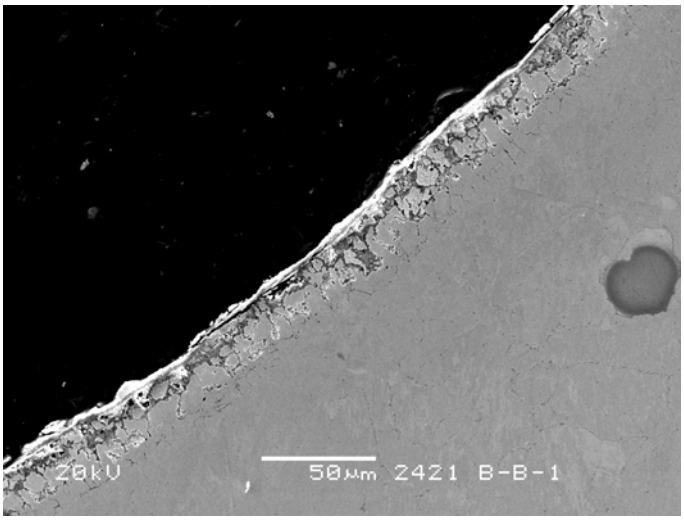

Figure 13. SEM SE image of the oxidation along the body of the same bolt shown in figure 12; notice the different scales.

This result corresponds nicely with the TEM results since it was speculated that the temperature in the bolt heads had been above the critical temperature for the formation of the ordered phase, while the body of the bolts had seen a lower service temperature.

3.5 Dilatometer

The material was heated up to 700ºC at a rate of 2ºC/min and the expansion of the material with temperature was recorded.

The tests show that the presence of the ordered phase indeed introduces a lattice contraction of about 0.1% in the lower part of the bolts.

Figure 16 shows the measured dilatometer curve for material from the lower part of bolt B3. During the first heating cycle an extra expansion is found due to the disappearance of the ordered phase at temperatures above T_c. After the specimen has been cooled to room temperature the experiment is repeated and the specimen is reheated. Now the extra expansion is no longer present in the curve (2nd cycle in Figure 14).

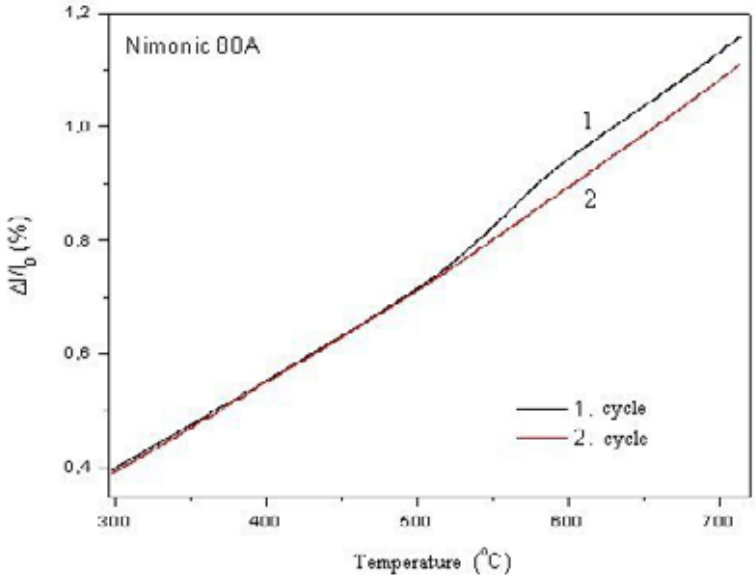

Figure 14. Dilatometer curve for lower part of B3.

This experiment shows that it is very easy to remove the ordering by holding specimens for a short while at a temperature above T_c. The second heating cycle does not show the same extra expansion because of the sluggish kinetics of the ordering formation. Like the initial formation of the ordering it will take several thousands of hours in the temperature regime 400–550ºC to again reestablish the ordering.

4. Discussion

The Nimonic 80A alloy does not normally suffer from excessive creep in the temperature regime 500–550ºC. However it has previously been found that negative creep in combination with an excessive prestraining of the bolts during tightening has led to failure of steam turbine bolts [6]. In the present case several different factors contribute and the sum of these factors may have led to the failure of the German gas turbine bolts.

Unlike steam turbine bolts the investigated bolts experience a temperature gradient during service. The temperatures are such that the Ni_2Cr ordered phase is thermodynamically stable in the lower part of the bolts but not in the bolt

heads. This leads to negative creep occurring in the lower part of the bolts but not in the bolt heads and will very likely result in a stress buildup in the exact area where the failure was found to initiate. Furthermore a notch is located at exactly this location (right below the bolt head) and acts as initiation site for the creep rupture. It is not believed that any of these factors by themselves can cause a failure, but the combination of differences in temperature, negative creep, the location of the notch and perhaps an initial overtightening may have lead to the observed failure of the German gas turbine bolts. The combination of factors contributing may also explain that the failure appeared as a typical creep failure, contrary to the brittle failures observed in steam turbine bolts.

5. Summary

Negative creep is the result of a solid-state transformation occurring during service or creep testing. For most applications the phenomenon is non-critical but for certain constrained components it may become critical.

For the alloy Nimonic 80A negative creep occurs due to ordering of the matrix phase resulting in the formation of the Ni_2Cr ordered phase. The negative creep is only observable after several thousand hours of exposure in the temperature regime 400–550ºC. The sluggish kinetics are probably caused by the deviation in composition from the 2:1 stoichiometry for Ni and Cr of the ordered phase. The ordering has in combination with other factors such as overtightening led to failure of steam turbine bolts.

A recent failure of Nimonic 80A gas turbine bolts in German gas turbines inspired an investigation of similar bolts from Danish gas turbines of the same type. Investigation in the TEM revealed the presence of the ordered phase in these bolts. The ordered phase was only found in the body of the bolts not in the bolt heads. This is because the temperature at the bolt heads was above the critical temperature for the ordering transformation.

It was shown by dilatometer experiments that the ordering transformation had resulted in a contraction of the lower part of the bolts of the order of size of 0.1%. It was also found that the ordering can be removed by a short heat treatment above the critical temperature for the ordering transformation.

It is believed that negative creep may have played a significant role in the failure of the German Nimonic 80A gas turbine bolts.

References

1. B. Reppich. Negatives Kriechen. Z. Metallkde. 75 (1984) 193.

2. R.W. Fountain & M. Korchynsky. The phenomenon of negative creep in alloys. Trans. ASM 51 (1959) 108.

3. K.H. Kloos, J. Granacher & H. Bartsch. Untersuchung des Kriechverhaltens hochwarmfester Gasturbinenwerkstoffe. Z. Werkstofftech 17 (1986), pp. 199–205.

4. E. Metcalfe, B. Nath & A. Wickens. Some effects of the ordering transformation in Nimonic 80A on stress relaxation behaviour. Materials Science and Engineering, 67 (1984), pp. 157–162.

5. E. Metcalfe & B. Nath. Proceedings of Conf. on Phase Transformations, York, 1979 Inst Metall. Conf. Ser. 3, 2(11) (1979) II-50.

6. S.M. Beech. 25 Years of experience of nickel based bolting materials. In: Strang, A. (Ed.) Performance of Bolting Materials in High Temperature Plant Applications, Conference Proceedings, 16–17 June 1994, York, UK. The Institute of Materials 1995. Pp. 259–270.

7. P. Vinders, R. Gommans, G. van Oppen & K. Verheesen. Brittle fracture of Alloy 80A stud bolts in a steam turbine. In: Strang, A. (Ed.) Performance of Bolting Materials in High Temperature Plant Applications, Conference Proceedings, 16–17 June 1994, York, UK. The Institute of Materials 1995. Pp. 271–283.

8. Marucco & B. Nath. Effects of ordering on the properties of Ni-Cr alloys. J. Materials Science 23 (1988), pp. 2107–2114.

9. A. Marucco & B. Nath. Effects of composition on ordering behaviour and rupture properties of Alloy 80A. In: High Temperature Materials for Power Engineering, Conference Proceedings, 24–27 September 1990, Liége, Belgium. Kluwer Academic Publishers 1990. Pp. 535–545.

10. Marucco and B. Nath. The effect of ordering on the high temperature deformation of nickel based alloys. In: Mechanical Behaviour of Materials – IV. Proceedings of the Fourth International Conference, 1984, 1, pp. 299–305.

11. S.M. Beech, S.R. Holdsworth, H.G. Mellor, D.A. Miller & B. Nath. An assessment of Alloy 80A as a high temperature bolting material for advanced steam conditions. Proceedings of Int. Conf. Advances in Material Technology for Fossil Power Plants, Chicago, 1987. Pp. 503–410.

12. A. Marucco. Atomic ordering in the Ni-Cr-Fe system. Materials Science and Engineering, A189, 1994, pp. 267–276.

13. K.H. Mayer & H. König. High temperature bolting of steam turbines for improved coal-fired power plants. Proceedings of Third International Conference on Improved Coal-Fired Power Plants (ICPP), San Francisco, 1991.

Lifetime prediction for TBC systems: Generation of appropriate input data for models

S. Osgerby, J.W. Nunn & S.R.J. Saunders
Materials Centre, National Physical Laboratory, Teddington, UK

Abstract

Reliable data on the properties of bondcoat and ceramic are vital to provide confidence in predictive models of TBC lifetime. Examples of the methods by which these data can be obtained are given together with examples of the properties of a commercial MCrAlY bondcoat and both EB-PVD and APS ceramic layers. In principle it is possible to measure all the required input data independently, thereby producing robust models with no arbitrary fitting parameters.

1. Introduction

Many components in gas turbines have a thermal barrier coating (TBC) to reduce the mean metal temperature. Accurate prediction of service lifetimes for these components relies upon many factors including identification and physical modelling of the appropriate failure mechanism, knowledge of the service conditions and accurate input data to the model. The latter of these factors is frequently ignored, as many inputs are difficult to measure, so values are assumed.

Examples of input data that are required include surface topology of the individual layers, growth kinetics for the alumina scale, growth stresses in this oxide, Young's modulus and Poisson's ratio of the individual layers and mechanical properties of the bondcoat. It is also important to know how these properties vary with temperature and evolve with the changing microstructure of the coating system over time.

This paper addresses methods by which the appropriate input data can be generated, together with the limitations of existing methods. The input data presented were generated on a system comprising a CMSX-4 substrate, a commercial MCrAlY bondcoat and either EB-PVD or APS zirconia.

2. General comments on model requirements

The common observation is that TBC systems fail by fracture associated with the thermally-grown oxide (TGO) between the bondcoat and ceramic. The fracture path may be through the TGO or at one of the interfaces – TGO/bondcoat or TGO/ceramic (1–3). There are significant differences between the behaviour of EB-PVD and APS TBC systems and any model developed for lifetime prediction must explain these.

3. Specific model requirements

The input data required for models to predict TBC lifetime can be classified into three sets, namely geometric, kinetic and mechanical. In the following sections these will be addressed individually and examples of the generation of robust input data will be given.

3.1 Geometrical factors

Most models of TBC systems fall into two broad categories. The first category assumes a planar interface between oxide and bondcoat (4) whereas the second category use a simplified geometry for the interface, similar to that shown in Figure 1. The bondcoat/ceramic interface is assumed to have a regular periodic variation in 3 dimensions. The interface can be characterised by the 2 parameters b and b/a.

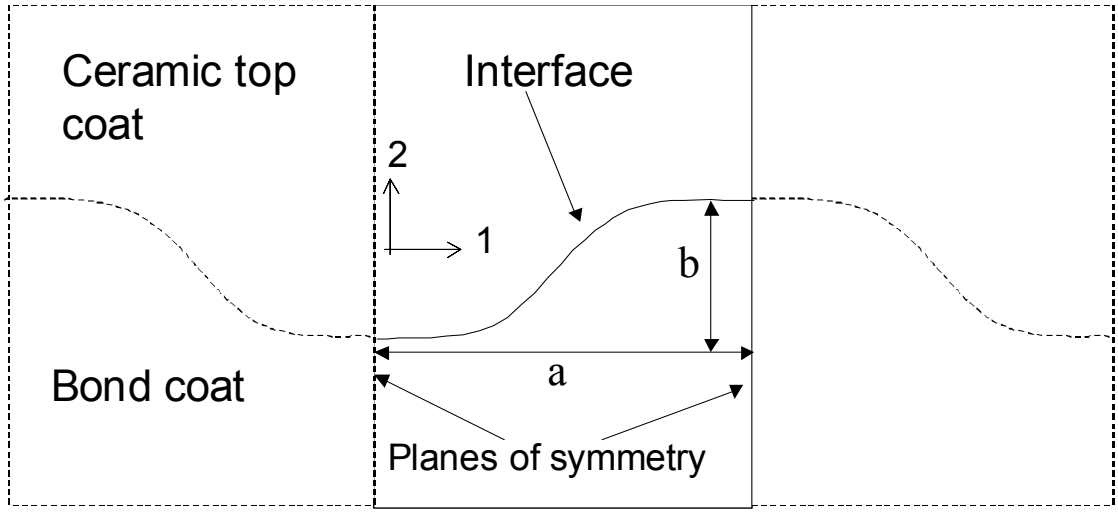

Figure 18. Generalised representation of TBC system.

Cross sections were prepared using standard metallographic procedure. The two parameters, a and b, were measured from scaled micrographs. The distribution

of the two parameters is shown in Figure 2. In both cases it can be seen that the parameters have a Gaussian distribution with easily defined mean and standard deviation.

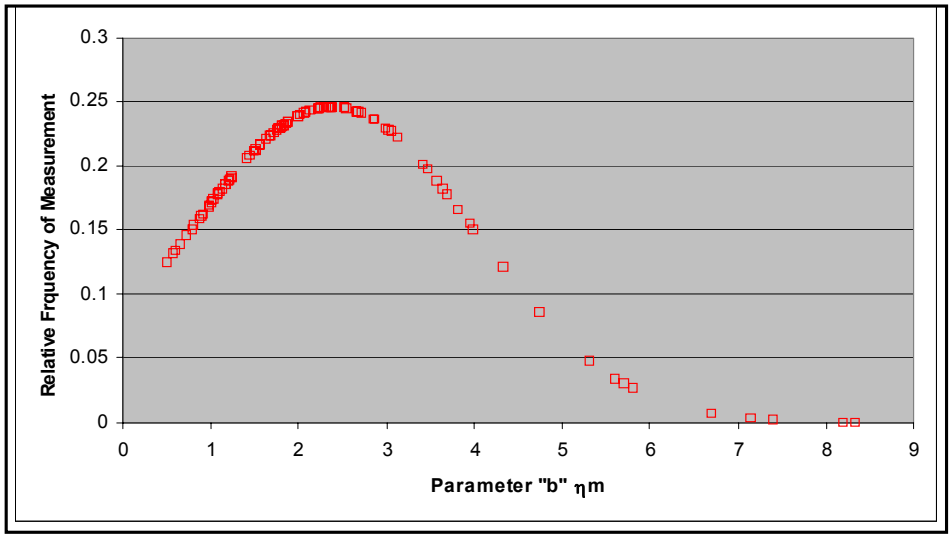

(a)

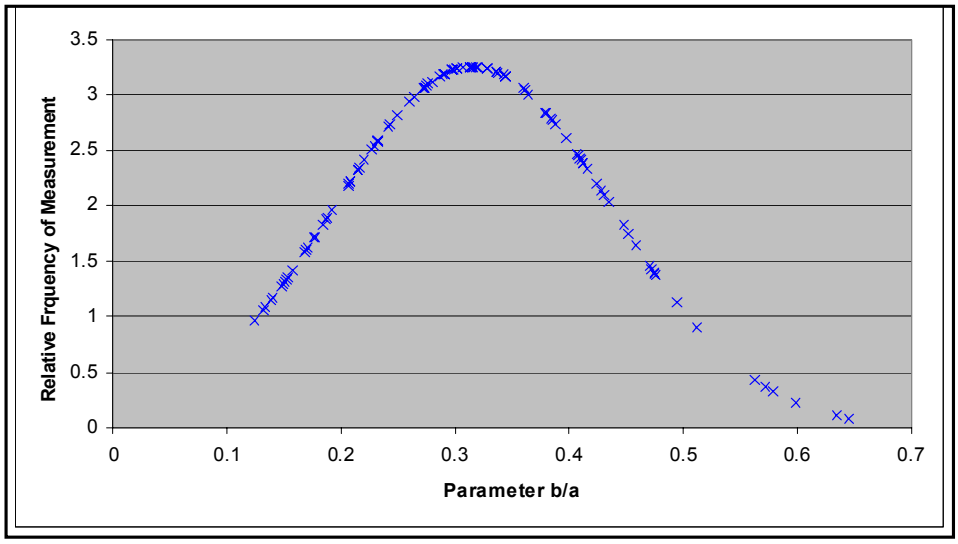

(b)

Figure 19. Distribution of interface geometry parameters for MCrAlY bondcoat/APS Zirconia TBC system (a) b parameter, mean= 2.39 μm, standard deviation = 1.62 μm (b) b/a parameter, mean= 0.32, standard deviation = 0.12.

3.2 Oxide growth kinetics

Samples comprising of CMSX-4 substrate and MCrAlY bondcoat were oxidised in air at temperatures between 1000°C and 1100°C for times up to 1000 h. The specimens were sectioned, prepared metallographically and the oxide thickness measured under an optical microscope incorporating x–y displacement measurement. The oxide thickness as a function of time is shown in Figure 3. For the exposures at 1050°C and 1100°C the oxide formed was indisputably

identified as alumina whereas at the lower temperature a mixed nickel/aluminium oxide was observed. This oxide has faster growth kinetics than alumina and the data from this exposure should be excluded from any constitutive expression of alumina growth rates.

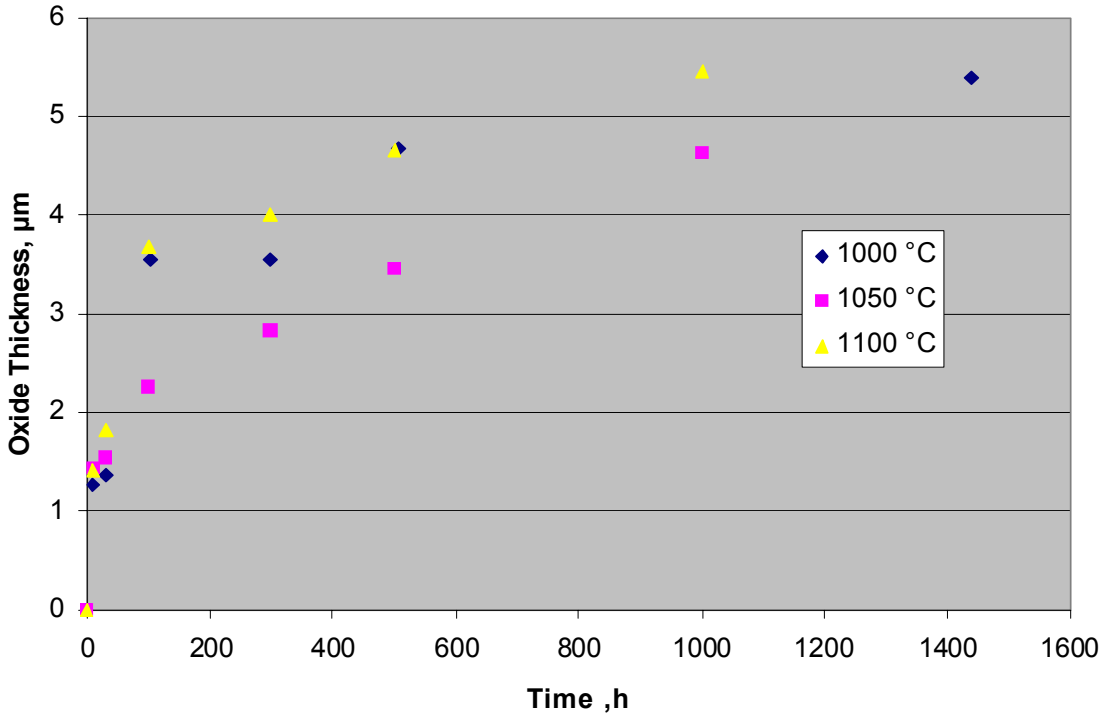

Figure 20. Growth kinetics for TGO on MCrAlY coating.

Data from the exposures at 1050°C and 1100°C were analysed to produce an analytical expression for the growth kinetics viz.

$$\lambda = 107 \exp\left(\frac{-58000}{RT}\right) t^{0.3} \qquad (1)$$

where λ is the oxide scale thickness measured in µm
T is the absolute temperature
t is the exposure time in hours.

The growth kinetics are sub-parabolic, which is a common observation for alumina (5). However the derived activation energy is very low compared to previously published values (6), perhaps indicating that some change in the composition or microstructure of the scale is operating between 1050 and 1100°C.

3.3 Oxide growth stresses

The importance of oxide growth stress on TBC failure is dependent upon the creep strength of the bondcoat at the oxide growth temperature. For 'rigid' bondcoats oxide growth stresses will continually increase and eventually initiate cracking leading to failure of the TBC system. However, as will be demonstrated in a later section of this paper, most bondcoats are relatively weak at high temperature and any stresses generated by oxide growth will relax due to creep processes in the bondcoat. In this case the oxide growth stresses can be safely ignored.

3.4 Young's modulus and Poisson's ratio

The Young's modulus and Poisson's ratio of both bond coat and ceramic are crucial inputs to any model of TBC performance. There are many methods available to measure Young's modulus and these have been compared in a recent publication (7). Some measurement techniques are limited to ambient temperature eg laser surface acoustic wave (LSAW) and nanoindentation, whereas others can be used at elevated temperatures eg impact excitation and mechanical straining.

Table 1. Young's modulus of freestanding MCrAlY using a range of techniques.

Technique	Room Temperature Modulus, GPa	Comment
Impact Excitation	177	
LSAW	197	
Nanoindentation (in plan)	60	Inaccurate value attributed to surface roughness of coating

A commercial bondcoat has been investigated using a several of these techniques - the results from which are shown in Table 1. It is apparent that the different techniques do not give the same value for Young's modulus. Great care must be taken in making measurements of modulus and assessing the data.

LSAW has also been used to measure the Young's modulus of EB-PVD zirconia in the longitudinal direction, yielding a value of 73 GPa. In this case the apparently low modulus is genuine and is a result of the columnar microstructure of the ceramic. The technique was also attempted on APS zirconia but no data were obtained due to excessive scattering of the acoustic waves by the internal boundaries. Using nanoindentation values of modulus between 40–160 GPa were obtained for EB_PVD zirconia and 40–120 GPa for APS zirconia. The range of

values is very high and probably related to cracking or other damage of the ceramic during indentation.

Techniques for measuring the Poisson's ratio of coatings have been developed by Maxwell et al. (8). One proposed method is to compare the Young's modulus obtained from the impact excitation method (E), where Poisson's ratio (υ) is not required in the derivation, to the indentation modulus (E^*). These values are related according to the expression:

$$\upsilon = \left(1 - \frac{E}{E^*}\right)^{0.5} \tag{2}$$

As yet no measurements of Poisson's ratio have been made on TBC system but, in principle, they are possible.

3.5 Creep Strength

The creep strength of the bondcoat is a measure of how quickly stresses that are developed during TGO growth or thermal cycles are relaxed. Two methods have been proposed to measure the creep response of bondcoats: firstly the bondcoat can be deposited to a thickness such that creep specimens can be machined directly from the coating, alternatively the creep properties of the coating can be derived from the behaviour of a composite specimen with known area fraction of coating and (well-defined) substrate.

The commercial MCrAlY bondcoat was produced with thickness approaching 10 mm. Creep specimens were machined from this coating and tested at 900 and 950°C. Creep curves are shown in Figure 4.

The coating showed high ductility at both temperatures with none of the specimens actually fracturing.

The creep response of the coating was analysed and expressed as an Arrhenius type equation viz.

$$\dot{\varepsilon} = 1x10^{10}\ \sigma^{2.28}\ \exp\left(\frac{-300000}{RT}\right) \tag{3}$$

where ε is the creep rate measured in hours
σ is the stress measured in MPa
T is the absolute temperature.

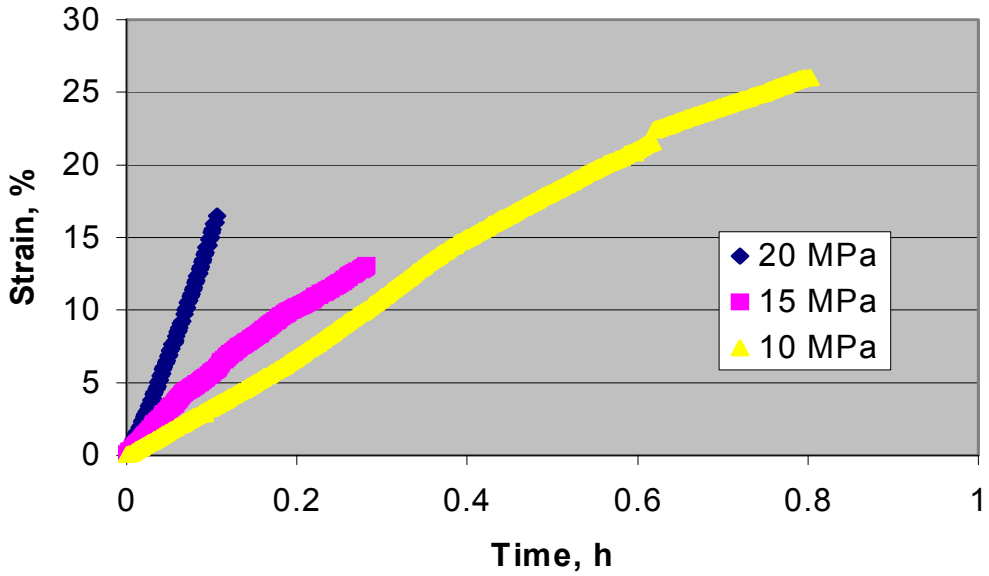

(a)

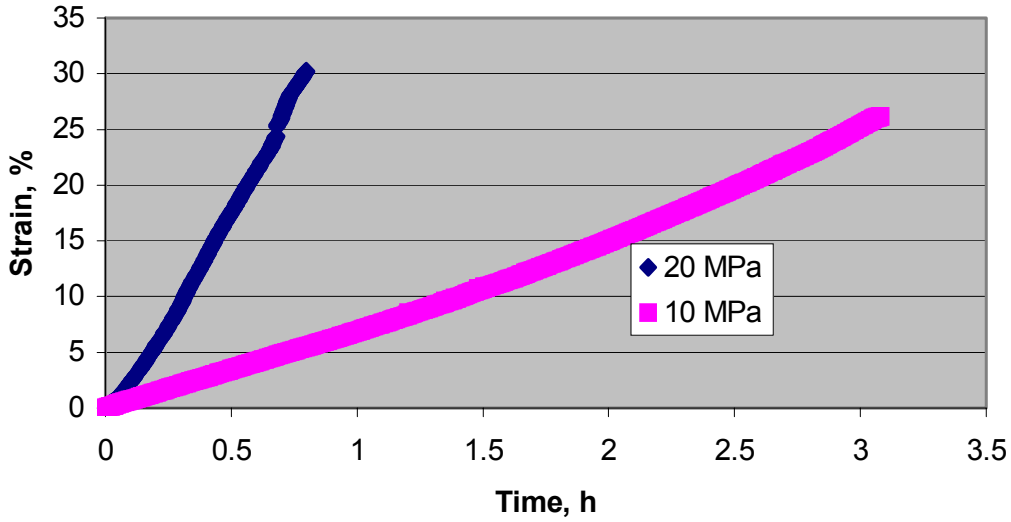

(b)

Figure 21. Creep curves obtained from free-standing coating at (a) 950°C and (b) 900°C.

Taylor et al. (9) demonstrated that the creep properties of MCrAlY coatings can be derived. Although no direct comparison is available, Taylor's results on APS 68Ni25Cr6Al0.4Y coating indicate creep rates more than two orders of magnitude lower than those observed in this work. This raises a question whether this difference is due to intrinsic material differences in the two pieces of work or whether there are inherent problems in producing thick coatings in that the microstructure is corrupted.

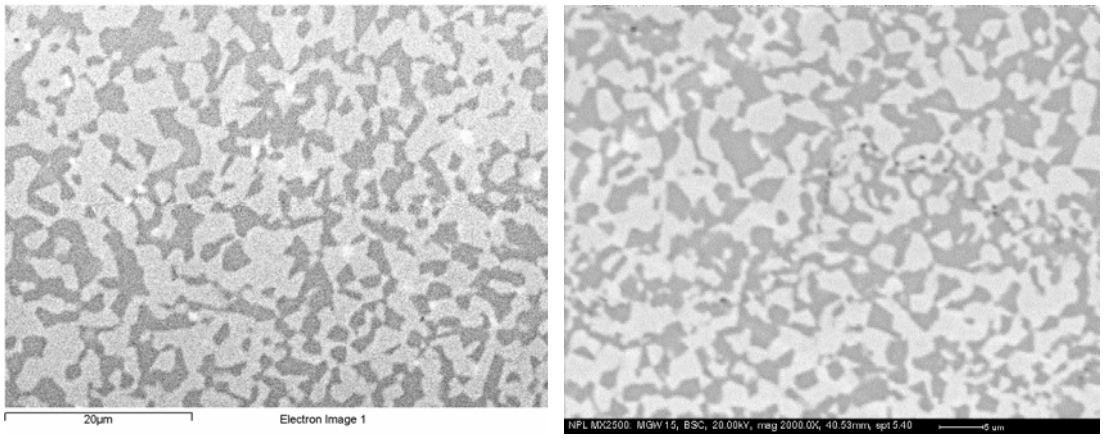

(a) (b)

Figure 22. SEM Images of commercial MCrAlY coating (a) produced as 'free standing' (b) coating on CMSX-4 substrate.

Figure 5 shows the differences in microstructure observed between 'coating' that is produced as free-standing and that deposited on a substrate. The deposited structure appears finer and there is a difference is the relative proportions of the constituent phases between the two production routes. This may be the cause of any differences in creep performance.

3.6 Ductility

The ductility of the coating can be measured by the onset of cracking under uniaxial or biaxial straining. Beam or disc testpieces are deformed in flexure, where the displacement of the central point on the testpiece can be correlated with surface strain, and cracking of the coating is detected by acoustic emission. Measurements are carried out at different temperatures to determine the ductile/brittle transition temperature (DBTT).

DBTT has been determined by a series of measurements using the small punch test. The displacement to initiate the first crack in the coating is shown in Figure 6 as a function of temperature. Although there is some scatter in the results the overall trend can be identified, giving a DBTT at ~575°C.

These data are reinforced by images of the cracking patterns at the different temperatures. Figure 7 shows examples of the cracking patterns obtained in both brittle and ductile failure.

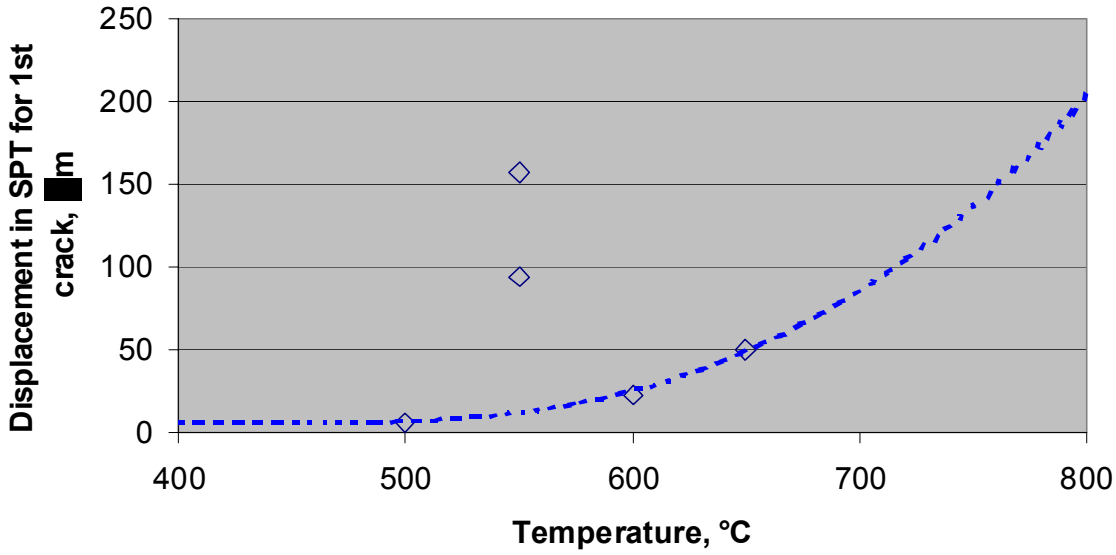

Figure 23. DBTT Determination for MCrAlY Coating.

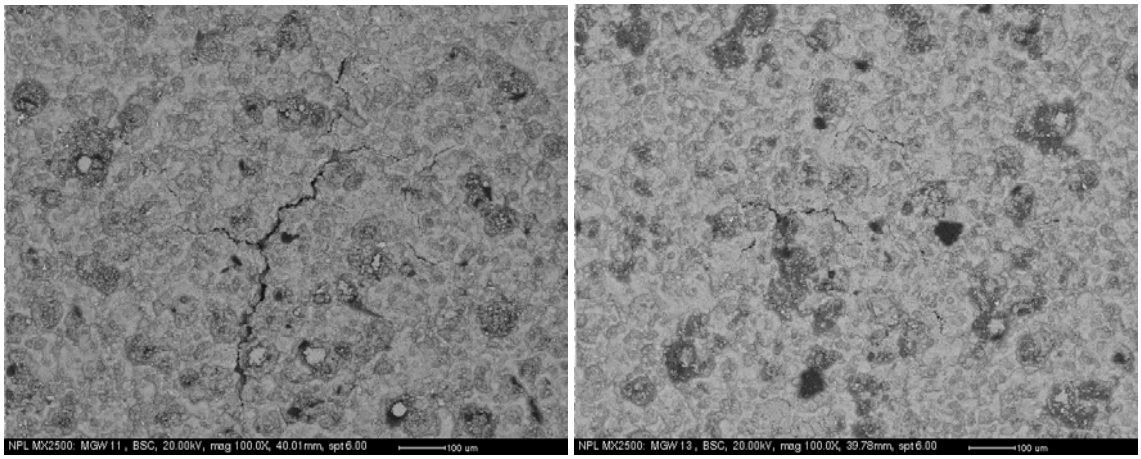

(a) (b)

Figure 24. SEM Images of cracking during small punch testing (a) brittle cracks at 500°C (b) ductile cracking at 650°C.

4. Conclusions

The availability of high quality input data is critical to the reliability of predictive models. This paper has demonstrated how such data can be generated for TBC systems.

5. Acknowledgements

This work was carried out under the Lifetime Performance of Materials Programme, a programme of research funded by the UK Department of Trade and Industry.

The authors are grateful to Dr Louise Brown and Mr Jim Banks who assisted with the testing and metallography.

References

1. J.H. Sun, E. Chang, C.H. Chao & M.J. Cheng. Oxid. Met. 40 (1993), pp. 465–481.

2. M.P Taylor, P. Niranatlumpong, H.E. Evans & C.B. Ponton. Proc. Conf 4th Int Conf on the Microscopy of Oxidation, Science Press New York 1999. Pp. 219–224.

3. N.P. Padture, M. Gell & E.H. Jordan. Science 296 (2002), pp. 280–284.

4. J.A. Nesbitt & R.W. Heckel. Thin Solid Films 119 (1984) 281.

5. G. Borchardt & G. Strehl. Proc. Int. Conf. on Materials Aspects in Automotive Catalytic Converters (MACC), held at Materials Week, Munich, 3–4 October 2001.

6. G. Strehl, D. Naumenko, H. Al-Badairy, L.M. Rodriguez Lobo, G. Borchardt, G.J. Tatlock & W.J. Quadakkers. Proc. Conf 4th Int. Conf. on the Microscopy of Oxidation, Science Press New York 1999. Pp. 87–92.

7. S. Osgerby, J.W. Nunn, J.P. Banks, A.S. Maxwell & G. Aldrich-Smith. Young's Modulus Measurement for Coatings used in Gas Turbines, National Physical Laboratory, MATC(MN)54, February 2004.

8. A.S. Maxwell, S. Owen-Jones & N.M. Jennett. Measurement of the Poisson's Ratio of Coatings, National Physical Laboratory, MATC(MN)51, June 2003.

9. M.P. Taylor, H.E. Evans, C.B. Ponton & J.R. Nicholls. Surface and Coatings Technology, 124 (2000), pp. 13–18.

Published by

Series title, number and report code of publication

VTT Symposium 233
VTT–SYMP–233

Author(s)
Veivo, Juha

Title

BALTICA VI
Life Management and Maintenance for Power Plants. Vol. 1

Abstract

BALTICA VI International Conference on Life Management and Maintenance for Power Plants, held on June 8–10, 2004 in Helsinki – Stockholm – Helsinki

This is one of the two volumes of the proceedings of the BALTICA VI Conference, which provides a forum for the transfer of technology from applied research to practice. The Conference focuses on reviewing new technology, recent experience and improvements in applied life management and maintenance for successful and economical operation of power plants.

Keywords
power plant, maintenance, boiler, machinery, equipment, inspection, monitoring, condition, life, performance, risk, reliability

Activity unit
VTT Industrial Systems, Kemistintie 3, P.O.Box 1704, FIN–02044 VTT, Finland

ISBN			Project number
951–38–6291–7 (soft back ed.) 951–38–6292–5 (URL: http://www.vtt.fi/inf/pdf/)			
Date May 2004	Language English	Pages 354 p.	Price G
Name of project BALTICA VI		Commissioned by	
Series title and ISSN VTT Symposium 0357–9387 (soft back ed.) 1455–0873 (URL: http://www.vtt.fi/inf/pdf/)		Sold by VTT Information Service P.O.Box 2000, FIN–02044 VTT, Finland Phone internat. +358 9 456 4404 Fax +358 9 456 4374	

BALTICA VI International Conference on Life Management and Maintenance for Power Plants, June 8–10, 2004 in Helsinki–Stockholm–Helsinki

This is one of the two volumes of the proceedings of the BALTICA VI Conference. The Conference focuses on reviewing new technology, recent experience and improvements in applied life management and maintenance for supporting successful and economical operation of power plants.

The BALTICA events:

BALTICA I. Materials Aspects in Life Extension of Power Plants, Helsinki–Stockholm–Helsinki, September 19–22, 1988

BALTICA II. International Conference on Plant Life Management & Extension, Helsinki–Stockholm–Helsinki, October 5–6, together with the International Symposium on Life and Performance of High Temperature Materials and Structures, Tallinn, Estonia, October 7–8, 1992

BALTICA III. International Conference on Plant Condition & Life Management, Helsinki-Stockholm-Helsinki, June 6–8, 1995

BALTICA IV. Plant Maintenance for Managing Life & Performance, Helsinki–Stockholm–Helsinki, September 7–9, 1998

BALTICA V. International Conference on Condition and Life Management for Power Plants, Hotel Haikko Manor, Porvoo, Finland, June 6–8, 2001

BALTICA VI. International Conference on Life Management and Maintenance for Power Plants, Helsinki–Stockholm–Helsinki, June 8–10, 2004

Tätä julkaisua myy	Denna publikation säljs av	This publication is available from
VTT TIETOPALVELU PL 2000 02044 VTT Puh. (09) 456 4404 Faksi (09) 456 4374	VTT INFORMATIONSTJÄNST PB 2000 02044 VTT Tel. (09) 456 4404 Fax (09) 456 4374	VTT INFORMATION SERVICE P.O.Box 2000 FIN–02044 VTT, Finland Phone internat. +358 9 456 4404 Fax +358 9 456 4374

ISBN 951–38–6291–7 (soft back ed.)
ISSN 0357–9387 (soft back ed.)

ISBN 951–38–6292–5 (URL: http://www.vtt.fi/inf/pdf/)
ISSN 1455–0873 (URL: http://www.vtt.fi/inf/pdf/)

VTT SYMPOSIUM 233 BALTICA VI. Life Management and Maintenance for Power Plants. Vol. 1